UNITED STATES DEPARTMENT OF THE INTERIOR

GEOLOGICAL SURVEY

Mafic and Ultramafic Xenoliths from Volcanic Rocks of the Western United States

H.G. Wilshire[1], C.E. Meyer[1], J.K. Nakata[1], L.C. Calk,[1]
J.W. Shervais[3], J.E. Nielson[1], and E.C. Schwarzman[2]

[1] Menlo Park, California 94025

[2] Woods Hole, Massachusetts 02543

[3] Universi[redacted]f [redacted]olina, Columbia South Carolina 29208

Open-File Report 85-139

MAFIC AND ULTRAMAFIC XENOLITHS FROM VOLCANIC ROCKS
OF THE WESTERN UNITED STATES

TABLE OF CONTENTS

ABSTRACT

Mafic and ultramafic xenoliths in the western United States occur in volcanic rocks ranging from lamprophyric to dacitic in composition, and are found in every major tectonic province from the Coast Ranges in California to the Great Plains. Xenoliths from 68 localities are described here, but new localities are being discovered, and much remains to be learned about their distribution with respect to the tectonic and geophysical framework of the western United States.

Xenoliths in volcanic rocks in the western United States are placed here in eight main groups: One group consists of accidental inclusions of crustal sedimentary, igneous, and metamorphic rocks. The seven other groups of interrelated inclusions comprise (2) gabbroids; (3) metagabbroids; (4) spinel peridotite, pyroxenite, and phlogopite-rich rocks of the Cr-diopside group; (5) spinel peridotite, pyroxenite, amphibole, and mica-rich rocks of the Al-augite group; (6) spinel peridotite and pyroxenite of the bottle-green pyroxene group; (7) spinel peridotite and pyroxenite of the feldspathic ultramafic group; and (8) peridotite and pyroxenite of the garnetiferous ultramafic group. Relative abundances of groups 2-8 vary from locality to locality, but in general peridotite of group 4 is dominant, and all other types, including pyroxenites of group 4, are very subordinate in abundance.

Composite xenoliths containing more than one rock type of the same group consistently show that peridotite forms the host rock for dikes and veins of the less mafic rocks. Composite xenoliths containing rock types representing more than one main group show that Cr-diopside peridotite, by far the dominant rock type, forms the host for rock types of the other main groups, and demonstrate that most principal xenolith rock types can occur in close proximity to one another in their place of origin. Peridotite members of the Al-augite group and possibly also of the feldspathic and bottle-green pyroxene groups formed by metasomatic alteration of Cr-diopside lherzolite in zones bordering dikes of those groups.

Structural evidence demonstrates that mafic dikes of all the main groups were emplaced in dilational fractures in solid peridotite. The fractures ranged from hairline to a few 10s of cm in width. Fractures discontinuously occupied by Cr-diopside and Al-augite glimmerite were healed before excavation, whereas other fractures associated with Al-augite hornblendite veins controlled excavation of the peridotite by the host magma. Minor element compositions of the dikes generally show that they no longer represent liquid compositions. This is interpreted to be the result of fractionation processes in which liquid residues were separted from basaltic intrusions during crystallization (and subsequently crystallized as hornblendite and glimmerite), wallrock reactions, and subsequent partial remelting.

Systematic probe traverses of composite xenoliths show that mafic dikes of all the main groups reacted with their wallrocks. The reactions generally resulted in enrichment in Fe and Ti of peridotite near Al-augite pyroxenite and hornblendite dikes. Unlike the pyroxenite reactions, however, the more volatile fluids that crystallized hydrous minerals and plagioclase effectively penetrated the wallrock along grain boundaries where secondary amphibole and

related minerals crystallized. The higher REE abundances and LREE-enriched patterns of the volatile fluids altered the REE compositions of clinopyroxene in the peridotite, and left leachable residues enriched in the same components in the peridotite. Composite xenoliths further show that reactions with both pyroxenite and hydrous mineral veins may change the isotopic composition of clinopyroxenes in the wallrock, producing a shift within the "mantle array" toward higher $^{87}Sr/^{86}Sr$ and lower $^{143}Nd/^{144}Nd$ compositions.

The relation between hydrous mineral veins and a complex system of planar fractures in peridotite suggests that the fracture system was propagated in front of the zone of liquid intrusion by a gas phase evolved from the hydrous liquids. Fractionation of LREE and other incompatible elements in the gas phase could extend the zone of metasomatic alteration beyond that in which new mineral phases crystallized in the altered rock.

Crosscutting relationships among dikes of different main groups in composite xenoliths combined with similar evidence from alpine peridotite massifs indicate a sequence of emplacement of dikes from oldest to youngest of: Cr-diopside pyroxenite (multiple generations); magnesian phlogopite glimmerite (±Cr-diopside); garnetiferous pyroxenite; bottle-green pyroxene pyroxenites; Al-augite pyroxenites, wehrlites, Ti-Fe hornblendite (± Ti-Fe mica and apatite), and Ti-Fe glimmerite (multiple generations); gabbroids (multiple generations).

An hypothesis for the origin of lithic variants of the inclusion suites consistent with field and laboratory investigations is that partial melting, differentiation of the melts, metasomatic interactions between the melts and wallrocks, and crystallization, recrystallization and remelting took place within diapirs of Cr-diopside peridotite and garnetiferous peridotite at progressively lower temperatures and pressures as the diapirs rose in the upper mantle, and, in places, into the lower crust. Differences in assemblages of xenoliths from locality to locality, with some populations comprising rocks of the Cr-diopside group alone, others comprising rocks of the Cr-diopside and Al-augite groups, and still others containing representatives of the feldspathic group, can be explained if volcanic eruption terminated diapirism at different levels in the upper mantle and lower crust.

The dikes representing all main groups of xenoliths are thus viewed as products of a broadly continuous episode of melting in the mantle and lower crust, and are regarded as quasi-cognate with the magma that brought fragments of them to the surface. Most peridotites, whether metasomatically altered or not, are accidental inclusions, but those modified by the multiple episodes of melting and reaction leading to generation of the host magmas cannot be considered broadly representative of the mantle. Metasomatic effects, including "cryptic," "patent," and "diffusion-reaction" types, are considered to be consequences of emplacement of the melts and their differentiates.

INTRODUCTION

Mafic and ultramafic inclusions are widespread in alkalic basalts and kimberlites of the western U.S. (fig. 1). Inclusions in basalts in this area have been the subject of study for several decades, but new discoveries are becoming more, not less, frequent. In the western United States more than 50 localities with inclusions sufficiently numerous and varied to be instructive are known (Appendix I), and many others of marginal value have been reported. These occurrences are found in widely varied geologic settings.

Whether the nature of the inclusion suites varies regionally with differences in setting, or independently, or not at all, is in part the subject of the work. We have as well concentrated our efforts on exploring the causes of variation within and between major types of inclusions. The first, and major step in our study was to determine the nature and distribution of inclusions by statistical field examination of a variety of physical parameters of the xenoliths, an approach pioneered by Jackson (1968). This focused our attention on the fact that there are at least five major varieties of ultramafic inclusions in these volcanic rocks, three of which are spinel-facies ultramafic rocks distinguished by different mineral compositions; a fourth group is characterized by spinel and plagioclase, and the fifth is garnetiferous. The ultramafic rocks occur with pyroxenite, metapyroxenite, gabbroid and metagabbroid rocks, and a variety of crustal inclusions at many localities. We present here a detailed account of the distribution, structural and textural relationships, and chemical characteristics of these xenoliths. Inclusions in kimberlites, breccia pipes, and in alkalic rocks of north-central Montana are not considered in this report.

PREVIOUS INVESTIGATIONS

The first important study of ultramafic inclusions in basalts of the western U. S. was that of Lausen (1927) who described peridotite inclusions and megacrysts of spinel, plagioclase, diopside, kaersutitic amphibole ("basaltic hornblende"), and biotite from San Carlos, Arizona (also called Rice Station and Peridot Cove). Brady and Webb (1943) described peridotite and upper crustal inclusions from vents in the San Francisco, Arizona volcanic field and from Dish Hill (Siberia Crater[1/]), California. Inclusions from the San Carlos (Peridot Cove), Arizona and Dish Hill (Ludlow), California localities were analyzed and described in the classic paper of Ross and others (1954) in which peridotite inclusions in basalt were compared with alpine-type peridotites.

Nakata (1977) described the first known xenolith occurrences in the California Coast Ranges. Rose (1959) reported dunite xenoliths in the Golden

---

1/ "Siberia Crater" is the cone called Dish Hill on the Bagdad 7 1/2 minute quadrangle. Wilshire and Trask (1971) used the name Siberia Crater to designate a satellite crater on the southwest flank of Dish Hill, but this has not been proven to be a vent. Wise (1966) considers it to be an eroded flow.

Gate Hill and Jackson Butte dacite domes near Jackson, California, which, along with the Big Creek, California assemblage of peridotite and lower crustal xenoliths in basaltic trachyandesite (discovered by J. P. Lockwood, U. S. Geological Survey), are very important localities in and at the margins of the Sierra Nevada batholith. Other important localities in the central Sierra Nevada include phlogopite-rich pyroxenite and peridotite xenoliths in upper Pliocene potassic basalts (Van Kooten, 1980). Moore (1963) briefly described peridotite inclusions in the Oak Creek basalt that was erupted along one of the east-bounding faults of the Sierra Nevada.

Brief mention was made by Barca (1966) of peridotite inclusions in young basalts of the Cima area, California. Other localities in that volcanic field have subsequently been discovered by our group, by I.D. MacGregor, University of California, Davis, and by A.L. Boettcher, University of California, Los Angeles. Stull and McMillan (1973) described small peridotite inclusions in the basalt of Malapai Hill in Joshua Tree National Monument, California. Basu (1979) described a prolific suite of ultramafic inclusions from the San Quintin volcanic field, Baja California. A reinterpretation of the origin of kaersutite megacrysts in the "camptonite" dikes near Hoover Dam (Campbell and Schenk, 1950) has been made by Pike and Nakata (1979).

Vitaliano and Harvey (1965) described megacrysts of olivine, pyroxene, and plagioclase from basalt at Black Rock Summit, Nevada (Lunar Crater volcanic field), a locality at which peridotite inclusions were subsequently discovered by H. G. Wilshire and D. H. Scott, and described in detail by Trask (1969) and Pike (1976).

New data on the Dish Hill and Oak Creek, California localities and on newly discovered localities near Dish Hill were presented by White (1966) in an important work that first seriously addressed the possibility of multiple origins of mafic and ultramafic inclusions in basalts. Also in 1966, Best and others first brought attention to the xenolith suites of the western Grand Canyon area of Arizona and Utah; their work has led to a series of important articles (Best and others, 1969, 1974; Best, 1970; 1974a, b; 1975a, b).

A significant contribution to our understanding of the diversity of ultramafic inclusions was made by Carter (1965; 1970) in his studies of inclusions from Kilbourne Hole and Potrillo Maar in southeastern New Mexico, and from the Knippa, Texas locality of the Balcones Province (Spencer, 1969).

Kudo and others (1971, 1972) reported the occurrence of abundant and varied peridotite xenoliths in a number of the Puerco basaltic necks northwest of Albuquerque, New Mexico. South of this area, Laughlin and others (1971, 1972) discovered a suite of peridotite inclusions in basaltic cinders of Bandera Crater and a richly xenolithic dike near Elephant Butte, New Mexico, about midway between Kilbourne Hole and the Puerco necks, was discovered by V. C. Kelley, University of New Mexico. Other localities in this area are described by Warren and others (1979).

Detailed study of peridotite, pyroxenite, and gabbroic inclusions from palagonitic tuff of Crater 160, San Francisco volcanic field, Arizona, was made by Cummings (1972). A comprehensive investigation of inclusion suites from many localities in this field was made by Stoesser (1973, 1974), and later studies were made by the U. S. Geological Survey (Ulrich and McKee, 1978).

P.H. Lewis (1973) described mica pyroxenite inclusions in limburgite from two localities in the Hopi Buttes, Arizona (Williams, 1936). We have subsequently found similar inclusions, as well as peridotites, amphibole-bearing inclusions, and megacrysts in other volcanoes of the Hopi field. We have also found spinel peridotite and pyroxenite xenoliths in minette intrusives of the Navajo volcanic field, Arizona. Ehrenberg (1979) described garnetiferous ultramafic inclusions from The Thumb, a minette neck in the Navajo field.

Topical studies, mainly on mineralogy, isotopic, and trace element compositions, have been made on xenoliths from several of these localities (Mason, 1968; Prinz and Nehru, 1969; Peterman and others, 1970; Hoffer and Hoffer, 1973; Zartman and Tera, 1973; Laughlin, 1974; Frey and Prinz, 1978; Basu, 1977, 1978). Comprehensive studies were made of Kilbourne Hole granulites by Padovani and Carter (1973; 1977) and of mafic and ultramafic inclusions at localities in the San Bernardino Valley field (Geronimo volcanic field), east of Douglas, Arizona (Lynch, 1978; Evans and Nash, 1979).

These studies have spanned a period in which major changes in views of the origin of the xenoliths have taken place and during which improvements in petrologic techniques have revealed the true complexity of these assemblages. Thus, the view of a simple cognate cumulate origin of the peridotites is well represented in the earlier papers. This has been supplanted, largely because of the work of Ross and others (1954), by the supposition that the peridotites represent fragments of the upper mantle. We are now in a period, given impetus in the United States by the outstanding work of White (1966), Jackson (1968), Jackson and Wright (1970), Carter (1970), and Best (1975), in which the true diversity of these rocks is recognized, and in which multiple origins are entertained as valid hypotheses.

DISTRIBUTION AND SETTING

Ultramafic and mafic xenoliths in basalts and other lavas are found in the area between the west coast (Gilroy, California) and west central Texas (Knippa), and south of latitude $38^{\circ}31'$ to and beyond the Mexican border. In the coterminous U. S. occurrences of mantle xenoliths are rare in Cenozoic volcanic rocks north of Black Rock summit, Nevada although such xenoliths have been reported in kimberlites near the Colorado-Wyoming border (McCallum and Eggler, 1971) and Montana (Hearn, 1979; Hearn and McGee, 1983) and in some phonolites in north-central Montana (Hearn, 1979). However, a thorough search for mantle xenoliths has not been made in much of the area lacking reported occurrences. The nearest localities in Canada are those described by Littlejohn (1972). Figure 1 shows the geographic distribution of the more important occurrences of ultramafic inclusions in basaltic and other volcanic rocks in the western U.S. superimposed on boundaries of principal tectonic provinces. Kimberlites are shown on the distribution map, but are not the subject of this study.

The westernmost localities (Table 1, nos. 1-2) are in basalt intruded into the moderately deformed Plio-Pleistocene Santa Clara Formation in the Coast Ranges of California. Associated flows of similar composition are interbedded and folded with sedimentary rocks of the Santa Clara Formation. Xenoliths in the San Quintin fields (nos. 4-6), occur mainly in the cinder ejecta of Holocene basalts (Basu, 1975; 1977). Tertiary dacite domes near

Jackson, California are intrusive into Paleozoic and Mesozoic metamorphic rocks and Tertiary volcanic rocks in the western foothills of the Sierra Nevada Province, while the Big Creek, California trachyandesites (no. 9) are intrusive into Mesozoic granitic rocks of the Sierran batholith. Upper Pliocene potassic basalts in the Merced Peak and Huntington Lake quadrangles of the central Sierra Nevada are intrusions in or flows on Cretaceous granitic rocks (Van Kooten, 1980). The Quaternary Oak Creek (nos. 10-11) and Waucoba (nos. 13-14) basalts were erupted along major faults that displace Cretaceous granitic rocks along the west and east sides of Owens Valley.

In southern California, xenolith-bearing basalts include: the late Cenozoic(?) Malapai Hill basalt (no. 20) is interpreted (Stull and McMillan, 1973) as a stock intrusive into middle Jurassic(?) quartz monzonite of the Transverse Ranges province in southern California. The Old Woman Springs basalts (nos. 21, 22), probably also late Cenozoic in age, were erupted along NW-trending fracture systems. These faults are oblique to both the San Andreas and Garlock faults and cross the dominant structural trend of the Transverse Ranges. Farther northeast in the Mojave Desert, Pliocene basalts that erupted through Mesozoic granitic rocks in the Deadman Lake and Bagdad quadrangles (nos. 23-36) appear to be controlled by a NNE-trending fracture system that is oblique to fold trends in nearby Miocene strata (Dibblee, 1967). Southeast of Baker, California, xenolith-bearing basalts were erupted through Mesozoic granitic rocks near the boundary of the Mojave Desert and Basin and Range provinces. Xenoliths are found here in basaltic rocks ranging in age from 0.01 to 9.2 m.y. (Oberlander, 1974; Dohrenwend and others, 1984).

The localities near Black Rock Summit (Lunar Crater field, nos. 16-19) in the Basin and Range province are in basalts (Scott and Trask, 1971) erupted from a NNE-trending fracture that cuts Tertiary silicic volcanic rocks of the Lunar Lake caldera (Ekren and others, 1974). Basaltic rocks in the Lunar Crater field range from at least 5.7 m.y. to Holocene (Dohrenwend and others, 1984). Xenoliths also occur in basaltic rocks of Pliocene age (Anderson and others, 1972) in parts of the Basin and Range province bordering the Colorado Plateau near Hoover Dam (no. 41) and near Wikieup, Arizona (no. 42). Basalts at both of these localities are intruded into alluvium derived from pre-Cambrian metamorphic rocks. Farther south in the Basin and Range province are the San Carlos locality (nos. 63-64) and localities (no. 65) in San Bernardino Valley (Geronimo volcanic field) east of Douglas, Arizona. The San Carlos locality is in Quaternary basalt erupted through Paleozoic sedimentary rocks and Tertiary volcanic rocks, whereas the Quaternary basalts of San Bernardino Valley were erupted through Cretaceous sedimentary rocks and Tertiary volcanic rocks.

Quaternary xenolithic basalts on the Uinkaret Plateau (nos. 44-46) were erupted onto Permian and Triassic sedimentary rocks of the Kaibab, Toroweap, and Moenkopi Formations of the Colorado Plateau close to the eastern edge of the Basin and Range province (Best and others, 1969). Localities in the Navajo-Hopi volcanic fields (nos. 49-56) occur in Quaternary alkalic flows and intrusives that lie on or intrude Triassic and Jurassic sedimentary rocks of the Glen Canyon and San Rafael groups well inside the Colorado Plateau. Those of the San Francisco volcanic field (nos. 47-48) are near the southern edge of the Colorado Plateau where the Quaternary basalts form an extrusive cap on Permian sedimentary rocks of the Kaibab and Toroweap Formations.

A number of localities are known in and near the Rio Grande depression which separates the southern Colorado Plateau and Great Plains provinces (Kelley, 1952; Lipman, 1969). Plio-Pliestocene basalts about 50 miles northwest of Santa Fe contain pyroxenite xenoliths (Baldridge, 1978, 1979). The Tertiary Puerco plugs (nos. 58-61) on the east flank of the Mt. Taylor volcano (Lipman, 1969) are about 20 miles west of the Rio Grande depression. The plugs intrude little-deformed Cretaceous sedimentary rocks of the Mesaverde Group. Bandera (no. 57) is a Quaternary basalt cinder cone, about 55 miles west of the Rio Grande depression. It was erupted onto Precambrian metamorphic rocks. The Elephant Butte dike (no. 62) intrudes deformed Cretaceous sedimentary rocks of the Mesaverde Group in the Rio Grande depression; it is presumed to be much younger than the rocks it intrudes, but no independent age information is available. Other localities in the Engle Basin contain lherzolite, pyroxenite, and two-pyroxene granulites (Warren and others, 1979). The southern-most localities marginal to the Rio Grande depression include the Quaternary Kilbourne Hole and Potrillo maars that were erupted through thick alluvial fill in or close to the edge of the Rio Grande depression. Kilbourne Hole erupted through a lava flow from Aden crater dated at 0.53 m.y.; A pre-Potrillo maar flow is 1.2 m.y. old and a post-maar flow is 0.18 m.y. old (Seager and others, 1984). These maars, as well as Hunts Hole, which has no ultramafic xenoliths,
were apparently controlled by a NE-trending fracture (Reeves and de Hon, 1965).

There are no known localities along the east side of the Rio Grande depression. The nearest locality to the east with peridotite inclusions is the Knippa, Texas intrusion (no. 68; Carter 1965), one of many Late Cretaceous mafic alkaline intrusions in the Balcones igneous province (Spencer, 1969). Miocene dikes more than 150 km southeast of the most southerly known extent of the Rio Grande depression contain megacrysts of feldspar, amphibole, biotite, apatite, and magnetite. The dikes intrude Cretaceous sedimentary rocks and Tertiary volcanic rocks (Dasch, 1969; Dasch and others, 1969). No peridotite inclusions have been found here, but they contain well-studied megacryst suites (Dasch, 1969; Irving and Frey, 1984).

Xenolithic volcanic rocks thus are not confined to any particular geologic environment. In fact, they occur in every major province between the Coast Ranges in California and the Balcones province in west Texas. A few xenolithic basalts, as at Gilroy, California (nos. 1-2) and Knippa, Texas (no. 68), are essentially contemporaneous with sedimentary rocks in which they occur, but most are much younger than their country rocks, and many (e.g., those in the Mojave Desert (nos. 23-36) were erupted along structures that are oblique to dominant structural trends in the country rock.

There is no correlation between the distribution of xenolith occurrences (fig. 2) or types of xenoliths (figs. 3-9) and crustal thickness, crustal age, or regional heat flow provinces. There is little overlap in distribution of xenolithic basalts and kimberlites (fig. 2) except in the Navajo field where no systematic comparison of their xenoliths has yet been made.

HOST ROCKS

The host rocks of the ultramafic xenoliths range from dacite to nepheline basanite, limburgite, and minette (Table 2). Full analyses of host rocks are

given in Appendix II. Plots of host rock compositions on an alkali-silica diagram (fig. 10) show a wide range of values, but the majority fall in the field of Hawaiian alkaline rocks. Xenolithic basalts that are marginally alkaline (e.g., those in the San Francisco volcanic field) tend to have dominantly crustal, pyroxenitic, and feldspathic xenolith suites. Where analyses are available of xenolithic and nonxenolithic basalts from the same locality, xenolithic basalts tend to be significantly more undersaturated than nonxenolithic ones (e.g., Waucoba, California and Black Rock Summit, Nevada, Table 1, nos. 13-14). However, the Deadman Lake cones (Table 1, nos. 23-31) show no such correlation, and there is no obvious correlation between occurrence of xenoliths and degree of undersaturation among the different localities. Thus, xenoliths are just as common in San Quintin basalts whose normative ne averages 5 percent as in the Toroweap basalt whose normative ne averages 20 percent.

Table 3 shows the ages, the normative ne values, and the K/Na ratios of xenolithic basalts in relation to heat flow. There are no obvious correlations in the degree of undersaturation and heat flow, nor is there any clear correlation between K/Na, taken as an index of heat-producing elements in the lava source area, and regional heat flow patterns whether the data points are lumped or treated separately according to age.

XENOLITHS

The types and relative abundances of xenoliths found at each locality are shown in Table 1. In general, we did not make statistical counts of xenoliths other than those in the gabbroid-peridotite groups. Hence, only qualitative guides to the relative abundances of different types of silicic igneous and metamorphic rocks and sedimentary xenoliths are given. The relative abundances of mafic-ultramafic types in Table 1 represent 100 or more field counts in which triaxial dimensions, shapes, grain sizes, lithologic heterogeneities, and estimates of modal composition were made systematically. A standard form, adapted from E. D. Jackson's (written communication, 1968) field description form, was used to systematize field observations (Appendix III, fig. 1).

We divide xenoliths in basaltic rocks of the western United States into eight main classes (fig. 11): (1) Xenoliths of crustal rocks, clearly unrelated to the basalt, including silicic and intermediate igneous and metamorphic rocks and sedimentary rocks; (2) Gabbroids, mostly gabbronorite or olivine gabbro, which grade into pyroxenites and olivine pyroxenites with decrease of feldspar content, and which grade texturally into metagabbroids; (3) Metagabbroids, mostly 2-pyroxene or olivine-pyroxene granulites, grading into metapyroxenites and olivine metapyroxenites with decrease of feldspar content; (4) Cr-diopside ultramafic group (Wilshire and Shervais, 1973; Type I of Frey and Prinz, 1978); (5) Al-augite ultramafic group (Wilshire and Shervais, 1973; Type II of Frey and Prinz, 1978); (6) Feldspathic ultramafic group; (7) Garnetiferous ultramafic group, and (8), An as-yet poorly defined group of spinel peridotites and pyroxenites with pyroxenes that are noticeably darker green (bottle-green) in hand specimen than Cr-diopside pyroxenes; this groups is provisionally labelled the bottle green pyroxene group. Groups (4), (5), (6), and (8) all contain spinel, and some in group (7) contain spinel in addition to garnet. The latter seven classes of xenoliths are not sharply defined groups and understanding their origin is as much dependent on

recognition of rock associations and intergradations as on chemical and textural criteria for their distinction.

Xenoliths other than accidental crustal inclusions are divided into two main groups--gabbroids and ultramafic rocks. This classification scheme poses difficulties because pyroxenite members of the Al-augite group are known to be modally gradational with some gabbroids, and a similar relationship may hold for pyroxenite members of the bottle-green pyroxene group and other gabbroids. Still other gabbroid xenoliths may be entirely unrelated to the ultramafic series. Because we cannot distinguish these possibilities with the data in hand, the gabbroids are lumped as a separate group. Each of the main groups is subdivded on the basis of textural and mineralogical criteria.

The gabbroids are subdivided primarily into igneous and metamorphic types and secondarily into modal groups, following orthodox treatment of xenolith populations. However, it would have been equally valid to subdivide primarily on a chemical-modal basis and secondarily on texture, which was the procedure followed for subdivision of the ultramafic group, again following orthodox approach. The textural criteria used to distinguish metamorphic from igneous rocks for purposes of classification include internal strain features in minerals; 120 degree triple junctions in recrystallized rocks; relic grains, either deformed or having exsolution textures, in finer-grained matrices lacking these features; and cataclastic flow textures (Pike and Schwarzman, 1977). Criteria used for identification of igneous rocks include hypidiomorphic-granular, porphyritic, and poikilitic textures. A well-populated class of coarse-grained peridotites and generally finer-grained pyroxenites and wehrlites have ambiguous allotriomorphic granular textures lacking relic grains, internal strain features, and exsolution textures.

The classification scheme and terminology we use for the ultramafic rocks (fig. 12) is that proposed by Streckeisen and others (1973) with appropriate modifiers for subdivisions of their groups. Detailed descriptions of the principal xenolith groups are given in Appendix III, bulk compositions are given in Appendix IV, and mineral compositions, mostly determined by electron-probe analysis, are given in Appendix V. The principal and secondry structural, lithologic, mineralogical, and chemical features of the ultramafic groups, to the extent known, are shown in Table 4. Too few systematic data are available to similarly characterize the gabbroid and metagabbroid groups. The following comments are a synthesis of the detailed descriptions.

The gabbroid group consists of rocks ranging from anorthosite to feldspathic pyroxenites with a wide variety of intermediate modal subtypes. Each main modal type (Appendix III) has both igneous and metamorphic representatives, and various intermediate stages of metamorphism of the igneous gabbroids are well-represented. Anorthosites are rare and small; the presence of thin nearly pure feldspar layers in layered gabbroids suggests an origin of "anorthosite" xenoliths by breakup of layered gabbroids. Rare composite xenoliths with sharp contacts between igneous and metamorphic gabbroids indicate a complex history of melting, crystallization, and subsolidus events. Thin gabbroid and metagabbroid dikes in Cr-diopside lherzolite do not differ materially from isolated gabbroid xenoliths, some of which may have been derived from larger dikes. There are unequivocal gradations from gabbroid to pyroxenite members of the Al-augite group. Gabbroid dikes in Cr-diopside lherzolites are found at localities where members of the feldspathic ultramafic group also occur.

The ultramafic xenoliths were subdivided into five groups on the basis of mineralogy and chemical characteristics. Each well-represented group has both pyroxene-rich and olivine-rich members, but the Cr-diopside group (fig. 13) has substantially greater modal variation than the Al-augite group (fig. 14). Although the proportions of xenoliths representing different groups varies from locality to locality, peridotite of the Cr-diopside group is, overall, by far the dominant lithology. Composite xenoliths containing different lithologies of the same or different groups are not common, but have been especially sought in this study because of the important information they yield. With rare exceptions, composite xenoliths containing the modal variants illustrated in figures 12 and 13 have thin layers of pyroxenite in a host rock rich in olivine, and crosscutting layers indicate that more than one generation of pyroxene-rich layers is present. Single pyroxenite layers may either be parallel to or crosscut foliation, when present, in the peridotite (Fig. 15a). Most peridotites, however, are not foliated whether or not they contain pyroxenite layers. In places, crosscutting pyroxenite layers are deformed by shearing parallel to the foliation (Fig. 15b). Especially in the Al-augite group, multiple igneous dikes of the same subtype, and sharp contacts between igneous and metamorphic varieties of the same subtype occur in single xenoliths. As with the gabbroids, the Al-augite group has both igneous and metamorphic members. While all members of the Cr-diopside group have metamorphic textures, relics of former igneous textures are common in the pyroxenite subtypes and unusual in the peridotite subtypes. In the feldspathic ultramafic group feldspar crystallized interstitially in peridotite and pyroxenite that have metamorphic textures. However, some rocks of this group recrystallized after the formation of plagioclase whereas others did not, so this group in a sense also has "igneous" and metamorphic varieties. As with the gabbroids, partial melting of both igneous and metamorphic members of all major groups is widespread and commonly extensive. This, along with composite igneous-igneous and igneous-metamorphic xenoliths of the same subtypes, indicates complex melting-crystallization-subsolidus histories.

Composite xenoliths reveal that Cr-diopside peridotite, by far the dominant lithology among the xenoliths, forms the host rock for a wide variety of dikes representing the gabbroid and metagabbroid groups and the Al-augite group. The Cr-diopside group grades with the appearance of feldspar into the feldspathic ultramafic group. Although only three specimens of garnet pyroxenite from localities dominated by peridotite xenoliths are known in the western United States, they are very similar (Shervais and others, 1973; Neville and others, 1983) to the garnet pyroxenite from Salt Lake Crater, Oahu (Beeson and Jackson, 1970) and to certain alpine occurrences (Kornprobst and Conquere, 1972; Conquere, 1977) which are dikes in spinel peridotite of the Cr-diopside group. The macroscopic relations of different lithologies in composite xenoliths, especially those involving members of the Al-augite group, not only establish relative ages of the Cr-diopside group and all other varieties, they also provide evidence of the close proximity in the source area of the xenoliths of all the principal lithic variants characteristic of western United States occurrences.

RELATIONSHIPS AMONG XENOLITH TYPES AS INDICATED BY COMPOSITE XENOLITHS

Proximity of Mafic-Ultramafic Lithologies in the Mantle and Sequence of Formation

The occurrence of composite xenoliths containing members of the subordinate groups in contact with Cr-diopside peridotite and in contact with one another show that all of the main types of lithologies can occur in very close proximity to one another at the time the xenoliths are incorporated into the magma that brought them to the surface. Crosscutting relationships between the different kinds of lithologies establish relative ages of emplacement. The sequence of emplacement deduced from these relationships is shown in figure 16. There are indications from crosscutting relationships that more than one generation of Cr-diopside pyroxenite occurs (Fig. 17), but they are not macroscopically distinguishable. The thin Mg-phlogopite (± Cr diopside) layers have not been observed to crosscut any other type of layering and are placed so as to be consistent with their counterparts in the Al-augite group; that is, derivative from pyroxenite. No direct evidence of the relative age of the garnet-bearing clinopyroxenites and bottle-green pyroxene rocks has been observed in xenoliths. The position of garnet pyroxenite in figure 16 is based on the relative age of similar dikes in the Lherz massif (Fig. 18a; Conquere, 1977). This is quite speculative and the position of the garnet pyroxenite could be earlier in the sequence as postulated by Obata (1980) for the Ronda massif. However, in most xenolith occurrences garnet formed both by exsolution from pyroxene and, by reaction, from hercynitic spinel. The position of bottle-green pyroxenite is speculative, but is in part based on apparent gradations between these rocks and gabbroids, and close association and textural similarity with Al-augite pyroxenites and peridotites at Crater 160 (no. 48). It is also possible there there is no distinction between bottle-green pyroxenites and garnet pyroxenites other than modal; garnet pyroxenite dikes in the Lherz massif have marginal (chill?) zones that are free of garnet.

Relative ages of subtypes of the Al-augite group and gabbroids are well-established. More than one generation of pyroxenite and wehrlite members of this group has been established in xenoliths from San Carlos and Kilbourne Hole (Fig. 18b). The close relationship between the occurrence of kaersutitic amphibole veins and amphibole-bearing Al-augite pyroxenites suggests a genetic link between these lithologies. This is well-substantiated in the Lherz massif where hornblendite segregations in pyroxenites are common (Fig. 19a); in places, derivation of hornblendite veins in peridotite from crosscutting pyroxenites is clear (Wilshire and others, 1980). The same relationship between hornblendite veins and pyroxenite is present but rare in xenoliths (Fig. 19b) (see also Francis, 1976, and reinterpretation by Roden and others , 1984). Crosscutting relationships between hornblendite veins and structures in Cr-diopside peridotite are well known (Wilshire and Trask, 1971). Also, hornblendite and phlogopite veins are closely associated with planar fracture systems in peridotite, and occupy some members of these fracture sets (Figs. 20, 21). The same relationships are seen in kimberlite xenoliths (Dawson, 1980, 1981, 1984). Gabbroid-metagabbroid dikes crosscut pyroxenites of both the Cr-diopside and Al-augite groups (Fig. 22), and modal gradations occur between these lithologies and Al-augite and bottle-green pyroxene pyroxenites.

The position of "basalt" in figure 16 is based solely on fine-grained texture. Xenoliths of basalt have been recognized at only one locality (no. 40) and have not been studied in detail. Fine-grained pyroxenite veins in Cr-diopside lherzolite from San Carlos may be related to the basalts in sequence.

Systematic Compositional Variations in Composite Xenoliths

The physical relationships of members of different major lithologies in composite xenoliths indicate that spinel peridotite of the Cr-diopside group made up the country rock in which the other lithologies formed. A transition from Cr-diopside peridotite to more Fe-rich peridotite of the Al-augite group was observed in a number of large composite xenoliths such that the more Fe-rich peridotite occurred in a zone bordering pyroxenite dikes of the Al-augite group. This observation led to the supposition that the Fe-rich peridotites of the Al-augite group represent Cr-diopside peridotite modified by metasomatic interaction with the dike forming magma. To test this, systematic electron-probe studies of mineral compositions in all the lithologies of typical composite Al-augite xenoliths were made in traverses normal to pyroxenite-peridotite contacts to assess whether compositions trended toward Cr-diopside compositions away from dike borders. The remarkable patterns of compositional variation found (Wilshire and Shervais, 1973, 1975) clearly established that compositional trends in the peridotite in fact progressively approach those of the Cr-diopside group with greater distance from the Al-augite pyroxenite dikes although this relationship was commonly not detectable in hand specimen. Similar reaction zones between garnet pyroxenites and peridotites in kimberlites were subsequently discovered by Harte and others (1977), Gurney and Harte (1980), and Harte (1983). Other studies (Wilshire and others, 1971; Best, 1974b) indicated that hydrous phases associated with hornblendite veins and anhydrous phases of the peridotite host rock of the veins also varied in composition systematically with proximity to the veins, a relationship that has subsequently been very amply documented (Francis, 1976; Stewart and Boettcher, 1977; Boettcher and others, 1979; Boettcher and O'Neil, 1980; Irving, 1980; Wilshire and others, 1980; Gurney and Harte, 1980). This clear evidence of common metasomatic alteration of mantle materials led us to undertake systematic probe studies of composite xenoliths containing all the common lithologies. All of these data are assembled in Appendix VI for the sake of completeness.

Systematic compostional data were obtained on seven composite xenoliths containing two or more subtypes of the Cr-diopside group, three composite xenoliths containing subtypes of the Al-augite group, three composite xenoliths in which the peridotite member is transitional between the Cr-diopside and Al-augite groups, one peridotite cut by a pyroxenite of the bottle-green pyroxene group, one peridotite of the Cr-diopside group in contact with garnet clinopyroxenite, three peridotites of the Cr-diopside or transitional groups cut by hornblendite veins, and one xenolith composed of two pyroxenitic subtypes of the Al-augite group and a hornblendite vein.

Significant compositional changes occur in peridotite adjacent to all the principal types of pyroxenite, gabbroid, and hydrous mineral layers over distances of 5 cm or more, and more subtle changes occur over larger distances (Appendix VI, figs. VI-2 to VI-21). Some composite xenoliths containing pyroxenitic and peridotitic members of the Cr-diopside group show no chemical variation, and others show strong variations that are not symmetrical to the layers. Asymetrical, but strong, compositional variations of spinel across Cr-diopside websterite layers in the Balmuccia alpine peridotite were documented by Sinigoi and others (1983). All other types of composite xenoliths that have been examined, however, show substantial compositional variation within the layers and in the peridotite with which they are in contact. The variations in the peridotite are commonly symmetrical with respect to proximity to the layers and are symmetrical across the width of layers.

The trends away from the mineral layers into adjacent peridotite are the same for xenoliths having pyroxenite layers of the Cr-diopside, Al-augite, bottle green pyroxene, and garnetiferous groups. The principal characteristics shared by these rocks (Appendix VI, figs. VI-2 to VI-8, VI-10 to VI-15 and VI-17) are decrease in Al/Cr ratio of spinel, increase of Mg/(Mg+Fe) ratio of the main silicate phases, decrease in Ti/Cr ratio of clinopyroxene, decrease in Al contents of both pyroxenes (and incrase in Al/Cr of clinopyroxenes), and a general, though commonly erratic, decrease in Ca content of olivine away from the pyroxenites into peridotite.

In contrast, peridotite xenoliths having amphibole-rich layers show chemical trends that are opposite for spinel composition and for Al contents of pyroxenes (Appendix VI, figs. VI-18 to VI-20) compared to those associated with pyroxenitic layers. Chemical variations in one composite xenolith with feldspathic layers have the same spinel trend as those with amphibole layers, but the Al contents of the pyroxenes decrease away from the feldspathic layers as they do away from pyroxenitic layers.

These differences are important in two respects: (1) trends of Al content in orthopyroxene that are opposite in reaction zones of amphibole and pyroxene veins extends the range of compositions due to metasomatic effects discussed by Wilshire and Jackson (1975) and Pike (1976) and exacerbates the problems of pyroxene geobarometry, and calls into question the use of pyroxenes as geothermometers (Tracy, 1980); (2) the metasomatic effects of hydrous and anhydrous mineral veins on peridotite compositions can be discriminated even when the veins are not in a particular sample. Thus, sample Ba-1-24 (Dish Hill, California; Appendix VI, fig. VI-9) clearly reveals significant metasomatic effects of hydrous mineral veining although the sample does not contain amphibole veins; indeed, it was selected for systematic study to determine the changes with respect to a pyroxenite layer. Small xenoliths containing hydrous- and anhydrous-mineral layers may, as in the case of sample Ba-1-15 (Appendix VI, fig. VI-22), yield complex chemical variations. Inasmuch as hydrous mineral veining post-dates most anhydrous mineral layering, the possibility exists for overprinting early metasomatic effects with younger ones that are qualitatively different. This has not been tested.

TRACE ELEMENTS AND ISOTOPES IN XENOLITHS AND HOST ROCKS

A substantial amount of information has been assembled on minor element and isotopic compositions of xenoliths, megacrysts, and host rocks in western U.S. occurrences. However, studies that deal systematically with the different lithologic associations in terms of their known structural-compositional relationship are few. In some studies the type of rock analyzed cannot be identified from the descriptions given, and in others the samples may have been misidentified. The latter problem stems largely from difficulty in distinguishing some kinds of xenoliths in hand specimen (e.g., Cr-diopside orthopyroxenite from Al-augite pyroxenite) and from the presence of significant chemical variability even within subordinate lithologic types. The more important conclusions regarding the genesis of the xenoliths and megacrysts are based on rare earth elements, and strontium, neodymium, and oxygen isotopes, so only these will be summarized here. The data from the literature are tabulated in Appendix VII.

Cr-diopside group. Chondrite-normalized rare earth element (REE) patterns for bulk rock samples described as Cr-diopside group peridotites from western U.S. localities show a complete range between and within localities from relative light REE (LREE) enrichment to relative LREE depletion (Frey and Prinz, 1978; Jagoutz and others, 1979b; Irving, 1980; W.P. Nash, written communication, 1981; A.J. Irving, written communication, 1979). Typically greater LREE enrichments are found in Cr-diopside lherzolites that contain phlogopite (Frey and Prinz, 1978, sample PA-51) or amphibole (W.P. Nash, written communication, 1981); some, but not all, fine-grained anhydrous lherzolites with tabular texture from Kilbourne Hole are slightly enriched in LREE compared to coarse-grained lherzolites (A. J. Irving, written communication, 1979). Pyroxenites of the Cr-diopside group generally have concave downward REE distributions, but higher abundances of REE than associated lherzolites (Frey and Prinz, 1978; Irving, 1980).

Composite Cr-diopside peridotite-Al-augite pyroxenite. Of three lherzolites described as members of the Cr-diopside group, but which represent wallrock of Al-augite pyroxenites (Irving, 1980) and may actually be Al-augite peridotites, one shows LREE enrichment relative to discrete Cr-diopside xenoliths from the same locality; the others have REE distributions within the range of the discrete Cr-diopside lherzolites. The LREE-enriched fine-grained tabular lherzolites from Kilbourne Hole are said to be commonly associated with Al-augite pyroxenite veins (Bussod, 1983), and all four composite samples from this and an adjacent locality (no. 66) for which we have systematic compositional data (Appendix VI) have fine-grained lherzolite with tabular texture.

Al-augite group. One peridotite from San Carlos described as a member of the Al-augite group (Frey and Prinz, 1978, sample PA-42) is enriched in REE compared to Cr-diopside lherzolites. Clinopyroxene-rich lithologies of the Al-augite group have concave downward REE patterns like their counterparts in the Cr-diopside group (Frey and Prinz, 1978; Irving, 1980; W.P. Nash, written communication, 1981; Irving, written communication, 1979), but they show substantially less LREE depletion than Cr-diopside pyroxenites. The one gabbro examined has a REE pattern like those of Al-augite pyroxenites (W.P. Nash, written communication, 1981).

Mineral separates and megacrysts, all groups. A substantial amount of REE data have been obtained on mineral separates from Cr-diopside group xenoliths (Kempton and others, 1984; Menzies and others, 1984), from garnetiferous ultramafic group xenoliths (Ehrenberg, 1982a), and from megacrysts (Ehrenberg, 1982a; Irving and Frey, 1984). The data for clinopyroxenes from lherzolites have resulted in identification of two subtypes of the Cr-diopside group (Kempton and others, 1984; Menzies, 1983; Menzies and others, 1984) as previously identified in Australian xenoliths by Frey and Green (1974). Type Ia is described by these authors as having LREE-depleted clinopyroxenes with chondrite-normalized Ce = 1.2-9.0 and Yb = 10-12 (the tabulated data given by Menzies and others, 1984, indicate that Ce values of type Ia clinopyroxenes range from 2.0-16.5). Type Ib is described as having LREE-enriched clinopyroxenes with chondrite-normalized Ce/Yb greater than 1, but such ratios may also occur in Type Ia (e.g., sample 20-6, Menzies and others, 1984). Chondrite-normalized values reported (Menzies and others, 1984) for Ce range

from 12.3-44.1, and for Yb from 2.9-14.8. The REE contents of clinopyroxenes thus do not uniquely separate Types Ia and b, and distinctions between "metasomatized" and "unmetasomatized" Ia and Ib (Menzies, 1983) are more theoretical than practical.

Bulk rock garnet lherzolites at one locality (Ehrenberg, 1982a) are relatively enriched in LREE whether they are from rocks with more or less than 12% modal clinopyroxene (the value chosen by Ehrenberg to separate high Ca-Al from low Ca-Al lherzolites), or from megacrystalline rocks. The low Ca-Al group has generally lower HREE than the other two groups, and higher La/Yb ratios than the high Ca-Al group.

Megacrysts of clinopyroxene, amphibole, mica, anorthoclase, and apatite from Kilbourne Hole (67), San Carlos (63), Dish Hill (32), Hoover Dam (41), and Mt. Riley, Alpine, and 96 Ranch, Texas were analyzed by Irving and Frey (1984). The clinopyroxenes, all Al-Ti augites, have REE patterns like those of Al-augite pyroxenites (Frey and Prinz, 1978). Kaersutite megacrysts, and one vein kaersutite, also have concave downward REE distributions, but abundances are much higher and LREE enrichment is substantially greater than in clinopyroxenes. The relatively high REE abundances in apatite shows the importance of this minor phase in the total REE budget of the rocks containing it.

Problems in interpreting REE data. Some problems with REE analytical data and approaches to obtaining the data remain unresolved. Independent analyses of the same sample may show discrepant REE values (Table VII-1D, nos. 64, 94). The differences do not change overall LREE enrichment patterns, but have a significant effect on light/heavy ratios used as parameters of REE behavior (Frey, 1983). In addition, the presence of microscopic inclusions can have a significant effect on the REE abundances (Jagoutz and others, 1979; Stosch and Seck, 1980; Kempton and others, 1984). The behavior of REE distributions with differing sample preparation techniques -- that is, acid washing -- is largely unexplored although this is especially significant in Sr isotopic measurements (Zindler and others, 1983). There is, moreover, a significant sampling problem that results from metasomatic interactions between melts and their wallrocks. Steep gradients in major element distributions documented for this process are not taken into account in selecting samples for REE analysis. For example, a single REE distribution pattern is presented for garnet pyroxenite in the garnet pyroxenite-spinel lherzolite composite sample 68 SAL 11 (Frey, 1980), yet the major element compositions of minerals in this sample vary drastically with proximity to the contact of the two lithologies (Wilshire and Jackson, 1975); which part of this chemically variable sample was analyzed for REE is unknown. The analytical and sampling problems could have particular significance where correlations such as $(Ce)_N/(Yb)_N$ with CaO bulk rock composition (Frey, 1983) and Cr/Al content vs $(Ce)_N/(Sm)_N$ of clinopyroxene (Kempton and others, 1984) are attempted. The latter is illustrated in figure 23 which shows $(Ce)_N/(Sm)_N$ vs Cr/Al of clinopyroxenes from depleted and enriched xenoliths determined by Kempton and others (1984). Superimposed on this diagram are the ranges and average value of Cr/Al of clinopyroxenes in two of the rocks whose REE compositions were determined by Menzies and others (1984). The clinopyroxenes from one "depleted" sample (Ba-2-1) have Cr/Al ratios that span the full range of the Cr/Al ratios in all the samples plotted by Kempton and others (1984). The other sample, Ba-1-72, has a similar wide range of Cr/Al values on the LREE-enriched side of the diagram. The locations

in the samples, which are quite heterogeneous (Wilshire and others, 1980), of the Cr/Al or the REE analyses are not given.

Sr, Nd Isotopes

Sr isotopes, Cr-diopside group. The Sr isotopic data available commonly show disequilibrium between xenoliths of the Cr-diopside group and their host rocks (Peterman and others, 1970; Laughlin and others, 1971; Kudo and others, 1972; Steuber and Ikramuddin, 1974; Basu, 1979), and commonly show apparent internal disequilibrium among the minerals composing these xenoliths (Peterman and others, 1970; Kudo and others, 1972; Steuber and Ikramuddin, 1974; Basu, 1979). However, more recent studies have revealed significant problems of grain boundary contamination (e.g., Zindler and others, 1983), and difficulty in obtaining meaningful Sr compositions of peridotite minerals other than clinopyroxene. One exception is the Malapai Hill occurrence (locality no. 20; Stull and Davis, 1973) in which Cr-diopside lherzolites have $^{87}Sr/^{86}Sr$ ratios close to those of their host rocks., Steuber and Murthy (1966) state that Sr isotopic data indicate that xenoliths in alkali basalts are genetically related to their host rocks, and give whole rock data on a Cr-diopside(?) peridotite from Dish Hill ($^{87}Sr/^{86}Sr$ = .7062), but no data on the host. Comparison with other data on basalt from Dish Hill ($^{87}Sr/^{86}Sr$ = .7031; Peterman and others, 1971) shows the same level of disequilibrium reported for most Cr-diopside lherzolites.

Sr isotopes, Al-augite group. Whole rock Sr isotopic data for Al-augite xenoliths are scarce, and all of those analyzed are hornblendites or kaersutite-bearing clinopyroxenites (Bergman and others, 1981; Bergman, 1982). Amphibole-bearing xenoliths from Black Rock Summit ($^{87}Sr/^{86}Sr$ = .70331-.70369) are commonly not in isotopic equilibrium with their host basalts, but they do fall in the range of isotopic values for the volcanic field ($^{87}Sr/^{86}Sr$ = .70304-.70508). Sr isotopic data on mineral separates from Al-augite xenoliths are more abundant (Appendix VII; Steuber and Ikramuddin, 1974; Basu, 1978, 1979; Wilshire and others, 1980; Menzies and others, 1984), and are even more abundant if megacrysts are considered as natural mineral separates from Al-augite (and other) xenoliths.

Analyses of more than one mineral in Al-augite xenoliths are rare. Steuber and Ikramuddin (1974) reported that clinopyroxene and olivine from an Al-augite wehrlite xenolith are not in equilibrium; the clinopyroxene, however, has the same isotopic composition as the host basalt. Bergman and others (1981) showed that feldspar and kaersutite from an Al-augite feldspathic hornblendite are in isotopic equilibrium with each other but not with the host basalt. Single mineral separates that have been analyzed include clinopyroxene from clinopyroxenites (Basu, 1979) and kaersutite from hornblendites (Basu, 1978; Wilshire and others, 1980; Menzies and others, 1984). Clinopyroxene from clinopyroxenites reported by Basu (1979) are substantially more radiogenic than their host rocks, whereas kaersutite from hornblendite (Basu, 1978) is substantially less radiogenic than its host rock. A number of analyses of clinopyroxene and amphibole megacrysts have been made (Steuber and Ikramuddin, 1974; Basu, 1979; Wilshire and others, 1980; Foland and others, 1980, 1983). Clinopyroxene megacrysts have isotopic compositions very similar to their host rocks (Steuber and Ikramuddin, 1974) or to basalts in the same volcanic field (Foland and others, 1983); kaersutite megacrysts commonly are somewhat less radiogenic than their host rocks (Basu, 1978; Foland and others, 1980), and where more comprehensive data are

available (Bergman, 1982; Foland and others, 1983), kaersutite megacrysts have Sr isotopic compositions at the low end of the range for all lavas in the same volcanic field. This important relationship was first noted by Stuckless and Irving (1976).

Sr isotopes, Feldspathic and bottle-green pyroxene groups. In a single sample of peridotite in the feldspathic ultramafic group (Basu, 1979) reported similar Sr compositions for plagioclase and clinopyroxene. Several xenoliths that we would classify in the bottle-green pyroxene group have been analyzed for Sr isotopes. These include harzburgite ($^{87}Sr/^{86}Sr$ = .70912, .70896), dunite ($^{87}Sr/^{86}Sr$ = .70418), and lherzolite ($^{87}Sr/^{86}Sr$ = .70502) classified by Bergman (1982) as Cr-diopside group, and olivine websterites (+ kaersutite) classifed as "green spinel lherzolites" by Laughlin and others (1971). The harzburgite analyzed by Bergman (1982) is well outside the range of isotopic ratios of lavas in the volcanic field (.70304-.70508), whereas the dunite and lherzolite fall within this range. The $^{87}Sr/^{86}Sr$ reported for four xenoliths from Bandera Crater, New Mexico by Laughlin and others (1971) range from .7023 to .7040 in comparison to the range of three host rocks of .7028-.7034. Isotopic compositions of two bottle-green pyroxene megacrysts (Foland and others, 1983) are .7038 and .7039, slightly more radiogenic than associated clinopyroxene and kaersutite megacrysts of the Al-augite group and well within the range of values for the Black Rock Summit volcanic field.

Sr, Nd isotopes, Cr-diopside group. Neodymium isotopic compositions, in addition to Sr isotopic compositions, have been determined for whole rocks and mineral separates from only a few Cr-diopside group xenoliths and their host rocks (Menzies and others, 1984; Roden and others, 1984), and for whole rock garnetiferous ultramafic group xenoliths and their host rocks (Domenick and others, 1983). Menzies and others (1984) divide the Cr-diopside group into two subgroups on the basis of absence or presence of LREE enrichment of clinopyroxene. In the Type Ia group of Menzies and others (1984) whole rock and clinopyroxene Sr and Nd isotopic compositions may or may not fall in the ranges given for lavas in the field. The six clinopyroxene compositions from Type Ia xenoliths given plot on the "mantle array" in the vicinity of oceanic basalts (Fig. 24; Menzies and others, 1984). Of five clinopyroxenes from Type Ib xenoliths analyzed, four fall near the "mantle array" and extend the field of xenolith compositions to the estimated value for bulk earth (Fig. 24; Menzies and others, 1984). One clinopyroxene, from a Geronimo volcanic field micaceous xenolith, falls well below the "mantle array" in a position not occupied by any xenoliths or alkali basalts previously analyzed.

Sr, Nd isotopes, composite xenoliths, Cr-diopside and Al-augite groups. Menzies and others (1984) also provide data for composite xenoliths from Dish Hill and the Geronimo volcanic field (Appendix VII). These include one Cr-diopside websterite-Cr-diopside lherzolite (I/I), one Al-augite pyroxenite-Cr-diopside lherzolite (II/I), one undescribed composite of two Al-augite lithologies (II/II), and three Al-augite hornblendite-Cr-diopside lherzolite composites (Fig. 25) (II/I). Two additional analyses of Al-augite group wallrocks are given without compositions of veins. Another sample (EN 01) is plotted as a vein (mica)-wallrock pair but is described only as micaceous lherzolite with intergranular mica (Menzies and others, 1984). With the exception of the last-named sample, isotopic compositions of wallrocks and veins are spread along the "mantle array" and have lower $^{87}Sr/^{86}Sr$ and higher $^{143}Nd/^{144}Nd$ ratios than bulk earth. Veins plot closer to bulk earth on the

Sr/Nd diagram than their wallrocks (Fig. 24b). Roden and others (1984) and M.F. Roden (written communication, 1984) derived data from two composite xenoliths from Kilbourne Hole (Appendix VII) which consist of Al-augite clinopyroxenite-Cr-diopside lherzolite (II/I). Clinopyroxenes from the clinopyroxenites and the lherzolites are isotopically equilibrated with respect to Sr for both samples and with respect to Nd in one sample; the second sample, however, has slightly higher $^{143}Nd/^{144}Nd$ than clinopyroxene from the lherzolite.

The pyroxenes in Cr-diopside websterite and Cr-diopside lherzolite of a composite xenolith from the Geronimo volcanic field are not in isotopic equilibrium either for Sr or Nd (Menzies and others, 1984). In contrast, Kudo and others (1972) reported indistinguishable whole rock Sr isotopic ratios for a Cr-diopside lherzolite-Cr-diopside websterite composite xenolith from the Puerco plugs, New Mexico (61).

Sr, Nd isotopes, garnetiferous ultramafic group. Whole rock Sr and Nd isotopic compositions of garnet lherzolite and Sr isotopic composition of grospydite and garnet pyroxenite are not in equilibrium with their trachyandesite host rock from Big Creek, California (9) (Domenick and others, 1983). The Nd isotopic ratio of the garnet pyroxenite, however, is identical to that of the host rock.

Sr, Nd isotopes, megacrysts. In the case of the Black Rock Summit volcanic field, Sr and Nd isotopic compositions for clinopyroxene megacrysts in the bottle-green pyroxene group (identified as Cr-diopside group by the authors), clinopyroxene and kaersutite megacrysts in the Al-augite group, and whole rock Al-augite xenoliths all fall in the range of Sr and Nd isotopic ratios of lavas in this volcanic field (Foland and others, 1983).

Problems in interpreting isotopic data. Problems akin to those encountered with REE determinations also exist for isotopic measurements Discrepant Sr isotopic ratios reported independently for the same samples remain unresolved. Dish Hill (locality no. 32) host basalt sample Ba-1-101 has two reported Sr isotopic values, .70281(11) (Wilshire and others, 1980) and .70379(5) (Basu, 1978); Dish Hill hornblendite kaersutite sample Ba-1-72 has reported values of .70269(5) (Basu, 1978) and .70289(3) (Menzies and others, 1984); and Dish Hill hornblendite kaersutite sample Ba-2-1 has reported values of .70323(15) (Wilshire and others, 1980) and .70281(3) (Menzies and others, 1984). Hoover Dam (locality no. 41) has reported host rock Sr values of .70399(8) (Basu, 1978) and .70456, untreated, or .70316, acid-washed (Foland and others, 1980). The effects of acid-leaching on Rb and Sr abundances, and Sr isotopic ratios reported by Basu and Murthy (1977), Basu (1979), and Foland and others (1980) suggest the need for some standard procedures so that analytical results may be compared. The problem is well-described by Zindler and others (1983). Moreover, the assumption that mineral phases of the xenoliths have escaped modification of their "mantle" compositions after exposure to the highly radiogenic leachable component hardly seems warranted on the basis of evidence presented by Jagoutz and others (1980) which illustrates presence of significant amounts of "contaminant" Sr even after acid-leaching. This is especially significant as the origin of the leachable component is not known, some authors ascribing it to crustal sources (e.g., Foland and others, 1980; Jagoutz and others, 1980), others to a mantle metasomatic fluid (e.g. Basu and Murthy, 1977; Basu, 1979). The sampling

problem, that is, the within-xenolith isotopic variability, is just as significant as it is for REE determinations. This is well-illustrated by local isotopic requilibration of wallrock with veins (Roden and Irving, 1984) and the significant local effects of infiltration metasomatism that are inferred by Menzies and others (1984) for Dish Hill sample Ba-1-72.

Oxygen Isotopes

Host alkalic basalts in the western U.S. have a $\delta^{18}O$ range from 5.6 to 6.4 (Appendix VII, Table VII-3A) compared to an overall average of 6.1 ± .27 for alkalic basalts and 5.5 ± .26 for tholeiitic basalts (Kyser, 1980). Large differences are found for samples of vesicular and nonvesicular portions of a single flow at San Carlos, Arizona (5.6 ± 0.3 and 6.4 ± 0.1 respectively, Rumble and others, 1979), and independent determinations of samples from the same flow gave ^{18}O values of 6.0 and 6.3 (Kyser, 1980). Mica and amphibole from a single hornblendite vein from Dish Hill (32) illustrate fractionation of oxygen isotopes with $\delta^{18}O$ values of 6.11 and 5.57 respectively (Boettcher and O'Neil, 1980). Amphibole occurring as hornblendite veins and megacrysts from Dish Hill may have very different $\delta^{18}O$ values (6.01 and 4.65 respectively, Boettcher and O'Neil, 1980), and amphibole megacrysts from the same volcanic field range from 4.65 to 5.55 (Boettcher and O'Neil, 1980).

Kyser (1980) suggested that Cr-diopside peridotites can generally be related to magma having $\delta^{18}O$ values like those of tholeiite whereas most pyroxenites appear to be related to alkalic basalts. However, Cr-diopside and Al-augite pyroxenites from San Carlos (Appendix VII, Table VII-3B, C) have the same $\delta^{18}O$. Moreover, the Al-augite xenoliths, considered by many authors to be cognate (e.g., Frey and Prinz, 1978; Irving, 1980), were considered by Kyser (1980) to have equilibrated with a liquid whose $\delta^{18}O$ was about 5.7 which is below most values reported for the host basalt (Appendix VII, Table VII-3A). The stable isotopes therefore do not appear to provide definitive evidence on the cognate or accidental origin of the xenoliths. Concordant temperatures of isotopic equilibration for some megacrysts and host rock from Black Rock Summit (locality 16) and Dish Hill (locality 32) support a genetic relation between them (Kyser and others, 1981).

ORIGIN AND CAUSES OF VARIATION AMONG XENOLITHS

Cognate vs Accidental Origin

Controversy about cognate vs accidental origin of mafic-ultramafic xenoliths has progressed from an either/or to a both/and status with recognition of more than one principal type of xenolith. The generally accepted hypothesis is that the dominant lithologies such as feldspathic peridotite, spinel peridotite, and garnet peridotite are accidental inclusions derived from a concentrically stratified upper mantle. The mineralogy of these concentric layers is considered to reflect differences in T and P of equilibrium, and differences in bulk chemical composition, if present, related to degree of withdrawal of partial melts. Concentric layering of the major lithologies is inferred from experimental results in simple systems and other considerations (Kushiro and Yoder, 1966; Green and Ringwood, 1967; Ringwood, 1969; O'Hara, 1969; Kornprobst, 1970; Green and Hibberson, 1970; Ringwood, 1975; Saxena and Eriksson, 1983), whereas concentric layering of common lithologies in the same main group, such as garnet harzburgite and garnet lherzolite, is inferred from hypothetical partial melting relations (Nixon and others, 1973; Dawson, 1980) or from density/composition relationships (Boyd

and McCallister, 1976). With few exceptions the prevailing view about the origin of members of the Cr-diopside, garnetiferous ultramafic, and feldspathic ultramafic groups is that they are accidental inclusions in the basaltic magmas that carried them to the surface. This view is supported by the complex histories of solid state events that have modified their textures, and by isotopic disequilibrium between xenoliths and their host rocks (e. g. Allsopp and others, 1969; Manton and Tatsumoto, 1971; Laughlin and others, 1971; Kudo and others, 1972; Stueber and Ikramuddin, 1974; Burwell, 1975; Dasch and Green, 1975; Stuckless and Irving, 1976; Kramers, 1977; Erlank and Shimizu, 1977; Allegre and others, 1978).

A cognate vs accidental origin of less abundant lithologies is highly controversial. Those who attempt stratigraphic reconstructions of the mantle and crust from minor components of xenolith populations consider all xenoliths to be accidental and attribute pyroxenites (including Al-augite pyroxenites), gabbroids, hornblendites, and granulites to laterally extensive layers in the mantle and crust (for example, Aoki, 1972, cited by Takahashi, 1978; Takahashi, 1978; Warren and others, 1979). Another view of laterally extensive layering commonly proposed for the minor lithologies and megacrysts of kimberlites is one of zones in which subordinate components of inclusion assemblages formed and that were subsequently sampled by magmas enroute to the surface (e.g. Nixon and Boyd, 1973, 1979; Dawson, 1977; Pasteris and others, 1979; Dawson. 1980). Still another concept of stratification is embodied in hypotheses of pervasive metasomatism or introduction of melts derived from lower levels into the upper mantle producing a widespread horizon in which basaltic melts are generated (Varne and Graham, 1971; Frey and Green, 1974, Lloyd and Bailey, 1975; Hanson, 1977; Frey and Prinz, 1978; Boettcher and others, 1979; Jagoutz and others. 1979; Wood, 1979; Boettcher and O'Neil, 1980; Wass and Rogers, 1980; Menzies and Murthy, 1980a; Bailey, 1982; Kramers and others, 1983; Dawson, 1984; Boettcher, 1984), or chemical stratification resulting from zone refining (Kay, 1979). A mantle stratified in distribution of incompatible elements is also postulated by some authors (e.g., Kay and Gast, 1973; Ito, 1977; Hofmann and others, 1978) to explain geochemical features of oceanic volcanic rocks, or to explain theoretical/experimental metasomatic fluid behavior (Schneider and Eggler, 1984).

Major compositional variants of peridotite within the same main group have similarly been ascribed to stratification of the mantle. Sheared garnetiferous and nongarnetiferous peridotites in kimberlites that typically have higher Fe and Ti than unsheared types, and also yield higher calculated pressures and temperatures of equilibration (Boyd, 1973), are attributed to lower, less-depleted layers of the upper mantle (Boyd and Nixon, 1973; Nixon and Boyd, 1973). Similar xenoliths in minette and those in kimberlite, however, are considered by Ehrenberg (1979, 1982), Gurney and Harte (1980), and Harte (1983) to result from metasomatic alteration of "depleted" rocks to produce the more Fe and Ti-rich rocks; the alteration is thought to occur in halos around melts emplaced at various depths.

The basic supposition of stratification of the source regions of the xenoliths also extends to the gabbroids. Metagabbroid xenoliths are almost universally ascribed to a lower crustal origin as accidental inclusions even where they are in isotopic equilibrium with the host rock (Lovering and Tatsumoto, 1968). In contrast, igneous gabbroids are more commonly considered to be cognate.

Concepts of a stratified mantle in which lithologic variants are unrelated to the volcanic rocks that brought them to the surface are not universally endorsed. Other authors (e.g., Wilshire and Pike, 1975; Irving, 1976; Gurney and Harte, 1980; Wilshire, 1984) have drawn attention to difficulties inherent in considering xenoliths to be representative of the upper mantle, and in extrapolating evidence drawn from xenoliths to delineate mantle stratigraphy. This is supported by the distribution of products of partial melting in peridotite massifs; these products of partial melting closely resemble veins in xenoliths, but their distribution in massifs indicate that lithologies, for example Cr-diopside, Al-augite, and garnet pyroxenites, gabbros, and hornblendites, commonly thought to represent widely separated "strata" in the mantle occur side-by-side (e.g., Boudier, 1972; Dick, 1977; Shervais, 1979; Quick and Albee, 1979; Quick, 1981). The similarity of mafic rock types and their mode of occurrence in xenoliths and peridotite massifs indicate that the lithologic variants in xenoliths do not represent stratification in the mantle, except that some garnet lherzolites probably represent deeper levels than Cr-diopside spinel lherzolites.

Designations of a cognate or accidental origin of the members of the Al-augite group are conflicting. The dominant view regarding anhydrous members of the group is that they are cognate, and the mechanisms causing mineralogic variation among them are considered to be cumulus (for example, Best, 1974; Frey and Prinz, 1978) or crystal-plating processes of fractionation (for example, Dickey and others, 1977; Irving, 1978, 1980; Suen and Frey, 1978). However, isotopic studies (Leggo and Hutchinson, 1968; Stueber and Ikramuddin, 1974) indicate that some of these rocks are not in isotopic equilibrium with the host basalts, and their textures commonly reveal complex histories of solid-state deformation and recrystallization. These are the principal lines of evidence used to support accidental origin of peridotite members of the other major xenolith groups. Other isotopic studies indicate that some Al-augite pyroxenites and wehrlites are in equilibrium with their host rocks (Paul, 1971), as are some garnet pyroxenites and their host rocks (O'Neil and others, 1970). Laughlin and others (1971) showed that Sr isotopic compositions of "green spinel lherzolite," which are like those we classify in the Al-augite group, are the same as those of the host basalt.

Opinions on the origin of hydrous members of the Al-augite group are also divided. Perhaps the dominant view is that kaersutitic amphibole with or without Ti-phlogopite is cognate or is related to earlier magmatic events in the same volcanic episode as represented by the host rock, but a substantial minority consider veins of these minerals to be precursors to generation of the host alkalic magma and thus surviving hydrous minerals are accidental inclusions (e.g., Lloyd and Bailey, 1975; Francis, 1976b; Wass, 1979 ; Boettcher and O'Neil, 1980; Menzies and Murthy, 1980a; Wass and others, 1980; Wass and Rogers, 1980; Stosch and Seck, 1980; Menzies and Wass, 1983; Menzies, 1983). Isotopic composition of the hydrous phases (Basu, 1978; Wilshire and others, 1980; Kempton and others, 1984) can be used in support of or opposition to either view.

In summary, the dominant views on the origin of the xenoliths are that peridotites and pyroxenites of the Cr-diopside, garnetiferous ultramafic, and feldspathic groups, and metagabbroids are accidental inclusions from stratified mantle source areas unrelated to the host basalt, and that pyroxenites of the Al-augite group and gabbroids are mantle-lower crustal

crystallization products of the host basalt or of a basaltic magma belonging to the same magmatic episode as the host; views are about equally divided on whether hydrous members of the Al-augite (and Cr-diopside) group are cognate or accidental (though essential in generating the host basalts). Megacrysts of hydrous and anhydrous minerals are almost always considered cognate in alkali basalt assemblages, whereas they are commonly considered to be accidental in kimberlite assemblages.

Origin of Lithologic Variants Within Major Ultramafic Groups

Salient features. The principal lithologic variants within each main group of ultramafic xenoliths comprise olivine-rich, pyroxene-rich, hydrous mineral-rich, or feldspar-rich rocks. With few exceptions composite xenoliths containing two or more subtypes of the same group show that pyroxene-, hydrous mineral-, and feldspar-rich rock types form comparatively thin layers in olivine-rich rock types; less commonly, hydrous mineral- and feldspar-rich rock types form thin layers in pyroxene-rich rock types. In addition, the relative abundances of the different rock types for all known localities as a whole (Table 1) indicate a subordinate volume of these rocks compared to peridotite. Large composite xenoliths show that Fe-rich peridotites, a subordinate lithology, form relatively thin septa separating pyroxene rich layers from magnesian peridotites. Pyroxene-rich members of the Cr-diopside group generally form plane-parallel layers in olivine-rich rock, but those of the Al-augite, bottle-green pyroxene and feldspathic peridotite groups commonly form irregular, anastomosing, and crosscutting layers in peridotite, as do the hydrous mineral subtypes of the Al-augite group. Some samples show crosscutting and anastomosing relationships between pyroxene-rich layers of the Cr-diopside group.

Pyroxenite and hydrous-mineral layers of the Cr-diopside and Al-augite groups commonly crosscut foliation in the peridotite. Layers of all groups may enclose fragments of olivine-rich rocks (J. L. Carter, oral communication, 1971; Wilshire and Shervais, 1975; Irving, 1980; Griffin and others, 1984), and the olivine in many olivine-bearing pyroxenites of the Cr-diopside and Al-augite groups may have been derived by disaggregation of peridotite wallrock. In places layers in peridotite of the Cr-diopside and Al-augite groups are sandwiched by especially olivine-rich peridotite interpreted as depletion zones by Boudier and Nicolas (1972) and as products of zone refining by Quick and Albee (1979). These relations are, however, comparatively rare in xenoliths (see, for example, Irving, 1980), and generally there is no change in modal composition of peridotite with distance from the layers. In other samples representing the same groups, irregular diffuse concentrations of pyroxene occur adjacent to or near the layers.

Hydrous-mineral layers (and, rarely, clinopyroxenite) of the Al-augite group are closely associated with complex, intersecting planar fracture systems (with spacings of 1 to 10 or more cm); some of the fractures are healed by the hornblendite and glimmerite veins, but most are open fractures. Xenoliths of peridotite were commonly excavated along these planes of weakness, but some have remained as planes of weakness within peridotite xenoliths. The same relationships have been observed in peridotite xenoliths from kimberlite (Dawson, 1980; 1981; 1984). Discontinuous hydrous mineral veins of the Al-augite and Cr-diopside groups are associated with trains of fluid inclusions in neighboring anhydrous minerals indicating that fractures

through which the fluids passed were later healed in individual mineral grains.

The peridotite host rocks of all the layer variants have metamorphic textures. Common textures include allotriomorphic-granular, porphyroclastic, and mosaic (Pike and Schwarzman, 1977). Tabular texture is locally well-developed, for example at Kilbourne Hole (no. 67) where it characterizes a subordinate class of fine-grained peridotites (Bussod, 1983). Pyroxene-rich rock types of the Cr-diopside and garnetiferous ultramafic groups commonly have metamorphic textures, in which relics of large pyroxenes contain exsolution lamellae. Rare samples of spinel pyroxenite have pre-metamorphic coarse-grained allotriomorphic granular textures. Pyroxene-rich members of the Al-augite group commonly have ambiguous textures; they too are allotriomorphic-granular, but orthopyroxene is a minor constituent and exsolution features are common. On the other hand, inequigranular textures in which very large clinopyroxene grains are surrounded by a mosaic of smaller clinopyroxene grains are common. Where olivine is a significant phase in Al-augite pyroxenite, textures commonly are clearly metamorphic, but some clearly igneous textures (subhedral olivine poikilitically enclosed in pyroxene) also occur. Even the igneous-textured layers show substantial signs of solid state deformation of olivine. Cataclastic texture is found rarely; in such rocks weakly annealed fragmented clinopyroxene surrounds olivine grains that now are completely recrystallized to a mosaic texture. Textures of hydrous-mineral layers usually are ambiguous; they are allotriomorphic granular, and generally undeformed or only weakly deformed. Best (1974b), however, reported recrystallized textures in some amphibole-rich xenoliths, and Pike and others (1980) noted deformation of mica in xenoliths. Feldspathic layers generally have igneous textures, but partial recrystallization is commonplace and some layers have been completely recrystallized to equigranular-mosaic textures.

Mineral compositions were studied systematically in composite xenoliths (Appendix VI). The results indicate significant variations within mineral layers and in their peridotite host rocks, usually with respect to proximity to the layers. These relations occur in all lithologic associations, but absence of variations or asymmetrical arrangement of variations about the mineral layers are more common in the Cr-diopside group. Compositional trends in peridotite members of the Al-augite group clearly show that the distinctive compositions of these rocks resulted from metasomatic alteration of Cr-diopside peridotite in zones adjacent to Al-augite pyroxenites and other mineral layers (Wilshire and Shervais, 1973, 1975; Wilshire and Jackson, 1975).

Physical conditions of emplacement and differentiation. The structural, textural, mineralogical, and chemical relationships cited above indicate that pyroxene-, hydrous mineral-, and feldspar-rich layers of all the main ultramafic rock groups were emplaced as fluids (including melts) in solid peridotite of Cr-diopside composition. Although there is much evidence of wallrock-fluid interaction, the structural evidence is decidely in favor of emplacement of the fluids in dilational fractures and not in favor of a replacement origin of pyroxenites such as proposed by Lloyd and Bailey (1975), Wass and others (1980), Lloyd (1981), Menzies and Wass (1983), and Menzies (1983). The physical conditions attending the opening of fractures into which the fluids were injected were quite variable. In places, the wallrocks were sheared and subsequently recrystallized to fine-grained mosaic or tabular

textures, in others there was substantial disaggregation of the wallrock and impregnation by the melts; disaggregation resulted in incorporation of variable, commonly large, amounts of lithic and crystal debris in both pyroxenite and, less commonly, in hornblendite (see Irving, 1984; Griffin and others, 1984). At the extremities of melt injection, networks of narrow, closely spaced planar fractures were opened, possibly by gas-induced hydraulic fracturing (see Nicolas and Jackson, 1982). Trains of gas bubbles associated with discontinuous hairline fractures occupied by mica veins indicate annealing of some of these fractures before incorporation of the xenoliths in the host basalt. The short life-expectancy under mantle conditions of fine-grained sheared textures (Goetz, 1975; Mercier, 1979) may also apply to the planar fracture systems. If so, such fracture systems were probably generated in the last stages of deformation, melting, and melt fractionation before incorporation in the host magma.

In general, pyroxenites of the Cr-diopside and Al-augite groups lack an array of minor and incompatible elements that should be present if they represented liquid compositions (Frey and Prinz, 1978; Frey, 1980, 1983). Various mechanisms of differentiation, including cumulus processes, crystal plating (Dickey and others, 1977; Irving, 1978, 1980; Suen and Frey, 1978; Sinigoi and others, 1983), filter pressing or dilation in a structurally dynamic environment (e.g., Kornprobst, 1969; Moores, 1969; Kornprobst and Conquere, 1972; Dick, 1977; Evarts, 1978; Wilshire and others, 1980), and partial refusion (Wilshire and Pike, 1975; Wilshire and others, 1980; Loubet and Allegre, 1982; Wilshire, 1984) have been advanced to explain the geochemistry of these rocks, and perhaps all have had an effect.

Residual fluids of differentiation of both Cr-diopside and Al-augite pyroxenites may include hydrous minerals which form vein systems within and independently of the pyroxenites. In western U.S. occurrences only phlogopite + Cr-diopside have been recorded for the Cr-diopside group, but both hornblendite and glimmerite are common (the former more abundant than the latter) in the Al-augite group. Where potassic lavas are the host rocks, peridotite xenoliths commonly contain phlogopite veins (e.g., Van Kooten, 1980; Ehrenberg, 1982a,b). As in kimberlite occurrences (Dawson, 1980, 1981; Erlank and others, 1982), mica-rich and amphibole-rich veins may occur side-by-side, and each commonly contains the characteristic mineral of the other as an accessory. There is, to our knowledge, no direct structural evidence of the relationship between these two lithologies. They may represent products of fractional crystallization or possibly immiscible liquids. The effectiveness of the processes that segregate them is clearly recorded in the rocks, however, and, because of the associated fractionation especially of Rb from Sr, may have significance in explaining some of the isotopic variability of xenoliths and their host rocks. Gabbroids and possibly garnet pyroxenites appear to be less modified than the spinel pyroxenites, but nevertheless have undergone some differentiation and loss of minor and incompatible elements. The inferred source and general character of processes responsible for minor rock types in the Cr-diopside, Al-augite, and feldspathic peridotite groups are shown in figure 26.

Wallrock reactions and metasomatism. Emplacement of basaltic partial melts and of residual, volatile-rich liquids derived from them in Cr-diopside lherzolite resulted in significant local chemical interchanges between the melts and wallrocks as previously documented. The close association in space

and time of hydrous minerals veins and intricate systems of planar fractures in the peridotite suggests the possibility of further chemical interchanges between a fluid phase derived from the differentiating silicate liquids and peridotite. Menzies and others (1984) present a model in which a fluid phase derived from hydrous liquids extends beyond the front of infiltration laterally from dikes. Neither model has been tested.

The nature of major-element effects of reaction between Cr-diopside peridotite and basaltic intrusions have been known for some time (e.g., Wilshire and Shervais, 1973, 1975), and were subsequently reported for garnetiferous ultramafic assemblages (Harte and others, 1977; Gurney and Harte, 1980; Ehrenberg, 1982b). The principal effects on wallrocks of the least differentiated intrusions (leaving residues of pyroxenite) are enrichment of the wallrock in Fe, Ti (Wilshire and Shervais, 1975; Wilshire and Jackson, 1975; Harte and others, 1977; Irving, 1980; Ehrenberg, 1982b) and sometimes LREE (Irving, 1980; Ehrenberg, 1982a; Roden and Murthy, 1985), and presumably other incompatible elements. As shown in table 5, the nature and magnitude of major element compositional changes in lherzolites of the Cr-diopside group resulting from reaction with igneous intrusions are the same as those for granular and sheared garnet lherzolite xenoliths in minette (Ehrenberg, 1982b) and kimberlite (Nixon and Boyd, 1973; Nixon and others, 1981). The main difference in western U.S. xenoliths is that the altered wallrock is less commonly sheared than it is in kimberlite samples, which may reflect differences in mechanical behavior of fractures at different pressures. However, both mosaic and tabular recrystallization of sheared rocks does occur, and is locally prominent (e.g., Lunar Crater, Nevada, nos. 16-19). It does not appear reasonable, solely on the grounds of chemical differences, to suppose that the Fe-enriched rocks are undepleted samples of the asthenosphere (Boyd, 1973; Boyd and Nixon, 1973), a conclusion also reached by Gurney and Harte (1980), Ehrenberg (1982b), and Harte (1983). The effect, if any, of Fe-Ti metasomatism on calculated pressures of sheared rocks remains to be tested. It is evident, however, that the sheared, metasomatized xenoliths in kimberlites generally show higher apparent pressures of equilibration for relic, unsheared minerals than for unsheared more magnesian rocks (Boyd, 1973, 1984; Schulze, 1984).

Differentiates of the basaltic intrusions include volatile-rich liquids that crystallize to hornblendite and glimmerite, and less volatile liquids that crystallize to anhydrous gabbroic assemblages. These liquids were mechanically separated from the parent intrusion and injected into surrounding unaltered Cr-diopside lherzolite with which they were not in equilibrium. Disaggregation of the wallrock allowed extensive local infiltration of liquids, as it did adjacent to pyroxenites. Unlike the pyroxenite reactions, however, the more volatile fluids that crystallized hydrous minerals effectively penetrated the wallrock along grain boundaries for distances of a few to 15 cm or more. Feldspathic melts also penetrated the wallrock peridotite forming interstitial deposits and microscopic veinlet networks (see Dick and Friesz, 1984). Although amphibole and plagioclase reaction rims on spinel are common, and replacement of clinopyroxene by amphibole occurs in places, much of the introduced amphibole and plagioclase is in apparent "textural equilibrium" with the peridotite so that distinctions between "primary" and "secondary" minerals are not always simple. Use of such internally contradictory terms as "primary metasomatic" (Harte and others, 1975; Gurney and Harte, 1980), however, seems unnecessarily misleading.

Many systematic studies have been made of major element variations in minerals in the hydrous vein-wallrock systems (Francis, 1976; Stewart and Boettcher, 1977; Boettcher and others, 1979; Boettcher and O'Neil, 1980; Irving, 1980; Wilshire and others, 1980), but far fewer data on bulk compositional effects are available than for reaction zones adjacent to Al-augite clinopyroxenites. The nature of the introduced phases and the compositional effects of reaction allow the generalization that likely effects are increased Fe, Ti, Al, Ca, alkalis, and LREE, and reduced Si, Mg, Cr, and Ni. This is supported, except for silica, by one analysis of Cr-diopside lherzolite sandwiched by hornblendite veins (Table VI-17) in comparison with unveined Cr-diopside lherzolites from the same locality (Appendix IV, Locality 32). It should be noted that, unlike the reaction zones adjacent to Al-augite pyroxenites, those adjacent to hornblendites and glimmerites are usually not conspicuous in hand specimen. The compositional effects of fluid-wallrock reactions are such that vein minerals are substantially richer in Fe, Ti and other components than intersititial hydrous minerals in adjacent wallrock. The same differences are found between micas of the MARID suite and interstitial micas in garnet lherzolites (Jones and others, 1982), so that a genetic relationship between micas of the two modes of occurrence is strongly indicated, contrary to the suggestion of Dawson and Smith (1977) and Delaney and others (1980).

The relatively high REE abundances and LREE-enriched patterns of kaersutitic amphibole, and, especially, of the commonly associated apatite (Wass and others, 1980; Irving and Frey, 1984; Menzies and others, 1984) indicate that a net result of the infiltration of fluids is a bulk enrichment of the peridotite in REE and other incompatible elements in minerals of the peridotite through reaction. It would be surprising if substantial quantities of introduced incompatible elements did not remain in the rocks as leachable intergranular deposits as suggested by Basu and Murthy (1977). Net enrichment of the REE is much less if only micas crystallize, although the micas also have LREE enriched patterns (Wass and others, 1980; Irving and Frey, 1984; Menzies and others, 1984).

The effects of addition of new mineral phases by hydrous fluid infiltration and reaction between the fluids and minerals comprising the wallrock have significant effects on isotopic compositions. Data on Dish Hill samples (Locality 32; Fig. 25) presented by Menzies and others (1984) are especially noteworthy. One of these samples (Ba-2-1) is composed of a thin selvage of mica-bearing hornblendite at one end of a lherzolite inclusion that is 17 cm long. Measurable major element reaction effects are localized in a zone about 2 cm wide (Wilshire and others, 1980; Appendix VI, Fig. VI-18), but a small amount of pargasite has crystallized throughout the body of the lherzolite. The second sample, Ba-1-72, is composed of two hornblendite selvages that sandwich a 7.2 cm thick slab of lherzolite; the lherzolite contains abundant amphibole adjacent to both selvages, so much of the lherzolite has been metasomatized. The isotopic characteristics of the two samples are quite different (Fig. 25); clinopyroxene from the least modified lherzolite (Ba-2-1) plots at the extreme depleted end of the "mantle array", whereas that of the more modified sample (Ba-1-72) plots close to amphibole from its selvage, and much closer to the estimated bulk earth composition. Menzies and others (1984) interpret this as the result of modification of the isotopic composition of clinopyroxene in Ba-1-72 lherzolite by reaction with vein fluids, with which we concur. This suggests that the clinopyroxene of

Ba-2-1 may have had an even higher $^{143}Nd/^{144}Nd$ and lower $^{87}Sr/^{86}Sr$ ratios before introduction of amphibole and mica than it now has, and that the vein minerals, especially Ba-1-72, may have crystallized from a fluid that had lower $^{143}Nd/^{144}Nd$ and higher $^{87}Sr/^{86}Sr$ ratios before reaction. In any case, it is significant that the isotopic effects of these relatively young intrusive events on their wallrocks is to shift the wallrock isotopic composition within the "mantle array" toward the estimated bulk earth composition, the same effect as produced by reaction with the parent pyroxenites. Varying degrees of reaction may thus alleviate the necessity of having a separate fluid of distinctive isotopic composition for every observed reaction product (Menzies and others, 1984).

The effectiveness of differentiation processes in separating fluids that crystallize amphibole from those that crystallize mica suggests additional causes of isotopic variability in the mantle inclusions and in lavas derived from the same mantle source areas. Micas, for example, do not show enrichment of Nd relative to Sm (Wass and others, 1980) so that crystallization of micas in wallrock can cause a significant change in the Rb/Sr ratio of the bulk rock but have little effect on the Sm/Nd ratio. Given time, a subject that will be discussed in a later section, fractionation of Rb from Sr and Sm from Nd in differentiates of partial melts and emplacement of the products in wallrocks can explain at least part of the isotopic variability in inclusions and host rocks without the need to invoke unrelated metasomatic events or separate "mantle reservoirs" for every isotopic variant in particular volcanic fields.

The relation between hydrous mineral veins and an intricate system of planar fractures in peridotite that are unoccupied by veins is quite clear in many western U.S. localities (Table 1) as well as other world-wide occurrences of xenoliths in basalts, for example, the Massif Central in France, Westeifel in Germany, eastern Australia, and the east African rift zone. Similar features are found in garnet lherzolite inclusions in kimberlite (Dawson, 1980, 1981, 1984). We postulate that propagation of a fracture system by hydraulic fracturing (Nicolas and Jackson, 1982) beyond the limits reached by hydrous liquids was caused by a CO_2-rich gas phase derived from the hornblendite-glimmerite liquids and their parent basaltic liquids. Evolution of a gas phase from these sources is attested by the abundance of macroscopic vesicles in amphibole and pyroxene megacrysts derived from vein systems, and in some wallrocks (Locality 47; Griffin and others, 1983). The gas phase is considered to be CO_2-rich from the abundance of CO_2 fluid inclusions in peridotites and associated minor lithologies (e.g., Bergman and others, 1981; Menzies and Wass, 1983). Menzies and others (1984) also postulate evolution of a CO_2-rich gas phase from hydrous silicate liquids that extends the zone of infiltration around veins. A macroscopic fracture system, such as is observed to exist in the peridotites, is likely to be much more efficient in distributing the gas phase than intergranular migration. Both hypotheses are, however, testable by looking for concentration gradients of fluid inclusions with proximity to structures in the peridotite, either veins or fractures.

The significance of distributing a gas phase beyond the limits reached by silicate liquids lies in fractionation of LREE into the gas phase (Wendlandt and Harrison, 1979; Harrison, 1981; Mysen, 1983). Such a process may allow LREE-enrichment of peridotite and its constituent clinopyroxene by infiltration and reaction with much less tangible influence on major element compositions than occurs when silicate liquids are involved. The process will

also affect the REE radiogenic system by decreasing the Sm/Nd ratio; potential major effects on the Rb/Sr system are indicated by the presence of Rb and radiogenic Sr in grain boundary locations of xenoliths (e.g., Basu, 1979; Jagoutz and others, 1980).

Thus, we see wallrock reactions and metasomatic events as an interrelated sequence: partial melting, injection of melts, reaction with and local infiltration of wallrock; differentiation of the intrusions, separation and injection of the liquid residues which themselves repeat the sequence of reaction and infiltration of the parent liquids; and, finally, separation of a gas phase and distribution of it through a fracture system propagated in front of the liquid injection zone. The gas phase also infiltrates the wallrock and reacts with it. This sequence is illustrated in figure 27, which shows three relationships that could occur between different rock types in composite xenoliths, and the cryptic effects of a gas phase evolved from the liquids: (1) the most common composite relationship seen in xenoliths results from injection of melts and liquid residues derived from these melts into peridotite with which they are not in equilibrium (Pt. A, Fig. 27). (2) residual liquids are segregated but not removed from their parent dikes (Pt. B, Fig. 27; see Wilshire and others, 1980, Plate 2); here there may be no chemical variations with proximity to lithologic contacts as is the rule in the Point A (Fig. 27) situation, and (3) (Pt. C, Fig. 27) in the zone of origin of the melts wallrock interactions with melts may be on a scale that is large compared to the size of the xenoliths so that chemical disequilibrium is not detectable. This could explain the relations observed by Bergman and others (1981) in a composite hornblendite/olivine-rich wehrlite, and lack of heterogeneity of mineral compositions in sheared metasomatized xenoliths reported by Ehrenberg (1979). A fourth situation (Pt. D, Fig. 27) arises where a gas phase is distributed through a fracture system propagated beyond the zone of hydrous liquid injection. This hypothetical reconstruction represents a single stage of melting. As will be discussed in a following section, a number of such events may be superimposed, and products of earlier ones may be deformed, recrystallized, and remelted.

Origin of the Main Xenolith Groups

Significant features of the xenolith assemblages of the western United States include: (1) Cr-diopside peridotite, mostly lherzolite, forms the host rock for a wide variety of mineral layers representing the Cr-diopside, Al-augite, bottle-green pyroxene, garnetiferous, feldspathic, and gabbroid groups; (2) peridotite members of the Al-augite group, and possibly those of the feldspathic, garnetiferous, and bottle-green pyroxene groups, formed by metasomatic alteration of Cr-diopside peridotite in contact with mineral layers rich in pyroxene and/or hydrous minerals, or plagioclase; (3) representatives of all the major lithologic groups can occur together in their source areas in such close proximity that individual xenoliths may contain members of more than one group; (4) the mineral layers were emplaced sequentially in the Cr-diopside peridotite country rock most probably in the order: Cr-diopside pyroxenite (more than one generation)--Cr-diopside plus phlogopite--garnet-bearing pyroxenite--bottle-green pyroxene pyroxenite--Al-augite pyroxenite and wehrlite (more than one generation)--hornblendite and glimmerite--gabbroid; (5) the relatively young layers -- gabbroids, hornblendites, Fe-Ti glimmerites, and Al-augite pyroxenites -- are commonly in

Sr isotopic equilibrium with the host basaltic magma or with other volcanic rocks in the same field. (6) older representatives of this sequence are in general more extensively metamorphosed than younger ones, and all show evidence of at least one episode of partial melting following their emplacement, consolidation, and, commonly, their metamorphism (Wilshire and Pike, 1975); (7) planar fractures in peridotites were commonly developed on a close-spaced polygonal pattern before or contemporaneously with emplacement of hydrous-mineral layers of the Al-augite group and before excavation by the basaltic magma. Shearing took place on some of these, and other, surfaces. The same relationships have been reported for xenoliths in kimberlite (Dawson, 1980, 1981, 1984).

These facts are consistent with a sequence of events in which partial melts of varying composition are concentrated and consolidate in comparatively thin layers in Cr-diopside peridotite under physical conditions that changed progressively toward lower pressure and temperature regimes with time. The simplest mechanical model to explain this sequence of events is that of diapirs of Cr-diopside peridotite rising through the upper mantle into the lower crust, successively crossing P-T regimes appropriate to crystallization of lithologic variants ranging from nonfeldspathic to feldspathic rocks (Wilshire and Pike, 1975). This dynamic model also explains mechanical separation of residual liquids of the intrusions as they crystallized, and the deformation, recrystallization, and partial remelting of the dikes, all of which result in dike compositions that no longer represent original liquid compositions. Evolution of fluid from basaltic intrusions and their differentiates may have induced hydraulic fracturing (Nicolas and Jackson, 1982) forming polygonal fracture systems in the peridotite before or during excavation of xenoliths. Differences in assemblages of xenoliths, with some populations comprising rocks of the Cr-diopside group alone, others comprising rocks of the Cr-diopside and Al-augite groups, and still others containing representatives of the feldspathic group, can be explained by termination of diapirism at different levels in the mantle-lower crust by volcanic eruptions (Wilshire and Pike, 1975); the eruptive stage occurs when there is an opportunity for generation of larger volumes of melt than represented by the dikes and veins frozen in the peridotite xenoliths.

Even veins that are isotopically in equilibrium with host rocks of the xenoliths commonly are recrystallized. This fact indicates that a dynamic interaction of melts and solid country rock persisted up to the time of eruption. The opportunity clearly existed, until eruption truncated the process, for isolation of small quantities of liquids as dikes, crystallization and differentiation of the liquids, recrystallization of the lithic products, and renewed partial melting, while still permitting incorporation of fragements of this system in erupted lavas. Thus, the evidence presented here suggests that the root zones of the volcanoes which yield xenoliths are sponge-like networks of dikes and mantle peridotite, which in places have risen into the crust. The root zones are not only structurally active, but also chemically active and involve metasomatic interchange between liquids and wallrock on scales that range from microscopic to large compared to the sizes of xenoliths.

According to this model, the layers of all the main groups of xenoliths are products of broadly continuous episodes of melting in the mantle and lower crust over an unknown period of time. We have not demonstrated, however, that

each of the main groups was derived from distinct partial melts during diapirism. In fact, the association of gabbroids and pyroxenites of the Al-augite and, less commonly, of the bottle green pyroxene group, suggest that they may be differentiates of a common parent. This relationship has been specifically suggested by Shervais (1979) and Sinigoi and others (1980; 1983) based on the occurrence of composite Al-augite and gabbroid dikes in the Balmuccia and Baldissero peridotite massifs. Sinigoi and others (1980; 1983) further suggest that Cr-diopside and Al-augite pyroxenites are also differentiates of a common parent magma. This is based on occurrence of composite dikes containing both lithologies and on continuity of pyroxene compositions. Although such an interpretation may be correct for specific occurrences, it does not explain the perfect regularity of crosscutting relationships among Cr-diopside, Al-augite, and gabbroid dikes as presently documented in both xenolith and massif occurrences. Inasmuch as there are multiple generations of dikes in each of the principal groups, a less systematic sequence of crosscutting relationships would be expected if all are directly related by fractionation. That is, an Al-augite pyroxenite or hornblendite or gabbroic derivative of an earlier generation of Cr-diopside dikes might be crosscut by any of the same set of rocks in a later generation. We have not observed such relationships. Combined with a dynamic process of diapirism in which the physical conditions of crystallization change with time as well as chemical composition of the liquids, however, a genetic link among all of the dikes is possible. In this model, the various layers may thus be viewed as quasi-cognate with the magma that ultimately brought fragments of them to the surface. Most peridotites, whether metasomatically altered or not, are accidental inclusions, but those that have been altered by the multiple episodes of melting and reaction before eruption cannot be considered broadly representative of the mantle. Our model suggests that the opportunity for the host basalts to sample peridotite that has been modified by the processes of melt generation is much greater than that for sampling peridotite more representative of the mantle. Because igneous gabbroids and metagabbroids share distinctive mineralogical features from locality to locality and because gabbroid layers are commonly partly recrystallized, isolated gabbroid and metagabbroid xenoliths may be quasi-cognate xenoliths, or accidental inclusions of crustal material, or individual xenolith populations may contain samples of both origins.

The time over which melting-metasomatic events in a diapir may take place is important in assessing causes of isotopic variability, but not much information is available. The Cima volcanic field (localities 37-40), however, is instructive. Here, episodic eruption of xenolith-bearing basalts has occurred over an interval of about 9 m.y. (Dohrenwend and others, 1984). The oldest rocks identified have xenoliths of feldspathic peridotite and gabbroid veins in peridotite as well as members of the Al-augite and Cr-diopside groups. According to our model 9 m.y. elapsed after the diapir reached the lower crust and igneous and metasomatic events continued over that period yielding episodic eruptions. If a similar period of time elapsed between the beginning of diapirism and arrival of the diapir in the crust, a modest amount of time (about 20 million years) is available for isotopic aging of the older metasomatic rocks and of the igneous intrusions. In particular, the time available may be significant for the more extreme products of Rb fractionation represented by mica. Thus, the basaltic magmas erupted can tap sources within the diapir with substantial isotopic variability. Considering the very small volumes of basaltic liquids erupted over a 9 m.y. period at

Cima (Dohrenwend and others, 1984), development of "mini-mantle reservoirs" as a built-in consequence of diapirism may suffice to explain some of the isotopic variability of basalts.

CURRENT CONCEPTS OF MANTLE METASOMATISM: CAUSE OR EFFECT OF ALKALINE BASALTIC MAGMATISM?

A plethora of models of mantle metasomatism have been advanced since the pioneering work of Bailey (1970, 1972), each seeking to explain phenomena observed in xenoliths in basalts and kimberlites, or to extrapolate theoretical-experimental considerations. Many authors consider the process of incompatible element enrichment of previously depleted mantle peridotites to be regional in extent and a necessary precursor to generation of alkaline magmas. These inferences are based on the wide geographic distribution of metasomatic effects observed in xenoliths (Bailey, 1972, 1982; Lloyd and Bailey, 1975; Wass and others, 1980; Boettcher and O'Neil, 1980; Menzies and Murthy, 1980a; Erlank and others, 1980), petrographic evidence that secondary hydrous minerals were emplaced before incorporation of the xenoliths in their host basalt (e.g., Wilshire and Trask, 1971; Pike and others, 1980; Dawson, 1980; Roden and others, 1984a), on limited rare gas data indicating that degassing of the earth is continuing and is symptomatic of much more comprehensive migration of mobile elements (Vollmer, 1983), on the supposition that fluids present (at the relatively shallow depths corresponding to stability limits of carbonate and amphibole) will move upward in the mantle and alter, by crystallizing amphibole and possibly carbonate, a zone about 70 km deep in both continental and oceanic areas (Schneider and Eggler, 1984), and on isotopic variability in xenoliths and magmas derived from the mantle, which has led to the supposition that enriched mantle reservoirs of unspecified size have existed for periods as long as 2 b.y. (O'Nions and others, 1979; Menzies and Murthy, 1980b; Basu and Tatsumoto, 1980; Cohen and others, 1984). Interpretation of the metasomatism as a necessary precursor to alkaline volcanism is based on the observation that some metasomatically altered peridotites are capable of yielding alkali basaltic magmas with substantial degrees of melting (Varne, 1970; Lloyd and Bailey, 1975; Menzies and Murthy, 1980a; Bailey, 1982; Menzies and Wass, 1983) whereas unaltered (depleted) peridotites cannot yield such compositions even with improbably low degrees of melting. Other authors ascribe the metasomatism to local interactions between magma and depleted wallrock, in part as we have represented them here (for example, Harte, 1975; Harte and others, 1977; Gurney and Harte, 1980; Wyllie, 1980; Ehrenberg, 1982a,b; Mysen, 1983; Roden and others, 1984a). In this view, the enrichment is a consequence of emplacement of alkaline melts in or passage of them through the depleted peridotite. The evidence on which this conclusion is based is recounted in the preceding chapters.

It is an unfortunate fact that with the explosion of models has come a terminology, fraught with genetic implications, that is confusing and internally contradictory. It is not likely to foster adequate testing of the various models. Current schemes of mantle metasomatism either ignore the Fe-Ti enrichment of wallrocks adjacent to pyroxenite dikes or treat it as an unrelated process, even though the nature of the reaction is the same as that involved in hydrous liquid reactions (see, for example, Menzies and Murthy, 1980a; Harte, 1983; Kramers and others, 1983; Dawson, 1984; O'Reilly and Griffin, 1984).

The current schemes divide mantle metasomatism into two unrelated parts: "patent" metasomatism in which hydrous phases are introduced into the metasomatized rock (Dawson, 1984), also called "modal" metasomatism (Harte, 1983), and "cryptic" metasomatism in which refractory peridotite is enriched in incompatible elements without introduction of hydrous phases (Dawson, 1984; Roden and Murthy, 1985). These processes are regarded as fundamentally different in origin and time of formation, clinopyroxenes of metasomatized rocks being modified by universally active "cryptic" processes operating well in advance of melting events related to eruption, and introduction of hydrous phases being local igneous phenomena related to the eruptive process or to preceding igneous events (Menzies, 1983; Kramers and others, 1983; Hawkesworth and others, 1983; Dawson, 1984; Menzies and others, 1984). Despite the limited amount of data available, further subdivisions of this classification scheme have been advanced: Menzies and others (1984) recognize a depleted type lacking LREE enrichment of clinopyroxene (Type Ia) and a depleted type with LREE enrichment of clinopyroxene (Type Ib), both of which have metasomatized and unmetasomatized and hydrous and anhydrous subtypes. This modification of the classification seems to mean that depleted rocks (Ia) may be cryptically metasomatized (yielding Ib), and that both Ia and Ib may be patently metasomatized, but patent metasomatism does not necessarily convert Ia to Ib.

In assessing the qualitative basis of this classification, it is well to remember that enrichment of refractory peridotites in incompatible elements (Nagasawa and others, 1969) was originally ascribed to introduced components that were harbored in clinopyroxenes and hydrous phases (Frey and Green, 1974), the enrichment sites now said to be genetically unlinked. The idea that these modes of metasomatism are unrelated is based in part on the supposition that cryptic processes are universal and patent processes are local (Kramers and others, 1983; Harte, 1983; Menzies, 1983; Dawson, 1984). Most commonly, however, analysis of a number of xenoliths shows that some (about 60% on the average at present count) from particular localities have LREE enrichments and others do not. Examination of the worldwide localities cited by Kramers and others (1983) and Dawson (1984) as examples of cryptic metasomatism reveals that many have rocks with introduced hydrous phases also; for example, the Victorian samples studied by Frey and Green (1974), the kimberlite samples studied by Menzies and Murthy (1980b), and the Westeifel samples studied by Stosch and Seck (1980). That the process has operated widely on a geographic basis is certainly true. The same is true of hydrous mineral veining. The same is true of anhydrous metasomatic alteration of wallrocks of pyroxenite and gabbroic intrusions. Frequency of occurrence and geographic distribution do not, therefore, distinguish either patent or cryptic metasomatism as more or less local than the other.

At the present time, it seems undesirable to attach highly restrictive definitions to the terms "patent" and "cryptic" metasomatism, and no a priori basis for considering them to be genetically unrelated is apparent. As purely descriptive terms, "patent" and "cryptic" are useful if they are extended as follows: "patent" metasomatism should include all reactions in which major and minor element compositions of the original minerals of the metasomatized rock are altered, and/or new mineral phases (hydrous or anhydrous) are formed in the metasomatized rock; "cryptic" metasomatism should refer to reactions in which minor element compositions are altered without conspicuous effects on major element compositions of the metasomatized rock, and without significant introduction of new mineral phases.

Inasmuch as both patent and cryptic metasomatism have the same effects on trace element distribution (Kramers and others, 1983), distinction of the processes as serial or unrelated events must rest on evidence other than trace element composition. This is essentially a question of timing of metasomatic events, especially important aspects of which are timing with respect to igneous phenomena with which they may be associated, or time of eruption of the host rock. Several independent lines of evidence give relevant information: crosscutting relations of different igneous intrusions directly associated with metasomatism; structures and textures of metasomatized rocks; zoning of minerals in metasomatized rocks; and isotopic compositions of metasomatized rocks.

Crosscutting relations among the various intrusive veins and dikes identified in this study, combined with geochemical evidence that all of the different varieties have reacted with their wallrocks, clearly indicates that local patent metasomatic events have occurred serially in the igneous history preceding eruption of the host basalts. If cryptic metasomatism is a consequence of evolution of gas from these melts as we and Menzies and others (1984) postulate, cryptic metasomatic events also may have occurred serially in the pre-eruption history. Because the various minor lithologies can occur in close proximity to one another in the host peridotite, superposition of patent and cryptic events is possible, if not likely.

The correlation between Fe-Ti metasomatism and fine-grained (sheared) textures in kimberlite xenoliths (and some basalt occurrences), suggest a close time relation between the metasomatism and eruption of kimberlite because such textures have a short life-expectancy under mantle conditions. Similarly, the spatial relation between hydrous mineral veins and unoccupied planar fractures in peridotite also suggest a time of formation contemporaneous with hydrous mineral emplacement and not greatly preceding eruption of the host basalt, again because such structures may not have long residence times at mantle T and P. Smith and Ehrenberg (1984) suggest that Fe-Mg zoning of garnets in metasomatized peridotite inclusions in minette could not have survived in the mantle longer than about a thousand years so that the metasomatism is essentially contemporaneous with eruption of the host minette. Boyd and others (1984) (see also, Pike and others, 1980) note the presence of zoned olivine in kimberlite dunites with sheared textures, and conclude that the metasomatism causing the zoning was contemporaneous with formation of the kimberlite.

The timing of metasomatic events as assessed from isotopic compositions of metasomatized rocks has been reviewed recently (Roden and Murthy, 1985). These authors discuss the difficulties in using Rb-Sr and U-Pb systems because of variability in fractionation of parent and daughter elements in metasomatic processes. The Sm-Nd system is said to be preferable because of the chemical similarity of Sm and Nd, consistent enrichment of Nd relative to Sm in metasomatized rocks, and the resistance of Sm and Nd to remobilization. However, the behavior of these elements and other parent-daughter pairs in a gas phase (probably generally rich in CO_2) under mantle conditions is poorly known (Wendlandt and Harrison, 1979; Mysen, 1983). Evidence from inclusions in basalts indicates that metasomatism commonly precedes basalt eruption by a time period shorter than the resolution of the Sm-Nd system ($<$ 200-500 m.y.; Menzies and Murthy, 1980a; Roden and others, 1984a; Roden and Murthy, 1984; Kempton and others, 1984). This is also consistent with common Sr isotopic

similarity of the younger vein assemblages (Al-augite hornblendite, pyroxenite) and the host basalts.

In contrast, metasomatism in African xenoliths, mostly from kimberlites, is commonly inferred to have predated the host kimberlite for periods from about 60 m.y. (Erlank and others, 1980; Hawkesworth and others, 1983) to as much as 2 b.y. (Menzies and Murthy, 1980b; Hawkesworth and others, 1983; Cohen and others, 1984). The "ages" of metasomatism of these rocks are inferred from high $^{87}Sr/^{86}Sr$, low $^{143}Nd/^{144}Nd$ ratios (Menzies and Murthy, 1980b), apparent isochronal relations of a number of xenoliths and megacrysts (Erlank and others, 1980; Hawkesworth and others, 1983), and a Nd model age of clinopyroxene (Cohen and others, 1984). The pitfalls of constructing "isochrons" from the type of data presented by Erlank and others (1980) and Hawkesworth and others (1983) are lucidly described by O'Reilly and Griffin (1984), even if the very great scatter of points used to define the isochrons is accepted as constraining the age of metasomatism and initial isotopic compositions of the metasomatizing fluids. In addition, the planar fracture systems, some of which were healed by hydrous mineral veins, in these xenoliths (Dawson, 1980, 1981, 1984) would have to survive at mantle T and P for about 60 m.y. before kimberlite eruption according to the present interpretation. The xenoliths described by Menzies and Murthy (1980b) and Cohen and others (1984) have clinopyroxenes that extend the "mantle array" well into the enriched quadrant of the Sr/Nd diagram (high $^{87}Sr/^{86}Sr$, low $^{143}Nd/^{144}Nd$) and for this reason are inferred to have undergone ancient metasomatic events. All of these rocks, however, have evidence of significant patent metasomatism in the form of introduced phlogopite. Isotopic compositions of two micas (Menzies and Murthy, 1980b) straddle and plot well off of the "mantle array." They are considered by Menzies and Murthy (1980b) to be secondary and unrelated to the process of enrichment of the clinopyroxene. All mineral components of the xenolith studied by Cohen and others (1984) have extreme Sr and Nd isotopic compositions, and the clinopyroxene is used to compute a model Nd age. A puzzling feature of this rock is that both garnet and clinopyroxene, with much lower Rb contents than the phlogopite, have higher $^{87}Sr/^{86}Sr$ ratios than the phlogopite so that an internal Sr isochron has a negative slope. It is not at all clear why the isotopic compositions and LREE contents of clinopyroxenes are considered to be "intrinsic features" (Roden and Murthy, 1985) or "most representative of mantle conditions" (Hawkesworth and others, 1983; Menzies and Murthy, 1980b) on which ages can be modelled, when leachable interstitial components or the products of patent metasomatism are present and either share to some extent the isotopic characteristics of the clinopyroxenes or depart radically from them.

A small amount of data available on patently metasomatized xenoliths (Menzies and others, 1984; Roden and others (1984b) (see Fig. 25) indicates that the isotopic composition of peridotite wallrock clinopyroxenes is shifted toward older apparent ages by a young intrusive-metasomatic event. That is, the resultant isotopic composition of the wallrock reflects the isotopic composition of the metasomatizing fluid, not the time of metasomatism. Although these data indicate that some caution is in order in interpreting the age of metasomatism, the extreme compositions of introduced phlogopite recorded by Menzies and Murthy (1980b) and Cohen and others (1984) cannot be obviously reconciled with fluids related to the host kimberlite or ankaramite.

Setting aside for the present whether or not large time gaps are demonstrable between metasomatism and eruption of host magmas, which would preclude any genetic relation between them, the record from all independent lines of evidence for xenoliths in alkali basalts is clearer. Here, the time elapsed between metasomatism identified with the Al-augite and younger groups and the time of eruption of host basalts is short, ranging from less than a thousand years to less than 500 m.y. depending on the sensitivity of the dating technique. A close time relation between metasomatism and eruption is consistent with both of the principal contending hypotheses: (1) that the metasomatism is not only a necessary precursor but is also a causal factor in alkaline magmatism (Bailey, 1972, 1982, 1984); (2) that the metasomatism is a consequence of alkaline magmatism as we assert here. In both hypotheses, the ultimate source of elements whose relative abundance characterizes alkali basaltic rocks is sought in the unknown depths of the mantle. Both have sought, as their strongest basis, the integration of field and geochemical data. Clearly, much has yet to be learned from all disciplines of earth science to resolve these differences, or to find new paths.

ACKNOWLEDGMENTS

We are especially indebted to B. Carter Hearn, Jr., Rosalind Helz, and Warren Hamilton, U.S. Geological Survey, and to Michael Roden, University of Georgia for their helpful criticisms of the manuscript. We are also grateful to Martin Menzies, Steven Bergman, and Michael Roden for making available as yet unpublished manuscripts and data.

REFERENCES

Allegre, C. J., Manhes, G., Richard, D., Rousseau, D., Shimizu, N., 1978, Systematics of Sr, Nd and Pb isotopes in garnet lherzolite nodules in kimberlites, in Zartman, R. E. (ed.), Short papers of the Fourth International Conference, Geochronology, Cosmochronology, Isotope Geology 1978: U.S. Geological Survey Open-File Report 78-701, p. 10-11.

Allsopp, H. L., Nicolaysen, L. D., and Hahn-Weinheimer, P., 1969, Rb/K ratios and Sr-isotopic compositions of minerals in eclogitic and peridotite rocks: Earth and Planetary Science Letters, v. 5, p. 231-244.

Anderson, R. E., Longwell, C. R., Armstrong, R. L., and Marvin, R. F., 1972, Significance of K-Ar ages of Tertiary rocks from the Lake Meade region, Nevada-Arizona: Geological Society of America Bulletin, v. 83, no. 2, p. 273-288.

Arculus, R. J., and Smith, Douglas, 1979, Eclogite, pyroxenite and amphibolite inclusions in the Sullivan Buttes Latite, Chino Valley, Yavapai County, Arizona: in F. R. Boyd and H. O. A. Meyer (eds), The mantle sample: inclusions in kimberlites and other volcanics: American Geophysical Union, Proceedings Second International Kimberlite Conference, v. 2, p. 309-317.

Bailey, D.K., 1970, Volatile flux, heat focusing and generation of magma: Geological Journal, Special Issue No. 2, p. 177-186.

Bailey, D.K., 1972, Uplift, rifting and magmatism in continental plates: Journal of Earth Sciences (Leeds), v. 8, p.225-239.

Bailey, D.K., 1982, Mantle metasomatism--continuing chemical change within the Earth: Nature, v. 296, p. 525-530.

Bailey, D.K. 1984, Kimberlite: "The mantle sample" formed by ultrametasomatism, in, J. Kornprobst (ed.), Kimberlites I: Kimberlites and Related Rocks: New York, Elsevier, p. 323-333.

Baldridge, W. S,, 1978, Mafic and ultramafic inclusion suites from the Rio Grande rift and their bearing on the composition and thermal state of the lithosphere: 1978 International Symposium on the Rio Grande rift, University of California, Los Alamos Scientific Laboratory, Program and Abstracts, p. 15-16.

Baldridge, W. S., 1979, Petrology and petrogenesis of Plio-Pleistocene basaltic rocks from the central Rio Grande rift, New Mexico, and their relation to rift structure, in Riecker, R. E. (ed.), Rio Grande rift: Tectonics and Magmatism: American Geophysical Union, p. 323-353.

Barca, R. A., 1966, Geology of the northern part of Old Dad Mountain quadrangle, San Bernardino County, California: California Division of Mines and Geology Map Sheet 7.

Basu, A. R., 1975, Hotspots, mantle plumes and a model for the origin of ultramafic xenoliths in alkalic basalts: Earth and Planetary Science Letters, v. 29, p. 261-274.

Basu, A. R., 1977, Textures, microstructures and deformation of ultramafic xenoliths from San Quentin, Baja California: Tectonophysics, v. 43, p. 213-246.

Basu, A. R., 1978, Trace elements and Sr-isotopes in some mantle-derived hydrous minerals and their significance: Geochimica et Cosmochimica Acta, v. 42, p. 659-668.

Basu, A. R., 1979, Geochemistry of ultramafic xenoliths from San Quentin, Baja California, in F. R. Boyd and Henry O. A. Meyer (eds.), The mantle sample: inclusions in kimberlites and other volcanics: American

Geophysical Union, Proceedings Second International Kimberlite Conference, v. 2, p. 391-399.
Basu, A. R., and Murthy, V. R., 1977, Ancient lithospheric lherzolite xenolith in alkali basalt from Baja California: Earth and Planetary Science Letters, v. 35, p. 239-246.
Basu, A. R. and Tatsumoto, M., 1980, Nd-isotopes in selected mantle-derived rocks and minerals and their implications for mantle evolution: Contributions to Mineralogy and Petrology, v. 75, p. 43-54.
Beeson, M. H., and Jackson, E. D., 1970, Origin of the garnet pyroxenite xenoliths at Salt Lake Crater, Oahu: Mineralogical Society of America Special Paper 3, p. 95-112.
Bergman, S. C. 1982, Petrogenetic aspects of the alkali basaltic layers and included megacrysts and nodules from the Lunar Crater volcanic field, Nevada, U.S.A.: Unpub. Ph.D. thesis, Princeton University, 432 p.
Bergman, S. C., Foland, K. A., and Spera, F. J. 1981, On the origin of an amphibole-rich vein in a periodotite inclusion form the lunar crater volcanic field, Nevada, U.S.A.: Earth and Planetary Science Letters, v. 56, p. 343-361.
Best, M. G., 1970, Kaursutite-peridotite inclusions and kindred megacrysts in basaltic lavas, Grand Canyon, Arizona: Contributions to Mineralogy and Petrology, v. 27, p. 25-44.
Best, M. G., 1974a, Contrasting types of chromium-spinel peridotite xenoliths in basaltic lavas, western Grand Canyon, Arizona: Earth and Planetary Science Letters, v. 23, no. 2, p. 229-237.
Best, M. G., 1974b, Mantle-derived amphibole within inclusions in alkalic-basaltic lavas: Journal of Geophysical Research, v. 79, no. 14, p. 2107-2114.
Best, M. G., 1975a, Amphibole-bearing cumulate inclusions, Grand Canyon and their bearing on undersaturated hydrous magmas in the upper mantle: Journal of Petrology, v. 16, p. 212-236.
Best, M. G., 1975b, Migration of hydrous fluids in the upper mantle and potassium variation in calc-alkalic rocks: Geology, v. 3, p. 429.
Best, M. G., and Brimhall, W. H., 1974, Late Cenozoic alkalic basaltic magmas in the western Colorado plateau and Basin and Range transition-zone, U.S.A., and their bearing on mantle dynamics: Brigham Young University, Geology Department Research Report 69-1, 39 p.
Best, M. G., Hamblin, W. K., and Brimhall, W. H., 1966, Preliminary petrology and chemistry of the Cenozoic basalts in the western Grand Canyon region: Brigham Young University, Geological Studies, v. 13, p. 105-123.
Binns, R. A., 1969, High-pressure megacrysts in basanitic lavas near Armidale, New South Wales: American Journal of Science, v. 267-A, p. 33-49.
Boettcher, A. L., 1984, The source regions of alkaline volcanoes, in Explosive Volcanism: Inception, Evolution and Hazards: Washington, D. L., National Academy Press, p. 13-22
Boettcher, A. L., O'Neil, J. R., Windom, K. E., Stewart, D. C., and Wilshire, H. G., 1979, Metasomatism of the upper mantle and the genesis of kimberlites and alkali basalts, in F. R. Boyd and Henry O. A. Meyer (eds.), The Mantle Sample: Inclusions in Kimberlites and other Volcanics: American Geophysical Union Proceedings Second International Kimberlite Conference, v. 2, p. 173-182.
Boettcher, H. L., and O'Neil, J. R., 1980, Stable isotope, chemical, and petrographic studies of high-pressure amphiboles and micas: evidence for metasomatism in the mantle source regions of alkali basalts and kimberlites: American Journal of Science, v. 280-A, The Jackson Volume, Part 2, p. 594-621.

Boudier, F., 1972, Relations Lherzolite-Gabbro-Dunite dans le Massif de Lanzo (Alpes piemontaises): Example de Fusion partielle: Unpub. Ph.D. thesis, Univ. Nantes, France, 106 p.

Boudier, F., and Nicolas, A., 1972, Fusion partielle gabbroique dans la lherzolite de Lanzo: Bull. suisse de Mineralogie et Petrographie, v. 52/1, p. 39-56.

Boyd, F.R., 1973, A pyroxene geotherm: Geochimica et Cosmochimica Acta, v. 37, p. 2533-2546.

Boyd, F.R., 1984, Siberian geotherm based on lherzolite xenoliths from the Udachnaya kimberlite, USSR: Geology, v. 12, p. 528-530.

Boyd, F.R., Jones, R.A., and Nixon, P.H., 1984, Mantle metasomatism: the Kimberley dunites: Geological Society of America, Abstracts with Programs, v. 16, p. 453.

Boyd, F. R. and McCallister, R. H., 1976, Densities of fertile and sterile garnet peridotites: geophysical Research Letters, v. 3, p. 509-512.

Boyd, F.R. and Nixon, P.H., 1973, Structure of the upper mantle beneath Lesotho: Carnegie Institute Year Book 72, p. 431-445.

Brady, L. F., and Webb, R. W., 1943, Cored bombs from Arizona and California volcanic cones: Journal of Geology, v. 51, no. 6, p. 398-410.

Burwell, A. D. M., 1975, Isotope geochemistry of lherzolites and their constituent minerals from Victoria, Australia: Earth and Planetary Science Letters, v. 28, p. 69-78.

Bussod, G. Y. A., 1983, Thermal and kinematic history of mantle xenoliths from Kilbourne Hole, New Mexico: U.S. Scientific Laboratory, Los Alamos, New Mexico, Publication LA-9616-T, 74 p.

Carter, J. L., 1965, The origin of olivine bombs and related inclusions in basalts: Ph.D. thesis, Rice University, Texas, 264 p.

Carter, J. L., 1970, Mineralogy and chemistry of the Earth's upper mantle based on the partial fusion-partial crystallization model: Geological Society of America Bulletin, v. 81, p. 2021-2034.

Cohen, R. S., O'Nions, R. K., and Dawson, J. B., 1984, Isotope geochemistry of xenoliths from East Africa: implications for development of mantle reservoirs and their interaction: Earth and Planetary Science Letters, v. 68, p. 209-220.

Conquere, F., 1977, Petrologie des pyroxenites litees dans les complexes ultramafiques de l'Ariege (France) et autres gisements de lherzolite a spinelle. I Compositions mineralogiques et chimiques, evolution des conditions de'equilibre des pyroxenites: Bull. Soc. fr. Mineral. Cristallogr., v. 100, p. 42-80.

Cummings, D., 1972, Mafic and ultramafic inclusions, Crater 160, San Francisco volcanic field, Arizona: U.S. Geological Survey Professional Paper 800-B, p. B95-B104.

Dasch, E. J., 1969, Strontium isotope disequilibrium in a porphyritic alkali basalt and its bearing on magmatic processes: Journal of Geophysical Research, v. 74, no. 2, p. 560-565.

Dasch, E. J.,Armstrong, R. L., and Clabaugh, S. E., 1969, Age of Rim Rock dike swarm, Trans-Pecos, Texas: Geological Society of America Bulletin, v. 80, p. 1819-1824.

Dasch, E. J., and Green, D. H., 1975, Strontium isotope geochemistry of lherzolite inclusions and host basaltic rocks, Victoria, Australia: American Journal of Science, v. 275, p. 461-469.

Dawson, J. B., 1977, Sub-cratonic crust and upper mantle models based on xenolith suites in kimberlite and nephelinitic suites: Journal of the Geological Society of London, v. 134, p. 173-184.

Dawson, J. B., 1979, Veined peridotites from the Bultfontein Mine: 2nd Kimberlite Symposium, Cambridge, England, Abstracts (unpaged).
Dawson, J. B., 1980, Kimberlites and their xenoliths: New York, Springer-Verlag, 252 p.
Dawson, J. B., 1981, The nature of the upper mantle: Mineralogical Magazine, v. 44, p. 1-18.
Dawson, J. B., 1984, Contrasting types of upper-mantle metasomatism?, in, J. Kornprobst (ed.), Kimberlites. II: The Mantle and Crust-Mantle Relationships: Amsterdam, Elsevier Science Publishers, p. 289-294.
Dawson, J. B., and Smith, J. V., 1977, The MARID (mica-amphibole-rutile-ilmenite-diopside) suite of xenoliths in kimberlite: Geochim. et Cosmochim. Acta, v. 41, p. 309-323.
Delaney, J. S., Smith, J. V., Carswell, D. A. and Dawson, J. B., 1980, Chemistry of micas from kimberlites and xenoliths, II. Primary- and secondary- textured micas from perdiotite xenoliths: Geochimica et Cosmochimica Acta, v. 44, p. 857-872.
Dibblee, T. W., Jr., 1967, Areal geology of the western Mojave desert, California: U.S. Geological Survey Professional Paper 522, 153 p.
Dick, H. J. B., 1977, Partial melting in the Josephine peridotite. I, The effect on mineral composition and its consequence for geobarometry and geothermometry: American Journal of Science, v. 277, p. 801-832.
Dick, H. J. B. and Friesz, B. L., 1984, Abyssal plagioclase peridotites and melt storage in the mantle beneath mid-ocean ridges: Geological Society of America Abstracts with Programs, v. 16, p. 487.
Dickey, J. G., Jr., Obata, M.,Suen, C. J., Frey, F. A., and Lundeen, M., 1977, The Ronda ultramafic complex, southern Spain (abs.): Geological Society of America, Abstracts with Programs, v. 9, p. 949-950.
Domenick, M.A., Kistler, R.W., Dodge, F.C.W., and Tatsumoto, M., 1983, Nd and Sr isotopic study of crustal and mantle inclusions from the Sierra Nevada and implications for batholith petrogenesis: Bulletin Geological Society of America, v. 94, no. 6, p. 713-719.
Dohrenwend, J. C., McFadden, L. D., Turrin, B. D., and Wells, S. G., 1984, K-Ar dating of the Cima volcanic field, eastern Mojave Desert, California: Late Cenozoic volcanic history and landscape evolution: Geology, v. 12, no. 3, p. 163-167.
Eggler, D. H., McCallum, M. E., and Smith,C. B., 1974, Megacryst assemblages in kimberlites from northern Colorado and southern Wyoming: Petrology, geothermometry-barometry, and areal distribution, in F. R. Boyd and H. O. A. Meyer (eds.), The Mantle Sample: Inclusions in Kimberlites and other Volcanics: American Geophysical Union, Proceedings Second International Kimberlite Conference, v. 2, p. 213-226.
Ehrenburg, S. N., 1979, Garnetiferous ultramafic inclusions in minette from the Navajo volcanic field, in F. R. Boyd and Henry O. A. Meyer (eds.), The Mantle Sample: Inclusions in Kimberlites and other Volcanics: American Geophysical Union, Proceedings Second International Kimberlite Conference, v. 2, p. 330-344.
Ehrenberg, S.N., 1982a, Rare earth element geochemistry of garnet lherzolite and megacrystalline nodules from minette of the Colorado Plateau province: Earth and Planetary Science Letters, v. 57, p. 191-210.
Ehrenberg, S.N., 1982b, Petrogenesis of garnet lherzolite and megacrystalline nodules from The Thumb, Navajo volcanic field: Journal of Petrology, v. 23, p. 507-547.
Ekren, E. B., Quinlivan, W. D., Snyder, R. P., and Kleinhampl, F. J., 1974, Stratigraphy, structure, and geologic history of the Lunar Lake caldera

of northern Nye County, Nevada: U.S. Geological Survey Journal Research, v. 2, no. 5, p. 599-608.
Erlank, A. J., Allsopp, H. L., Hawkesworth, C. J., and Menzies, M. A., 1982, Chemical and isotopic characterisation of upper mantle metasomatism in peridotite nodules from the Bultfontein kimberlite: Terra Cognita, v. 2, p. 261-263.
Erlank, A. J., and Shimizu, N., 1977, Strontium and strontium isotope distributions in some kimberlite nodules and minerals: Second International Kimberlite Conference, Santa Fe, New Mexico, Abstract (unpaged).
Erlank, A. J. Allsop, H. L., Duncan, A. R., and Bristow, J. W., 1980, Mantle heterogeneity beneath southern Africa; evidence from the volcanic record: Phil. Trans. Royal Soc., London, Ser. A, v. 297, p. 295-307.
Evans, S. H., Jr., and Nash, W. P., 1979, Petrogenesis of xenolith-bearing basalts from southeastern Arizona: American Mineralogist, v. 64, nos. 3-4, p. 249-267.
Evarts, R. C., 1978, The Del Puerto ophiolite complex, California: A structural and petrologic investigation (Ph.D. thesis): Stanford, California, Stanford University, 409 p.
Foland, K. A., Spera, F.J., and Bergman, S.C., 1980, Strontium isotope relations in megacryst-bearing camptonites from northwest Arizona (abs.): Geological Society of America Abstracts with Programs, v. 12, no. 1, p. 36.
Francis, D. M., 1976a, Amphibole pyroxenite xenoliths: cumulate or replacement phenomena from the upper mantle, Nunivak Island, Alaska: Contributions to Mineralogy and Petrology, v. 58, p. 51-61.
Francis, D. M., 1976b, The origin of amphibole in lherzolite xenoliths from Nunivak Island, Alaska: Journal of Petrology, v. 17, p. 357-378.
Frey, F. A., 1979, Trace element geochemistry: Applications to the igneous petrogenesis of terrestrial rocks: Reviews of Geophysics and Space Physics, American Geophysical Union, v.17, p. 803-823.
Frey, F. A., 1980, The origin of pyroxenites and garnet pyroxenites fromn Salt Lake Crater, Oahu, Hawaii: Trace element evidence: American Journal of Science, v. 280-A, p. 427-449.
Frey, F. A., 1983, Rare earth element abundances in upper mantle rocks, in, P. Henderson (ed.), Rare Earth Geochemistry: Amsterdam, Elsevier Science Publishers, Chapt. 5.
Frey, F. A., and Green, D. H., 1974, The mineralogy, geochemistry, and origin of lherzolite inclusions in Victoria basanites: Geochimica et Cosmochimica Acta, v. 38, p. 1023-1059.
Frey, F. A., and Prinz, M., 1978, Ultramafic inclusions from San Carlos, Arizona: Petrologic and geochemical data bearing on their petrogenesis: Earth and Planetary Science Letters, v. 34, p. 129-176.
Ghent, E. P., Coleman, R. G., and Hadley, D., 1980, Ultramafic inclusions and host alkali olivine basalts of SE coastal plain of the Red Sea, Saudi Arabia: America Journal of Science, v. 280-A, The Jackson Volume, Part 2, p. 499-527.
Giletti, B. J., 1981, Mantle inhomogeneity, isotope exchange, and diffusion effects: Geolgical Society of America, Abstracts with Programs, v. 13, no. 7, p. 459.
Goetze, C., 1975, Sheared lherzolites: From the point of view of rock mechanics: Geology, v. 3, p. 172-173.
Green, D. H., and Hibberson, W., 1970, The instability of plagioclase in peridotite at high pressures: Lithos, v. 3, p. 209-222.

Green, D. H., and Ringwood, A. E., 1967, The stability fields of aluminous pyroxene peridotite and garnet peridotite and their relevance in upper mantle structure: Earth and Planetary Science Letters, v. 3, p. 151-160.

Griffin, W. L., Wass, S. Y. and Hollis, J. D., 1984, Ultramafic xenoliths from Bullenmerri and Gnotuk, maars, Victoria, Australia: Petrology of a subcontinental crust-mantle transition: Journal of Petrology, v. 25, p. 53-87

Gurney, J. J., and Harte, B., 1980, Chemical variations in upper mantle nodules from southern African kimberlites: Philosophical Transactions of the Royal Society of London, v. 297, p. 273-293.

Hanson, G. N., 1977, Evolution of the suboceanic mantle: Journal of Geological Sciences, London, v. 134, pt. 2, p. 235-254.

Harrison, W. J., 1981, Partitioning of REE between minerals and coexisting melts during partial melting of a garnet lherzolite: American Mineralogist, v. 66, p. 242-252.

Harte, B., 1977, Rock nomenclature with particular relation to deformation and recrystallization textures in olivine-bearing xenoliths: Journal of Geology, v. 85, p. 279-288.

Harte, B., 1983, Mantle peridotites and processes -- the kimberlite sample, in, C.J. Hawkesworth and M. J. Norry (eds.), Continental Basalts and Mantle Xenoliths: United Kingdom, Shiva Publishing Ltd., p. 46-91.

Harte, B., Cox, K. G., and Gurney, J. J., 1975, Petrography and geological history of upper mantle xenoliths from the Matsoku kimberlite pipe, Physics and Chemistry of the Earth, v. 9, p. 477-506.

Harte, B., Gurney, J. J., and Cox, K. G., 1977, Clinopyroxene-rich sheets in garnet-peridotite: Xenolith specimens from the Matsoku kimberlite pipe, Lesotho: Second International Kimberlite Conference, Extended abstracts, not paginated.

Hawkesworth, C. J., Erlank, A. J., Marsh, J. S., Menzies, M. A., and Calsteren, P. van, 1983, Evolution of the continental lithosphere: Evidence from volcanics and xenoliths in southern Africa, in, C. J. Hawkesworth and M. J. Norry (eds.), Continental Basalts and Mantle Xenoliths: United Kingdom, Shiva Publishing Ltd., p. 111-138.

Hearn, B.C., Jr., 1979, Preliminary map of diatremes and alkalic ultramafic intrusions in the Missouri River Breaks and vicinity, north-central Montana: U.S. Geological Survey Open File Report 79-1128.

Hearn, B.C., Jr. and McGee, E.S., 1983, Garnet peridotites from Williams kimberlites, north-central Montana, USA: U.S. Geological Survey Open File Report 83-172, 26 p.

Hoefs, J., and Wedepohl, 1968, Strontium isotope studies on young volcanic rocks from Germany and Italy: Contributions to Mineralogy and Petrology, v. 19, p. 328-338.

Hoffer, J. M., and Hoffer, R. L., 1973, Composition and structural state of feldspar inclusions from alkaline olivine basalt, Potrillo Basalt, southern New Mexico: Geological Society of America Bulletin, v. 84, p. 2139-2142.

Hofmann, A. W., White, W. M., and Whitford, D. J., 1978, Geochemical constraints on mantle models: the case for a layered mantle: Carnegie Institute, Yearbook 77, p. 548-562.

Hofmann, A. W., and Hart, S. R., 1978, An assessment of local and regional isotopic equilibrium in the mantle: Earth and Planetary Science Letters, v. 38, p. 44-62.

Hofman, A. W., White, W. M., and Whitford, D. J., 1978, Geochemical constraints on mantle models: the case for a layered mantle: Carnegie Institute Yearbook 77, p. 548-562.

Hofmann, A. W., and Hart, S. R., 1978, An assessment of local and regional isotopic equilibrium in the mantle: Earth and Planetary Science Letters, v. 38, p. 44-62.

Hutchinson, R., and Dawson, J. B., 1970, Rb, Sr and $^{87}Sr/^{86}Sr$ in ultrabasic xenoliths and host-rocks, Lashaine Volcano, Tanzania: Earth and Planetary Science Letters, v. 9, no. 1, p. 87-92.

Irving, A. J., 1976, On the validity of paleogeotherms determined from xenolith suites in basalts and kimberlites: American Mineralogist, v. 4, p. 638-642.

Irving, A. J., 1977, Origin of megacryst suites in basaltic dikes near 96 Ranch, west Texas and Hoover Dam, Arizona (abs): EOS, American Geophysical Union Trans., v. 56, no. 6, p. 526.

Irving, A. J., 1978, Flow crystallization: A mechanism for fractionation of primary magmas at mantle pressures (abs.): EOS, American Geophysical Union Trans., v. 59, p. 1214.

Irving, A. J., 1980, Petrology and geochemistry of composite ultramafic xenoliths in alkalic basalts and implications for magmatic processes within the mantle: American Journal of Science, v. 280-A, The Jackson Volume, p. 389-426.

Irving, A. J. and Frey, F. A., 1984, Trace element abundances in megacrysts and their host basalts: Constraints on partition coefficients and megacryst genesis: Geochemica et Cosmochimica Acta, v. 48, p. 1201-1221.

Ito, L., 1977, Magma genesis in a dynamic mantle: in H. Imai (ed.), Genesis of metalliferous ore deposits in Japan and East Asia: Tokyo, Tokyo University Press.

Jackson, E. D., 1968, The character of the lower crust and upper mantle beneath the Hawaiian Islands: Proc. 23rd International Geological Congress, Prague, v. 1, p. 135-150.

Jagoutz, E., Carlson, R.W., and Lugmair, G.W., 1980, Equilibrated Nd-unequilibrated Sr isotopes in mantle xenoliths: Nature, v. 286, p. 708-710.

Jagoutz, E., Lorenz, V., and Wanke, H., 1979a, Major trace elements of Al-augites and Cr-diopsides from ultramafic nodules in European alkali basalts, in Boyd, F. R., and Meyer, H. O. A. (eds.), The Mantle Sample: Inclusions in Kimberlites and other Volcanics: Proceedings Second International Kimberlite Conference, p. 382-390.

Jagoutz, E. Palme, H. Baddenhansen, H., Blum, K., Candales, M., Dreibus, G., Spettel, B., Lorenz, V., and Wanke, H., 1979b, The abundances of major, minor, and trace elements in the Earth's mantle as dervied from primitive ultramafic nodules: Proceedings of Lunar Scientific Conference, 10th, Geochimica et Cosmochimica Acta, Suppl. 11, p. 2031-2050.

Jones, A. P., Smith, J. V., and Dawson, J. B., 1982, Mantle metasomatism in 14 veined peridotites from Bultfontein Mine, South Africa: Journal of Geology, v. 90, p. 435-453.

Katz, M. and Boettcher, A.L., 1980, The Cima volcanic field, in, Fife, D.L. and Brown, A.R. (eds.), Geology and mineral wealth of the California desert: South Coast Geological Society, p. 236-241.

Kay, R. W., 1979, Zone refining at the base of lithospheric plates: a model for a steady-state asthenosphere: Tectonophysics, v. 55, p. 1-9.

Kay, R. W., and Gast, P. W., 1973, The rare earth contact and origin of alkali-rich basalts: Journal of Geology, v. 81, p. 653k-682.

Kelley, V. L., 1952, Tectonics of the Rio Grande depression of central New Mexico, in New Mexico Geological Society Guidebook, 3rd Field Conference, October 1952, p. 93-105.

Kempton, P.D., 1983, Peridotites from the Geronimo volcanic field: evidence for multiple interactions between basaltic magma and the upper mantle beneath SE Arizona: Geological Society of America Abstracts with Programs, v. 15, no. 5, p. 302.

Kempton, P. D., Menzies, M. A., and Dungan, M. A., 1984, Petrography, petrology and geochemistry of xenoliths and megacrysts from the Geronimo volcanic field, southeastern Arizona, in J. Kornprobst (ed.), Kimberlites II: The Mantle and Crust-Mantle Relationships: Amsterdam, Elsevier Science Publishers, p. 71-83.

Kornprobst, J., 1969, Le massif ultrabasique des Beni Bouchera (Rif Interne, Maroc): Etude des peridotites de haute temperature et de haute pression, et des pyroxenolites a grenat ou sans grenat, qui leur sont associees: Contributions to Mineralogy and Petrology, v. 23, p. 283-322.

Kornprobst, J., 1970, Les peridotites et les pyproxenolites du massif ultrbasique des Beni Bouchera: une etude experimental entre 1100 et 1550°C, sons 15 a 30 kilobars de pression seche: Contributions to Mineralogy and Petrology, v. 29, p. 290-309.

Kornprobst, J., and Conquere, F., 1972, Les pyroxenolites a grenat du massif de lherzolite de Moncaup (Haute Garonne-France): Caracteres communs avec certaines enclaves des basaltes alcalins: Earth and Planetary Science Letters, v. 1, p. 1-14.

Kramers, J., 1977, Lead and strontium isotopes in Cretaceous kimberlites and mantle-derived xenoliths from southern Africa: Earth and Planetary Science Letters, v. 34, p. 419-431.

Kramers, J. D., Roddick, J. C. M., and Dawson, J. B., 1983, Trace element and isotope studies on veined, metasomatic and "MARID" xenoliths from Bultfontein, South Africa: Earth and Planetary Science Letters, v. 65, p. 90-106.

Krieger, M.H., 1965, Geology of the Prescott and Paulden quadrangles, Arizona: U.S. Geological Survey Professional Paper 467, 127 p.

Kudo, A. M., Aoki, K., and Brookins, D. G., 1971, The origin of Pliocene-Holocene basalts of New Mexico in the light of strontium-isotopic and major-element abundances: Earth and Planetary Science Letters, v. 13, p. 200-204.

Kudo, A. M., Brookins, D. G., and Laughlin, A. W., 1972, Sr isotopic disequilibrium in lherzolites from the Puerco necks, New Mexico: Earth and Planetary Science Letters, v. 15, p. 291-295.

Kurat, G., Palme, H., Spettel, B., Baddenhansen, H., Hofmeister, H., Palme, C., and Wanke, H., 1980, Geochemistry of ultramafic xenoliths from Kapfenstein, Austria; evidence for a variety of upper mantle processes: Geochimica et Cosmochimica Acta, v. 44, no. 1, p. 45-60.

Kushiro, I., and Yoder, H. S., Jr.,1966, Anorthite-forsterite and anorthite-enstatite reactions and their bearing on the basalt-eclogite transformation: Journal of Petrology, v. 7, no. 3, p. 337-362.

Kyser, T. K., O'Neil, J. R., and Carmichael, I. S. E., 1982, Genetic relations among basic lavas and ultramafic nodules: Evidence from oxygen isotope compositions: Contributions to Mineralogy and Petrology, v. 81, p. 88-102.

Larsen, J. G., 1979, Glass-bearing gabbro inclusions in hyaloclastites from Tindfjallajokull, Iceland: Lithos, v. 12, p. 289-302.

Laughlin, A. W., Brookins, D. G., and Causey, J. D., 1972, Late Cenozoic basalts from the Bandera lava field, Valencia County, New Mexico: Geological Society of America Bulletin, v. 82, p. 1543-1557.

Laughlin, A. W., Brookins, D. G., Kudo, A. M., and Causey, J. D., 1971, Chemical and strontium isotopic investigations of ultramafic inclusions

and basalt, Bandera Crater, New Mexico: Geochimica et Cosmochimica Acta, v. 35, p. 107-113.
Laughlin, A. W., Manzer, G. K., Jr., and Carden, J. R., 1974, Feldspar megacrysts in alkali basalts: Geological Society of America Bulletin, v. 85, p. 403-412.
Lausen, C., 1927, The occurrence of olivine bombs near Globe, Arizona: American Journal of Science, v. 14, p. 293-306.
Leggo, P. J., and Hutchinson, R., 1968, A Rb-Sr isotope study of ultrabasic xenoliths and their basaltic host rocks from the Massif Central, France: Earth and Planetary Science Letters, v. 5, no. 2, p. 71-75.
Lewis, J. F., 1973, Petrology of the ejected plutonic blocks of the Soufriere volcano, St. Vincent, West Indies: Journal of Petrology, v. 14, p. 81-112.
Lewis, P. H., 1973, Mica pyroxenite inclusions in limburgite, Hopi Buttes volcanic field, Arizona: Brigham Young University Geology Studies, v. 20, pt. 4, p. 191-225.
Lipman, P. W., 1969, Alkalic and tholeiitic basaltic volcanism related to the Rio Grande depression, southern Colorado and northern New Mexico: Geological Society of America Bulletin, v. 80, p. 1343-1354.
Littlejohn, A. L., 1972, A comparative study of lherzolite nodules in basaltic rocks from British Columbia: Unpub. M.S. thesis, University of British Columbia, 113 p.
Lloyd, F. E., 1981, Upper-mantle metasomatism beneath a continental rift: clinopyroxenes in alkali mafic lavas and nodules from south west Uganda: Mineralogical Magazine, v. 44, p. 315-323.
Lloyd, F. E., and Bailey, D. K., 1975, Light element metasomatism of the continental mantle: the evidence and the consequences: in L. H. Ahrens, J. B. Dawson, A. R. Duncan, and A. J. Erlank (eds.), Phys. Chem. of the Earth, v. 9, p. 389-416.
Loubet, M. and Allegre, C. J., 1982, Trace elements in orogenic lherzolites reveal the complex history of the upper mantle: Nature, v. 298, p. 809-814.
Lovering, J. F., and Tatsumoto, M. 1968, Lead isotopes and the origin of granulite and eclogite inclusions in deep-seated pipes: Earth and Planetary Science Letters, v. 4, p. 350-356.
Lynch, D. J., 1978, The San Bernardino volcanic field of southeastern Arizona: New Mexico Geological Society Guidebook, 24th Field Conference, Land of Cochise, p. 261-268.
MacDonald, G. A. and Katsura, T., 1964, chemical composititon of Hawaiian lavas: journal of Petrology, v.5, p.82-133.
Manton, W. I., and Tatsumoto, M., 1971, Some Pb and Sr isotopic measurements in eclogites from Roberts Victor mine, South Africa: Earth and Planetary Science Letters, v. 10, p. 217-226.
Mason, B., 1968, Kaersutite from San Carlos, Arizona, with comments on the paragenesis of this mineral. Mineralogical Magazine, London, v. 36. no. 283, p. 997-1002.
McCallum, M.E. and Eggler, D.H., 1971, Mineralogy of the Sloan diatreme, a kimberlite pipe in northern Larimer County, Colorado: American Mineralogist, v. 56, p. 1735-1749.
McGetchin, T.R. and Silver, L.T., 1970, Compositional relations in minerals from kimberlite and related rocks in the Moses Rock dike, San Juan County, Utah: American Mineralogist, v. 55, p. 1738-1771.
Menzies, M. A., 1983, Mantle ultramafic xenoliths in alkaline magmas: evidence for mantle heterogeneity modified by magmatic activity, in, C.J.

Hawkesworth and M.J. Norry (eds.), Continental Basalts and Mantle Xenoliths: United Kingdom, Shiva Publishing Ltd., p. 92-110.

Menzies, M. A., Kempton, P., and Dungan, M., 1984, Multiple enrichment events in residual MORB like mantle below the Geronimo volcanic field, Arizona, U.S.A.: Journal of Petrology (in press).

Menzies, M. A., Leeman, W.P., and Hawkesworth, C.J., 1983, Isotope geochemistry of Cenozoic volcanic rocks reveals mantle heterogeneity below western U.S.A.: Nature, v. 303, p. 205-209.

Menzies, M. A. and Murthy, V. R., 1980a, Mantle metasomatism as a precursor to the genesis of alkaline magmas--isotopic evidence: American Journal of Science, v. 280-A, p. 622-638.

Menzies, M. A. and Murthy, V. R., 1980b, Nd and Sr isotopes in diopsides from kimberlite nodules: Nature, v. 283, p. 634-636.

Menzies, M. A. and Wass, S. Y., 1983, CO_2- and LREE-rich mantle below eastern Australia: a REE and isotopic study of alkaline magmas and apatite-rich mantle xenoliths from the southern highlands province, Australia: Earth and Planetary Science Letters, v. 65, p. 287-302.

Mercier, J. C., and Nicols, A., 1975, Textures and fabrics of upper-mantle peridotites as illustrated by xenoliths from basalts: Journal of Petrology, v. 16, p. 454-487.

Mercier, J. C., 1979, Peridotite xenoliths and the dynamics of kimberlite intrusion, in, F. R. Boyd and H. O. A. Meyer (eds.), The Mantle Sample: Inclusions in Kimberlites and Other Volcanics: Washington, D.C., American Geophysical Union, p. 197-212.

Moore, J. G., 1963, Geology of the Mount Pinchot quadrangle, southern Sierra Nevada, California: U.S. Geological Survey Bulletin 1130, 152 p.

Moore, J.G. and Dodge, F.C.W., 1980a, Late Cenozoic volcanic rocks of the southern Sierra Nevada, California: I. Geology and petrology: Summary: Geological Society of America Bulletin, Part I, v. 91, p. 515-518.

Moore, J.G. and Dodge, F.C.W., 1980b, Late Cenozoic volcanic rocks of the southern Sierra Nevada, California: I. Geology and petrology: Geological Society of America Bulletin, Part II, v. 91, p. 1995-2038.

Moores, E. M., 1969, Petrology and structure of the Vourinos ophiolitic complex, northern Greece: Geological Society of America Special Paper 118, 74 p.

Mysen, B. O., 1983, Rare earth element partitioning between (H_2O + CO_2) vapor and upper mantle minerals: experimental data bearing on the conditions of formation of alkali basalt and kimberlite: Neues Jahrbuch fur Mineralogie Abhandlungen, v. 146, p. 41-65.

Nagasawa, H., Wakita, H., Higuchi, H., and Onuma, N., 1969, Rare earths in peridotite nodules: an explanation of the genetic relationships between basalt and peridotite nodules: Earth and Planetary Science Letters, v. 5, p. 377-381.

Nakata, J. K., 1977, Distribution and petrology of the Anderson-Coyote Reservoir volcanic rocks: U.S. Geological Survey Open-File Report 80-1286.

Neville, S.L., Schiffman, P., and Sadler, P.M., 1983, New discoveries of spinel lherzolite and garnet websterite nodules in alkaline basalts form the south-central Mojave Desert and northeast Transverse Ranges, California: Geological Society of America Abstracts with Programs, v. 15, no. 5, p. 302.

Nicolas, A. and Jackson, M., 1982, High temperature dikes in peridotites: origin by hydraulic fracturing: Journal of Petrology, v. 23, p. 568-582.

Nixon, P. H., and Boyd, F. R., 1973, Petrogenesis of the granular and sheared ultrabasic nodule suite in kimberlites, in Nixon, P. H. (ed.), Lesotho kimberlites: Cape Town, Cape and Transvaal Printers, Ltd., p. 48-56.

Nixon, P. H., 1973, The discrete nodule association in kimberlites from northern Lesotho, in Nixon, P. H. (ed.), Lesotho kimberlites: Cape Town, Cape and Transvaal Printers, Ltd., p. 67-75.

Nixon, P. H., 1979, Garnet bearing lherzolites and discrete nodule suites from the Malatia alnoite, Solomon Islands, S-W Pacific, and their bearing on oceanic mantle composition and geotherm, in F. R. Boyd and Henry O. A. Meyer (eds.), The Mantle Sample: Inclusions in Kimberlites and other Volcanics: American Geophysical Union, Proceedings Second International Kimberlite Conference, v. 2, p. 400-423.

Nixon, P. H., Boyd, F. R., and Boullier, A-M., 1973, The evidence of kimberlite and its inclusions on the constitution of the outer part of the earth, in Nixon, P. H. (ed.), Lesotho kimberlites: Cape Town, Cape and Transvaal Printers, Ltd., p. 312-318.

Nixon, P. H., Rogers, N. W., Gibson, I. L., and Grey, A., 1981, Depleted and fertile mantle xenoliths from southern African kimberlites: Annual Review of Earth and Planetary Sciences, v. 9, p. 285-309.

Obata, M., 1980, The Ronda peridotite: garnet-, spinel-, and plagioclase-lherzolite facies and the P-T trajectories of a high-temperature mantle intrusion: Journal of Petrology, v. 21, no. 3, p. 533-572.

Oberlander, T., 1974, Landscape inheritance, and the pediment problem in the Mojave Desert of Southern California: American Journal of Science, V. 274, p. 849-875.

O'Hara, M. J., 1967, Mineral facies in ultrabasic rocks, in P. J. Wyllie (ed.), Ultramafic and related rocks: New York, John Wiley & Sons, p. 7-17.

O'Hara, M. J., 1969, Phase equilibrium studies relevant to upper mantle petrology, in P. J. Hart (ed.), The Earth's crust and upper mantle: American Geophysical Union, Geophysical Monograph 13, p. 634-637.

O'Neil, J. R., Hedge, C. E., and Jackson, E. D., 1970, Isotopic investigations of xenoliths and host basalts from the Honolulu Volcanic Series: Earth and Planetary Science Letters, v. 8, p. 253-257.

O'Nions, R.K., Carter, S.R., Evensen, N.M., and Hamilton, P.J., 1979, Geochemical and cosmochemical applications of Nd isotope analysis: Annual Reviews of Earth and Planetary Sciences, v. 7, p. 11-38.

O'Reilly, S. Y. and Griffin, W. L., 1984, Sr isotopic heterogeneity in primitive basaltic rocks, southeastern Australia: correlation with mantle metasomatism: Contributions to Mineralogy and Petrology, v. 87, p. 220-230.

Padovani, E. R., and Carter, J. L., 1973, Mineralogy and mineral chemistry of a suite of anhydrous, quartzo-feldspathic, garnet-bearing granulites from Kilbourne Hole maar: Geological Society of America Abstracts with Programs, v. 5, no. 7, p. 761-762.

Padovani, E. R., 1977, Non-equilibrium fusion due to decompression and thermal effects in crustal xenoliths, in H. J. B. Dick (ed.), Magma Genesis: Oregon Department of Geological Mineral Industries Bulletin 96, p. 43-57.

Pakiser, L. C., and Zietz, I., 1965, Transcontinental crustal and upper mantle structures: Reviews of Geophysics, v. 3, p. 505-520.

Pasteris, J. D., Boyd, F. R., and Nixon, P. H., 1979, The ilmenite association at the Frank Smith mine, R. S. A., in F. R. Boyd and Henry O. A. Meyer (eds.), The Mantle Sample: Inclusions in Kimberlites and other Volcanics: American Geophysical Union, Proceedings Second International Kimberlite Conference, v. 2, p. 265-278.

Paul, D. K., 1971, Strontium isotope studies of ultramafic inclusions from Dreiser Weiher, Eifel, Germany: Contributions to Mineralogy and Petrology, v. 4, p. 22-28.

Peterman, Z. E., Carmichael, I. S. E., and Smith, A. L., 1970, Strontium isotopes in Quaternary basalts of southeastern California: Earth and Planetary Science Letters, v. 7, p. 381-384.

Pike, J. E. N., 1976, Pressures and temperatures calculated from chromium-rich pyroxene compositions of megacrysts and peridotite xenoliths, Black Rock Summit, Nevada: American Mineralogist, v. 61, p. 725-731.

Pike, J. E. N., Meyer, C. E., and Wilshire, H. G., 1980, Petrography and chemical composition of a suite of ultramafic xenoliths from Lasbaine, Tanzania: Journal of Geology, v. 88, p. 343-352.

Pike, J. E. N., and Nakata, J. K., 1979 Flow-sorting of a fragmented kaersutite-peridotite assemblage and crustal xenoliths in mafic alkalic dikes, Black Canyon, Arizona: Geological Society of America Abstracts with Programs, v. 11, no. 9, p. 541.

Pike, J. E. N. and Schwarzman, E. C., 1977, Classification of textures in ultramafic xenoliths: Journal of Geology, v. 85, p. 49-61.

Prinz, M., and Nehru, C. E., 1969, Comment on "Kaersutite from San Carlos, Arizona, with comments on the paragenesis of this mineral" by Brian Mason: Mineralogical Magazine, London, v. 37, no. 287, p. 333-337.

Quick, J. E., 1981, Petrology and petrogenesis of the Trinity peridotite, northern California: unpub. Ph.D. thesis, California Institute of Technology, 288 p.

Quick, J. E., and Albee, A. L., 1979, Dike-wall rock interactions in the Trinity peridotite, North California--zone refining in the upper mantle: Geological Society of America, Abstracts with Programs, v. 11, no. 7, p. 500.

Reeves, C. C., Jr., and de Hon, R. A., 1965, Geology of Potrillo maar, New Mexico and northern Chihuahua, Mexico: American Journal of Science, v. 263, p. 401-409.

Reid, J. B., Jr., and Frey, F. A., 1971, Rare earth distributions in lherzolite and garnet pyroxenite and the constitution of the upper mantle: Journal of Geophysical Research, v. 76, no. 5, p. 1184-1196.

Ringwood, A. E., 1969, Composition and evolution of the upper mantle, in P. J. Hart (ed.), The Earth's crust and mantle: American Geophysical Union, Geophysical Monogr. 13, p. 1-17.

Ringwood, A. E., 1975, Composition and Petrology of the Earth's Mantle: New York, McGraw Hill, 618 p.

Roden, M. F., Frey, F. A., and Franics, D. M., 1984, An example of consequent mantle metasomatism in peridotite inclusions from Nunivak Island, Alaska: Journal of Petrology, v. 25, p. 546-577.

Roden, M. F. and Murthy, V. R., 1984, Mantle metasomatism: Annual Reviews of Earth and Planetary Sciences (in press).

Roden, M. F., Murthy, V. R., and Irving, A. J., 1984, Isotopic heterogeneity and evolution of uppermost mantle, Kilbourne Hole, New Mexico, EOS, v. 65, p. 306.

Rose, R. L., 1959, Tertiary volcanic domes near Jackson, California: California Division of Mines, Special Report, 21 p.

Ross, C. W., Foster, M. D., and Myers, A. T., 1954, Origin of dunites and of olivine-rich inclusions in basaltic rocks: American Mineralogist, v. 39, p. 693-737.

Rumble, D., III, Hoering, T. L., and Boctor, N., 1979, Oxygen isotopic composition of ultramafic nodules and basanite from San Carlos, Arizona: Carnegie Institution Yearbook 78, p. 492-493.

Sass, J. H., Blackwell, D. D., Chapman, D. S., Costain, J. K., Decker, E. R., Lawver, L. A., and Swanberg, C. A., 1980, Heat flow from the crust of the United States, in Y. S. Tonolonkian, W. R. Judd, and R. F. Roy (eds.): Physical properties of Rocks and Minerals: New York, McGraw-Hill, in press.

Saxena, S. K. and Eriksson, G., 1983, Theoretical computation of mineral assemblages in pyrolite and lherzolite: Journal of Petrology, v. 24, p. 538-555.

Schneider, M. E. and Eggler, D. H., 1984, Compositions of fluids in equilibrium with peridotite: Implications for alkaline magmatism-metasomatism, in, J. Kornprobst (ed.), Kimberlites II: The Mantle and Crust-Mantle Relationships: Amsterdam, Elsevier Science Publishers, p. 333-345.

Schulze, D.J., 1984, Inhomogeneities in garnet peridotite xenoliths from eastern Kentucky kimberlites: Geological Society of America Abstracts with Program, v. 16, p. 648.

Schulze, D. J., and Helmstaedt, H., 1979, Garnet pyroxenite and eclogite xenoliths from the Sullivan Buttes latite, Chino Valley, Arizona, in F. R. Boyd and Henry O. A. Meyer (eds.), The Mantle Sample: Inclusions in Kimberlites and other Volcanics: American Geophysical Union, Proceedings Second International Kimberlite Conference, v. 2, p. 318-329.

Scott, D. H., and Trask, N. J., 1971, Geology of the Lunar Crater volcanic field, Nye County, Nevada: U.S. Geological Survey Professional Paper 599-I, p. Ii-I22.

Seager, W. A., Shafigullah, M., Hawley, J. W., and Marvin, R. F., 1984, New K-Ar dates from basalts and the evolution of the southern Rio Grande rift: Geological Society fo America Bulletin, v.95, p. 87-99.

Shervais, J. W., Wilshire, H. G., and Schwarzman, E. C., 1973, Garnet clinopyroxenite xenolith from Dish Hill, California: Earth and Planetary Science Letters, v. 19, no. 2, p. 120-130.

Shervais, J.W., 1979, Ultramafic and mafic layers in the alpine-type lherzolite massif at Balmuccia (Italy): Universita di Padova Memorie di Scienze Geologiche, v. 33, p. 135-145.

Sinigoi, S., Momin-Chiaramonti, P., and Albeti, A., 1980, Phase relations in the partial melting of the Baldissero spinel-lherzolite (Ivrea-Verbaro zone, western Alps, Italy): Contributions to Mineralogy and Petrology, v. 75, p. 111-121.

Sinigoi, S., Comin-Chiaramonti, P., Demarchi, G., and Siena, F., 1983, Differentiation of partial melts in the mantle: Evidence from the Balmuccia peridotite, Italy: Contributions to Mineralogy and Petrology, v. 82, p. 351-359.

Smith, D. and Ehrenberg, S. N., 1984, Zoned minerals in garnet peridotite nodules from the Colorado Plateau: implications for mantle metasomatism and kinetics: Contributions to Mineralogy and Petrology, in press.

Spencer, A. B., 1969, Alkalic igneous rocks of the Balcones province, Texas: Journal of Petrology, v. 10, pt. 2, p. 272-306.

Stewart, D. C., and Boettcher, A. L., 1977, Chemical gradients in mantle xenoliths (abs.): Geological Society of America Abstracts with Programs, v. 9, p. 1191-1192.

Stoesser, D. B., 1973, Mafic and ultramafic xenoliths of cumulus origin, San Francisco volcanic field, Arizona: Ph.D. thesis, University of Oregon, 260 p.

Stoesser, D. B., 1974, Xenoliths of the San Francisco volcanic field, northern Arizona, in Geology of Northern Arizona, Pt. II, Area studies and field guides: Geological Society of America, p. 530-545.

Stosch, H.-G., and Seck, H. A., 1980, Geochemistry and mineralogy of two spinel peridotite suites from Dreiser Weiher, West Germany: Geochemica et Cosmochemica Acta, v. 44, p. 457-470.
Streckeisen, A. L., and others, 1973, Plutonic rocks, classification and nomenclature recommended by the IUGS Subcommission on the Systematics of Igneous Rocks: Geotimes, October, 1973, p. 26-30.
Stuckless, J. S., and Erickson, R. L., 1976, Strontium isotopic geochemistry of the volcanic rocks and associated megacrysts and inclusions from Ross Island and vicinity, Antarctica: Contributions to Mineralogy and Petrology, v. 58, p. 111-126.
Stuckless, J. S., and Irving, A. J., 1976, Strontium isotope geochemistry of megacrysts and host basalts from southeastern Australia: Geochimica et Cosmochimica Acta, v. 40, p. 209-213.
Stueber, A. M., and Ikramuddin, M., 1974, Rubidium, strontium, and the isotopic composition of strontium in ultramafic nodule minerals and host basalts: Geochimica et Cosmochimica Acta, v. 38, p. 207-216.
Stueber, A. M., and Murthy, V. R., 1966, Strontium isotope and alkali element abundance in ultramafic rocks: Geochimica et Cosmochimica Acta, v. 30, p. 1243-1259.
Stull, R. J., and Davis, T. E., 1973, Strontium isotopic composition of lherzolite xenoliths and alkali olivine basalt from Malapai Hill, California: Geological Society of America Abstracts with Programs, v. 5, no. 1, p. 113.
Stull, R. J., and McMillan, K., 1973, Origin of lherzolite inclusions in the Malapai Hill basalt, Joshua Tree National Monument, California: Geological Society of America Bulletin, v. 84, p. 2343-2350.
Suen, C. J., and Frey, F. A., 1978, Origin of mafic layers in alpine peridotite bodies as indicated by the geochemistry of the Ronda Massif, Spain (abs.): EOS, American Geophysical Union Trans., v. 59, p. 401.
Takahashi, E., 1978, Petrologic model of the crust and upper mantle of the Japanese island arcs: Bulletin Volcanologique, v. 41, no. 4, p. 529-547.
Tracy, R. J., 1980, Petrology and genetic significance of an ultramafic xenolith suite from Tahiti: Earth and Planetary Science Letters, v. 48, p. 80-96.
Trask, N. J., 1969, Ultramafic xenoliths in basalt, Nye County, Nevada: U.S. Geological Survey Professional Paper 650-D, p. D43-D48.
Ulrich, G. W., and McKee, E. H., 1978, Silicic and basaltic volcanism at Bill Williams Mountain, Arizona: Geological Society of America Abstracts with Programs, v. 10, no. 3, p. 151.
Van Kooten, G. K., 1980, Mineralogy, petrology, and geochemistry of an ultrapotassic basaltic suit, central Sierra Nevada, California, U.S.A.: Journal of Petrology, v. 21, part 4, p. 651-684.
Varne, R., 1970, Hornblende lherzolite and the upper mantle: Contributions to Mineralogy and Petrology, v. 27, p. 45-51.
Varne, R., and Graham, A. L., 1971, Rare earth abundances in hornblende and clinopyroxene of a hornblende lherzolite xenolith: implications for upper mantle fractionation processes: Earth and Planetary Science Letters, v. 13, p. 11-18.
Vernon, R. H. 1970, Comparative grain-boundary studies of some basic and ultrabasic granulites, nodules, and cumulates: Scottish Journal of Geology, v. 6, pt. 4, p. 337-351.
Vitaliano, C. J., and Harvey, R. D., 1965, Alkali basalt from Nye County, Nevada: American Mineralogist, v. 50, p. 73-84.

Vollmer, R., 1983, Earth degassing, mantle metasomatism, and isotopic evolution of the mantle: Geology, v. 11, p. 452-459.
Wager, L. R., 1962, Igneous cumulates from the 1902 eruption of Soufriere, St. Vincent: Bulletin Volcanologique, v. 24, p. 93-99.
Warren, R. G., Kudo, H. M., and Keil, K., 1979, Geochemistry of lithic and single-crystal inclusions in basalt and a characterization of the upper mantle-lower crust in the Engle Basin, Rio Grande rift, New Mexico, in Riecker, R. E. (ed.) Rio Grande Rift: Tectonics and Magmatism: American Geophysical Union, p. 393-415.
Wass, S. Y., 1979, Fractional crystallization in the mantle of late-stage kimberlitic liquids--evidence in xenoliths from the Kiama area, N.S.W., Australia, in, F. R. Boyd and H. O. A. Meyer (eds.), The Mantle Sample: Inclusions in Kimberlites and Other Volcanics: Washington, D.C., American Geophysical Union, p. 366-373.
Wass, S. Y., Henderson, P., and Elliott, C. J., 1980, Chemical heterogeneity and metasomatism in the upper mantle: evidence from rare earth and other elements in apatite-rich xenoliths in basaltic rocks from eastern Australia: Philasophical Transactions of the Royal Society of London, v. A297, p. 333-346.
Wass, S. Y., and Rogers, N. W., 1980, Mantle metasomatism--precursor to continental alkaline volcanism: Geochimica et Cosmochimica Acta, v. 44, no. 11, p. 1811-1823.
White, R. W., 1966, Ultramafic inclusions in basaltic rocks from Hawaii: Contributions to Mineralogy and Petrology, v. 12, p. 245-314.
Wendlandt, R. F. and Harrison, W. J. 1979, Rare Earth partitioning between immiscible carbonate and silicate liquids and CO_2 vapor: Results and implications for the formation of light Rare Earth-enriched rocks: Contributions to Mineralogy and Petrology, v. 69, p. 409-419.
Wilkinson, J. F. G., 1975a, Ultramafic inclusions and high pressure megacrysts from a nephelinite sill, Nandewar Mountains, northeastern New South Wales, and their bearing on the origin of certain ultramafic inclusions in alkaline volcanic rocks: Contributions to Mineralogy and Petrology, v. 51, p. 235-262.
Wilkinson, J. F. G., 1975b, An Al-spinel ultramafic-mafic inclusion suite and high pressure megacrysts in an analcimite and their bearing on basaltic magma fractionation at elevated pressures: Contributions to Mineralogy and Petrology, v. 53, p. 71-104.
Wilkinson, J. F. G., 1976, Some subcalcic clinopyroxenites from Salt Lake Crater, Oahu, and their petrogenetic significance: Contributions to Mineralogy and Petrology, v. 58, p. 181-201.
Williams, H., 1936, Pliocene volcanoes of the Navajo-Hopi Country: Geological Society of America Bulletin, v. 47, p. 111-122.
Wilshire, H. G., 1980, Comment on 'A variably veined suboceanic mantle--genetic significance for mid-ocean ridge basalts from geochemical evidence: Geology, v. 8, p. 99-100.
Wilshire. H. G., 1984, Mantle metasomation: The REE story: geology, v. 12, p. 395-398.
Wilshire, H. G., Calk, L. C., and Schwarzman, E. L., 1971, Kaersutite--a product of reaction between pargasite and basanite at Dish Hill, California: Earth and Planetary Science Letters, v. 10, p. 281-284.
Wilshire, H. G., and Jackson, E. D., 1975, Problems in determining mantle geotherms from pyroxene compositions of ultramafic rocks: Journal of Geology, v. 83, p. 313-329.

Wilshire, H. G. and Pike, J. E. N., 1975, Upper-mantle diapirism: Evidence from analogous features in alpine peridotite and ultramafic inclusions in basalt: Geology, v. 3, p. 467-470.

Wilshire, H. G., Pike, J. E. N., Meyer, C. E., and Schwarzman, E. L., 1980, Amphibole-rich veins in lherzolite xenoliths, Dish Hill and Deadman Lake, California: American Journal of Science, v. 280-A, The Jackson Volume, Part 2, p. 576-593.

Wilshire, H. G., and Shervais, J. W., 1973, Al-Augite and Cr-Diopside ultramafic xenoliths in basaltic rocks from western United States: Structural and textural relationships: International Conference on Kimberlites, South Africa, Extended Abstracts, p. 321-324.

Wilshire, H. G., and Shervais, J. W., 1975, Al-Augite and Cr-Diopside ultramafic xenoliths in basaltic rocks from western United States: Structural and textural relationships: Physics and Chemistry of the Earth, v. 9, p. 257-272.

Wilshire, H. G. and Trask, N. J., 1971, Structural and textural relationships of amphibole and phlogopite in peridotite inclusions, Dish Hill, California: American Mineralogist, v. 56, p. 240-255.

Wise, W. S., 1966, Zeolitic basanite from southeastern California: Bulletin Volcanologique v. 29, p. 235-252.

Wood, D. A., 1979, A variably veined suboceanic upper mantle -- genetic significance for mid-ocean ridge basalts from geochemical evidence: Geology, v. 7, p. 499-503.

Wyllie, P. J., 1980, The origin of kimberlite: Journal of Geophysical Research, v. 85, p. 6902-6910.

Zartman, R. E. and Tera, F., 1973, Lead concentration and isotopic composition in five peridotite inclusions of probable mantle origin: Earth and Planetary Science Letters, v. 20, p. 54-66.

Zindler, A., 1979, REE and major element geochemistry of lherzolite and harzburgite nodules: implications for magma petrogenesis in the mantle: Hawaii Symposium on Interplate Volcanism and Submarine Volcanism, Hilo, Hawaii, July 16-22, 1979, Abs. Vol., p. 106.

Zindler, A., Staudigel, H., Hart, S. R., Endres, R., and Goldstein, S., 1983, Nd and Sr isotopic study of a mafic layer from Ronda ultramafic complex: Nature, v. 304, p.226-230.

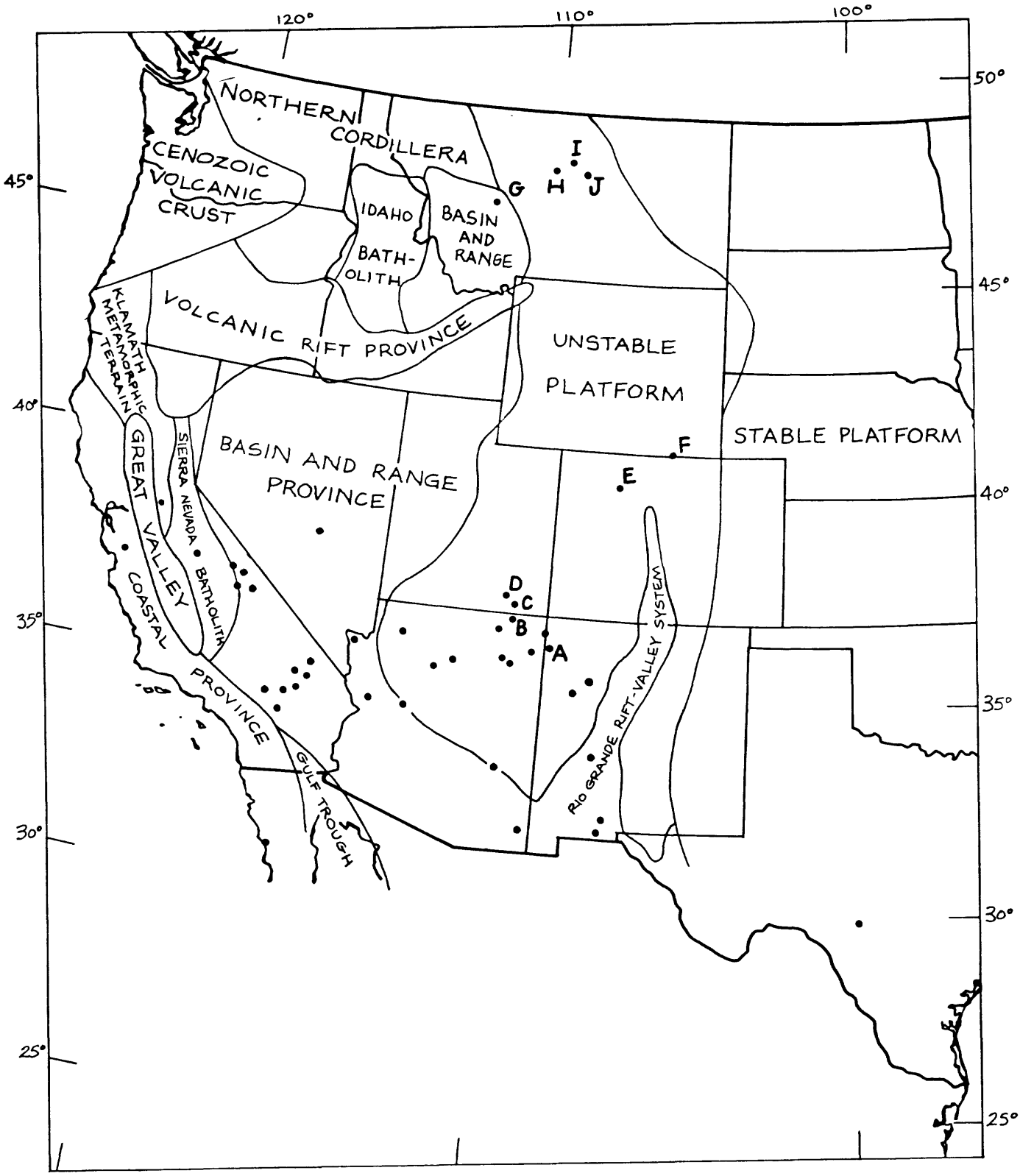

Fig. 1. Distribution of xenolith localities with respect to Cenozoic tectonic provinces (after Hamilton and Meyers, 1966). Xenolith occurrences in kimberlites and phonolites identified by letters.

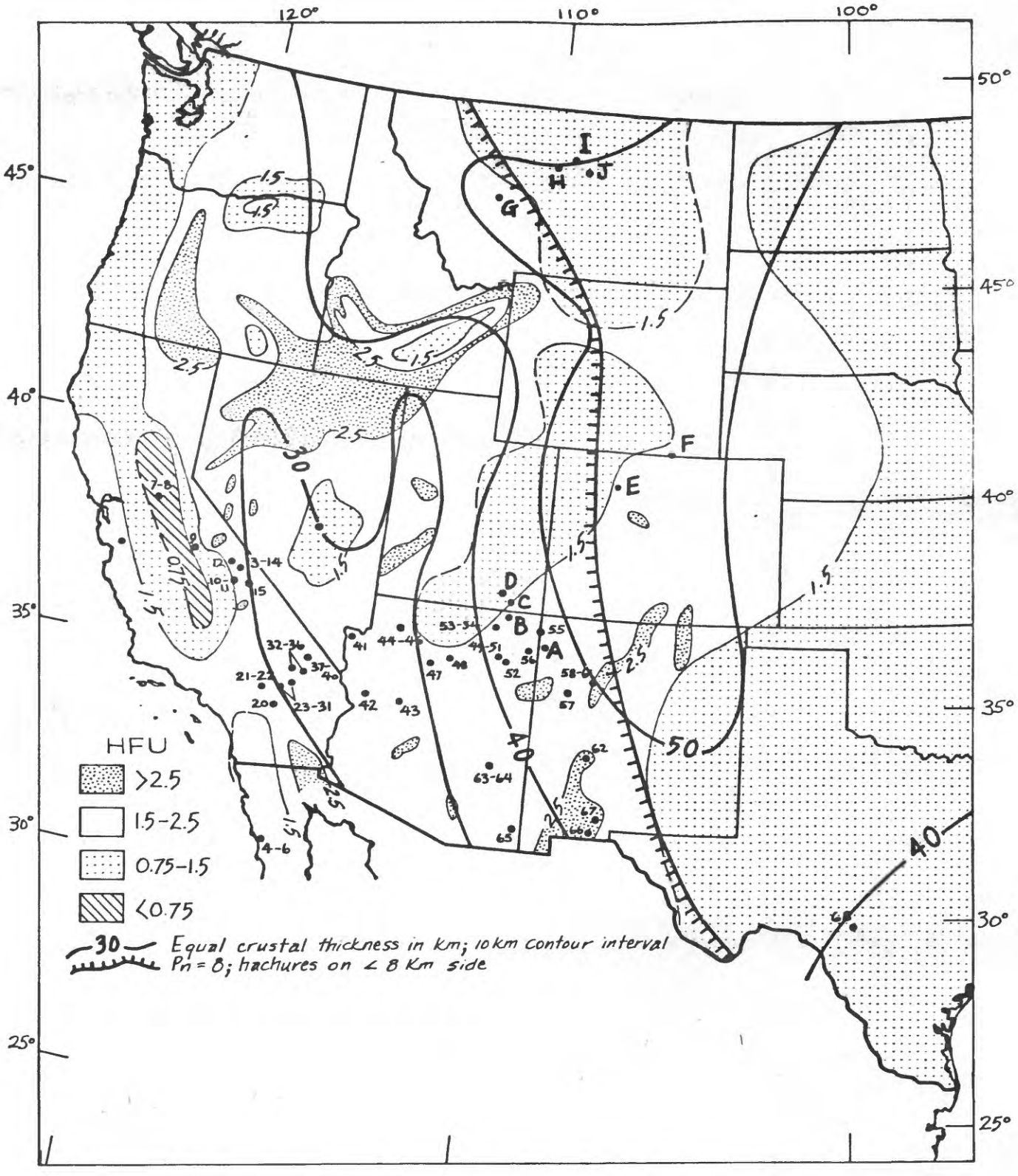

Fig. 2. Distribution of xenoliths with respect to heat flow provinces (after Sass and others, 1980), and crustal thickness, P-wave velocity (after Pakiser and Zietz, 1965). Kimberlites and phonolites identified by letters.

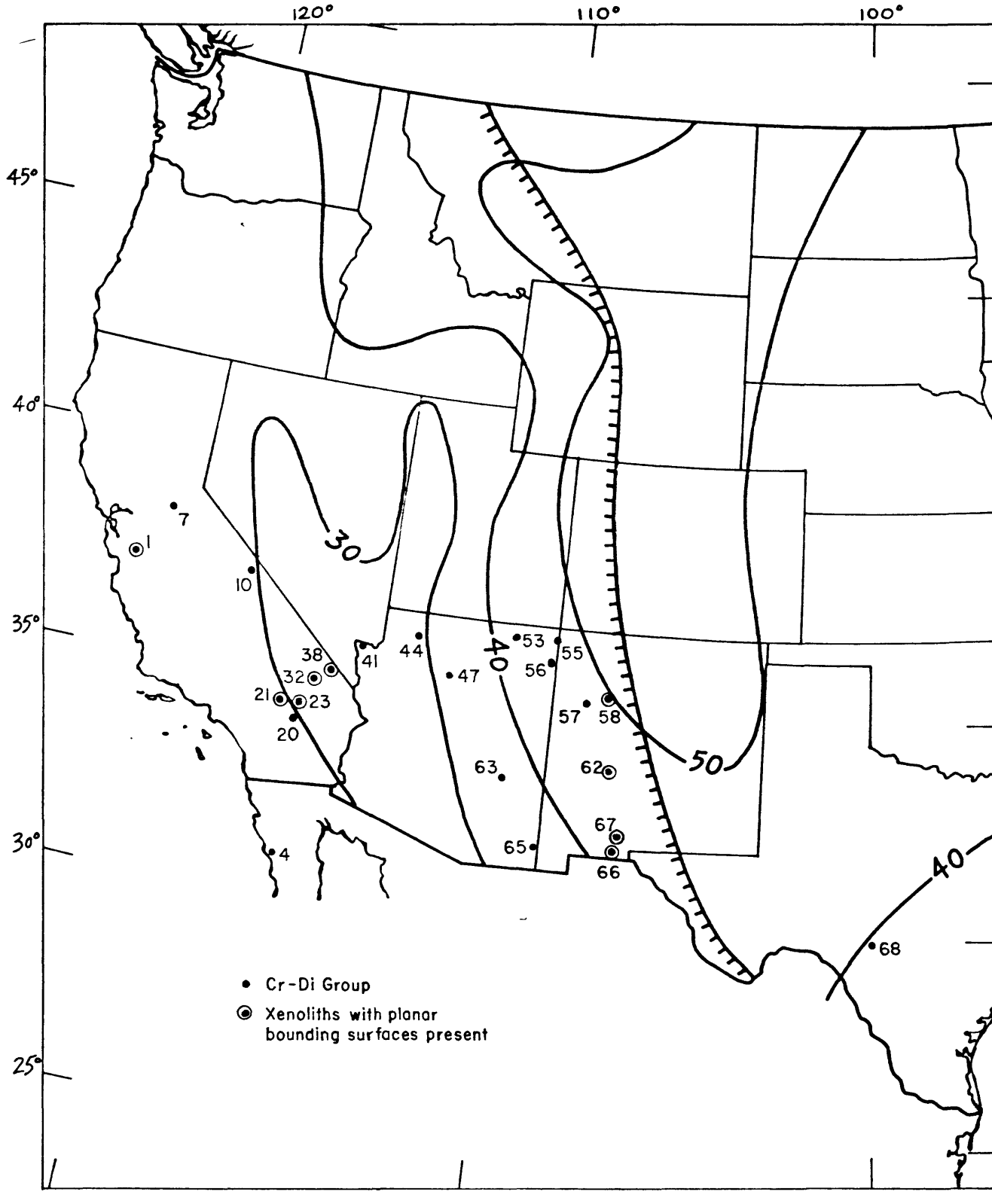

Fig. 3. Distribution of xenoliths in the Cr-diopside group.

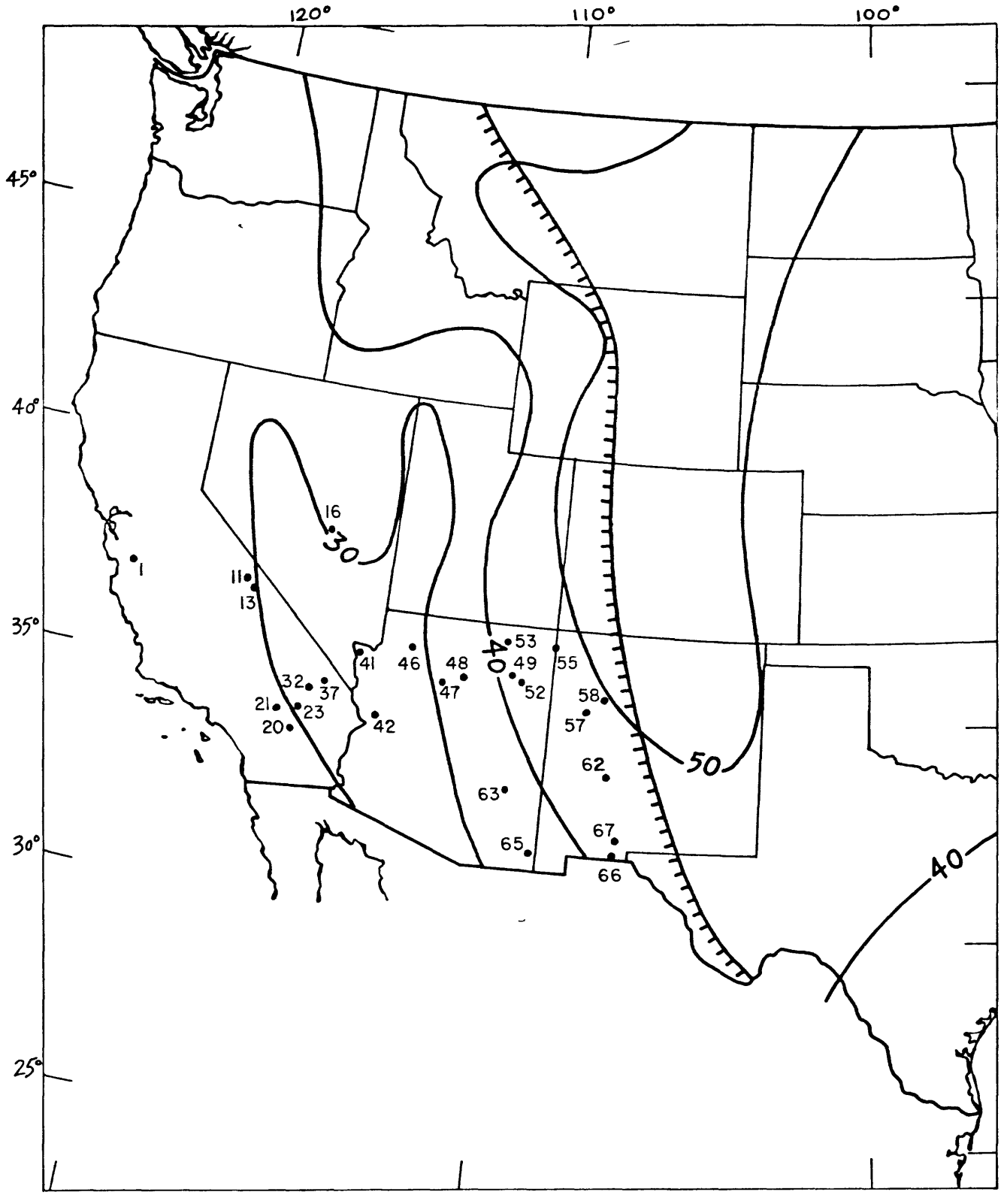

Fig. 4. Distribution of xenoliths in the Al-augite group.

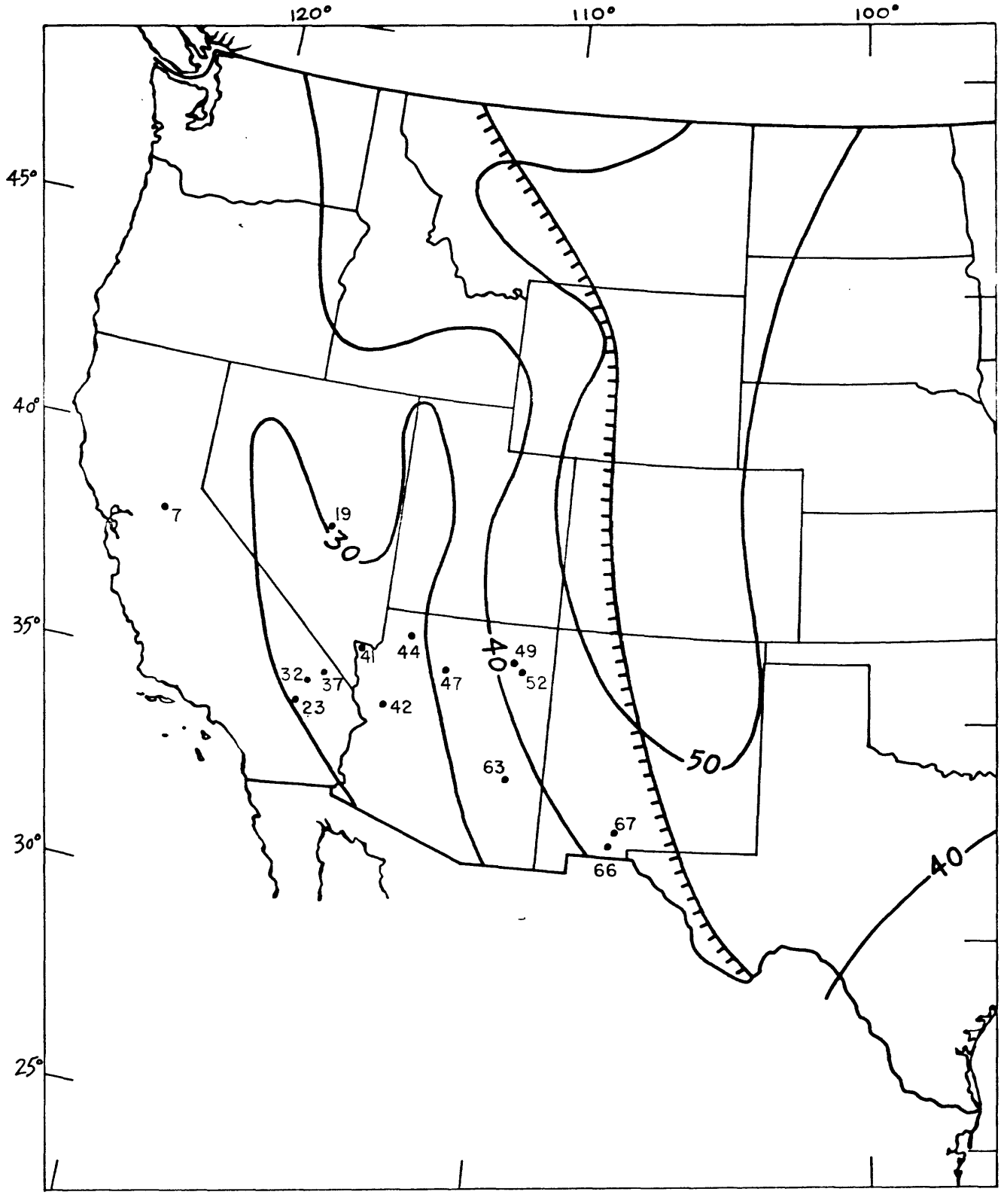

Fig. 5. Distribution of xenoliths with hydrous phases.

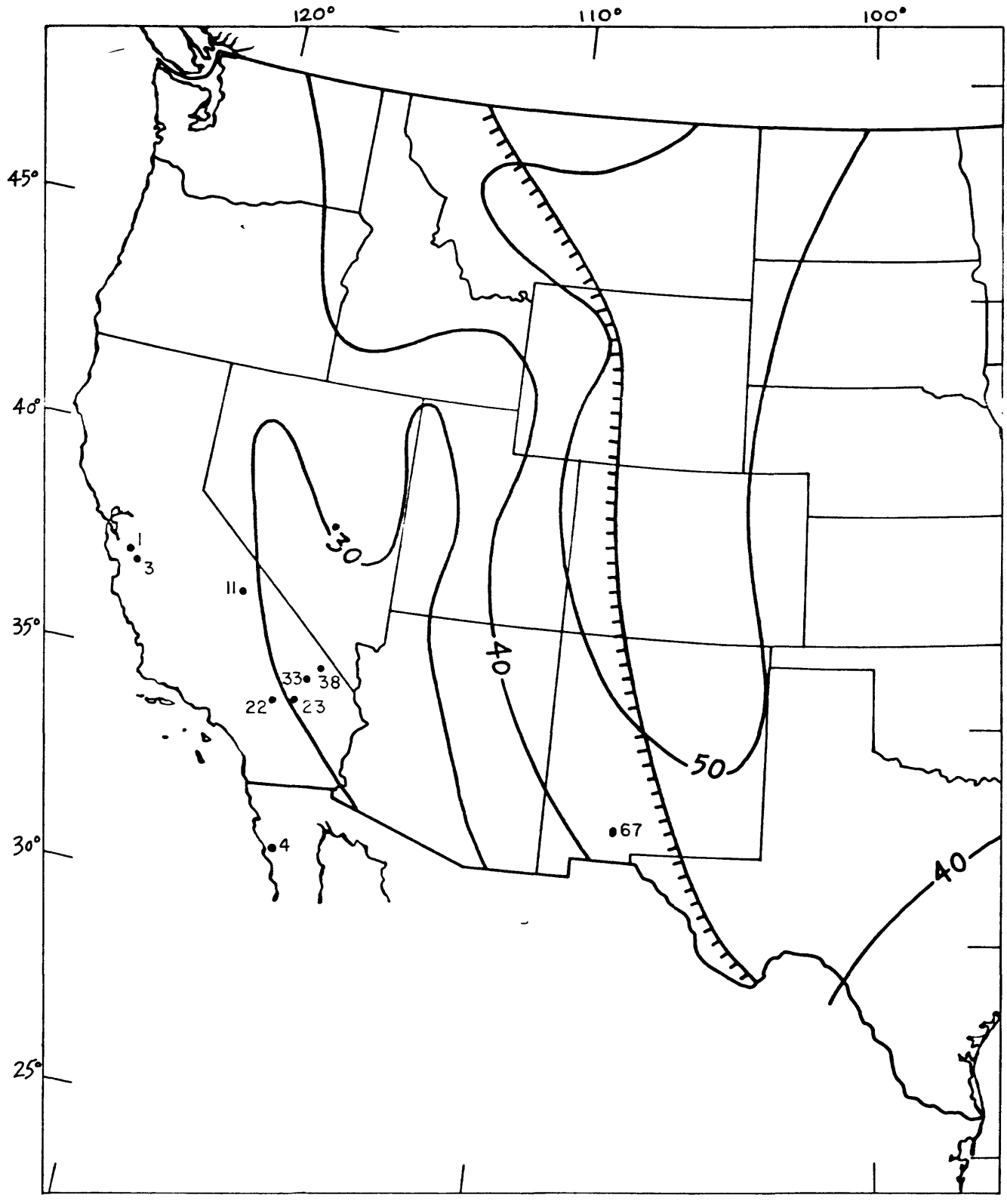

Fig. 6. Distribution of xenoliths in the feldspathic ultramafic group.

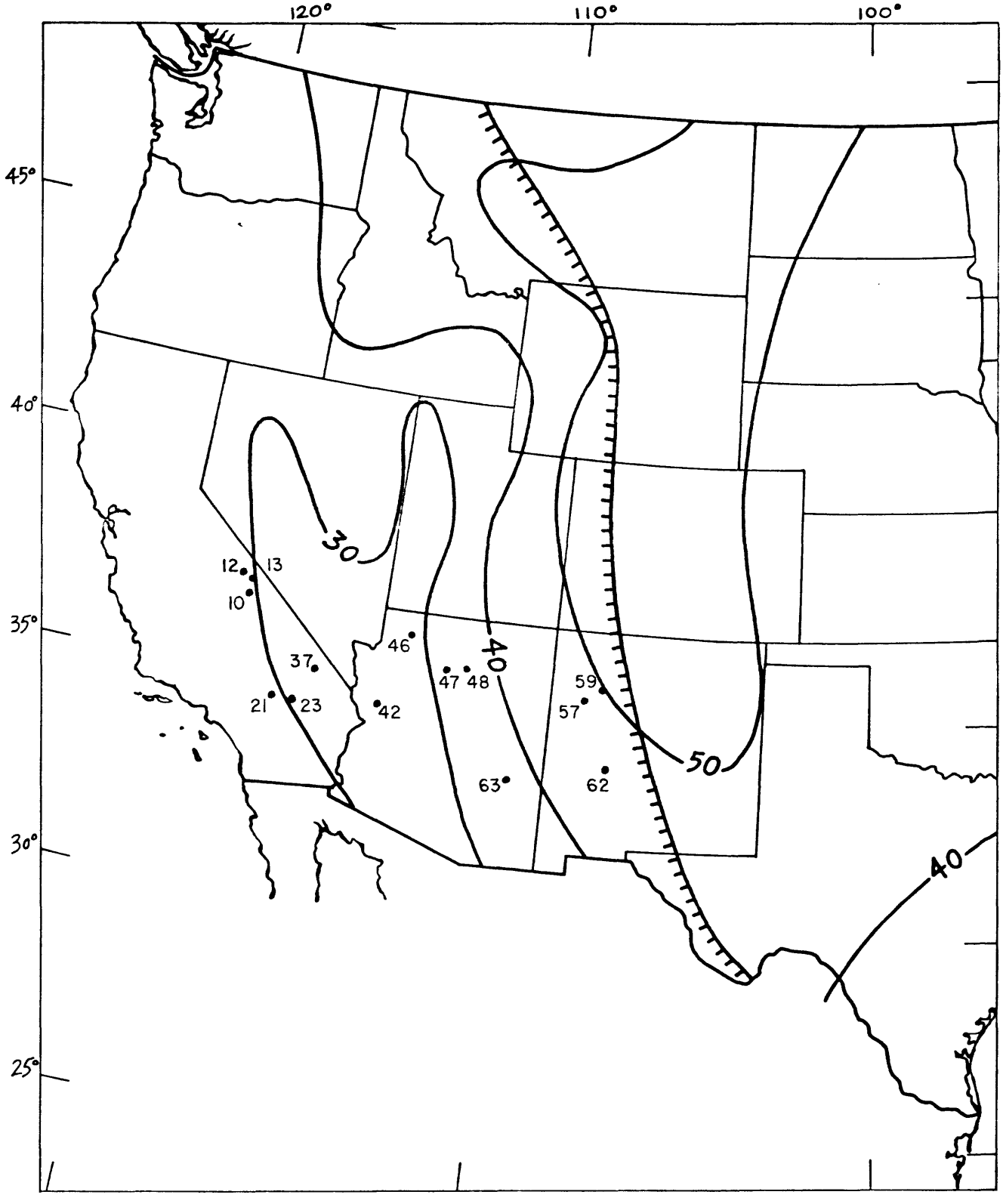

Fig. 7. Distribution of xenoliths in the bottle-green pyroxene group.

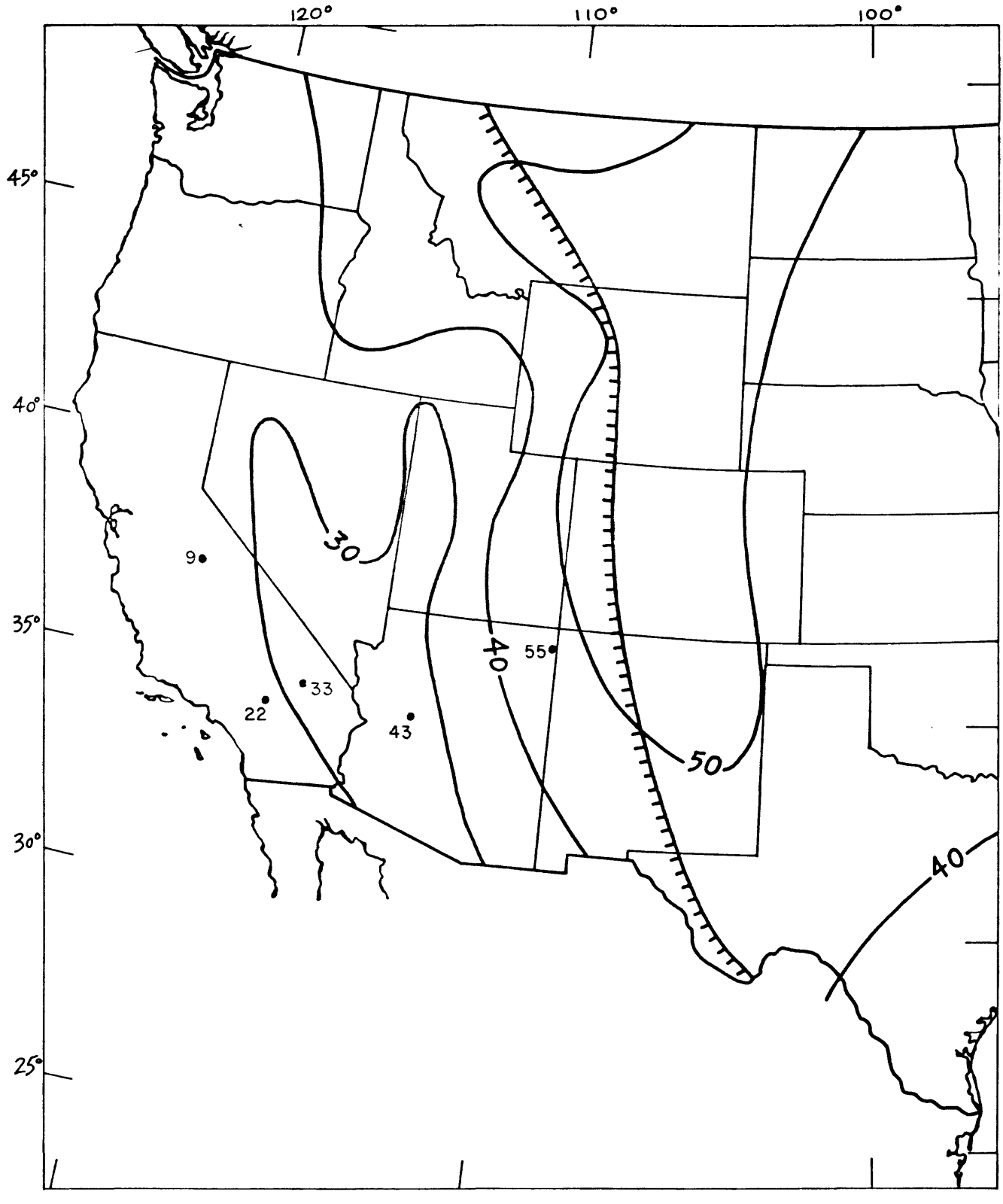

Fig. 8. Distribution of xenoliths in the garnetiferous ultramafic group.

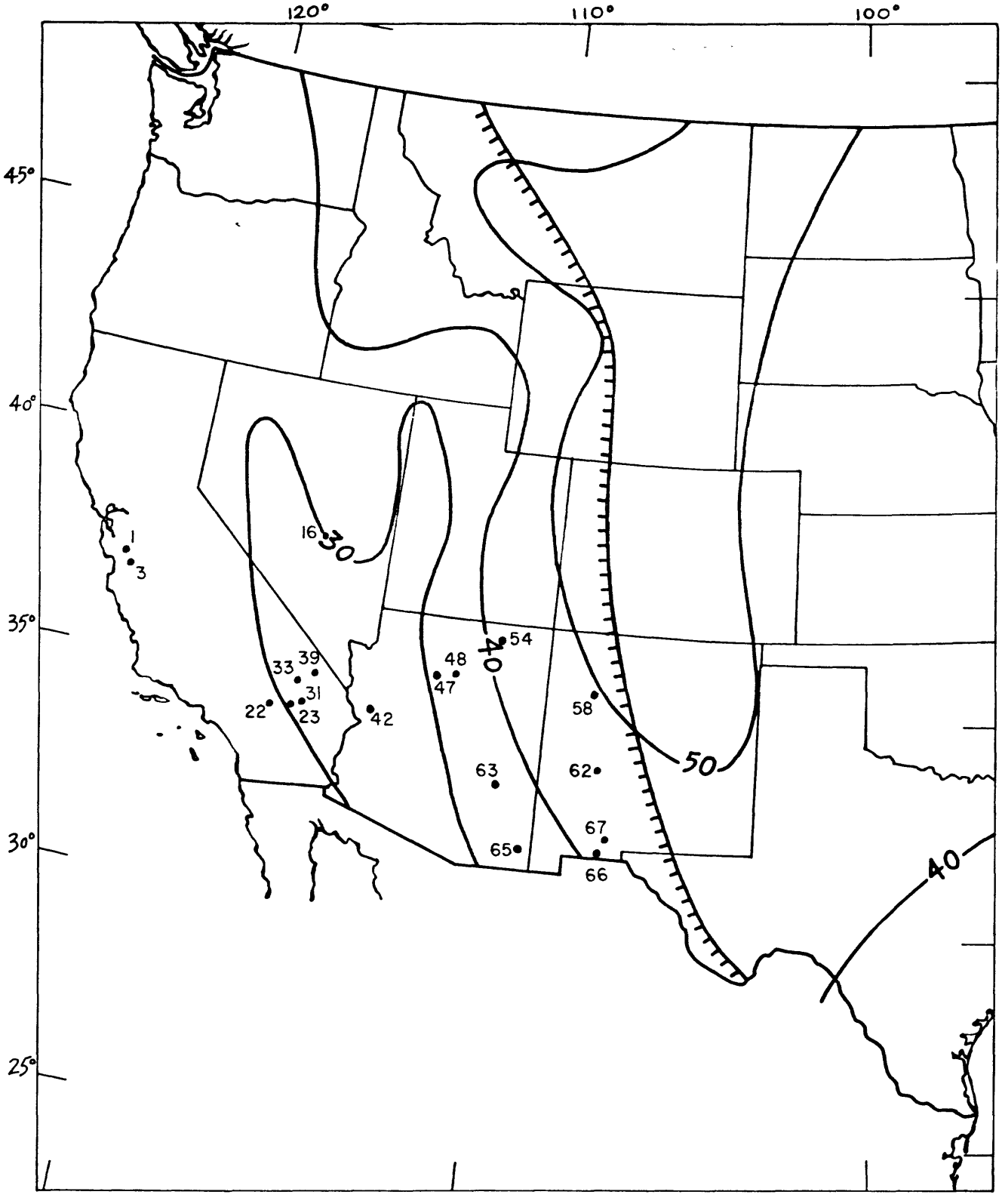

Fig. 9. Distribution of xenoliths in the gabbroid and metagabbroid groups.

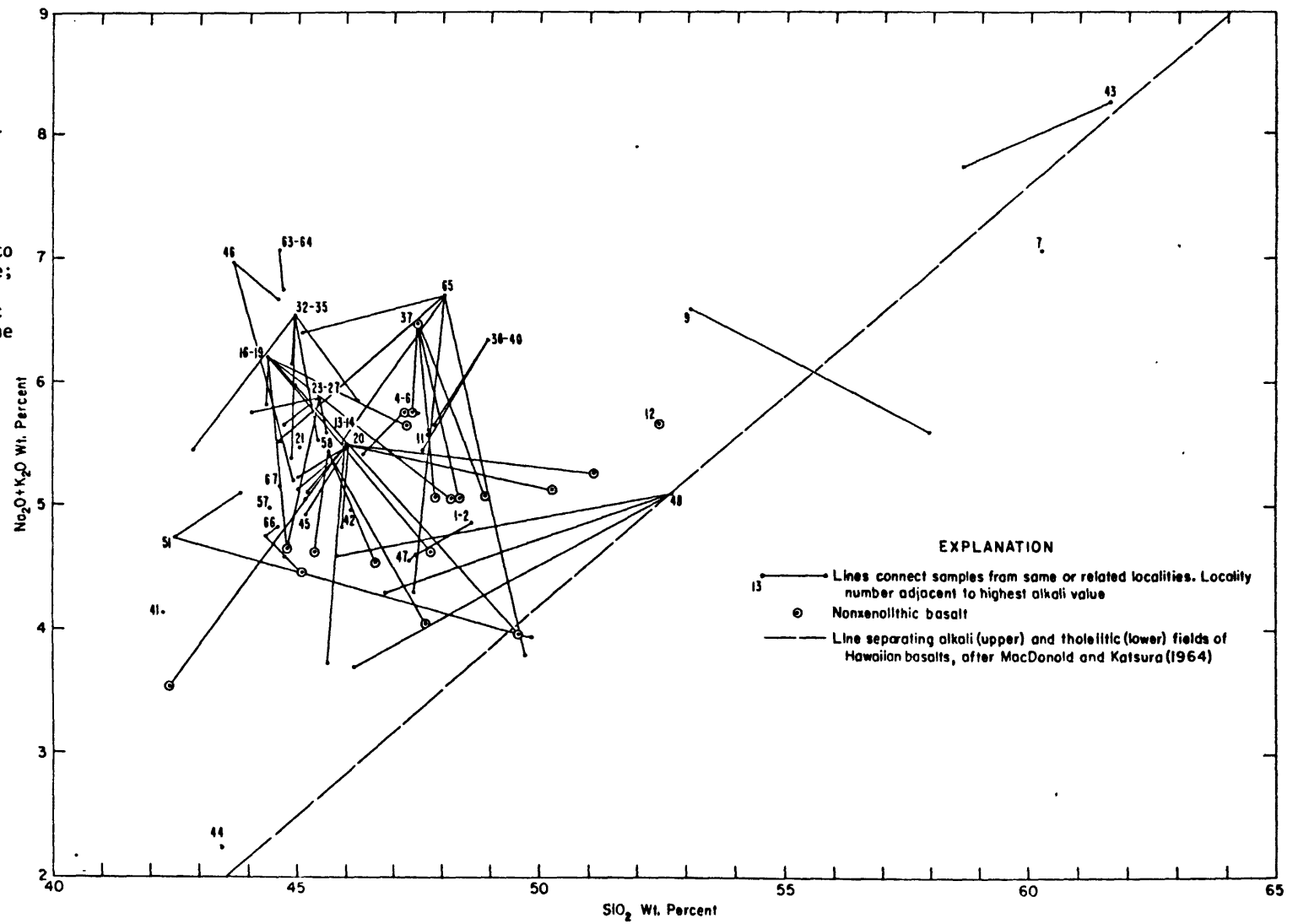

Fig. 10. Alkali-silica variations of host rocks. Solid lines connect samples from the same or related localities; locality number is adjacent to highest alkali value; circled points represent nonxenolithic basalts. Dashed line separates alkalic (upper) and tholeiitic fields, Hawaiian basalts (after MacDonald and Katsura, 1964)

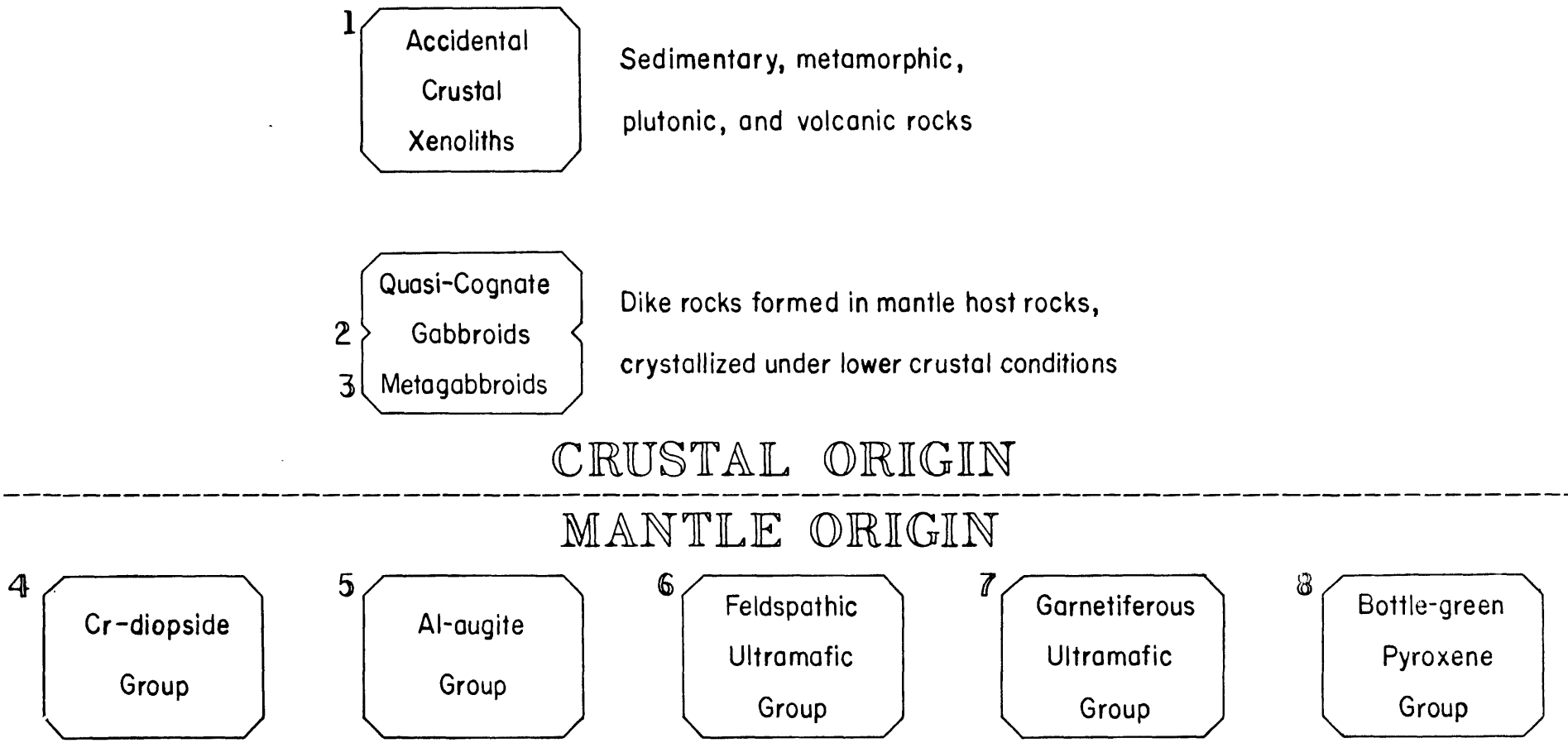

Fig. 11. Main xenolith groups recognized in this report.

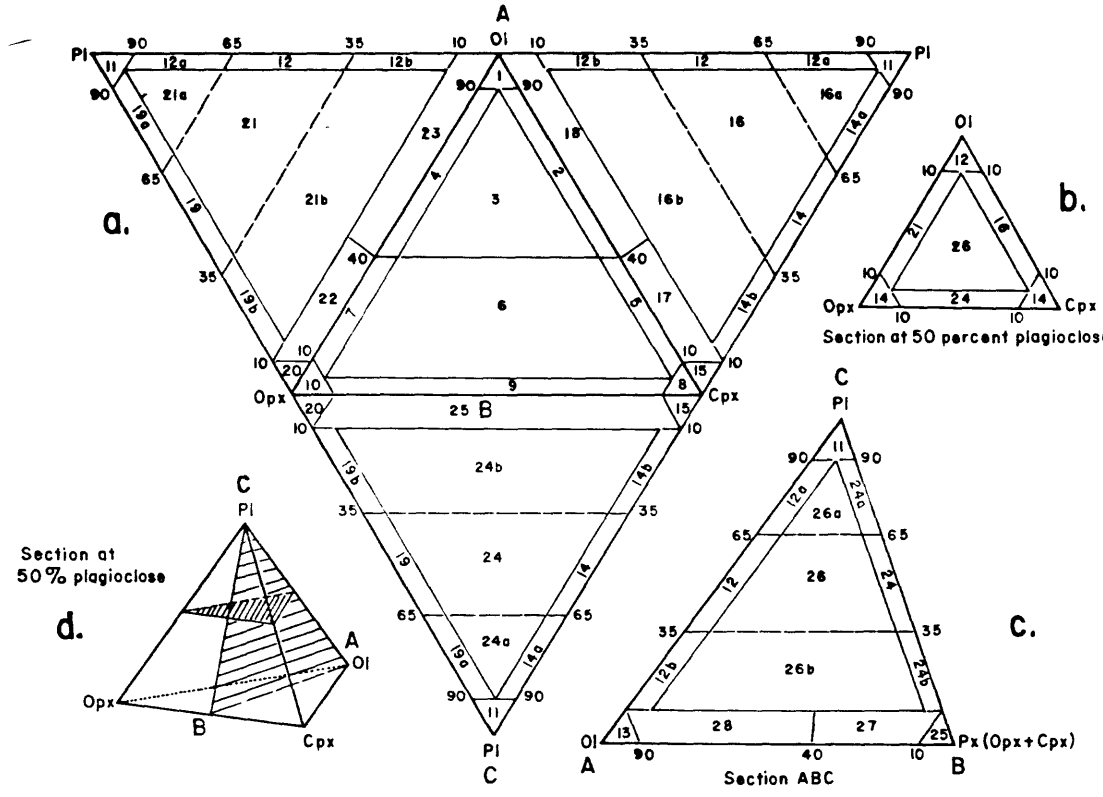

Fig. 12. Classification and nomenclature of ultramafic and gabbroic rocks in the tetrahedron olivine-plagioclase-orthopyroxene-clinopyroxene (from Streckeisen, 1976). a. Faces of the tetrahedron. b. Section parallel to the base Ol-Opx-Cpx at 50% plagioclase content. c. Section of the tetrahedron along the line A-B-C. d. Tetrahedron showing classification scheme: 1. dunite; 2. wehrlite; 3. lherzolite; 5. olivine clinopyroxenite; 6. olivine websterite; 7. olivine orthopyroxenite; 8. clinopyroxenite; 9. websterite; 10. orthopyroxenite; 11. anorthosite; 12. troctolite (a = leuco- b = mela-); 15. plagioclase-bearing clinopyroxenite; 16. olivine gabbro (a = leuco-, b = mela-); 17. plagioclase-bearing olivine clinopyroxenite; 18. plagioclase-bearing wehrlite; 19. norite (a = leuco-, b = mela-); 20. plagioclase-bearing orthopyroxenite; 21. olivine norite (a = leuco-, b = mela-); 22. plagioclase-bearing olivine orthopyroxenite; 23. plagioclase-bearing harzburgite; 24. gabbronorite (a = leuco-, b = mela-); 25. plagioclase-bearing websterite; 26. olivine gabbronorite (a = leuco-, b = mela-); 27. plagioclase-bearing olivine websterite; 28. plagioclase-bearing lherzolite.

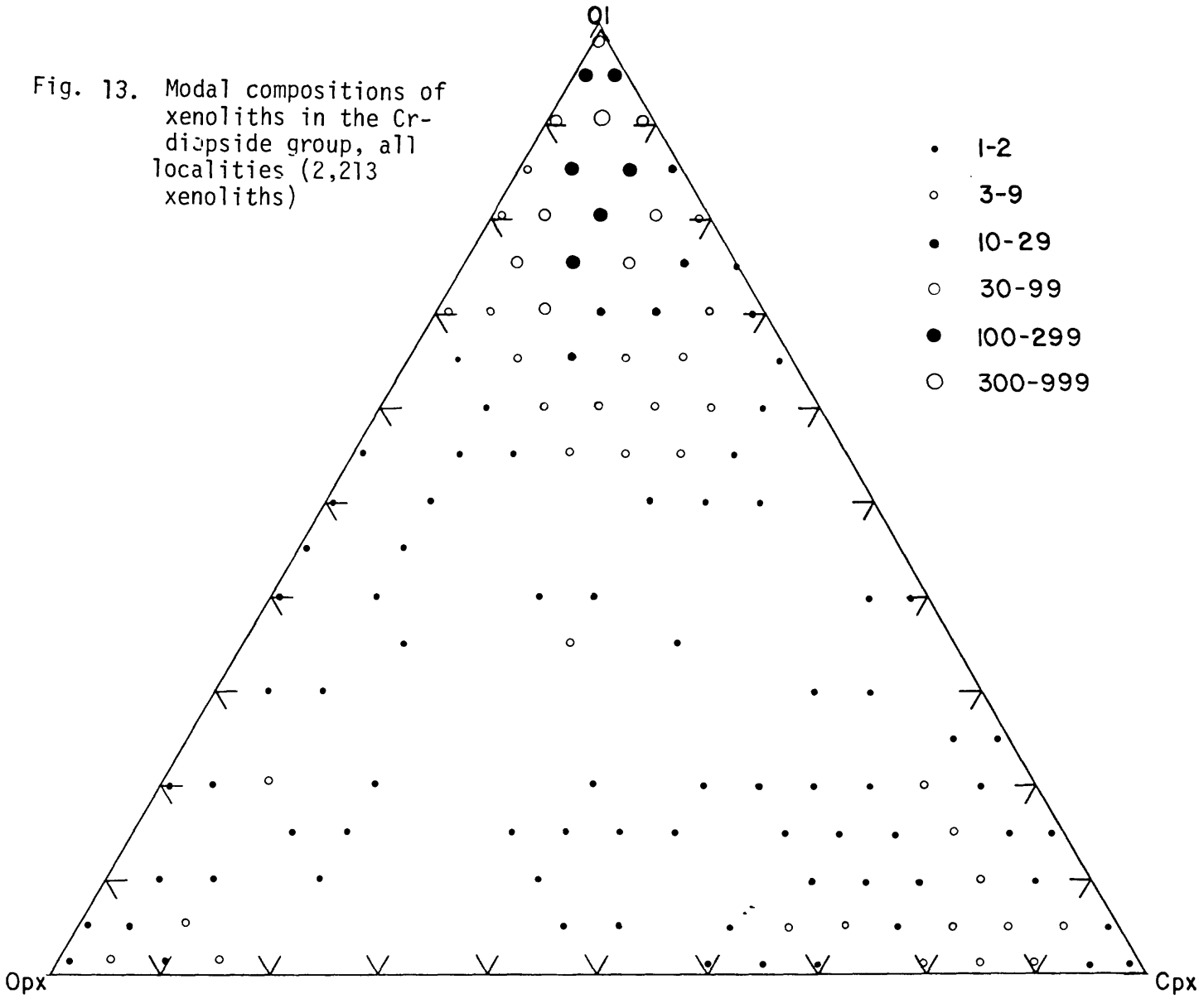

Fig. 13. Modal compositions of xenoliths in the Cr-diopside group, all localities (2,213 xenoliths)

Fig. 14. Modal compositions of xenoliths in the Al-augite group, all localities (705 xenoliths)

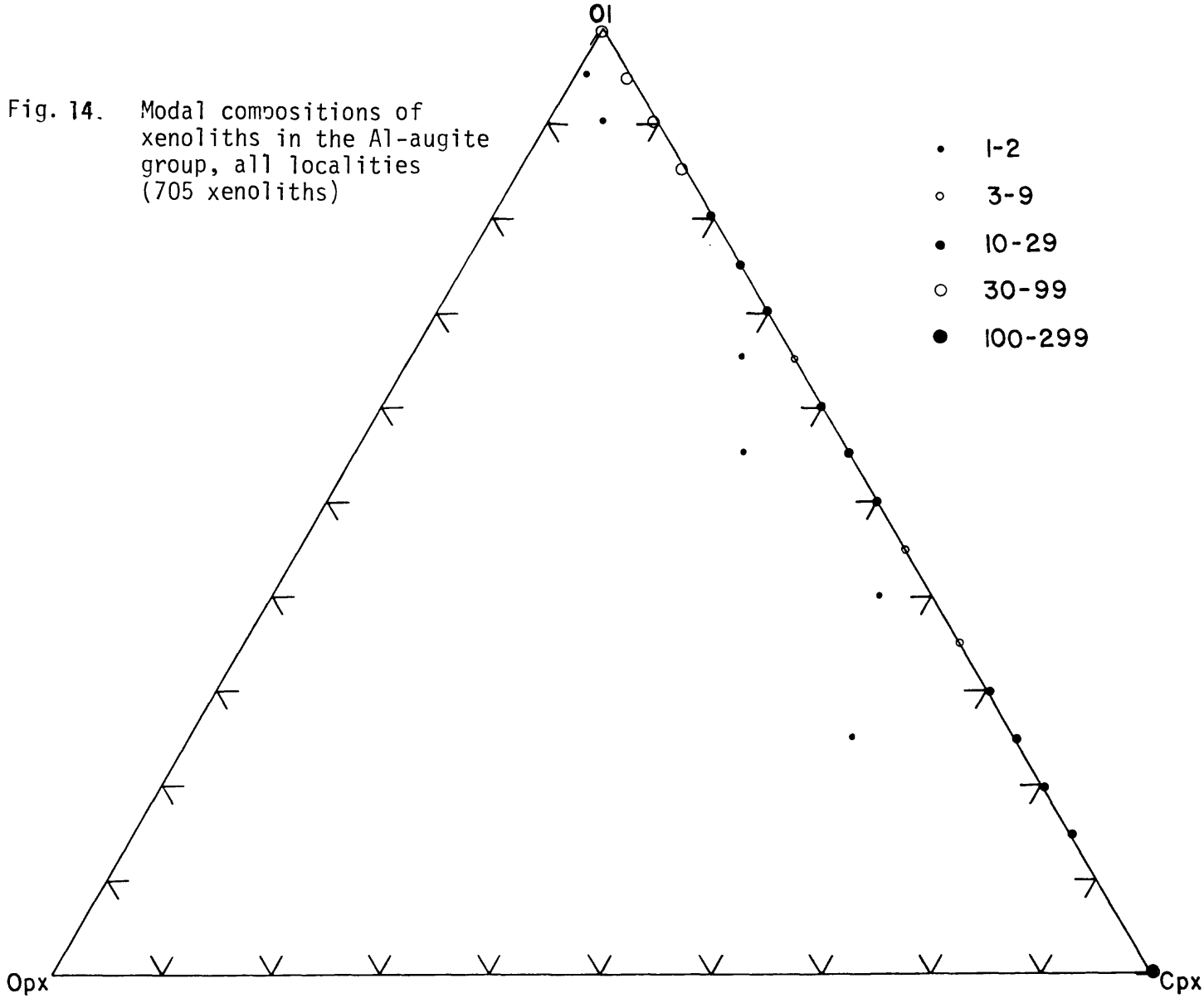

Figure 15a. Cr-diopside websterite dike crosscuts foliation (parallel to pencil) of Cr-diopside lherzolite. Xenolith, San Carlos, Arizona.

Figure 15b. Shearing parallel to foliation in Cr-diopside lherzolite produced lenses of peridotite parallel to the foliation in a crosscutting Cr-diopside websterite dike. Xenolith, San Carlos, Arizona.

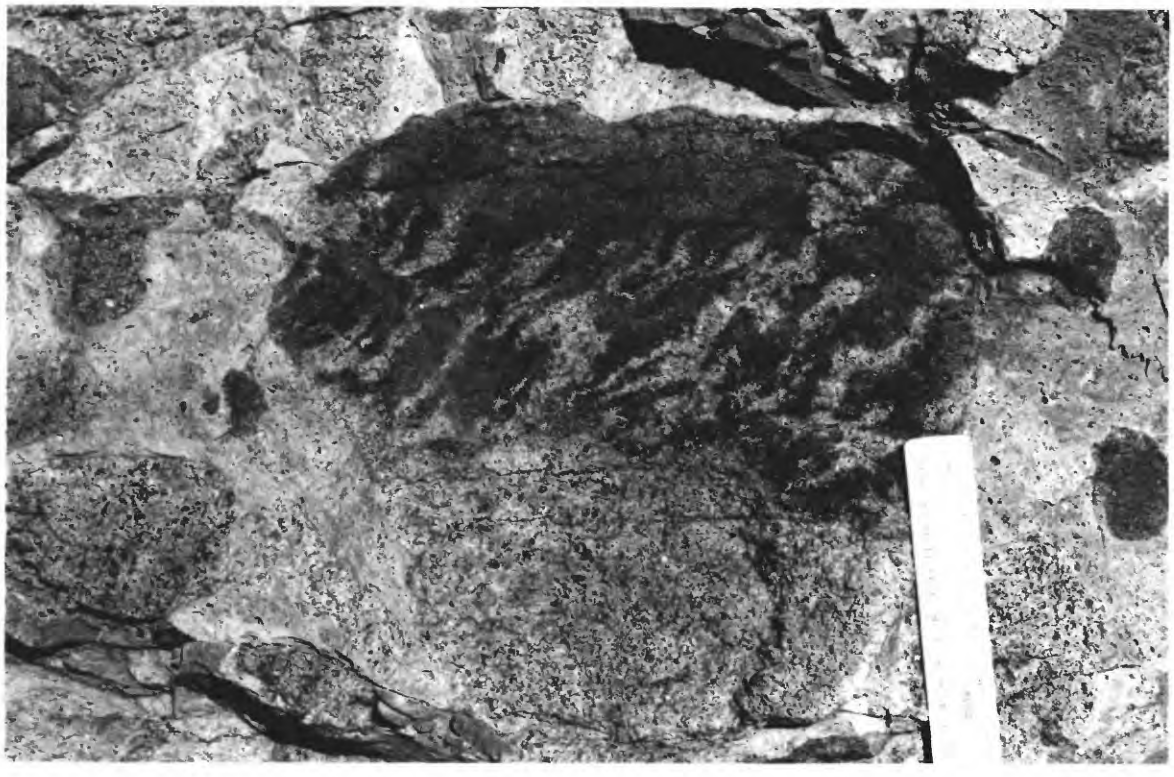

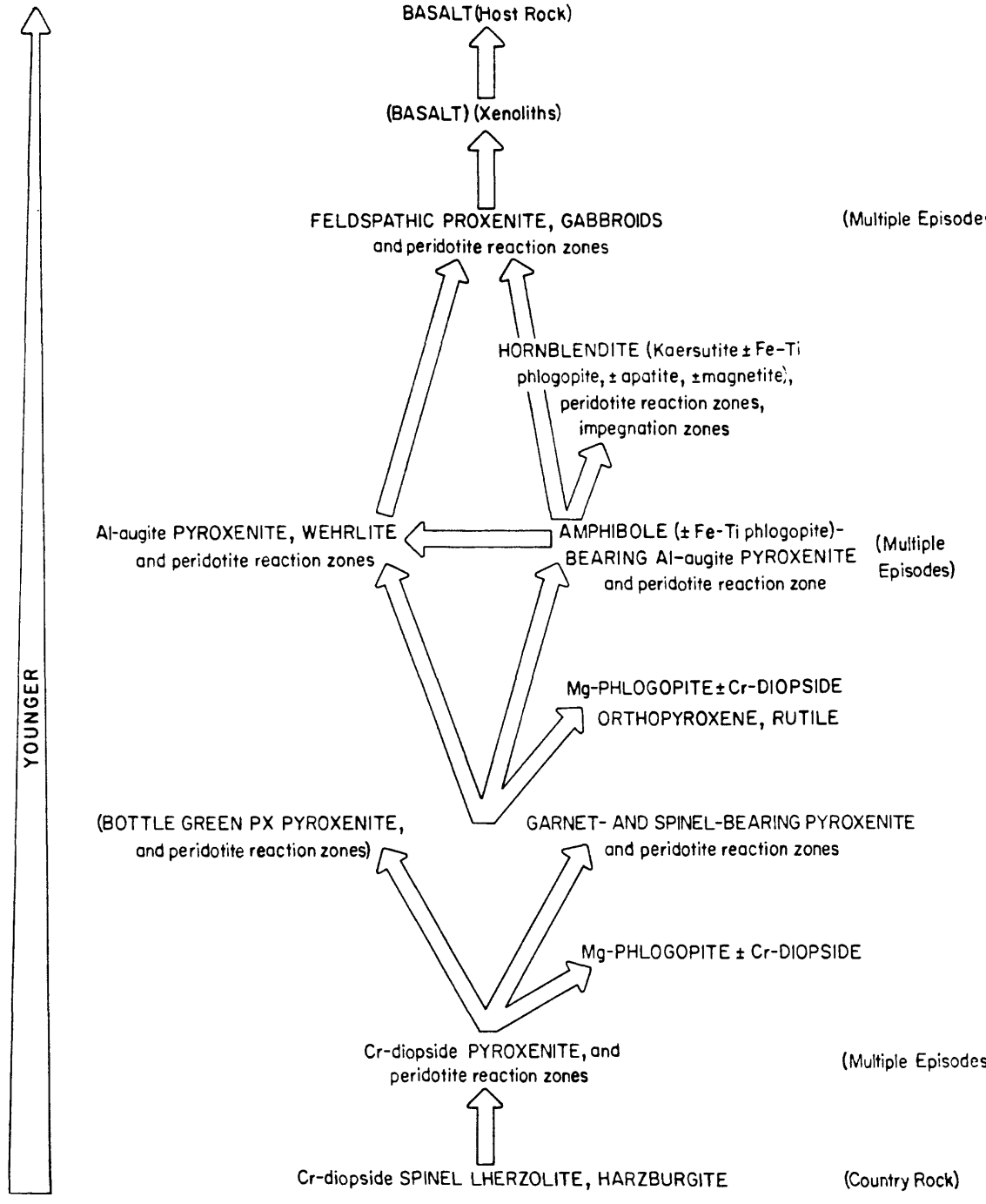

Fig. 16. Schematic diagram showing sequence of emplacement of dike rocks and associated reaction zones in xenoliths. No direct evidence for the position shown is known for rock types in brackets.

Figure 17a. Crosscutting Cr-diopside websterite dikes in Cr-diopside lherzolite. Near vertical dike offsets the other. Note small lherzolite xenolith in websterite at the junction of the two dikes. Xenolith, San Carlos, Arizona.

Figure 17b. Crosscutting Cr-diopside websterite dikes in Cr-diopside lherzolite. Note dilational offset of thin dikes by the thick one. Balmuccia peridotite massif.

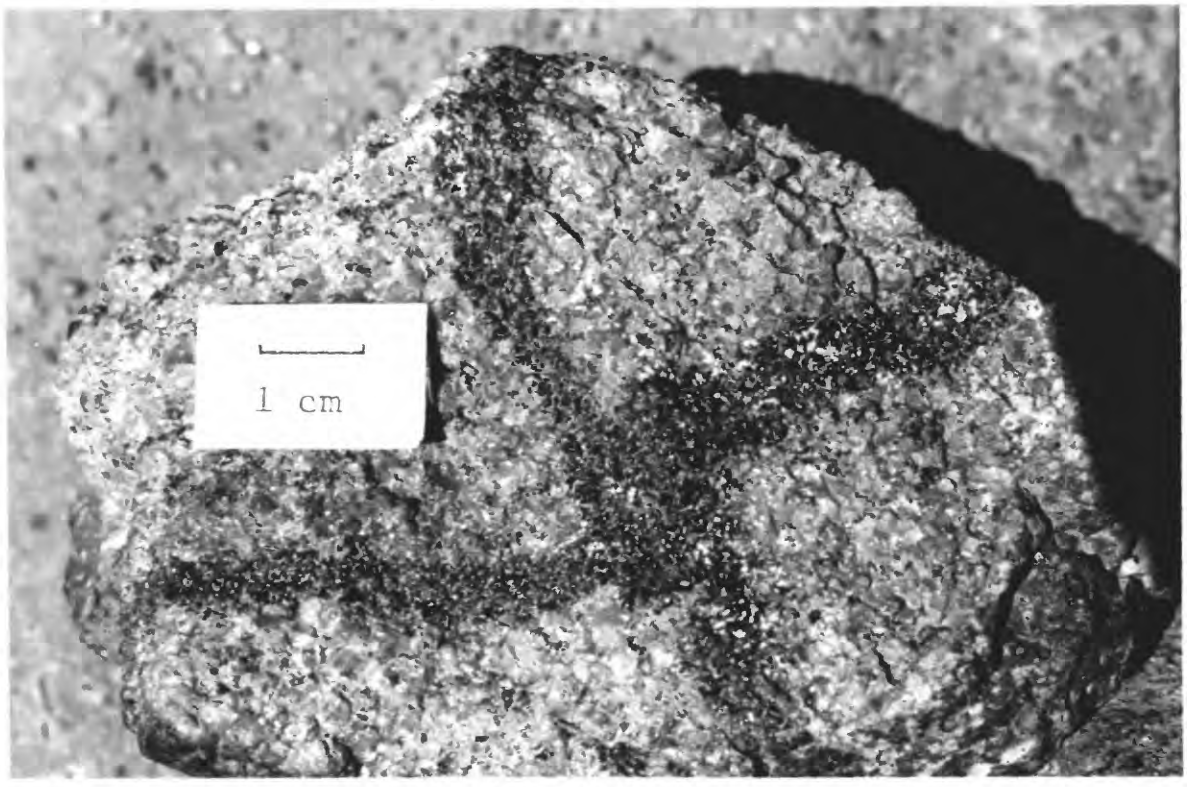
1 cm

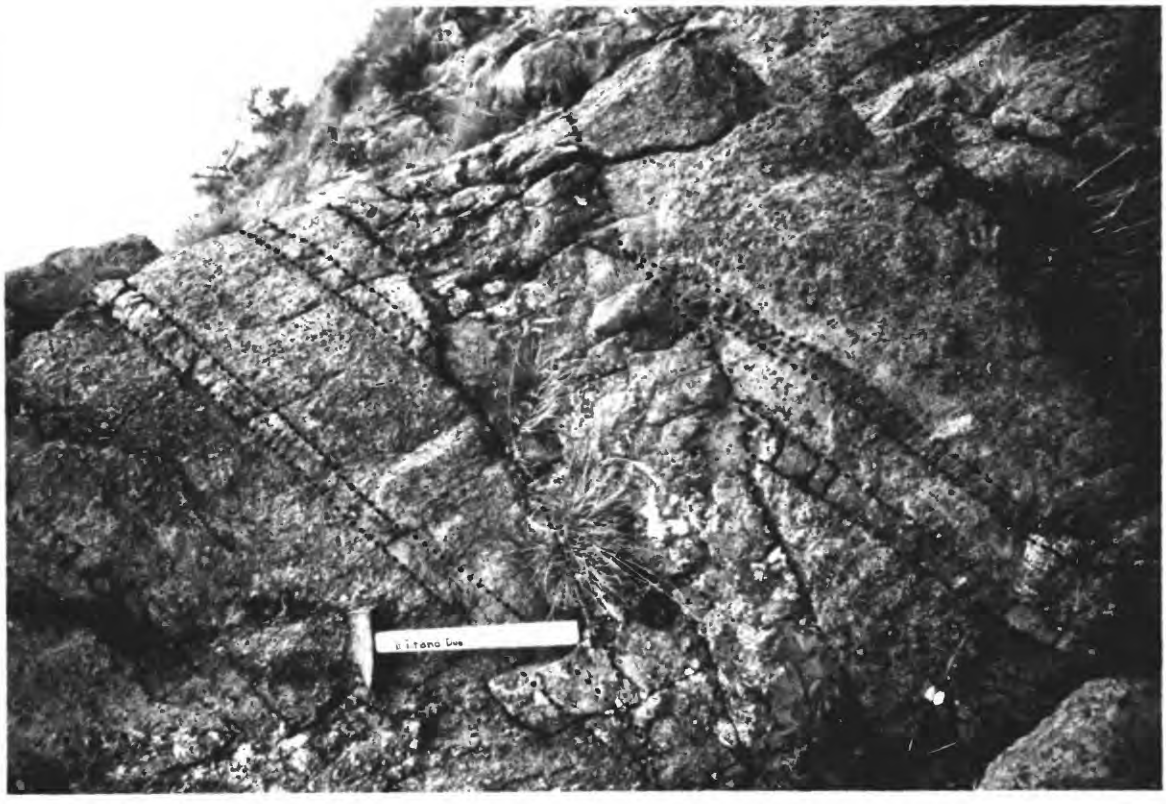
Titano Due

Figure 18a. Garnet pyroxenite (top right, marked by tape inclined to right) crosscuts Cr-diopside spinel pyroxenite layers (center, marked by tape inclined to left). Two Al-augite hornblendite dikes (largest one in center just above hammer head, marked by horizontal tape) crosscut the spinel pyroxenites and are at a high angle to the garnet pyroxenite (contact relationships not exposed). Lherz peridotite massif.

Figure 18b. Branching Al-augite pyroxenite dike isolates an angular inclusion of Al-augite peridotite. This pyroxenite is crosscut by another on right side of xenolith; note large spinels in dike on right. A vaguely defined zone in peridotite at the junction of the two dikes is especially enriched in clinopyroxene. Xenolith, San Carlos, Arizona.

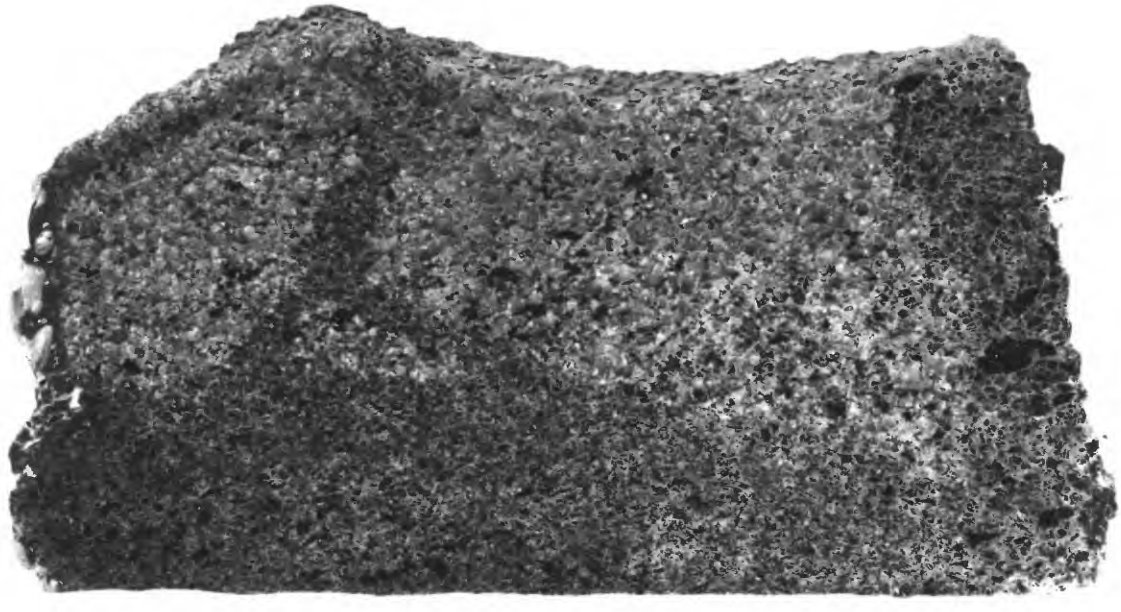
0
3
CM

Figure 19a. Hornblendite segregations in hornblende pyroxenite dikes (steep left dips). Segregation in thin dike, left side, splits off of the pyroxenite dike near bottom of photo and crosscuts the host Cr-diopside lherzolite. Lherz peridotite massif.

Figure 19b. Hornblendite derived from fine-grained hornblende pyroxenite (nearly horizontal in photo) crosscuts Cr-diopside lherzolite. Both junctions of the hornblendite and pyroxenite are contained within the xenolith. Pyroxenite has axial concentration of amphibole. Xenolith, San Carlos, Arizona.

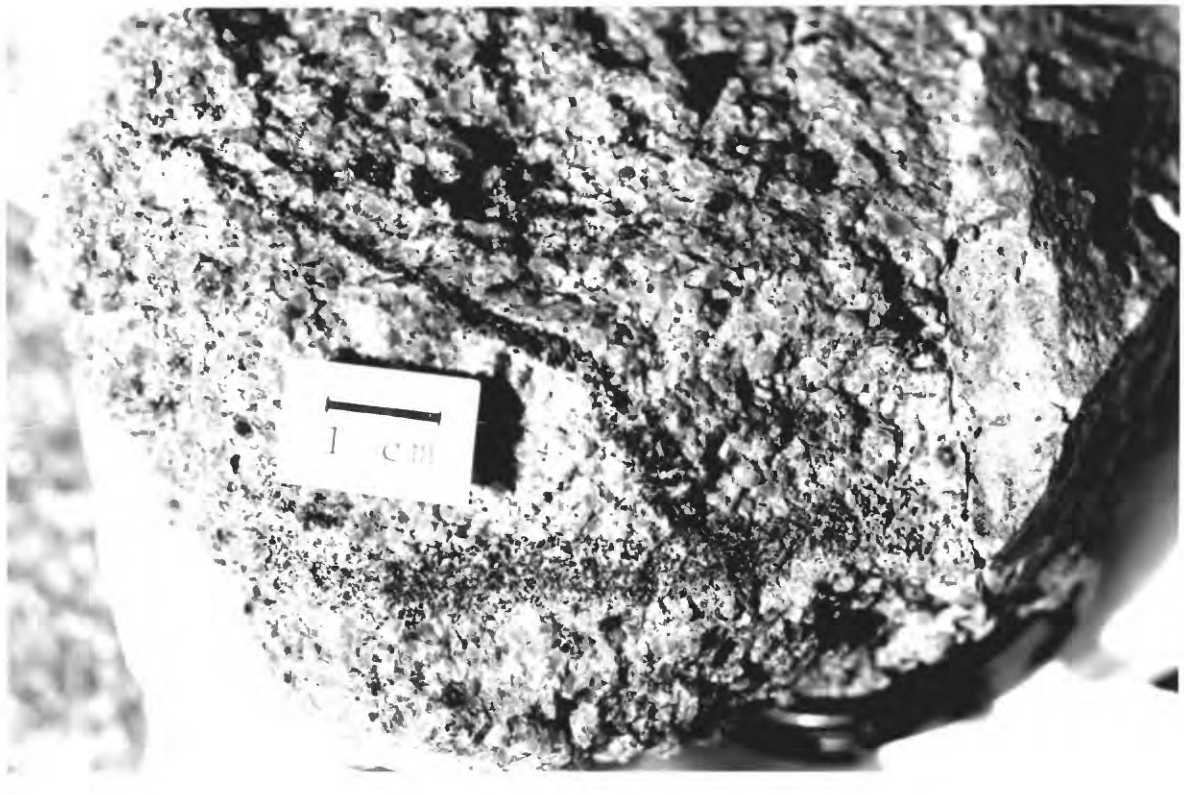
1 cm

Figure 20a. Hornblendite crosscuts Cr-diopside websterite dike in Cr-diopside lherzolite. Xenolith, Deadman Lake, California.

Figure 20b. Hornblendite intruded into planar fracture in Cr-diopside lherzolite. Xenolith broke along the vein which is now a rind along the bottom edge of the xenolith. Deadman Lake, California.

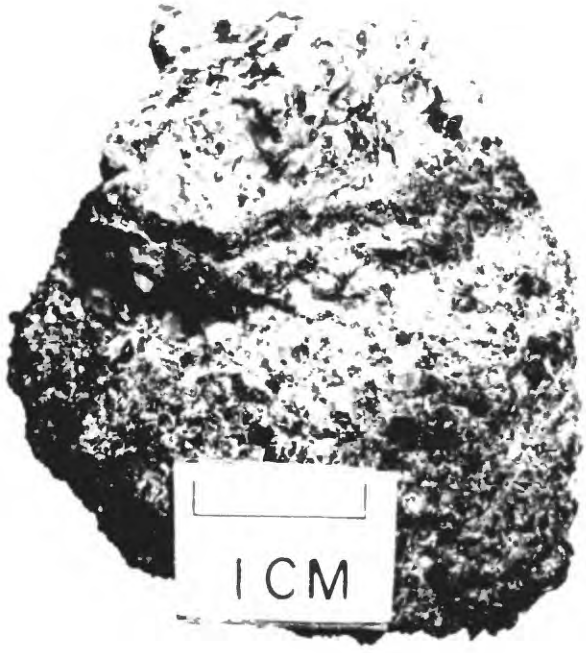
1 CM

Figure 21a. Two differently oriented hornblendite (+ apatite) dikes in planar fractures (left and top-right sides) in Cr-diopside lherzolite. Three additional sets of fractures in the lherzolite are unoccupied. Xenolith, Dish Hill, California.

Figure 21b. Cr-diopside lherzolite xenolith excavated along a complex system of intersecting planar fractures. Xenolith, Dish Hill, California.


1 CM

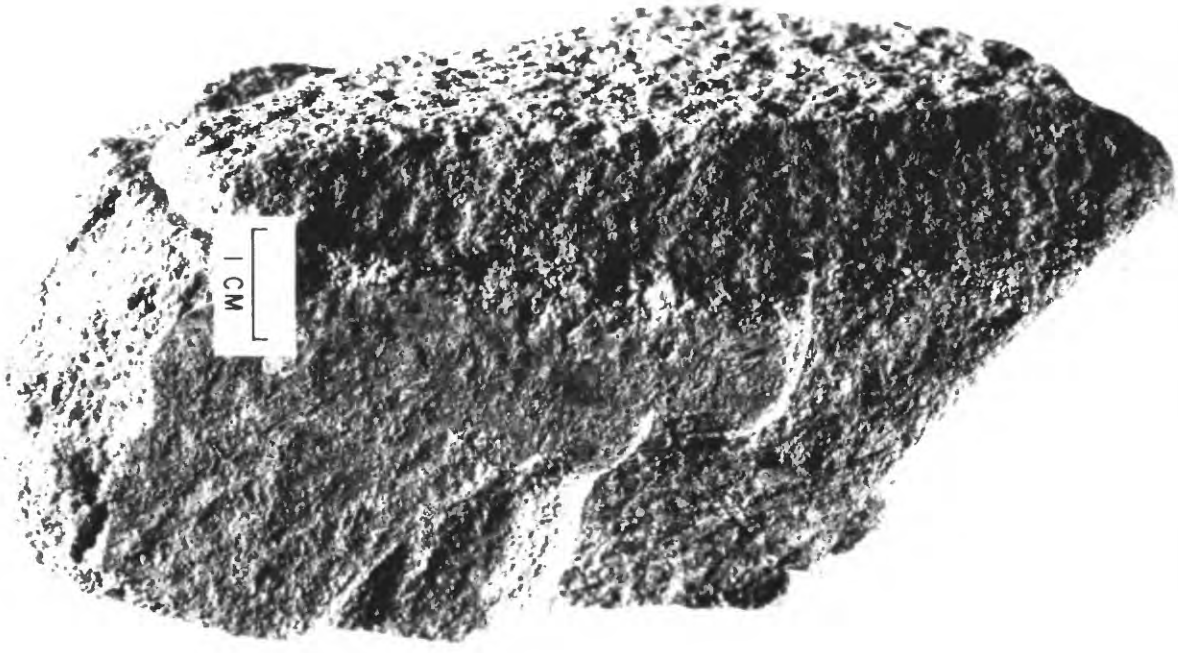
1 CM

Figure 22a. Fine-grained gabbro dike (inclined to right, top-right) crosscuts two Cr-diopside websterite layers (vertical) in Cr-diopside lherzolite. Xenolith, Cima, California.

Figure 22b. Thin feldspar-rich vein in Al-augite clinopyroxenite. Xenolith, Cima, California.

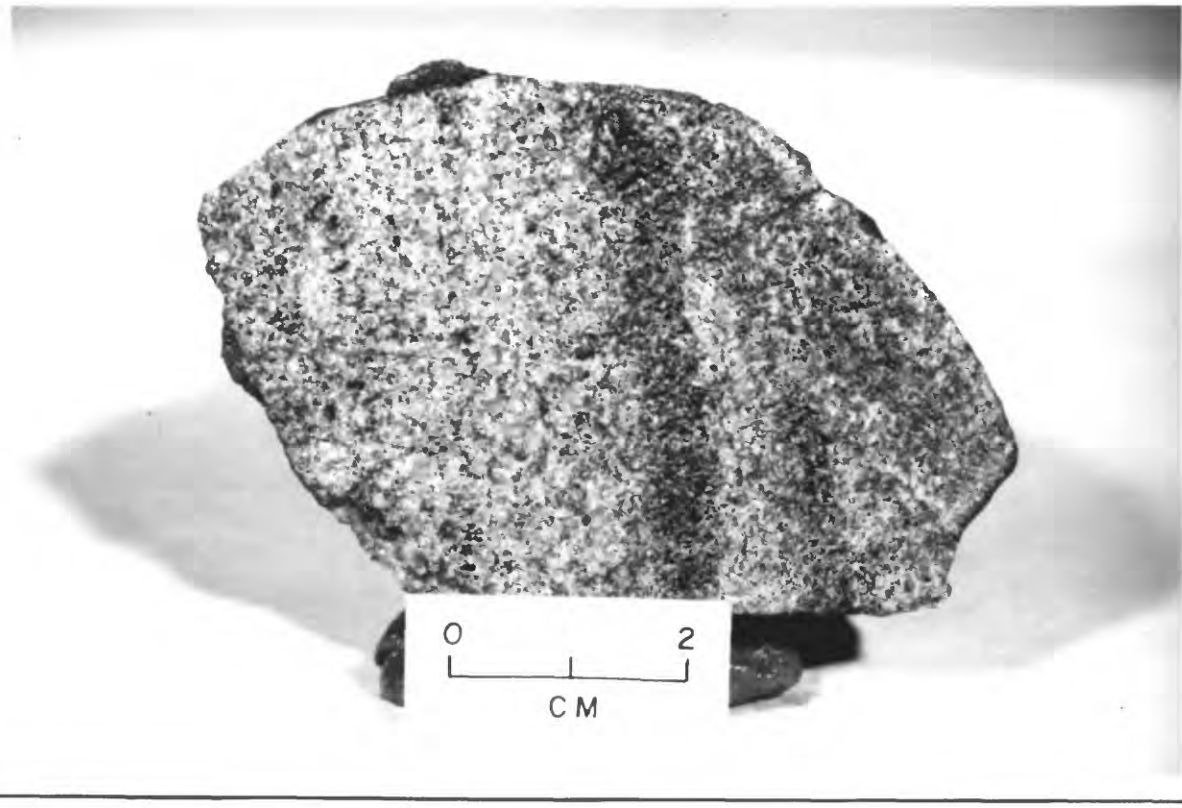
0
2
CM

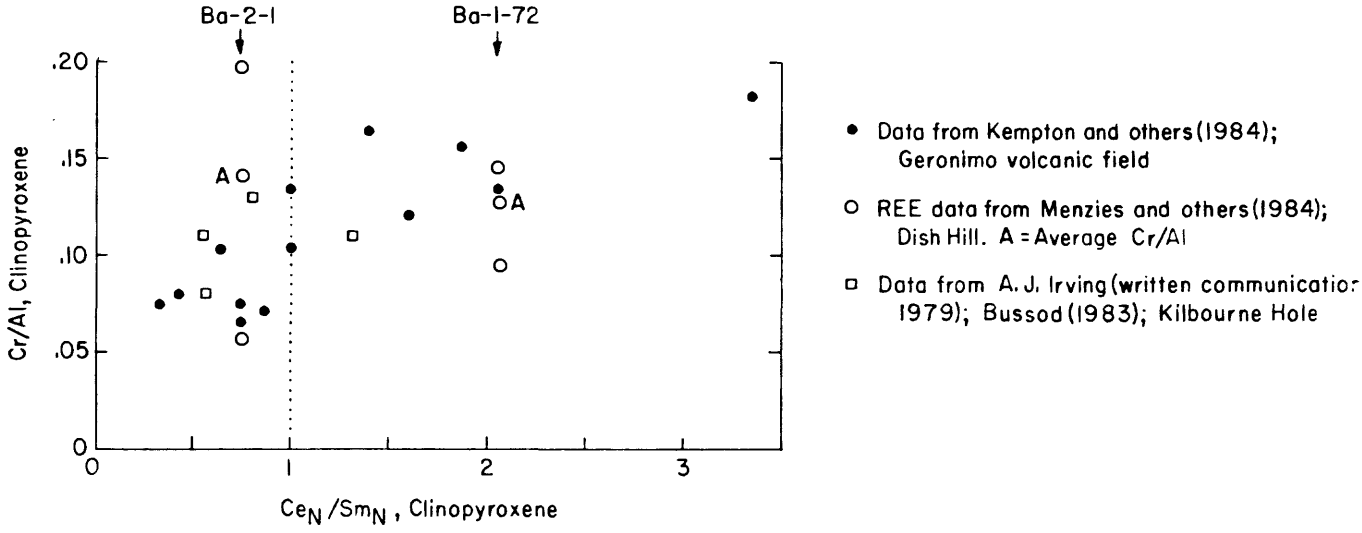

Fig. 23. Ranges and average value of Cr/Al of clinopyroxene in wallrocks of hornblendite dikes (Ba-2-1; Ba-1-72) plotted against Ce_N/Sm_N (after Kempton and others, 1984)

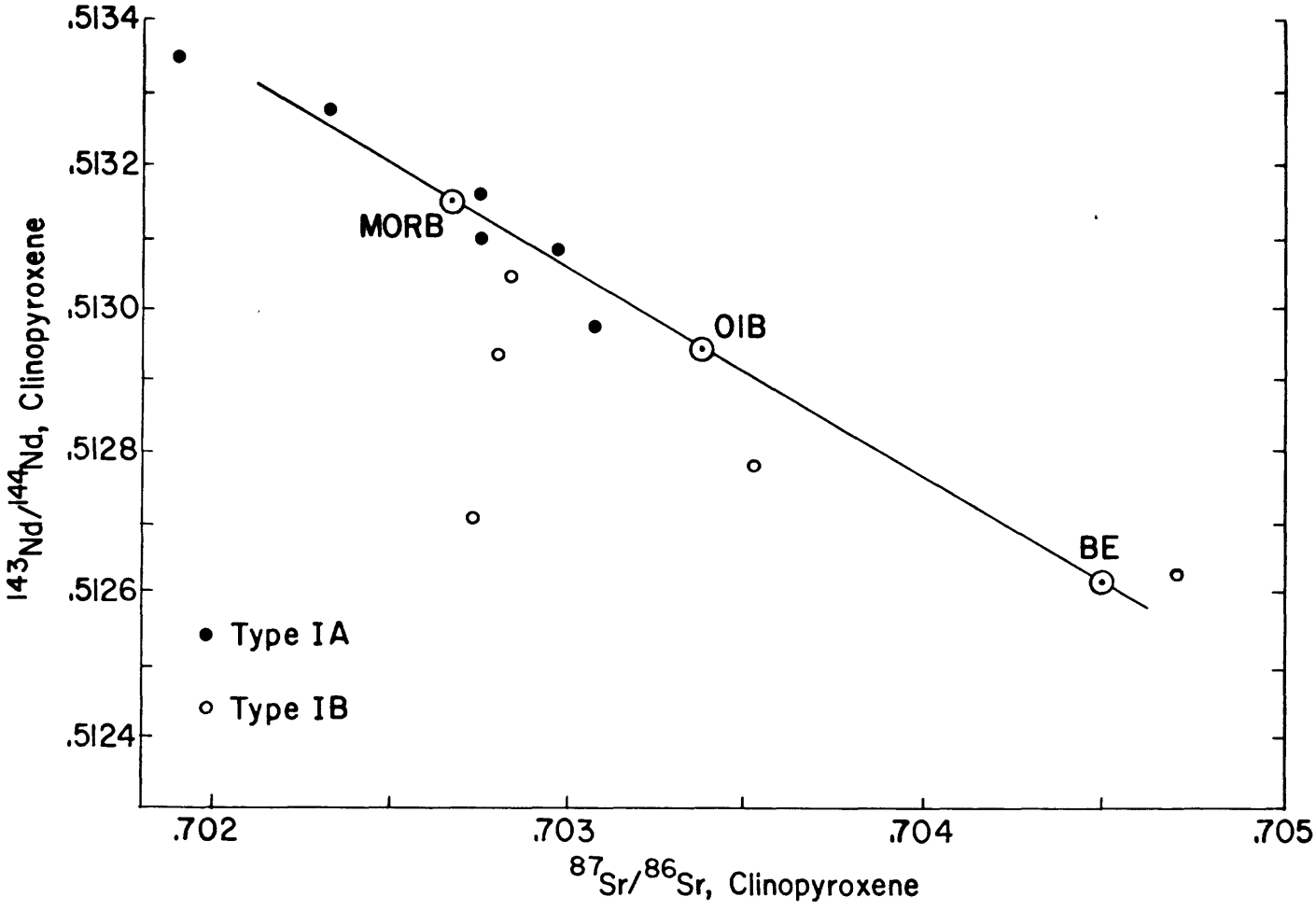

Fig. 24. Nd/Sr plot of Type Ia and Type Ib xenoliths showing their positions on the "mantle array" (from Menzies and others, 1984).

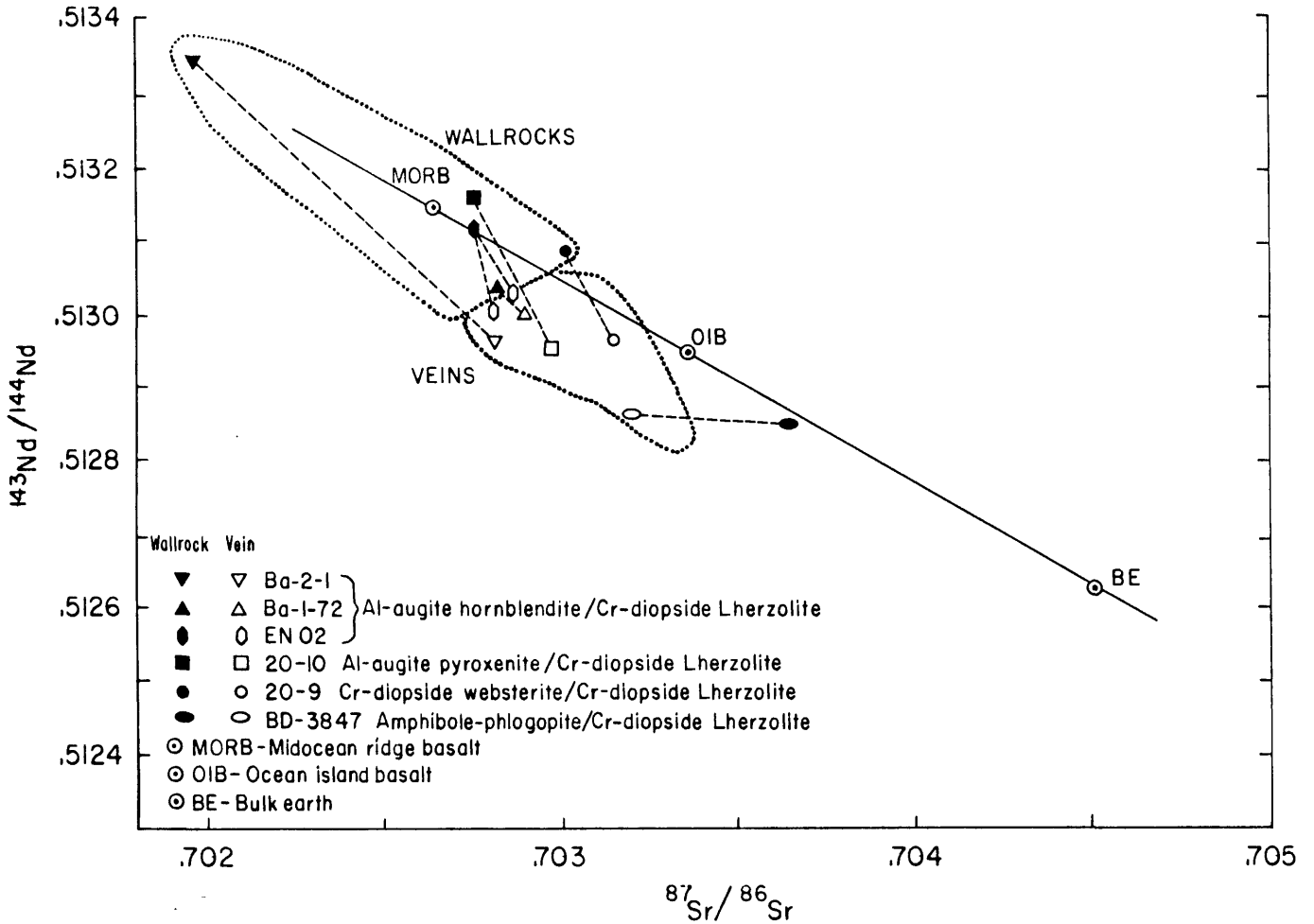

Fig.25. Nd/Sr plot of composite xenoliths (from Menzies and others, 1984).

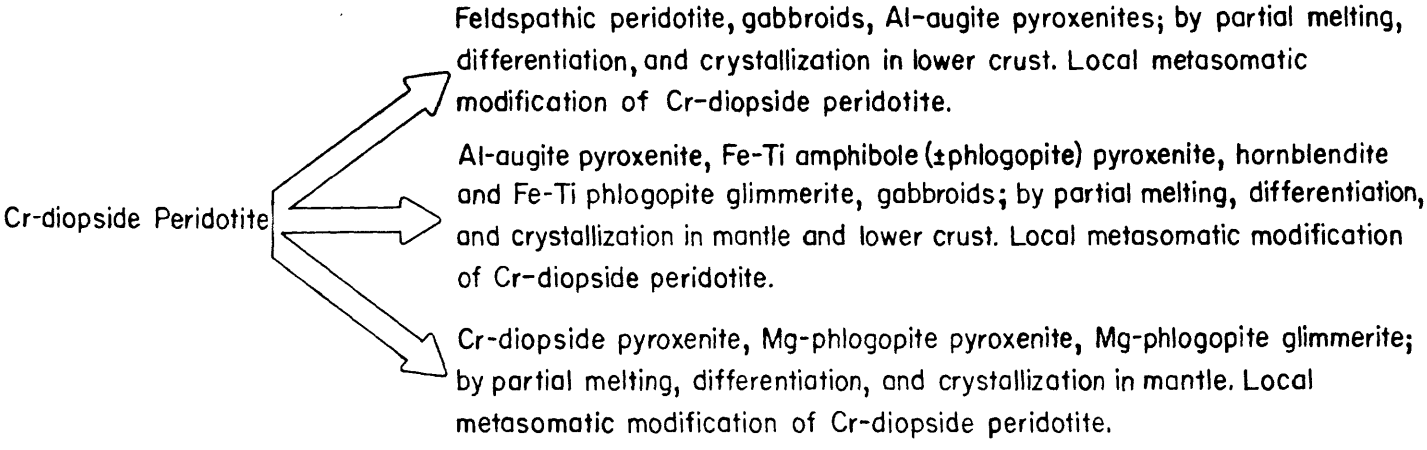

Fig. 26. Inferred source, products, and processes in formation of common xenolith groups.

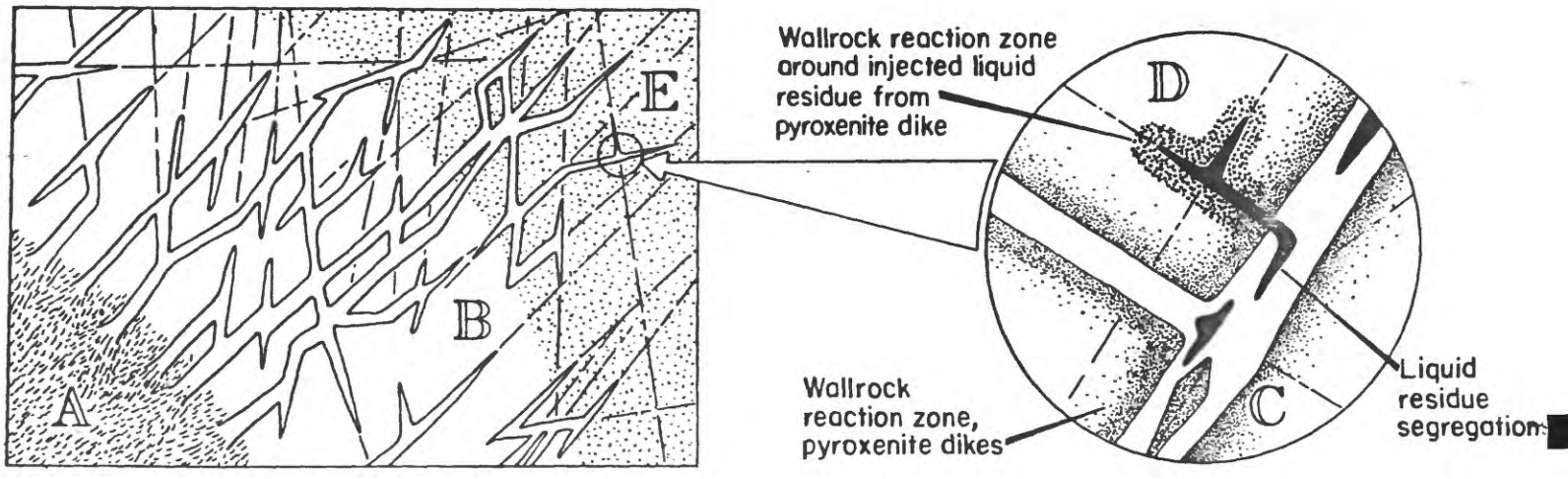

Fig. 27. Schematic representation of source and emplacement zones of one generation of dikes. Pt. A identifies a condition in which melts are concentrated in dikes and veins within the zone of melting. Pt. B identifies zone of melt injection in which melts are not in equilibrium with adjacent peridotite. Pt. C identifies a condition in which liquid residues are segregated within, but are not separated from their parent dike. Pt. D identifies liquid residues separated from their parent dike. Pt. E identifies a planar fracture system that is propagated in front of the zone of hydrous liquid intrusion by a gas phase evolved from the hydrous liquid. Reaction between melt or gas phases and wallrock can be anticipated under conditions of Pts. B and D, but not of Pts. A and C.

MPM29-wilshire-draft-8/5/81 includes tables 1, tables 2, tables 3 and tables 4; revised 11/12/81; sw 3/15/84; 4/23/81; wilshire/sw

Table 1. Distribution and Relative Abundancies of Xenoliths and Megacrysts

Locality[1/]	Crustal Xenoliths				Gabbroid and Metagabbroid Groups				Cr-diopside Group	
	Sedimentary	Silicic Igneous	Mafic Igneous	Metamorphic	Black Pyroxene		Green Pyroxene		Peridotite	Pyroxenite
					Gabbroid	Metagabbroid	Gabbroid	Metagabbroid		
1. Gilroy, California (Gi-1)				X			X	XY	XXY	XY
2. Gilroy, California (Gi-2)							XY	X	XXY	XY
3.										
4. San Quintin, Baja, CA (SQ-1)								(X)	XXY	Y
5. San Quintin, Baja, CA (SQ-4)	X							(X)	XXY	XY
6. San Quintin, Baja, CA (SQ-7)									XXY	Y
7. Jackson, California										
Jackson, Butte				X					(XX)	
8. Jackson, California										
Golden Gate Hill				X					(XX)	
9. Big Creek, California										
10. Pinchot, California (Pi-1)		X							XX	
11. Pinchot, California (Pi-2)		X							XXY	XY
12. Mariposa, California (Ma-1)		X		X						
13. Waucoba, California (Wu-2)										
14. Waucoba, California(Wu-4)										
15. Panamint Valley, CA (DV-7)										
16. Black Rock Summit, NV (LC)					X				X	
17. Black Rock Summit, NV (TM-1)					X				X	
18. Black Rock Summit, NV (TM-2)					X					
19. Black Rock Summit, NV (EC-1)					XXY	X?				
20. Malapais Hill, CA (LH-1)		X							XXY	Y
21. Old Woman Springs, CA (OW-1)									XXY	XY
22. Old Woman Springs, CA (OW-3)		X		X				(X)	XXY	Y
23. Deadman Lake, CA (DL-5)						X		X	XXY	Y
24. Deadman Lake, CA (DL-6)										
25. Deadman Lake, CA (DL-7)									XX	
26. Deadman Lake, CA (LM-1)									XX	X
27. Deadman Lake, CA (DL-8)									XXY	XY
28. Deadman Lake, CA DL-9)									XXY	X
29. Deadman Lake, CA (DL-10)									XX	
30. Deadman Lake, CA (DL-11)									XX	
31. Deadman Lake, CA (DL-16)						X			XXY	XY
32. Dish Hill, CA (Ba-1)									XXY	Y
33. Dish Hill, CA (Ba-2)						X		X	XXY	XY
34. Hill 1933, CA (Ba-3)		X							XXY	XY

35. Hill 1933, CA (Ba-4)											~~	
36. Dish Hill, CA (Ba-5)											XX	
37. Cima Field, CA (Sb-4)									X		X	
38. Cima Field, CA (Ki-1)		X		X					X		XXY	XY
39. Cima Field, CA (Ki-2)		X			XY						XY	
40. Cima Field, CA (Ki-5)					XX	X?					XXY	XY
41. Hoover Dam, AZ (BC-1)		X		X							XXY	
42. Wikieup, AZ (WK-1)	X	X		X	XY							
43. Chino Valley, AZ												
44. Grand Canyon, AZ (GC-1)	X										XX	X
45. Grand Canyon, AZ (GC-2)	X	X									XX	
46. Grand Canyon, AZ (GC-3)											XXY	XY
47. Williams, AZ (Wi-1)	X	X	(X)		X	X					X	X
48. Crater 160, AZ (SP-1)					X							
49. Hopi Field, AZ (FC-1)												
50. Hopi Field, AZ (FG-2)	X	X		X								
51. Hopi Field, AZ (FC-3)												
52. Hopi Field, AZ (GL-1)												
53. Navajo Field, AZ (MC-1)	X			X							X	
54. Navajo Field, AZ (MC-2)		X			(XX)							
55. Navajo Field, AZ (The Thumb)				X							(X)	
56. Hopi Field, AZ (GL-2)		X	X	X							XX	
57. Bandera, NM				X							XX	
58. Puerco Plugs, NM (MQ-1,2	X	X			X						XXY	XY
59. Puerco Plugs, NM (MG-3)											X	
60. Puerco Plugs, NM (GP-1)	X										XXY	XY
61. Puerco Plugs, NM (GP-2)	X										XXY	XY
62. Elephant Butte, NM (TR-1)		X				X					XXY	XY
63. San Carlos, AZ (SC-1)					XY						XXY	XY
64. San Carlos, AZ (SC-2)											XXY	XY
65. San Bernardino Valley, AZ (Pm-1)					X?	X?					XX	
66. Potrillo maar, NM (Ep-1)	X	X	X	X	(X)						XXY	XY
67. Kilbourne Hole, NM (EP-3)	X	X	X	X	X	XY					XXY	XY
68. Knippa, Texas (Sa-1)											XX	

X = present XX = abundant type in the mafic-ultramafic suites Y = present as a component of composite xenoliths (X) = present, classification uncertain

1/ See Appendix A for locality descriptions. Sample codes shown in parantheses

2/ (B) = Fe-rich olivine, black Al-Ti augite

3/ NR = Information not recorded

Table 1 (2)

	Al-augite Group			Feldspethic Ultramafic Group		Garnetiferous Ultramafic Group		"Bottle Green" Px Group		Structures	
	Peridotite	Pyroxenite Wehrlite	Hornblendite	Peridotite	Pyroxenite	Peridotite	Pyroxenite	Peridotite	Pyroxenite	Planar Fecets, Internal Fractures	Polished Frecture
1.	X	XY			X						
2.	X			X						X	
3.											
4.										X	X
5.										X	X
6.										X	
7.											
8.											
9.										NR[3/]	
10.									X	NR	
11.	Y	XY			X				X	NR	
12.											
13.								(X)	(X)	NR	
14.								(X)	(X)	NR	
15.	X	X								NR	
16.	X	X						XXY	XY	NR	
17.	X	X						XXY	XY	NR	
18.	X	X						XXY	XY	NR	
19.	X	XXY	X?	X	X					X	
20.	X?	X								NR	
21.		X							X	X	
22.								X		X	
23.		XY	Y						X	X	X
24.		X									
25.										NR	
26.										NR	
27.										NR	
28.		X	Y							NR	
29.										NR	
30.										NR	
31.	X									X	
32.		X	Y							X	
33.	Y	XY	Y				X			X	X
34.		X?								X	
35.											
36.	Y	XY								NR	
37.	(XX)	X						(XX)	(X)		
38.	XXY	XXY		X						NR	
39.	XXY	XXY	X						(X)	NR	
40.		X	Y	XXY	Y					X	
41.	(X)		Y								
42.	XXY	XXY	X					XXY	XY	NR	
43.											
44.										NR	
45.										NR	
46.	X	X							X		
47.	Y	XY	X					XX	XX		
48.	X	XX						X	XX		
49.		X?									
50.			X								
51.	X	XX									
52.	Y	XY	X								
53.		(X)								NR	
54.											
55.	(X)					XX	X				
56.											
57.	X	X						X	XX	X	
58.		X									
59.	X	X							(X)		
60.	XY	XY								X	
61.		X								X	
62.	X?	X							X?	X	
63.	XY	XY	XY						X		
64.									X		
65.	X?	X									
66.		X								X	
67.	XY	XY	Y							X	
68.											

pg 86

Table 1 (3)

	Megacrysts					
	Olivine	Pyroxene	Amphibole	Mica	Feldspar	Spinel
1.	X(B)[2/]	X(B)			X	
2.	X(B)	X(B)			X	
3.						
4.						
5.						
6.						
7.						
8.						
9.						
10.						
11.	X X(B)	X(B)				
12.		X(B)				
13.		X(B)				
14.						
15.	X(B)	X(B)				
16.	X X(B)	X X(B)			X	
17.	X X(B)	X X(B)			X	
18.	X X(B)	X X(B)			X	
19.						
20.		X(B)				
21.	X X(B)					
22.						
23.						
24.		X(B)	X			
25.		X(B)	X			
26.		X(B)				
27.		X(B)				
28.		X(B)	X			X
29.		X(B)				
30.						
31.						
32.						
33.		X(B)	X			X
34.						
35.						
36.						
37.						
38.		X(B)				
39.		X	X		X	
40.						
41.	X(B)	X(B)	X	X	X	
42.			X			
43.						
44.						
45.						
46.		X(B)				
47.						
48.		X(B)				
49.		X(B)	X			
50.		X(B)	X			
51.						
52.			X			
53.						
54.						
55.						
56.						
57.	X(B)				X	
58.	X					
59.	X(B)	(XB)				X
60.						
61.						
62.		X(B)				
63.	X(B)	X(B)	X		X	
64.	X(B)	X(B)	X		X	
65.						
66.		X(B)	X			
67.	X X(B)	X(B)				
68.						

Table 2. Chemical Parameters of Host Rocks of the Xenoliths[1/]

Locality	Normative Ne	Mg/Mg+Fe X100	$Na+K/SiO_2$	References and notes
1. Gilroy, CA (Gi-1)	0.0	57.8	0.10	Nakata (1977)
2. Gilroy, CA (Gi-2)	0.0	60.3	0.10	Nakata (1977)
4. San Quintin (SQ-1)	5.0	49.3	0.13	
5. San Quintin (SQ-4)	3.5	57.8	0.12	
San Quintin (SQ-6)	4.5	57.2	0.12	Nonxenolithic
6. San Quintin (SQ-7)	5.2	58.0	0.12	
7. Jackson, CA (RJ-7)	0.0	64.0	0.12	
9. Big Creek, CA	0.0	55.1*	0.12	
Big Creek, CA	0.0	72.1	0.10	
11. Pinchot, CA (Pi-2)	5.9	66.5	0.12	
12. Mariposa, CA (Ma-1)	0.0	63.1	0.11	
13. Waucoba, CA (Wu-1)	0.0	62.6	0.10	Nonxenolithic
Waucoba, CA (Wu-2)	8.7	67.5	0.12	
Waucoba, CA (Wu-3)	0.0	65.5	0.08	Nonxenolithic
14. Waucoba, CA (Wu-4)	8.0	67.4	0.12	
Waucoba, CA (Wu-5)	0.0	61.6	0.09	Nonxenolithic
16. Black Rock Summit, NV (LC)	11.6	65.6	0.12	Vitaliano & Harvey (1965)
16. Black Rock Summit, NV (LC)	11.0	59.3	0.12	Scott and Trask (1971) #9
16. Black Rock Summit, NV (LC)	13.7	58.3	0.13	Scott and Trask (1971) #10
17-19. Black Rock Summit, NV (TM, EC)	11.3	55.0	0.13	Scott and Trask (1971) #8
17-19. Black Rock Summit, NV (TM, EC)	12.9	53.8	0.14	Scott and Trask (1971) #7
Black Rock Summit, NV	0.0	43.0	0.10	Scott and Trask (1971) #1 Nonxenolithic
Black Rock Summit, NV	0.0	43.8	0.08	Scott and Trask (1971) #2 Nonxenolithic
Black Rock Summit, NV	0.0	59.6	0.09	Scott and Trask (1971) #3 Nonxenolithic
Black Rock Summit, NV	4.3	48.8	0.12	Scott and Trask (1971) #4 Nonxenolithic
Black Rock Summit, NV	0.0	48.8	0.10	Scott and Trask (1971) #5 Nonxenolithic
Black Rock Summit, NV	6.3	56.7	0.10	Scott and Trask (1971) #6 Nonxenolithic

[1/]Complete analyses in Appendix II

Table 2. Chemical Parameters of Host Rocks of the Xenoliths[1/]

Locality	Normative Ne	Mg/Mg+Fe	$Na+K/SiO_2$	References and notes
20. Malapai Hill, CA	4.2	52.8	0.12	Stull and McMillan (1973)
Malapai Hill, CA	8.1	53.7	0.11	Stull and McMillan (1973)
Malapai Hill, CA	9.3	53.2	0.12	Stull and McMillan (1973)
Malapai Hill, CA	5.6	53.9	0.11	Stull and McMillan (1973)
Malapai Hill, CA	7.0	53.2	0.11	Stull and McMillan (1973)
Malapai Hill, CA	10.2	52.6	0.12	Stull and McMillan (1973)
Malapai Hill, CA	9.2	51.0	0.11	Stull and McMillan (1973)
21. Old Woman Spring CA (OW-1)	3.9	57.9	0.12	
Deadman Lake, CA (DL-1)	8.7	63.8	0.13	Nonxenolithic
Deadman Lake, CA (DL-4)	4.0	55.8	0.12	Nonxenolithic
23. Deadman Lake, CA (DL-5)	2.1	61.8	0.10	
27. Deadman Lake, CA (DL-8)	7.3	61.1	0.13	
Deadman Lake, CA (DL-13)	4.9	53.6	0.12	
Deadman Lake, CA (DL-14)	7.9	56.7	0.13	
32. Dish Hill, CA (Ba-1)	12.2	58.1	0.14	
33. Dish Hill, CA (Ba-2)	9.2	59.3	0.13	Bomb
33. Dish Hill, CA (Ba-2)	5.7	58.7	0.13	Flow
34. Hill 1933, CA (Ba-3)	5.6	56.7	0.12	Flow
34. Hill 1933, CA (Ba-3)	6.8	60.0	0.12	Bomb
36. Dish Hill, CA (Ba-5)	9.5	62.2	0.15	
Cima Field, CA (Sb-2)	6.2	52.8	0.14	Nonxenolithic
37. Cima Field, CA (Sb-4)	5.6	58.1	0.12	
38. Cima Field, CA (Ki-1)	3.5	55.9	0.13	
39. Cima Field, CA (Ki-2)	2.4	58.3	0.12	
Cima Field, CA (Ki-3)	5.5	60.1	0.12	Nonxenolithic
40. Cima Field, CA (Ki-5)	2.7	55.9	0.12	
41. Hoover Dam, AZ (BC-1)	0.0	53.7	0.10	
42. Wikimup, AZ (WK-1)	4.8	63.8	0.11	
43. Chino Valley, AZ	0.0	59.7	0.13	
Chino Valley, AZ	0.0	55.1	0.13	

1/Complete analyses in Appendix II

Table 2. Chemical Parameters of Host Rocks of the Xenoliths[1/]

Locality	Normative	Mg/Mg+Fe	$Na+K/SiO_2$	References and notes
66. Potrillo, NM				
(Ep-1)	9.9	65.7	0.11	Bomb
Potrillo, NM				
(Ep-1)	9.2	64.8	0.11	Pre-maar flow
Hunts Hole, NM				Nonxenolithic pre-maar flow
(Ep-2)	8.4	64.2	0.10	from Aden Crater
67. Kilbourne Hole, NM				
(Ep-3)	10.9	66.3	0.12	

1/ Complete analyses in Appendix II

MPM-29; HW-sw; 3/16/84;

Table 3. Normative ne, K/Na, and Heat Flow Province

Locality	Normative ne	K/Na	Heat Flow Province (μ cal/cm^{2}sec)
1	0	.25-.48	1.5-2.5
4	3.5-5.2	.48-.51	.75-1.5
7	0	.56	< .75
9	0	.87-1.20	.75-1.5
10	5.9	.63	1.5-2.5
13	0-.87	.35-.54	1.5-2.5
19	0-13.7	.32-.51	.75-1.5
20	4.2-10.2	.30-.55	1.5-2.5
21	4.0-8.7	.58	1.5-2.5
23	2.1-8.2	.35-.46	1.5-2.5
32	5.7-12.3	.17-.76	1.5-2.5
37	2.4-5.6	.37-.64	1.5-2.5
41	0	.56	1.5-2.5
42	4.9	.55	1.5-2.5
43	0	1.97-2.00	1.5-2.5
44	0-22.3	.43-.71	1.5-2.5
47	2.8	.34	1.5-2.5
48	0-0.7	.32-.54	1.5-2.5
55			
57	6.0	.47	1.5-2.5
58	0-4.8	.25-.40	> 2.5
63	12.3	.62-.66	1.5-2.5
65	0-11.8	.27-.52	1.5-2.5
66	9.3-9.9	.46-.48	> 2.5
67			

Table 4. Principal features of the ultramafic xenolith groups

GROUP

		Cr-diopside	Al-augite
A.	Rock Types	LHERZOLITE; dunite; ol-websterite; websterite; wehrlite; ol-clinopyroxenite; harzburgite; clinopyroxenite; (ol-orthopyroxenite); (orthopyroxenite); (glimmerite)	OLIVINE CLINOPYROXENITE; WEHRLITE; CLINOPYROXENITE; HORNBLENDITE; dunite; lherzolite; glimmerite (ol-websterite); (websterite)
	1. lherzolite	abundant	moderate abundance
	2. wehrlite	uncommon	abundant; opx exsolution lamellae uncommon to locally abundant
	3. harzburgite	locally common	not reported
	4. dunite	common	common; irregularly "soaked" in cpx near pyroxenite bands
	5. websterite	common; all modal variants	common; usually cpx-rich
	6. clinopyroxenite	uncommon	common; can be extremely inequigranular; large grains have ovoid and tubular cavities
	7. orthopyroxenite	uncommon	very rare, putative
	8. megacrysts	olivine; possible opx, cpx	CPX; OL; KAERSUTITE; feldspar; spinel; mica; cpy and kaersutite contain ovoid and tubular cavities
B.	Structures		
	1. layering and cross-cutting	CONCORDANT LAYERS; branching, but rarely cross-cutting	BRANCHING AND CROSS-CUTTING IGNEOUS LAYERS; pyroxene-rich dikes cross foliation of ol-rich wall rock
	2. contact relations	SHARP; PLANAR; GRADATIONAL; nonplanar	SHARP; IRREGULAR; PLANAR; GRADATIONAL
	3. inclusions	ol-rich inclusions in cpx-rich rocks	OL-RICH INCLUSIONS IN CPX-RICH ROCKS; (px-rich inclusions in ol-rich rocks)
	4. grain orientation	common	uncommon
C.	Textures	TECTONITE; RECRYSTALLIZATION; unmixing (in relics)	px-rich rocks: (?) IGNEOUS VEIN; unmixing; recrystallization; reaction; cumulus; cataclastic ol-rich rocks: RECRYSTALLIZATION; tectonite
D.	Mineralogy		
	1. relative abundance	OL; OPX; cpx; spinel; pargasite; phlogopite	CPX; OL; spinel; opx; kaersutite; Ti-phlogopite

2. composition[1/]

		Cpx	SD	Opx	SD	Ol	SD	Cpx	SD	Opx	SD	Ol	SD
*	Ca	46.1	1.4	1.8	.4			45.0	2.4	2.1	.7		
	Mg	48.5	1.6	88.2	1.3	88.9	.9	45.4	1.1	80.4	3.7	82.1	1.9
	Fe	5.4	.8	10.0	1.3	11.1	.9	9.6	2.8	17.6	3.3	17.9	1.9
**	Al	5.5	1.1	4.1	.9			6.6	1.7	5.3	1.9		
	Cr	.93	.31	.17	.13			.17	.13				
	Ti	.50	.20	1.10	.54			1.10	.54				

		Sp				Sp	
*	Fe	13.8	3.6			21.6	4.0
	Al	60.0	10.1			55.1	6.1
	Mg	20.1	2.7			17.6	2.3
	Cr	14.5	8.9			4.2	4.7

	no. samples:	48		29		19		13		16		13	
		30						19					
E.	Isotope data	Xenolith isotopic compositions not in equilibrium with host basalt; minerals usually not in internal equilibrium						Xenolith isotopic composition in apparent equilibrium with host basalt; minerals usually not in internal equilibrium; data available only for pyroxenites, wehrlites					

[1/] Compositions reported for Cr-Di, Al-Aug, and bottle-green px groups are averages of analyses from noncomposite xenoliths lacking macroscopic evidence of metasomatic effects. Insufficient data for feldspathic ultramafic group.

* Normalized atomic%
** Weight %

Feldspathic Ultramafic Group	Bottle-Green Pyroxene Group	Garnetiferous Ultramafic Group
LHERZOLITE; ol-websterite; websterite; dunite; clinopyroxenite	OL-WEBSTERITE; HARZBURGITE; WEBSTERITE; lherzolite(?); clinopyroxenite	CLINOPYROXENITE; WEBSTERITE; LHERZOLITE; amphibolite; garnet-kaersutite rock; glimmerite
common	difficult to distinguish macroscopically from Cr-Di lherzolite	locally common
none reported	none reported	none reported
none reported	locally common	none reported
rare	identifiable only by association	none reported
moderate abundance; wide modal variation	common; cpx usually dominant	locally common eclogite locally common
rare	uncommon	common
none reported	none reported	locally moderately common
not distinguishable from Cr-diopside group	CPX; OPX locally common; ol not	CPX; OPX; garnet
concordant websterite-lherzolite layering; branching, cross-cutting gabbroic layers	branching rare	concordant phase layering; cross-cutting garnet pyroxenite; pyroxenite, phlogopite-bearing layers
SHARP; PLANAR; IRREGULAR	sharp; gradational	SHARP; GRADATIONAL; PLANAR
none reported	ol-rich inclusions in px-rich rocks	ol-rich inclusions in px-rich rocks
common	uncommon	uncommon
TECTONITE; Recrystallization; replacement	TECTONITE; RECRYSTALLIZATION; unmixing in relics	TECTONITE; recrystallization; unmixing in relics
OL; OPX; CPX; plagioclase; spinel	CPX; OPX; OL; spinel	Variable location to location. CPX, OPX; OL; garnet; spinel
Insufficient data	Cpx SD Opx SD Ol SD 35.5 1.4 4.3 1.7 56.9 1.3 87.4 1.4 88.5 1.0 7.9 1.0 8.3 .6 11.2 1.0	See Arculus and Smith (1979); Schulze and Helmstaedt (1979); Ehrenberg (1979)
	6.0 1.6 3.4 .9 1.5 .2 .38 .26	
	Sp 16.0 1.6 29.4 12.0 16.8 2.1 37.3 14.2	
	23 18 10 6	
One sample: internal equilibrium between cpy and plagioclase, disequilibrium with host basalt	Xenolith isotopic compositions not in equilibrium with host basalt.	None available

Table 5. Comparison of Bulk Cehmical Differences Between Cr-diopside Lherzolite/Al-augite Lherzolite And Garnet Lherzolite/Sheared or Fertile Lherzolite

	Cr-diopside Lherzolite Aveg. (31)[1]	Al-augite Lherzolite Aveg. (11)	Coarse Gnt. Lherzolite [2] Aveg. (16)	Sheared Gnt. Lherzolite [2] Aveg. (11)	Granular Gnt. Lherzolite [3] Aveg. (4)	Sheared Gnt. Lherzolite [3] Aveg. (6)
SiO_2	44.2	42.9	43.0	43.1	44.8	42.9
Al_2O_3	2.76	2.43	1.41	1.60	.49	1.81
Fe_2O_3	.96	1.01			1.84	1.48
FeO	7.34	10.79	8.05	9.48	4.43	7.06
MgO	41.37	38.11	43.6	41.6	45.04	41.99
CaO	2.17	2.63	1.32	1.54	.80	1.82
Na_2O	.17	.13	.08	.14	.06	.21
K_2O	.04	.03	.01	.03	.03	.04
TiO_2	.09	.20	.11	.26	.03	.16

	Garnet Lherzolite & Harzburgite [4] Aveg. (11)	Fertile Lherzolite [4] Aveg. (6)
SiO_2	43.9	41.7
Al_2O_3	1.03	2.56
Fe_2O_3	2.02	2.67
FeO	5.27	7.83
MgO	42.92	39.83
CaO	.73	1.98
Na_2O	.07	.22
K_2O	.12	.06
TiO_2	.06	.19

[1] Number in paranthesis is number of samples. [2] Ehrenberg (1982b). [3] Nixon and Boyd (1973). [4] Nixon and others (1981)

Appendix I. Locality Descriptions

Localities 1, 2. Located on Gilroy 7.5' quadrangle, California, 37°05'N 121°32'W. Discovered June, 1971 by J.K. Nakata (Nakata, 1977). Xenoliths are generally small but fairly abundant. Mostly Cr-diopside lherzolite. Scarce gabbroids and Cr-diopside and feldspathic group websterite. Black clinopyroxene megacrysts common; some brown olivine and feldspar megacrysts. One composite xenolith has thin feldspar-rich vein in Cr-diopside lherzolite.

Localities 5, 6. San Quintin, Baja, California, 30°25'N 116°00'W. Sampled by H.G. Wilshire April, 1970. Basu (1977; 1979). Locality has 12 main cinder cones and several smaller advantitious cones, including Isle San Martin. SQ-1 (numbered north to south)(locality #4): small cone on SE side of main cone has moderately abundant Cr-diopside lherzolite inclusions in blocks and bombs. Scattered water-worn pebbles as at Cones 4 and 6. Xenoliths are abundant to top of Cone 1, but there is probably not much section involved. SQ-4 (locality #5): xenoliths, dominantly Cr-diopside lherzolite, most abundant in agglutinates in about the upper 1/4 of the section. Xenoliths very abundant in youngest agglutinate at crest of cone. Rare siltstone inclusions. More common, but still subordinate to lherzolite, are strongly foliated green pyroxene granulites. Some gabbro xenoliths. Largest lherzolite seen 165mm X 145 X 50. SQ-7(locality #6): Quarry exposes about middle 1/2 of section. Abundant very large xenoliths in quarry dumps. Colluvium above quarry has abundant, but generally smaller, xenoliths. Xenoliths mostly highly oxidized Cr-diopside lherzolite. Xenoliths small and scarce in Cone 8, absent in Cone 10.

Localities 7, 8. #7, Jackson Butte, located on Mokelumne Hill 7.5' quadrangle, California, 38°20'30"N 120°43'W. #8, Golden Gate Hill, located on San Andreas 7.5' quadrangle, California, 38°15'N 120°44'30"W. Discovered by R.L. Rose (Rose, 1959). Sampled by H.G. Wilshire and J.E.N. Pike, June, 1979. Cr-diopside lherzolite to 80 mm X 50 dominant. Olivine generally altered to clay minerals. Many, but not all, xenoliths have fibrous orthopyroxene reaction rims; less commonly the orthopyroxene rim is surrounded by a dark amphibole rim. Xenoliths smaller than about 20 mm are commonly entirely reacted. Amphibolite xenoliths with prominent lineations are common, as are gneiss and schist inclusions.

Locality 9. Located on Huntington Lake 15' quadrangle, California. Discovered by J.P. Lockwood. Other localities in the same general area subsequently discovered by Van Kooten (1980) and F.C.W. Dodge (Domenick and others, 1983; Moore and Dodge, 1980a,b). These localities include Chinese Peak, Huntington Lake 15' quadrangle, California. 37°13'N 119°09'W, and Hill 8056 (also known as "Blue Knob"), Merced Peak 15' quadrangle, California, 37°33'N 119°19'W. Localities sampled August, 1981 by H.G. Wilshire and J.E.N. Pike. Chinese Peak contains moderately abundant bottle-green pyroxene pyroxenites to 75 mm X 65, generally medium to fine-grained and equigranular, but some have individual grains to 11 mm. Banded coarse and fine gabbro and unbanded very fine-grained gabbro inclusions present. Micaceous clinopyroxenites to 40 mm are uncommon, and clinopyroxene-bearing orthopyroxenite is rare. Granitic inclusions are abundant. Scarce peridotite to 25 mm; bottle-green pyroxene, brownish olivine. Megacrysts of dark green

clinopyroxene to 11 mm, possibly to 52 mm. "Blue Knob" contains abundant granite and granitic gneiss inclusions, moderately abundant bottle-green pyroxene pyroxenites to 90 mm X 90, some clinopyroxene-rich bottle-green pyroxene websterite, possible Cr-diopside lherzolite to 15 mm X 15. Rare Cr-diopside (?) wehrlite to 20 mm.

Locality 10. Located on Mount Pinchot 15' quadrangle, California, 36°50'N 118°16'W. Discovered by J.G. Moore (Moore, 1963). Sampled by H.G. Wilshire and N.J. Trask, October, 1968. Abundant Cr-diopside lherzolite to 60 mm, fairly abundant "bottle-green" pyroxene pyroxenites and wehrlite, rarely with a little plagioclase; in a few of these, olivine forms loose-knit layers. Lherzolites commonly have well developed foliation with elongate orthopyroxene relics. This texture contrasts with equigranular texture of the clinopyroxenites. No composite xenoliths of lherzolite and bottle-green pyroxene pyroxenites found, but Cr-diopside websterite and olivine websterite form thin bands in some lherzolites. Al-augite clinopyroxenite and wehrlite with brown olivine and rarely with a little plagioclase are present. Some are layered with bands rich in olivine and those rich in pyroxene. One composite xenolith has Al-augite pyroxenite in contact with Cr-diopside lherzolite; olivine in the lherzolite is decidely browner closer to the contact, and the clinopyroxene loses its bright apple green color. Black clinopyroxene megacrysts to 40 mm occur, and rarely brown olivine to 20 mm and green olivine to 10 mm. Granitic inclusions very common.

Locality 12. Located on Mariposa 2° sheet, 37°01'N 118°18'W. Discovered by H.G. Wilshire and N.J. Trask, October, 1968. No published information. Rare olivine gabbro inclusions. Moderately abundant black clinopyroxene megacrysts to 8 mm. Very abundant granitic and metamorphic inclusions.

Localities 13, 14. Located on Waucoba 15' quadrangle, California. 37°00'N 118°10'W. Discovered by W.S. Wise. Sampled by H.G. Wilshire and E.C. Schwarzman, December, 1969 and subsequent dates. No published information. Small xenoliths are moderately abundant in a flow on the north side of the highest of 3 cinder cones, and in the ejecta of that cone. Xenoliths are dominantly peridotites with bottle-green pyroxene. Moderately abundant black clinopyroxene megacrysts to 40 mm. Some bottle-green pyroxene wehrlite, rare possible Cr-diopside lherzolite, some Al-augite pyroxenites.

Locality 15. Located on Death Valley 2° sheet, 36°21'N 117°32'W. Discovered by H.G. Wilshire and J.E.N. Pike, March, 1980. No published information. Very small Cr-diopside lherzolites common, larger Al-augite pyroxenite and coarse wehrlite present. Gabbro present. Scarce black pyroxene megacrysts.

Localities 16-19. Lunar Crater volcanic field; Black Rock Summit. #16 located on The Wall 7.5' quadrangle, Nevada, 38°30'N 116°00'W. #17 located on Lunar Crater 7.5' quadrangle, Nevada, 38°27'N 116°02'W. #18-19 include xenoliths from both of the other localities. Megacrysts discovered by Vitaliano and Harvey (1965). Xenoliths discovered by H.G. Wilshire and N.J. Trask, October, 1968. Subsequent studies by Trask (1969), Pike (1976), and comprehensive study by Bergman (1982). Locality 17 is flows and ejecta on the west side of Easy Chair crater. Xenoliths are mostly small (less than about 60 mm). Dominant types are Al-augite pyroxenites with or without kaersutite; wehrlites and gabbroids (with or without amphibole and biotite) are less abundant. Many xenoliths have poikilitic amphibole; in these the pyroxene is much finer

grained than in other xenoliths. Megacrysts are abundant and include black clinopyroxene, feldspar, amphibole, and green and brown olivine (to 20 mm). A few bottle-green pyroxene pyroxenites and wehrlites are present as well as scarce bottle-green pyroxene megacrysts. Dunites, both magnesian and relatively iron-rich types, are scarce. Lherzolites are reported by Bergman (1982). Locality 16 is the cone from which the conspicuous fresh flow immediately north of HW 50 was erupted. Xenoliths are moderately abundant from the lowest parts of the cone to the crest. Most are bomb cores or inclusions in basalt blocks. Xenoliths are dominantly Al-augite pyroxenite, bottle-green pyroxene wehrlite (Bergman, 1982, considers these to be members of the Cr-diopside group), Al-augite wehrlite and dunite, and magnesian dunite that is probably related to the bottle-green pyroxene wehrlite. The dunites and olivine portions of wehrlites are commonly mylonitized and have well developed foliation; pyroxenes in the wehrlites are more resistant to crushing and remain as large, deformed or undeformed relics. Mylonitized xenoliths commonly have cavities suggesting partial melting. Cr-diopside (?) lherzolites are scarce and gabbroic rocks very scarce. Composite xenoliths of Cr-diopside (?) lherzolite with net veins of bottle-green pyroxene pyroxenite are rare. Megacrysts are abundant and are dominantly black pyroxene (to sizes larger than 65 mm), green and brown olivine (to 50 mm X 50), bottle-green pyroxene (to 65 mm X 38 X 28), and feldspar. The flow that issued from this cone has abundant inclusions, dominantly Al-augite pyroxenite and wehrlite, and uncommon gabbros. Al-augite pyroxene and bottle-green pyroxene megacrysts are abundant. Counts of the inclusions in the south and north lobes of the flow, respectively, are as follows: Black pyroxene megacrysts (29%, 39%); Al-augite pyroxenite (3%, 2%); Al-augite wehrlite (10%, 5%); Gabbro (1%, 0%); bottle-green pyroxene megacrysts (16%, 16%); bottle-green pyroxene wehrlite (5%, 1%); green olivine megacrysts (12%, 14%); brown olivine megacryst (8%, 3%); dunite mylonite (8%, 0%); Cr-diopside (?) lherzolite (1%, 1%); feldspar megacrysts (8%, 20%). Pyroxene and olivine megacrysts of all types show a range of color from light to dark; there may be a continuous gradation between the black and bottle-green pyroxenes and between green and brown olivines.

Locality 20. Located on Lost Horse Mountain 15' quadrangle, California, 33°56'N 116°05'W. Discovered by Stull and McMillan (1973). Sampled by H.G. Wilshire, August, 1973. Xenoliths are mostly small (less than 20 mm) Cr-diopside lherzolite. Al-augite pyroxenites present but uncommon; possible Al-augite olivine-rich types. Granitic xenoliths common.

Locality 21. Located on Old Woman Springs 15' quadrangle, California, 34°26'N 116°41'30"W. Neville and others (1983). Sampled by H.G. Wilshire, June, 1970. Fairly abundant small xenoliths. Dominantly Cr-diopside lherzolite, minor Cr-diopside websterite. Moderately abundant Al-augite pyroxenite. Black and green pyroxene megacrysts present.

Locality 22. Located at boundary between Lucerne Valley and Old Woman Springs 15' quadrangles, California. Neville and others (1983). Sampled by H.G. Wilshire and J.K. Nakata, April, 1971. Moderate abundance of Cr-diopside lherzolites, rounded and faceted, to 300 mm, scarce Cr-diopside websterite (some as thin bands in lherzolite). Neville and others (1983) report a single garnet websterite xenolith from this locality.

Localities 23-31. #23-25, 27-31 located on Deadman Lake NE 7.5' quadrangle, California, 34°27'N-34°30'N at 116°01'W. #26 located on Lead Mountain 7.5'

quadrangle, California, 34°29'N 115°59'W. Locality 23 has summit elevation 2237; #24, 2275; #26, 2333; #27, 2232; #28, 2284; #31, 2232. All localities are on the Twenty Nine Palms Marine Corps base. Discovered by W.S. Wise, H.G. Wilshire, and J.W. Shervais, January, 1970. Wilshire and others (1980) provide information on amphibole-bearing xenoliths. There are 12, possibly 13, deeply eroded agglutinate cones and associated small flows aligned on a NE trend that, extended, includes localities 32-36. Southernmost cone contains abundant granitic inclusions, but only very small and sparse peridotites and black pyroxene megacrysts. Cone 2 contains sparse, very small lherzolite xenoliths. Cone 3 contains moderately abundant but small (about 10 mm) lherzolites and black pyroxene megacrysts in the flow on west side of the cone. Cone 4 contains no xenoliths or megacrysts. Cone 5 (locality 23) is exceptional. The agglutinate cone is offset slightly to the west from preceding maar phase tuffs. The latter contain abundant Cr-diopside lherzolite xenoliths (to 160 mm). Well-developed Cr-diopside websterite banding in lherzolites. Relatively abundant kaersutite selvages, with or without phlogopite, on planar surfaces of Cr-diopside lherzolite inclusions; some selvages, and internal veins, are dominantly phlogopite. Kaersutite veins cross cutting Cr-diopside websterite bands in lherzolite present but rare. Black pyroxene and kaersutite megacrysts common. Cone 6 has abundant black pyroxene and kaersutite megacrysts. Dike on south flank of Cone 6 has marked axial concentration of xenoliths; large Cr-diopside lherzolites, many bounded by planar facets, some by kaersutite selvages on planar facets. Pegmatitic Al-augite pyroxenite with individual grains to 90 mm. Cone 7 has sparse weathered lherzolites and black pyroxene megacrysts. The cone making up Hill 2333 (locality 26) has badly weathered Cr-diopside lherzolite and websterite xenoliths and black pyroxene megacrysts in oldest to youngest agglutinates. A dike on the south flank contains fresher inclusions of the same types. Cone 8 has fairly common Cr-diopside lherzolite and websterite xenoliths throughout. One orthopyroxenite seen. All olvine-bearing inclusions are badly weathered. Flow exposed in the crater has abundant xenoliths, mostly Cr-diopside lherzolite, some of which are banded by websterite; orthopyroxene-rich bands are present but rare. Sparse black pyroxene megacrysts. Locality 28 is agglutinate overlying a flow. The flow contains many weathered Cr-diopside lherzolites; these are less abundant in the agglutinate. Agglutinate contains abundant kaersutite and pyroxene megacrysts and some poikilitic kaersutite pyroxenites. Euhedral spinel megacrysts rare. Cone 10 is at the northern end of the chain and is nearly buried by alluvium. Inclusions are dominantly rhyolite, granite, and badly weathered lherzolite; megacrysts are rare. Cone 11 contains mostly Cr-diopside lherzolite inclusions in agglutinate and a flow. Locality 31 is a flow in Hill 2232. Inclusions are dominantly Cr-diopside lherzolite.

Localities 32-33 and 36. Located on Bagdad SW 7.5' quadrangle, California, 34°36'30" 115°57'W. Dish Hill, described by Brady and Webb (1943), Ross and others (1954), White (1966), Wilshire and Trask (1971). Xenoliths are abundant and are dominantly Cr-diopside lherzolite with less abundant Cr-diopside websterite, Al-augite pyroxenite, scarce 2 pyroxene granulite, and rare garnet websterite (as at locality 22, only a single garnet websterite xenolith has been found here). Lherzolite xenoliths are commonly faceted; some facets are coated by kaersutite selvages (the kaersutite is commonly accompanied by phlogopite, magnetite, and apatite). Of 257 xenoliths collected randomly at locality 33 (SE flank of cone, basal tuffs), 69% had at least one set of planar bounding facets lacking amphibole selvages; 16% had no

facets and no selvages, 15% had kaersutite selvages on one set of facets, and less than 1% had kaersutite selvages on 2 or more sets of facets. One xenolith had an internal kaersutite vein. Of the xenoliths with selvages, 26 of the selvages have glazed surfaces and 14 are rough, exposing many fresh cleavage faces on the amphiboles. 19 of the kaersutite selvages also contain apatite and one also contains phlogopite. These same xenoliths consist of 65% medium grained Cr-diopside lherzolite, 13% medium grained Cr-diopside lherzolite with amphibole, 10% fine grained Cr-diopside lherzolite, 6% Cr-diopside websterite, 3% relatively iron-rich lherzolite with kaersutite and 3% relatively iron-rich lherzolite lacking amphibole. Megacrysts are abundant. They are dominantly black pyroxene (to 70 mm) and kaersutite (to 40 mm); the megacrysts are generally broken fragments, the pyroxenes having conchoidal fracture, the amphiboles generally breaking along prismatic cleavages; many, however, have smoothed and glazed surfaces. A small percentage of the pyroxene megacrysts are euhedral or have some crystal faces. Euhedral inclusions of apatite, magnetite, and spinel are common as are tubular cavities; these are especially common in euhedral pyroxene megacrysts. Scarce bottle-green pyroxene megacrysts to 25 mm; small green olivine megacrysts.

Localities 34-35. Located on Bagdad 15' quadrangle, California, 34°37'15"N 115°55'W. Hill 1933 and flow. Discovered by White (1966). Sampled by H.G. Wilshire, July, 1969. Xenoliths in the agglutinate are dominantly weathered Cr-diopside lherzolite. Fresher inclusions are present in the flow which breached the north side of the cone and turned southward down the valley on the east side of Hill 1933. The xenolith assemblage is similar to that of Dish Hill, but no kersutite selvages were seen, and amphibole megacrysts are scarce.

Localities 37-40. #37 located on Trona 2° sheet, California, 35°13'N 115°47'W. First described by Barca (1966). #38-39 located on Kingman 2° sheet, Arizona, California, 35°21'N 115°40'W. Discovered by H.G. Wilshire, February, 1969. #40 located on Kingman 2° sheet, Arizona, California. 35°18'N 115°44'W. Discovered by I.D. Macgregor. Sampled by H.G. Wilshire, April, 1971, Katz and Boettcher (1980). #38 is a deeply eroded remnant of a flow and cinder cone. Abundant small Cr-diopside lherzolite (to 35 mm); a small percentage of lherzolites are feldspathic. Black pyroxene megacrysts are abundant. #39 is a deeply eroded agglutinate cone and remnant of a flow. Xenoliths are abundant and large. The dominant type is Al-augite pyroxenite, but Cr-diopside lherzolite is common, and relatively iron-rich lherzolites are present. Composite xenoliths contain both lherzolite and Al-augite pyroxenite. Bottle-green pyroxene pyroxenite present, some gabbro xenoliths. One composite xenolith of Al-augite pyroxenite cut by gabbro vein. Moderately abundant megacrysts of black pyroxene, amphibole (to 30 mm), glassy feldspar. #40 is adjacent to the cone containing Aiken Quarry. This cone is much younger than #38-39. Xenoliths are abundant and are dominantly Cr-diopside lherzolite, many of which have planar bounding faces. About 15-20% of lherzolites are feldspathic. Cr-diopside and feldspathic websterite is present as isolated xenoliths and as bands in Cr-diopside lherzolite. Medium to fine grained gabbros are moderately common, and medium to fine grained gabbro veins are present in several lherzolite xenoliths. Rare Cr-diopside lherzolites have kaersutite veins; pyroxenite (Al-augite?) with phlogopite veins rare. Chalky and glassy feldspar megacrysts to 30 mm moderately common.

Locality 41. Located on Black Canyon 15' quadrangle, Arizona, 35°56'30"

114°38'W. Megacrysts first described by Campbell and Schenk (1950). Xenoliths discovered by H.G. Wilshire, April, 1970; subsequent studies by Pike and Nakata (1979). Megacrysts and xenoliths are abundant in dikes intrusive into fanglomerate. The dikes are zoned such that larger inclusions are concentrated in the center. Inclusions are dominated by kaersutite megacrysts (to 72 mm) with lesser amounts of black pyroxene, feldspar, and olivine megacrysts and assorted silicic metamorphic inclusions and Cr-diopside lherzolite; Al-augite pyroxenites are rare. Small inclusions with kaersutite poikilitically enclosing olivine are uncommon. Lherzolites range to 150 mm, and some are faceted; one contains a thin vein of kaersutite, and another has an 8 mm thick websterite band. The kaersutite megacrysts are generally irregular in shape except for the faces controlled by prismatic cleavages.

Locality 42. Located on Wikieup 7.5' quadrangle, Arizona, 34°39'N 113°36'30"W. Discovered by Richard Shepherd. Sampled by H.G. Wilshire, November, 1970. Occurrence is a short dike intruded into a cone-shaped (?) breccia mass about 130 m in diameter in fanglomerate. The breccia is composed mostly of reworked fanglomerate in the vent and basalt bombs and blocks. The basalt blocks are conspicuously more abundant closer to the dike. The xenoliths are dominantly lherzolite whose clinopyroxenes appear darker green than normal for the Cr-diopside group; some have websterite bands. Al-augite pyroxenite and wehrlite are abundant. Lherzolites cut by anastomosing veins of Al-augite pyroxenite are moderately common. Megacrysts and aggregates of black amphibole to 110 mm are moderately abundant, along with black pyroxene. One peridotite has a 30 mm thick band of gabbro.

Locality 43. Located on Paulden 15' quadrangle, Arizona, 34°47'N 112°19'30"W. Discovered by Krieger (1965). Arculus and Smith (1979), Schulze and Helmstaedt (1979). Xenoliths abundant; Arculus and Smith (1979) report that about 60% of the xenoliths are eclogite with minor amphibole, apatite, rutile, and opaque oxides. Phase layering with varying proportions of garnet and clinopyroxene is common. 30% of the xenoliths are dominantly pargasitic amphibole with minor diopside, garnet, phlogopite, apatite, and oxides. Pyroxenites form 2-4% of the population, and the remainder is made up of various crustal rocks.

Localities 44-46. North rim of Grand Canyon, Toroweap, 36°10'N to 36°25'N 113°05'W to 113°10'W. Localities described by Best and others (1966, 1969, 1974) and Best (1970, 1974a,b, 1975a,b).#44 is Vulcans Throne. Most xenoliths appear to have been derived from a thin agglutinate bed about 2/3 of the way up the cone. Most are small (to 20 mm), but Best reports inclusions to 150 mm. Most inclusions are Cr-diopside lherzolites, a few are Cr-diopside websterite. #45 is north of Mt. Emma on the west fence line of Grand Canyon National Park. Xenoliths are abundant and range to several hundred mm across. No field count was made, but Cr-diopside lherzolite is dominant. #46 is the Toroweap flow, sampled close to the lip of the canyon. Xenoliths are moderately abundant and range to about 150 mm. Most are Cr-diopside lherzolite. Al-augite pyroxenites and wehrlites are scarce, and black pyroxene megacrysts fairly scarce. One bottle-green pyroxene pyroxenite; individual grains have tubular cavities about 1/2 mm in diameter and a few mm long. Best reported the presence of small kaersutite-garnet xenoliths.

Locality 47. Located on Williams 15' quadrangle, Arizona, 35°21'N 112°09'W. First described by Lausen (1927). Brady and Webb (1943), Stoesser

(1973; 1974). Sampled by H.G. Wilshire and N.J. Trask, October, 1968. Xenoliths are abundant, most are rounded but some are faceted. Xenoliths commonly have a distinctive irridescence caused by thin intergranular films of vesicular glass; glassy xenoliths commmonly contain vugs adjacent to which amphibole or pyroxene may display crystal faces. Most common type is bottle-green pyroxene wehrlite or lherzolite. Possible scarce Cr-diopside lherzolite. Some Al-augite pyroxenites, rarely with a small amount of plagioclase. One xenolith is composed of green clinopyroxene and phlogopite. Kaersutite is present but uncommon. Banded granulites are uncommon, gabbros fairly common; two gabbro xenoliths have "Willow Lake" type layering with alternating bands of pyroxene, plagioclase, and glass.

Locality 48. Located on S P Mountain 15' quadrangle, Arizona, 35°32'30"N 111°38'W. Xenoliths first described by Cummings (1972). Stoesser (1973; 1974). Sampled by H.G. Wilshire and N.J. Trask, October, 1968. Xenoliths abundant in 5 m thick palagonite tuff. Dominant types are Al-augite and bottle-green pyroxene pyroxenites, wehrlites, and gabbros.

Localities 49-52. The Colliseum. Located on Flagstaff 2° sheet, Arizona. Near highest point on east rim is a conspicuous gray bed in the maar deposits. Above this and in contact with it is a series of beds as much as 3 m thick rich in pyroxene and amphibole megacrysts; possible small pyroxene (?)-amphibole xenoliths. Rare granulite xenoliths. #50 is a maar crater southeast and across the road from The Colliseum. Very scarce amphibole and pyroxene xenoliths. Fair abundance of large kaersutite and pyroxene debris in volcanic blocks and in tuffs. #51, first described by Lewis (1973), is a very inconspicuous maar crater about 5 miles north of the junction of road from Dilkon and paved highway (5 miles north of Bidahochi Trading Post). Xenoliths are abundant; mostly Al-augite biotite and amphibole pyroxenites, some hornblendites (lherzite). One relatively iron-rich peridotite found. #52 located on Gallup 2° sheet, New Mexico, Arizona. 35°29'N 110°00'W. 34.1 miles west of Window Rock on Tuba City road, 8.6 miles west of Greasewood. Coalescing maar craters. At the top of the first cliff in the maar beds is a zone with volcanic bomb fragments. These have fairly abundant kaersutite megacrysts. One Al-augite peridotite with a band of biotite pyroxenite (?). Possible kaersutite-feldspar aggregates scarce.

Localities 53-54. Located on Marble Canyon 2° sheet, Arizona, 36°50'N 110°14'W. #53, Agathla Peak. Sampled by H.G. Wilshire, May, 1968. Scarce small lherzolite inclusions, one with interstitial amphibole. Scarce Al-augite pyroxenites (?). #54 is a small plug 1 and 1/4 mi west of Chaistla Butte. 36°47'N 110°14'W. Xenoliths moderately abundant; composed of varying proportions of phlotopite, green pyroxene, and plagioclase; some may have amphibole. Inclusions are as much as 150 mm across, well rounded. Most are medium grained, nonfeldspathic.

Locality 55. Located on Red Valley 7.5' quadrangle, Arizona, 36°35'30"N 109°02'30"W. The Thumb. First described by Ehrenberg (1979). Ultramafic xenoliths are moderately abundant, and are mostly garnet lherzolite, harzburgite, and dunite. One spinel lherzolite and one websterite were reported by Ehrenberg. The peridotites are mostly coarse-granular types, but a substantial minority are sheared (porphyroclastic). A few peridotites contain thin veins of variable combinations of phlogopite, chromite, clinopyroxene, orthopyroxene, and rutile. Megacrysts and very coarse grained

polycrystalline aggregates of clinopyroxene, orthopyroxene, garnet, olivine, phlogopite, and ilmenite are present.

Locality 56. Located on Gallup 2° sheet, New Mexico, Arizona, 35°56'N 109°05'W. Buell Park. Circular complex of kimberlite with a ring dike of minette on E-S sides. Buell Mtn., on the north and northwest sides is a complex of intrusive minette, kimberlite and possible minette lava lake remnant. In center of east side is a knob that stands above the surrounding kimberlite. The knob is also kimberlite and is the best place to find ultramafic inclusions. Most of these appear to be coarse-grained harzburgitic rocks that are partly to extensively altered. Abundant granitic rocks, hornblende diorite, amphibolites, rhyolite, mica schist; scarce granulite. Ultramafics, where fresh enough, are clearly spinel-bearing.

Locality 57. Bandera crater, about 20 miles southwest of Mt. Taylor, New Mexico, 35°00'N 108°04'30"W. Small ultramafic xenoliths are moderately abundant. There are three types: (1) most common, but not by much, is Cr-diopside lherzolite found as bomb cores, inclusions in blocks, and as thinly coated, faceted blocks to 90 mm. There is some modal variation, but no banding was seen; (2) bottle-green pyroxene pyroxenite and wehrlite. Most of these are small (less than 30 mm) pyroxenites. There is a range in color of the pyroxene from very dark green to pale green (not nearly as bright as the Cr diopside). The olivines are darker brown the darker the pyroxene in wehrlites. One sample has small dunite inclusions in pale green pyroxenite; (3) light dirty brown pyroxenite, wehrlite, dunite. All are small (less than 30 mm), and most are wehrlites. Olivines of the wehrlites and dunites have a distinct brown color. Megacrysts include olivine to 2-3 mm and feldspar to 30 mm. No black pyroxenes seen.

Localities 58-59. Puerco plugs. #58-59 located on Moquino 7.5' quadrangle, New Mexico. # 58 is Cerro Negro, #59 Seboyeta. Xenoliths first described by Kudo (Kudo and others, 1971, 1972). Sampled by H.G. Wilshire and J.K. Nakata, October, 1969, October, 1974. Cerro Negro is actually 3 plugs, 2 large ones and a very small outcrop on the south end. The basalt of the two main plugs (the small one may be breccia) contains abundant inclusions of sedimentary rocks to 2 m across and abundant peridotite xenoliths, mostly Cr-diopside lherzolite (to 140 mm), rarely with thin bands of websterite. Scarce isolated Cr-diopside websterite xenoliths. Rare lherzolites have bands (?) of coarse grained dunite. Moderate abundance of Al-augite pyroxenite; one has 3mm dunite inclusions. One gabbro was seen, and two bottle-green pyroxene megacrysts were found. Seboyeta is a large breccia pipe composed of broken sedimentary rocks and basalt irregularly intruded by basalt. Some of the basalt injections are themselves brecciated. The relief on the plug is due entirely to the relative abundance of basalt, the higher northern part having more basalt injections. Inclusions are not abundant and are mostly small (less than 10 mm, but as large as 30 mm). The dominant inclusion type is Al-augite pyroxenite, dunite, and wehrlite; about 10% are Cr-diopside lherzolite, a few of which have poorly developed pyroxene-rich bands. Black pyroxene and brown olivine megacrysts are common. Possible members of the bottle-green pyroxene group are reprsented by rare pyroxenites.

Localities 60-61. Puerco Plugs. Located on the Guadalupe 7.5' quadrangle, New Mexico. #60 is Cerro de Guadalupe, #61 is Cerro de Santa Clara. Cerro de

Guadalupe is a plug composed in part of breccia that is irregularly intruded by basalt. Inclusions are abundant, Cr-diopside lherzolite being dominant; these range up to 210 mm. Some lherzolites contain thin bands of Cr-diopside websterite and isolated inclusions of Cr-diopside websterite are moderately common. Al-augite pyroxenites and wehrlites are moderately abundant and range to 68mm; one has a 5mm dunite inclusion in pyroxenite. Composite inclusions with pyroxene-rich and olivine-rich members of the Al-augite group in contact are present but rare. Lherzolites intermediate between Cr-diopside types and Al-augite types are present; they are identified by the fact that orthopyroxene and clinopyroxene are still distinguishable but have noticeably darker color than their counterparts in the Cr-diopside group; the two pyroxenes are not distinguishable in hand specimen in the Al-augite group. Banded granulites present but rare. Cerro de Santa Clara is composed dominantly of basalt with a small proportion of breccia. Inclusions are abundant; Cr-diopside lherzolite is dominant. Banded types are sufficiently common that they can be found without great effort; one Cr-diopside lherzolite with a 3mm thick spinel layer was seen. Isolated xenoliths of Cr-diopside olivine websterite are moderately common. Al-augite pyroxenite and wehrlite are substantially less common than at Cerro de Guadalupe.

Locality 62. Located on Tularosa 2° sheet, New Mexico, 33°08'N 107°13'W. Discovered by V.C. Kelley. Sampled by H.G. Wilshire and J.K. Nakata, October, 1974. Exposed in a road cut directly across New Mexico HW 51 from the Elephant Butte Dam. The occurrence is in a thin (85 cm) sill-dike of basalt. Inclusions are abundant and are concentrated in the lower 40 cm of the intrusion where its dip is low. Cr-diopside lherzolite is dominant and ranges up to 230 mm. Granulites are uncommon (about 3%), and range up to about 500 mm. Al-augite pyroxenites are moderately common and range to about 300 mm. Black pyroxene megacrysts to 20 mm are sparse. Inclusions of sedimentary rock and granitic gneiss are rare. The peridotites resemble those from Kilbourne Hole in being mostly medium grained and having orthopyroxene dominant over clinopyroxene. One very small bottle-green pyroxene (?) pyroxenite was seen.

Localities 63-64. San Carlos. Located on the San Carlos 7.5' quadrangle, Arizona. #63, the agglutinate cone, is located at 33°19'30"N 110°29'30"W, #64, the flow, is located at 33°20'30"N 110°28'W. The locality was first described by Lausen (1927); subsequent studies by Ross and others (1954); Frey and Prinz (1978). The locality is rather surprising in that the cinder cone, breached by erosion on the south side, is still preserved but the flow that came from this vent caps a plateau substantially above the surrounding country. The eruption began as a maar, the distinctive beds of which are exposed east of the cinder cone and below the flow on the south side of the mesa. Apparently two flows, the lower of which is poorly exposed in the main drainage that dissects the plateau on the north, came from the vent following the maar stage of eruption, and these were followed by formation of the cinder cone as cinders mantle the upper flow over most of the plateau. #63: No xenoliths were seen in the maar beds, but they are abundant in both flows and in the cinder cone, especially in the agglutinate beds on the east side of the cone. The agglutinate and cinders on the north and east sides of the cone contain abundant Al-augite pyroxenites and wehrlites, many of which contain kaersutite. These seem on the average bigger (to 215 mm) than the Al-augite pyroxenite veins so well displayed in the flow (#64); some Al-augite pyroxenites have scattered exceptionally large grains (to 25 mm), and others

have bands of especially large grains. Composite xenoliths containing both pyroxene-rich and olivine-rich lithologies are uncommon. Cr-diopside lherzolites are present but subordinate to Al-augite types. Layered members of this group were not seen, but scarce Cr-diopside websterite inclusions were seen; these commonly have abundant large clinopyroxene relics with coarse exsolution lamellae of orthopyroxene. Pyroxenites, possibly in the bottle-green pyroxene group with dull gray-green pyroxenes are moderately common; some have relic (?) grains of pyroxene to 7 mm X 5 with conspicuous exsolution lamellae. One green pyroxenite has grain size banding. Black pyroxene, kaersutite, and feldspar megacrysts are common. #64: The younger and larger flow is incised by a north-flowing stream channel that originates at the north edge of the cone. Xenoliths are gravity sorted in the flow. The thickest zone of inclusions is quarried for peridot and the waste material is dumped along the sides of the channel. Over the years, this has resulted in exposure of literally tens of thousands of fresh xenoliths. The xenoliths are dominantly Cr-diopside lherzolite (79%) with lesser amounts of Cr-diopside websterite and orthopyroxenite (8%), Al-augite peridotite (3%) and Al-augite pyroxenite and wehrlite (10%). Some lherzolites of the Cr-diopside group have layers of pyroxene-rich members of the group; generally when more than one layer is present the layers are parallel, but some contain cross-cutting layers. Cr-diopside websterite layers that cross-cut foliation of the lherzolite are present. Three types of Cr-diopside pyroxenites are recognized, each with or without olivine: (1) Cr-diopside rich pyroxenite with as much as 15% orthopyroxene; no orthopyroxene relics, abundant clinopyroxene relics. These were clinopyroxenites before recrystallization. (2) websterites with 15-45% orthopyroxene; relics of both orthopyroxene and clinopyroxene common. These were websterites at the time of original crystallization. (3) websterites with as much as 15% clinopyroxene; orthopyroxene relics common, no clinopyroxene relics. These were orthopyroxenites before recrystallization. The orthopyroxene-rich layers commonly have a zoning such that clinopyroxene is much more abundant at the edges of the layer. Clinopyroxene-rich layers are commonly zoned such that the pyroxene becomes darker in color toward the interior of the layer, and olivine, if present, drops off rapidly in abundance toward the interior. Several lherzolites have been found that contain thin layers of Cr-diopside phlogopite pyroxenite, or just phlogopite. Kaersutite veins in Cr-diopside lherzolite are rare. Cr-diopside lherzolites containing anastomosing or cross-cutting veins of Al-augite pyroxenite and wehrlite are moderately abundant; the Cr-diopside lherzolite is generally separated from the veins by a reaction zone in which the lherzolite is conspicuously browner in color and orthopyroxene and clinopyroxene are difficult to distinguish in hand specimen (these are Al-augite lherzolites). Rare samples clearly show gradations from Mg-rich to Fe-rich peridotite with no Al-augite pyroxenite in the sample. "Depletion" zones of dunite separating pyroxene-rich and olivine-rich lithologies are uncommon. Rounded and angular inclusions of peridotite are fairly common in both Cr-diopside and Al-augite pyroxenites, a feature first noted by J.L. Carter in samples from Kilbourne Hole. Cross-cutting relationships in which Al-augite pyroxenites cross-cut foliation or pyroxene-rich bands in Cr-diopside lherzolite occur rarely. Al-augite peridotites, with or without Al-augite pyroxenite layers, commonly show highly irregular "soaking" by black pyroxene. Gabbro inclusions are rare. Black pyroxene, feldspar, olivine, and kaersutite megacrysts are uncommon.

Locality 65. Geronimo volcanic field; San Bernardino volcanic field. Located on Pedregosa Mountains 15' quadrangle, Arizona, 31°33'30"N 109°16'W. first

described by Lynch (1978). Subsequent studies by Kempton (1983) and Kempton and others (1984). Sampled by H.G. Wilshire, April, 1971. Xenoliths are very abundant at a number of individual localities in the San Bernardino Valley volcanic field. The most common types are Cr-diopside group and Al-augite group. Kaersutite pyroxenite, lherzolite, and hornblendite are moderately abundant. Gabbros are subordinate. Locality 65 has sparse, small Cr-diopside lherzolite and dunite xenoliths as inclusions in scoria blocks and in bombs. Black pyroxene, yellow-brown olivine, and feldspar megacrysts to 18 mm are sparse.

Locality 66. Potrillo maar. Located on El Paso 2° sheet, Texas, New Mexico, 31°46'N 106°59'W. First described in detail by Carter (1965, 1970). Sampled by H.G. Wilshire and J.W. Shervais, November, 1968. The maar crater is presumed to be located on a fault that also localized Hunts Hole and Kilbourne Hole maars to the northeast. Potrillo maar is located immediately south of the East Potrillo Mts. (a block of tilted Paleozoic rocks). The maar is located on thick colluvium forming the upper terrace of the Rio Grande River, on the west edge of the Rio Grande rift. Potrillo is about 1/3 in the United States and 2/3 in Mexico. Two small cinder cones in the center of the structure are in Mexico. The part of the crater on the U.S. side of the border consists of eroded well-bedded maar ejecta with thin crossbedded layers (low angle foresets away from crater) alternating with plane parallel air-fall deposits. Bomb sags are scarce and indicate steep trajectories; one has two totally different kinds of rock fragments in the same sag--remarkable considering the sparsity of the sags. The bedded ejecta consists of pulverized La Mesa material (colluvium) with sideromelane and partly crystllized vitrophyres fragments and pellets. Basalt blocks to 1 m are present along with large fragments of granitic and gabbroic rocks. At the north end of the exposures, fragments of a petrocalcic horizon to 2 m thick on La Mesa colluvium occur in the ejecta blanket. A small basalt spatter cone and flow occur at the north end of the exposures. These have fairly abundant small inclusions of Cr-diopside peridotite. Basalt blocks and bombs in the ejecta commonly contain Cr-diopside peridotite and gabbro-metagabbro inclusions; these are also common as isolated blocks. Cr-diopside websterite is very scarce both as isolated inclusions and as bands in Cr-diopside lherzolite. Al-augite pryoxenites and wehrlites are uncommon, as are black pyroxene (to 60 mm X 60 X 20) and kaersutite megacrysts. Several of the Al-augite pyroxenites and wehrlites have conspicuous cataclastic textures. The most abundant xenoliths are gabbro-diorite, a clear contrast with the Kilbourne Hole population which has abundant granulites and garnetiferous silicic gneiss); a moderate abundance of sandstone and limestone fragments occur, along with some granitic gneiss, rhyolite, pink granite, and marble. Most are rounded, and the largest is about 70 cm across.

Locality 67. Kilbourne Hole. Located on El Paso 2° sheet, Texas, New Mexico, 31°59'N 106°58'W. First described in detail by J.L. Carter (1965, 1970). Sampled by H.G. Wilshire and J.W. Shervais, November 1968. Kilbourne Hole is somewhat modified by erosion, and has no associated basalt flows or spatter cones as do Potrillo and Hunts Hole maars. A basalt flow that came from the Aden crater to the north is cut by the maar crater. It forms a prominent bench on the east side of the crater, and slivers of it collapsed into the crater during eruption. Blocks of the Aden basalt are also found in the ejecta. Both Kilbourne Hole and Hunts Hole have prominent east-side welts of ejecta, suggesting westerly winds during eruption. Xenoliths are very

abundant and occur as isolated blocks, inclusions in basalt blocks, and inclusions in basalt bombs. Xenoliths consist of common limestone, sandstone, and quartzite (scarce conglomerate fragments contain these lithologies). Abundant granulites are found, some consisting of alternating black (pyroxene) and white (plagioclase) bands; many of these are partly melted. Granitic gneiss, commonly garnetiferous, xenoliths are abundant. Rhyolite fragments to 35 cm occur locally. Peridotites are dominantly coarse grained orthopyroxene-rich lherzolites of the Cr-diopside group. Cr-diopside websterite inclusions and bands are scarce. Al-augite pyroxenites and wehrlites are moderately abundant, and composite xenoliths with pyroxene-rich bands in Fe-rich peridotite hosts can be found without difficulty. Specimens showing apparent transition between the Fe-rich and Cr-diopside peridotites occur. One Al-augite pyroxenite with two cross-cutting Al-augite wehrlite bands was found. Two Cr-diopside peridotite xenoliths with phlogopite veins and one with interleaved Cr-diopside lherzolite and granulite have been found. One xenolith has been found in which a single Cr-diopside websterite band in Cr-diopside lherzolite is cross-cut by coarse Al-augite pyroxenite.

OTHER, UNNUMBERED, LOCALITIES

MH-1 Moses Rock. Located on Mexican Hat 15' quadrangle, Arizona, 37°07'N 109°47'W. First described in detail by T.R. McGetchin (McGetchin and Silver, 1970). Sampled by H.G. Wilshire and E.C. Schwarzman, May, 1974. Inclusions are very abundant. Nonsedimentary types include abundant mafic granulites, garnet granulites, gneisses. Moderate amount of completely serpentinized harzburgite with conspicuous bastite pseudomorphs after orthopyroxene. These are rounded and tend to be substantially larger than other peridotite xenoliths. Cr-diopside group spinel lherzolites are moderately abundant, generally small and commonly partly altered. These are much finer grained than the serpentinized harzburgites. Scarce Cr-diopside olivine websterites; one small garnet-Cr-diopside rock(?), and two eclogite inclusions like those at Garnet Ridge. It seems possible that the xenoliths represent two distinct peridotite assemblages, one comprising fine-grained, relatively fresh Cr-diopside spinel lherzolite-websterite xenoliths like those in typical basalt occurrences, and another comprising coarse-grained, highly altered harzburgite-eclogite xenoliths, although a close relationship of the latter types in their place of origin has not been established.

BP-1. Located on the Burnett Peak 7.5' quadrangle, California, 35°48'N 121°11'W. Discovered by V.M. Seiders, June, 1983. Inclusions are in a small basalt intrusion-crater fill that cross-cuts serpentinite and Franciscan melange in the southern California coast ranges. The xenoliths are dominantly small (to 35mm) Cr-diopside lherzolite, some of which are bounded by 1 set of planar facets. Some lherzolites are equigranular, others are porphyroclastic. Cr-diopside websterite is uncommon. Black pyroxene (to 15 mm) and glassy and chalky feldspar (to 30 mm) megacrysts are moderately common.

Appendix II. Bulk Chemical Compositions and CIPW Norms of Host Rocks

Locality #:	1	2	4	5	(6)*	6	7	9
SiO_2	48.6	47.6	46.49	46.40	47.22	47.50	60.23	53.1
Al_2O_3	17.9	16.8	16.08	15.70	15.75	15.97	16.16	14.9
Fe_2O_3	4.8	3.6	4.07	5.64	3.50	2.02	4.83	3.9
FeO	4.4	5.8	8.46	5.90	7.38	8.65	.05	3.9
MgO	6.7	7.7	6.62	8.44	7.90	8.11	4.39	5.1
CaO	8.4	8.5	8.13	8.70	8.31	8.18	5.37	7.3
Na_2O	3.9	3.1	3.97	3.59	3.89	3.86	4.53	3.0
K_2O	.98	1.5	1.98	1.82	1.85	1.88	2.53	3.6
H_2O^+	1.3	2.59	.16	.10	.70	.21	.33	.90
H_2O^-			.14	.08	.08	.11	.05	2.1
TiO_2	.96	.88	2.77	2.66	2.37	2.55	.80	.93
P_2O_5	.51	.64	.76	.61	.67	.63	.33	.56
MnO	.15	.15	.20	.19	.18	.18	.08	.10
CO_2	.02	.20	.04	.02	.01	.01		.42
Cl			.05	.04	.06	.03	.01	
F			.08	.07	.07	.07	.08	
S								
Cr_2O_3			.02	.02	.02	.03		
NiO			.01	.02	.02	.03		
Subtotal			100.03	100.00	99.98	100.02	99.77	
Less O			.04	.04	.04	.04	.03	
Total	98.62	99.06	99.99	99.96	99.94	99.98	99.74	99.81
q							9.03	3.16
or	5.95	9.19	11.70	10.76	10.93	11.11	15.04	21.97
ab	33.91	27.19	24.00	23.62	24.25	22.82	38.49	26.22
an	29.22	28.50	20.40	21.51	20.29	20.81	16.43	17.10
lc								
ne			4.99	3.50	4.46	5.21		
hl			.08	.07	.10	.05	.02	
di	7.94	7.67	11.82	13.71	13.19	12.55	4.31	10.94
hy	3.86	6.44					9.00	10.61
ol	8.83	11.86	13.56	11.84	14.72	17.75		
cm			.03	.03	.03	.04		
mt	7.15	5.41	5.90	8.18	5.08	2.93		5.84
hm							4.86	
il	1.87	1.73	5.26	5.05	4.50	4.84	.28	1.83
ap	1.24	1.57	1.80	1.45	1.59	1.49	.79	1.37
cc	.05	.47	.09	.05	.02	.02		.99
fr			.03	.03	.02	.03	.11	
tn							1.62	

*Sample from same volcanic field, but not host rock of xenoliths. Data Sources listed in Table 2.

Appendix II. Bulk Chemical Compositions and CIPW Norms of Host Rocks

Locality #:	(9)	11	12	(13)	13	13	14	(14)	(16)
SiO_2	57.9	47.84	52.40	51.08	45.97	42.4	45.64	50.27	48.46
Al_2O_3	13.5	16.25	17.61	17.25	15.70	15.6	15.78	17.47	16.19
Fe_2O_3	1.4	2.16	1.16	3.38	3.41	7.4	2.47	5.43	6.60
FeO	4.4	6.30	5.85	4.57	5.59	.84	6.20	2.90	6.30
MgO	8.2	9.16	6.62	7.14	10.09	8.0	9.79	7.00	5.17
CaO	5.0	9.66	8.08	8.86	10.22	13.3	10.41	9.07	8.37
Na_2O	3.0	3.42	3.77	3.79	3.67	2.6	3.42	3.67	3.78
K_2O	2.6	2.16	1.91	1.50	1.81	.92	1.84	1.45	1.25
H_2O^+	2.0		.08	.06	.13	1.8	.63	.43	.14
H_2O^-	.79	.07	.06	.05	.08	.59	.30	.03	.15
TiO_2	.63	1.67	1.34	1.39	1.93	1.6	1.89	1.40	2.73
P_2O_5	.02	.77	.45	.45	.84	.71	.88	.46	.49
MnO	.10	.15	.12	.15	.16	.14	.15	.15	.18
CO_2	.03	.01	.01	.07	.14	3.8	.27	.04	.05
Cl		.01	.03	.01	.02		.02	.02	
F		.12	.07	.06	.10		.10	.08	.06
S									
Cr_2O_3		.05	.03	.02	.03		.04	.02	.01
NiO		.03	.02	.02	.03		.03	.01	.01
Subtotal		99.83	99.61	99.85	99.92	99.70	99.86	99.90	99.94
Loss on		.05	.04	.03	.04		.04	.03	.03
Total	99.57	99.78	99.57	99.82	99.88	99.70	99.82	99.87	99.91
q	7.07								
or	15.88	12.79	11.33	8.88	10.70		11.00	8.58	7.41
ab	26.23	18.07	31.80	32.04	14.89		14.44	30.95	32.10
an	16.21	22.69	25.71	25.70	21.12		22.60	27.03	23.60
lc									
ne		5.87			8.69		7.95		
hl		.02	.05	.02	.03		.03	.03	
di	7.26	15.88	9.14	11.73	18.27		17.49	11.46	11.39
hy	23.90		6.89	4.66				6.16	8.94
ol		16.22	9.46	7.98	15.02		16.41	4.20	.41
cm		.07	.04	.03	.04		.06	.03	.02
mt	2.10	3.14	1.69	4.91	4.95		3.62	5.79	9.60
hm								1.45	
il	1.24	3.18	2.56	2.64	3.67		3.63	2.66	5.20
ap	.05	1.83	1.07	1.07	1.99		2.11	1.00	1.17
cc	.07	.02	.02	.16	.32		.62	.09	.11
fr		.11	.06	.04	.05		.05	.09	.03

Appendix II. Bulk Chemical Compositions and CIPW Norms of Host Rocks

Locality #:	(16)	(16)	(16)	(16)	(16)	16	16	16
SiO_2	49.59	47.67	47.24	47.76	44.79	44.37	44.66	44.41
Al_2O_3	18.01	14.55	16.52	15.29	15.27	15.65	15.35	15.45
Fe_2O_3	5.47	5.41	3.38	5.98	4.21	4.44	3.39	2.74
FeO	4.88	6.45	8.75	6.84	8.12	7.94	7.92	8.66
MgO	4.28	9.37	6.30	6.53	8.75	7.80	8.96	8.74
CaO	9.71	9.06	8.42	9.06	10.02	9.62	10.40	10.49
Na_2O	2.81	3.05	4.15	3.45	3.51	4.32	3.67	3.99
K_2O	1.17	1.00	1.52	1.16	1.11	1.88	1.84	1.80
H_2O^+	.43	.34	.12	.14	.41	.22	.16	.11
H_2O^-	.76	.27	.06	.10	.21	.17	.04	.01
TiO_2	1.88	1.84	2.40	2.57	2.65	2.43	2.33	2.34
P_2O_5	.54	.33	.51	.48	.52	.74	.65	.73
MnO	.15	.18	.19	.18	.19	.22	.21	.22
CO_2	.10	.28	.19	.27	.03	.08	.07	.04
Cl	.01		.04	.02	.03	.04	.07	.05
F	.07	.04	.06	.06	.07	.09	.08	.08
S								
Cr_2O_3	.01	.05	.02	.03	.03	.03	.06	.06
NiO		.03	.01	.01	.02	.02	.03	.03
Subtotal	99.87	99.92	99.88	99.93	99.94	100.06	99.89	99.95
Less O	.03	.02	.04	.03	.04	.05	.05	.04
Total	99.84	99.90	99.84	99.90	99.90	100.01	99.84	99.91
q	5.14							
or	7.01	5.95	9.00	6.88	6.60	11.15	10.91	10.66
ab	24.02	25.99	26.98	29.13	18.09	12.65	10.33	8.23
an	33.56	23.22	22.16	22.96	22.91	17.98	20.31	19.16
lc								
ne			4.28		6.28	12.86	11.00	13.66
hl	.02		.07	.03	.05	.07	.12	.08
di	8.60	14.29	11.73	13.63	18.73	19.59	21.35	22.49
hy	8.39	8.04		7.79				
ol		9.58	14.35	4.13	14.71	12.57	14.76	15.33
cm	.02	.07	.03	.04	.04	.04	.09	.09
mt	8.04	7.90	4.91	8.70	6.15	6.46	4.93	3.98
hm								
il	3.62	3.52	4.57	4.90	5.07	4.63	4.44	4.45
ap	1.30	.79	1.47	1.14	1.24	1.76	1.54	1.73
cc	.23	.64	.43	.62	.07	.18	.16	.09
fr	.05	.02	.01	.04	.05	.05	.05	.03

Appendix II. Bulk Chemical Compositions and CIPW Norms of Host Rocks

Locality #:	19	19	20	20	20	20	20	20	20
SiO_2	44.8	44.88	45.31	45.20	46.10	45.90	45.20	45.00	45.00
Al_2O_3	16.5	15.60	14.76	14.94	14.81	14.95	14.70	14.81	14.72
Fe_2O_3	2.23	4.29	4.03	12.73	12.32	12.21	12.40	12.37	12.79
FeO	8.10	7.47	8.63						
MgO	10.8	7.76	7.70	8.28	7.85	8.02	7.90	7.69	7.46
CaO	10.1	9.94	7.85	7.97	8.45	8.34	8.26	8.34	8.25
Na_2O	3.43	4.13	3.64	3.33	3.58	3.11	3.19	4.01	3.86
K_2O	1.76	1.83	1.70	1.77	1.91	1.71	1.75	1.20	1.26
H_2O^+	.23	.11		2.50	2.09	2.56	2.97	2.34	2.85
H_2O^-		.13							
TiO_2	1.67	2.44	2.77	2.50	2.74	2.73	2.70	2.79	2.83
P_2O_5	.64	.73	.58						
MnO	.22	.21	.19	.21	.22	.21	.21	.21	.21
CO_2		.03							
Cl		.06							
F		.08							
S									
Cr_2O_3		.04							
NiO		.02							
Subtotal		99.75							
Less O		.04							
Total	100.48	99.71	97.16	99.43	100.07	99.74	99.28	98.76	99.23
q									
or		10.87	10.34	10.79	11.52	10.40	10.74	7.35	7.73
ab		13.87	24.01	14.18	13.78	16.68	15.12	16.41	16.85
an		18.95	19.47	21.24	19.09	22.41	21.41	19.57	19.84
lc									
ne		11.27	4.17	8.07	9.28	5.63	6.99	10.17	9.23
hl		.10							
di		20.45	13.48	16.15	19.57	16.63	17.46	19.29	18.74
hy									
ol		11.66	15.73	24.68	21.45	22.91	22.96	21.71	22.04
cm		.06							
mt		6.25	6.01						
hm									
il		4.66	5.42	4.90	5.31	5.34	5.32	5.50	5.58
ap		1.74	1.41						
cc		.07							
fr		.03							

Appendix II. Bulk Chemical Compositions and CIPW Norms of Host Rocks

Locality #:	21	(23)	(23)	23	27	(30)	(30)	32
SiO_2	45.02	45.45	45.62	44.77	44.74	45.62	44.05	44.85
Al_2O_3	14.46	15.44	16.48	15.17	15.29	16.05	15.45	15.87
Fe_2O_3	4.95	3.10	6.34	6.38	6.54	4.61	6.35	3.10
FeO	6.30	7.21	3.60	4.37	4.60	6.19	5.02	8.18
MgO	8.29	9.88	6.59	9.18	9.25	6.70	7.87	8.52
CaO	8.92	8.45	8.30	9.85	8.94	9.10	8.74	9.37
Na_2O	3.47	3.71	4.56	3.49	3.76	4.31	4.39	4.00
K_2O	2.01	2.15	1.03	1.07	1.91	1.00	1.37	2.16
H_2O^+	.84	.66	1.71	1.01	.83	1.70	1.94	
H_2O^-	.65	.10	1.03	.31	.38	.77	.82	
TiO_2	3.47	2.56	2.62	2.47	2.58	2.56	2.65	2.97
P_2O_5	.96	.59	.77	.72	.65	.81	.68	.62
MnO	.19	.18	.17	.20	.20	.21	.20	.19
CO_2	.20	.06	.16	.67	.07	.02	.18	.01
Cl	.01	.04	.02	.01	.01	.03	.02	.04
F	.07	.07	.07	.07	.07	.08	.07	.08
S								
Cr_2O_3	.04	.04	.02	.05	.04	.03	.08	.05
NiO	.03	.03	.02	.04	.03	.01	.02	.02
Subtotal	99.88	99.72	99.11	99.83	99.89	99.80	99.90	100.03
Less O	.03	.04	.03	.03	.03	.04	.03	.04
Total	99.85	99.68	99.08	99.08	99.86	99.76	99.87	99.99
q								
or	11.89	12.74	6.14	6.33	11.30	5.92	8.10	12.76
ab	22.11	15.17	31.39	25.62	18.28	27.25	22.39	10.94
an	18.00	19.34	21.73	22.65	19.26	21.66	18.50	19.12
lc								
ne	3.91	8.67	4.01	2.11	7.31	4.91	7.93	12.24
hl	.02	.07	.03	.02	.02	.05	.03	.07
di	14.75	14.63	10.67	13.47	15.85	14.38	14.98	18.53
hy								
ol	11.23	17.57	8.14	11.67	11.01	9.72	8.88	14.56
cm	.06	.06	.03	.07	.06	.04	.12	.07
mt	7.19	4.51	4.64	7.64	8.04	6.70	9.10	4.49
hm			3.20	1.12	1.00		.08	
il	6.60	4.88	5.02	4.70	4.91	4.87	5.04	5.64
ap	2.28	1.40	1.84	1.71	1.54	1.92	1.61	1.47
cc	.46	.14	.37	1.53	.16	.05	.41	.02
fr		.04		.01	.03	.02	.02	.05

Appendix II. Bulk Chemical Compositions and CIPW Norms of Host Rocks

Locality #:	33	33	34	34	36	37	38	38	39
SiO_2	42.84	46.25	44.86	45.47	44.96	47.54	48.98	47.37	47.83
Al_2O_3	15.07	16.63	15.95	15.82	15.82	16.63	16.92	16.06	17.33
Fe_2O_3	5.39	3.55	5.67	5.74	3.43	4.34	3.37	2.08	3.55
FeO	5.58	5.80	5.04	4.68	6.72	6.39	5.70	8.32	5.31
MgO	8.53	7.18	7.45	8.30	9.06	6.47	6.21	7.93	6.68
CaO	9.46	8.75	8.99	8.93	8.89	8.19	8.61	8.56	9.15
Na_2O	4.64	3.87	4.11	4.54	3.73	4.42	4.32	3.94	3.45
K_2O	.81	1.98	1.27	1.00	2.23	2.05	2.02	1.79	2.21
H_2O^+	2.61	1.60	2.12	1.79	.89	.14	.22	.24	.91
H_2O^-	.47	.89	1.02	.34	.20	.01	.21	.04	.43
TiO_2	2.73	2.46	2.52	2.31	2.66	2.69	1.74	2.67	1.97
P_2O_5	.60	.68	.70	.62	.61	.70	.63	.68	.52
MnO	.19	.17	.21	.20	.17	.18	.17	.18	.17
CO_2	.92	.05	.07	.10	.11	.02	.61	.05	.31
Cl	.03	.03	.01	.05	.04	.06	.04	.04	.04
F	.07	.07	.07	.06	.07	.07	.07	.07	.07
S					.01				
Cr_2O_3	.04	.03	.03	.04	.05	.02		.03	.02
NiO	.02	.02	.01	.02	.03	.01		.02	.01
Subtotal	100.00	100.01	100.10	100.01	99.68	99.93	99.82	100.07	99.96
Less O	.04	.04	.03	.04	.05	.04	.04	.04	.04
Total	99.96	99.97	100.07	99.97	99.63	99.89	99.78	100.03	99.92
q									
or	4.79	11.70	7.50	5.91	13.37		11.97	10.57	13.07
ab	22.06	21.95	24.42	25.44	14.13		29.81	22.71	24.51
an	18.02	22.27	21.34	20.03	20.29		21.02	20.99	25.44
lc									
ne	9.20	5.73	5.55	6.83	9.53		3.54	5.59	2.38
hl	.05	.05	.02	.08	.07		.07	.07	.07
di	14.95	12.96	14.19	15.25	15.60		11.06	13.44	11.49
hy									
ol	11.21	11.21	8.95	9.82	14.99		11.03	16.45	10.76
cm	.06	.04	.04	.06	.08			.04	.03
mt	7.82	5.15	8.21	8.32	5.05		4.90	3.01	5.15
hm									
il	5.19	4.67	4.78	4.39	5.13		3.31	5.07	3.74
ap	1.42	1.61	1.66	1.47	1.47		1.50	1.61	1.23
cc	2.09	.11	.16	.23	.25		1.39	.11	.71
fr	.03	.02	.02	.01	.03			.02	.05

Appendix II. Bulk Chemical Compositions and CIPW Norms of Host Rocks

Locality #:	Ki-3 (39)	Ki-5 40	41	42	43	43	44	45
SiO_2	47.64	47.75	42.26	46.08	61.61	58.58	43.49	45.20
Al_2O_3	15.92	16.33	14.61	16.02	13.89	14.47	13.66	15.50
Fe_2O_3	1.52	2.96	5.38	1.83	4.14	5.21	4.30	11.88
FeO	7.69	7.19	4.56	7.78	.72		6.21	
MgO	7.64	6.83	6.12	9.30	3.69	3.59	12.76	8.55
CaO	8.90	8.81	9.40	9.33	4.63	4.62	11.26	9.52
Na_2O	3.95	3.88	2.64	3.20	2.79	2.57	1.42	3.31
K_2O	1.97	1.73	1.48	1.76	5.49	5.15	.82	1.74
H_2O^+	.44	.53	3.93	1.11	.73	1.46	1.75	
H_2O^-	.19	.10	2.72	.37	.31	1.66	1.34	
TiO_2	2.50	2.40	3.18	2.17	.76	.78	1.93	2.80
P_2O_5	.63	.58	.62	.55	.36	.36	.63	
MnO	.16	.17	.05	.17	.08	.09	.17	
CO_2	.38	.48	2.99	.32		.01	.07	
Cl	.05	.04		.01			.01	
F	.06	.06		.06			.05	
S		.01	.09	.01				
Cr_2O_3		.04	BaO .16				.11	
NiO		.02					.04	
Subtotal	99.64	99.91		100.07			100.02	
Less O	.04	.05		.04			.02	
Total	99.60	99.86	100.19	100.03	99.20	98.55	100.00	98.50
q			1.97		12.69	7.91		
or	11.76	10.23	9.35	10.39	33.05	31.89	4.85	10.44
ab	23.19	27.62	23.88	18.11	24.05	22.79	11.94	9.16
an	20.29	22.21	25.28	24.17	9.33	13.35	28.51	22.64
lc								
ne	5.53	2.68		4.81				10.44
hl	.08	.07		.02			.02	
di	14.07	11.80	.27	13.20	9.08	6.72	18.01	20.79
hy			16.17		5.15	14.90	6.24	
ol	15.59	13.31		18.96			15.63	21.14
cm		.06					.16	
mt	2.23	4.30	5.69	2.65	.39		6.23	
hm			1.83		3.95			
il	4.80	4.56	6.46	4.12	1.47	1.55	3.67	5.40
ap	1.51	1.38	1.57	1.30	.87	.89	1.49	
cc	.87	1.09	7.27	.73		.02	.16	
fr	.09	.02		.02				
pr		.02	.18	.02				

Appendix II. Bulk Chemical Compositions and CIPW Norms of Host Rocks

Locality #:	46	46	46	47	48	48	48	48
SiO_2	44.30	43.70	44.90	47.31	46.2	46.8	45.8	52.7
Al_2O_3	14.55	14.18	14.18	15.47	12.7	12.2	13.0	16.3
Fe_2O_3	13.07	13.79	13.20	3.43	5.8	9.9	10.1	8.4
FeO				7.23	4.9		.20	1.0
MgO	7.55	7.64	7.89	9.31	9.6	9.3	7.9	5.4
CaO	9.10	9.31	9.10	9.68	12.2	11.8	12.0	8.2
Na_2O	4.66	4.79	3.04	3.43	2.7	2.8	3.0	3.7
K_2O	2.02	2.17	2.16	1.13	1.0	1.5	1.6	1.4
H_2O^+				.10				
H_2O^-				.09				
TiO_2	2.84	2.84	2.67	1.96	2.5	2.1	2.1	1.7
P_2O_5				.57	.80	.90	1.6	.60
MnO				.17	.20	.20	.20	.20
CO_2				.02				
Cl				.02				
F				.05				
S								
Cr_2O_3				.07				
NiO				.02				
Subtotal				100.06				
Less O				.02				
Total	98.09	98.42	97.14	100.04	98.60	97.50	97.50	99.60
q								4.73
or	12.17	11.11	13.14	6.67	5.99	9.09	9.70	8.31
ab	3.35		8.33	23.71	21.81	24.30	26.03	31.43
an	13.07	10.96	19.22	23.54	19.86	16.71	17.72	23.83
lc		1.50						
ne	19.96	22.31	9.83	2.79	.74			
hl				.03				
di	27.29	29.84	22.56	16.50	28.25	23.82	20.79	9.19
hy								9.24
ol	18.66	18.80	21.71	16.35	8.13	8.91	7.39	
cm				.10				
mt				4.97	8.53			
hm						10.15	10.36	8.43
il	5.50	5.48	5.22	3.72	4.82	.44	.87	2.55
ap				1.35	1.92	2.19	3.89	1.43
cc				.05				
tn						3.82	1.48	.89
pf						.62	1.86	

Appendix II. Bulk Chemical Compositions and CIPW Norms of Host Rocks

Locality #:	52	52	52	55	57	58	(58)	(58)	63-64
SiO_2	42.50	44.95	43.81	48.8	44.47	45.65	46.63	45.41	44.68
Al_2O_3	12.21	10.70	11.22	8.60	15.22	14.00	13.78	13.55	14.20
Fe_2O_3 —	12.74	12.16	12.25	3.89	4.39	2.98	3.37	5.88	4.72
FeO				3.85	8.42	9.94	9.72	6.49	7.85
MgO	7.92	6.81	8.33	12.3	9.30	8.38	9.13	8.28	8.82
CaO	13.58	12.88	13.00	8.81	8.80	7.71	7.87	7.27	8.30
Na_2O	3.61	2.48	3.71	1.74	3.38	3.67	3.25	3.73	4.13
K_2O	1.11	1.47	1.39	4.72	1.60	1.74	1.30	.91	2.73
H_2O^+					.28	1.28	1.63	3.72	.97
H_2O^-					.08	.74	.48	1.79	.35
TiO_2	3.69	5.20	4.44	2.44	3.04	2.88	2.13	2.06	2.84
P_2O_5	1.53	1.51	1.46	1.08	.58	.66	.43	.47	.97
MnO	.40	.21	.20	.16	.15	.19	.19	.17	.18
CO_2									
Cl									
F									
S									
Cr_2O_3									
NiO									
L.O.I.								.03	
Subtotal				2.46					
Less O									
Total	99.29	98.37	99.87	98.85	99.71	99.82	99.91	99.73	100.77
q					9.53	10.51	7.85	5.71	16.22
or	6.61	8.83	8.22		17.74	22.88	26.86	33.50	12.41
ab	2.56	16.06	5.78		21.81	16.96	19.60	18.62	12.21
an	13.93	13.95	9.87						
lc					6.01	4.81	.68		12.31
ne	15.28	2.86	13.90						
hl					14.69	14.40	14.14	13.00	18.22
di	36.17	33.70	37.00				2.13		
hy					16.64	18.87	20.71	12.70	14.04
ol	14.83	11.01	13.41					.04	
cm					6.42	4.42	5.00	9.05	6.88
mt									
hm					5.82	5.59	4.14	4.15	5.42
il	7.06	10.04	8.44		1.39	1.60	1.04	1.18	2.31
ap	3.65	3.64	3.46						
cc									

Appendix II. Bulk Chemical Compositions and CIPW Norms of Host Rocks

Locality #:	63-64	65	65	65	66	66	(67)	67	67
SiO_2	44.61	49.7	45.9	44.58	44.61	44.34	45.05	44.63	44.11
Al_2O_3 —	14.15	15.2	15.3	15.66	14.29	14.22	15.06	14.45	15.09
Fe_2O_3	6.66	10.4	11.6	2.84	1.99	2.34	1.91	2.07	
FeO	6.38			7.38	9.45	9.14	8.86	8.58	11.55
MgO	8.62	8.3	9.4	9.92	12.08	11.63	10.65	11.55	9.56
CaO	8.15	10.0	9.3	10.27	9.59	9.60	10.70	9.93	9.78
Na_2O	4.38	3.0	3.7	3.63	3.30	3.25	3.02	3.45	3.34
K_2O	2.70	.80	1.8	1.87	1.51	1.52	1.45	1.70	1.93
H_2O^+	.98			.50	.09	.72	.32	.06	.66
H_2O^-	.29			.09	.05	.11	.10	.07	
TiO_2	2.73	1.8	2.4	2.40	2.20	2.21	2.07	2.11	2.51
P_2O_5	.95			.54	.48	.48	.46	.54	.53
MnO	.20			.18	.20	.19	.18	.19	.19
CO_2				.08	.09	.05	.02	.21	
Cl				.06	.03	.06	.04	.05	
F				.08	.06	.07	.06	.05	
S				.01					
Cr_2O_3								.07	
NiO								.04	
Subtotal				100.09	100.02	99.93	99.95	99.75	
Less O				.05	.04	.04	.04	.03	
Total	100.80	99.20	99.40	100.04	99.98	99.89	99.91	99.72	99.28
q		.57							
or	16.03	4.77	10.70	11.04	8.92	8.99	8.57	10.07	
ab	14.51	25.59	22.95	8.65	9.45	10.10	9.76	8.70	
an	11.03	25.85	19.94	21.13	19.83	19.97	23.42	19.17	
lc									
ne	12.31		4.63	11.70	9.88	9.20	8.41	10.94	
hl				.10	.05	.10	.07	.08	
di	18.36	13.89	14.06	20.40	19.26	19.34	21.31	20.37	
hy		14.40							
ol	10.64		11.94	16.13	24.00	22.53	20.14	21.62	
cm								.10	
mt	9.70			4.11	2.89	3.40	2.77	3.01	
hm		10.48	11.67						
il	5.21			4.55	4.18	4.20	3.93	4.02	
ap	2.26			1.28	1.14	1.14	1.09	1.28	
cc				.18	.21	.11	.05	.48	
pf			4.11						
fr				.07	.04	.06	.04		
pr				.02					
tn		4.45							

Appendix III. Detailed Descriptions of Principal Xenolith Groups and Composite Xenoliths.

Xenoliths, other than accidental crustal xenoliths, are divided into two main groups--gabbroids and ultramafic rocks -- each of which is subdivided on the basis of textural, chemical (Appendix IV), and mineralogical (Appendix V) criteria.

Gabbroid Group

Gabbroid xenoliths with igneous textures occur as xenoliths in at least 17 localities. Most commonly the gabbroids occur as isolated, homogeneous xenoliths that range from 2 cm to 15 cm in maximum dimension. The average of 173 samples is 7 cm in largest dimension. Composite xenoliths are found at a number of localities. Most of these involve grain-size layering or compositional layering resulting from variations in proportions of mafic and felsic minerals. Layered xenoliths with comb structure are present but rare (Table 1, locality 47). Contacts between layers of different composition or grain size range from sharp to gradational. Both planar and highly irregular contacts occur. The compositionally layered xenoliths establish the close spatial relationship of rocks ranging from anorthositic to pyroxenitic in their source area.

Textures of the gabbroids are dominantly hypidiomorphic-granular, but range from those with tabular palgioclase to those in which plagioclase oikocrysts enclose mafic minerals. In some poikilitic rocks plagioclase, amphibole and clinopyroxene form oikocrysts that enclose euhedra of orthopyroxene. Several xenoliths from locality no. 40 have oikocrysts of olivine that enclose plagioclase euhedra. These unusual rocks also contain glomeroporphyritic clots of clinopyroxene formed by liquid-orthopyroxene reaction. Gabbroids with flow-alined plagioclase are uncommon but were found at two localities (nos. 64, 40). Opaque oxides and deep green hercynitic spinels occur about equally commonly as inclusions in pyroxene and as isolated grains. In some rocks vermiform clusters of oxide mineral grains are enclosed in plagioclase; they may represent the residue of clinopyroxene + spinel --- plagioclase + olivine (orthopyroxene) reaction (fig. II-2a). Some gabbroids appear to have crystallized originally as spinel clinopyroxenites, with modal coarse plagioclase having formed as a consequence of the aforementioned reaction (see Ghent and others, 1980).

Modal variants among the gabbroids include gabbronorite, olivine gabbronorite, norite, gabbro, anorthosite, olivine-hornblende gabbro, and hornblende gabbronorite. There are unequivocal gradations from these rocks through plagioclase-bearing pyroxenites to plagioclase-free pyroxenites of the Al-augite and bottle-green pyroxene groups. Gabbronorites range from orthopyroxene-dominant to augite-dominant; some contain olivine (locality no. 40) and some contain amphibole (locality nos. 16-19, 47). Considerable variation in modal composition is reflected by bulk compositions (Appendix IV). Plagioclase in gabbronorites has progressive normal zoning or, uncommonly, oscillatory zoning. Exsolution lamellae are common in orthopyroxenes in all the gabbronorites but occur only sporadically in

clinopyroxene. Clinopyroxenes in a few gabbronorites have complex exsolution(?) features. Discontinuous reaction relations observed are: olivine-orhopyroxene, olivine-clinopyroxene, and orthopyroxene-clinopyroxene. The gabbronorites grade modally to feldspathic websterite and to anorthosite.

Olivine gabbros and gabbros are about equally abundant; considerable modal variation is reflected by major variations in bulk composition (Appendix IV). Orthopyroxene is absent except as exsolution lamellae in clinopyroxene in about half of the gabbros. Olivine is commonly subhedral, but is rarely abundant. At certain localities (no. 19) amphibole is a major constituent and the rocks are classified as olivine hornblende gabbro. The amphibole poikilitically encloses clinopyroxene, both where clinopyroxene is interstitial to plagioclase and where the clinopyroxene is enclosed by plagioclase. None of the minerals shows prominent zoning. Most highly feldspathic rocks contain orthopyroxene.

Although a variety of gabbroic lithologies may be found at a single locality, certain features characterize the majority from each locality. Thus, most gabbroids from the Black Rock Summit locality (nos. 16-19) are olivine hornblende gabbros with amphibole as an important constituent. In contrast, most gabbroids from one Cima locality (no. 40) are amphibole-free gabbronorites or olivine gabbronorites, and from another Cima locality (no. 39) are gabbros with green spinel. Gabbroids from Kilbourne Hole (no. 67) are mostly amphibole-free norites and gabbronorites; moreover, anorthosites are more common there than elsewhere.

A great many gabbroids of all types have been incipiently to extensively melted and quenched. Most commonly, melting proceeded along grain boundaries until low melting components, especially amphibole and pyroxenes in the more felsic rocks, were largely or entirely melted. In a few cases, however, all mafic minerals in one part of a xenolith were melted, but remained unmelted in other parts (fig. III-2b); these melting relationships are not related to the present shapes or boundaries of the xenoliths. In many, the melt has partly crystallized yielding plagioclase, olivine, and oxide quench crystals in pale yellow to nearly opaque vesicular. In some, large skeletal olivines crystallized from the melt. Some of the medium-grained feldspathic rocks have evidently formed by partial fusion of pyroxenites followed by crystallization of olivine and plagioclase from the melt or by solid state clinopyroxene-spinel reactions. That the melts were products of partial fusion and not residual liquids resulting from incomplete crystallization (cf. J.F. Lewis, 1973; Wager, 1962; Larsen, 1979) is evident from the distribution of melt (fig. III-2b) in some gabbroids, and from the fact that metagabbroids have also undergone partial melting.

Metagabbroid Group

Gabbroids with metamorphic textures occur in at least 17 xenolith localities (Table 1), where their abundance ranges from rare to common. For the most part these are distinctive, pyroxene-bearing rocks that are easily distinguished from metamorphic rocks of crustal origin which are locally common and include mafic gneisses containing green amphibole and chlorite. The varied and complex assemblages of metamorphic rocks found at localities such as Kilbourne Hole and Potrillo maar (Padovani and Carter, 1973; 1977), however, may prove difficult to subdivide on the basis we use here. The

metagabbroids most commonly occur as isolated xenoliths that range from 2 cm to 12.5 cm (average of 25 samples is 7.7 cm in largest dimension). Many of the xenoliths are compositionally layered, mafic and felsic layers alternating (fig. III-2c). The dimensions of many of the layers are such that homogeneous xenoliths of various compositions were likely produced by mechanical breakdown of layered rocks. Layers range from lenticular to plane-parallel with sharp to gradational contacts. These layered xenoliths establish that, in the source areas, there was a close spatial relationship of rocks ranging from meta-anorthosite to metapyroxenite, and from coarse to fine grain size.

Although partly metamorphosed gabbroids are common (fig. III-2d), composite xenoliths in which igneous-textured gabbroid and metagabbroid occur as distinct masses in sharp contact with one another are rare; they are, however, difficult to recognize in the field. Composite xenoliths have been found at locality 19 in which basalt is in contact with metagabbro (fig. III-2e); the basalt bears no resemblance to the host lava of the xenoliths. The solid basalt and attached gabbro were clearly dislodged as a xenolith from the place of basalt crystallization. Isolated rounded or faceted xenoliths of basalt that is distinctly different from the host basalt also form part of the xenolith population at locality no. 40.

Textures of the metagabbroids are tabular in strongly foliated rocks or equigranular-mosaic. Many have porphyroclastic textures with deformed plagioclase relics and undeformed pyroxene relics in recrystallized matrices. The recrystallization of pyroxenes in metaggabroids yields mosaic textures that are virtually indistinguishable from those of clinopyroxenites and websterites. Symplectite intergrowths of pyroxene and green spinel are common. Unmixing textures are rare, even in relic mineral grains, as is compositional zoning. Oxide minerals, commonly hercynitic spinel, occur as equant grains or are moulded on other mineral grains. Brown amphibole partly replaces clinopyroxene as in the gabbroids; it is often difficult to determine whether the amphibole predates or postdates the recrystallization.

Modal variants among the metagabbroids are virtually identical to those of the igneous gabbroids; metagabbronorites and metagabbros are most abundant, followed by meta-olivine gabbros. Meta-anorthosites occur as discrete, homogeneous xenoliths but are uncommon. As with the gabbroids, there are unequivocal gradations from metagabbroids through metafeldspathic pyroxenites to metapyroxenites. The modal variations are reflected by ranges of bulk composition (Appendix IV) that are like those of the gabbroids.

The distinctive features that characterize the gabbroids of each locality are shared by the metagabbroids. Thus, metagabbroids from localities at which olivine hornblende gabbros dominate (e.g., no. 19), are also dominantly metamorphosed olivine hornblende gabbros. Where amphibole-free norites and gabbronorites are common, (locality nos. 40, 67) amphibole-free metanorites are also common. Certain bulk chemical features of igneous and metamorphic gabbroids are also characteristic of specific localities. For example all samples (Appendix IV) from San Quintin, including metagabbronorites and metagabbro have high Al_2O_3 and Ca/(Na+K) ratios leading to low differentiation index (D.I.). It is, however, noteworthy that all the gabbroids in contact with peridotite so far examined from locality no. 40 are olivine gabbros and meta-olivine gabbros, even though gabbronorite xenoliths are common at this locality. The metagabbronorite in contact with peridotite from Kilbourne Hole closely resembles isolated metagabbronorite xenoliths from that locality.

Partial melting has affected all varieties of metagabbroids in the same way that the gabbroids were affected. The melting ranges from incipient fusion along grain boundaries to extensive fusion of low-melting components, especially amphibole. The melt was quenched to vesicular glass plus small crystals of olivine, plagioclase, and oxides.

Mafic-Ultramafic Xenolith Groups

Rocks ranging from mafic to ultramafic in composition occur in widely varying proportions at all localities listed in Table 1. We have subdivided these rocks on the basis of modal composition, chemical composition of minerals, and textures into five types according to the plan shown in Figure 11. This classification is based principally on distinctive characteristics as seen in hand specimen; chemical gradations between types create difficulties in classification (Table 4). Nonetheless, typical members of each group are distinctive rocks in hand specimen as well as in chemical composition.

Five groups of mafic-ultramafic xenoliths are recognized. Four groups -- Cr-diopside, Al-augite, feldspathic, and bottle-green pyroxene -- are spinel-bearing, and the remaining one is garnet-bearing with or without spinel. The most abundant and widespread of these is the Cr-diopside Group (Tables 1, III-1A; fig. 12). The essential characteristics of this group include highly magnesian compositions of silicate phases, and relatively Cr-rich compositions of diopside and spinel (Table 4). All members except orthopyroxenite (dark brown to black) are bright green in hand specimen. Modal compositions are extremely variable (figs. III-3,4). The Al-augite group is also widespread (Table 1), but is generally very subordinate in abundance compared to the Cr-diopside group (Table III-1). The essential characteristics of this group are more ferruginous compositions of silicate phases than those of the Cr-diopside group, yielding yellow-brown and black colors of the rocks, relatively high Al, Ti, and Fe contents of clinopyroxene, and much higher Al/Cr ratios of spinel than in the Cr-diopside group (Table 4). Modal compositions of this group are not as variable as those of the Cr-diopside group (Fig. III-4). Rocks of the feldspathic peridotite group occur at only seven localities (Table 1), and representatives of it are not abundant at any of them. Members of this group are only distinguishable from those of the Cr-diopside group in hand specimen by the presence of feldspar. Insufficient data are available to define special chemical characteristics of this group. The bottle-green pyroxene group is moderately widespread in occurrence, but is generally subordinate in abundance to the Cr-diopside group (Table 1). The essential characteristics of this group include highly magnesian compositions of silicate phases so that the xenoliths are green in hand specimen (Table 4). However, differences that are not yet quantified yield a darker green color of clinopyroxenes than seen in Cr-diopside group xenoliths, and, at least at some localities, green color of orthopyroxene. Olivines have the same compositions as those in the Cr-diopside group, so distinguishing the groups requires the presence of clinopyroxene or green orthopyroxene. Modal compositions of a small number of xenoliths are similar to those of the Al-augite group (Fig. III-5). The garnetiferous peridotite group is very restricted in its distribution (Table 1), and generally also subordinate in abundance; it is defined by the presence of garnet, although spinel may occur (Table 4). Spinels in these rocks generally are much more like those of the Al-augite group than of the Cr-diopside group.

Cr-diopside Ultramafic Group. Members of the Cr-diopside group (Wilshire and Shervais, 1973, 1975) are characterized by highly magnesian olivine and pyroxenes and by chromian diopside and spinel (Table 4). The dominant peridotite members of this group (fig. III-3) have four phases, olivine, orthopyroxene, clinopyroxene, and spinel, whose average compositions are given in Table 4. Cr-diopside peridotites usually occur as isolated, moderately homogeneous xenoliths that range from 1 to 40 cm (average of 2,179 samples is 6 cm) in largest dimension. There is an enormous range of modal compositions (fig. III-3) and grain sizes. Field data allow the generalizations that more olivine-rich members of the group tend to have coarser grain sizes, and that modal variants with more than about 20 or 25 percent total pyroxene probably represent layers in lherzolite. Pyroxene-rich members of the Cr-diopside group (fig. III-3) are much less abundant than olivine-rich members and occur as isolated, homogeneous xenoliths that range from 1 cm to 16 cm (average of 32 samples is 5 cm), or, more commonly, as layers in composite xenoliths.

Composite xenoliths, in which pyroxene-rich and olivine-rich subtypes of the Cr-diopside group are in contact are widespread but not abundant. The modal compositions of rocks in contact in single xenoliths are variable (Fig. III-6). Most commonly only a single contact between pyroxene-rich and olivine-rich rocks is seen. Nevertheless a great many composite Cr-diopside group xenoliths have multiple contacts; usually, the pyroxene-rich rocks occur as thin layers in olivine-rich host rocks. The thickness of pyroxene-rich layers ranges from 1 mm to 182 cm (average of 149 samples is 2 cm; Table III-2. The layering is typically planar and regular, and contacts are sharp to gradational (see table III-2); the spectacular exposures of xenoliths at San Carlos, Arizona show that rocks with pyroxene contents ranging from 100 percent down to 20 or 25 percent repressent layering in normally much more olivine-rich lherzolite host rocks because parallel layers with high and low pyroxene contents are seen in the same xenolith (Table III-2). It is important to recognize that at least some of the pyroxene rich rocks of this group are younger than the peridotites; this is based on crosscutting relationships between pyroxenite layers, and between pyroxenite layers and foliation in the peridotite. In a small percentage of xenoliths from many localities, pyroxene-rich layers are separated from normal lherzolite by exceptionally olivine-rich zones ("depletion zones", Boudier and Nicolas, 1972). These dunitic rocks are commonly much coarser-grained than either the lherzolite or pyroxenite with which they are in contact. Multiple plane-parallel layering, in places deformed, is uncommon, and several xenoliths have en echelon dunite slivers in websterite. Branching layers enriched in Cr-diopside are uncommon, and crosscutting Cr-diopside layers are still less common. Inclusions of olivine-rich rock ranging in size from a few millimeters to more than 3 cm across are fairly common in pyroxene-rich layers (fig. III-2f). Generally, peridotite inclusions in the pyroxenites are irregular and roughly equant, but a few are thin screens that are isolated in the pyroxenite and oriented parallel to the pyroxenite contacts. Pyroxene-rich layers generally are parallel to foliation in the peridotite, but crosscut it in rare samples.

An important, though uncommon, type of composite xenolith consists of thin phlogopite ± Cr-diopside layers in lherzolite, and was found at San Carlos and Kilbourne Hole. The mica in these rocks has a distinctly different composition from that in the lherzolites of the Al-augite group (M. Prinz, written commun., 1973). These layers, as thin and uncommon as they are in

spinel lherzolites, provide a link with the very common phlogopite ± Cr-diopside lithology in garnetiferous xenoliths in kimberlite (glimmerite and MARID-suite rocks of Dawson and Smith, 1977; Dawson, 1980).

Textures of rocks in the Cr-diopside ultramafic group all appear to be metamorphic (Mercier and Nicolas, 1975; Pike and Schwarzman, 1977) and include allotriomorphic-granular, porphyroclastic, mosaic, and tabular textures. Allotrimorphic-granular texture is common in lherzolites. The texture is equigranular, medium-grained with interstitial spinel moulded on other grains. Olivine is commonly kink-banded. Xenoliths with porphyroclastic texture in which orthopyroxene forms porphyroclasts in lherzolite are common at localities 4, 10, and 11; those in which clinopyroxene forms porphyroclasts in lherzolite are common at San Quintin locality (no. 4) and very rare elsewhere. Olivine porphyroclasts are abundant in Cr-diopside lherzolites from San Quintin (nos. 4-6) but less common elsewhere. In contrast, porphyroclastic Cr-diopside pyroxenites with orthopyroxene and/or clinopyroxene porphyroclasts are of widespread occurrence. The pyroxenites are characterized by deformed relics of pyroxene with exsolution lamellae. Generally, the relics are set in a matrix with mosaic texture, but in places the matrix texture is allotriomorphic-granular. Medium- to fine-grained mosaic texture is common in peridotite and pyroxenite members of the Cr-diopside group at many localities. Rocks with tabular texture are comparatively scarce. It is noteworthy that the beginnings of textures strongly resembling tabular textures containing intergrowths of pyroxene and elongate euhedral olivine prisms are found in partly melted pyroxenites from which new olivine has crystallized; it is possible, as suggested by A. Nicolas (oral commun., 1973), that some peridotites with tabular texture have been partly melted.

Typical modal variants in the Cr-diopside group are shown in a composite diagram (fig. 12) that includes all field data, and figure III-5 that shows modal variants in composite xenoliths from San Carlos, Arizona. These data show that the great majority of rocks in this group are very rich in either olivine or pyroxene. As already detailed, these variants are expressed as pyroxene-rich layers in olivine-rich host rock, with olivine-rich lherzolite by far the dominant host lithology. Additional information from field counts of San Carlos, Arizona xenoliths indicates that websterites with about 15 percent or less orthopyroxene contain no orthopyroxene porphyroclasts, and websterites with less than about 15 percent clinopyroxene contain no clinopyroxene porphyroclasts. Websterites with intermediate proportions of the two pyroxenes commonly contain porphyroclasts of both mineral species, each type containing exsolution lamellae. This suggests that some websterites originally crystallized as orthopyroxenites with about 15 percent clinopyroxene in solid solution, whereas others originally crystallized as websterites, and that subsolidus unmixing and recrystallization have greatly modified the modal compositions.

Partial fusion of members of the Cr-diopside group is not commonly extensive. In a few places, incipient fusion is localized along spinel grain boundaries, but this is probably a consequence of fusion of hydrous minerals or plagioclase that commonly occur around the spinels. We believe that the Ti-rich to pargasitic amphiboles, and probably much of the plagioclase as well, crystallized in already solid peridotite (Wilshire and Trask, 1971), so that partial melting of the hydrous minerals and plagioclase is the last of a

multi-stage history. Glass and quench crystals of this origin are, as Frey and Green (1974) have noted, both common and widespread. Partial fusion of Cr-diopside websterite is extensive at locality 40 (fig. III-2g).

Al-augite Ultramafic Group--Members of the Al-augite ultramafic group (Wilshire and Shervais, 1975) are characterized by comparatively Fe-rich compositions of olivine and pyroxenes, high Al and Ti contents of clinopyroxene, and high Al/Cr ratio of spinel compared to the same minerals in rocks of the Cr-diopside group (Table 4). Some peridotite members of this group have four phases (olivine, clinopyroxene, orthopyroxene, spinel), but they are more commonly (fig. III-4) composed of olivine, clinopyroxene, and spinel whose range and average compositions are given in Table 4. Al-augite peridotites are about equally abundant as isolated, moderately homogeneous xenoliths and as composite xenoliths with pyroxene-rich and olivine-rich lithologies together (Table III-1A). Discrete peridotite xenoliths range from 1 cm to 21 cm (average of 205 samples is 5 cm), while isolated pyroxene-rich xenoliths range from 1 cm to 26 cm (average of 302 samples is 6 cm). As with the Cr-diopside group, these rocks show an enormous range of grain sizes and modal compositions; in the Al-augite group, however, coarse-grained olivine commonly occurs in websterite with equally coarse-grained clinopyroxene.

Composite xenoliths in which pyroxene-rich and olivine-rich subtypes of the Al-augite group are in contact are widespread in occurrence but are not especially abundant. Xenoliths with multiple contacts between pyroxenite and peridotite are common (fig. III-2h). Generally, the pyroxene-rich rocks occur as comparatively thin layers in olivine-rich rocks (Fig. III-7). Contacts between the two lithologies range from sharp to gradational, and are planar to highly irregular. In contrast to the Cr-diopside group, Al-augite pyroxenites commonly form irregular net veins in peridotite (fig. III-8a), whereas plane-parallel layering is scarce. Moreover, crosscutting relations between different Al-augite pyroxenite layers are considerably more common than seen in the Cr-diopside group; an exceptional example from Kilbourne Hole (fig. III-8b) has three generations of Al-augite olivine pyroxenite and wehrlite in a single xenolith. A small percentage of xenoliths have olivine-rich "depletion zones" separating pyroxenite from more pyroxene-rich peridotite. Much more common are irregular concentrations of pyroxene in peridotite adjacent to pyroxenite forming patchy wehrlite (fig. III-7h), and diffuse concentrations of pyroxene in layers parallel to dense concentrations. As in the case of the Cr-diopside group, rocks with pyroxene contents greater than about 20 percent appear to represent layers of local "soaking" adjacent to pyroxenite dikes in peridotite. Inclusions of olivine-rich rock, as much as 3 to 5 cm across, are common in the pyroxenites. These xenoliths-within-xenoliths range from equidimensional (fig. III-7h) to thin screens parallel to the pyroxenite contacts.

Composite xenoliths containing lithologies rich in hydrous phases in contact with peridotite or pyroxenite containing much lower proportions of hydrous phrases are very common. These are mostly kaersutite-rich veins in peridotite, but some are phlogopite-rich veins. The mica is considerably richer in Fe and Ti than most of the veins in the Cr-diopside group (Martin Prinz, written commun., 1973). Textures of rocks in the Al-augite group are complex and commonly ambiguous (Pike and Schwarzman, 1977). Olivine-rich

members appear generally to have metamorphic textures with allotriomorphic-granular, mosaic, and porphyroclastic textures the most commonly represented. Some of the more pyroxene-rich peridotites, however, have igneous allotriomorphic- and hypidiomorphic-granular textures, and some are probably mixtures of metamorphic olivine-rich rock and added igneous pyroxene. Originally coarse-grained Al-augite wehrlites from locality 66 are partly to extensively mylonitized, yielding distinctive porphyroclastic textures with relics of olivine and clinopyroxene in a layered matrices of fine angular fragments of clinopyroxene and recrystallized olivine with mosaic texture. The pyroxenes are broken down less readily than the olivines so that very large clinopyroxenes may be attached to finely mylonitized and recrystallized olivine pyroxenite and wehrlite. Disaggregation of such rocks doubtless yielded at least some of the common black clinopyroxene megacrysts found at many localities.

Pyroxene-rich members of the Al-augite group have both igneous and metamorphic textures, but a large group has textures lacking distinctive igneous or metamorphic features. Igneous textures of pyroxenites are mostly hypidiomorphic- to allotriomorphic-granular intergrowths in which pyroxene-pyroxene boundaries are commonly sutured. Oxide minerals occur interstitially molded on silicate minerals or as isolated grains comparable in size to the silicate minerals. Small anhedral to euhedral oxide grains are commonly enclosed in pyroxene and olivine where oxides are abundant, and in xenoliths that are especially rich in oxides, the opaque minerals may poikilitically enclose silicate grains. Orthopyroxene is generally very subordinate to clinopyroxene in abundance, and occurs either as small interstitial grains or as isolated grains of the same size as clinopyroxene. Exsolution lamellae of clinopyroxene in orthopyroxene are rare. Exsolution lamellae of orthopyroxene, ilmenite, and, uncommonly, spinel in clinopyroxene are poorly to moderately developed in these rocks. The variety of possible igneous textures in wehrlites is well illustrated by figure III-8b in which three distinctively different Al-augite pyroxenites-wehrlites are in contact. The oldest lithology is coarse-grained (allotriomorphic-granular) with clusters of large interstitial equidimensional opaque oxides and interstitial deformed olivine. The intermediate lithology is fine-grained olivine-rich wehrlite with an allotriomorphic-granular texture. Deformed olivine occurs interstitially and opaque oxides are mostly isolated equidimensional grains, but in places are anhedral inclusions in pyroxene. The youngest lithology is fine-grained olivine-poor wehrlite or olivine clinopyroxenite with anhedral to subhedral oxide grains commonly enclosed in pyroxene. Another igneous texture in some wehrlite members of the group consists of olivine subhedra poikilitically enclosed in clinopyroxene. Some such rocks have been subsequently mildly deformed and the olivine crystals kinked. Rocks with these textures have been found at four localities (nos. 13, 47, 48, 64). Kaersutite and phlogopite pyroxenites in which the hydrous phases poikilitically enclose pyroxenes and olivine are found at many localities (nos. 23, 33, 46, 19, 51) (Best, 1975a; Trask, 1969; P.H. Lewis, 1973), but are abundant at only a few (e.g., no. 51). Metamorphic textures are dominantly fine- to medium-grained mosaic and porphyroclastic textures in which 120° triple junctions of pyroxene and/or amphibole and interstitial spinel moulded on other grains characterize the recrystallized textures. These textures are considered to be metamorphic on the basis of gradations to igneous texture in the same rock (see Best, 1974b), as is fairly common, or on the basis of scattered relics of previous textures (fig. III-8c). In the

clinopyroxenites, large clinopyroxene relics (as much as 6 cm x 3 cm) are fairly common in medium-grained matrices with mosaic texture. The relics are ragged grains, commonly broken and invaded by the finer-grained mosaic pyroxenite. Unlike pyroxene relics in the Cr-diopside pyroxenites, these rarely show any signs of internal deformation. Considering the difficulties of distinguishing igneous and metamorphic textures in monomineralic rocks (Vernon, 1970), it remains possible, even where relics are present, that the later history of the matrix is igneous not metamorphic. Unfortunately, many pyroxenite members of the Al-augite group have these ambiguous textures, and most lack even the large relics. Although the mode of occurrence of many Al-augite pyroxenites as delicate net veins strongly suggest igneous emplacement (Wilshire and Shervais, 1975), we believe now that this interpretation is too simple, and one or more episodes of solid deformation may have affected them.

Typical modal variants of the Al-augite group are shown in figure 13. It should be emphasized here that orthopyroxene and clinopyroxene in rocks of this group cannot be distinguished in hand specimen. Hence, "clinopyroxene" on the triangular plots may and often does, include a small amount of orthopyroxene. Of the hundreds of thin sections cut, however, orthopyroxene is nearly always a minor component; one occurrence has been reported (Frey and Prinz, 1976) in which orthopyroxene constitutes 20% of the rock. Others (e.g. as reported by Evans and Nash, 1979 and Irving, components) with more than 40% orthopyroxene are, in our opinion, members of the Cr-diopside group in which such rocks are fairly common. Modal data for the Al-augite group show a preponderance of dunite, wehrlite, olivine clinopyroxenite, and clinopyroxenite, that contrast with dominant lherzolite in the Cr-diopside group. These variants are expressed mainly as complex clinopyroxene-rich dikes in olivine-rich host rocks. Also in contrast to the Cr-diopside group, clinopyroxene-rich and olivine-rich rocks of the Al-augite group are much more nearly equal in abundance. Oxide minerals in these rocks range from green to gray or brown, hercynitic spinel to opaque oxides. Assemblages dominantly of three phases (spinel, olivine, clinopyroxene ±minor orthopyroxene) grade modally to kaersutite (±Ti-rich mica) pyroxenites to hornblendites. Both amphibole and mica occur in discrete layers within pyroxenites, and both occur as poikilitic grains enclosing anhydrous minerals.

Partial fusion of members of the Al-augite group is seen at many localities and ranges from incipient melting along grain boundaries to extensive fusion of both hydrous (fig. III-8d) and anhydrous assemblages. The melt typically has been quenched to vesicular glass with crystallites of olivine, plagioclase, and oxide minerals. Marked zoning of relic grains is common adjacent to the glass. The melting occurred in thin dikes in peridotite of composite xenoliths as well as large, monolithologic xenoliths of the group. As with the gabbroids, igneous and metamorphic members alike of this group have undergone partial melting.

Bottle-green Pyroxene Group.--Peridotite and pyroxenite xenoliths whose pyroxene components have a distinctive deep green color that contrasts with the bright apple-green Cr-diopside and black Al-augite of the Cr-diopside and Al-augite groups occur widely (Table 1) although they are rarely abundant; they are, however, the dominant lithology at three of the central Sierra Nevada localities described by Van Kooten (1980) and at some Black Rock Summit localities described by Bergman, (1982). Only one suite of these rocks has been examined systematically for its chemical signature (Black Rock Summit,

locality 16; Pike, 1976); these rocks contain abundant Cr-rich orthopyroxene that is difficult to distinguish in hand specimen from clinopyroxene. The clinopyroxene has low Ca contents compared to those of the Cr-diopside and Al-augite groups (Pike, 1976). If these chemical compositions prove characteristic of the group, it can be called the Low-Ca clinopyroxene group. However, certain peridotites of the Cr-diopside group that have been metasomatically altered by pyroxenite or hydrous mineral veins resemble the rocks of the bottle-green pyroxene group in hand specimen but are chemically transitional between Cr-diopside and Al-augite groups. Also, the feldspathic peridotites may fall in the same compositional category. Thus, this group will remain only tentatively separable until more data are available on mineral compositions.

Clinopyroxenes of the sort occurring in pyroxenites of the bottle-green pyroxene group are found as megacrysts also (loc. nos. 16-18, 39, 48; Bergman, 1982). Similar megacrysts, also with low Ca contents, were reported by Binns (1969) and pyroxenites containing the same types of clinopyroxenes were reported by Wilkinson (1975a, b; 1976) from Australian occurrences. Stoesser (1973) reported bottle-green pyroxene pyroxenites and wehrlites from some San Francisco volcanic field occurrences, and we have found them to be abundant at the Williams locality (no. 47) and moderately abundant at Crater 160 (no. 48) in the San Francisco volcanic field. Pyroxenite members of this group appear to grade into gabbroic rocks with similar pyroxenes although this is not an established relationship.

Peridotite members of the bottle-green pyroxene group mostly have 3 or 4 of the phases olivine, clinopyroxene, orthopyroxene (mostly as exsolution lamellae in clinopyroxene where clinopyroxene is dominant), and spinel. Modal compositions are combined with those of the Al-augite group in figure III-4 and III-7. Isolated, moderately homogeneous peridotite xenoliths range from 1 to 14 cm in largest dimension (average of 244 samples is 4 cm). Pyroxenite members are composed either dominantly of clinopyroxene or dominantly of orthopyroxene; websterites with nearly equal proportions of the two have not been found. Pyroxenites occur generally as isolated, moderately homogeneous xenoliths ranging from 1 cm to 14 cm (average of 116 samples is 5 cm). Only two composite xenoliths containing two subtypes of this group have been found. One is harzburgite(?) cut by anastomizing veins of pyroxenite which contain small, irregular fragments of dunite, a xenolith-in-xenolith relationship also found in the Cr-diopside and Al-augite groups. Irving (1980) described a large composite xenolith in which a thick layer of probable bottle-green pyroxenite is in contact with lherzolite. Similar, though small, dunite inclusions in other pyroxenites of this group have been found at three localities (nos. 11, 16, 57).

Textures of rocks in the bottle-green pyroxene group range from igneous to metamorphic, with hypidiomorphic-granular and poikilitic igneous textures and porphyroclastic and allotriomorphic granular metamorphic textures dominating. Some bottle-green pyroxene peridotites have poikilitic textures in which olivine euhedra or anhedra are enclosed in clinopyroxene. Most of these appear to be igneous textures, but some have marked variations of grain size of inclusions in the pyroxenes and bizarre exsolution features. Commonly the grain size of the peridotites is too coarse to determine textural relations in the small xenoliths, but some have either hypidiomorphic- or allotriomorphic-granular igneous textures with sutured intergrowths of olivine

and clinopyroxene. Mylonitized members of the bottle-green pyroxene group are common at the same localities (nos. 16-18). These rocks consist of porphyroclasts of clinopyroxene and olivine in a matrix of fragmental clinopyroxene and spinel and recrystallized olivine with mosaic texture (figs. III-8e, f, g). In some rocks, clinopyroxene resisted the mylonitization so that the texture consists of large clinopyroxenes in finely mylonitized dunite. There can be little doubt that further mechanical breakdown of such assemblages could yield the common bottle-green pyroxene megacrysts and dunite mylonites found at the locality (Bergman, 1982).

Typical modal variants of the bottle-green pyroxene group are shown in figure III-5. The similarity of these rocks to those of the Cr-diopside Al-augite groups in most physical aspects other than in frequency of occurrence of composite inclusions, strongly suggests that the pyroxenite members of this group also formed layers in olivine-rich rock before disaggregation in the conduits.

Partial fusion of bottle-green pyroxene group rocks is widespread though generally not extensive. As with the other lithologic groups, partial melting has affected metamorphic as well as igneous members. At locality 47 (Williams, Arizona) olivine pyroxenites are commonly partly melted and vuggy. Amphibole and pyroxene adjacent to vugs display crystal faces similar to relationships noted by Griffin and others (1984) in their wehrlite suite of xenoliths. Partial fusion appears to have been contemporaneous with mylonitization of some rocks from the Black Rock Summit, Nevada field.

Feldspathic Ultramafic Group.--The feldspathic ultramafic group is macroscopically distinguished from the Cr-diopside group only by the presence of plagioclase. Moreover, at all occurrences of feldspathic peridotite xenoliths (Table 1), nonfeldspathic Cr-diopside lherzolite xenoliths are abundant. Feldspathic peridotites normally occur as isolated, moderately homogeneous xenoliths ranging from 1 cm to 14 cm (average of 25 samples is 6 cm) in largest dimension. The proportion of plagioclase is, however, quite variable within single xenoliths. Some composite xenoliths have layers of feldspathic pyroxenite in peridotite host rock. These relationships clearly establish the close proximity of feldspathic and non-feldspathic peridotites in their place of origin.

The same textural types found in the Cr-diopside group characterize the feldspathic ultramafic rocks as well. All rocks of this group appear to have metamorphic textures, the most common of which are allotriomorphic-granular, porphyroclastic, and mosaic. In all these rocks plagioclase occurs as interstitial grains molded on other grains.

Plagioclase commonly forms coronas on spinel, probably as a consequence of partial melting along spinel-clinopyroxene grain boundaries. Euhedral olivine (fig. III-8h) has crystallized along with plagioclase at these loci. Solid-state spinel-clinopyroxene reaction is a possible explanation for the coronas, but the occurrence of gabbroid dikes in lherzolite (localities 2 and 40) suggests that melting is a more likely explanation. Relic grains in porphyroclatic feldspathic ultramafic rocks are always pyroxene or olivine, and never plagioclase. Mosaic texture has formed by recrystallization of all phases, including plagioclase in some rocks. In many feldspathic peridotites, however, plagioclase appears to have formed after metamorphism and is not

recrystallized.

Typical modal variants of the feldspathic ultramafic group are like those of the Cr-diopside group with olivine-rich lherzolites dominant. Plagioclase content ranges from less than a percent to about 15 percent of the rock.

Partial fusion of feldspathic ultramafic rocks is common, but it is often difficult to determine texturally whether glass and quench crystals are residual liquids from incomplete crystallization of the feldspathic component or are the result of partial melting. Rare unambiguous examples consist of relatively coarse plagioclase and olivine and vesicular glass with small olivine crystals.

Garnetiferous Ultramafic Group:--Garnet-bearing mafic and ultramafic xenoliths have a very limited distribution in western United States basalt occurrences, and are common at only three localities (Table 2, nos. 9, 43, 55). A single garnet websterite xenolith has been found at Dish Hill (locality 33; Shervais and others, 1973), another at Fry Mountain (locality 22; Neville and others, 1983), and two garnet and kaersutite-bearing xenoliths were found at the Toroweap locality (no. 46), Best, 1975a). These rocks have very different mineralogical and textural characteristics at different localities, and probably have different origins. Most are also different from the garnet lherzolite and harzburgite that are common in kimberlites (Dawson, 1980). Garnetiferous mafic and ultramafic xenoliths in basalts are dominantly pyroxenite. The garnet peridotite and pyroxenite from Big Creek (no. 9) are pyrope lherzolite and websterite. Garnet lherzolite and harzburgite from The Thumb minette (Ehrenberg, 1979) are composed of allotriomorphic-granular, porphyroclastic, and mosaic-porphyroclastic rocks, a few of which contain pyroxene-rich lenses or 1 to 2 mm thick discontinuous vein-like concentrations of phlogopite, orthopyroxene, clinopyroxene and chromite. The allotriomorphic-granular rocks are composed of pyropic garnet and other minerals with compositions like those of the Cr-diopside group, whereas those of the porphyroclastic rocks are generally richer in Fe, Ti, and other components. Textures indicative of partial melting were described by Ehrenberg (1979).

By contrast, the garnetiferous xenolith assemblage from Chino Valley (no. 43) (Arculus and Smith, 1979; Schulze and Helmstaedt, 1979) is composed of eclogite, amphibolite, garnet websterite, and garnet clinopyroxenite. No olivine-bearing xenoliths have been found. Eclogites are commonly layered as a result of varying proportions of garnet and pyroxene, and eclogite is interlayered with amphibolite in some inclusions. Textures of the pyroxene-rich rocks are allotriomorphic-granular, porphyroclastic, and equigranular mosaic. A few samples contain substantially higher almandine and grossular components than garnet in garnet websterite from Dish Hill (Shervais and others, 1973; Beeson and Jackson, 1970).

The garnet websterite found at Dish Hill, California (Shervais and others, 1973) has a porphyroclastic texture with large deformed clinopyroxenes set in a matrix with mosaic texture. The clinopyroxene relics have exsolution lamellae of orthopyroxene and garnet. The matrix is composed of isolated grains of undeformed orthopyroxene, clinopyroxene, garnet, and spinel. In places garnet is aligned in its original position as exsolution lamellae, but the pyroxene around it has been recrystallized. Garnet of the same pyropic

composition occurs as reaction rims on green spinel. Reconstruction of the pre-exsolution composition of the pyroxenes (Shervais and others, 1973; Table III-3) shows that the rock originally crystallized as a clinopyroxenite, possibly with a few percent garnet and spinel.

This rock is virtually identical to some garnet pyroxenites from Salt Lake Crater, Oahu (Beeson and Jackson, 1970) where they have been found in contact with spinel lherzolites. Beeson and Jackson interpret the garnet pyroxenite as dikes that were emplaced in spinel lherzolites at depth in the mantle. This interpretation is probably applicable to the Dish Hill sample as well. Moreover, garnet pyroxenite also occur as dikes in spinel lherzolite in some alpine peridotites (Kornprobst, 1969; Kornprobst and Conquere, 1972; Conquere, 1977).

Best (1975a) reported two specimens of garnet-kaersutite pyroxenite from the Grand Canyon area. In these rocks, garnet and amphibole are interstitial to earlier-crystallized clinopyroxene. They appear to be rather similar to garnet-kaersutite assemblages within complex pyroxenite dike systems in the Lherz massif described by Conquere (1977).

Specimen no._____ Locality_____

Collected(?)_____

Bomb_____ Block_____ Inclusion_____ Color_____

Size of inclusion(mm) a_____ b_____ c_____

Volume(cc)_____

Angular_____ Subangular_____ Subrounded_____ Rounded_____

Slabby_____ Blocky_____ No. of facets_____

No. of internal planar fractures_____ Polished?_____

Compositional layering_____

No. of layers_____ Thickness_____

Contact: sharp_____ gradational_____

Veins

Internal_____ Selvage_____ No._____ Parallel(?)_____ Angle_____

Thickness_____ Angle to layering_____ Angle to folia_____

Size layering_____

Foliation_____ Lineation_____

Grain size(avg.)_____ Sorting g_____ m_____ p_____

Mineral proportions and textures

	Ol		Opx		Cpx		Pc	Sp	Gar	
	α	β	α	β	α	β				
% (host)										
% (layer)										
Color										
Poik. size										
Shape										
Cumulate										
Postcumulus										
Alteration %										

Remarks:_____

Fig. III-1. Field count-book form

Figure III-2. Photomicrographs and outcrop photographs of xenoliths. Number at bottom of photomicrographs indicates width of field of view. a) Deep green vermiform spinel enclosed in plagioclase of a hornblende olivine gabbro. Amphibole, generally intergrown with clinopyroxene, is locally intergrown with the spinel. b) Gabbro composed of a zone in which clinopyroxene is largely fused (right side) in relatively sharp contact with a zone containing unfused clinopyroxene. c) Layered metawebsterite (bottom) and metagabbro. The metawebsterite contains large deformed relics of orthopyroxene and a small amount of amphibole. The metagabbro is very rich in plagioclase. Both lithologies show substantial grain boundary fusion (quenched to glass). Crossed polarizers. d) Relic plagioclase in partly recrystallized 2-pyroxene gabbro. Crossed polarizers. e) Olivine basalt (left) in contact with fine-grained gabbro. f) Rounded dunite inclusion in Cr-diopside websterite xenolith. g) Extensively fused Cr-diopside websterite. Quench products include pyroxene, olivine, opaque oxide, plagioclase, and glass. h) Al-augite wehrlite cut by branhcing and cross-cutting veins of Al-augite pyroxenite. Note angular inclusion of wehrlite in pyroxenite left center.

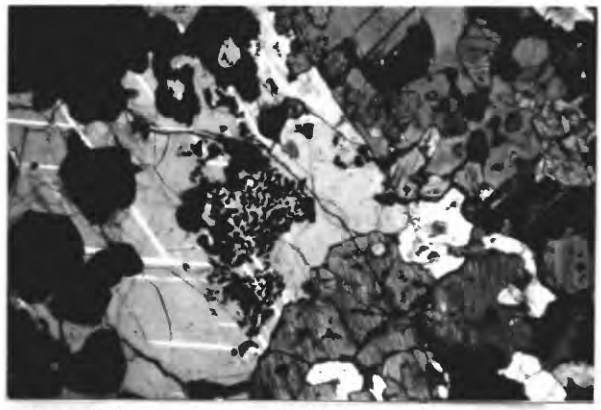

Ec-58 8.3mm a

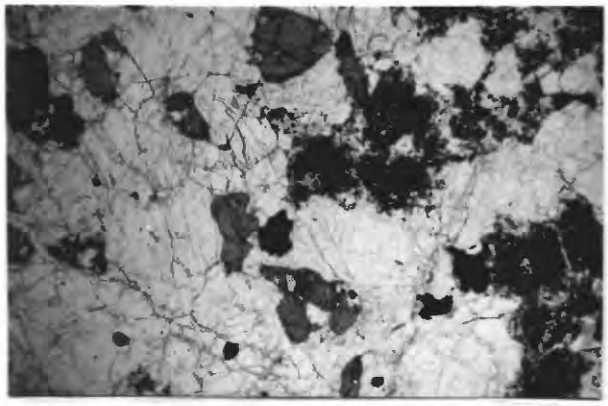

Ba-3-1 8.3mm b

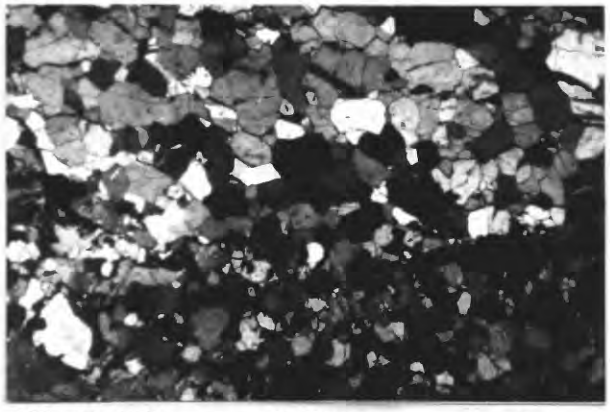

DL-5-58 8.3mm c

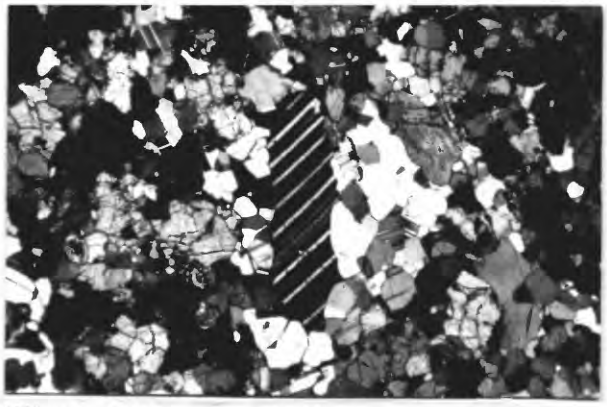

Wi-1-106 8.3mm d

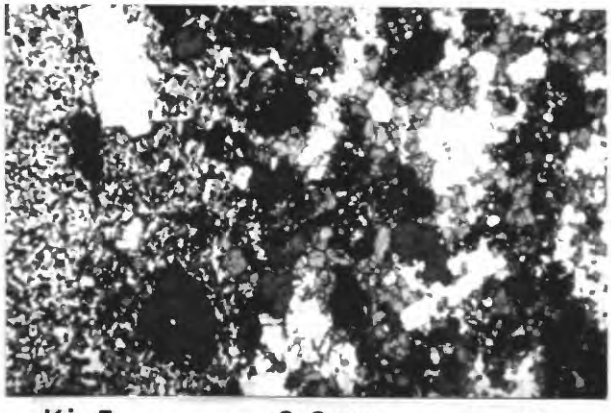

Ki-5 8.3mm e

San Carlos Scale, inches f

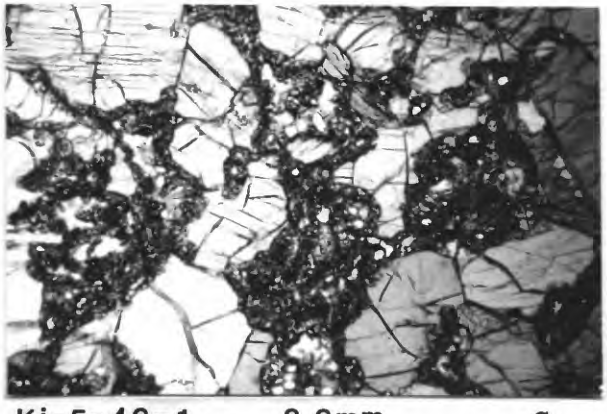

Ki-5-46-1 8.3mm g

SC-1-10 13cm h

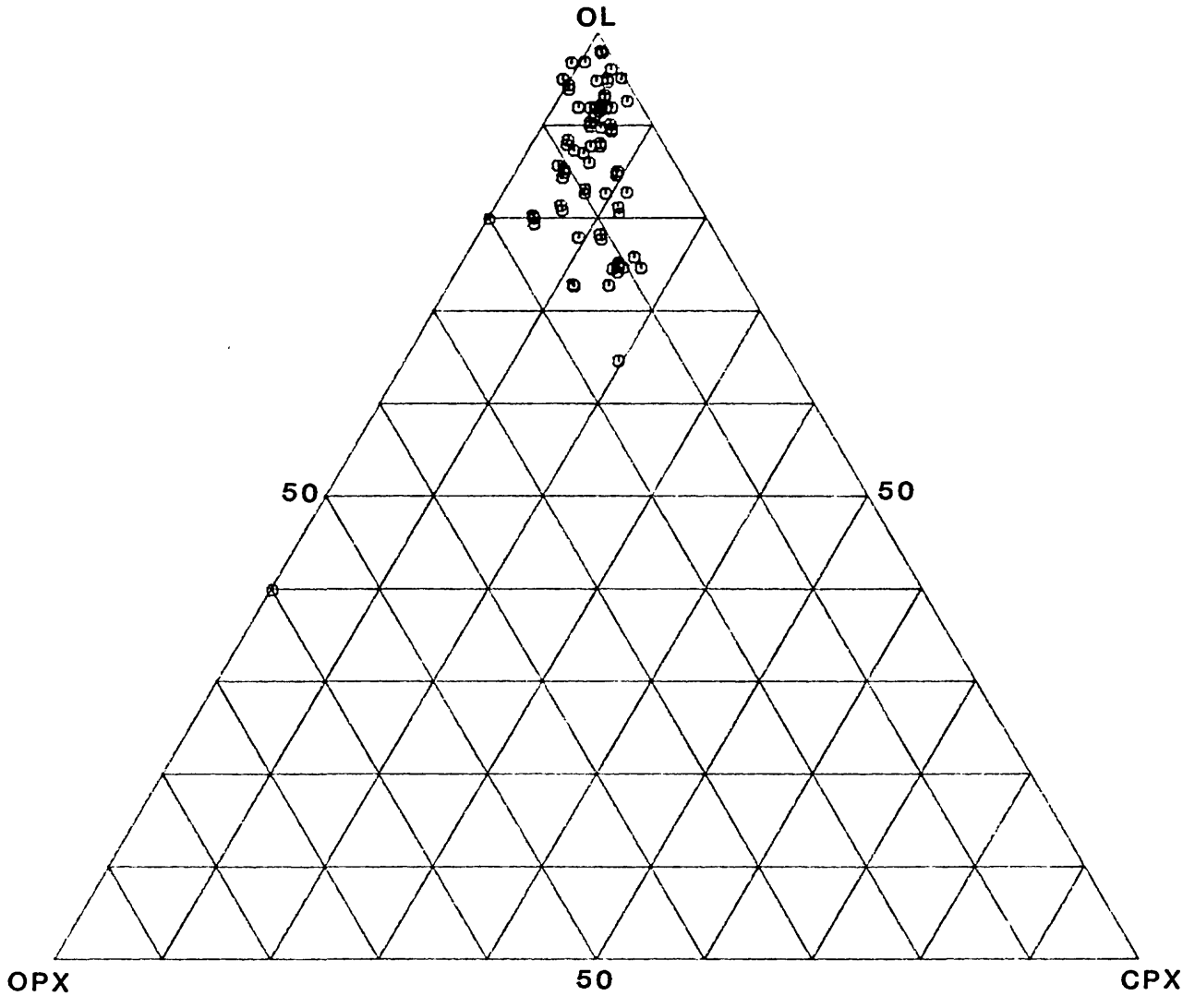

Fig. III-3a. Modal compositions of xenoliths in the Cr-diopside group. Locality No. 1.

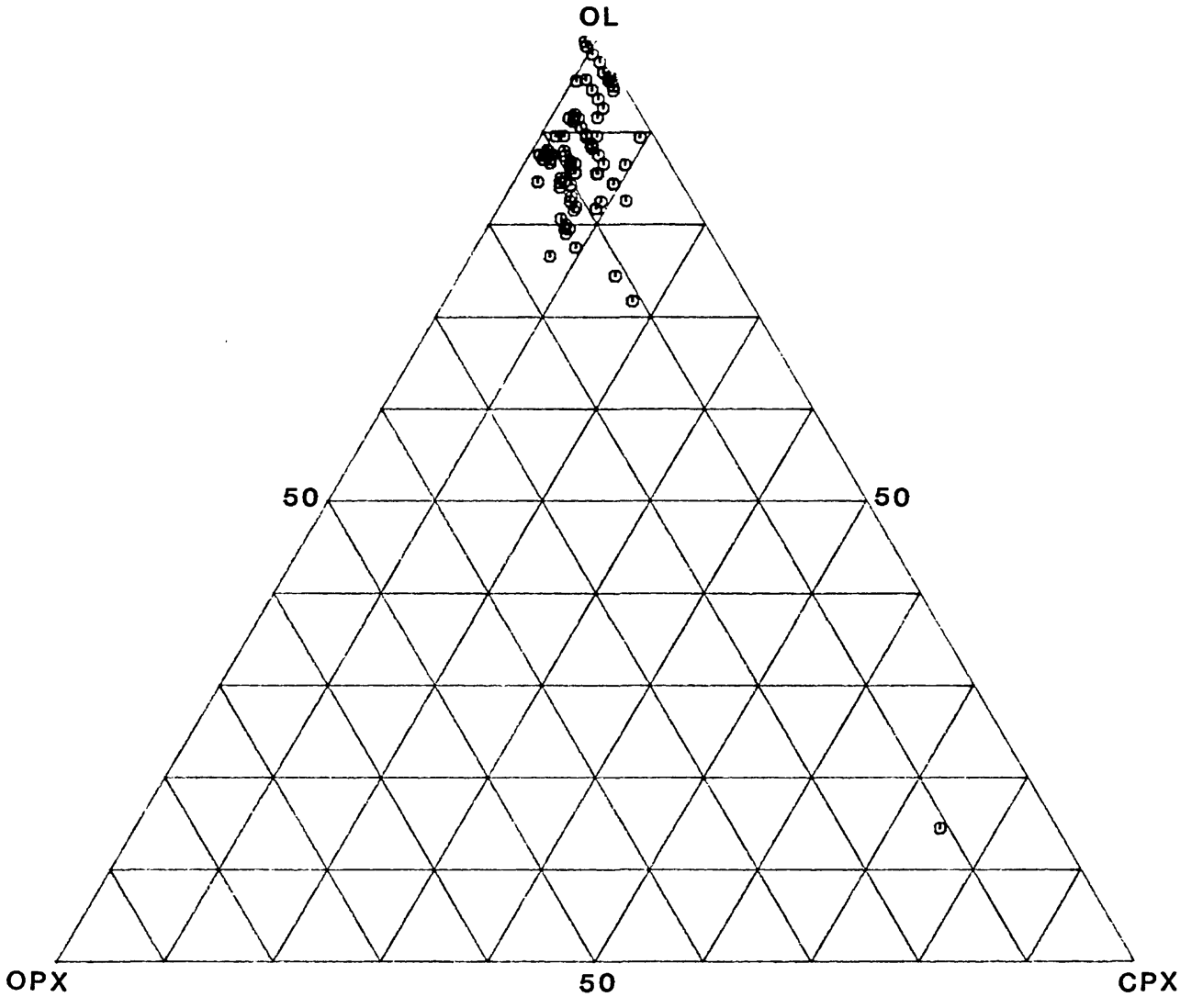

Fig. III-3b. Modal compositions of xenoliths in the Cr-diopside group. Locality No. 2.

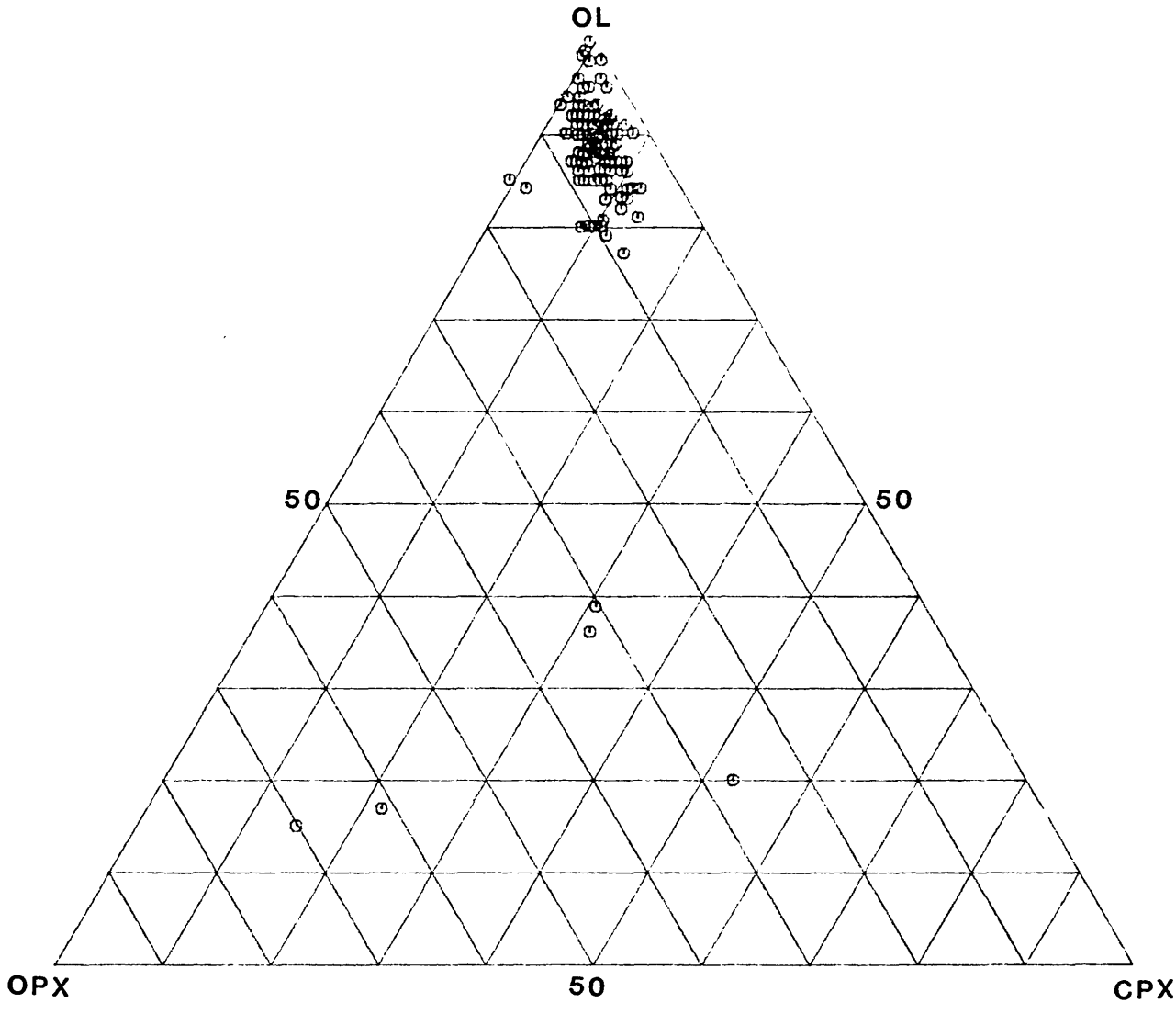

Fig. III-3c. Modal compositions of xenoliths in the Cr-diopside group. Locality No. 4.

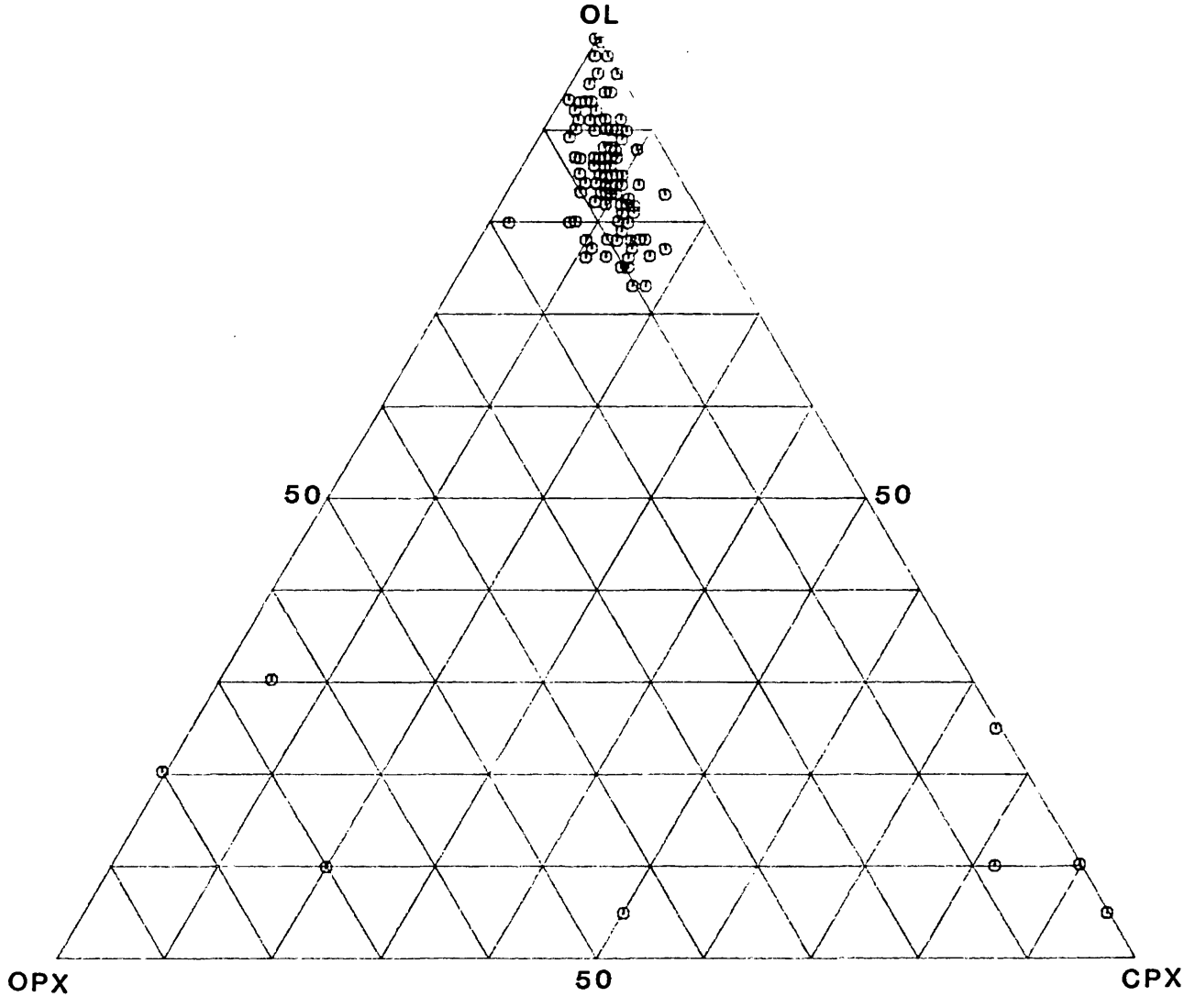

Fig. III-3d. Modal compositions of xenoliths in the Cr-diopside group. Locality No. 5.

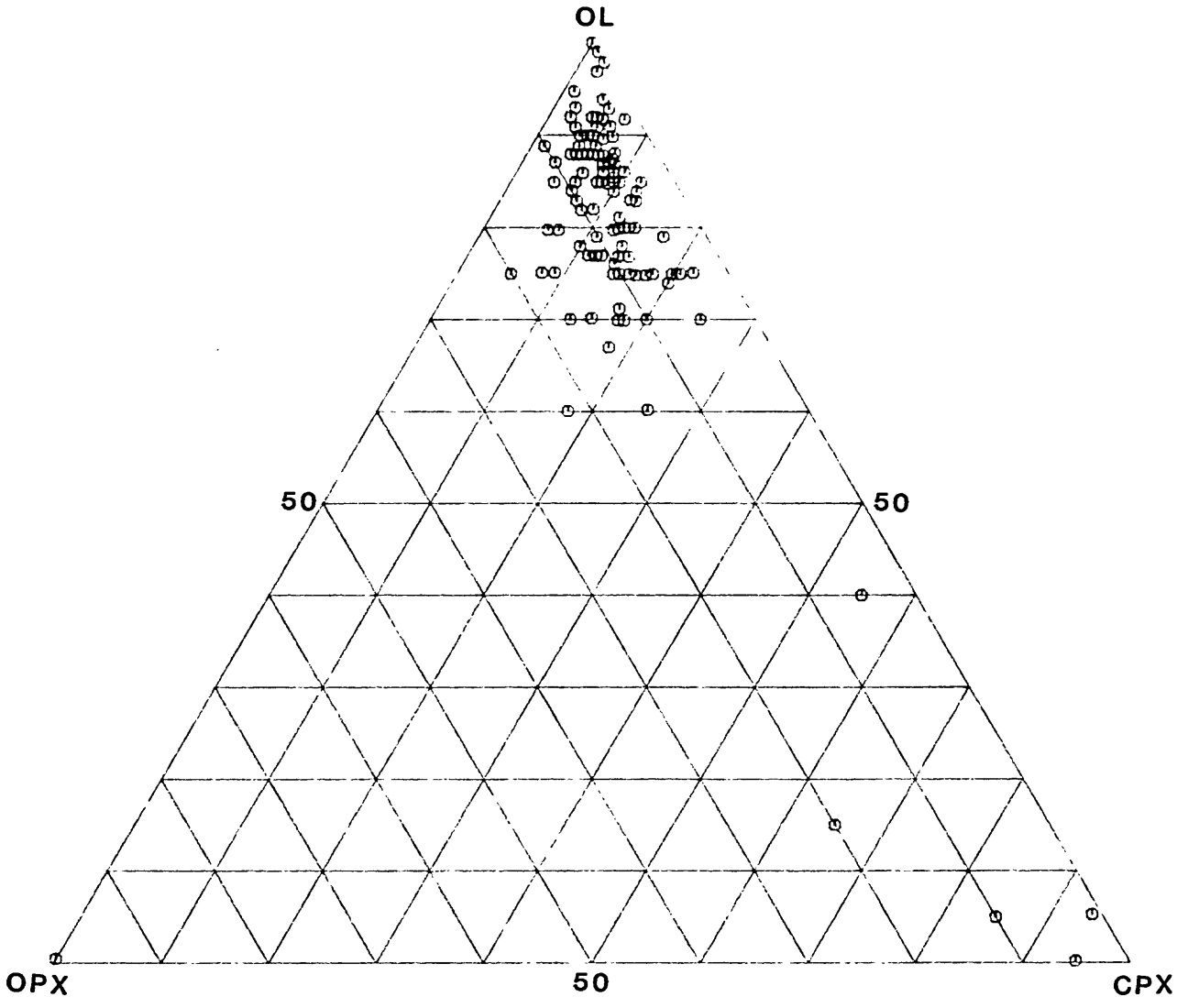

Fig. III-3e. Modal compositions of xenoliths in the Cr-diopside group. Locality No. 6.

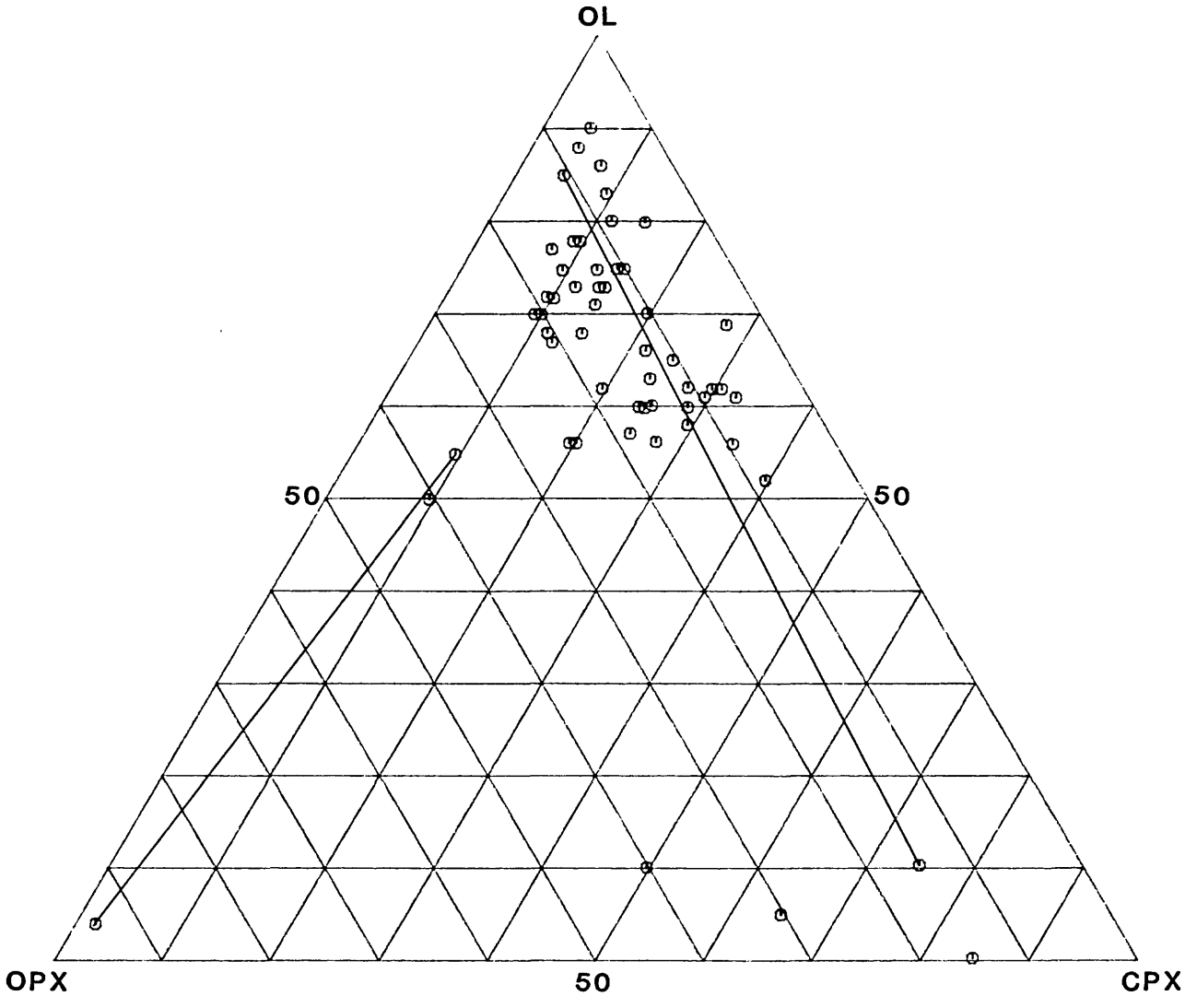

Fig. III-3f. Modal compositions of xenoliths in the Cr-diopside group. Lines connect different lithologies in the same xenolith. Locality No. 11.

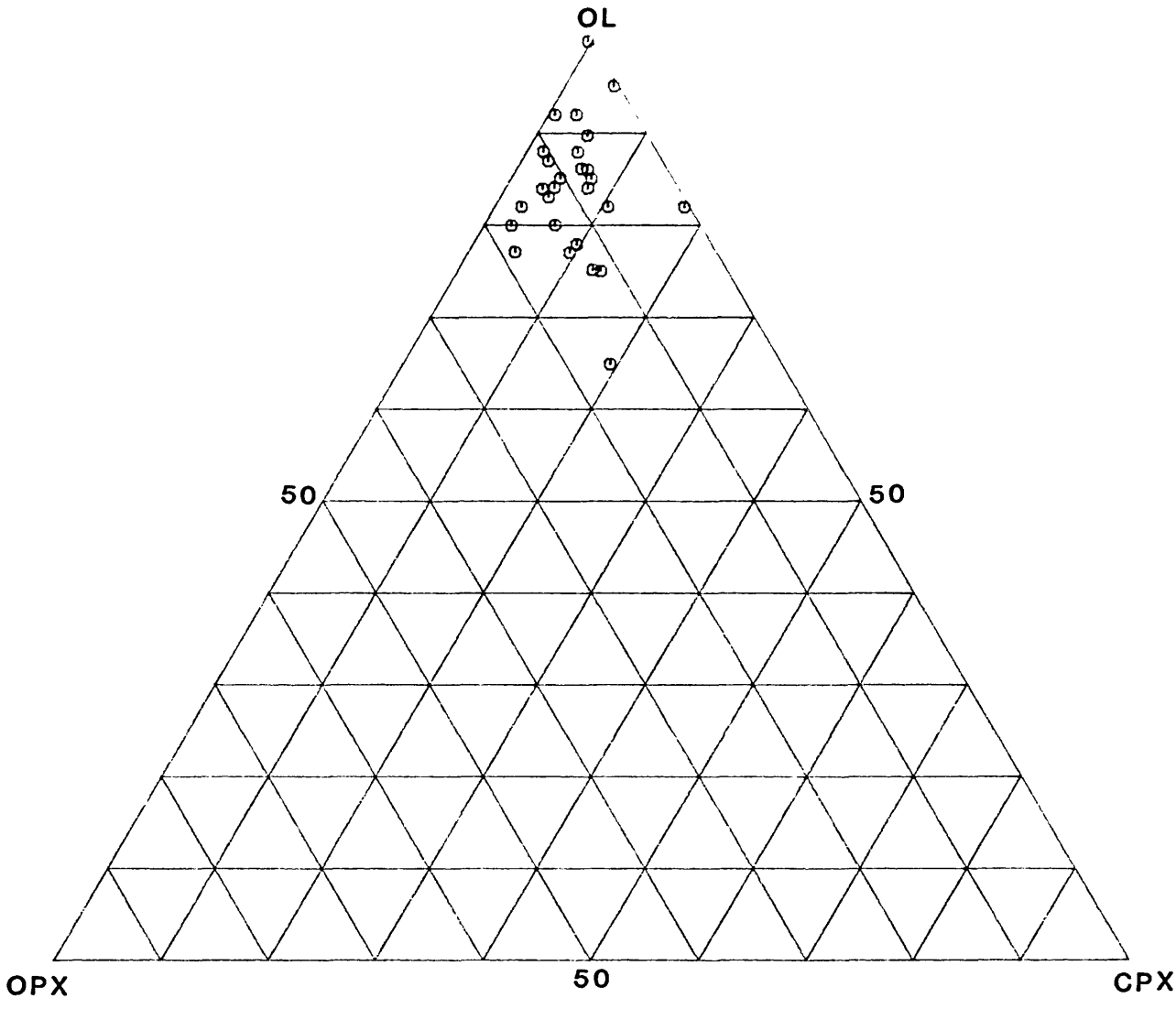

Fig. III-3g. Modal compositions of xenoliths in the Cr-diopside group. Locality No. 16.

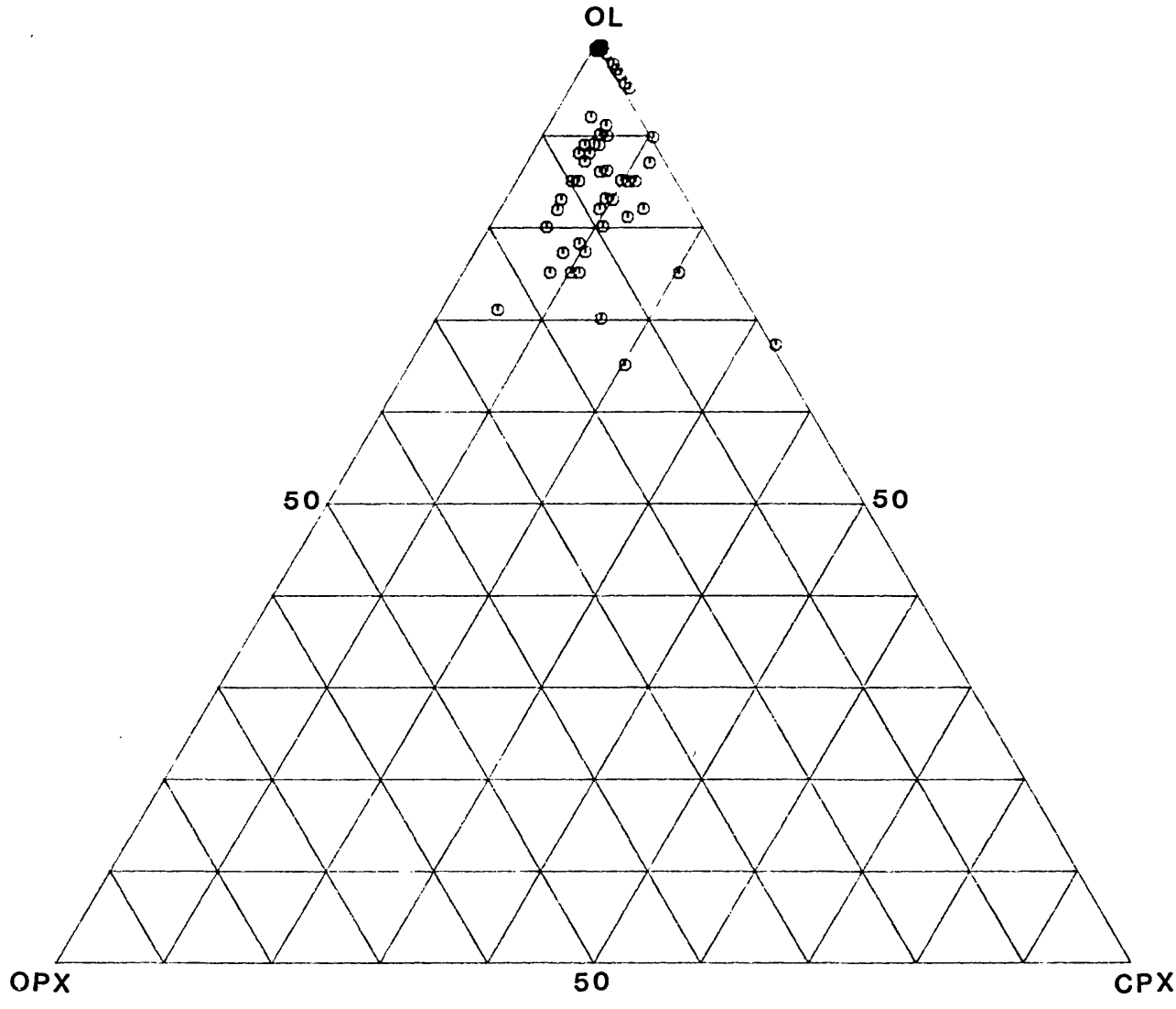

Fig. III-3h. Modal compositions of xenoliths in the Cr-diopside group. Locality No. 17.

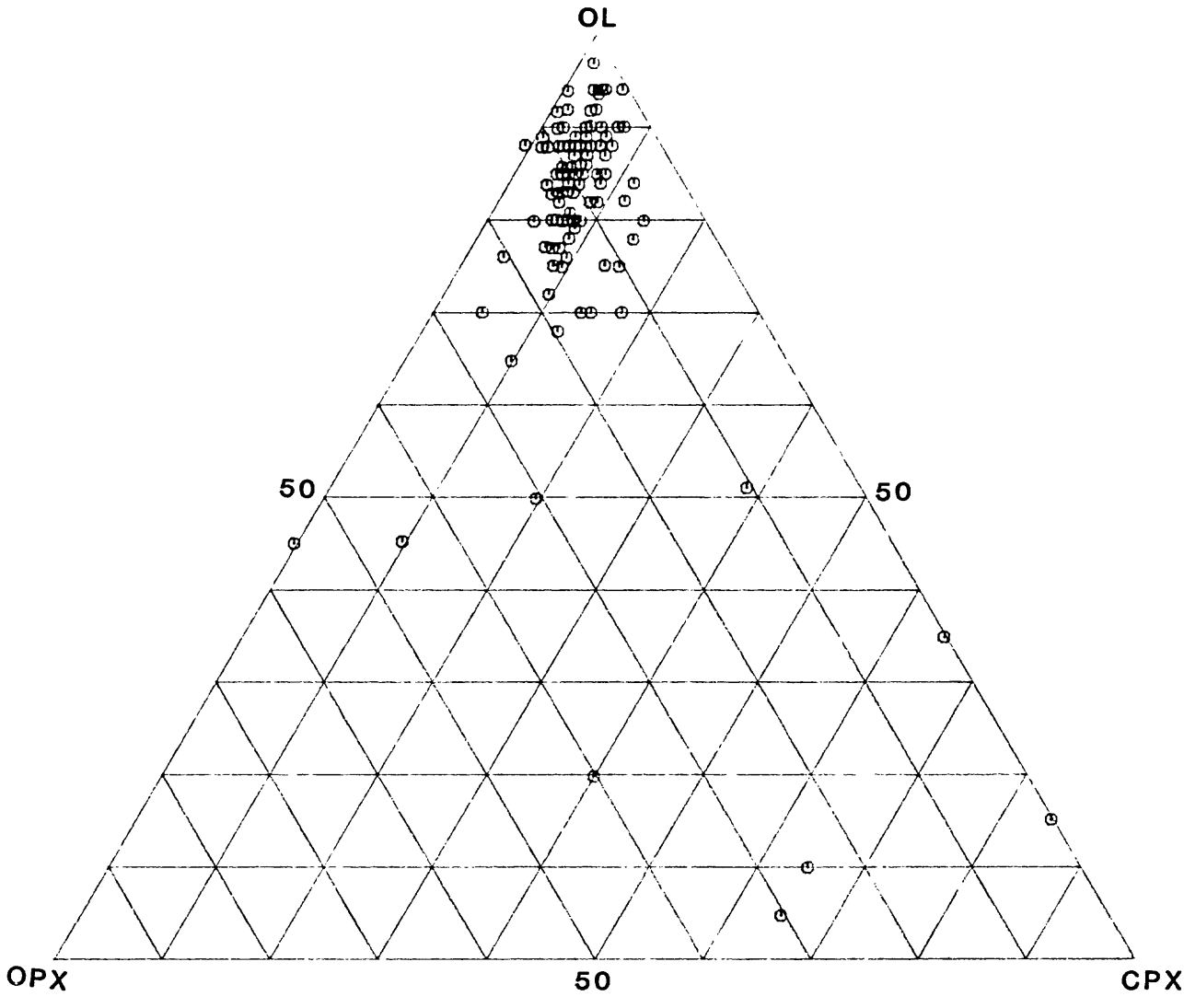

Fig. III-3i. Modal compositions of xenoliths in the Cr-diopside group. Locality No. 21.

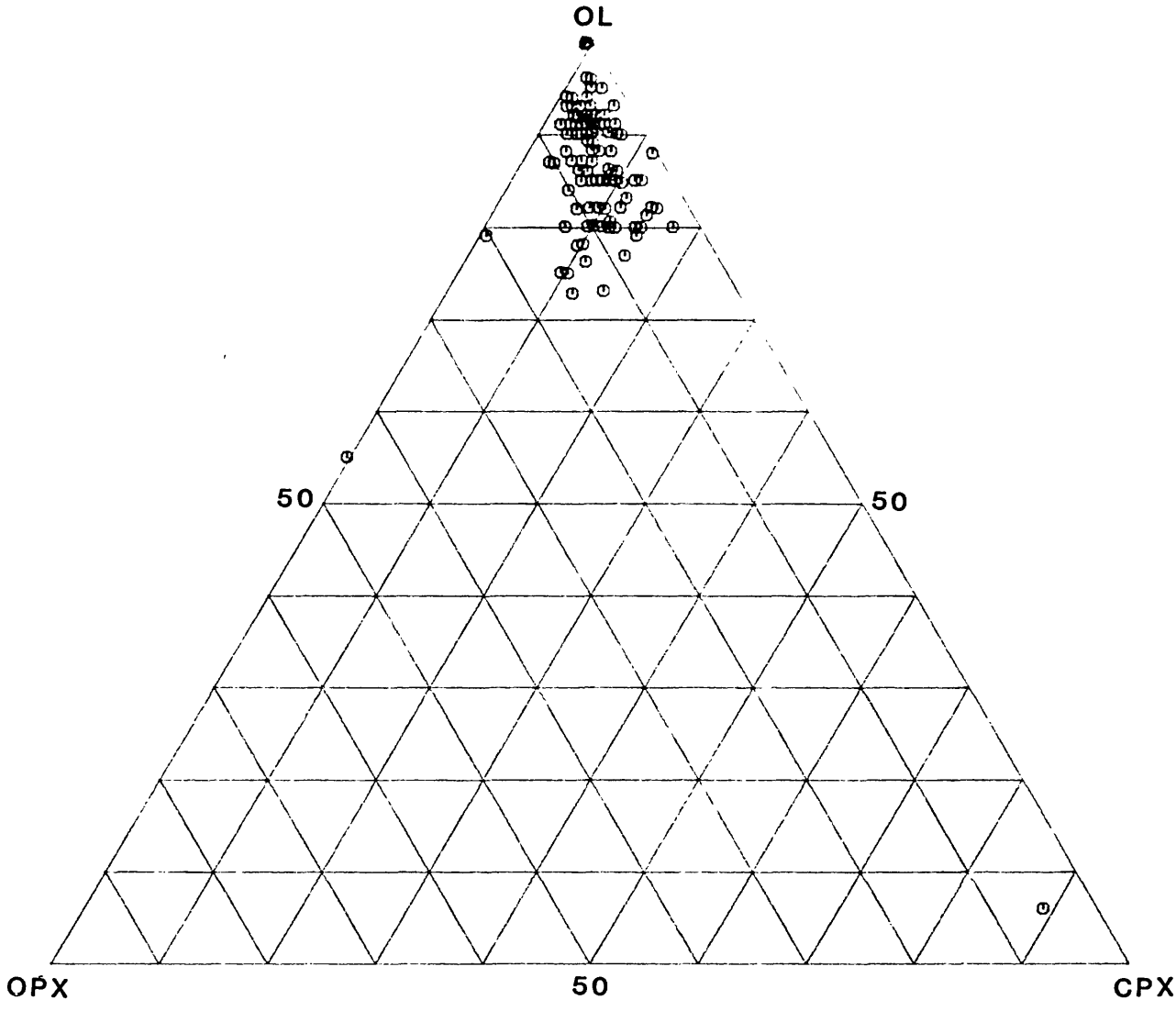

Fig. III-3j. Modal compositions of xenoliths in the Cr-diopside group. Locality No. 22.

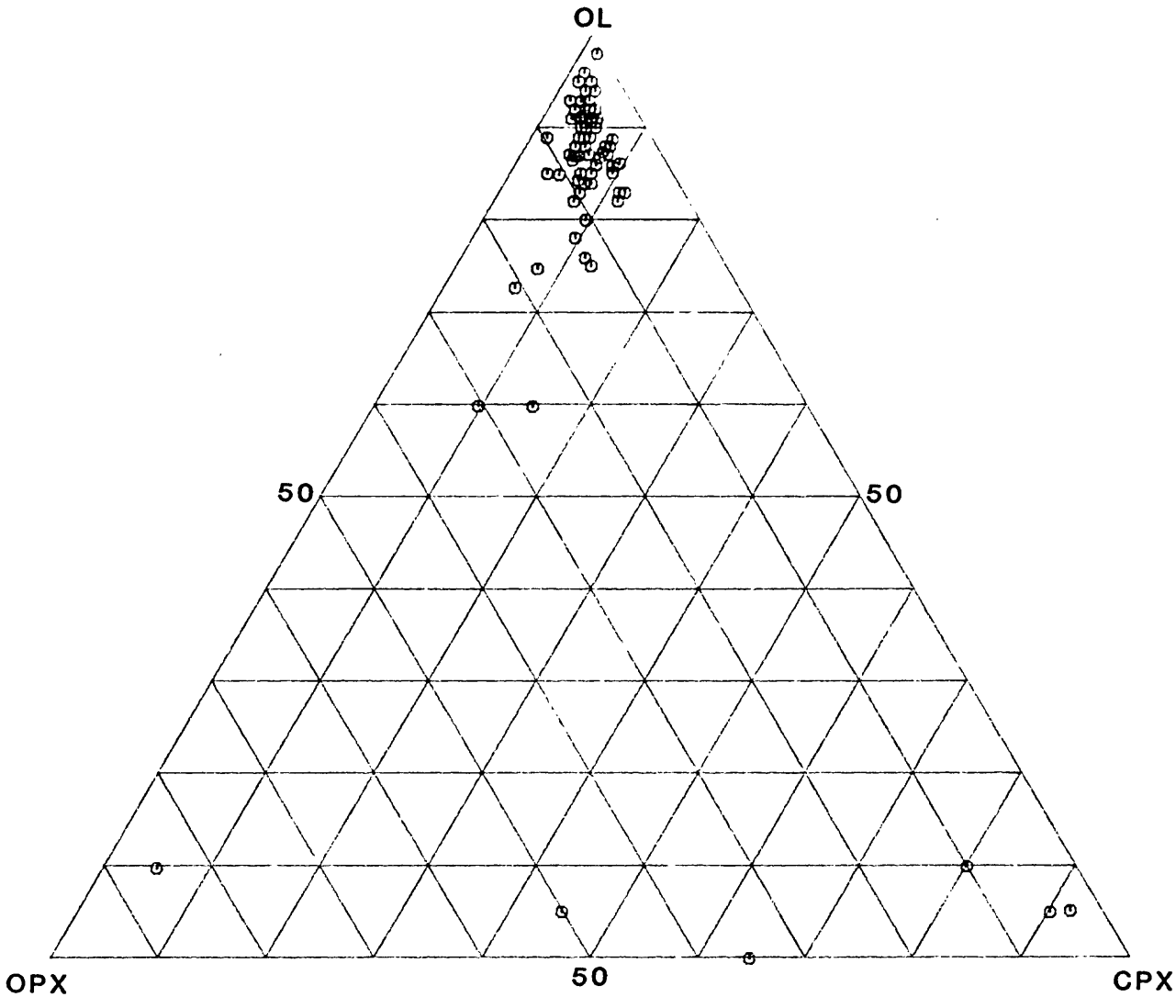

Fig. III-3k. Modal compositions of xenoliths in the Cr-diopside group. Locality No. 23.

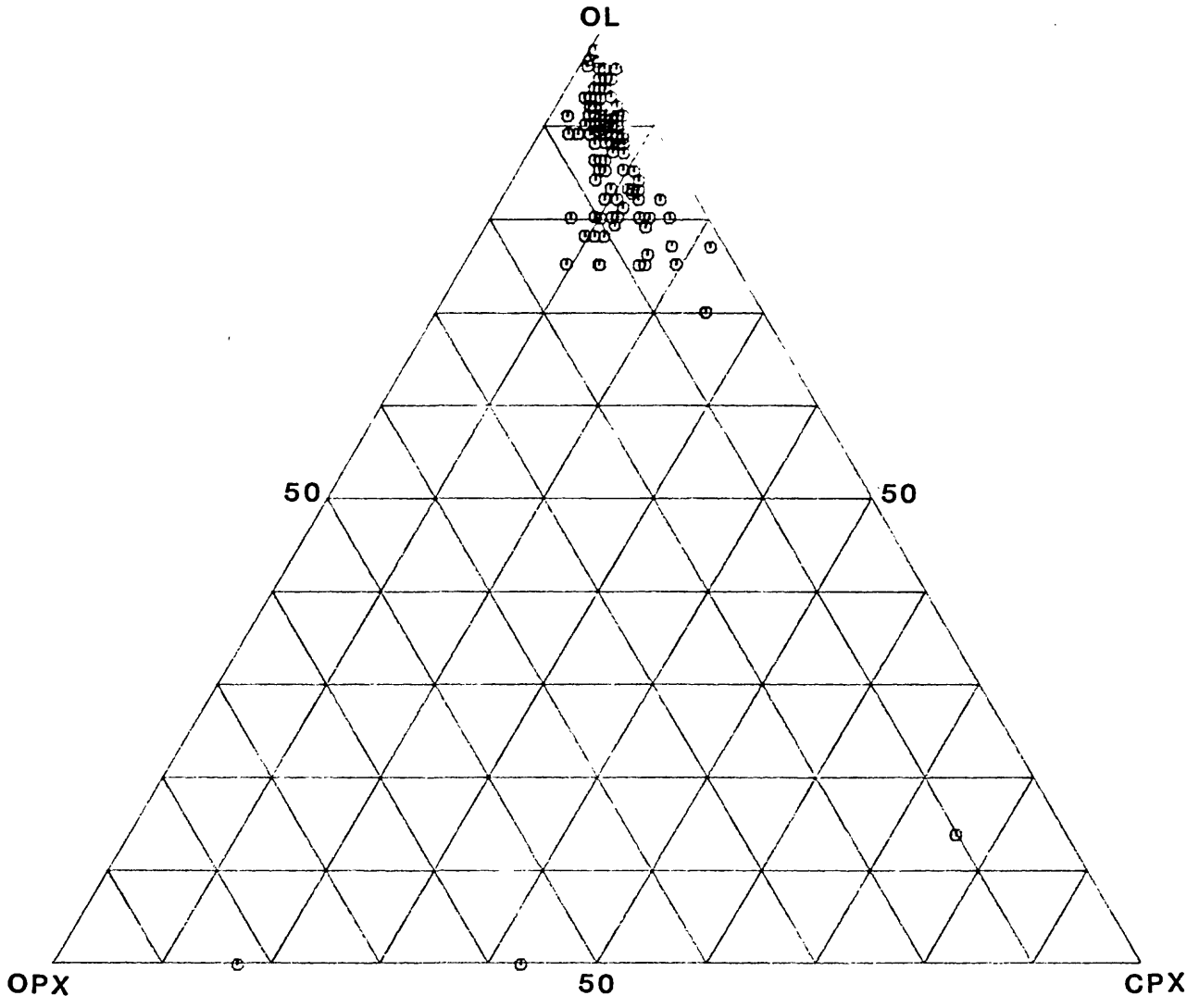

Fig. III-31. Modal compositions of xenoliths in the Cr-diopside group. Locality No. 31.

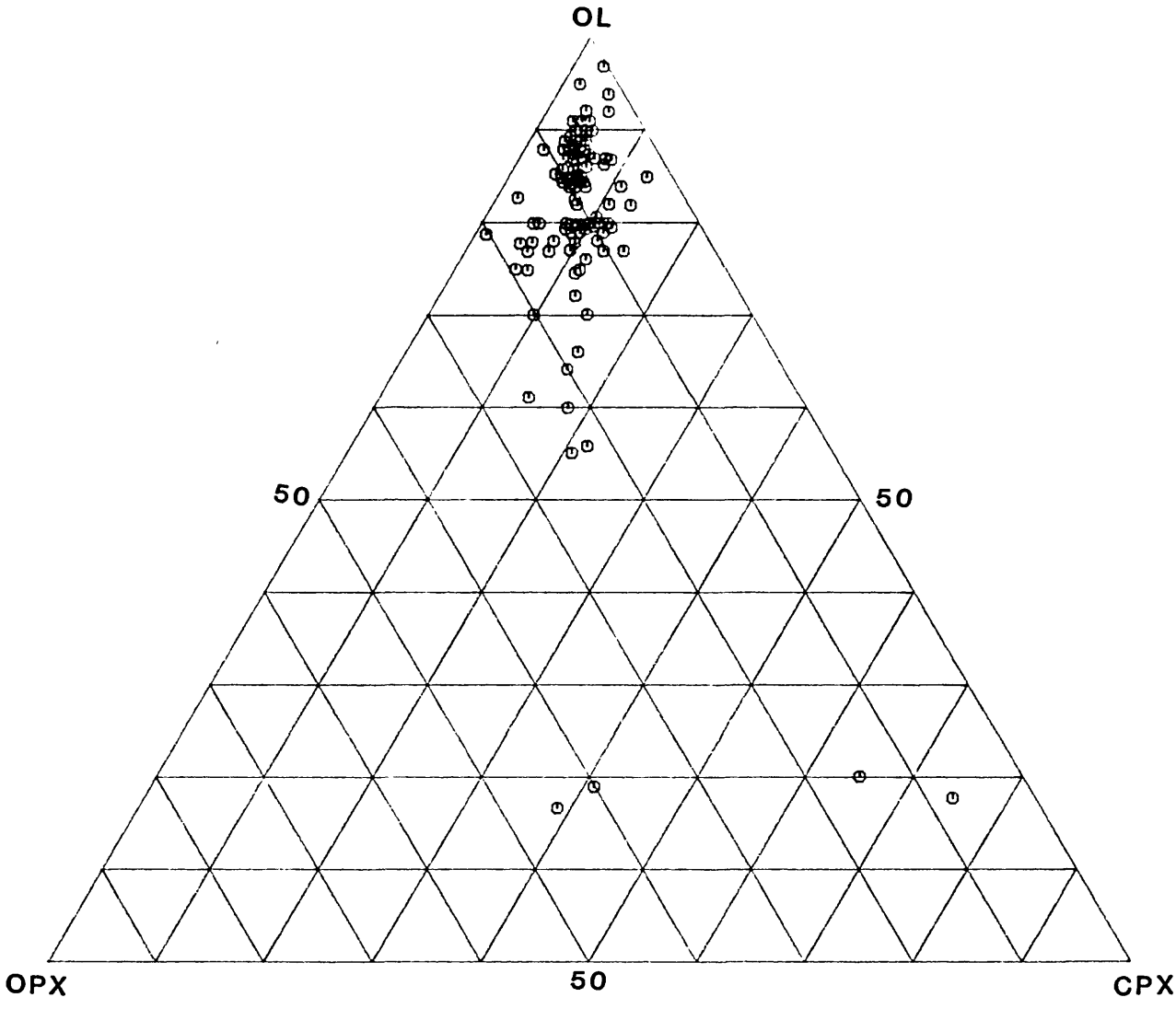

Fig. III-3m. Modal compositions of xenoliths in the Cr-diopside group. Locality No. 32.

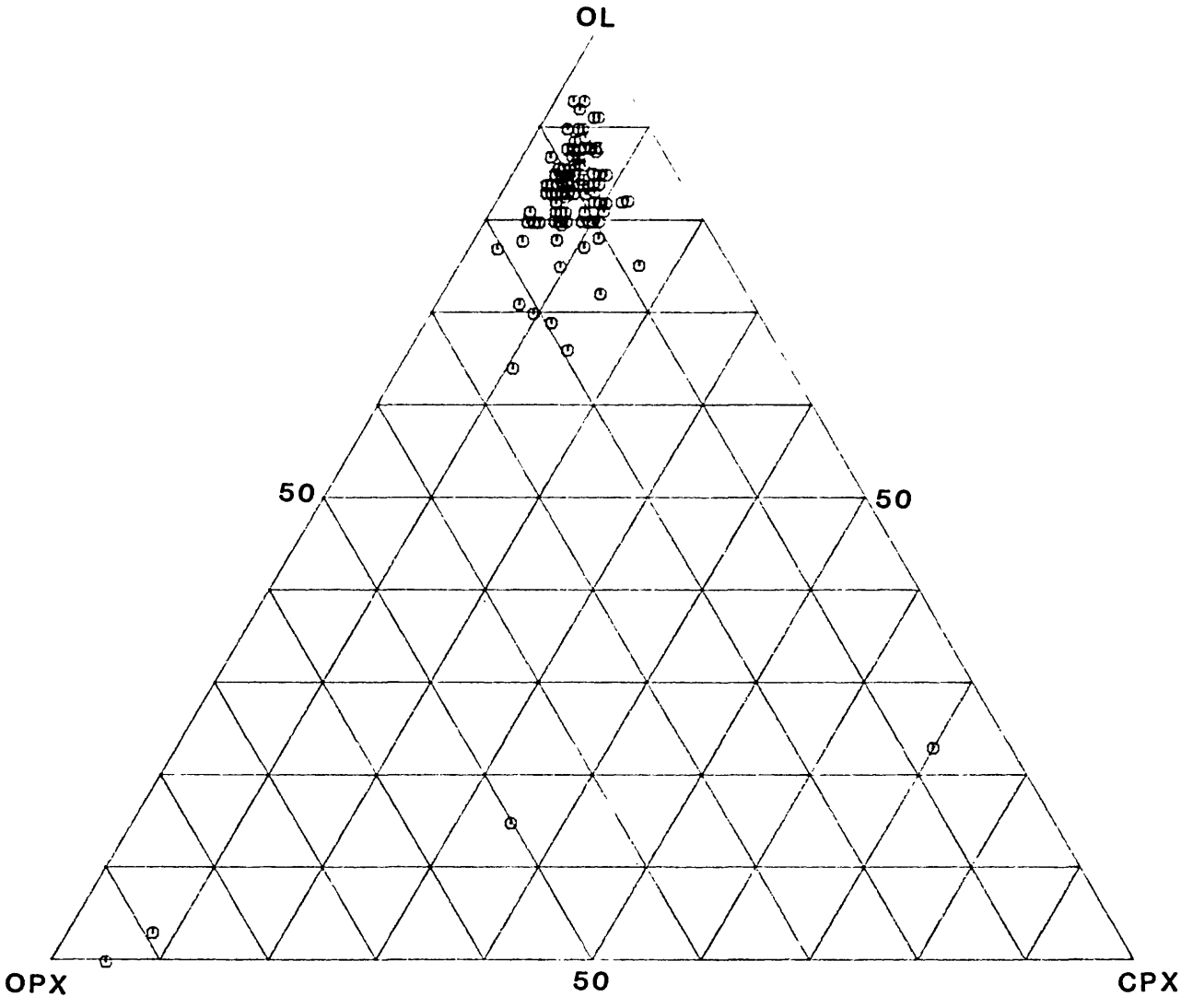

Fig. III-3n. Modal compositions of xenoliths in the Cr-diopside group. Locality No. 33.

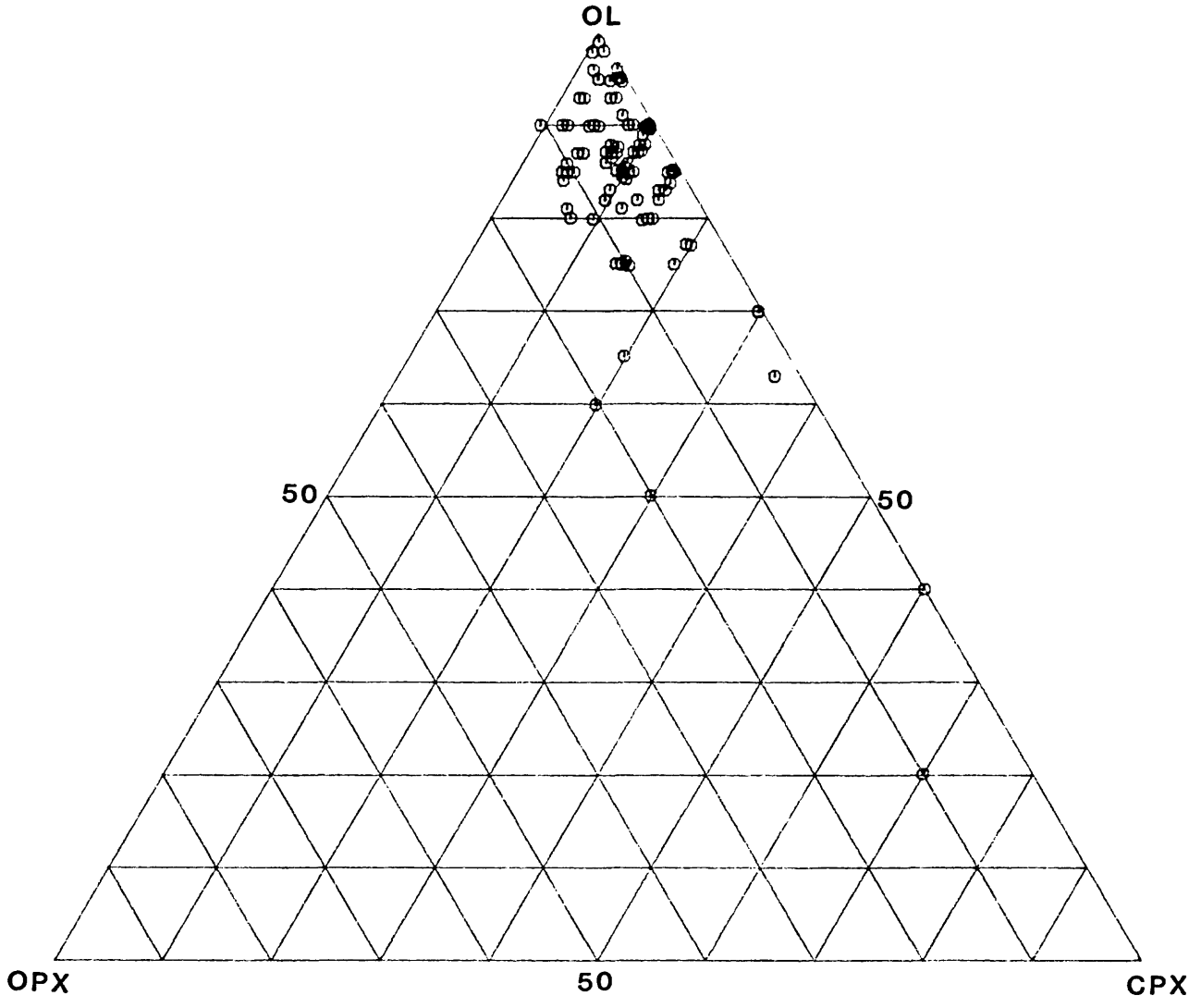

Fig. III-3o. Modal compositions of xenoliths in the Cr-diopside group. Locality No. 34.

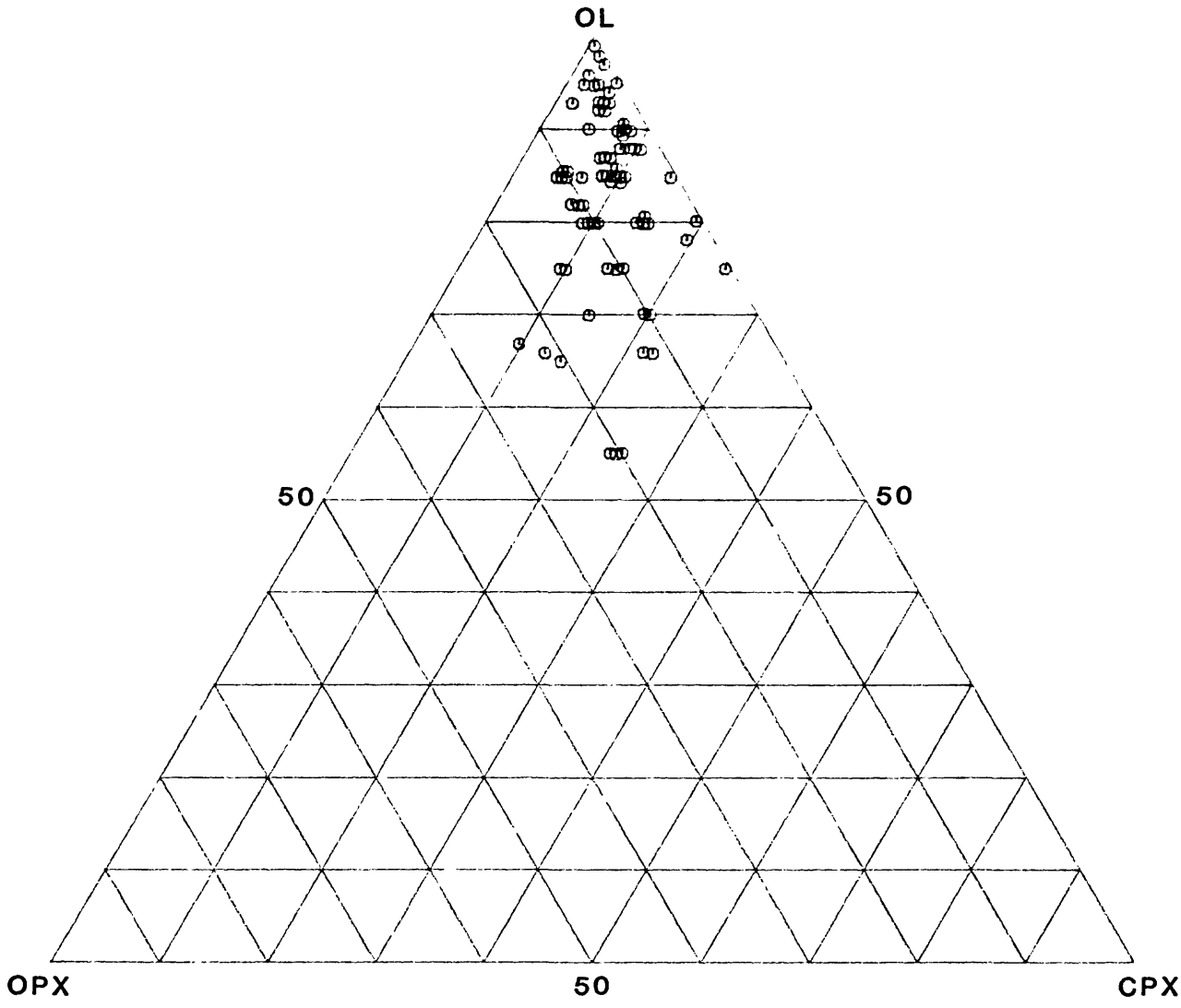

Fig. III-3p. Modal compositions of xenoliths in the Cr-diopside group. Locality No. 35.

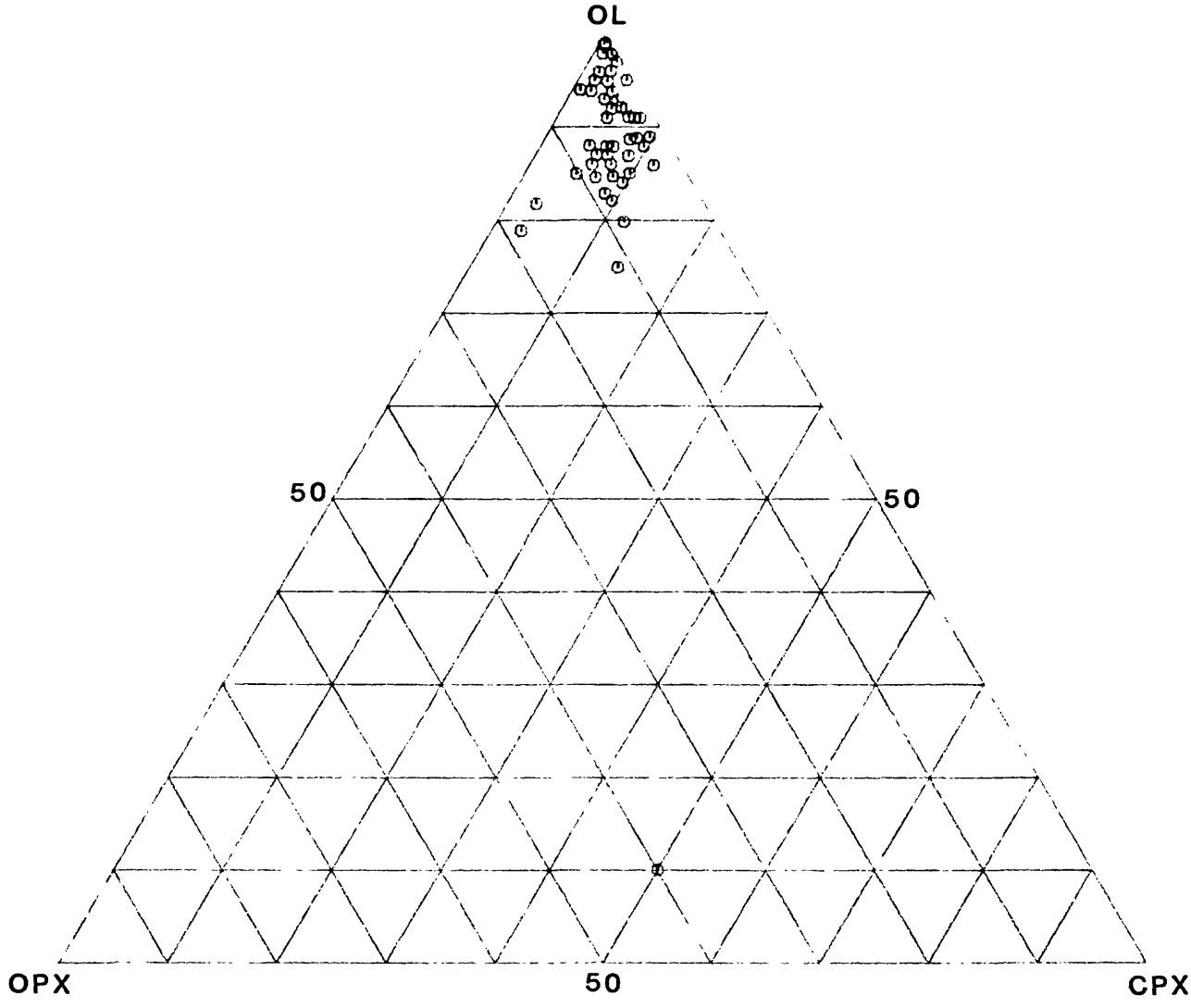

Fig. III-3q. Modal compositions of xenoliths in the Cr-diopside group. Locality No. 38.

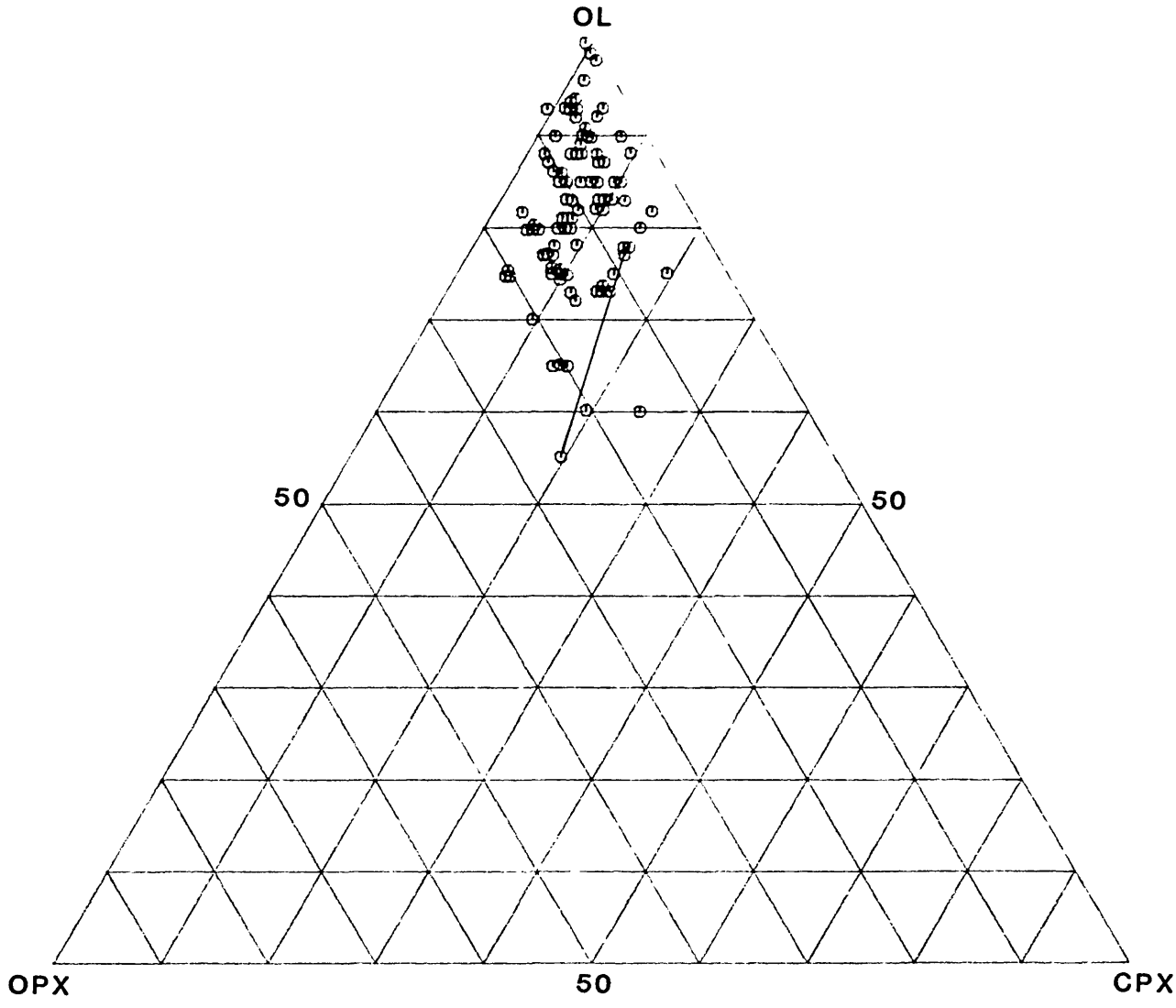

Fig. III-3r. Modal compositions of xenoliths in the Cr-diopside group. Line connects different lithologies in the same xenolith. Locality No. 46.

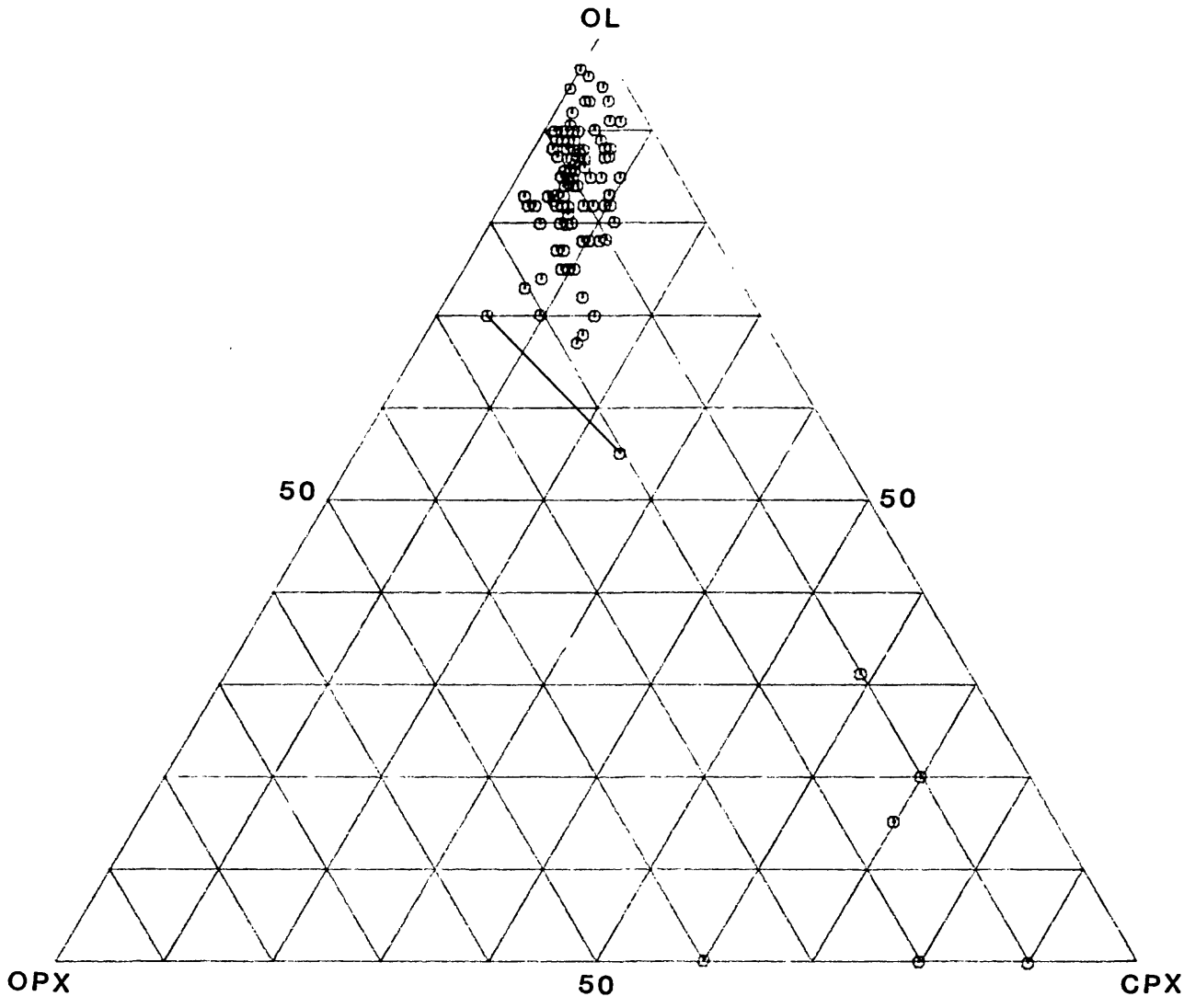

Fig. III-3s. Modal compositions of xenoliths in the Cr-diopside group. Line connects different lithologies in the same xenolith. Locality No. 58.

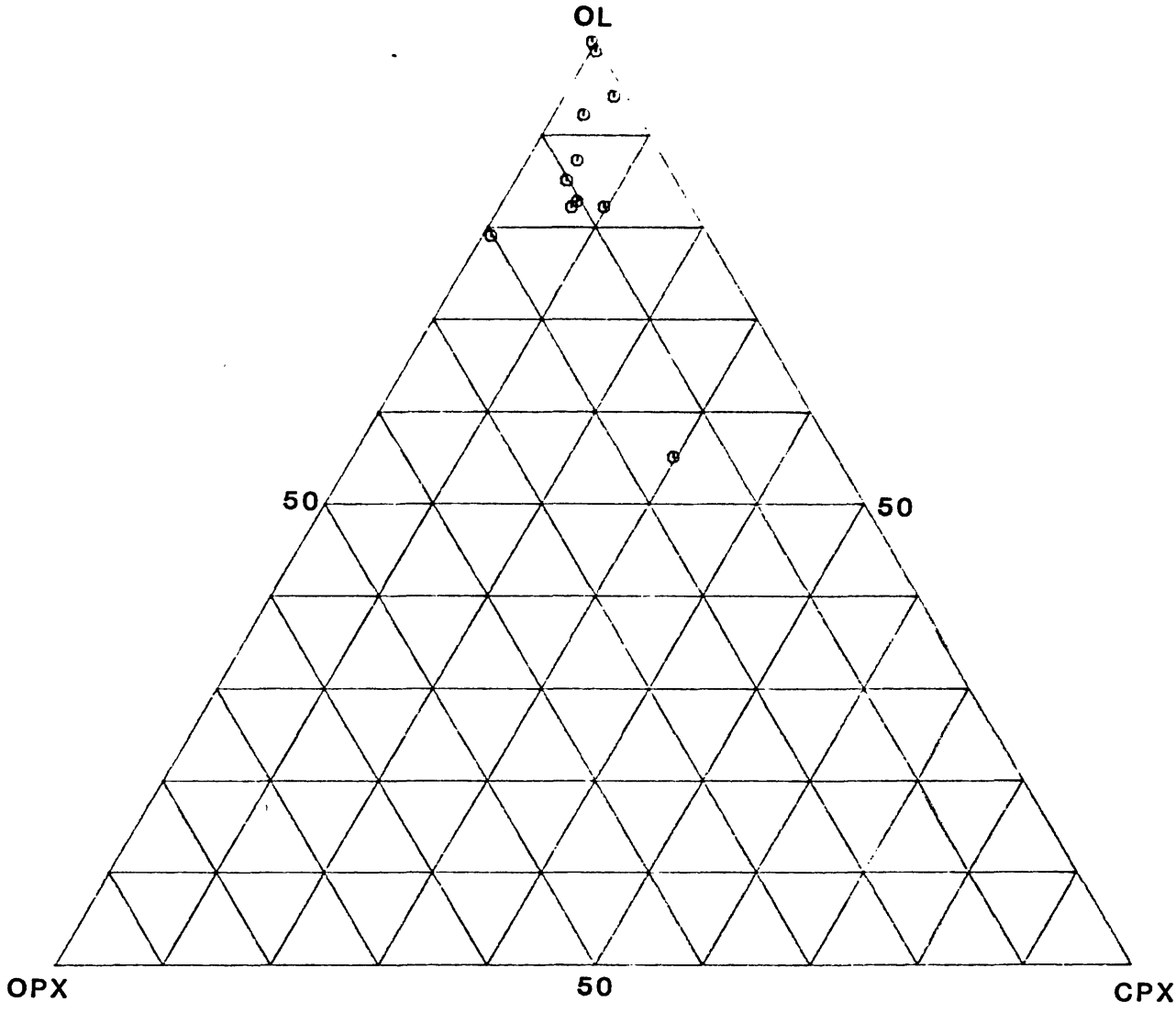

Fig. III-3t. Modal compositions of xenoliths in the Cr-diopside group. Locality No. 59.

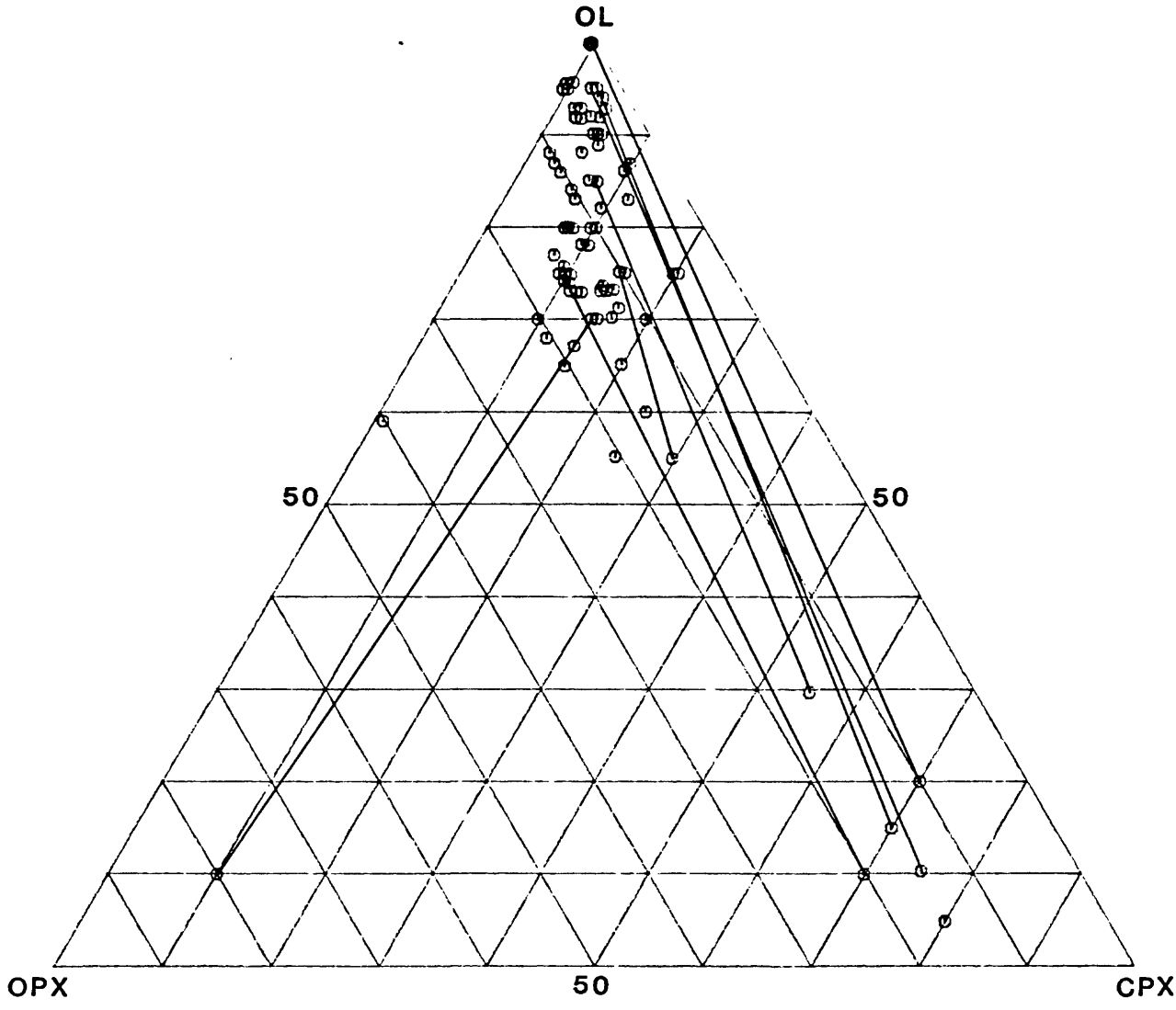

Fig. III-3u. Modal compositions of xenoliths in the Cr-diopside group. Lines connect different lithologies in the same xenolith. Locality No. 60.

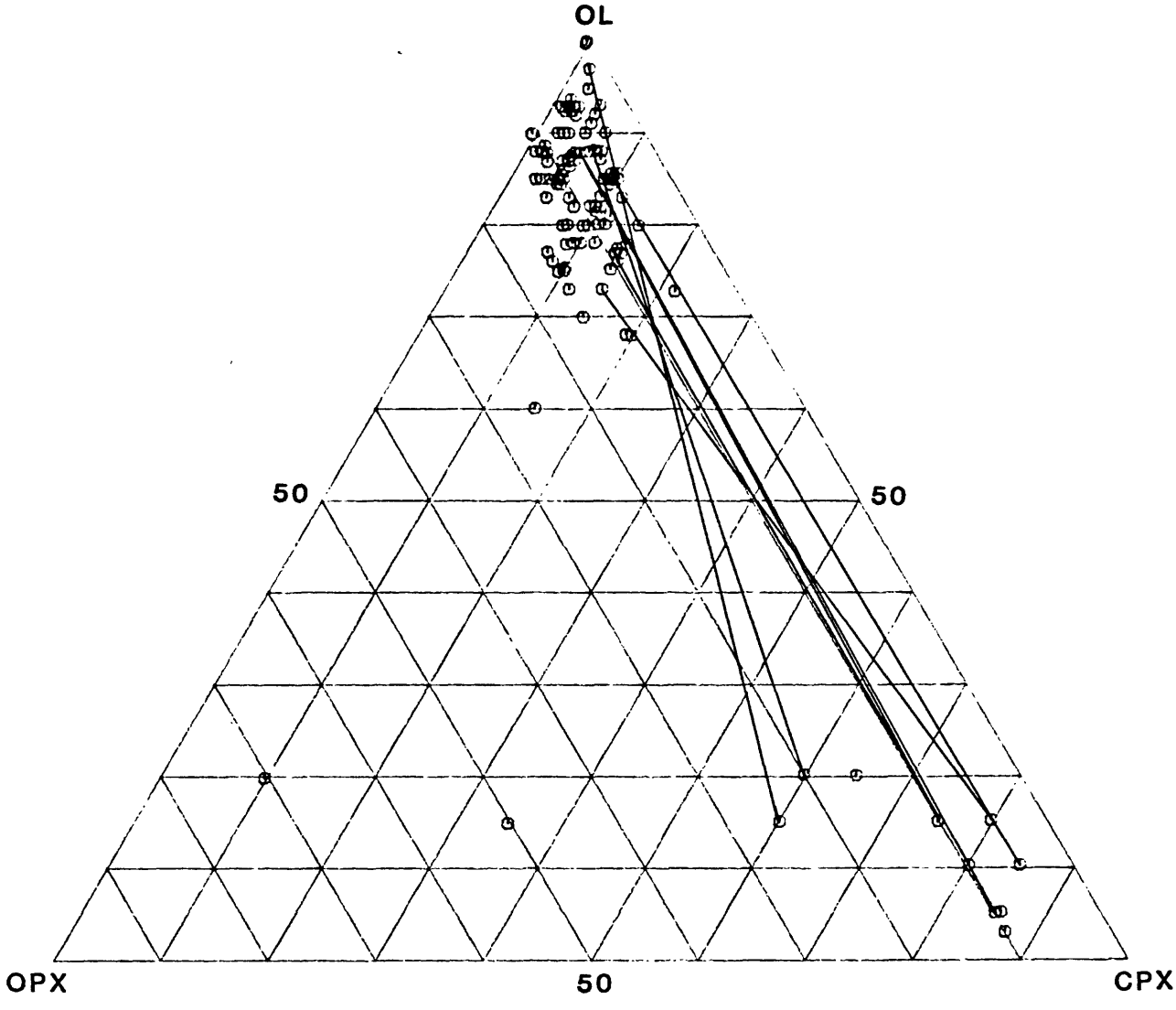

Fig. III-3v. Modal compositions of xenoliths in the Cr-diopside group. Lines connect different lithologies in the same xenolith. Locality No. 61.

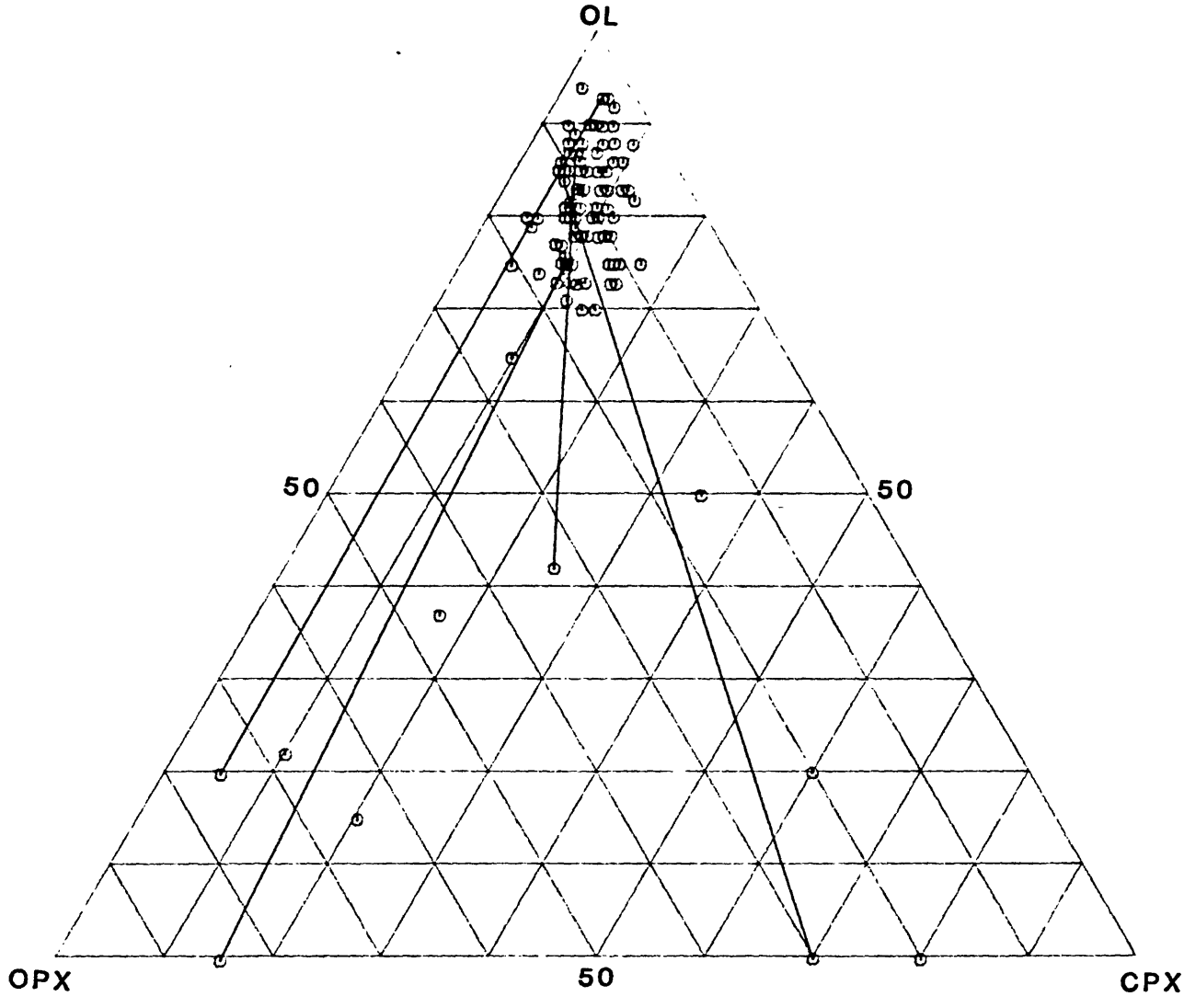

Fig. III-3w. Modal compositions of xenoliths in the Cr-diopside group. Lines connect different lithologies in the same xenolith. Locality No. 62.

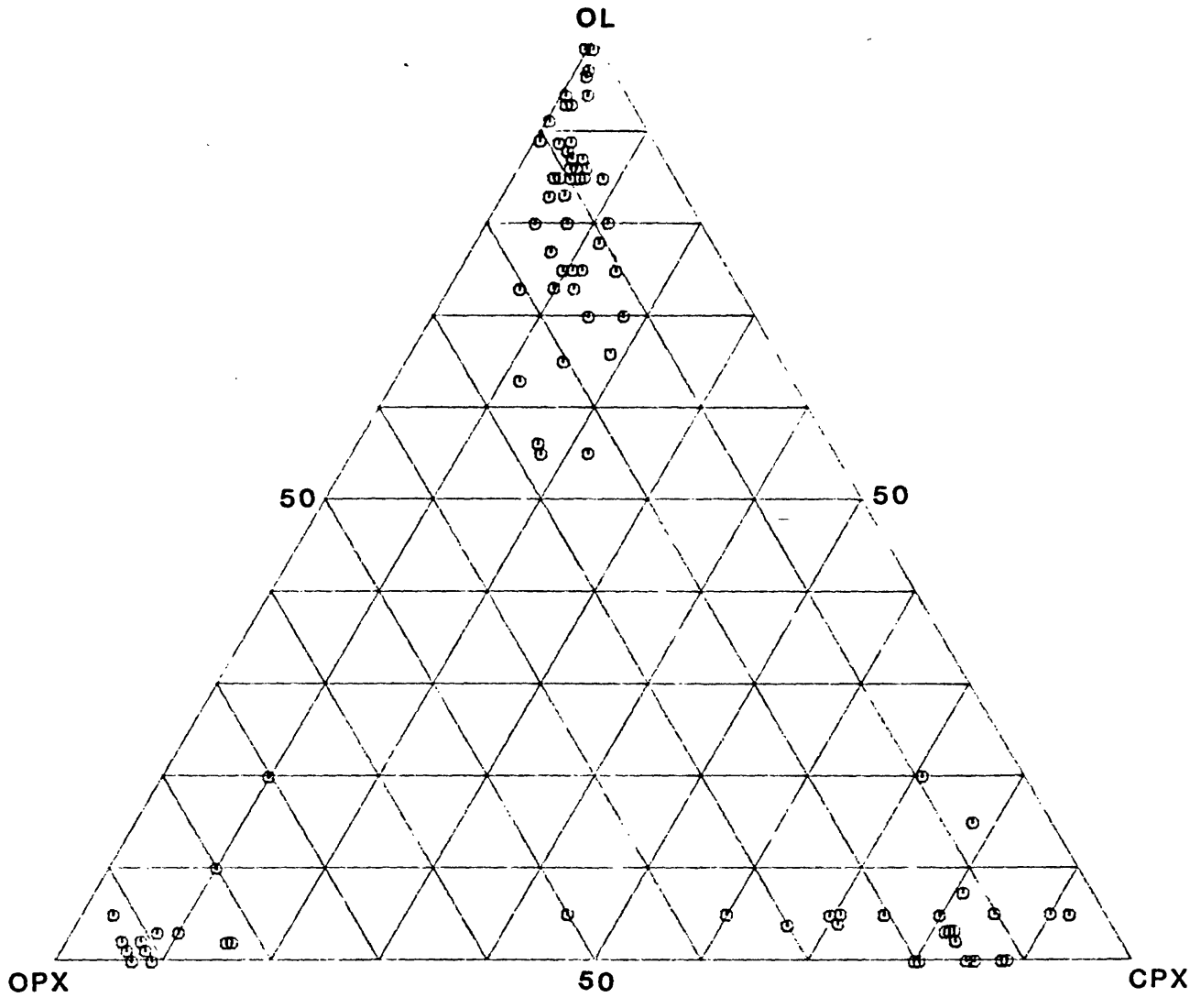

Fig. III-3x. Modal compositions of xenoliths in the Cr-diopside group. Locality No. 63.

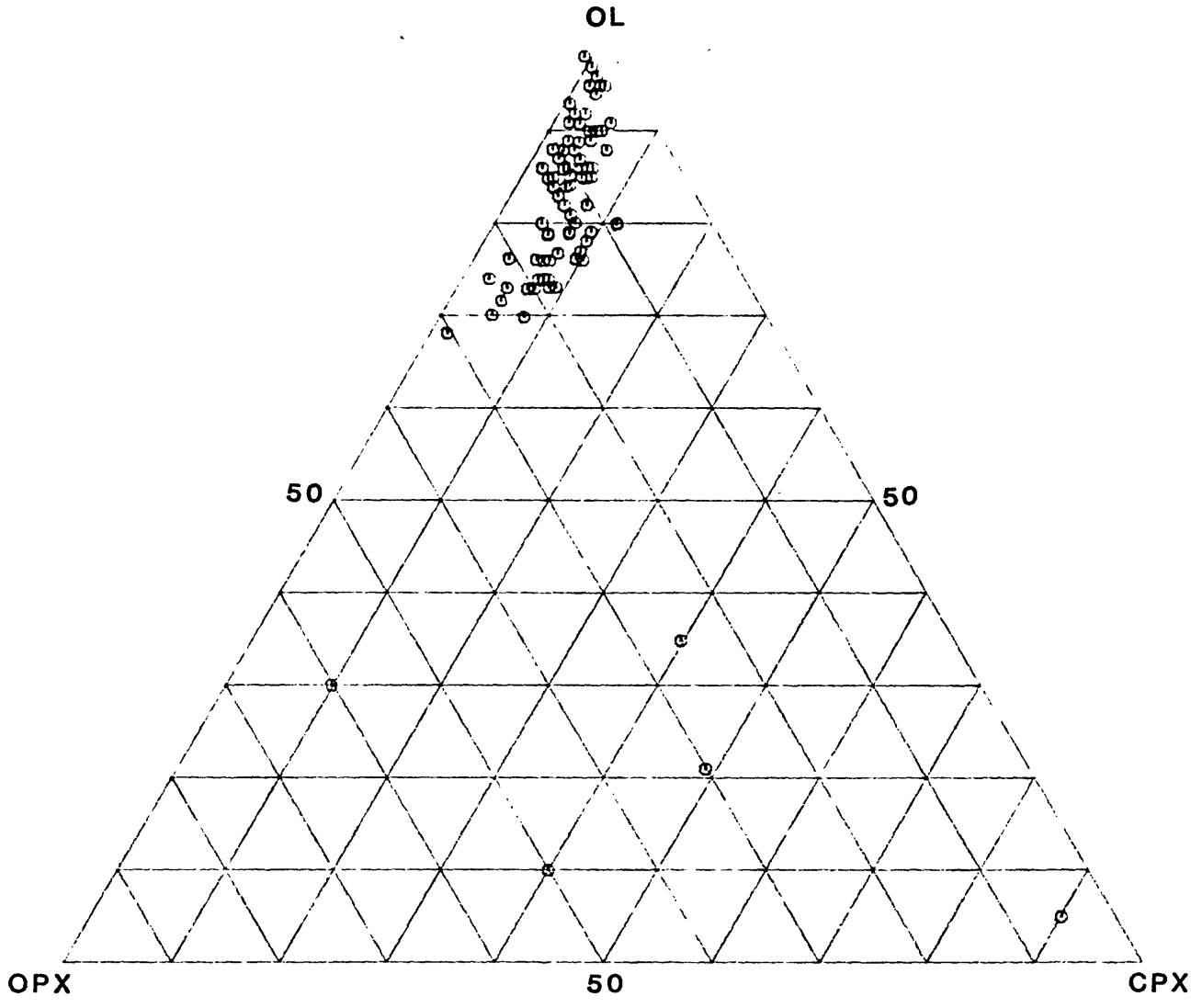

Fig. III-3y. Modal compositions of xenoliths in the Cr-diopside group. Locality No. 63.

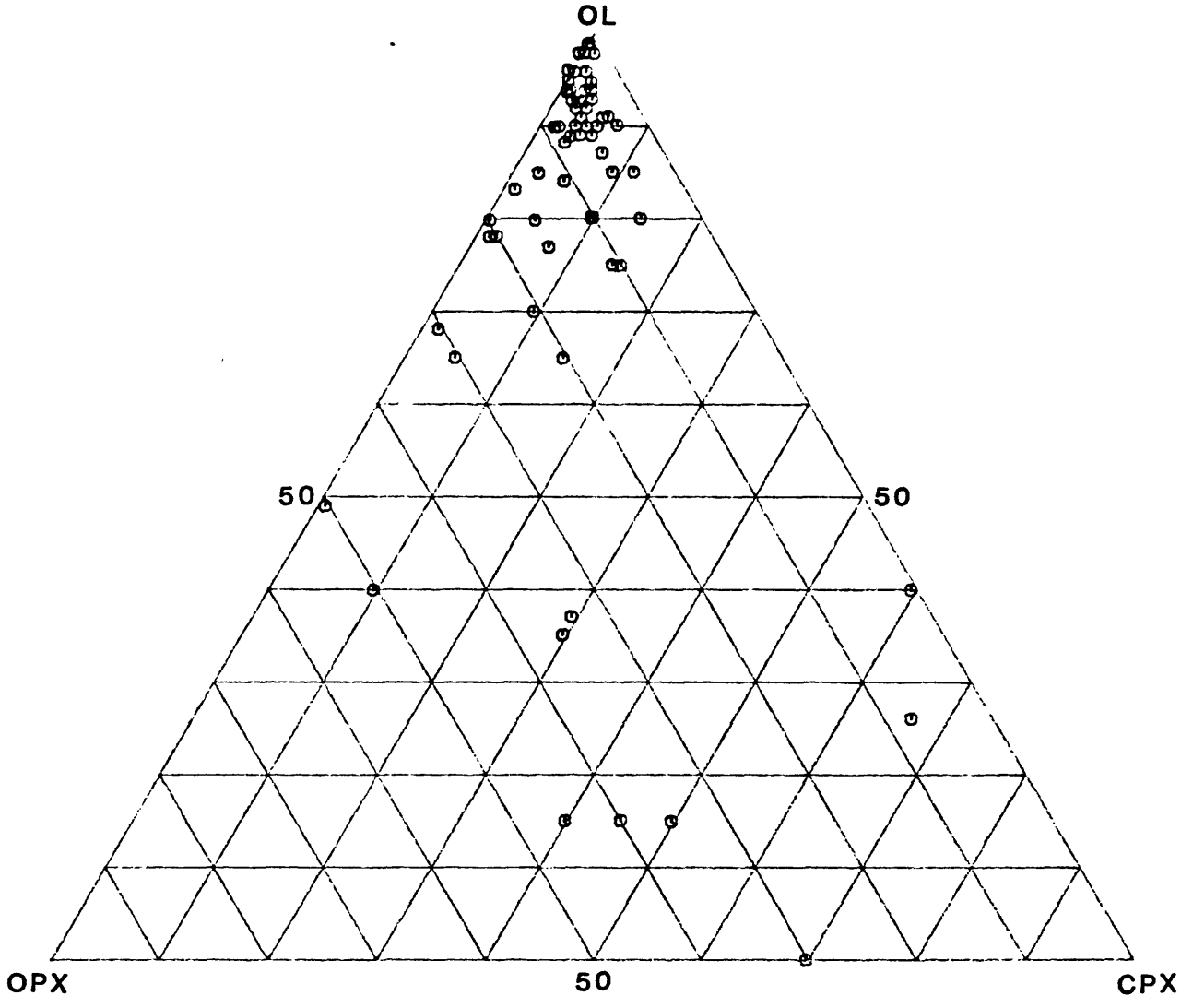

Fig. III-3z. Modal compositions of xenoliths in the Cr-diopside group. Locality No. 64.

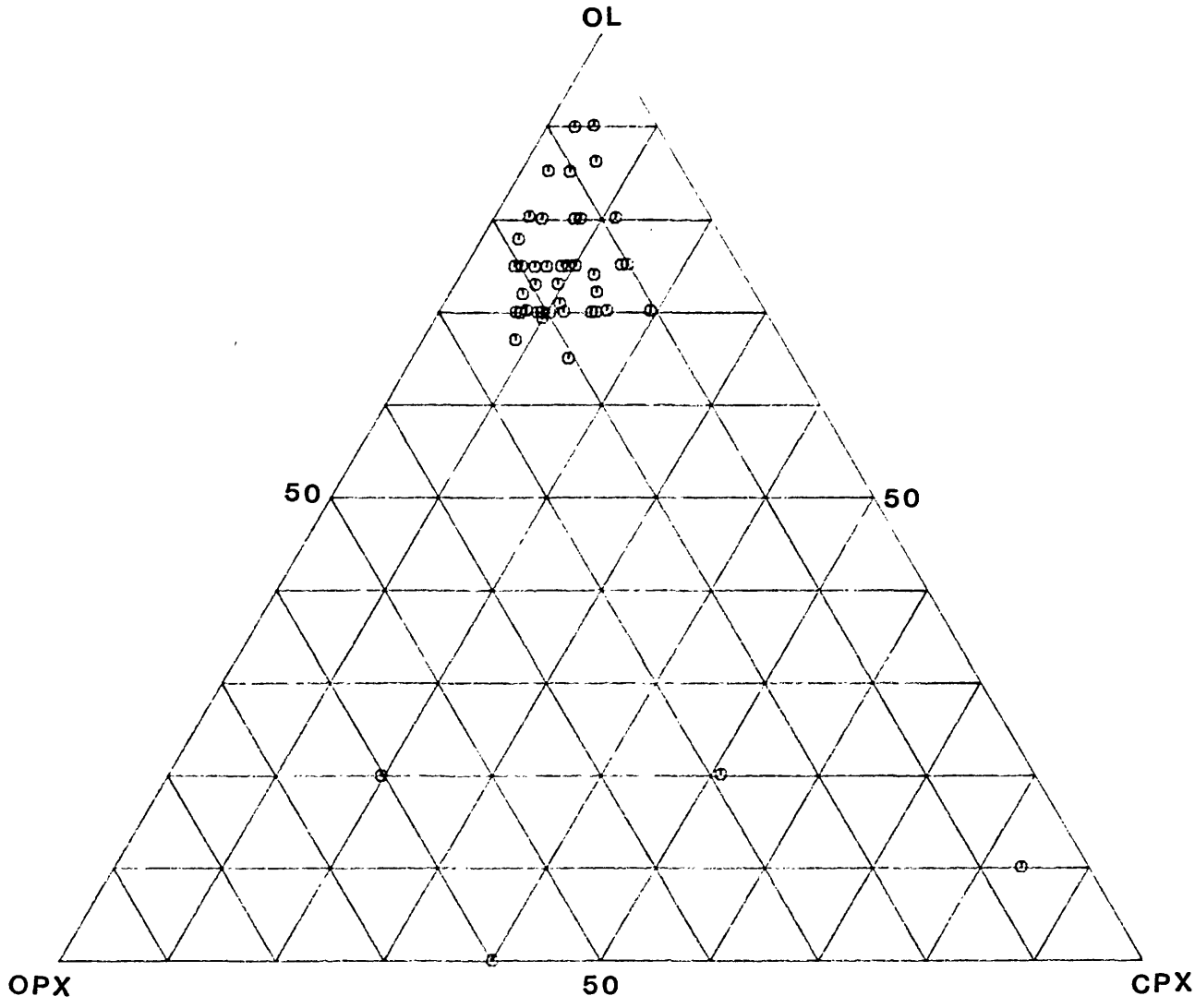

Fig. III-3aa. Modal compositions of xenoliths in the Cr-diopside group. Locality No. 66.

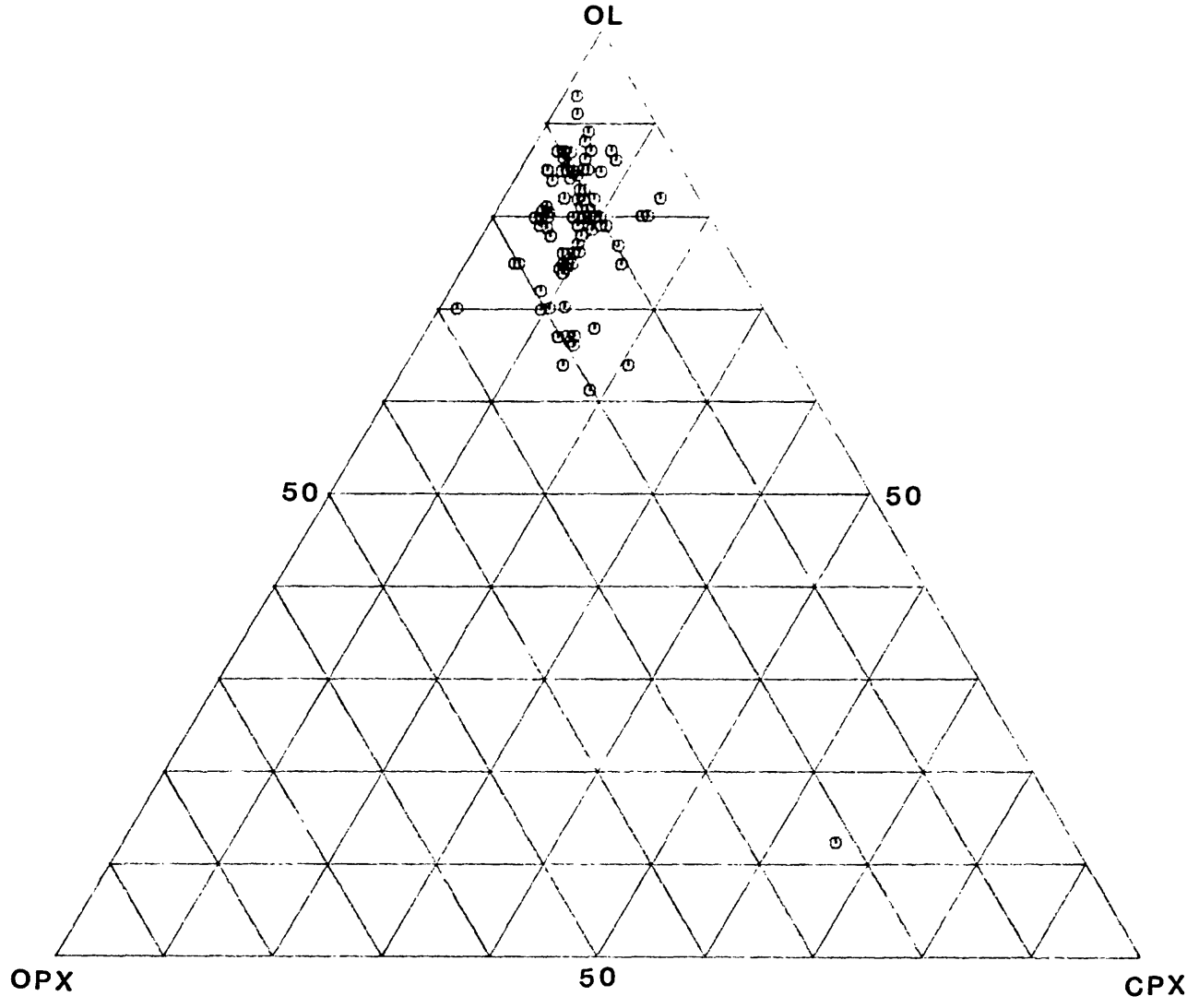

Fig. III-3bb. Modal compositions of xenoliths in the Cr-diopside group. Locality No. 67.

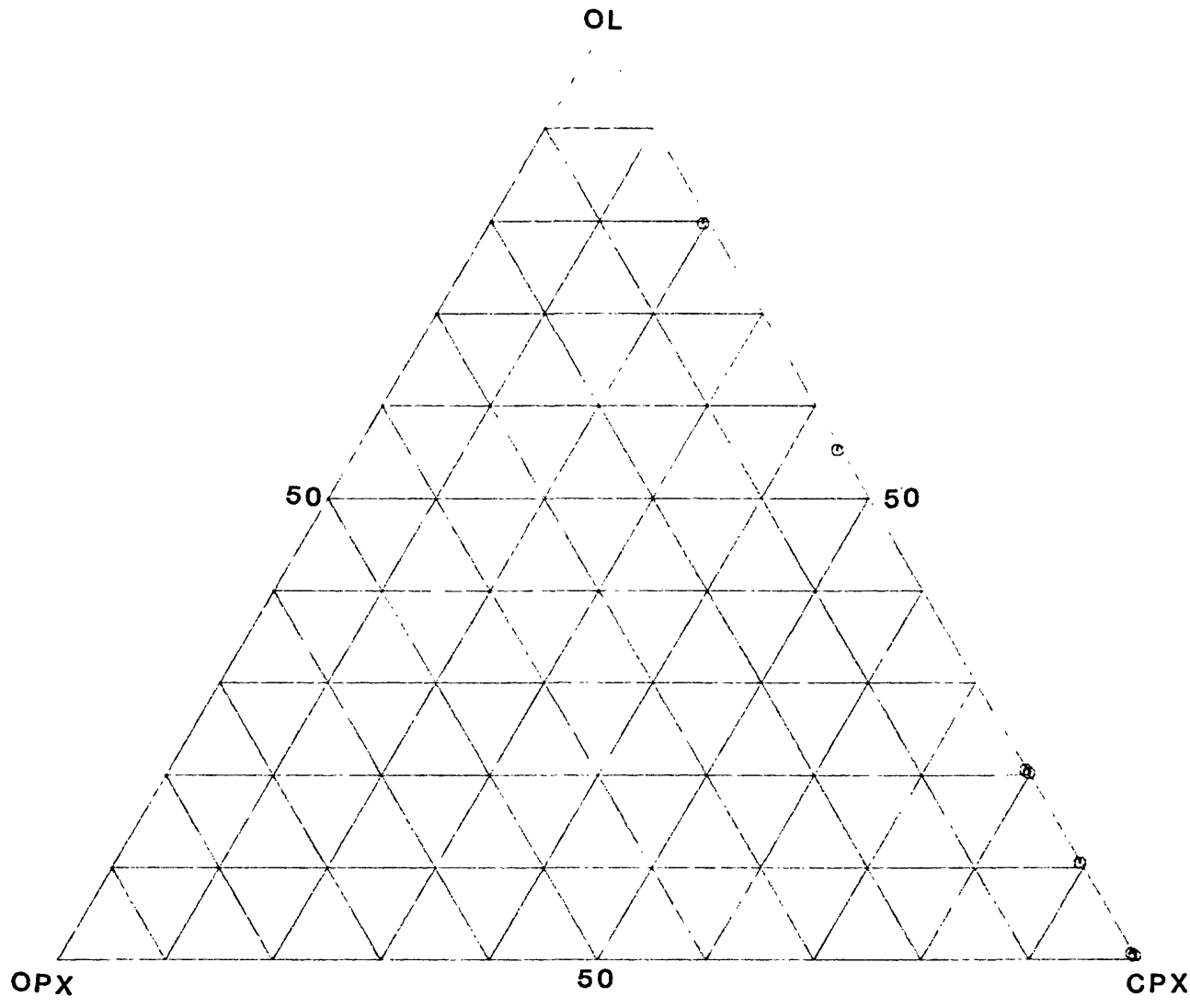

Fig. III-4a. Modal compositions of xenoliths in the Al-augite group. Locality Nos. 1-2.

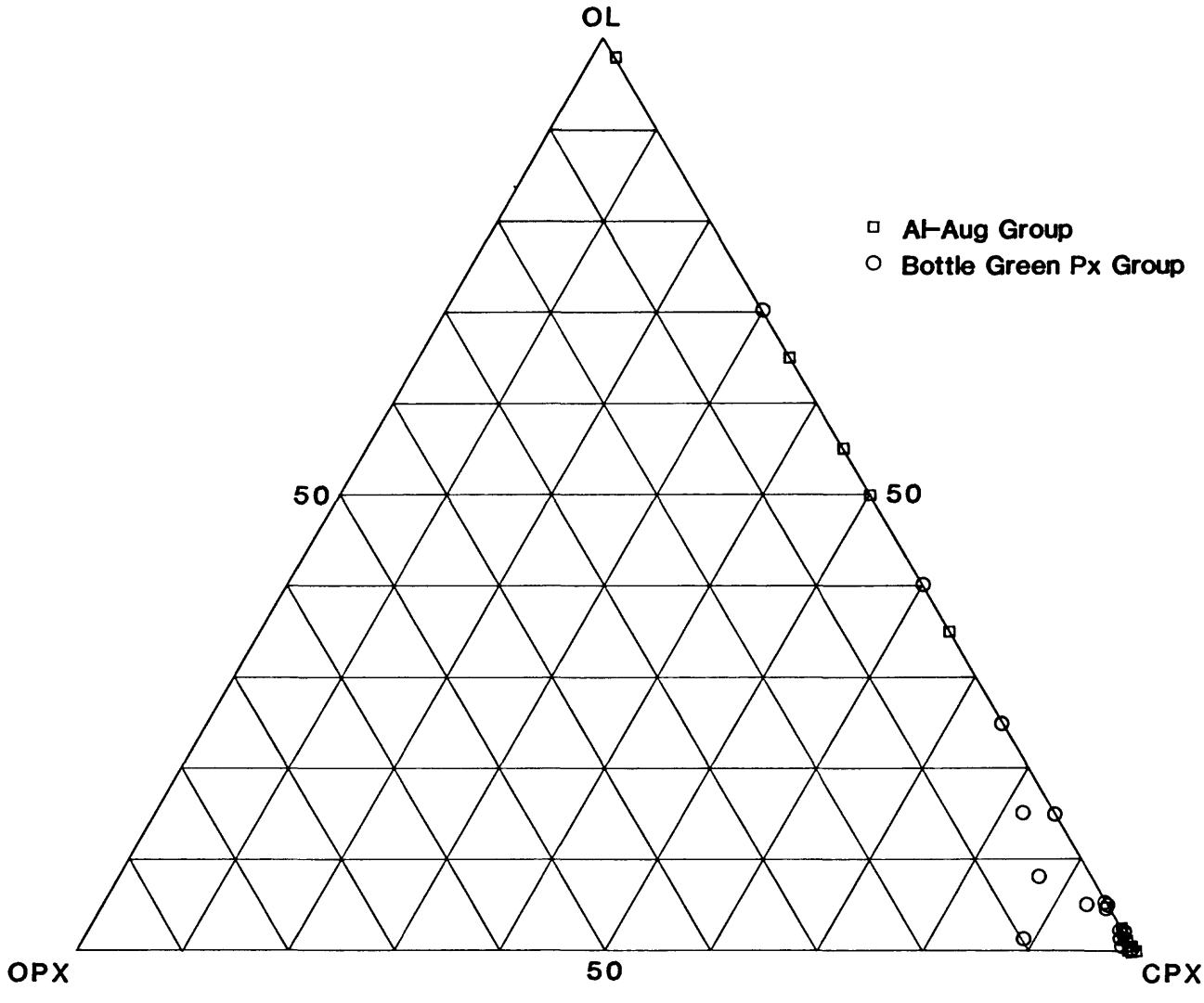

Fig. III-4b. Modal compositions of xenoliths in the Al-augite and bottle green pyroxene groups. Locality No. 11.

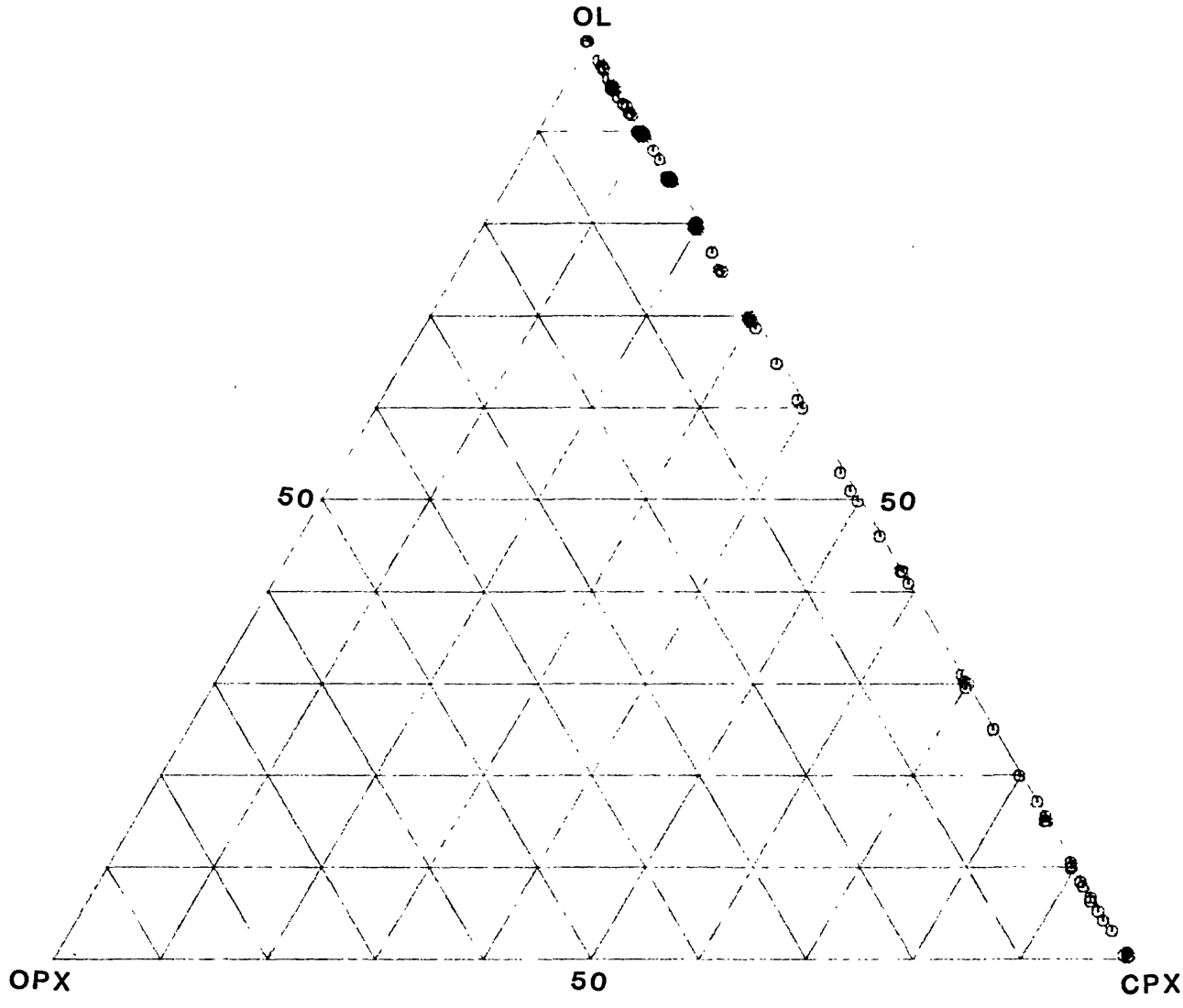

Fig. III-4c. Modal compositions of xenoliths in the Al-augite group. Locality No. 13.

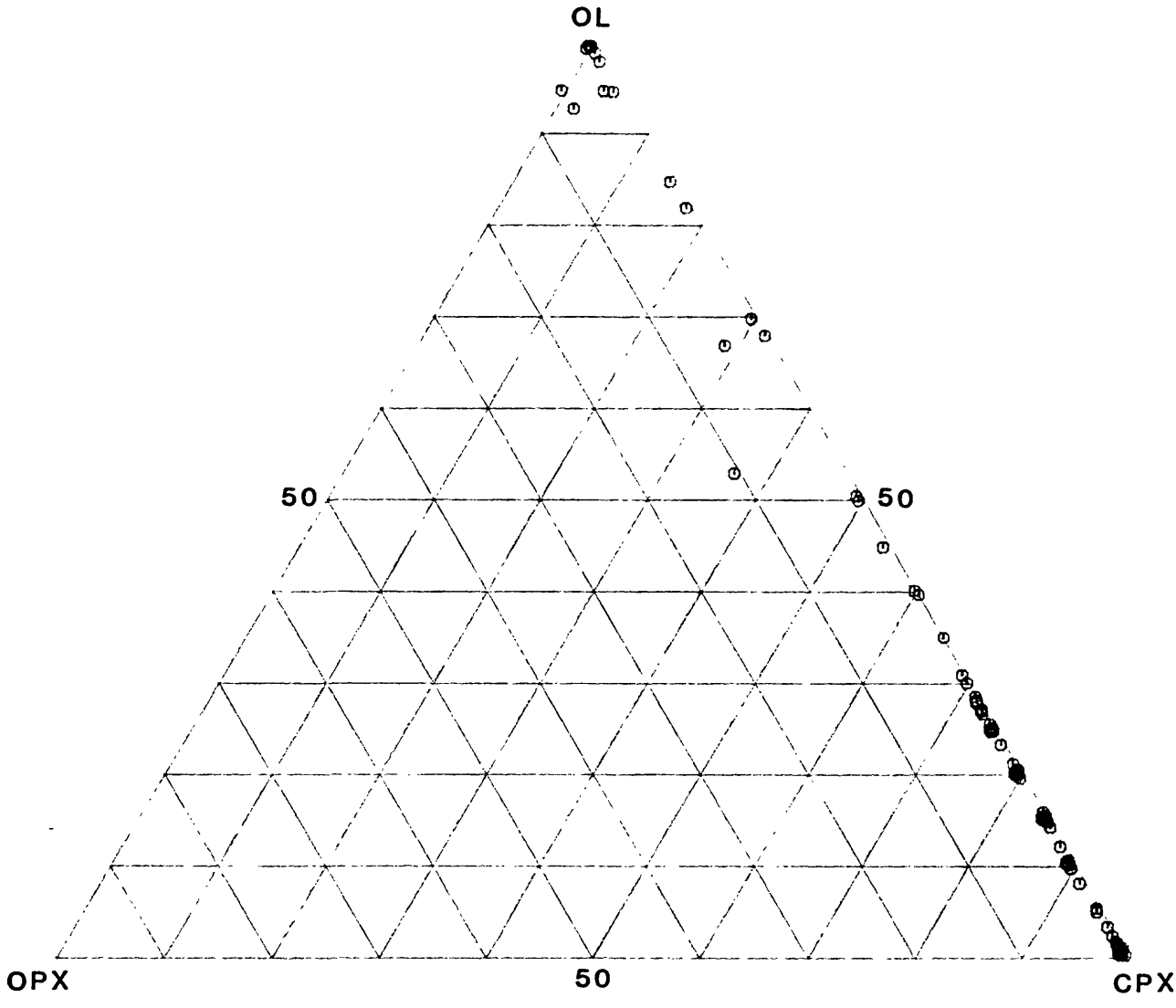

Fig. III-4d. Modal compositions of xenoliths in the Al-augite group. Locality No. 16.

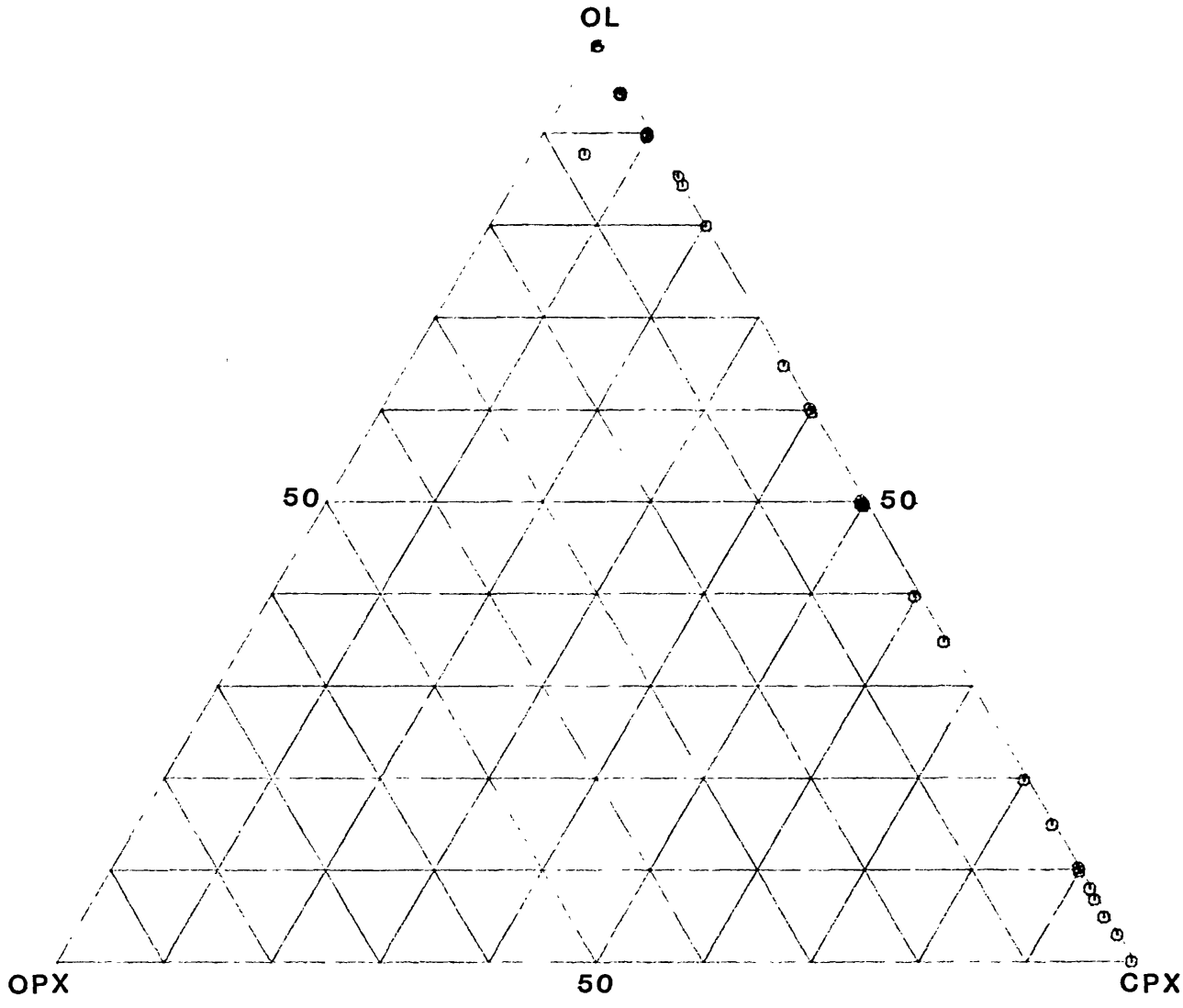

Fig. III-4e. Modal compositions of xenoliths in the Al-augite group. Locality No. 17.

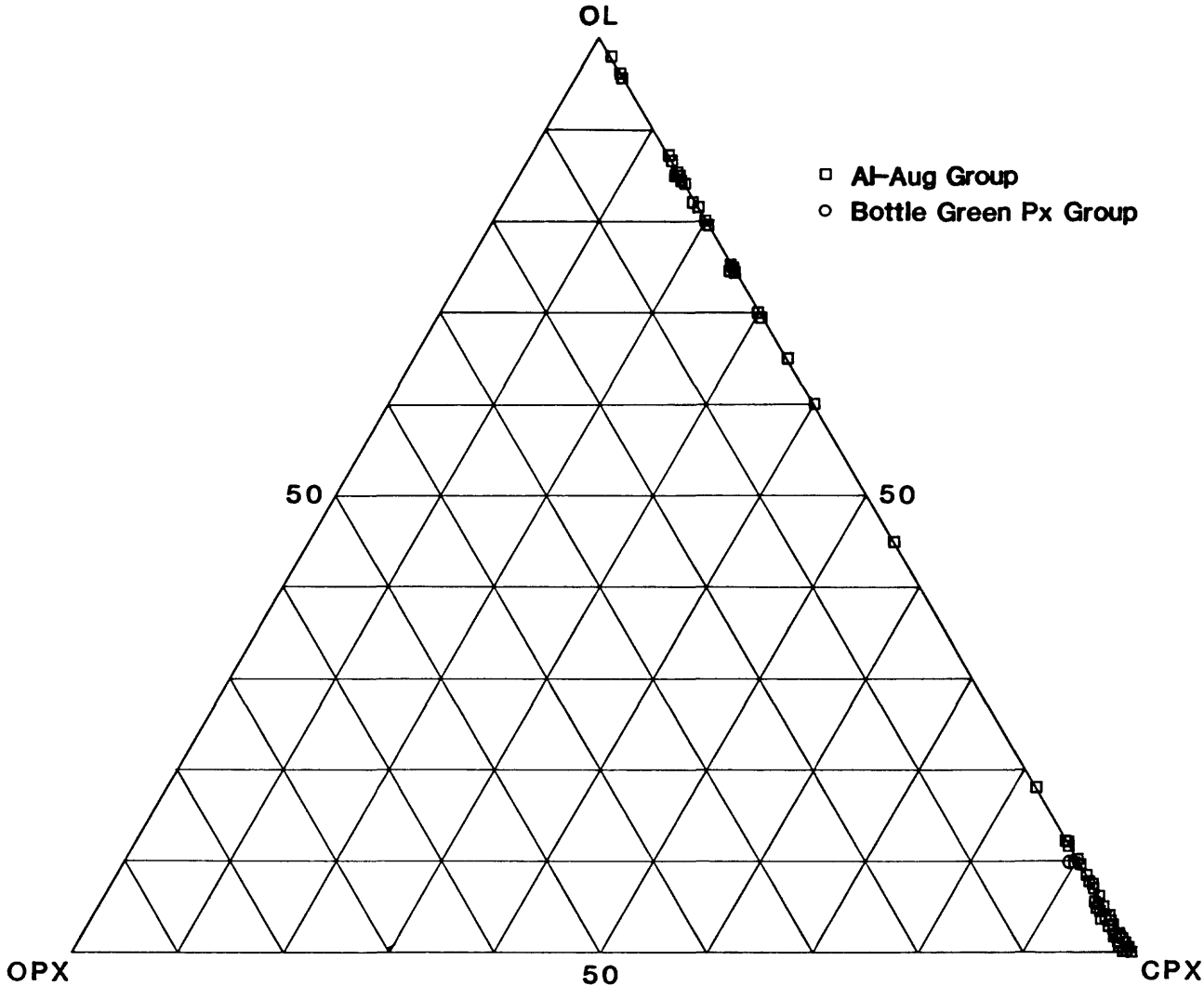

Fig. III-4f. Modal compositions of xenoliths in the Al-augite and bottle green pyroxene groups. Locality No. 39.

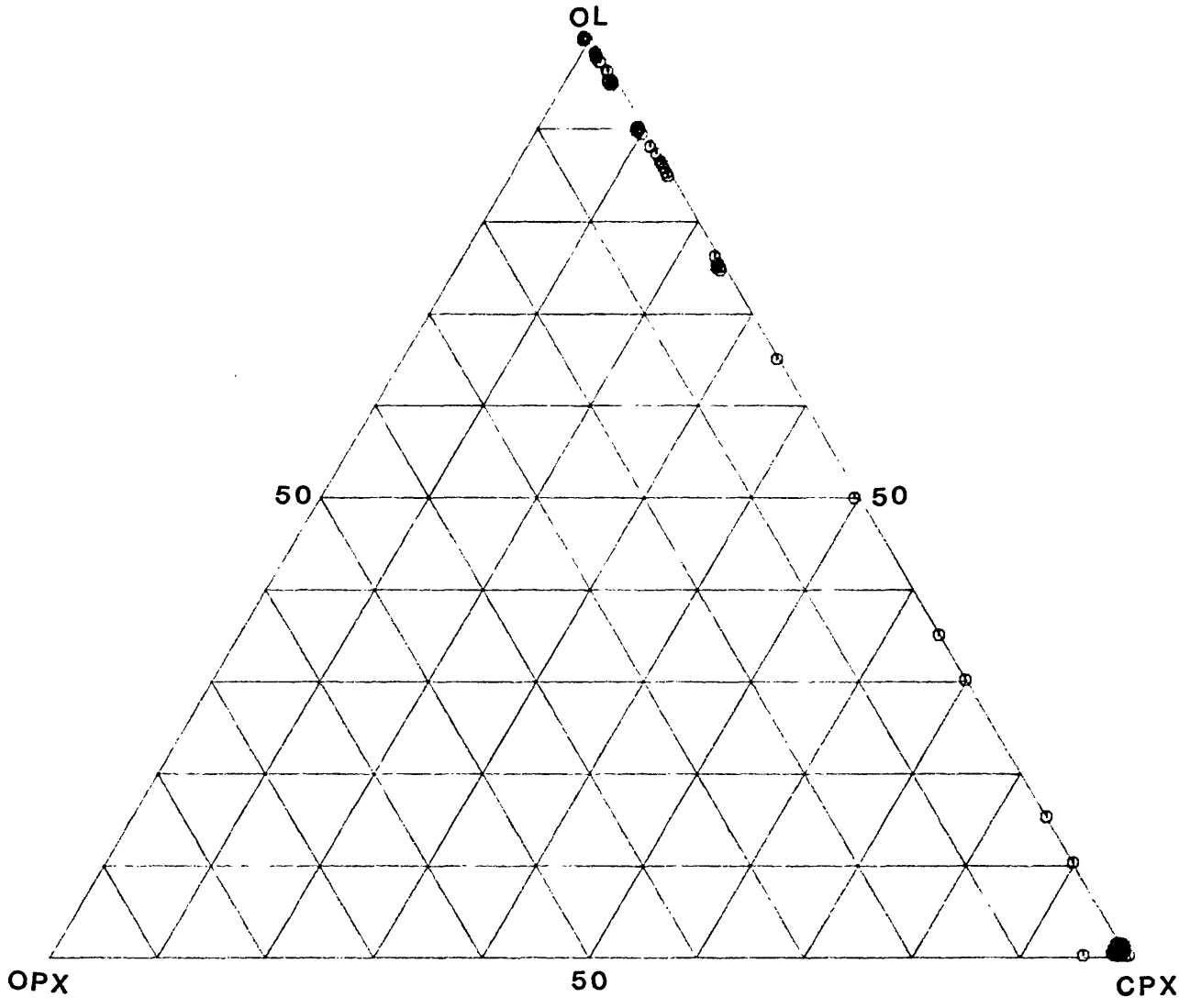

Fig. III-4g. Modal compositions of xenoliths in the Al-augite group. Locality No. 42.

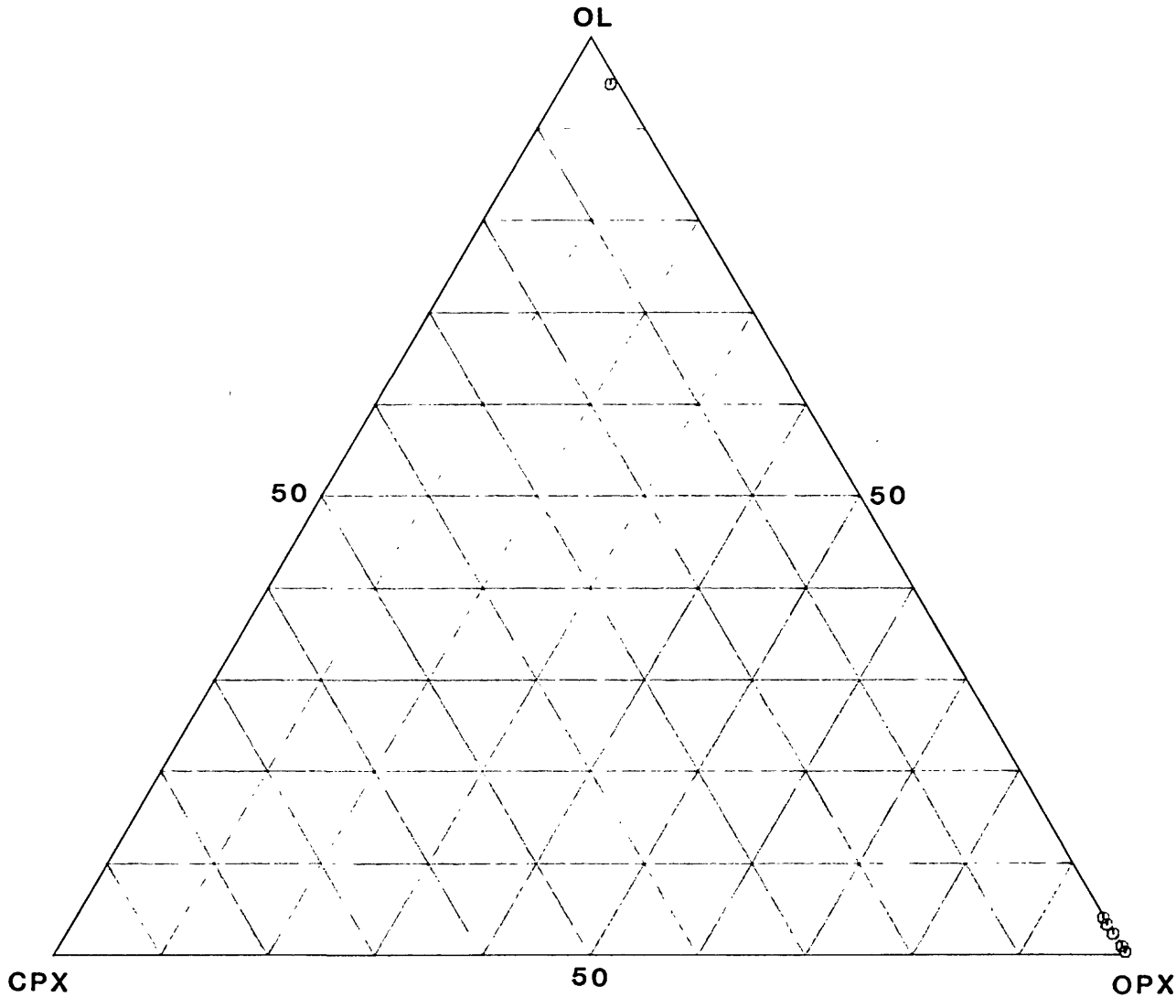

Fig. III-4h. Modal compositions of xenoliths in the Al-augite group. Locality No. 46.

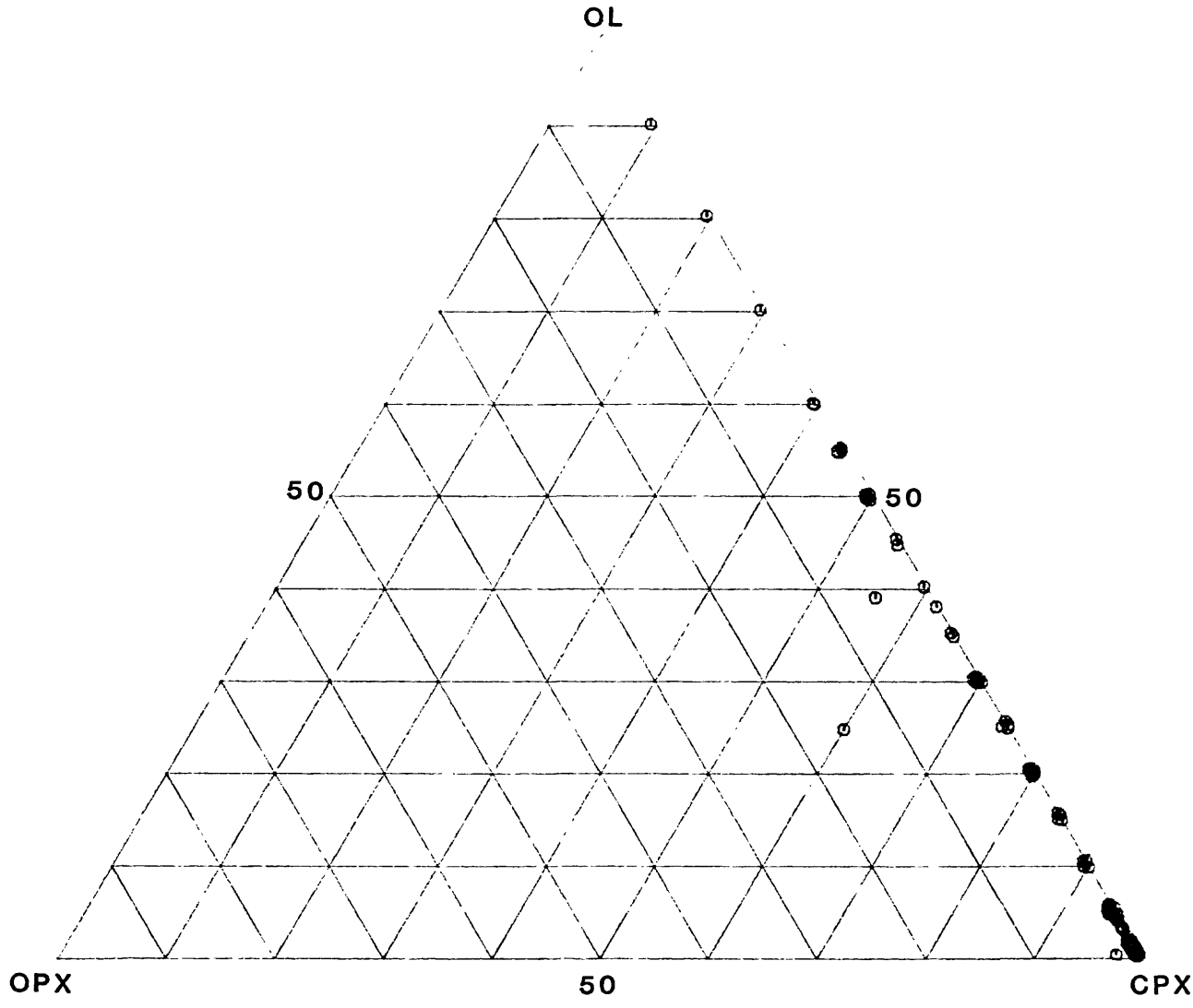

Fig. III-4i. Modal compositions of xenoliths in the Al-augite group. Locality No. 48.

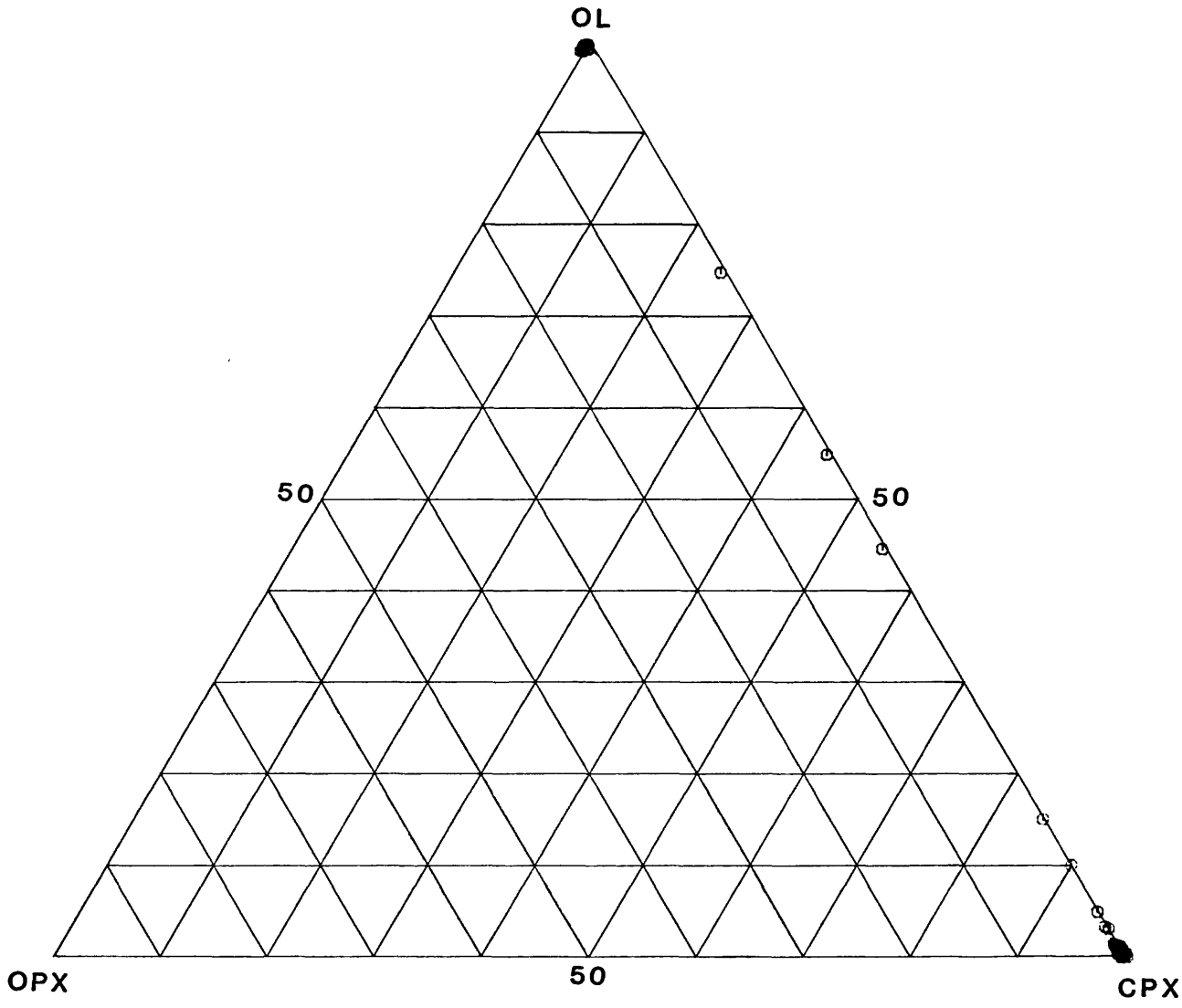

Fig. III-4j. Modal compositions of xenoliths in the Al-augite group. Locality No. 59.

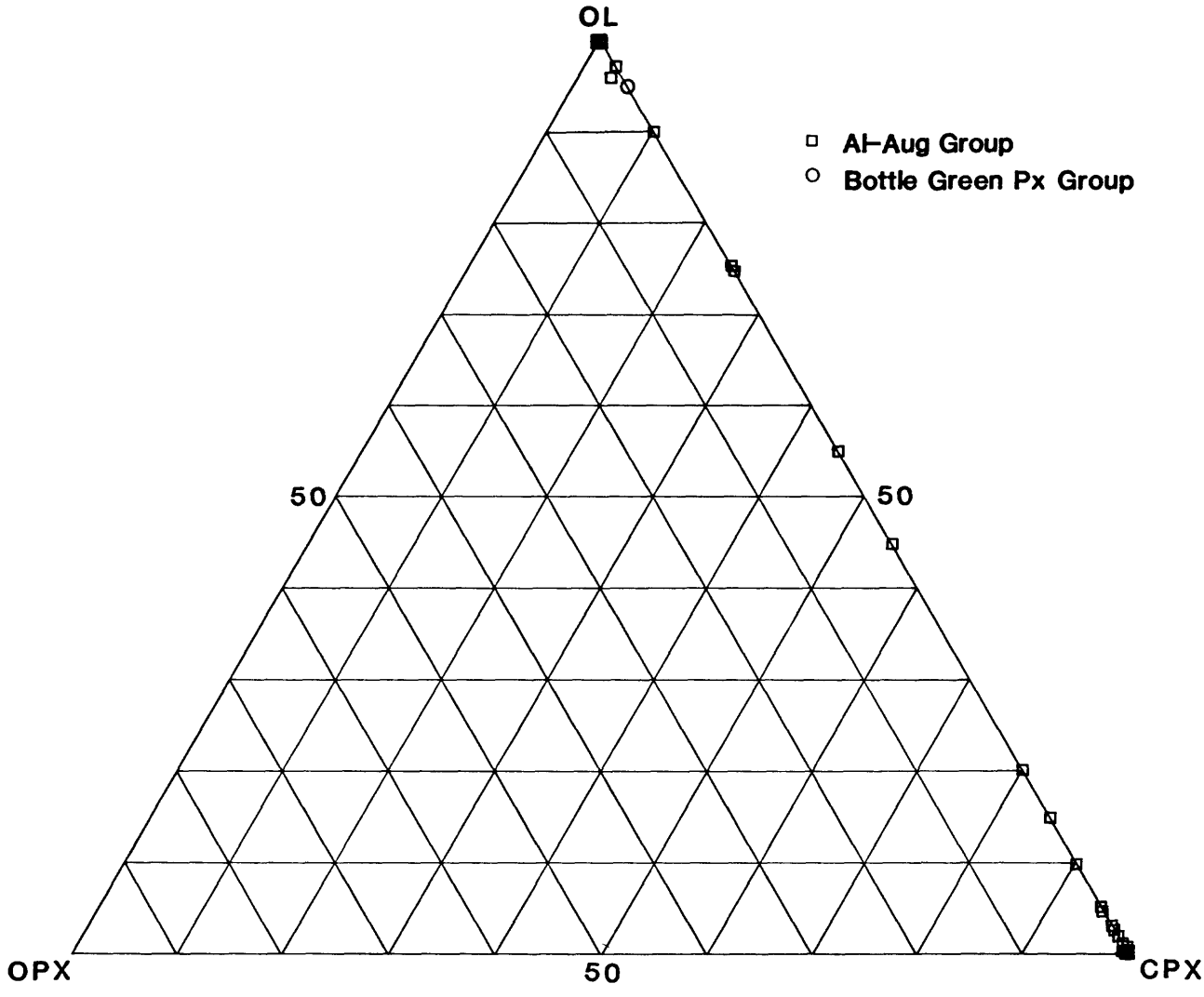

Fig. III-4k. Modal compositions of xenoliths in the Al-augite and bottle green pyroxene groups. Locality No. 60.

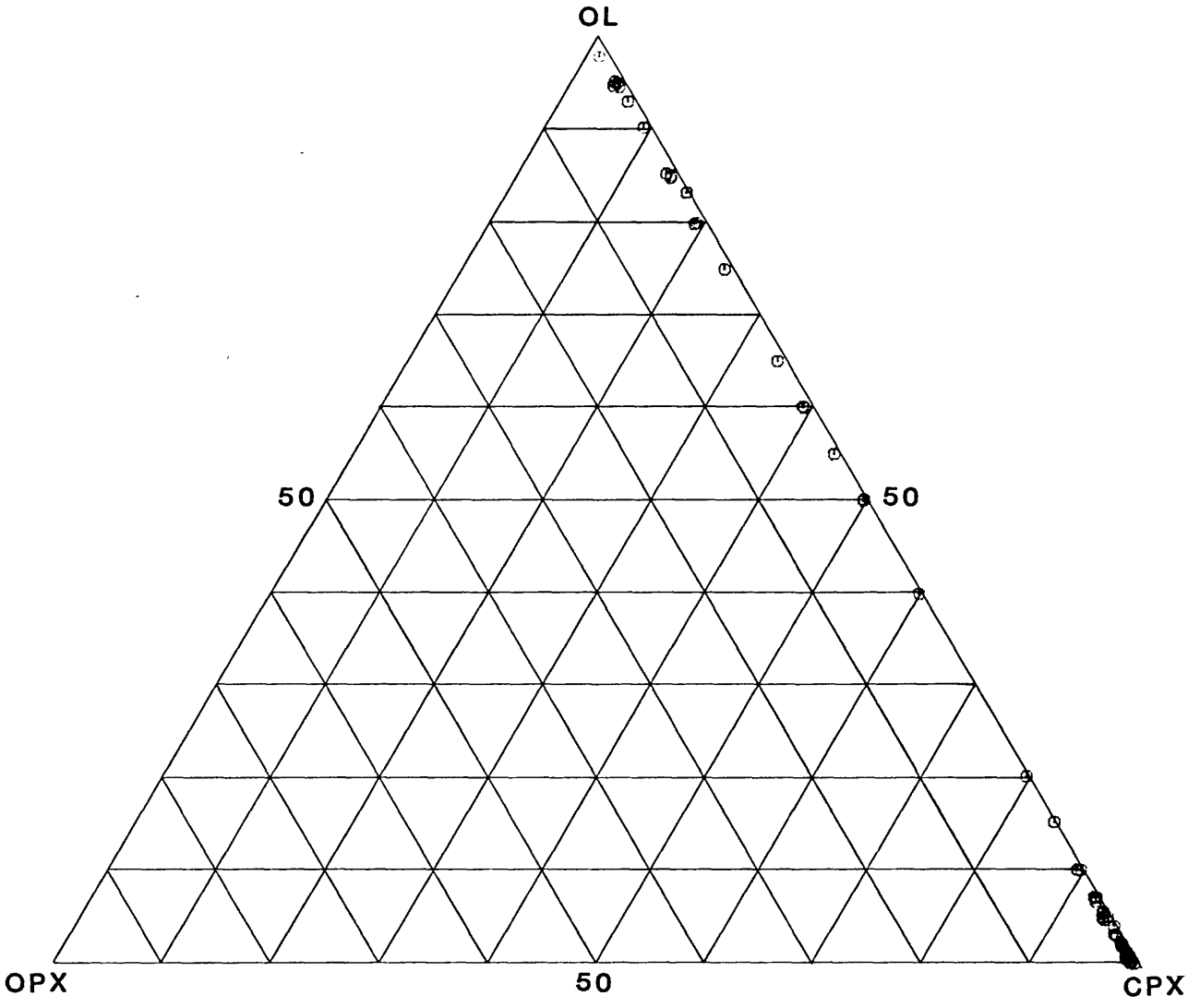

Fig. III-41. Modal compositions of xenoliths in the Al-augite group. Locality No. 63.

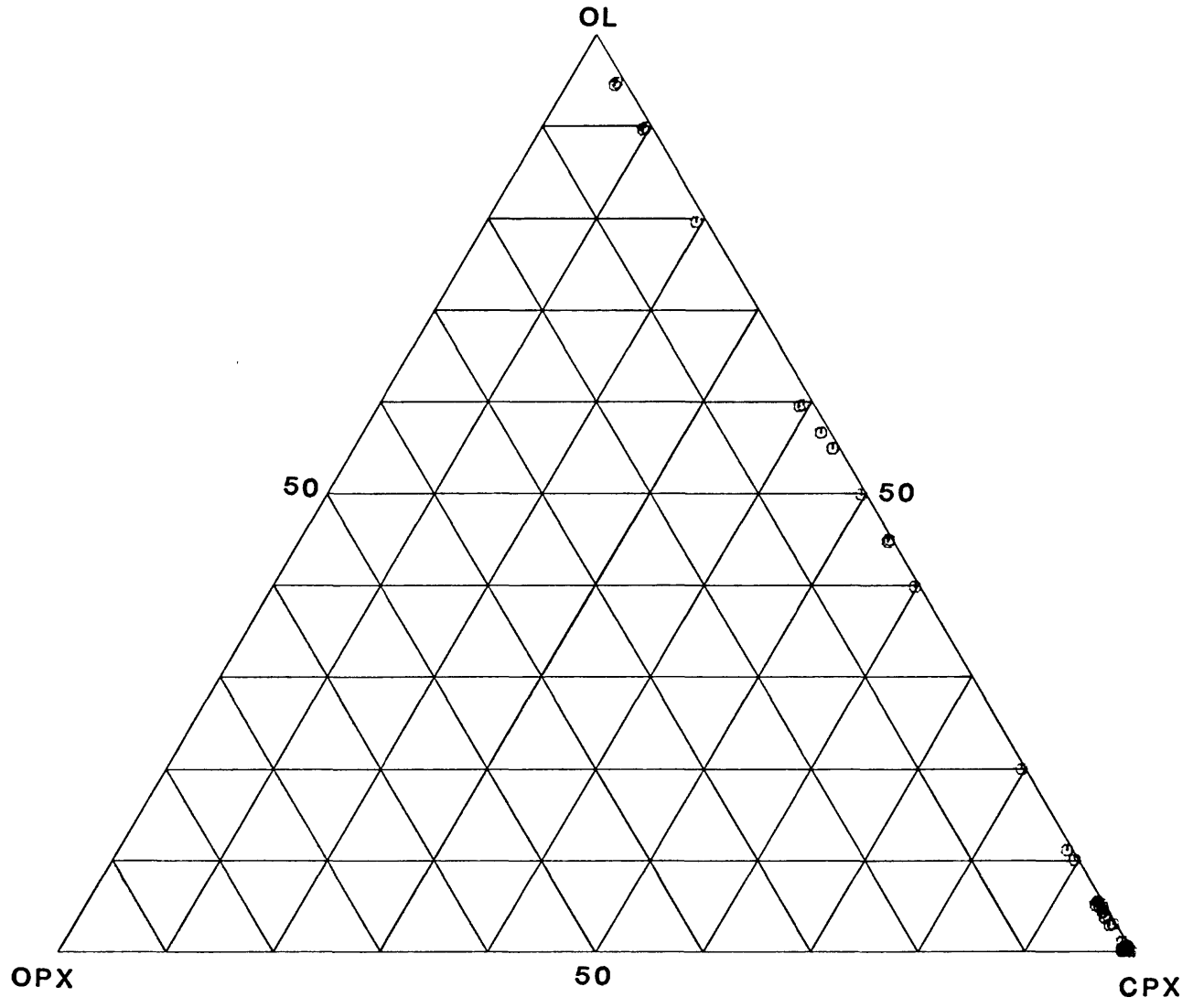

Fig. III-4m. Modal compositions of xenoliths in the Al-augite group. Locality No. 64.

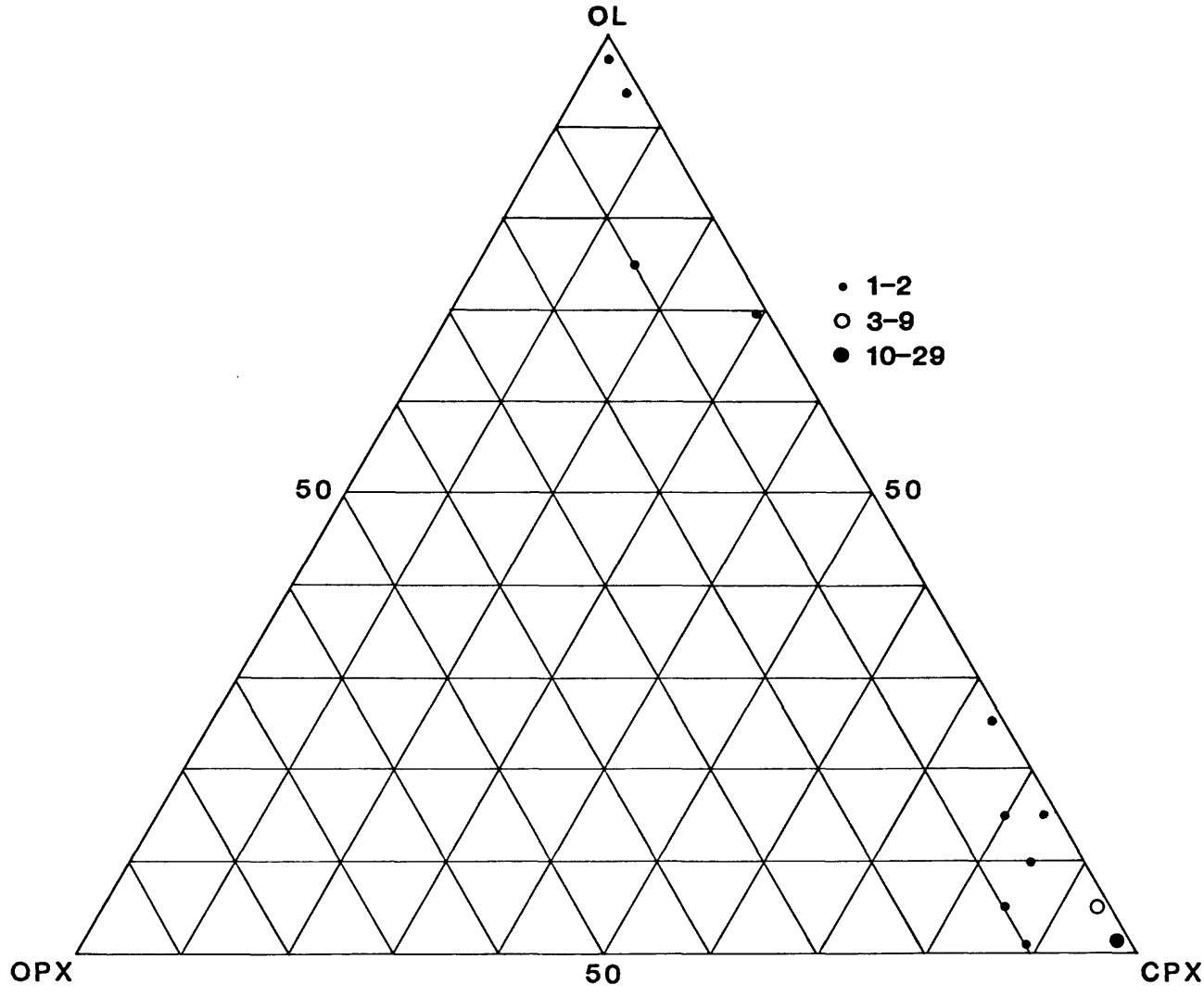

Fig. III-5. Modal compositions of xenoliths in the bottle green pyroxene group. All localities, 34 xenoliths.

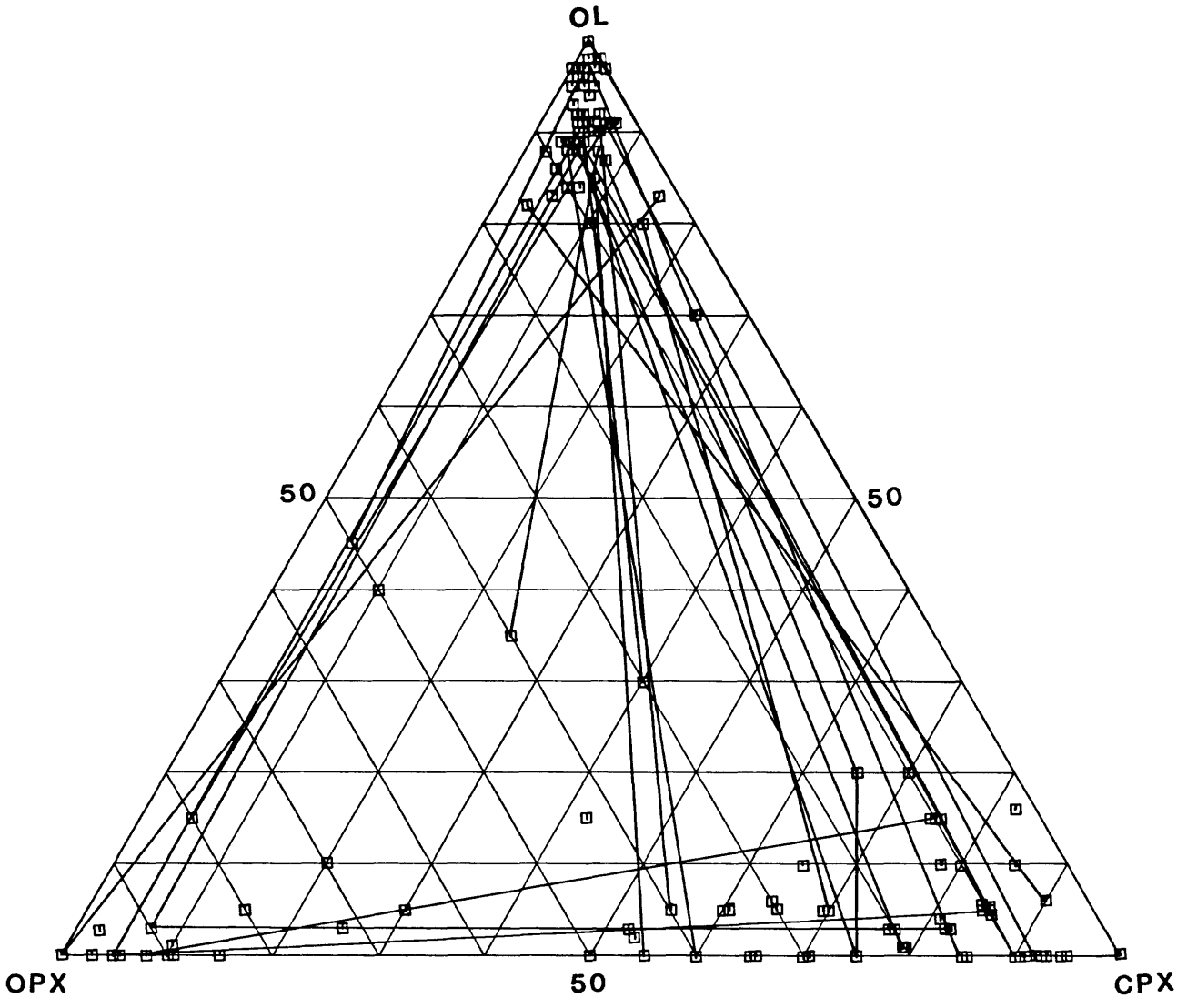

Fig. III-6. Modal compositions of composite xenoliths in the Cr-diopside group. Lines join lithologies in the same xenolith. Locality No. 63.

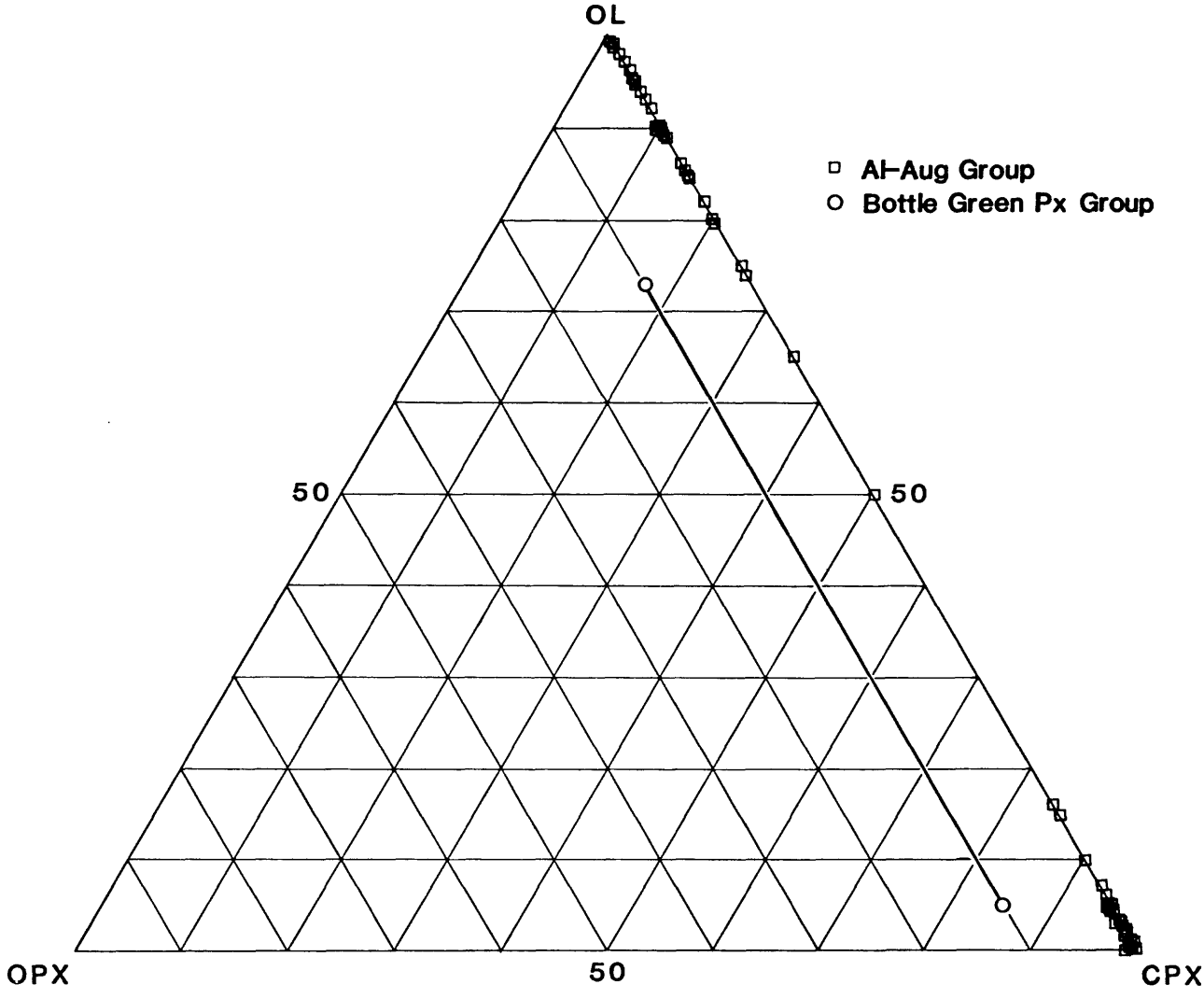

Fig. III-7. Modal compositions of composite xenoliths in the Al-augite and bottle green pyroxene groups. Line joins lithologies in the same xenolith. Locality No. 63.

Figure III-8. Photomicrographs and outcrop photographs of xenoliths. Number at bottom of photomicrographs indicates the width of the field of view. a) Al-augite wehrlite cut by net veins of Al-augite pyroxenite. b) Composite Al-augite pyroxenite comprising a coarse clinopyroxenite (sliver on diagonal from lower right corner) intruded by fine-grained clinopyroxenite (top); both lithologies are crosscut by a medium-grained olivine clinopyroxenite (bottom). c) Al-augite clinopyroxenite with large (relic?) grain surrounded by a mosaic of small grains. d) Al-augite amphibole clinopyroxenite. Amphibole in field of view is largely fused single poikilitic grain (black and dark gray). e) Wehrlite composed of relic clinopyroxene in finely recrystallized olivine matrix. f) Same as e), crossed polarizers. g) Two large clinopyroxene relics in wehrlite; olivine is finely recrystallized, and margins of clinopyroxene relics have undergone cataclasis. h) Small euhedral olivine grains and plagioclase form corona on spinel in feldspathic spinel lherzolite.

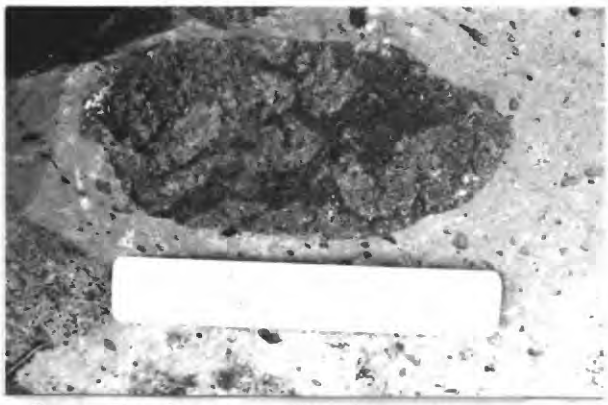

San Carlos Scale, cm a

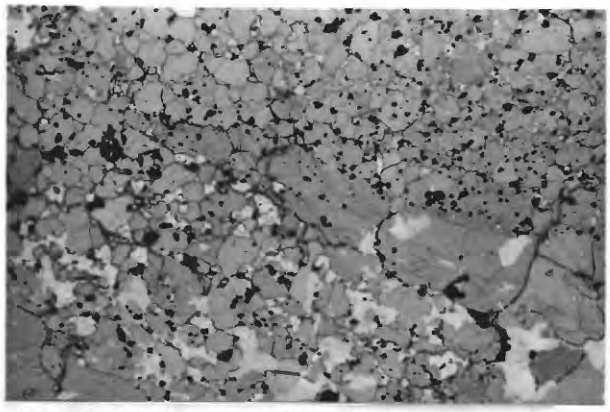

Ep-3-77 8.3mm b

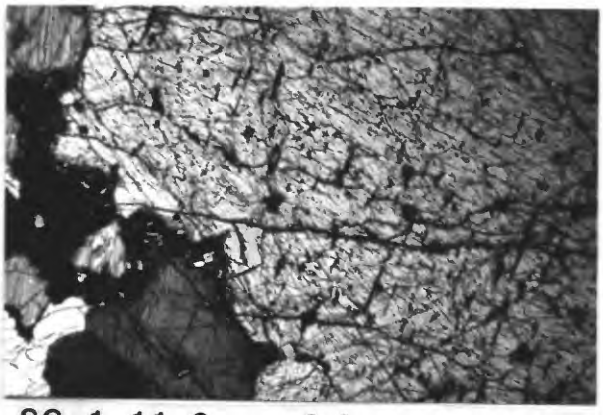

SC-1-11-2 8.3mm c

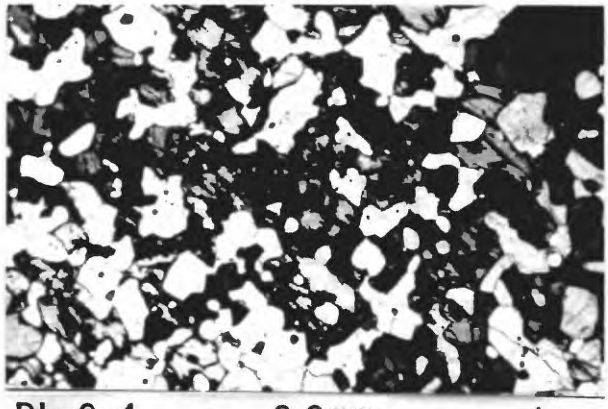

DL-9-4 8.3mm d

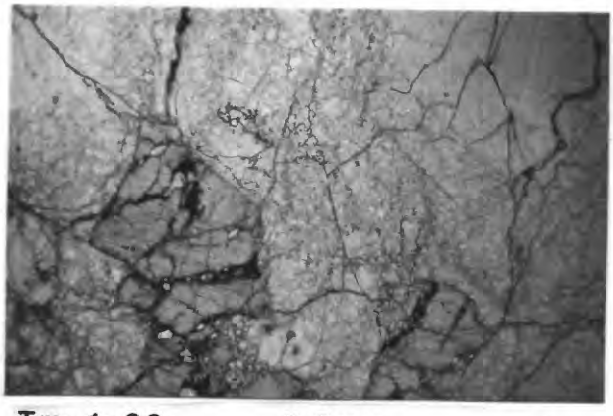

Tm-1-36 8.3mm e

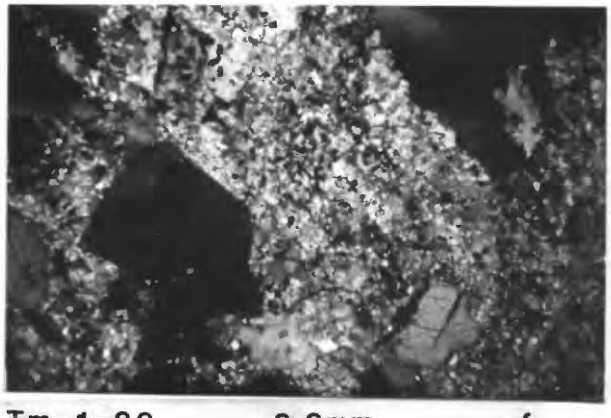

Tm-1-36 8.3mm f

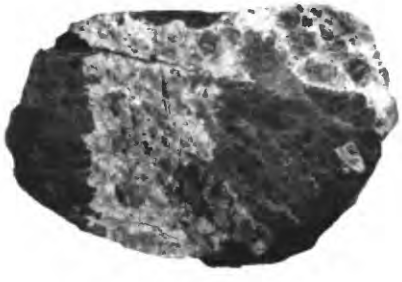

Tm-1-36 g

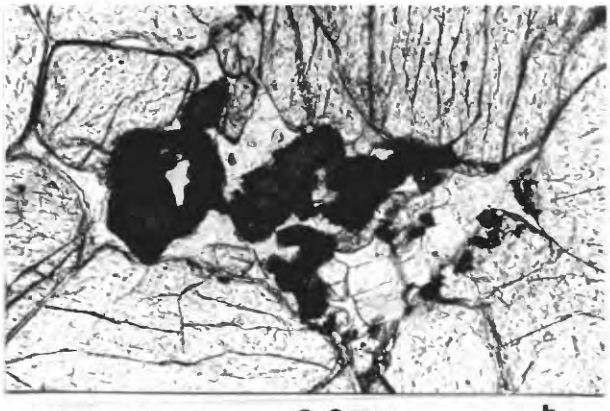

Ki-5-13-1 0.9mm h

Disk 10-xenoliths pp 1-6; Wilshire-sw; 2/15/84;3/7/84

Table III-1A. Relative abundances (100 counts, each location) of Cr-diopside and Al-augite xenoliths, San Carlos, Arizona

	Cr-diopside Lherzolite	Cr-diopside Pyroxenites, Banded Pyroxenite/ Peridotite	Al-augite Lherzolite	Al-augite Pyroxenites, Banded Pyroxenite/ Peridotite
1	78%	8%	6%	8%
2	76	10	5	9
3	79	7	4	10
4	83	7	1	9
5	78	9	1	12
Aveg.	79	8	3	10

All measurements made in quarried parts of flow.

Table III-1B. Relative abundances (100 counts, each location) of Bottle Green Pyroxene, Al-augite, and Cr-diopside xenoliths and megacrysts from two portions of a lava flow, Black Rock Summit, Nevada

		South Lobe	North Lobe
Al-augite Group	Clinopyroxene Megacryst	29%	39%
	Olivine Megacryst	8	3
	Clinopyroxenite	3	2
	Wehrlite	10	5
	Gabbro ± Amphibole	1	0
Bottle Green Pyroxene Group	Clinopyroxene Megacryst	16	16
	Olivine Megacryst	12	14
	Wehrlite/ Harzburgite	5	1
	Dunite Mylonite	8	0
Cr-diopside Group	Lherzolite	1	1
	Feldspar Megacryst	9	20

Table III-2. Data on composite xenoliths, San Carlos, Arizona

Cr-diopside Group					Al-augite Group			
Modal Oliv.	Composition Cpx	Opx	Thickness (mm)	No. of Contacts	Modal Oliv.	Composition Cpx + Opx	Thickness (mm)	No. of Contacts
	90	10	32	1	15	80	14-30	2
88	4	7	34	1	80	18		
	85	15	26	2	79	20		
97	1	1		2	8	97		
	75	25	14	1		100	27	1
20	64	15	17	2	95	5		
86	8	5	27	3				
	74	25	18	1	90	10		multiple
87	5	7	11	1		97		
10	5	85	13	1	87	10	2	
89	6	4		1		98	21	2
3	81	15	14	1	5	93	2-12	mulitple
3	6	90	19	2	95	5		
90	5	4		3	1	99	22	mulitple
82	15	2	33	2	94-98	1-5		
	100			2	83-96	2-15	1	
5	84	10	23	2	3	95	97	1
89	5	5		2	89	10	2	
5	69	25	10	2	5	95	12-32	2
78	15	5		2	50	50	2	
						98	35	2
97	1	1	3	2	90	9	2	
45	5	49	26	2		100	1-30	2
	10	89	43	1	5	91	18	1
79	10	10		1	89-98	1-10	1	
5	54	40	98	1	89	10	1	
91	5	3		1	1-5	95	28	1
5	84	10		zoned, rims	84-97	2-15	2	
	5	94		core		98	45	2
89	4	6						
	55	45	16	2	89-98	1-10		multiple
84	8	7		2	0-10	10-90	2-25	

Table III-2. - Continued

Table III-2. - Continued

1	79	20	62	1
88	4	7		1
15	75	10	zoned, rims	
	8	91	core	
69	25	5	20	2
97	1	1		3
10	89	10	20	2
91	3	5		2
	65	35	gradational	
10	84	5	182	1
	89	10	28	1
90	7	2	27	1
	59	40	35	2
87	4	8		2
5	84	10	25	1
97	1	1		1
1	10	87		
	98		85	1
3	52	45	47	2
88	5	6		2
	92	8	37	1
90	6	3		1
30	39	30	33	2
90	4	5		2
5	49	35	60	1
92	2	5		1
5	90	4	10	2
81	3	15		2
2	77	20	28	1
92	2			1
15	82	2	10	2
83	7	9		2
34	25	40	25	2
87	7	5		2
	93	7	22	1
85	4	10		1
89-90	1-10			2
5	95	10		2
75-88	2-25			multiple
1-3	97	1-7		
65-99	1-35			1
7	93	30		1
85-96	3-15			multiple
1-5	95	12-25		
15	85	55		1
84	15			1
1	99	42		2
74	25			2
2	98	15		1
89	10	0		1
2-3	97-98	40		1
85-99	1-15			1
1	99	15		2
84	15			2
1	99	7		2
97	2			2

Table III-2. - Continued

15	75	10	22	2
94	2	3		2
10	64	25	7	1
88	4	7		1
	92	7	11	2
88	4	7		2
5	15	79	10	2
88	3	8		2
10	20	69	14	1
89	5	5		1
	50	50	27	2
96	2	1		2
	95	5	11	1
99				1
39	10	50	65	1
90	6	3		1
5	84	10	8	2
95	2	2		2
5	84	10		zoned 1
	3	96		
95	2	2		1
5	70	25	7	2
5	70	25	8	2
90	4	5		4
15	75	10	60	1
91	3	5		1
	70	30	11	1
90	5	4		1
	95	5	16	1
95	1	3		1
10	77	12	26	1
96	3			1
3	81	15	18	2
94	1	4		2
3	2	95	30	2
96	1	2		2

Table III-2. - Continued

3	76	20	17	2
96	3			2
15	41	42	15	2
15	41	42	15	2
83	6	10		2
3	81	15	21	2
93	3	3		2
	15	84	30	1
94	3	2		1
5	59	35	6	2
87	2	10		2
5	30	64	12	2
82	5	12		2
2	52	45	40	2
96	1	2		2

Table III-3. Mineral compositions, garnet clinopyroxenite

	Clinopyroxene					Orthopyroxene		Garnet			Spinel
	Wet Chem.	Unrecrys-tallized	Recrys-tallized	Recon-structed	Whole rock	Exsolu-tion	Recrys-tallized	Exsolu-tion	Isolated	Rims on spinel	
SiO_2	50.09	49.7	50.3	49.1	47.92	50.0	50.9	41.1	41.1	41.2	
Al_2O_3	9.41	9.1	8.7	10.9	12.61	7.5	7.2	25.2	24.9	23.7	63.9
Fe_2O_3	0.86				1.63						
		4.7	4.7	5.8		10.0	10.3	11.7	11.7	11.5	14.3
FeO	3.99				5.26						
MgO	14.23	14.0	14.3	15.4	15.43	28.5	28.0	18.2	18.7	18.1	18.9
CaO	19.40	19.4	19.0	16.8	15.49	0.94	0.90	5.5	5.6	5.6	
Na_2O	1.23	0.92	1.0	1.03	0.79						
K_2O	0.015	0.03	0.05	0.02	0.04						
H_2O+					0.07						
H_2O-	0.00				0.09						
TiO_2	0.40	0.55	0.56	0.36	0.31	0.11	0.07	0.15	0.06	0.21	0.01
P_2O_5	0.00				0.01						
MnO	0.13			0.15	0.18			0.40	0.34	0.40	
F	0.00				0.00						
Cr_2O_3	0.19	0.09	0.10	0.16	0.14			0.06	0.07	0.08	2.7
NiO	0.08			0.07	0.05						0.26
V_2O_5	0.09			0.07							
Ign. loss (750°C)	0.03			(CO_2)	0.03						
Total	100.15	98.49	98.71	99.86	100.05	97.05	97.37	102.31	102.47	100.79	100.07

Appendix IV. Bulk Chemical Compositions and CIPW Norms of Xenoliths [1/]

	Olivine Gabbro						Gabbro	
Locality #:	39	40	40	40	40	63	5	23
Sample #:	Ki-2-28	Ki-5-27A	Ki-5-55	Ki-5-91	Ki-5-4B	SC-1-15	SQ-4-105	Dl-5-56
SiO_2	42.87	44.33	45.5	47.2	48.26	45.8	44.66	42.94
Al_2O_3	20.16	13.49	16.3	12.5	12.40	11.5	23.03	9.35
Fe_2O_3	4.70	3.87	5.9	5.7	1.05	4.0	1.77	2.37
FeO	3.38	10.71	6.8	8.7	3.57	6.3	3.62	9.45
MgO	10.23	13.52	7.5	11.7	16.19	16.9	8.95	10.37
CaO	15.95	8.07	10.6	9.4	14.76	12.3	16.98	17.28
Na_2O	1.36	2.36	2.7	2.1	1.69	1.4	.50	.71
K_2O	.10	.35	.22	.12	.10	.15	.03	.02
H_2O^+	.03	.16	.26	.57	.14	.18	.09	.25
H_2O^-	.07	.08	.20	.05	.12	.32	.08	.02
TiO_2	1.09	2.40	2.8	1.2	1.16	.74	.14	6.00
P_2O_5	.04	.13	.12	.09	.04	.10	.03	.05
MnO	.12	.19	.14	.20	.09	.20	.11	.15
CO_2	.02			.15				.09
Cl		.01						
F	.01	.02			.01		.01	.01
S	.03	.02						.09
Cr_2O_3		.09			.19			
NiO		.04			.10			
Subtotal	100.16	99.84	99.04	99.68	99.87	99.89	100.00	99.15
Less O	.01	.02						.05
Total	100.15	99.82	99.04	99.68	99.87	99.89	100.00	99.10
q								
or	.59	2.06	1.32	.72	.59	.89	.18	.12
ab	2.89	19.77	23.11	17.94	11.48	11.90	4.23	5.67
an	48.53	25.06	32.08	24.56	26.01	24.76	60.52	22.48
lc								
ne	4.66				1.55			.22
hl		.02						
di	23.45	11.09	16.09	16.80	36.99	28.40	18.68	50.17
hy		3.83	8.48	22.85		2.02	.21	
ol	10.69	26.16	4.34	5.94	19.00	24.38	13.10	5.77
cm		1.30			.28			
mt	6.80	5.58	8.65	8.34	1.53	5.83	2.57	3.47
hm								
il	2.07	4.53	5.38	2.30	2.21	1.41	.27	11.50
ap	.10	.31	.29	.22	.10	.24	.07	.12
cc	.05			.34				.21
fr	.01	.02			.01		.02	.01
pr	.06	.04						

[1/] See Appendix VI for additional bulk compositions of xenoliths.

Appendix IV, Continued

	Norite		Gabbronorite					
Locality #:	66	67	4	4	67	42	40	40
Sample #:	Ep-1-53	Ep-3-133	SQ-1-107	SQ-1-106	Ep-3-112	Wk-1-76	Ki-5-47	Ki-5-112
SiO_2	50.7	52.6	43.77	44.56	46.57	46.66	51.5	51.7
Al_2O_3	18.7	22.1	17.45	18.26	14.57	20.57	16.5	10.4
Fe_2O_3	3.6	2.2	5.33	2.24	2.95	2.68	1.3	1.5
FeO	4.4	4.2	9.50	4.37	5.99	2.50	6.5	8.5
MgO	10.4	4.6	7.95	15.52	12.23	8.09	7.8	17.0
CaO	8.0	7.9	13.66	14.03	15.05	15.06	11.0	7.1
Na_2O	2.6	4.0	.91	.46	1.40	2.05	2.7	1.7
K_2O	.30	.64	.05	.03	.10	.10	.26	.28
H_2O^+	.35	.18	.08	.24	.09	.55	.77	.59
H_2O^-	.05	.04	.09	.14	.02	.66	.06	.05
TiO_2	.31	.76	1.04	.07	.97	.53	.96	.79
P_2O_5	.06	.07	.01	.02	.03	.01	.14	.10
MnO	.18	.08	.18	.11	.16	.08	.13	.18
CO_2		.21	.01		.04	.56	.25	
Cl				.01				
F			.01	.01	.02	.02		
S			.02		.02			
Cr_2O_3								
NiO								
Subtotal	99.65	99.58	100.06	100.07	100.21	100.12	99.87	99.89
Less O			.01		.02	.01		
Total	99.65	99.58	100.05	100.07	100.19	100.11	99.87	99.89
q		1.70					.65	
or	1.78	3.80	.30	.18	.59	.59	1.54	1.66
ab	22.09	34.00	7.70	3.82	11.17	17.16	22.89	14.41
an	38.62	37.58	43.36	47.68	33.11	46.57	32.20	19.95
lc								
ne					.35	.09		
hl				.02				
di	.66		19.67	17.15	32.49	19.08	16.17	11.75
hy	30.25	16.32	11.48	4.11			21.17	41.44
ol			7.56	23.23	15.83	9.07		6.30
cm								
mt	1.18	3.21	7.73	3.25	4.27	3.88	1.89	2.18
hm								
il	.99	1.45	1.97	.13	1.84	1.01	1.83	1.50
ap	.29	.17	.02	.05	.07	.02	.33	.24
cc		.48	.02		.09	1.27	.57	
fr			.02	.02	.04	.04		
pr					.04			

Appendix IV, Continued

	Olivine Metagabbro			Metanorite		Metagabbronorite		
Locality #:	19	4	40	67	67	5	47	67
Sample #:	Ec-103	SQ-1-108	Ki-5-98	Ep-3-162-1	Ep-3-124	SQ-4-106	Wi-1-112	Ep-3-153
SiO_2	44.80	45.18	49.7	50.14	57.7	43.41	46.39	46.8
Al_2O_3	13.50	21.07	14.6	11.92	16.3	22.02	21.77	17.8
Fe_2O_3	7.55	1.39	3.0	1.29	2.1	2.96	2.71	5.4
FeO	6.26	4.77	7.6	3.87	7.2	5.51	3.78	8.9
MgO	11.79	10.28	8.6	20.37	4.9	13.64	9.39	7.6
CaO	10.79	16.52	10.8	9.88	6.7	11.31	13.18	5.7
Na_2O	2.29	.47	2.8	1.51	2.6	.51	1.92	3.1
K_2O	.20	.02	.26	.06	.75	.06	.05	.30
H_2O^+	.08	.06	.35	.04	.36	.23	.20	.44
H_2O^-	.08	.09	.04	.04	.06	.21	.13	.02
TiO_2	1.49	.12	1.9	.46	1.0	.08	.45	2.7
P_2O_5	.06	.01	.12	.02	.13	.11	.05	.07
MnO	.19	.11	.18	.11	.14	.14	.09	.21
CO_2	.91	.02		.03		.01	.01	
Cl						.01		
F	.02	.01				.02	.01	
S	.01			.01		.01		
Cr_2O_3				.19			.03	
NiO				.11			.02	
Subtotal	100.02	100.12	99.95	100.05	99.94	100.24	100.18	99.04
Less O	.02			.01		.02		
Total	100.00	100.12	99.95	100.04	99.94	100.22	100.18	99.04
q					14.22			.72
or	1.18	.12	1.54	.35	4.44	.18	.30	1.79
ab	19.37	3.97	23.71	12.74	22.03	3.82	16.24	26.49
an	25.96	55.26	26.53	25.49	30.63	47.68	50.68	28.10
lc								
ne								
hl						.02		
di	16.77	21.06	21.19	18.16	1.48	17.15	11.27	
hy	10.59	1.89	14.62	20.69	21.60	4.11	2.22	27.01
ol	9.93	15.23	3.83	19.33		23.23	6.99	
cm				.28				
mt	10.95	2.01	4.35	1.87	3.05	3.25	3.93	7.91
hm								
il	2.83	.23	3.61	.87	1.90	.13	.85	5.18
ap	.14	.02	.28	.05	.31	.05	.12	.17
cc	2.07	.05		.07			.02	
pf	.03	.02				.02	.01	
fr	.02			.02				
c								2.20

Appendix IV, Continued

Locality #:	67	47	67	33	66	36
Sample #:	Ep-3-104	Wi-1-106	Ep-3-127	Ba-2-112	Ep-1-54	Ba-5-24
SiO_2	48.15	49.39	50.0	51.49	51.5	52.2
Al_2O_3	18.46	14.20	17.0	19.95	26.8	19.7
Fe_2O_3	2.14	1.99	2.5	2.19	1.0	2.4
FeO	7.67	4.16	6.1	2.14	1.2	5.5
MgO	12.08	11.41	9.4	3.05	2.7	3.9
CaO	8.23	15.99	10.3	13.79	11.8	10.0
Na_2O	2.14	1.52	2.4	3.90	3.8	3.6
K_2O	.22	.04	.30	.58	.32	.64
H_2O^+	.01	.15	.69	.17	.27	.39
H_2O^-	.10	.17	.05	.15	.06	.07
TiO_2	.51	.64	.62	1.11	.13	1.1
P_2O_5	.05	.08	.06	.21	.03	.33
MnO	.17	.11	.15	.07	.07	.17
CO_2	.14	.02		.82		
Cl	.01					
F	.03	.01		.03		
S		.02		.07		
Cr_2O_3		.07				
NiO		.02				
Subtotal	100.11	99.99	99.57	99.72	99.68	100.00
Less O	.01	.01		.05		
Total	100.10	99.98	99.57	99.67	99.68	100.00
q				.97		2.03
or	1.30	.24	1.78	3.44	.89	3.79
ab	18.01	12.87	20.41	33.09	11.90	30.48
an	39.39	32.01	34.89	35.32	24.76	35.73
lc						
ne						
hl	.02					
di		36.97	12.89	16.95	28.40	9.61
hy	22.16	6.23	20.79		2.02	11.64
ol	14.18	6.99	3.59		24.38	
cm						
mt	3.10	2.89	3.64	3.18	5.83	3.48
hm						
il	.97	1.22	1.18	2.11	1.41	2.09
ap	.12	.19	.14	.50	.24	.78
cc	.32	.05		1.87		
fr	.05	.01		.02		
c	.27					
pr		.04		.13		

Appendix IV, Continued

	Cr-diopside Lherzolite							
Locality #:	32	32	32	33	36	36	66	66
Sample #:	Ba-1-22	Ba-1-48	Ba-1-52	Ba-2-3	BA-5-12	Ba-5-18	Ep-1-13	Ep-1-19
SiO_2	44.31	43.68	44.43	44.82	44.81	44.06	44.09	43.5
Al_2O_3	3.25	1.58	3.19	2.85	4.14	3.21	3.77	2.5
Fe_2O_3	.81	.71	2.00	.80	1.13	.86	.72	.76
FeO	7.19	7.33	7.24	7.02	6.84	7.54	7.53	7.4
MgO	40.56	44.64	39.14	40.85	39.18	40.97	39.11	41.7
CaO	2.67	.97	2.78	2.39	3.13	2.41	3.44	2.5
Na_2O	.23	.06	.27	.16	.22	.19	.37	.22
K_2O	.01	.01	.01		.02	.01		.09
H_2O^+	.03	.02	.10	.02	.13	.12	.01	.56
H_2O^-	.02	.05	.10	.07	.02	.02		.06
TiO_2	.10	.04	.08	.06	.13	.10	.14	.11
P_2O_5	.01	.01			.01	.01	.01	.05
MnO	.13	.13	.17	.13	.13	.13	.14	.17
CO_2	.03	.02	.05	.06	.03	.05	.02	
Cl		.01				.01		
F	.01		.01		.01			
S								
Cr_2O_3	.39	.40	.41	.41	.04	.31	.37	
NiO	.28	.30	.24	.28	.03	.27	.25	
Subtotal	100.03	100.26	100.22	99.92	100.00	100.27	99.97	99.62
Less O								
Total	100.03	100.26	100.22	99.92	100.00	100.27	99.97	99.62
q								
or	.06	.06	.06		.12	.06		.53
ab	1.95	.43	2.28	1.36	1.86	1.53	3.13	1.87
an	7.80	4.05	7.45	7.06	10.25	7.89	8.63	5.59
lc								
ne								
hl		.02				.02		
di	4.03	.45	4.67	3.49	3.91	2.88	6.51	5.15
hy	16.37	17.59	19.84	21.01	19.08	16.37	11.52	11.39
ol	67.67	75.55	61.71	64.98	62.58	69.08	68.27	73.46
cm	.57	.59	.60	.60	.60	.46	.55	
mt	1.17	1.03	2.89	1.16	1.64	1.24	1.04	1.11
hm								
il	.19	.08	.15	.11	.25	.19	.27	.21
ap	.02	.02			.02	.02	.02	.12
cc	.07	.05	.11	.14	.07	.11	.05	
fr	.02		.02	.02				

Appendix IV, Continued

	Cr-diopside Lherzolite							
Locality #:	67-C*	67	67	67	67	67	67-C	40
Sample #:	Ep-3-162-2	Ep-3-44	Ep-3-61	Ep-3-72	Ep-3-87	Ep-3-94	EP-3-163-G	Ki-5-12
SiO_2	44.74	45.0	45.2	44.7	46.0	45.1	44.6	45.9
Al_2O_3	3.75	2.6	2.5	2.1	3.3	2.9	3.4	3.7
Fe_2O_3	.95	.58	1.0	1.0	.89	.78	3.7	1.1
FeO	7.85	7.2	6.9	7.2	7.2	7.2	6.2	7.1
MgO	39.03	40.0	40.2	41.8	37.7	40.0	37.1	37.4
CaO	2.62	3.1	2.7	2.3	3.2	2.7	3.7	3.4
Na_2O	.20	.30	.22	.20	.19	.14	.22	.43
K_2O		.06	.07	.08	.09	.03	.07	.05
H_2O^+	.01	.40	.36	.10	.39	.53	.44	.46
H_2O^-	.04	.03	.03	.10	.03	.02	.02	.02
TiO_2	.12	.11	.09	.10	.13	.10	.23	.13
P_2O_5	.01	.04	.05	.05	.04	.10	.04	.04
MnO	.14	.16	.17	.18	.19	.16	.26	.13
CO_2	.02							
Cl								
F.	.01							
S								
Cr_2O_3	.37							
NiO	.26							
Subtotal	100.12	99.58	99.49	99.91	99.35	99.76	99.98	99.86
Less O								
Total	100.12	99.58	99.49	99.91	99.35	99.76	99.98	99.86
q								
or		.36	.42	.47	.54	.18	.41	.30
ab	1.70	2.55	1.87	1.70	1.62	1.19	1.86	3.64
an	9.35	5.60	5.66	4.61	7.94	7.22	8.09	8.03
lc								
ne								
hl								
di	2.69	7.56	5.89	5.12	6.14	4.38	7.87	6.78
hy	21.23	16.53	21.09	17.63	26.56	22.60	23.02	21.76
ol	63.11	65.86	62.96	68.62	55.18	62.35	52.41	57.09
cm	.16							
mt	1.38	.85	1.46	1.45	1.30	1.13	5.37	1.60
hm								
il	.23	.21	.17	.19	.25	.19	.44	.25
ap	.02	.10	.12	.12	.10	.24	.10	.10
cc	.05							
fr	.02							

* "C" designates member of a composite sample

Appendix IV, Continued

	Cr-diopside Lherzolite					
Locality #:	40	40	40	63	63	63
Sample #:	Ki-5-20	Ki-5-39	Ki-5-110	SC-1-1	SC-1-30	SC-1-36
SiO_2	44.9	44.7	44.3	43.5	43.97	45.1
Al_2O_3	3.2	2.9	1.9	2.8	2.05	6.4
Fe_2O_3	1.0	.46	.36	1.4	.69	1.9
FeO	7.5	7.4	7.4	6.9	7.93	6.0
MgO	40.0	39.4	44.1	40.5	43.91	35.1
CaO	2.7	3.3	1.5	3.2	.90	3.6
Na_2O	.30	.27	.10	.36	.05	.31
K_2O	.03	.06	.08	.05	.01	.02
H_2O^+		.34	.05	.30		.29
H_2O^-	.02	.02	.02	.08	.06	.09
TiO_2	.13	.15	.06	.13	.05	.17
P_2O_5	.04	.04	.04	.06	.01	.06
MnO	.13	.18	.11	.18	.14	.18
CO_2					.02	
Cl						
F						
S						
Cr_2O_3						
NiO						
Subtotal	99.95	99.22	100.02	99.46	99.79	99.22
Less O						
Total	99.95	99.22	100.02	99.46	99.79	99.22
q						
or	.18	.36	.47	.30	.06	.12
ab	2.54	2.30	.85	3.07	.42	2.65
an	7.30	6.58	4.50	5.91	4.28	16.15
lc						
ne						
hl						
di	4.61	7.63	2.11	7.61		1.16
hy	18.00	15.90	16.07	9.42	20.12	25.93
ol	65.59	65.84	75.22	70.96	73.50	50.47
cm						
mt	1.45	.67	.52	2.04	1.00	2.78
hm						
il	.25	.29	.11	.25	.10	.33
ap	.10	.10	.10	.14	.02	.14
cc.					.05	
c					.39	

Appendix IV, Continued

	Cr-diopside Websterite			Cr-diopside Olivine Ortho-Pyroxenite		Harzburgite		
Locality #:	32	32	63	63	63	33	66	16
Sample #:	Ba-MC-24	Ba-MC-12	SC-1-2	SC-1-16	SC-1-45	Ba-2-991	Ep-1-79	Ep-1-92
SiO_2	51.65	49.92	51.3	52.7	49.6	54.4	44.6	44.1
Al_2O_3	6.47	9.41	5.8	4.9	7.6	4.6	1.3	1.2
Fe_2O_3	1.46	1.80	2.0	3.1	2.4	2.8	.52	
FeO	4.12	3.42	3.3	4.9	3.6	4.2	6.8	7.4
MgO	19.96	23.41	20.6	30.7	19.7	30.8	45.5	46.4
CaO	13.97	9.50	15.2	2.6	15.0	1.6	.61	.69
Na_2O	.83	.88	.66	.17	.63	.19	.08	.03
K_2O	.05	.04	.06		.05	.12	.19	.04
H_2O^+	.11	.11	.41	.48	.28	.62	.35	.29
H_2O^-	.05	.05	.07	.07	.04	.03	.06	.05
TiO_2	.25	.33	.41	.22	.48	.22	.07	.02
P_2O_5	.02	.02	.07	.07	.08		.10	.04
MnO	.15	.12	.18	.20	.19	.08	.16	.15
CO_2	.04	.04				.02	.02	
Cl								
F	.01	.01						
S								
Cr_2O_3	.85	.94						
NiO	.07	.12						
Subtotal	100.06	100.12	100.06	100.11	99.65	99.68	100.34	100.41
Less O								
Total	100.06	100.12	100.06	100.11	99.65	99.68	100.34	100.41
q						1.20		
or	.30	.24	.36		.30	.71	1.12	.24
ab	7.03	7.45	5.59	1.44	5.35	1.61	.68	.25
an	13.80	21.62	12.69	12.44	17.83	7.84	2.37	3.01
lc								
ne								
hl								
di	43.41	19.67	48.87		44.25			.11
hy	22.91	30.08	18.04	74.85	14.54	82.18	19.40	16.03
ol	8.55	16.17	10.21	5.67	12.85		74.88	79.94
cm	1.25	1.39						
mt	2.12	2.61	2.90	4.49	3.49	4.07	.75	
hm								
il	.48	.63	.78	.42	.92	.42	.13	.04
ap	.05	.05	.17	.17	.19		.24	.09
cc	.09	.09				.05		
c				.06		1.20	.09	
fr	.02	.02						

Appendix IV, Continued

	Harzburgite								
Locality #:	67	67	67	40	40	40	40-C	16	63-C
Sample #:	Ep-3-165	Ep-3-46	Ep-3-164	Ki-5-4A	Ki-5-8	Ki-5-16	Ki-5-45A	LC-157	SC-1-41
SiO_2	43.70	45.0	41.8	44.14	44.7	42.5	43.78	43.9	40.1
Al_2O_3	1.18	1.2	2.1	1.44	1.7	.68	1.59	1.1	6.6
Fe_2O_3	.52	1.0	.51	.69	1.1	.53	.80	.36	.66
FeO	7.18	7.3	8.9	8.24	7.0	7.7	7.83	.77	6.9
MgO	45.18	44.3	44.7	43.77	43.2	46.9	44.26	8.3	43.2
CaO	.52	1.1	.93	.71	1.2	.40	.69	43.5	1.2
Na_2O	.06	.04	.07	.04	.07		.03	1.1	.03
K_2O	.01	.02	.12	.03	.07	.08	.01	.10	.04
H_2O^+	.03	.21	.45	.05	.23	1.1		.07	.76
H_2O^-	.06	.05	.03	.02	.02		.04	.40	.14
TiO_2	.04	.02	.04	.05	.04	.02	.08	.02	.06
P_2O_5	.01	.06	.14	.01	.04	.04	.02	.07	.07
MnO	.12	.17	.16	.15	.11	.12	.15	.04	.17
CO_2	.04			.03			.09	.19	
Cl	.01			.01					
F	.01								
S									
Cr_2O_3	.51			.33			.37		
NiO	.32			.28			.30		
Subtotal	99.69	100.47	99.95	99.99	99.48	100.07	100.04	99.56	99.93
Less O									
Total	99.69	100.47	99.95	99.99	99.48	100.07	100.04	99.56	99.93
q									
or	.06	.12	.71	.18	.42	.47	.06	.42	.24
ab	.44	.34	.59	.27	.60		.25	.85	.25
an	2.20	3.02	3.70	3.27	4.14	1.62	2.72	2.36	5.51
lc									
ne									
hl	.02								
di		1.59			1.25	.08		2.26	
hy	19.37	23.14	8.09	22.04	23.37	11.46	21.29	18.37	8.22
ol	75.83	69.97	84.82	72.32	68.21	84.37	72.99	73.98	79.29
cm	.75			.49			.55		
mt	.76	1.44	.74	1.00	1.60	.77	1.16	1.12	.96
hm									
il	.08	.04	.08	.10	.08	.04	.15	.13	.11
ap	.02	.14	.33	.02	.10	.10	.05	.10	.17
cc	.09			.07			.21		
c	.28		.50	.16			.53		4.50
fr	.02								

Appendix IV, Continued

	Harzburgite			Cr-diopside		Olivine Websterite		
Locality #:	67	16	63	66	66	40	40	63-C
Sample #:	Ep-3-165	LC-161	SC-1-7	Ep-1-88	Ep-1-93	Ki-5-46	Ki-5-120	Sc-1-4-2
SiO_2	44.12	42.7	43.8	49.8	50.1	50.6	51.9	50.7
Al_2O_3	1.65	.78	1.0	6.6	8.8	4.3	4.2	3.8
Fe_2O_3	.52	.46	.54	1.2	1.9	1.2	2.1	1.5
FeO	7.36	8.4	7.6	3.6	3.7	7.6	4.8	2.6
MgO	45.16	45.2	45.2	21.4	21.8	28.5	18.9	24.5
CaO	.59	1.1	1.0	15.1	12.4	6.2	15.9	14.8
Na_2O	.04	.11	.06	1.2	1.0	.33	.61	.50
K_2O	.02	.07		.05	.04	.06	.05	.02
H_2O^+		.41	.36	.41	.28	.37	.43	1.0
H_2O^-	.06	.02	.09	.06	.04	.06		.05
TiO_2	.03	.05	.02	.43	.24	.35	.40	.22
P_2O_5	.01	.11	.06	.07	.02	.11	.14	.07
MnO	.13	.16	.18	.16	.13	.18	.16	.15
CO_2	.05							
Cl	.01							
F								
S								
Cr_2O_3								
NiO								
Subtotal	99.75	99.57	99.91	100.08	100.45	99.86	99.59	99.91
Less O								
Total	99.75	99.57	99.91	100.08	100.45	99.86	99.59	99.91
q								
or	.12	.42		.30	.24	.36	.30	.12
ab	.34	.94	.51	10.19	8.43	2.80	5.18	4.24
an	2.55	1.43	2.46	12.52	19.33	10.10	8.61	8.08
lc								
ne								
hl								
di		2.62	1.67	48.92	32.86	15.84	55.01	50.89
hy	20.73	10.17	16.76	.10	16.13	46.89	22.01	14.11
ol	74.62	82.98	77.29	25.24	19.50	20.98	4.32	18.81
cm								
mt	.76	.67	.78	1.75	2.74	1.74	3.06	2.18
hm								
il	.06	.10	.04	.82	.45	.67	.76	.42
ap	.02	.26	.14	.17	.05	.26	.33	.17
cc	.11							
c	.63							

Appendix IV, Continued

	Cr-diopside Olivine Websterite	Transitional Cr-diopside/ Al-augite Lherzolite		Al-augite Dunite
Locality #:	63	32	35	17
Sample #:	Sc-1-51	BA-1-57	Ba-4-1	Tm-1-4
SiO_2	51.3	44.65	44.38	40.8
Al_2O_3	4.9	3.98	3.89	.71
Fe_2O_3	1.8	.98	1.23	
FeO	2.2	8.16	7.03	10.8
MgO	22.6	37.43	39.06	46.1
CaO	15.1	3.27	2.96	.62
Na_2O	.71	.32	.23	.06
K_2O		.02	.02	.04
H_2O^+	.10	.07	.01	.43
H_2O^-	.04	.02	.08	.03
TiO_2	.27	.20	.14	.07
P_2O_5	.10	.01	.01	.11
MnO	.15	.15	.14	.19
CO_2		.04	.03	
Cl				
F		.01		
S				
Cr_2O_3		.35	.35	
NiO		.23	.24	
Subtotal	99.27	99.89	99.80	99.96
Less O				
Total	99.27	99.89	99.80	99.96
q				
or		.12	.12	.24
ab	6.05	2.71	1.95	.51
an	10.26	9.38	9.54	1.55
lc				
ne				
hl				
di	50.49	5.12	3.88	.64
hy	15.74	18.78	18.61	1.53
ol	13.97	61.34	63.15	94.69
cm		.52	.52	
mt	2.63	1.42	1.79	
hm				
il	.52	.38	.27	.13
ap	.24	.02	.02	.26
cc		.09	.07	
fr		.02		

Appendix IV, Continued

	Al-augite Lherzolite		Transitional Al-augite Lherzolite/wehrlite		Al-augite Wehrlite	
Locality #:	40	63-C	63-C	63-C	66-C	66-C
Sample #:	Ki-5-27B	SC-1-27G	SC-1-10A	SC-1-100	Ep-1-42-1	Ep-1-42-2
SiO_2	42.28	40.9	41.2	39.0	43.1	44.2
Al_2O_3	3.96	2.5	4.2	3.2	3.7	4.1
Fe_2O_3	2.28	.15	.40	1.2	1.0	1.5
FeO	15.39	15.5	15.0	17.7	9.6	8.8
MgO	32.01	33.8	29.4	34.0	33.0	29.5
CaO	2.59	5.2	7.3	3.2	7.2	9.3
Na_2O	.18	.40	.45	.22	.50	.61
K_2O	.02	.06	.03	.04	.20	.12
H_2O^+	.03	.40	.58	.41	.66	1.0
H_2O^-	.04	.18	.03	.04	.06	.05
TiO_2	.28	.38	.74	.36	.56	.48
P_2O_5	.03	.09	.10	.23	.10	.09
MnO	.28	.26	.24	.26	.20	.22
CO_2	.07					
Cl						
F	.01					
S	.01					
Cr_2O_3	.34					
NiO	.14					
Subtotal	99.94	99.82	99.67	99.86	99.88	99.97
Less O	.01					
Total	99.93	99.82	99.67	99.86	99.88	99.97
q						
or	.12			.24	1.18	.71
ab	1.52			.99	.203	3.57
an	9.94	4.87	9.39	7.64	7.27	8.10
lc		.28	.14			
ne		1.84	2.07	.48	1.20	.87
hl						
di	1.78	15.15	20.33	5.43	22.10	29.73
hy	22.34					
ol	59.61	75.84	64.96	81.86	62.81	52.73
cm	.50					
mt	3.31	.22	.58	1.74	1.45	2.18
hm						
il	.53	.72	1.41	.69	1.07	.91
ap	.07	.21	.24	.55	.24	.21
cc	.16					
fr	.02					
pr	.02					
cs		.47	.30			

Appendix IV, Continued

	Al-augite Clinopyroxenite							
Locality #:	33	36	36	66	66	66	66	66
Sample #:	Ba-2-107	Ba-5-14	Ba-5-20	Ep-1-6	Ep-1-7	Ep-1-24	Ep-1-49	Ep-1-63
SiO_2	42.82	41.92	43.8	46.3	42.6	44.5	42.1	38.3
Al_2O_3	12.81	15.87	10.3	6.8	14.8	13.7	15.9	18.7
Fe_2O_3	6.41	4.85	3.7	1.5	3.7	2.3	3.5	7.2
FeO	5.42	4.55	5.4	8.0	4.5	5.1	4.6	4.1
MgO	12.96	15.76	15.3	21.5	13.5	16.5	13.5	12.0
CaO	13.45	13.69	16.7	13.3	18.0	15.8	17.9	15.8
Na_2O	1.84	.87	.85	.71	.81	.86	.67	.69
K_2O	.54	.04	.12	.11	.02	.03	.07	.04
H_2O^+	.35	.10	.44	.57	.28	.31	.37	.40
H_2O^-		.09	.23	.05	.05	.05	.06	.06
TiO_2	2.96	1.24	1.7	.84	1.4	.98	1.2	1.2
P_2O_5	.02	.05	.05	.06	.06	.05	.06	.04
MnO	.17	.14	.16	.19	.20	.18	.18	.21
CO_2	.17	.20	.17	.11				
Cl	.01							
F	.08	.01						
S								
Cr_2O_3	.04	.02						
NiO	.04	.04						
Subtotal	100.09	100.44	98.92	100.04	99.92	100.36	100.11	98.74
Less O	.04							
Total	100.05	100.44	98.92	100.04	99.92	100.36	100.11	98.74
q								
or	3.20	.24	.72	.65		.18		
ab	8.23	3.49	.73	6.01		.25		
an	25.21	39.11	24.25	15.04	36.74	33.33	40.15	48.45
lc					.09		.32	.19
ne	3.96	2.08	3.55		3.72	3.79	3.07	3.21
hl	.02							
di	31.09	21.17	45.89	39.66	31.67	35.15	25.92	14.58
hy								
ol	12.67	23.77	15.20	33.03	15.62	21.70	17.94	16.49
cm	.06	.03						
mt	9.32	7.00	5.44	2.18	5.37	3.32	5.07	10.56
hm								.01
il	5.64	2.35	3.27	1.60	2.66	1.86	2.28	2.31
ap	.05	.12	.12	.14	.14	.12	.14	.10
cc	.39	.45	.39	.25				
fr	.16	.01						
cs					.372		4.74	3.71

Appendix IV, Continued

	Al-augite Clinopyroxenite							
Locality #:	66	67	67	67	67	67	67-C	63-C
Sample #:	Ep-1-83	Ep-3-43	Ep-3-45B	Ep-3-76	Ep-3-118	Ep-3-137	Ep-3-163B	SC-1-10B
SiO_2	42.9	49.6	43.8	44.5	40.4	41.3	47.0	42.3
Al_2O_3	15.1	8.0	10.7	8.3	15.5	14.9	8.2	16.4
Fe_2O_3	3.2	1.5	3.5	3.0	5.6	3.5	1.7	3.4
FeO	4.1	5.8	6.3	7.3	5.8	5.2	4.9	5.5
MgO	13.8	18.4	16.4	18.2	15.3	14.1	20.5	13.6
CaO	17.4	14.6	14.9	14.9	14.5	17.4	14.7	16.2
Na_2O	.85	.67	.94	.93	.88	.61	.98	.87
K_2O	.25	.09	.04	.08	.08	.14	.07	
H_2O^+	.50	.53	.62	.60	.36	.47	.44	.29
H_2O^-	.06	.05	.05	.04	.10	.06	.04	.16
TiO_2	1.2	.66	1.4	1.3	1.4	1.2	1.2	1.4
P_2O_5	.11	.04	.05	.06	.07	.03	.04	.08
MnO	.18	.15	.19	.22	.19	.18	.15	.18
CO_2				.14	.15	.37		
Cl								
F								
S								
Cr_2O_3								
NiO								
Subtotal	99.65	100.09	98.89	99.57	100.33	99.46	99.92	100.38
Less O								
Total	99.65	100.09	98.89	99.57	100.33	99.46	99.92	100.38
q								
or		.53	.24	.48			.41	
ab		5.67	3.42	2.7			6.02	
an	36.80	18.55	25.15	18.32	38.02	37.73	17.79	40.75
lc	1.16				.37	.65		
ne	3.91		2.51	2.82	4.03	2.81	1.24	3.98
hl								
di	30.98	42.48	39.00	43.38	22.54	25.43	43.29	27.08
hy		14.94						
ol	16.43	13.79	21.12	24.39	22.29	20.15	25.97	18.70
cm								
mt	4.66	2.17	5.13	4.37	8.10	5.11	2.47	4.92
hm								
il	2.29	1.25	2.69	2.48	2.65	2.29	2.28	2.65
ap	.26	.10	.12	.14	.17	.07	.10	.19
cc				.32	.34	.85		
cs	3.02				1.15	4.44		1.44

Appendix IV, Continued

	Al-augite Clinopyroxenite							
Locality #:	63-C	63	63	63	63-C	17	17	17
Sample #:	SC-1-10C	SC-1-11	SC-1-22	SC-1-25	SC-1-27B	Tm-1-7	Tm-1-21	Tm-1-43
SiO_2	40.6	43.4	41.0	40.5	42.1	43.5	39.0	43.1
Al_2O_3	17.1	13.8	16.5	16.0	15.9	9.2	17.7	9.6
Fe_2O_3	4.2	3.9	5.0	6.6	3.8	2.7	3.8	3.9
FeO	5.0	5.2	4.9	5.6	4.5	8.5	8.7	7.0
MgO	13.8	14.5	14.1	12.0	13.5	17.0	12.3	16.4
CaO	15.8	16.6	15.9	15.9	16.7	15.0	15.0	15.7
Na_2O	.85	.84	1.0	.83	.89	.96	.90	.78
K_2O		.04	.04	.03	.06	.25	.16	.12
H_2O^+	.37	.32	.44	.41	.46	.46	.55	.44
H_2O^-	.03	.15	.13	.12	.13	.03	.10	.03
TiO_2	1.5	1.4	1.4	1.7	1.8	1.7	1.8	1.7
P_2O_5	.07	.06	.07	.06	.05	.20	.14	.14
MnO	.20	.20	.16	.20	.19	.19	.20	.19
CO_2							.12	
Cl								
F								
S								
Cr_2O_3								
NiO								
Subtotal	99.52	100.41	100.64	99.95	100.08	99.69	100.47	99.10
Less O								
Total	99.52	100.41	100.64	99.95	100.08	99.69	100.47	99.10
q								
or								.36
ab								
an	43.06	33.68	40.21	39.91	39.23	20.12	43.86	22.54
lc		.19	.18	.14	.28	1.16	.74	.28
ne	3.92	3.84	4.56	3.81	4.08	4.41	4.13	3.61
hl								
di	20.33	36.67	22.57	28.92	28.99	42.40	12.31	43.65
hy								
ol	20.26	16.41	19.22	13.28	15.94	23.78	25.19	19.80
cm								
mt	6.12	5.64	7.21	9.59	5.51	3.93	5.52	5.71
hm								
il	2.86	2.65	2.65	3.23	3.42	3.24	3.43	3.26
ap	.17	.14	.17	.14	.12	.48	.33	.34
cc							.27	
cs	2.92	.48	2.81	.58	1.98	.01		

Appendix IV, Continued

	Al-augite Clinopyroxenite	Al-augite Harzburgite	Al-augite Websterite	
Locality #:	42	33	36	40
Sample #:	WK-1-77	Ba-2-2	Ba-5-11	Ki-5-17
SiO_2	43.2	39.52	49.25	53.0
Al_2O_3	14.6	2.97	8.55	3.9
Fe_2O_3	3.8	2.00	2.28	1.3
FeO	3.6	13.86	7.15	5.7
MgO	13.6	37.53	20.17	22.2
CaO	18.1	2.00	10.67	12.5
Na_2O	.40	.19	.70	.63
K_2O	.03	.14	.03	.10
H_2O^+	.79	.10		.12
H_2O^-	.41	.11	.06	
TiO_2	.94	.21	.82	.38
P_2O_5	.01	.04	.03	.07
MnO	.13	.25	.16	.16
CO_2	.85	.30	.05	
Cl		.01	.01	
F		.01	.01	
S			.01	
Cr_2O_3		.30	.06	
NiO		.34	.05	
Subtotal	100.46	99.84	100.05	100.06
Less O			.01	
Total	100.46	99.84	100.04	100.06
q				
or	.18	.83	.18	.59
ab	.56	1.54	5.85	5.33
an	37.93	6.89	20.13	7.51
lc				
ne	1.53			
hl		.02	.02	
di	36.35	.67	25.56	42.72
hy		4.20	30.00	33.15
ol	13.42	81.10	13.04	7.82
cm		.44	.09	
mt	5.51	2.90	3.30	1.88
hm				
il	1.78	.40	1.56	.72
ap	.02	.10	.07	.17
cc	1.93	.68	.11	
fr		.01	.02	
pr			.02	

Appendix IV, Continued

	Feldspathic Lherzolite	Garnet-Spinel Websterite
Locality #:	40-C	33
Sample #:	Ki-5-45B	Ba-2-204
SiO_2	49.23	47.92
Al_2O_3	6.77	12.61
Fe_2O_3	1.37	1.63
FeO	5.51	5.26
MgO	31.30	15.43
CO	3.66	15.49
Na_2O	.51	.79
K_2O	.05	.04
H_2O^+	.06	.07
H_2O^-	.04	.09
TiO_2	.26	.31
P_2O_5	.02	.01
MnO	.14	.18
CO_2	.11	.03
Cl		
F	.01	
S		
Cr_2O_3	.85	.14
NiO	.15	.05
Subtotal	100.04	100.05
Less O		
Total	100.04	100.05
q		
or	.30	.24
ab	4.31	6.68
an	16.02	30.73
lc		
ne		
hl		
di	.45	36.38
hy	46.92	5.93
ol	27.64	16.62
cm	1.25	.21
mt	1.98	2.36
hm		
il	.49	.59
ap	.05	.02
cc	.25	.07
fr	.20	
pr		.02

Appendix V. Mineral Analyses

The following tables give the full analyses determined for principal mineral components of xenoliths examined in detail in this study. Most of the analyses were made with an LRL microprobe; a separate listing is made of wet chemical analyses. There are few data available on compositions of principal phases of rocks in the feldspathic ultramafic group, the bottle-green pyroxene group, and gabbroids. No data were obtained on minor phases such as sulfides and apatite.

Ranges of compositions of principal phases in the Cr-diopside and Al-augite groups indicate substantial overlap of the two groups as distinguished by hand-specimen characteristics. Table 4 lists average compositions of the principal phases of these two groups; following are ranges of important oxide weight percentages and the Mg/Mg+Fe ratio for the dominant phases:

		Cr-diopside Group	Al-augite Group
Clino-pyroxene	Cr_2O_3	.17 - 1.90	.003 - .92
	Al_2O_3	2.0 - 8.4	3.7 - 8.9
	TiO_2	.00 - 1.2	.32 - 2.5
	FeO	1.5 - 6.3	2.0 - 7.5
	Mg/Mg+Fe	.79 - .92	.76 - .89
Ortho-pryoxene	Al_2O_3	2.4 - 6.7	1.5 - 6.8
	FeO	5.4 -12.2	6.3 - 13.3
	Mg/Mg+Fe	.81 - .92	.79 - .90
Olivine	FeO	9.5 -22.0	10.3 - 20.4
	Mg/Mg+Fe	.65 - .84	.67 - .83
Spinel	Al_2O_3	26.2 - 62.9	43.6 - 65.2
	Cr_2O_3	4.0 -35.9	.01 - 20.8

1/ First number is locality number (see Table 1), second is sample number, third is grain number; capital letters following third number identify different probe mounts.

2/ "Systematic" refers to minerals analyzed in probe traverses across composite xenoliths; lithologies are identified in Appendix VI. "Transitional" refers to minerals in rocks transitional between the Cr-diopside and A1-augite groups. Groups to which other samples belong are identified as follows: Cr-Di (Cr-diopside group), A1-Aug (A1-augite group), B-G (Bottle-green pyroxene group), F (Feldspathic group), G (Garnetiferous group).

3/ Rock types are identified as follows: L= lherzolite; D= dunite; Web= websterite; H= harzburgite; OWeb= olivine websterite; CP= clinopyroxenite; OCP= olivine clinopyroxenite; Weh= wehrlite; OP= orthopyroxenite; GWeb= garnet websterite; GCP= garnet clinopyroxenite; Gb= gabbroid; FP= feldspathic pyroxenite; MGb=metagabbroid; Ho= hornblendite. Mineral identifications are: Mega.= megacryst; Amph.= amphibole; Cpx= clinopyroxene; Opx= orthopyroxene.

4/ Center and edge refer to position of analysis on individual mineral grains.

WET CHEMICAL ANALYSES OF MINERALS

	Cr-diopside Group						Al-augite Group			
Loc. sample[1/]	44-46	67-5	47-89	10-100	66-13	33-24	32-1	67-7-1	67-7	39-9
Rock Type[3/]	OWeb	L	L	L	L	OWeb	Mega.	OCP	L	CP
Mineral[3/]	Cpx	Cpx	Cpx	Opx	Opx	Cpx	Cpx	Cpx	Cpx	Cpx
SiO_2	53.80	51.04	52.70	53.80	54.00	50.80	47.08	49.39	50.07	48.27
Al_2O_3	2.02	7.41	3.35	5.15	5.28	7.51	8.65	7.90	6.64	8.94
Fe_2O_3	.84	1.03	1.81	1.51	1.49	1.28	4.04	1.76	1.56	2.21
FeO	1.54	2.96	1.80	5.40	5.02	1.97	5.33	3.53	3.51	4.34
MgO	17.70	15.72	16.00	31.60	32.30	15.29	11.73	14.22	14.69	14.06
CaO	23.10	18.44	22.00	1.05	1.09	20.36	19.76	20.89	20.95	19.97
Na_2O	.21	1.47	.85	.19	.11	1.20	1.30*	.93	.89	.74
K_2O	.04	.009	.03	.05	.03	.01	.006	.005	.004	.008
H_2O+	.35	.21				.10	.00	.11	.18	.10
H_2O-		.03	.00	.42	.23	.00	.00	.00	.00	.00
TiO_2	.00	.44	.32	.14	.13	.67	1.75	1.02	.90	1.20
P_2O_5	.02	.10	.02	.01	.01	.80		.00	.10	.10
MnO	.10	.11	.11	.16	.14	.09	.19	.16	.19	.17
F	.01	.01	.01	.01	.01	.00		.02	.01	.01
Cr_2O_3	.50	.74	1.23	.44	.46	.04		.003	.37	.005
NiO		.06				.11		.05	.05	.03
V_2O_5										
Subtotal										
Less O=F										
Total	100.23	99.80	100.23	99.93	100.30	100.23	99.84	99.99	100.11	100.15
Ca	46.7	43.3	48.2	2.1	2.2	46.2	45.9	48.1	47.5	46.5
Mg	49.7	51.3	48.7	87.4	90.0	48.3	37.9	45.5	46.3	45.6
Fe	3.6	5.4	3.1	10.5	7.8	5.5	16.2	6.3	6.2	7.9

WET CHEMICAL ANALYSES OF MINERALS

	Al-augite Group				Bottle-green Px Group			Garnet. Group
Loc. sample[1]	16-93	16-141	67-7	32-72	17-22	48-12	16-131	33-204
Rock Type[3]	CP	Weh	L	H∅	Weh	OCP	Mega.	CP
Mineral[3]	Cpx	Cpx	Opx	Amph.	Cpx	Cpx	Cpx	Cpx
SiO_2	49.03	49.39	53.34	40.34	50.98	48.91	51.17	50.09
Al_2O_3	7.82	8.36	4.69	13.81	6.25	8.89	6.41	9.41
Fe_2O_3	1.46	1.43	.89	4.80	.82	2.11	.80	.86
FeO	5.56	5.12	8.67	6.33	3.94	4.89	3.83	3.99
MgO	13.48	15.43	28.75	13.59	17.16	14.63	17.80	14.23
CaO	19.74	17.45	2.67	11.13	17.54	17.90	17.06	19.40
Na_2O	1.00	1.03	.12	2.74	.83	.83	.81	1.23
K_2O	.012	.057	.003	1.39	.041	.016	.011	.015
H_2O+	.06	.14	.06	1.00	.10	.11	.00	.03
H_2O-	.04	.00	.00	.01	.00	.00	.15	
TiO_2	1.27	.93	.34	4.36	.51	.96	.38	.40
P_2O_5	.10	.40	.20		.60	.10	.05	.00
MnO	.25	.16	.25	.14	.10	.18	.18	.13
F	.01	.01	.01	.14	.01	.01	.00	.00
Cr_2O_3	.31	.27	.23		1.05	.11	1.17	.19
NiO	.03	.04	.07		.16	.06	.08	.08
V_2O_5								.09
Subtotal				99.78				
Less O=F				.06				
Total	100.17	100.22	100.29	99.72	100.09	99.71	99.90	100.15
Ca	46.1	40.7	5.3		38.9	41.1	37.5	45.2
Mg	43.7	50.0	79.9		53.0	46.7	55.3	46.1
Fe	10.2	9.3	14.8		8.1	12.2	7.2	8.7

Olivine

Loc., Sample[1]	32-15-1	32-15-2	32-15-3	32-15-4	31-15-5	32-15-6	32-15-7	32-22-2
Group[2]	Systematic							Cr-Di
Rock Type[3]	OWeb							L
SiO_2	39.5	39.7	39.5	39.0	39.3	39.6	39.5	39.8
FeO	13.1	13.6	13.6	13.7	13.5	15.3	14.1	10.5
MgO	46.7	46.6	46.5	46.4	46.5	45.4	46.2	49.1
MnO	.22	.22	.22	.22	.20	.29	.25	.21
Cr_2O_3								
NiO	.18	.17	.18	.19	.18	.18	.19	.32
CaO	.18	.17	.15	.13	.19	.21	.17	.10
TiO_2								
Total	99.88	100.46	100.15	99.64	99.87	100.98	100.41	100.03
Fo	86.2	85.7	85.7	85.7	85.8	84.0	85.2	89.3
Fs	13.8	14.3	14.3	14.3	14.2	16.0	14.8	10.7

Loc., Sample	32-22-3	32-24-1	32-24-2	32-24-3	32-24-1A	32-24-2A	32-24-3A	32-24-1B
Group		Systematic						
Rock Type		OWeb						
SiO_2	39.3	40.5	40.3	40.5	40.0	41.0	40.6	39.2
FeO	10.8	10.5	10.3	10.3	10.3	10.6	10.6	15.0
MgO	49.5	48.7	49.0	49.0	48.2	48.7	48.8	45.3
MnO	.16							
Cr_2O_3								
NiO	.31	.26	.27	.28	.24	.26	.26	.24
CaO	.06	.09	.10	.10	.10	.08	.09	.12
TiO_2		.01	.01	.01	.01	.01	.01	
Total	100.13	100.06	99.98	100.19	98.95	100.65	100.36	99.86
Fo	89.1	89.2	89.5	89.5	89.3	89.1	89.1	84.3
Fs	10.9	10.8	10.5	10.5	10.7	10.9	10.9	15.7

Olivine

Loc., Sample[1]	32-15-1	32-15-2	32-15-3	32-15-4	32-15-5	32-15-6	32-15-7	32-22-2	32-22-3	32-24-1
Group[2]	Systematic							Cr-Di		Systematic
Rock Type[3]	OWeb							L		OWeb
SiO_2	39.5	39.7	39.5	39.0	39.3	39.6	39.5	39.8	39.3	40.5
FeO	13.1	13.6	13.6	13.7	13.5	15.3	14.1	10.5	10.8	10.5
MgO	46.7	46.6	46.5	46.4	46.5	45.4	46.2	49.1	49.5	48.7
MnO	.22	.22	.22	.22	.20	.29	.25	.21	.16	
Cr_2O_3										
NiO	.18	.17	.18	.19	.18	.18	.19	.32	.31	.26
CaO	.18	.17	.15	.13	.19	.21	.17	.10	.06	.09
TiO_2										.01
Total	99.88	100.46	100.15	99.64	99.87	100.98	100.41	100.03	100.13	100.06
Fo	86.2	85.7	85.7	85.7	85.8	84.0	85.2	89.3	89.1	89.2
Fs	13.8	14.3	14.3	14.3	14.2	16.0	14.8	10.7	10.9	10.8

Loc., Sample	32-24-2	32-24-3	32-24-1A	32-24-2A	32-24-3A	32-24-1B	32-24-2B	32-24-3B	32-29-1
Group									Al-Aug
Rock Type									Web
SiO_2	40.3	40.5	40.0	41.0	40.6	39.2	39.5	39.9	39.3
FeO	10.3	10.3	10.3	10.6	10.6	15.0	14.6	14.0	14.7
MgO	49.0	49.0	48.2	48.7	48.8	45.3	45.7	46.1	45.5
MnO									
Cr_2O_3									
NiO	.27	.28	.24	.26	.26	.24	.24	.26	.22
CaO	.10	.10	.10	.08	.09	.12	.12	.11	.11
TiO_2	.01	.01	.01	.01	.01				
Total	99.98	100.19	98.85	100.65	100.36	99.86	100.16	100.37	99.83
Fo	89.5	89.5	89.3	89.1	89.1	84.3	84.8	85.4	84.7
Fs	10.5	10.5	10.7	10.9	10.9	15.7	15.2	14.6	15.3

Olivine

Loc., Sample[1]	32-29-2	32-29-3	32-29-4	32-52-1	32-52-3	32-72-1	32-72-2	32-72-3	32-72-4	32-72-5
Group[2]				Cr-Di		Systematic				
Rock Type[3]				L		L				
SiO_2	39.5	39.5	39.8	40.8	41.3	38.4	39.1	39.5	39.7	39.5
FeO	14.7	14.8	14.7	12.3	12.7	15.1	14.7	14.2	13.9	13.3
MgO	45.5	45.7	45.7	46.0	47.4	45.4	46.7	46.1	46.3	46.7
MnO						.23	.22	.22	.21	.18
Cr_2O_3										
NiO	.22	.22	.21	.20	.18	.16	.15	.16	.16	.17
CaO	.12	.13	.12	.09	.08	.16	.17	.16	.15	.19
TiO_2	.02	.03	.02							
Total	100.6	100.38	100.55	99.39	101.66	99.45	101.04	100.34	100.42	100.04
Fo	84.7	84.6	84.6	87.0	86.9	84.3	84.7	85.3	85.6	86.3
Fs	15.3	15.4	15.4	13.0	13.1	15.7	15.3	14.7	14.4	13.7

Loc., Sample	32-72-6	32-72-7	32-72-8	32-72-1A	32-72-2A	32-72-3A	32-72-4A	32-72-5A	32-72-6A	32-72-A
Group										
Rock Type										
SiO_2	39.7	40.3	39.8	40.0	40.2	39.9	39.9	41.2	40.0	40.2
FeO	12.6	12.1	11.8	11.1	11.0	11.3	11.3	11.5	11.7	11.7
MgO	47.3	47.5	47.9	47.7	47.8	48.0	48.1	47.4	47.5	47.7
MnO	.19	.16	.14	.15	.15	.15	.13	.15	.17	.18
Cr_2O_3										
NiO	.18	.18	.18	.17	.17	.18	.19	.18	.17	.18
CaO	.15	.16	.14	.16	.16	.15	.19	.17	.16	.15
TiO_2										
Total	100.12	100.39	99.96	99.28	99.48	99.68	99.81	100.60	99.70	100.11
Fo	87.0	87.5	87.9	88.5	88.6	88.4	88.4	88.0	87.9	87.9
Fs	13.0	12.5	12.1	11.5	11.4	11.6	11.6	12.0	12.1	12.1

Olivine

Loc., Sample[1]	32-72-8A	32-74-1	32-90-1	32-90-2	32-90-3	33-1-1	33-1-2	33-1-3	33-1-4	33-1-5
Group[2]		Transitional	Cr-Di			Systematic				
Rock Type[3]		L	L			L				
SiO_2	40.2	40.2	40.2	40.2	40.3	39.0	39.0	38.8	39.0	39.1
FeO	12.0	11.3	9.7	9.6	9.8	15.9	15.8	15.5	15.1	14.3
MgO	47.4	48.0	49.2	48.8	49.6	44.5	44.8	44.9	45.2	45.7
MnO	.17	.16	.08	.11	.11	.29	.31	.29	.28	.26
Cr_2O_3										
NiO	.18	.29	.22	.22	.24	.13	.14	.16	.15	.15
CaO	.15	.10	.17	.18	.10	.18	.21	.15	.13	.19
TiO_2										
Total	100.10	100.05	99.57	99.11	100.15	99.79	100.26	99.80	99.86	99.70
Fo	87.6	88.3	90.0	90.1	90.0	83.3	83.5	83.8	84.2	85.1
Fs	12.4	11.7	10.0	9.9	10.0	16.7	16.5	16.2	15.8	14.9

Loc., Sample	33-1-6	33-1-7	33-1-1A	33-1-2A	33-1-3A	33-1-4A	33-1-5A	33-1-6B	33-1-1B	33-1-2B
Group										
Rock Type										
SiO_2	39.4	39.4	39.5	39.4	39.5	39.6	40.0	40.1	40.4	39.8
FeO	13.7	12.6	12.9	12.0	11.4	11.2	11.3	10.6	10.7	10.6
MgO	46.5	47.1	47.1	47.5	47.9	48.1	48.7	48.4	48.8	48.9
MnO	.24	.19	.22	.18	.17	.15	.15	.15	.14	.13
Cr_2O_3										
NiO	.17	.16	.18	.17	.17	.18	.18	.17	.19	.18
CaO	.15	.12	.13	.14	.13	.15	.14	.11	.13	.12
TiO_2										
Total	100.16	99.57	100.03	99.39	99.27	99.38	100.47	99.53	100.36	99.73
Fo	85.8	86.9	86.6	87.6	88.2	88.5	88.5	89.0	89.1	89.1
Fs	14.2	13.1	13.4	12.4	11.8	11.5	11.5	11.0	10.9	10.9

Olivine

Loc., Sample[1]	33-1-3B	33-1-4B	33-1-5B	33-1-1C	33-1-2C	33-1-3C	33-2-1	33-2-2	33-2-3	33-2-24
Group[2]							Al-Aug			
Rock Type[3]							L			
SiO_2	40.2	40.1	39.8	40.1	40.4	39.8	37.9	37.4	38.1	37.4
FeO	10.8	10.3	10.3	10.4	10.8	10.5	17.5	17.5	17.6	17.5
MgO	49.0	48.8	48.8	48.9	49.0	48.8	43.4	43.4	43.5	43.5
MnO	.13	.15	.14	.14	.14	.15	.23	.19	.22	.27
Cr_2O_3										
NiO	.18	.17	.19	.17	.17	.18	.20	.19	.20	.20
CaO	.12	.11	.14	.12	.11	.09	.14	.15	.15	.12
TiO_2										
Total	100.43	99.63	99.37	99.83	100.62	99.52	99.37	98.83	99.77	98.99
Fo	89.0	89.4	89.4	89.3	89.0	89.2	81.4	81.4	82.2	81.3
Fs	11.0	10.6	10.6	10.7	11.0	10.8	18.6	18.6	18.8	18.7

Loc., Sample	33-2-5	33-2-6	33-2-7	33-2-8	33-3-1	33-3-2	33-3-3	35-1-1	35-1-2	35-1-3
Group					Cr-Di			Cr-Di		
Rock Type					L			L		
SiO_2	38.3	38.6	38.3	37.9	39.4	39.0	38.8	40.9	40.1	49.3
FeO	17.6	17.7	17.5	17.5	10.1	10.2	10.3	10.9	11.1	11.3
MgO	43.7	43.5	43.5	43.5	48.9	48.7	48.8	47.7	47.4	48.0
MnO	.19	.22	.21	.23	.17	.17	.16			
Cr_2O_3										
NiO	.20	.20	.21	.18	.19	.21	.20	.17	.19	.24
CaO	.14	.16	.13	.14	.10	.11	.09	.10	.08	.10
TiO_2										
Total	100.19	100.38	99.85	99.45	98.86	98.39	98.35	99.77	98.87	99.94
Fo	81.3	81.2	81.4	81.4	89.4	89.4	89.3	88.6	88.4	88.3
Fs	18.7	18.8	18.6	18.6	10.6	10.6	10.7	11.4	11.6	11.7

	Olivine						
Loc., Sample[1/]	36-11-1	36-12-1	36-12-2	36-12-3	36-18-1	36-18-2	36-18-3
Group[2/]	Al-Aug	Cr-Di			Cr-Di		
Rock Type[3/]	Web	L			L		
SiO_2	38.1	40.1	40.1	39.9	40.0	40.0	40.0
FeO	20.4	10.7	10.7	10.7	11.1	11.0	11.1
MgO	42.0	48.5	48.6	48.6	48.3	48.3	48.2
MnO							
Cr_2O_3	.19	.30	.32	.30	.29	.28	.27
NiO							
CaO							
TiO_2							
Total	100.69	99.60	99.72	99.5	99.69	99.58	99.57
Fo	78.6	89.0	89.0	89.0	88.6	88.7	88.6
Fs	21.4	11.0	11.0	11.0	11.4	11.3	11.4

Loc., Sample	
Group	
Rock Type	
SiO_2	
FeO	
MgO	
MnO	
Cr_2O_3	
NiO	
CaO	
TiO_2	
Total	
Fo	
Fs	

Olivine

Loc., Sample[1]	23-11-1	23-11-2	23-11-3	23-11-4	23-11-5	23-11-6	23-11-1A	23-11-2A	23-11-3A	23-11-4A
Group[2]	Systematic									
Rock Type[3]	L									
SiO_2	38.7	39.1	39.0	38.9	39.8	39.2	39.4	39.5	39.5	39.9
FeO	16.1	16.0	15.6	14.4	12.9	12.3	11.3	11.1	11.1	11.0
MgO	44.6	44.7	45.0	45.9	47.2	47.4	48.2	48.3	48.5	48.4
MnO	.24	.23	.24	.20	.16	.17	.15	.15	.15	.14
Cr_2O_3										
NiO	.15	.16	.16	.17	.19	.18	.18	.18	.18	.19
CaO	.17	.19	.16	.14	.14	.17	.16	.13	.13	.13
TiO_2										
Total	99.96	100.38	100.16	99.71	100.39	99.42	99.39	99.36	99.56	99.76
Fo	83.2	83.3	83.7	85.0	86.7	87.2	88.4	88.6	88.6	88.7
Fs	16.8	16.7	16.3	15.0	13.3	12.8	11.6	11.4	11.4	11.3

Loc., Sample	23-11-5A	23-11-1B	23-11-2B	23-11-3B	23-11-4B
Group					
Rock Type					
SiO_2	40.0	39.9	39.7	39.9	40.7
FeO	11.1	11.1	11.1	11.1	11.1
MgO	48.6	48.6	48.5	48.6	48.4
MnO	.13	.13	.14	.14	.14
Cr_2O_3					
NiO	.19	.19	.19	.18	.18
CaO	.18	.14	.11	.12	.15
TiO_2					
Total	100.20	100.06	99.74	100.04	100.67
Fo	88.7	88.6	88.7	88.6	88.6
Fs	11.3	11.4	11.3	11.4	11.4

Olivine

Loc., Sample[1]	66-10-1	66-10-1a	66-10-2	66-10-2a	66-10-3	66-10-1A	66-10-2A	66-10-3A	66-10-3Aa	66-10-4A
Group[2]	Systematic					Systematic		Systematic		
Rock Type[3]	L					OCP		L		
SiO_2	39.7	39.5	39.7	39.5	39.5	39.6	39.5	39.8	39.6	39.7
FeO	13.7	13.7	13.8	13.7	13.7	12.2	13.8	13.9	13.6	13.7
MgO	47.0	46.8	46.8	46.8	46.5	46.9	46.6	46.6	46.7	46.9
MnO	.18	.17	.16	.17	.17	.12	.17	.18	.18	.16
Cr_2O_3										
NiO	.17	.16	.17	.17	.16	.18	.16	.18	.17	.17
CaO	.08	.12	.22	.11	.13	.15	.16	.18	.13	.14
TiO_2										
Total	100.83	100.45	100.85	100.45	100.16	99.15	100.45	100.84	100.38	100.21
Fo	85.9	85.9	85.8	85.9	85.8	87.3	85.8	85.7	86.0	85.9
Fs	14.1	14.1	14.2	14.1	14.2	12.7	14.2	14.3	14.0	14.1

Loc., Sample	66-10-5A	66-10-6A	66-10-7A	66-10-8A	66-10-9A	66-10-10A	66-10-11A	66-10-12A	66-10-13A	66-123-1
Group					Systematic					Systematic
Rock Type					OCP					L
SiO_2	39.7	39.7	39.7	39.6	39.6	39.6	39.7	39.7	39.9	40.0
FeO	13.6	13.6	13.6	13.6	13.7	13.9	13.3	12.8	13.1	11.4
MgO	46.8	46.8	46.9	46.9	46.8	46.6	47.2	47.2	47.1	48.2
MnO	.19	.19	.17	.18	.17	.17	.18	.16	.18	.14
Cr_2O_3										
NiO	.18	.17	.18	.19	.17	.16	.18	.18	.17	.19
CaO	.10	.12	.11	.14	.17	.20	.18	.15	.15	.15
TiO_2										
Total	100.57	100.58	100.66	100.61	100.61	100.63	100.74	100.19	100.60	100.08
Fo	86.0	86.0	86.0	86.0	86.9	85.7	86.3	86.8	86.5	88.3
Fs	14.0	14.0	14.0	14.0	14.1	14.3	13.7	13.2	13.5	11.7

Olivine

Loc., Sample[1]	66-123-2	66-123-3	66-123-4	66-123-5	66-123-1A	66-123-2A	66-123-3A	66-123-4A	67-7-1	67-7-2
Group[2]			Systematic		Systematic		Systematic		Systematic	
Rock Type[3]			Web		L		Web		OCP	
SiO_2	39.9	40.1	40.2	40.2	40.3	40.3	40.1	40.0	39.2	39.0
FeO	11.4	11.7	11.7	11.5	11.5	11.7	11.6	11.5	18.2	18.2
MgO	48.3	48.3	48.3	48.5	48.2	48.3	48.4	48.3	44.5	44.4
MnO	.13	.14	.16	.16	.13	.13	.13	.14		
Cr_2O_3										
NiO	.20	.20	.19	.19	.20	.21	.22	.20	.14	.16
CaO	.10	.14	.12	.12	.13	.13	.10	.11		
TiO_2										
Total	100.03	100.58	100.67	100.67	100.46	100.77	100.55	100.25	102.04	101.76
Fo	88.3	88.0	88.0	88.3	88.2	88.0	88.1	88.2	81.3	81.3
Fs	11.7	12.0	12.0	11.7	11.8	12.0	11.9	11.8	18.7	18.7

Loc., Sample	67-7-3	67-7-4	67-7-5	67-7-6	67-7-7	67-7-1A	67-7-2A	67-7-3A	67-7-4A	67-7-5A
Group									Systematic	
Rock Type									L	
SiO_2	38.8	39.0	39.2	39.1	39.1	38.6	38.7	38.8	39.2	39.2
FeO	18.0	17.8	17.6	18.0	17.9	17.2	17.1	17.2	16.8	16.9
MgO	44.4	44.4	44.3	44.8	44.5	44.3	44.2	44.2	44.5	44.7
MnO									.20	.19
Cr_2O_3										
NiO	.18	.17	.15	.15	.14	.17	.18	.16	.25	.26
CaO	.02	.01			.03				.18	.16
TiO_2	.02	.01	.01	.02	.01					
Total	101.42	101.39	101.26	102.07	101.68	100.27	100.18	100.36	101.13	101.40
Fo	81.5	81.6	81.8	81.6	81.6	82.1	82.2	82.1	82.5	82.5
Fs	18.5	18.4	18.2	18.4	18.4	17.9	17.8	17.9	17.5	17.5

Olivine

Loc., Sample[1/]	67-7-6A	67-7-7A	67-7-8A	67-84-1	67-84-2	67-84-1A	67-84-2A	67-84-3A	67-84-1B
Group[2/]				Systematic		Systematic			
Rock Type[3/]				OCP		L			
SiO_2	39.1	38.8	38.8	39.3	39.2	39.5	40.1	40.0	39.7
FeO	16.9	16.9	16.1	13.9	13.5	13.5	13.3	13.5	13.5
MgO	44.7	44.3	44.8	44.5	46.4	47.0	46.3	46.5	46.7
MnO	.23	.22	.21		.16				
Cr_2O_3									
NiO	.25	.25	.27	.21	.36	.23	.23	.23	.26
CaO	.21	.18	.18	.11	.15	.06	.07	.08	.08
TiO_2							.01	.02	.01
Total	101.39	100.65	100.26	98.02	99.77	100.29	100.01	100.33	100.25
Fo	82.5	82.4	83.2	85.1	86.0	86.1	86.1	86.0	86.0
Fs	17.5	17.6	16.8	14.9	14.0	13.9	13.9	14.0	14.0

Loc., Sample	67-84-2B	67-84-3B	67-136-1	67-136-2	67-136-3	67-136-4	67-136-5	67-136-6	67-136-7
Group			Systematic			Systematic			
Rock Type			CP			L			
SiO_2	39.9	39.1	38.5	37.9	38.3	38.6	38.6	38.4	38.8
FeO	13.3	13.4	16.3	16.0	16.1	15.8	15.7	15.7	15.8
MgO	46.5	47.0	44.0	44.1	44.4	44.6	44.8	44.7	44.8
MnO			.22	.22	.23	.24	.22	.24	.21.
Cr_2O_3									
NiO	.26	.26	.17	.18	.17	.19	.17	.16	.17
CaO	.07	.09	.18	.16	.11	.13	.11	.11	.11
TiO_2	.03	.01							
Total	100.06	99.86	99.37	98.56	99.31	99.56	99.60	99.31	99.89
Fo	86.2	86.2	82.8	83.1	83.1	83.4	83.6	83.5	83.5
Fs	13.8	13.8	17.2	16.9	16.9	16.6	16.4	16.5	16.5

Olivine

Loc., Sample[1]	67-136-1A	67-136-2A	67-136-3A	67-136-4A	67-136-5A	67-136-6A	67-136-1B	67-136-2B	67-136-3B	67-136-4B
Group[2]	Systematic			Systematic						
Rock Type[3]	CP			L						
SiO_2	38.6	38.5	39.5	39.2	39.4	39.2	39.0	38.8	39.7	39.4
FeO	14.2	14.2	13.6	13.6	13.6	13.3	13.3	13.2	13.4	13.5
MgO	45.2	45.5	46.2	46.3	46.3	46.4	46.4	46.3	46.6	46.4
MnO	.20	.19	.19	.18	.18	.19	.18	.19	.20	.19
Cr_2O_3										
NiO	.21	.24	.24	.24	.24	.22	.23	.24	.23	.23
CaO	.16	.18	.12	.10	.09	.11	.10	.08	.14	.10
TiO_2										
Total	99.07	98.81	99.85	99.62	99.81	99.42	99.21	98.81	100.27	99.82
Fo	85.2	85.1	85.8	85.9	85.9	86.1	86.1	86.2	86.1	86.0
Fs	14.8	14.9	14.2	14.1	14.1	13.9	13.9	13.8	13.9	14.0

Loc., Sample	
Group	
Rock Type	
SiO_2	
FeO	
MgO	
MnO	
Cr_2O_3	
NiO	
CaO	
TiO_2	
Total	
Fo	
Fs	

Olivine

Loc., Sample[1]	40-1-1	40-1-2	40-1-3	40-1-4	40-1-5	40-1-6	40-1-7	40-1-8	40-1-9	40-1-1A
Group[2]	Systematic			Systematic						Systematic
Rock Type[3]	OWeb			L						OWeb
SiO_2	39.3	39.9	39.0	40.1	39.6	39.6	40.4	39.8	39.9	39.7
FeO	10.0	9.9	9.9	10.2	10.0	10.0	10.0	10.0	9.9	9.8
MgO	48.8	48.9	49.1	49.2	49.0	49.2	49.1	49.1	49.1	48.9
MnO	.14	.16	.16	.15	.15	.15	.14	.15	.15	.14
Cr_2O_3										
NiO	.27	.29	.28	.28	.29	.29	.29	.29	.26	.28
CaO	.09	.11	.10	.10	.12	.10	.10	.08	.10	.09
TiO_2										
Total	98.60	99.26	99.44	100.03	99.16	99.34	100.03	99.42	99.41	98.91
Fo	89.7	89.8	89.8	89.6	89.7	89.8	89.7	89.7	89.8	89.9
Fs	10.3	10.2	10.2	10.4	10.3	10.2	10.3	10.3	10.2	10.1

Loc., Sample	40-1-2A	40-1-3A	40-1-4A	40-1-5A	40-1-6A	40-2-2	40-2-3	40-2-4	40-2-5	40-2-6
Group			Systematic			Cr-Di				
Rock Type			L			L-Web				
SiO_2	39.9	40.1	39.9	39.7	39.9	41.1	40.6	40.5	40.5	40.1
FeO	9.8	9.9	10.0	10.0	10.0	10.1	10.0	10.0	10.1	10.0
MgO	49.0	49.1	48.9	49.0	48.9	50.1	49.9	49.7	49.8	49.5
MnO	.14	.14	.14	.16	.15					
Cr_2O_3						.32	.28	.31	.28	.29
NiO	.29	.28	.29	.29	.27					
CaO	.14	.12	.11	.09	.10					
TiO_2										
Total	99.27	99.64	99.34	99.24	99.32	101.62	100.78	100.51	100.68	99.89
Fo	89.9	89.8	89.7	89.7	89.7	89.8	89.9	89.9	89.8	89.8
Fs	10.1	10.2	10.3	10.3	10.3	10.2	10.1	10.1	10.2	10.2

Olivine

Loc., Sample[1]	40-2-7	40-2-8	40-4-1	40-4-6	40-4-8	40-127-1	40-127-2	40-127-3	40-127-4	40-127-4a
Group[2]			Cr-Di	Gb		Systematic			Systematic	Systematic
Rock Type[3]			L			L			FP	L
SiO_2	40.7	40.4	37.8	39.3	36.8	39.1	38.8	38.2	38.3	38.1
FeO	10.0	9.9	15.8	15.5	19.7	15.9	17.1	18.8	19.8	19.8
MgO	49.7	49.5	44.8	44.3	41.6	45.3	44.1	42.9	42.5	42.3
MnO						.17	.23	.23	.23	.25
Cr_2O_3	.30	.31	.29	.24	.24					
NiO						.18	.18	.13	.10	.12
CaO			.05	.09	.08	.16	.13	.19	.17	.22
TiO_2			.20	.36	.43					
Total	100.70	100.11	98.94	99.79	98.85	100.81	100.54	100.45	101.10	100.79
Fo	89.9	89.9	83.5	83.6	79.0	83.5	82.1	80.3	79.3	79.2
Fs	10.1	10.1	16.5	16.4	21.0	16.5	17.9	19.7	20.7	20.8

Loc., Sample	40-127-4b	40-127-5	40-127-5a	40-127-6	40-127-7	40-127-1A	40-127-2A	40-127-3A	40-127-4A	40-127-5A
Group									Systematic	
Rock Type									Gb	
SiO_2	38.4	39.0	39.5	40.1	40.0	38.5	38.1	37.9	36.9	36.9
FeO	18.6	16.5	13.4	11.5	11.4	18.3	20.6	21.3	26.4	26.5
MgO	42.9	44.6	47.2	48.3	48.2	42.6	41.9	41.1	37.5	37.0
MnO	.24	.20	.15	.13	.13	.24	.28	.28	.33	.35
Cr_2O_3										
NiO	.14	.17	.20	.19	.19	.18	.16	.13	.09	.09
CaO	.18	.20	.17	.11	.13	.16	.18	.26	.25	.26
TiO_2										
Total	100.46	100.61	100.62	100.33	100.05	99.98	101.22	100.97	101.47	101.10
Fo	80.4	82.8	86.3	88.2	88.3	80.6	78.4	77.5	71.7	71.3
Fs	19.6	17.2	13.7	11.8	11.7	19.4	21.6	22.5	28.3	28.7

Olivine

Loc., Sample[1]	40-127-6A	40-127-7A	40-127-8A	40-127-1B	40-127-2B	40-127-2B	40-127-2B	40-127-3B	40-127-3aB	40-127-4B	40-127-4B
Group[2]				Systematic	Center[4]	> to Edge	Edge[4]			Center	> to Edge
Rock Type[3]				L							
SiO_2	36.3	36.7	36.6	38.7	38.5	38.6	38.3	38.1	37.7	37.7	37.7
FeO	28.7	25.9	28.1	16.4	17.5	17.6	17.7	18.6	20.4	21.2	21.5
MgO	36.0	37.6	36.0	43.8	43.1	43.1	43.0	42.2	40.6	40.5	39.
MnO	.36	.33	.38								
Cr_2O_3											
NiO	.10	.09	.10								
CaO	.31	.27	.24								
TiO_2											
Total	101.77	100.89	101.42	98.9	99.1	99.3	99.0	98.9	98.7	99.4	99.1
Fo	69.1	72.1	69.5	82.6	81.4	81.4	81.2	80.2	78.0	77.3	76.8
Fs	30.9	27.9	30.5	17.4	18.6	18.6	18.8	19.8	22.0	22.7	23.2

Loc., Sample	40-127-4B	40-127-5B	40-127-6B	40-127-7B	40-127-10B	40-127-10B	40-127-10B	40-127-11B	40-127-11B	40-127-11B
Group	Edge		Systematic	Systematic	Center	> to Edge	Edge	Center	> to Edge	Edge
Rock Type					Systematic					
			L-G	G	L					
SiO_2	37.6	37.8	37.5	37.9	39.4	39.2	38.8	38.7	38.9	38.9
FeO	21.5	22.0	22.3	22.8	16.8	17.0	17.2	18.2	18.3	18.1
MgO	39.8	39.6	29.2	38.8	43.8	43.8	43.7	43.1	43.1	42.9
MnO										
Cr_2O_3										
NiO										
CaO										
TiO_2										
Total	98.9	99.4	99.0	99.5	100.0	100.0	99.7	100.0	100.3	99.9
Fo	76.7	76.2	75.8	75.2	82.3	82.1	81.9	80.8	80.8	80.9
Fs	23.3	23.8	24.2	24.8	17.7	17.9	18.1	19.2	19.2	19.1

Olivine

Loc., Sample[1] / Group[2] / Rock Type[3]	40-127-12B Center	40-127-12B ½ to Edge	40-127-12B Edge	40-127-13B Center	40-127-13B ½ to Edge	40-127-13B Edge	40-127-14B Center	40-127-14B ½ to Edge	40-127-14B Edge	40-127-15B Center Systematic L-Gb
SiO_2	38.3	38.8	38.7	38.5	38.3	38.5	37.9	38.0	37.9	38.1
FeO	19.1	19.1	19.1	20.9	20.9	20.7	21.9	22.0	21.5	22.0
MgO	42.3	42.2	42.3	40.9	40.9	39.9	40.3	40.3	40.5	40.5
MnO										
Cr_2O_3										
NiO										
CaO										
TiO_2										
Total	99.1	100.1	100.1	100.3	100.1	99.1	100.1	100.3	99.9	100.6
Fo	79.8	79.7	79.8	77.7	77.7		76.6	76.6	77.1	76.7
Fs	20.2	20.3	20.2	22.3	22.3		23.4	23.4	22.9	23.3

Loc., Sample Group Rock Type	40-127-15B ½ to Edge	40-127-15B Edge	40-127-16B Center Systematic Gb	40-127-16B ½ to Edge	40-127-16B Edge	40-127-16B Edge	40-127-17B Center	40-127-17B Edge	40-127-17B Edge	40-127-18B Center
SiO_2	38.2	37.2	36.7	36.8	37.4	37.5	36.9	37.3	37.0	36.4
FeO	21.3	24.8	25.7	25.2	22.7	23.0	26.0	23.0	25.7	27.6
MgO	40.9	37.7	37.6	37.8	39.6	39.2	37.5	39.5	37.4	36.1
MnO										
Cr_2O_3										
NiO										
CaO										
TiO_2										
Total	100.4	99.7	100.0	99.8	99.7	99.7	100.4	99.8	100.1	100.1
Fo	77.4	73.1	72.3	72.8	75.7	75.2	72.0	75.4	72.2	70.0
Fs	22.6	26.9	27.7	27.2	24.3	24.8	28.0	24.6	27.8	30.0

	Olivine							
Loc., Sample[1]	40-127-18B	40-127-18B	40-127-19B	40-127-19B	40-127-19B	40-127-20B	40-127-20B	40-127-20B
Group[2]	Edge	Edge	Center	Edge	Edge	Center	Edge	Edge
Rock Type[3]								
SiO_2	37.0	37.7	36.4	37.4	37.4	36.7	37.2	36.7
FeO	25.4	23.1	28.0	23.6	22.9	28.4	26.7	26.0
MgO	37.9	39.2	35.6	39.0	39.6	35.6	36.8	37.3
MnO								
Cr_2O_3								
NiO								
CaO								
TiO_2								
Total	100.3	100.0	100.0	100.0	99.9	100.1	100.7	100.0
Fo	72.7	75.2	69.4	74.7	75.5	69.1	71.1	71.9
Fs	27.3	24.8	30.6	25.3	24.5	30.9	28.9	28.1

Loc., Sample	
Group	
Rock Type	
SiO_2	
FeO	
MgO	
MnO	
Cr_2O_3	
NiO	
CaO	
TiO_2	
Total	
Fo	
Fs	

Olivine

Loc., Sample[1]	63-3-1	63-3-2	63-3-3	63-3-4	63-3-5	63-3-1A	63-3-2A	63-3-3A	63-3-4A	63-3-5A
Group[2]	Systematic					Systematic				
Rock Type[3]	L					OWeb				
SiO_2	39.8	39.9	39.7	39.8	40.1	39.6	39.8	39.6	39.6	40.4
FeO	11.2	11.1	11.1	11.0	11.1	11.5	11.4	11.3	11.0	11.1
MgO	48.3	48.4	48.3	48.3	48.4	48.2	48.3	48.1	48.4	48.5
MnO	.13	.14	.14	.15	.15	.15	.14	.16	.15	.14
Cr_2O_3										
NiO	.19	.18	.19	.19	.18	.18	.18	.18	.18	.17
CaO	.12	.14	.18	.16	.18	.17	.10	.15	.18	.12
TiO_2										
Total	99.74	99.86	99.51	99.60	100.11	99.80	99.92	99.49	99.51	100.43
Fo	88.5	88.6	88.6	88.7	88.6	88.2	88.3	88.4	88.7	88.6
Fs	11.5	11.4	11.4	11.3	11.4	11.8	11.7	11.6	11.3	11.4

Loc., Sample	63-3-6A	63-3-7A	63-3-1B	63-3-2B	63-3-3B	63-3-4B	63-3-5B	63-6-1	63-6-1	63-6-2
Group	Systematic	Systematic						Systematic		
Rock Type	L-OWeb	L						L Center	Edge	
SiO_2	39.7	39.9	39.9	40.0	39.6	39.4	39.4	40.7	40.8	40.6
FeO	11.0	11.1	11.4	11.4	11.4	11.4	11.3	9.6	9.6	9.7
MgO	48.4	48.4	48.1	48.2	48.1	48.1	48.2	49.7	49.7	49.7
MnO	.15	.15	.15	.15	.15	.15	.15	.11	.11	.13
Cr_2O_3										
NiO	.18	.18	.18	.16	.18	.18	.16	.19	.17	.19
CaO	.14	.13	.15	.16	.08	.15	.17	.13	.09	.13
TiO_2										
Total	99.57	99.86	99.88	100.07	99.51	99.38	99.38	100.43	100.47	100.45
Fo	88.7	88.6	88.3	88.3	88.3	88.3	88.4	90.2	90.2	90.1
Fs	11.3	11.4	11.7	11.7	11.7	11.7	11.6	9.8	9.8	9.9

Olivine

Loc., Sample[1]	63-6-3	63-6-1A	63-6-2A	63-6-3A	63-6-1B	63-6-2B	63-6-3B	63-6-4B	63-6-5B	63-6-6B
Group[2]			Systematic	Systematic						
Rock Type[3]			L-OWeb	OWeb						
SiO_2	40.7	40.5	40.7	40.9	40.7	40.7	40.7	40.5	40.5	40.7
FeO	9.6	9.6	9.6	9.7	9.7	9.6	9.7	9.5	9.9	9.7
MgO	49.7	49.6	49.5	49.7	50.1	49.8	49.8	49.7	49.6	49.8
MnO	.11	.12	.12	.13	.12	.12	.13	.13	.13	.14
Cr_2O_3										
NiO	.19	.19	.19	.20	.19	.19	.19	.23	.19	.19
CaO	.10	.11	.14	.11	.10	.08	.10	.18	.20	.14
TiO_2										
Total	100.40	100.12	100.25	100.74	100.91	100.49	100.62	100.14	100.52	100.67
Fo	90.2	90.2	90.2	90.1	90.2	90.2	90.1	90.3	89.9	90.1
Fs	9.8	9.8	9.8	9.9	9.8	9.8	9.9	9.7	10.1	9.9

Loc., Sample	63-6-7B	63-6-1C	63-6-2C	63-6-3C	63-6-4C	63-9-1	63-9-2	63-9-3	63-9-4	63-9-5
Group						Systematic				
Rock Type						L				
SiO_2	40.5	40.5	40.4	40.1	40.4	39.4	39.8	39.4	39.6	39.5
FeO	9.9	10.1	10.1	10.2	10.1	13.7	13.7	13.9	13.6	13.6
MgO	49.8	49.1	49.2	49.3	49.3	46.3	46.6	46.5	46.5	46.2
MnO	.13	.14	.15	.14	.14	.18	.17	.17	.17	.16
Cr_2O_3										
NiO	.18	.19	.19	.20	.20	.15	.19	.18	.17	.19
CaO	.15	.12	.13	.13	.14	.15	.11	.17	.13	.12
TiO_2										
Total	100.66	100.15	100.17	100.07	100.20	99.88	100.57	100.32	100.17	99.77
Fo	90.0	89.7	89.7	89.6	89.7	85.8	85.8	85.6	85.9	85.8
Fs	10.0	10.3	10.3	10.4	10.3	14.2	14.2	14.4	14.1	14.2

Olivine

Loc., Sample[1]	63-9-1A	63-9-2A	63-9-3A	63-9-4A	63-9-5A	63-9-6A	63-9-1B	63-9-2B	63-9-3B	63-9-4B
Group[2]		Systematic		Systematic					Systematic	
Rock Type[3]		CP		L					CP	
SiO_2	39.4	39.7	39.7	39.6	39.4	39.2	39.2	39.3	38.1	39.2
FeO	14.0	14.0	14.4	14.4	14.3	14.3	14.1	14.4	13.8	14.5
MgO	46.6	46.5	46.7	46.6	46.4	46.3	46.1	46.0	44.6	45.9
MnO	.16	.18	.17	.16	.17	.16				
Cr_2O_3										
NiO	.17	.16	.18	.17	.18	.18				
CaO	.12	.17	.17	.13	.15	.12				
TiO_2										
Total	100.45	100.71	101.32	101.12	100.60	100.26	99.4	99.7	96.5	99.6
Fo	85.6	85.5	85.3	85.2	85.3	85.2	85.4	85.1	85.2	84.9
Fs	14.4	14.5	14.7	14.8	14.7	14.8	14.6	14.9	14.8	15.1

Loc., Sample	63-9-5B	63-9-6B	63-9-7B	63-9-8B	63-9-9B	63-12-1	63-12-2	63-12-3	63-12-4	63-12-5
Group						Systematic				
Rock Type						OWeb				
SiO_2	39.2	39.2	39.2	39.2	39.5	39.2	39.0	39.4	39.3	39.5
FeO	15.3	15.3	15.3	15.3	15.1	14.0	14.0	14.1	14.1	14.1
MgO	45.2	45.1	45.0	45.0	45.1	46.3	46.2	46.2	46.3	46.4
MnO						.15	.15	.14	.16	.14
Cr_2O_3										
NiO						.20	.19	.20	.21	.21
CaO						.12	.13	.13	.11	.12
TiO_2										
Total	99.7	99.6	99.5	99.5	99.7	99.97	99.67	100.17	100.18	100.47
Fo	84.0	84.0	84.0	84.0	84.2	85.5	85.5	85.4	85.4	85.4
Fs	16.0	16.0	16.0	16.0	15.8	14.5	14.5	14.6	14.6	14.6

Olivine

Loc., Sample[1]	63-12-6	63-12-7	63-12-8	63-12-9	63-12-10	63-12-11	63-12-12	63-12-13	63-17-1	63-17-2
Group[2]	Systematic			Systematic	Systematic		Systematic	Systematic	Systematic	
Rock Type[3]	L			L-OWeb	OWeb		L	OWeb	L	
SiO_2	39.4	39.6	40.2	40.2	40.5	38.2	38.9	39.4	40.2	38.8
FeO	14.1	14.1	14.3	14.5	14.3	13.8	13.9	13.8	11.9	12.4
MgO	46.5	46.7	47.0	47.3	47.1	46.1	46.1	46.0	48.1	47.9
MnO	.15	.14	.15	.15	.14	.14	.19	.18	.03	.06
Cr_2O_3										
NiO	.21	.20	.20	.20	.19	.20	.19	.20	.17	.17
CaO	.13	.12	.13	.14	.17	.17	.19	.16	.16	.09
TiO_2										
Total	100.49	100.86	101.98	102.49	102.40	98.61	99.47	99.74	100.56	99.42
Fo	85.5	85.5	85.4	85.3	85.4	85.4	85.4	85.4	87.8	87.3
Fs	14.5	14.5	14.6	14.7	14.6	14.6	14.6	14.6	12.2	12.7

Loc., Sample	63-17-3	63-17-4	63-17-1A	63-17-2A	63-17-3A	63-17-5A	63-17-6A	63-17-7A	63-17-1B
Group					Systematic	Systematic		Systematic	
Rock Type					OWeb	L		OWeb	
SiO_2	39.9	39.6	39.2	39.5	39.6	39.3	39.6	40.0	39.6
FeO	11.9	12.0	11.8	11.6	11.8	12.0	11.8	11.9	11.6
MgO	47.7	47.8	47.4	47.4	47.6	47.7	47.7	47.6	47.3
MnO	.04	.01	.03	.05	.04		.07	.05	
Cr_2O_3									
NiO	.17	.16	.15	.18	.18	.18	.18	.19	.17
CaO	.04		.08	.09	.08	.10	.07	.08	.12
TiO_2									
Total	99.75	99.57	98.66	98.82	99.30	99.28	99.42	99.82	98.79
Fo	87.7	87.7	87.7	87.9	87.8	87.6	87.8	87.7	87.9
Fs	12.3	12.3	12.3	12.1	12.2	12.4	12.2	12.3	12.1

Olivine

Loc., Sample[1]	63-17-2B	63-17-3B	63-17-4B	63-17-5B	63-17-1C	63-17-2C	63-17-3C	63-17-4C	63-17-5C	63-17-6C
Group[2]	Systematic		Systematic							
Rock Type[3]	OWeb		L							
SiO_2	39.5	39.6	39.4	39.6	39.3	38.8	39.4	39.4	39.8	39.2
FeO	11.8	11.9	11.9	11.7	11.7	11.8	11.7	11.5	11.9	11.7
MgO	47.7	47.8	47.8	47.8	47.4	47.7	47.5	47.4	47.7	47.5
MnO	.03	.06	.06	.04	.03	.04	.04	.05	.05	.03
Cr_2O_3										
NiO	.20	.16	.16	.19	.19	.20	.21	.16	.18	.17
CaO	.06	.17	.17	.14	.12	.08	.06	.07	.09	.06
TiO_2										
Total	99.29	99.69	99.49	99.47	98.74	98.62	98.91	98.58	99.72	98.66
Fo	87.8	87.7	87.7	87.9	87.8	87.8	87.9	88.0	87.7	87.9
Fs	12.2	12.3	12.3	12.1	12.2	12.2	12.1	12.0	12.3	12.1

Loc., Sample	63-17-1D	63-17-2D	63-17-3D	63-17-4D	63-17-5D	63-31-1	63-31-2	63-31-3	63-31-4	63-33-1
Group						Al-Aug				Al-Aug
Rock Type						L-OCP				OCP
SiO_2	39.6	40.0	39.9	39.9	39.5	39.8	40.2	40.4	39.8	39.9
FeO	11.9	11.9	12.0	12.2	12.1	10.9	11.1	11.0	10.9	11.0
MgO	47.5	48.0	48.1	48.1	47.9	49.1	48.5	47.9	48.7	48.4
MnO	.18	.14	.13	.16	.17	.03	.02		.02	.08
Cr_2O_3										
NiO	.19	.20	.20	.20	.18	.02				
CaO	.18	.16	.15	.20	.16	.25	.01	.22	.19	.59
TiO_2										
Total	99.55	100.40	100.48	100.76	100.01	100.10	99.83	99.82	99.61	99.97
Fo	87.7	87.8	87.7	87.5	87.6	88.9	88.6	88.6	88.8	88.7
Fs	12.3	12.2	12.3	12.5	12.4	11.1	11.4	11.4	11.2	11.3

Olivine

Loc., Sample[1]	63-33-2	63-33-3	63-36-1	63-36-2	63-36-3	63-36-4	63-36-5	63-36-6	63-36-7	63-36-8	63-36-9
Group[2]			Cr-Di								
Rock Type[3]			L								
SiO_2	39.5	39.5	40.0	39.8	39.6	39.8	39.1	39.6	39.8	39.5	39.7
FeO	11.0	11.0	11.1	11.0	10.9	11.0	10.9	10.9	11.0	11.0	11.0
MgO	48.9	48.9	48.5	48.7	48.9	48.4	48.4	49.2	48.6	49.1	49.0
MnO	.09	.06	.06		.01	.01		.09		.02	
Cr_2O_3											
NiO										.15	
CaO	.57	.53	.49	.49	.61	.48	.28	.13	.18	.06	.21
TiO_2											
Total	100.06	99.99	100.15	99.99	100.02	99.69	98.68	99.92	99.58	99.83	99.91
Fo	88.8	88.8	88.7	88.8	88.9	88.7	88.8	88.9	88.7	88.8	88.8
Fs	11.2	11.2	11.3	11.2	11.1	11.3	11.2	11.1	11.3	11.2	11.2

Loc., Sample
Group
Rock Type
SiO_2
FeO
MgO
MnO
Cr_2O_3
NiO
CaO
TiO_2
Total
Fo
Fs

Olivine

Loc., Sample[1]	4-80-1	4-80-2	4-80-3	4-80-4	4-80-5	4-80-6	4-80-1A	4-80-2A	4-80-3A	40-80-4A	4-80-5A
Group[2]	Systematic					Systematic	Systematic			Systematic	
Rock Type[3]	L					OWeb	L			OWeb	
SiO_2	39.7	39.4	39.5	39.7	39.1	39.4	39.3	39.5	39.2	39.4	37.8
FeO	12.7	12.7	12.6	12.6	12.5	12.4	12.4	12.4	12.5	12.5	12.4
MgO	47.3	47.5	47.2	44.4	47.2	47.1	47.4	47.5	47.4	47.3	46.6
MnO	.16	.17	.16	.15	.14	.15	.15	.15	.15	.15	.15
Cr_2O_3											
NiO	.16	.18	.19	.19	.18	.19	.18	.20	.17	.20	.20
CaO	.20	.21	.16	.17	.13	.13	.16	.13	.15	.14	.21
TiO_2											
Total	100.22	100.69	99.81	97.21	99.25	99.37	99.59	99.88	99.57	99.69	97.36
Fo	86.9	87.0	87.0	86.3	87.1	87.1	87.2	87.2	87.1	87.1	87.0
Fs	13.1	13.0	13.0	13.7	12.9	12.9	12.8	12.8	12.9	12.9	13.0

Loc., Sample
Group
Rock Type

SiO_2
FeO
MgO
MnO
Cr_2O_3
NiO
CaO
TiO_2
Total
Fo
Fs

Olivine

Loc., Sample[1/]	18-9-1	18-9-2	18-9-3	18-31-1	18-31-2	18-75-1	18-75-2	18-75-3	18-75-4
Group[2/]	B-G			B-G		B-G			
Rock Type[3/]	L			W		L			
SiO_2	39.7	40.6	40.6	40.5	40.2	40.6	39.6	39.7	39.9
FeO	9.5	9.7	9.6	11.9	11.9	11.1	11.1	11.2	11.4
MgO	49.1	49.1	48.9	47.3	47.3	47.4	47.6	47.7	47.6
MnO	.11	.13	.12	.15	.15	.14	.12	.15	.12
Cr_2O_3									
NiO	.29	.26	.29	.22	.23	.25	.25	.22	.26
CaO	.25	.24	.24	.25	.27	.22	.21	.24	.18
TiO_2									
Total	98.95	100.03	99.75	100.32	100.05	99.71	98.88	99.21	99.46
Fo	90.0	89.9	89.9	87.5	87.5	88.2	88.3	88.3	88.1
Fs	10.0	10.1	10.1	12.5	12.5	11.8	11.7	11.7	11.9

Loc., Sample	18-75-5	18-78-1	18-78-2	18-78-3	18-78-4	18-78-5	18-78-6	18-78-7
Group		Systematic						
Rock Type		L						
SiO_2	39.5	39.4	39.3	38.6	39.8	39.4	39.7	38.9
FeO	10.9	13.6	13.2	13.3	13.4	13.0	13.2	13.2
MgO	47.6	46.0	46.0	46.3	46.1	46.0	46.3	46.2
MnO	.13	.15	.15	.14	.15	.16	.15	.14
Cr_2O_3								
NiO	.24	.24	.24	.22	.23	.24	.25	.22
CaO	.20	.16	.16	.16	.17	.14	.15	.17
TiO_2								
Total	98.57	99.55	99.05	98.72	99.85	98.94	99.75	98.83
Fo	88.6	85.7	86.0	86.0	85.8	86.2	86.1	86.1
Fs	11.4	14.3	14.0	14.0	14.2	13.8	13.9	13.9

Olivine

Loc., Sample[1]	SAL-1	SAL-2	SAL-3	SAL-4	SAL-5	SAL-6	SAL-7	SAL-8	SAL-9	SAL-10	SAL-11
Group[2]	Systematic										
Rock Type[3]	L										
SiO_2	39.0	39.0	38.9	38.9	39.1	38.8	39.1	39.0	38.9	38.8	38.7
FeO	13.8	13.8	14.1	13.9	14.2	14.6	14.4	14.7	14.7	14.8	15.2
MgO	46.0	46.0	46.1	45.8	45.8	46.0	45.7	45.8	45.6	45.3	45.5
MnO	.04	.04	.04	.03	.04	.03	.05	.03	.07	.04	.04
Cr_2O_3											
NiO	.19	.18	.17	.17	.19	.19	.17	.18	.17	.18	.15
CaO	.04	.07	.04	.06	.03	.05	.07	.06	.08	.05	.05
TiO_2											
Total	99.07	99.09	99.35	98.86	99.36	99.67	99.49	99.77	99.52	99.17	99.64
Fo	85.6	85.6	85.4	85.4	85.2	84.9	85.0	84.7	84.7	84.5	84.2
Fs	14.4	14.4	14.6	14.6	14.8	15.1	15.0	15.3	15.3	15.5	15.8

Loc., Sample	
Group	
Rock Type	
SiO_2	
FeO	
MgO	
MnO	
Cr_2O_3	
NiO	
CaO	
TiO_2	
Total	
Fo	
Fs	

CLINOPYROXENE

Loc., Sample[1]	40-1-1	40-1-2	40-1-3	40-1-6	40-1-7	40-1-8	40-1-9	40-1-1A	40-1-2A
Group[2]	Systematic			Systematic				Systematic	
Rock Type[3]	OWeb			L				OWeb	
SiO_2	52.1	52.6	52.5	52.6	52.6	52.8	52.9	52.6	52.5
Al_2O_3	4.5	4.8	5.1	5.1	5.0	4.8	5.0	4.5	4.8
FeO	2.8	2.9	2.9	2.8	2.8	2.8	2.9	2.8	2.9
MgO	16.1	16.5	16.4	16.2	16.4	16.5	16.5	16.2	16.4
CaO	21.0	20.9	21.3	21.0	21.4	21.5	20.9	21.2	20.2
Na_2O	.93	.90	.90	.91	.88	.88	.84	.93	.91
K_2O	.02	.02	.02	.02	.03	.02	.13	.02	.02
TiO_2	.37	.30	.34	.35	.33	.30	.33	.38	.39
Cr_2O_3	.88	.75	.87	.90	.73	.68	.80	.90	.92
NiO									
Total	98.70	99.67	100.33	99.88	100.17	100.28	100.30	99.53	99.04
Ca	46.1	45.3	45.9	45.9	46.1	46.1	45.3	46.2	44.6
Fe	4.8	4.9	4.9	4.8	4.7	4.7	4.9	4.8	5.0
Mg	49.1	49.8	49.2	49.3	49.2	49.2	49.8	49.1	50.4

Loc., Sample	40-1-3A	40-1-4A	40-1-5A	40-1-6A	40-2-1	40-2-2	40-2-3	40-2-4	40-2-5
Group		Systematic			Cr-Di				
Rock Type		L			L-OWeb				
SiO_2	52.5	52.4	52.9	52.4	52.7	52.8	53.2	53.1	53.0
Al_2O_3	4.9	4.6	4.5	4.6	3.9	3.9	3.7	3.6	3.5
FeO	2.8	2.8	2.8	2.8	2.6	2.6	2.5	2.5	2.5
MgO	16.2	16.5	16.7	16.5	15.8	15.9	16.0	16.3	16.2
CaO	21.4	20.9	21.4	20.9	20.7	20.6	20.7	20.5	20.6
Na_2O	.92	.89	.88	.94	1.4	1.4	1.3	1.3	1.3
K_2O	.02	.03	.02	.02	.02	.03	.03	.03	.03
TiO_2	.40	.42	.40	.45	.45	.52	.49	.51	.47
Cr_2O_3	.96	.94	.86	.96	1.7	1.6	1.7	1.4	1.6
NiO									
Total	100.10	99.48	100.46	99.51	99.27	99.35	99.62	99.24	99.20
Ca	46.4	45.4	45.7	45.4	46.3	46.0	46.1	45.4	45.7
Fe	4.7	4.7	4.7	4.7	4.5	4.5	4.3	4.3	4.3
Mg	48.9	49.9	49.6	49.9	49.2	49.4	49.6	50.3	50.0

CLINOPYROXENE

Loc., Sample[1/]	40-2-6
Group[2/]	
Rock Type[3/]	
SiO_2	53.2
Al_2O_3	4.0
FeO	2.5
MgO	15.9
CaO	20.6
Na_2O	1.4
K_2O	.03
TiO_2	.66
Cr_2O_3	1.5
NiO	
Total	99.79
Ca	46.1
Fe	4.4
Mg	49.5

CLINOPYROXENE

Loc., Sample[1]	40-4-1	40-4-2	40-127-1	40-127-2	40-127-3	40-127-4	40-127-5	40-127-6	40-127-7	40-127-8
Group[2]	Cr-Di		Systematic							
Rock Type[3]	L		L							
SiO_2	50.0	48.7	51.6	51.4	51.8	51.8	52.0	51.4	51.1	50.1
Al_2O_3	6.7	6.2	5.4	5.5	5.1	5.3	5.2	5.4	5.2	6.7
FeO	3.2	3.4	2.9	2.8	3.0	3.0	3.3	3.5	4.9	6.0
MgO	15.4	16.2	15.9	15.8	16.1	15.9	16.0	15.9	15.3	14.4
CaO	22.7	23.8	21.2	21.1	21.3	21.5	21.2	21.6	20.8	20.0
Na_2O	.76	.87	.88	.90	.82	.87	.82	.78	.82	.90
K_2O										
TiO_2	1.1	.84	.70	.71	.62	.64	.62	.65	.63	1.2
Cr_2O_3			.94	.92	.77	.84	.75	.85	.76	.35
NiO			.05	.04	.06	.04	.05	.05	.04	.04
Total	99.86	100.01	99.57	99.17	99.57	99.89	99.94	100.13	99.55	99.69
Ca	48.7	48.6	46.5	46.6	46.3	46.8	46.1	46.5	45.3	
Fe	5.4	5.4	5.0	4.8	5.1	5.1	5.6	5.9	8.3	
Mg	45.9	46.0	48.5	48.6	48.6	48.1	48.3	47.6	46.4	

Loc., Sample	40-127-9	40-127-10	40-127-11	40-127-12	40-127-13	40-127-14	40-127-15	40-127-1A	40-127-2A	40-127-3A
Group	Systematic				Systematic					Systematic
Rock Type	Gb				L					Gb
SiO_2	48.5	48.4	48.7	50.2	51.5	51.9	51.6	51.9	50.8	50.6
Al_2O_3	7.6	7.6	7.7	6.5	5.1	5.5	6.0	5.1	5.7	6.1
FeO	6.4	6.6	6.4	5.7	5.0	3.0	2.9	3.7	6.0	7.4
MgO	13.7	13.7	13.7	14.7	15.5	15.8	15.6	15.9	14.8	14.3
CaO	20.1	19.9	20.1	20.0	20.5	21.3	21.2	20.8	19.9	19.4
Na_2O	.88	.93	.89	.93	.63	.89	.91	.84	.77	.84
K_2O										
TiO_2	1.9	2.0	1.8	1.5	.73	.65	.63	.53	1.0	1.1
Cr_2O_3	.34	.31	.49	.65	.52	.93	1.0	.73	.24	.17
NiO	.04	.02	.04	.04	.04	.04	.06	.04	.04	.06
Total	99.46	99.46	99.82	100.22	99.52	100.01	99.90	99.54	99.25	99.97
Ca	45.5	45.1	45.5	44.5	44.6	46.7	46.9	45.4	44.1	43.0
Fe	11.3	11.7	11.3	9.9	8.5	5.1	5.0	6.3	10.4	12.8
Mg	43.2	43.2	43.2	45.5	46.9	48.2	48.0	48.3	45.5	44.1

CLINOPYROXENE

Loc., Sample[1] Group[2] Rock Type[3]	40-127-4A	40-127-5A	40-127-6A	40-127-7A	40-127-8A	40-127-1B Center L	40-127-1B ½ to Edge	40-127-1B Edge	40-127-1B Edge	40-127-2B Center
SiO_2	49.1	49.1	50.8	49.9	48.8	51.3	51.7	51.4	51.4	51.0
Al_2O_3	7.5	6.8	5.0	6.4	7.5	5.4	5.3	5.7	5.2	5.4
FeO	6.9	7.2	7.1	6.8	7.2	4.0	4.3	5.0	4.8	5.7
MgO	14.1	14.0	15.0	14.3	14.5	15.6	15.7	15.3	15.7	14.9
CaO	19.9	19.7	20.7	19.3	18.8	21.0	20.9	20.6	20.8	21.0
Na_2O	.73	.87	.49	.84	.69	.79	.78	.86	.82	.83
K_2O						.04	.03	.04	.04	.02
TiO_2	1.6	1.7	1.0	1.3	2.0	.43	.42	.45	.41	.47
Cr_2O_3	.54	.52	.24	.64	.25	.82	.77	.74	.87	.90
NiO	.06	.02	.05	.04	.05					
Total	100.43	99.91	100.38	99.52	99.79	99.38	99.90	100.09	100.04	100.22
Ca	44.3	44.0	43.9	43.4	42.2	45.8	45.3	45.0	44.8	45.5
Fe	12.0	12.5	11.8	11.9	12.6	6.8	7.3	8.5	8.1	9.6
Mg	43.7	43.5	44.3	44.7	45.2	47.4	47.4	46.5	47.1	44.9

Loc., Sample Group Rock Type	40-127-2B ½ to Edge	40-127-2B Edge	40-127-2B Edge	40-127-3B Center	40-127-3B ½ to Edge	40-127-3B Edge	40-127-4B Center Gb	40-127-4B ½ to Edge	40-127-4B Edge	40-127-5B Center
SiO_2	51.3	50.6	51.0	51.6	51.4	50.9	49.3	49.5	49.8	49.3
Al_2O_3	5.4	6.0	6.2	5.6	5.5	6.1	7.3	7.4	7.2	7.6
FeO	5.9	6.1	6.3	5.1	5.0	5.3	6.7	6.7	7.0	7.0
MgO	14.7	14.6	14.8	15.3	15.4	15.1	13.9	13.9	14.1	13.6
CaO	20.2	20.0	19.8	20.7	20.9	20.7	19.6	19.7	19.6	19.6
Na_2O	.83	.87	.85	.84	.82	.86	.95	.95	.94	.90
K_2O	.03	.03	.03	.04	.04	.03	.03	.04	.04	.04
TiO_2	.54	.76	.83	.45	.47	.56	1.4	1.3	1.3	1.4
Cr_2O_3	.85	.67	.56	.79	.80	.71	.67	.54	.44	.41
NiO										
Total	99.75	99.63	100.37	100.42	100.33	100.26	99.85	100.03	100.42	99.85
Ca	44.6	44.4	43.7	45.0	45.2	45.2	44.4	44.5	43.9	44.6
Fe	10.2	10.6	10.9	8.7	8.4	9.0	11.8	11.8	12.2	12.4
Mg	45.2	45.1	45.4	46.3	46.3	45.8	43.8	43.7	43.9	43.0

CLINOPYROXENE

Loc., Sample[1]	40-127-5B	40-127-6B	40-127-6B	40-127-6B	40-127-6B
Group[2]	Center	Center	1/2 to Edge	Edge	Edge
Rock Type[3]					
SiO_2	49.9	48.9	49.7	49.1	49.5
Al_2O_3	6.6	7.3	6.3	7.5	6.3
FeO	6.7	7.3	7.0	6.9	6.7
MgO	14.0	13.6	14.1	13.6	14.5
CaO	20.3	19.5	19.4	19.5	20.0
Na_2O	.87	.86	.86	.89	.68
K_2O	.04	.03	.03	.03	.17
TiO_2	1.0	1.4	1.1	1.4	1.2
Cr_2O_3	.39	.39	.66	.41	.17
NiO					
Total	99.80	99.28	99.15	99.33	99.22
Ca	45.1	44.2	43.6	44.5	44.1
Fe	11.6	12.9	12.3	12.3	11.5
Mg	43.3	42.9	44.1	43.2	44.4

Loc., Sample
Group
Rock Type
SiO_2
Al_2O_3
FeO
MgO
CaO
Na_2O
K_2O
TiO_2
Cr_2O_3
NiO
Total
Ca
Fe
Mg

CLINOPYROXENE

Loc., Sample[1]	32-15-1	32-15-2	32-15-3	32-15-5	32-15-6	32-15-7	32-15-8	32-22-1	32-22-2	32-22-3
Group[2]	Systematic							Cr-Di		
Rock Type[3]	OWeb							L		
SiO_2	51.5	51.0	51.7	51.5	51.7	51.6	51.1	51.8	51.4	52.7
Al_2O_3	6.8	6.7	6.9	7.1	6.8	7.0	6.9	6.6	6.9	6.7
FeO	4.1	4.4	4.0	3.8	3.8	4.0	4.7	2.8	2.8	2.8
MgO	15.3	15.0	15.4	15.2	15.3	15.2	14.9	15.2	15.3	15.3
CaO	20.1	20.8	20.3	19.9	19.8	19.8	19.5	20.0	20.3	20.6
Na_2O	1.1	1.1	1.1	1.1	1.1	1.1	1.2	1.6	1.6	1.6
K_2O										
TiO_2	.43	.46	.44	.45	.32	.34	.40	.55	.51	.51
Cr_2O_3	.44	.47	.43	.48	.50	.55	.50	.82	.90	.90
NiO	.09	.07	.07	.08	.09	.07	.06			
Total	99.86	100.00	100.34	99.61	99.41	99.66	99.26	99.37	99.71	101.11
Ca	45.0	46.0	45.3	45.1	45.0	45.0	44.5	46.2	46.4	46.7
Fe	7.2	7.7	7.0	6.8	6.8	7.1	8.3	5.0	5.0	5.0
Mg	47.8	46.3	47.7	48.1	48.2	47.9	47.2	48.8	48.6	48.3

Loc., Sample	32-24-10	32-24-11	32-24-13	32-24-14	32-24-15	32-24-16	32-24-1A	32-24-2A	32-24-3A	32-24-4C
Group	Systematic									
Rock Type	OWeb									
SiO_2	51.6	51.2	51.2	51.5	51.5	51.7	51.4	51.8	51.1	51.6
Al_2O_3	7.0	7.5	6.9	7.1	6.6	6.6	6.5	6.8	6.4	5.9
FeO	3.2	3.2	3.3	3.2	3.3	3.3	3.2	3.2	3.3	4.4
MgO	15.4	15.2	15.3	15.4	15.5	15.4	15.3	15.5	15.7	14.8
CaO	20.2	20.2	20.4	20.5	20.6	20.3	20.8	20.8	20.7	19.9
Na_2O	.98	1.2	1.1	1.1	1.1	1.1	1.1	1.2	1.2	1.3
K_2O							.01	.01	.01	
TiO_2	.72	.85	.76	.75	.73	.73	.70	.75	.70	.51
Cr_2O_3	.13	.11	.31	.36	.36	.42	.48	.49	.45	.62
NiO	.10	.10	.09	.11	.08	.08				.08
Total	99.33	99.56	99.36	100.32	99.77	99.77	99.49	100.55	99.56	99.11
Ca	45.8	46.1	46.1	46.1	46.0	45.8	46.7	46.4	45.9	45.3
Fe	5.7	5.7	5.8	5.6	5.8	5.8	5.6	5.6	5.7	7.8
Mg	48.5	48.2	48.1	48.2	48.2	48.4	47.7	48.0	48.4	46.9

CLINOPYROXENE

Loc., Sample[1]	32-24-5C	32-24-6C	32-24-7C	32-29-1	32-29-2	32-29-3	32-29-4	32-35-1	32-35-2	32-35-3
Group[2]				Al-Aug				Cr-Di		
Rock Type[3]				Web				L		
SiO_2	51.2	51.8	52.0	49.6	50.3	50.7	50.5	52.1	52.2	52.00
Al_2O_3	6.3	6.1	6.0	7.8	7.7	7.6	7.5	6.5	6.2	6.20
FeO	4.0	4.1	3.7	4.2	4.3	4.2	4.2	3.0	3.1	3.20
MgO	14.9	15.2	15.5	14.5	14.6	14.6	14.8	15.4	15.5	15.60
CaO	20.2	19.8	20.5	20.0	20.1	20.0	20.1	20.4	20.8	20.70
Na_2O	1.2	1.2	1.1	1.2	1.3	1.2	1.2	1.4	1.3	1.30
K_2O										
TiO_2	.62	.51	.51	.82	.85	.86	.93	.54	.47	.44
Cr_2O_3	.66	.60	.54	.17	.17	.20	.20	.76	.79	.82
NiO	.10	.39	.10							
Total	99.18	99.70	99.95	98.29	99.32	99.36	99.43	100.10	100.36	100.26
Ca	45.9	44.9	45.6	46.0	45.9	45.9	45.7	46.2	46.4	46.1
Fe	7.1	7.2	6.4	7.5	7.7	7.5	7.5	5.3	5.4	5.6
Mg	47.0	47.9	48.0	46.4	46.4	46.6	46.8	48.5	48.2	48.3

Loc., Sample	32-35-4	32-57-1	32-57-2	32-57-3	32-57-4	32-71-1	32-71-2	32-71-3	32-71-4	32-72-1
Group		Transitional				Cr-Di				Systematic
Rock Type		L				L				L
SiO_2	51.5	51.1	51.1	50.9	50.8	51.2	52.1	52.1	52.1	52.5
Al_2O_3	6.8	7.9	7.7	7.6	7.9	6.6	6.7	6.9	7.3	4.6
FeO	3.0	5.1	4.5	4.8	5.1	3.1	3.1	3.2	3.1	4.8
MgO	15.3	15.5	15.6	15.7	15.4	15.6	15.7	15.8	15.5	16.0
CaO	20.2	18.8	18.8	18.8	18.7	20.1	19.8	20.2	20.0	19.8
Na_2O	1.5	1.3	1.3	1.3	1.3	1.5	1.5	1.4	1.6	1.3
K_2O						.05	.04	.05	.04	
TiO_2	.61	1.1	.59	.69	1.1	.53	.56	.43	.51	.48
Cr_2O_3	.84	.66	.74	.67	.52	.73	.75	.67	.72	.31
NiO										.09
Total	99.75	101.46	100.33	100.46	100.82	99.41	100.25	100.75	100.87	99.88
Ca	46.1	42.4	42.7	42.4	42.4	45.4	44.9	45.2	45.5	43.2
Fe	5.3	9.0	8.0	8.4	9.0	5.5	5.5	5.6	5.5	8.1
Mg	48.6	48.6	49.3	49.2	48.6	49.1	49.6	49.2	49.0	48.7

CLINOPYROXENE

Loc., Sample[1]	32-72-2	32-72-3	32-72-4	32-72-5	32-72-6	32-72-7	32-72-8	32-72-1A	32-72-2A	32-72-3A
Group[2]										
Rock Type[3]										
SiO_2	52.4	51.7	51.3	51.3	51.8	51.4	51.8	52.0	51.3	51.3
Al_2O_3	5.4	6.7	6.7	7.2	6.8	7.2	7.1	6.6	7.4	7.2
FeO	4.7	4.7	4.5	4.3	4.1	3.9	3.8	3.6	3.7	3.7
MgO	15.5	14.9	14.8	14.8	15.2	15.2	15.3	15.5	15.1	15.2
CaO	19.8	19.6	19.9	19.7	19.9	19.9	19.7	20.1	19.9	19.9
Na_2O	1.3	1.4	1.4	1.4	1.4	1.4	1.4	1.3	1.4	1.4
K_2O										
TiO_2	.30	.38	.35	.45	.35	.49	.50	.34	.56	.55
Cr_2O_3	.62	.73	.73	.74	.70	.75	.68	.59	.70	.66
NiO	.09	.10	.07	.10	.11	.10	.11	.11	.07	.09
Total	100.11	100.21	99.75	99.99	100.36	100.34	100.39	100.14	100.13	100.00
Ca	43.9	44.6	45.2	45.0	45.0	45.2	44.9	45.2	45.5	45.3
Fe	8.2	8.3	8.0	7.7	7.2	6.9	6.7	6.2	6.5	6.6
Mg	47.9	47.1	46.9	47.3	47.8	47.9	48.4	48.5	48.0	48.2

Loc., Sample	32-72-4A	32-74-1	32-85-1	32-85-2	32-85-3	32-85-4	32-90-1	32-90-2	32-90-3	32-103-1
Group		Transitional	Cr-Di				Cr-Di			Cr-Di
Rock Type		L	L				L			L
SiO_2	51.7	51.4	52.2	52.3	52.3	52.4	52.1	51.8	52.3	52.0
Al_2O_3	6.7	7.7	5.6	5.6	5.7	5.8	4.6	4.5	3.9	6.1
FeO	3.8	3.5	2.6	2.6	2.7	2.6	2.8	2.8	2.7	3.5
MgO	15.7	15.7	15.7	15.5	15.4	15.5	14.6	14.7	14.5	16.5
CaO	19.9	19.00	21.7	21.3	20.9	21.6	21.7	22.1	22.7	20.3
Na_2O	1.3	1.4	1.2	1.3	1.3	1.2	1.5	1.6	1.4	.99
K_2O		.04	.03	.02	.03	.03				.05
TiO_2	.39	.20	.42	.40	.37	.42	.18	.17	.18	.40
Cr_2O_3	.68	.63	.69	.70	.66	.68	1.1	1.0	.93	.88
NiO	.11									
MnO							.08	.07	.05	
Total	100.28	99.57	100.14	99.72	99.36	100.23	98.66	98.74	98.66	100.72
Ca	44.6	43.6	47.6	47.4	47.0	47.8	49.1	49.4	50.5	44.1
Fe	6.6	6.3	4.5	4.5	4.7	4.5	4.9	4.9	4.7	5.9
Mg	48.8	50.1	47.9	48.0	48.2	47.7	46.0	45.7	44.8	49.9

CLINOPYROXENE

Loc., Sample[1]	32-103-2	32-103-3	32-103-4	33-1-1	33-1-A	33-1-2	33-1-3	33-1-4	33-1-5	33-1-6
Group[2]				Systematic						
Rock Type[3]				L						
SiO_2	51.8	51.7	51.8	51.6	53.1	50.9	51.4	51.7	51.9	51.9
Al_2O_3	5.5	5.9	5.6	5.6	3.8	6.7	6.6	7.1	7.0	6.1
FeO	3.6	3.4	3.4	4.8	5.0	5.0	4.7	4.1	4.2	4.1
MgO	16.4	16.7	16.4	15.1	16.1	14.7	15.0	15.0	15.1	15.6
CaO	19.4	19.8	19.5	19.9	20.2	19.6	19.7	19.4	19.7	20.0
Na_2O	1.1	1.0	.93	1.3	1.1	1.4	1.4	1.5	1.5	1.2
K_2O	.06	.04	.06							
TiO_2	.33	.40	.42	.59	.50	.48	.36	.51	.52	.26
Cr_2O_3	.87	.86	.91	.85	.17	.81	.84	.85	.81	.77
NiO				.50	.41	.39	.47	.42	.38	.45
Total	99.06	99.80	99.02	100.24	100.28	99.98	100.47	100.58	101.11	100.38
Ca	43.1	43.3	43.4	44.6	43.5	44.6	44.6	44.6	44.7	44.6
Fe	6.2	5.8	5.9	8.4	8.4	8.8	8.2	7.4	7.5	7.1
Mg	50.7	50.9	50.7	47.0	48.1	46.6	47.2	48.0	47.8	48.3

Loc., Sample	33-1-7	33-1-1A	33-1-2A	33-1-3A	33-1-4A	33-1-5A	33-1-1B	33-1-2B	33-1-3B	33-1-4B
Group										
Rock Type										
SiO_2	51.8	51.4	51.6	51.9	51.5	51.8	51.9	52.5	52.0	51.9
Al_2O_3	6.8	7.1	6.9	6.7	7.3	6.7	6.9	6.8	6.9	6.9
FeO	4.0	3.4	3.4	3.6	3.6	3.9	3.3	3.4	3.4	3.3
MgO	15.3	15.4	15.3	15.6	15.4	15.4	15.4	15.6	15.5	15.6
CaO	19.8	20.3	20.3	20.4	19.6	20.1	20.2	20.5	20.0	20.4
Na_2O	1.3	1.4	1.3	1.3	1.5	1.3	1.3	1.3	1.4	1.4
K_2O										
TiO_2	.43	.46	.44	.40	.52	.44	.49	.45	.52	.44
Cr_2O_3	.79	.87	.85	.78	.86	.80	.82	.81	.77	.83
NiO	.42	.34	.47	.43	.38	.47	.43	.45	.46	.41
Total	100.64	100.67	100.56	101.11	100.66	100.91	100.74	101.81	100.95	101.18
Ca	44.9	45.7	45.9	45.4	44.8	45.1	45.7	45.7	45.2	45.7
Fe	7.1	5.9	5.9	6.3	6.4	6.9	5.9	5.8	5.9	5.8
Mg	48.0	48.4	48.2	48.3	48.8	48.0	48.4	48.5	48.8	48.5

CLINOPYROXENE

Loc., Sample[1]	33-1-1C	33-1-2C	33-1-3C	33-2-1	33-2-2	33-2-3	33-2-4	33-3-1	33-3-2	33-3-3
Group[2]				Al-Aug				Cr-Di		
Rock Type[3]				L				L		
SiO_2	52.2	52.0	52.2	51.1	51.6	52.0	51.7	52.3	52.9	52.8
Al_2O_3	7.1	7.1	7.0	4.5	4.1	3.7	4.1	4.7	4.8	4.7
FeO	3.3	3.3	3.3	4.3	4.3	4.6	4.5	2.6	2.7	2.7
MgO	15.4	15.4	15.5	14.7	15.4	15.3	15.4	15.8	15.9	15.8
CaO	20.0	20.1	20.3	22.2	22.4	22.6	22.2	21.5	21.0	21.2
Na_2O	1.5	1.4	1.4	.47	.45	.40	.51	1.3	1.3	1.3
K_2O										
TiO_2	.54	.50	.46	.52	.64	.41	.60			
Cr_2O_3	.86	.83	.80	.25	.20	.16	.51	.74	.77	.79
NiO	.49	.39	.42							
Total	101.39	101.02	101.38	98.04	99.09	99.17	99.52	99.02	99.37	99.29
Ca	45.4	45.5	45.8	48.3	47.5	47.6	47.1	47.2	46.4	46.8
Fe	5.8	5.9	5.8	7.3	7.1	7.6	7.4	4.5	4.7	4.7
Mg	48.7	48.6	48.4	44.4	45.4	44.8	45.5	48.3	48.9	48.5

Loc., Sample	33-3-4	33-40-1	33-40-2	33-40-3	33-99-1	33-99-2	33-99-3	33-99-4	35-4-1	35-4-2
Group		Cr-Di			Cr-Di				Cr-Di	
Rock Type		L			OP				L	
SiO_2	53.0	52.8	53.6	53.1	51.4	52.2	52.3	52.1	51.1	50.9
Al_2O_3	4.2	4.6	4.2	3.6	5.3	5.1	5.1	5.0	6.1	5.8
FeO	2.6	4.1	3.4	4.3	3.6	3.7	3.7	3.6	3.7	3.7
MgO	16.0	15.2	15.6	15.7	15.3	15.6	15.5	15.5	15.3	15.6
CaO	21.4	20.4	21.0	20.7	20.1	19.8	19.9	20.0	19.7	19.7
Na_2O	1.2	1.5	1.3	1.4	1.5	1.5	1.5	1.5	1.5	1.5
K_2O					.04	.03	.03	.03		
TiO_2		.12	.10	.07	.82	.56	.63	.56	.67	.64
Cr_2O_3	.71	.69	.60	.72	1.2	1.2	1.3	1.2	.67	.64
NiO										
MnO		.09	.08	.09						
Total	99.11	99.50	99.88	99.68	99.26	99.69	99.96	99.49	98.74	98.47
Ca	46.8	45.6	46.3	45.1	45.5	44.6	44.9	45.1	44.9	44.5
Fe	4.4	7.2	5.9	7.3	6.4	6.5	6.5	6.3	6.6	6.5
Mg	48.7	47.2	47.8	47.6	48.2	48.9	48.6	48.6	48.5	49.0

CLINOPYROXENE

Loc., Sample[1]	35-4-3	36-11-1	36-11-2	36-11-3	36-12-1	26-12-2	36-12-4	36-14-1	36-14-2	36-18-1
Group[2]		Al-Aug			Cr-Di			Al-Aug		Cr-Di
Rock Type[3]		Web			L			CP		L
SiO_2	51.4	49.0	48.9	48.7	51.4	51.6	51.4	48.2	48.0	51.8
Al_2O_3	5.9	7.5	7.3	7.6	6.3	6.3	6.4	7.9	7.9	6.2
FeO	3.7	7.0	7.3	6.8	3.3	3.3	3.3	7.4	7.5	3.2
MgO	15.5	13.9	14.7	14.0	15.9	15.8	15.2	13.5	13.4	15.1
CaO	19.4	18.4	18.0	18.6	19.2	18.9	18.9	18.2	18.3	20.1
Na_2O	1.6	1.1	1.1	1.1	1.3	1.3	1.3	1.2	1.2	1.5
K_2O		.03	.03	.03	.03	.02	.02	.02	.03	.01
TiO_2	.67	1.6	1.5	1.6	.53	.55	.52	1.8	2.0	.63
Cr_2O_3	.63	.09	.09	.08	.83	.82	.77	.02	.01	.81
NiO		.05	.05	.04	.06	.06	.05	.04	.04	.05
Total	98.80	98.61	98.97	98.55	98.85	98.65	97.86	98.28	98.38	99.40
Ca	44.2	42.6	40.8	42.9	43.7	43.5	44.3	42.6	42.8	46.1
Fe	6.6	12.6	12.9	12.2	5.9	5.9	6.0	13.5	13.7	5.7
Mg	49.2	44.8	46.3	44.9	50.4	50.6	49.6	43.9	43.5	48.2

Loc., Sample	36-18-2	36-18-3
Group		
Rock Type		
SiO_2	51.9	51.7
Al_2O_3	6.0	5.9
FeO	3.1	3.2
MgO	15.2	15.2
CaO	19.6	20.3
Na_2O	1.5	1.4
K_2O	.02	.02
TiO_2	.62	.58
Cr_2O_3	.76	.78
NiO	.27	.05
Total	98.91	99.13
Ca	45.4	46.2
Fe	5.6	5.7
Mg	49.0	48.1

CLINOPYROXENE

Loc., Sample[1]	66-10-1	66-10-2	66-10-3	66-10-4	66-10-1A	66-10-2A	66-10-3A	66-10-4A	66-10-5A	66-10-6A
Group[2]	Systematic								Systematic	
Rock Type[3]	L								OCP	
SiO_2	51.4	51.6	51.4	51.6	51.5	51.2	51.0	50.9	50.2	50.5
Al_2O_3	6.5	6.2	6.2	6.3	6.3	6.4	6.8	7.0	7.8	8.0
FeO	3.9	3.8	3.8	3.9	3.8	3.8	3.8	3.9	3.8	3.9
MgO	15.0	15.1	15.2	15.0	15.1	14.9	14.9	14.8	14.7	14.7
CaO	21.1	21.7	20.8	20.9	20.5	21.1	21.6	21.3	21.1	20.1
Na_2	1.1	1.1	1.1	1.1	1.1	1.1	1.1	1.1	1.1	1.1
K_2O										
TiO_2	.81	.75	.72	.78	.92	1.1	1.3	1.4	1.5	1.5
Cr_2O_3	.54	.54	.55	.58	.56	.56	.39	.20	.24	.04
NiO	.04	.04	.03	.04	.04	.03	.04	.04	.05	.05
Total	100.39	100.83	99.80	100.20	99.82	100.19	100.93	100.64	100.49	99.89
Ca	46.9	47.5	46.3	46.6	46.1	47.1	47.7	47.4	47.4	46.1
Fe	6.8	6.5	6.6	6.8	6.7	6.6	6.5	6.8	6.7	7.0
Mg	46.4	46.0	47.1	46.6	47.2	46.3	45.8	45.8	45.9	46.9

Loc., Sample	66-10-7A	66-123-1	66-123-2	66-123-3	66-123-4	66-123-1A	66-123-2A	66-123-3A	66-123-4A
Group		Systematic		Systematic		Systematic	Systematic		
Rock Type		L		Web		L	Web		
SiO_2	50.5	51.9	51.7	52.0	51.6	51.3	51.8	51.2	51.1
Al_2O_3	7.9	7.5	7.7	7.7	8.2	7.5	7.7	8.3	8.4
FeO	3.7	3.2	3.2	3.2	3.2	3.2	3.3	3.3	3.2
MgO	14.7	15.2	15.0	15.1	14.9	15.1	15.1	14.9	14.5
CaO	20.7	20.1	18.8	19.2	19.0	19.4	19.3	18.9	19.4
Na_2O	1.2	1.6	1.6	1.6	1.7	1.6	1.6	1.7	1.7
K_2O									
TiO_2	1.5	.76	.76	.72	.79	.74	.76	.70	.80
Cr_2O_3	.18	.60	.66	.60	.69	.58	.62	.64	.64
NiO	.04	.03	.05	.05	.05	.05	.04	.06	.05
Total	100.42	100.89	99.47	100.17	100.13	99.47	100.22	99.70	99.79
Ca	47.0	45.9	44.6	45.0	45.0	45.2	45.0	44.8	46.1
Fe	6.6	5.7	5.9	5.8	5.9	5.8	6.0	6.1	5.9
Mg	46.4	48.3	49.5	49.2	49.1	49.0	49.0	49.1	48.0

CLINOPYROXENE

Loc., Sample[1]	67-7-1	67-7-2	67-7-3	67-7-2A	67-7-4A	67-7-3A	67-84-1	67-84-2	67-84-3	67-84-4
Group[2]	Systematic			Systematic			Systematic			
Rock Type[3]	OCP			L			OCP			
SiO_2	47.4	47.8	48.6	48.6	48.0	48.8	49.8	49.9	49.2	49.2
Al_2O_3	7.7	7.8	7.6	6.7	7.4	6.6	8.3	7.8	8.3	8.7
FeO	5.1	5.3	5.3	5.1	5.2	5.2	4.6	4.2	4.7	4.9
MgO	14.0	14.4	14.5	14.6	14.3	14.5	14.7	14.9	14.4	14.4
CaO	20.5	21.1	21.0	21.3	20.8	21.4	21.2	21.2	21.0	20.7
Na_2O	.82	.79	.81	.87	.75	.82	.88	.83	.88	.89
K_2O	.06	.05	.05	.05	.06	.08	.02	.01	.01	.01
TiO_2	1.6	1.7	1.6	1.3	1.6	1.2	1.6	1.6	1.7	1.7
Cr_2O_3	.07	.04	.08	.44	.10	.42	.01	.02	.01	.01
NiO										
Total	97.25	98.98	99.54	98.96	98.21	99.02	101.11	100.46	100.20	100.51
Ca	46.6	46.6	46.3	46.7	46.5	46.9	46.9	46.9	47.0	46.4
Fe	9.1	9.1	9.1	8.7	9.1	8.9	7.9	7.2	8.2	8.6
Mg	44.3	44.3	44.5	44.5	44.4	44.2	45.2	45.9	44.8	45.0

Loc., Sample	67-84-1A	67-84-2A	67-84-3A	67-84-4A	67-84-5A	67-84-6A	67-84-7A	67-84-1B	67-84-2B	67-84-3B
Group	Systematic				Systematic			Systematic		
Rock Type	L				OCP			L		
SiO_2	50.8	50.0	50.7	50.8	49.8	49.8	50.1	51.2	51.4	51.7
Al_2O_3	6.9	7.7	6.7	6.6	8.3	8.2	7.9	6.7	6.5	6.6
FeO	4.0	4.2	4.0	3.9	4.3	4.4	4.1	3.9	4.1	4.1
MgO	15.3	14.9	15.3	15.3	14.7	14.7	14.9	15.1	15.3	15.2
CaO	21.4	21.1	20.8	21.1	20.6	21.5	21.6	21.0	20.9	20.9
Na_2O	.87	.90	.88	.87	.92	.82	.87	.94	1.0	.95
K_2O	.01	.01	.01	.01	.02	.01	.01			
TiO_2	1.0	1.3	.92	.90	1.5	1.5	1.4	.68	.53	.61
Cr_2O_3	.46	.16	.51	.49	.20	.01	.06	.55	.71	.61
NiO										
Total	100.74	100.27	99.82	99.97	100.34	100.94	100.94	100.07	100.44	100.67
Ca	46.7	46.8	46.0	46.4	46.4	47.4	47.4	46.6	46.1	46.2
Fe	6.8	7.3	6.9	6.7	7.6	7.6	7.0	6.8	7.0	7.1
Mg	46.5	45.9	47.1	46.9	46.0	45.0	45.5	46.6	46.9	46.7

CLINOPYROXENE

Loc., Sample[1]	67-136-1	67-136-2	67-136-3	67-136-4	67-136-5	67-136-6	67-136-1A	67-136-2A	67-136-3A	67-136-4A
Group[2]	Systematic			Systematic			Systematic			Systematic
Rock Type[3]	CP			L			CP			L
SiO_2	49.4	49.8	50.4	50.5	50.7	50.5	49.8	50.1	50.4	51.2
Al_2O_3	7.5	7.2	7.2	6.8	6.6	6.6	7.5	7.6	7.2	6.4
FeO	4.6	4.7	4.7	4.8	4.5	4.7	4.3	4.3	4.2	3.8
MgO	14.4	14.8	14.7	14.8	15.2	15.0	14.7	15.0	14.9	15.5
CaO	21.1	21.4	21.3	21.2	21.5	21.3	21.2	21.3	20.8	21.7
Na_2O	.88	.74	.87	.86	.76	.84	.83	.89	.90	.82
K_2O	.03	.03	.03	.02	.02	.03	.03	.02	.02	.02
TiO_2	1.6	1.5	1.5	1.4	1.4	1.4	1.7	1.6	1.5	1.3
Cr_2O_3	.02	.08	.22	.35	.33	.36	.02	.02	.18	.36
NiO										
Total	99.53	100.25	100.92	100.73	101.01	100.73	100.08	100.83	100.10	101.10
Ca	47.2	46.9	46.9	46.6	46.6	46.5	47.1	46.8	46.4	46.9
Fe	8.0	8.0	8.1	8.2	7.6	8.0	7.5	7.4	7.3	6.4
Mg	44.8	45.1	45.0	45.2	45.8	45.5	45.4	45.8	46.3	46.6

Loc., Sample	67-136-5A	67-136-6A	67-136-1B	67-136-2B	67-136-3B	67-136-4B	67-162-3	67-162-6	67-162-7
Group							MGb	Cr-Di	
Rock Type								L	
SiO_2	50.7	51.3	51.1	50.8	51.2	51.5	50.3	52.4	49.4
Al_2O_3	6.8	5.8	5.6	5.8	5.8	6.0	8.5	7.1	7.0
FeO	4.0	4.0	3.9	4.0	3.8	3.8	3.2	3.1	3.3
MgO	15.2	15.5	15.3	15.4	15.5	15.5	14.8	15.2	15.7
CaO	21.5	21.3	21.1	21.4	21.7	21.5	21.2	19.8	20.7
Na_2O	.89	.85	.86	.87	.84	.80	1.3	1.3	1.4
K_2O	.02	.03	.03	.03	.03	.02			
TiO_2	1.3	.92	.71	.89	1.0	1.1	1.1	.94	.87
Cr_2O_3	.37	.63	.80	.64	.60	.47	.06	.10	.11
NiO									
Total	100.78	100.33	99.40	99.83	100.47	100.69	100.46	99.94	98.38
Ca	47.0	46.3	46.4	46.6	46.9	46.7	47.9	45.7	45.9
Fe	6.8	6.8	6.7	6.8	6.4	6.4	5.6	5.6	5.7
Mg	46.2	46.9	46.9	46.6	46.6	46.8	46.5	48.8	48.4

CLINOPYROXENE

Loc., Sample[1]	4-80-1	4-80-2	4-80-3	4-80-4	4-80-5	4-80-6	4-80-7	4-80-1A	4-80-2A	4-80-3A
Group[2]	Systematic						Systematic			
Rock Type[3]	OWeb						L			
SiO_2	51.1	51.7	51.3	52.5	52.5	51.1	52.5	52.4	52.6	52.3
Al_2O_3	7.8	6.7	7.2	5.9	5.9	7.5	5.9	5.8	6.0	5.7
FeO	3.3	3.3	3.3	3.3	3.2	3.3	3.2	3.2	3.2	3.3
MgO	15.1	15.6	15.6	16.1	16.0	15.1	15.9	16.2	16.1	16.3
CaO	20.7	21.2	20.7	21.4	20.7	21.3	21.4	21.1	21.6	21.8
Na_2O	.94	.85	.92	.83	.85	.92	.87	.88	.92	.86
K_2O										
TiO_2	.41	.37	.36	.33	.32	.35	.32	.39	.39	.39
Cr_2O_3	.53	.44	.59	.42	.57	.61	.41	.56	.56	.49
NiO	.09	.09	.09	.09	.09	.10	.10	.09	.10	.11
Total	99.97	100.25	100.06	100.87	100.13	100.28	100.60	100.62	101.47	101.25
Ca	46.7	46.6	46.0	46.1	45.5	47.5	46.5	45.7	46.5	46.3
Fe	5.8	5.7	5.7	5.6	5.5	5.7	5.4	5.4	5.4	5.5
Mg	47.4	47.7	48.3	48.3	49.0	46.8	48.1	48.9	48.2	48.2

Loc., Sample	4-80-4A	4-80-5A	4-80-6A	4-80-7A	4-80-8A	4-80-9A	4-80-10A	4-80-11A	4-80-12A
Group		Systematic							
Rock Type		OWeb							
SiO_2	52.5	51.9	52.0	52.2	52.4	52.2	52.0	51.9	51.5
Al_2O_3	5.7	6.2	6.1	6.0	6.2	6.2	6.7	6.7	6.5
FeO	3.3	3.2	3.2	3.2	3.2	3.2	3.3	3.3	3.3
MgO	16.3	15.9	16.0	16.0	16.0	16.0	15.6	15.6	15.6
CaO	21.3	20.9	21.6	21.8	21.6	21.3	21.1	21.0	21.1
Na_2O	.86	.89	.90	.86	.86	.90	.94	.89	.87
K_2O									
TiO_2	.37	.39	.36	.41	.38	.35	.36	.34	.33
Cr_2O_3	.55	.59	.55	.55	.54	.56	.55	.39	.40
NiO	.10	.07	.10	.11	.08	.09	.10	.10	.08
Total	100.98	100.04	100.81	101.13	101.26	100.79	100.65	100.22	99.68
Ca	45.8	45.9	46.6	46.8	46.6	46.3	46.5	46.4	46.5
Fe	5.5	5.5	5.4	5.4	5.4	5.4	5.7	5.7	5.7
Mg	48.7	48.6	48.0	47.8	48.0	48.3	47.8	47.9	47.8

CLINOPYROXENE

Loc., Sample[1]	63-3-1	63-3-2	63-3-3	63-3-4	63-3-1A	63-3-2A	63-3-3A	63-3-4A	63-3-5A	63-3-6A
Group[2]	Systematic									
Rock Type[3]	L-Web									
SiO_2	52.2	51.1	52.0	52.5	52.4	52.9	52.9	52.2	52.7	52.6
Al_2O_3	4.3	4.8	4.5	4.5	4.7	4.7	4.6	4.7	4.5	4.7
FeO	2.9	2.9	2.9	2.9	2.9	3.0	3.0	3.0	3.0	3.0
MgO	16.5	16.1	16.3	16.4	16.4	16.7	16.8	16.5	16.7	16.7
CaO	20.5	20.6	20.5	20.6	21.0	21.7	21.6	22.1	21.1	21.6
Na_2O	.74	.79	.80	.77	.73	.73	.68	.72	.71	.71
K_2O										
TiO_2	.36	.40	.41	.41	.42	.42	.41	.45	.41	.41
Cr_2O_3	.94	1.3	.99	.95	1.0	.95	.90	1.0	.94	1.0
NiO	.12	.11	.12	.10	.07	.08	.09	.08	.09	.10
Total	98.56	98.05	98.52	99.13	99.62	101.18	100.98	100.75	100.15	100.82
Ca	44.9	45.5	45.0	45.1	45.6	45.9	45.7	46.6	45.2	45.8
Fe	4.9	5.0	5.0	5.0	4.9	5.0	4.9	4.9	5.0	5.0
Mg	50.2	49.5	50.0	49.9	49.5	49.1	49.4	48.4	49.8	49.2

Loc., Sample	63-3-7A	63-3-8A	63-3-9A	63-3-1B	63-3-2B	63-3-3B	63-3-4B	63-3-5B	63-3-1C	63-3-2C
Group										
Rock Type										
SiO_2	53.0	52.4	52.4	51.2	51.2	51.0	51.9	51.1	52.0	52.1
Al_2O_3	4.7	5.2	4.7	5.4	5.7	5.9	5.8	5.8	4.9	5.0
FeO	3.0	3.1	3.0	2.9	3.1	3.0	3.1	3.0	3.0	3.1
MgO	16.8	16.4	16.5	16.0	16.0	15.9	15.9	15.9	16.3	16.3
CaO	22.3	21.0	22.0	20.5	20.3	20.4	20.5	20.4	21.3	22.0
Na_2O	.72	.77	.72	.78	.75	.78	.81	.81	.73	.71
K_2O										
TiO_2	.42	.44	.45	.52	.52	.55	.55	.55	.46	.44
Cr_2O_3	.93	1.3	.96	1.1	.83	.90	.92	.96	.88	.88
NiO	.09	.08	.09	.09	.09	.12	.13	.11	.09	.07
Total	101.96	100.69	100.82	98.49	98.49	98.55	99.61	98.63	99.66	100.60
Ca	46.4	45.4	46.5	45.5	45.1	45.5	45.4	45.4	46.0	46.7
Fe	4.9	5.2	5.0	5.1	5.3	5.3	5.4	5.3	5.1	5.1
Mg	48.7	49.4	48.5	49.4	49.6	49.2	49.2	49.3	48.9	48.2

CLINOPYROXENE

Loc., Sample[1]	63-3-3C	63-3-4C	63-3-5C	63-3-6C	63-3-7C	63-3-8C	63-3-1D	63-3-2D	63-3-3D	63-3-4D
Group[2]										
Rock Type[3]										
SiO_2	52.5	52.2	51.9	52.1	52.5	52.6	51.4	52.0	53.0	52.3
Al_2O_3	5.0	5.0	5.0	4.7	4.6	4.6	5.1	5.0	5.0	5.1
FeO	3.1	3.0	3.0	3.0	2.9	2.9	3.1	3.1	3.0	3.0
MgO	16.3	16.2	16.1	16.3	16.5	16.6	16.0	16.3	16.3	16.2
CaO	21.7	21.7	21.3	21.7	21.6	21.6	21.7	20.9	22.0	21.6
Na_2O	.71	.71	.78	.73	.73	.74	.72	.70	.72	.73
K_2O										
TiO_2	.47	.47	.45	.39	.40	.43	.51	.51	.52	.53
Cr_2O_3	.92	.99	1.3	1.2	.97	.99	.87	.90	.93	.93
NiO	.10	.08	.09	.08	.10	.10	.08	.09	.08	.06
Total	100.80	100.35	99.92	100.20	100.30	100.56	99.48	99.50	101.55	100.45
Ca	46.4	46.6	46.3	46.5	46.1	46.0	46.8	45.4	46.8	46.5
Fe	5.2	5.0	5.1	5.0	4.8	4.8	5.2	5.3	5.0	5.0
Mg	48.4	48.4	48.6	48.5	49.0	49.2	48.0	49.3	48.2	48.5

Loc., Sample	63-3-5D	63-3-1E	63-3-2E	63-3-3E	63-3-4E	63-3-5E	63-6-1	63-6-2	63-6-3	63-6-2A
Group							Systematic			
Rock Type							L			
SiO_2	52.3	52.1	52.1	52.1	52.7	52.6	53.4	53.7	53.7	53.4
Al_2O_3	4.9	5.1	4.8	4.7	4.6	4.6	3.6	3.5	3.5	3.6
FeO	3.1	2.9	2.9	2.9	2.9	3.0	2.7	2.6	2.6	2.6
MgO	16.3	16.1	16.4	16.5	16.5	16.4	17.4	17.4	17.3	17.4
CaO	21.7	20.3	20.2	20.5	20.5	20.5	20.5	21.0	20.7	21.1
Na_2O	.71	.74	.83	.76	.71	.77	.88	.86	.89	.74
K_2O							.03	.03	.03	.04
TiO_2	.50	.50	.47	.49	.48	.48	.19	.18	.17	.26
Cr_2O_3	.89	1.1	1.0	.97	.96	.94	1.3	1.3	1.3	1.2
NiO	.08	.11	.11	.10	.16	.18				
Total	100.48	98.95	98.81	99.02	99.51	99.42	100.00	100.57	100.19	100.34
Ca	46.4	45.1	44.6	44.8	44.8	44.9	43.8	44.5	44.2	44.6
Fe	5.2	5.0	5.1	5.0	5.0	5.1	4.5	4.3	4.3	4.3
Mg	48.4	49.9	50.3	50.2	50.2	50.0	51.7	51.2	51.4	51.1

CLINOPYROXENE

Loc., Sample[1]	63-6-3A	63-6-4A	63-6-1B	63-6-2B	63-6-3B	63-6-4B	63-6-1C	63-6-2C	63-6-3C	63-6-4C
Group[2]			Systematic		Systematic					
Rock Type[3]			OWeb		L					
SiO_2	53.7	53.5	52.7	53.0	53.0	53.2	52.3	52.3	52.4	52.3
Al_2O_3	3.6	3.6	3.9	3.6	3.2	3.4	5.3	5.5	5.5	5.7
FeO	2.6	2.6	2.6	2.7	2.6	2.6	2.9	2.8	2.9	2.8
MgO	17.3	17.3	17.0	17.1	17.5	17.4	16.8	16.5	16.6	16.3
CaO	20.8	21.1	21.4	21.7	20.8	21.4	21.2	20.7	20.5	21.2
Na_2O	.76	.75	.70	.71	.67	.67	.71	.74	.75	.76
K_2O	.03	.04					.02	.03	.03	.04
TiO_2	.26	.26	.37	.37	.35	.34	.38	.41	.40	.42
Cr_2O_3	1.2	1.2	1.2	1.3	1.1	1.1	1.9	1.1	1.0	1.2
NiO			.06	.05	.06	.03				
Total	100.25	100.35	99.93	100.53	99.28	100.14	101.51	100.08	100.08	100.72
Ca	44.4	44.7	45.5	45.6	44.1	44.9	45.3	45.2	44.7	46.0
Fe	4.3	4.3	4.3	4.4	4.3	4.3	4.8	4.8	4.9	4.7
Mg	51.3	51.0	50.2	50.0	51.6	50.8	49.9	50.1	50.4	49.2

Loc., Sample	63-9-1	63-9-2	63-9-3	63-9-4	63-9-1A	63-9-2A	63-9-3A	63-9-4A	63-9-1B	63-9-1B
Group	Systematic					Systematic			Center	Edge
Rock Type	L					OWeb				
SiO_2	50.9	51.0	50.9	51.3	49.7	49.3	49.6	49.6	49.4	49.6
Al_2O_3	6.1	6.0	6.4	5.9	7.5	8.5	8.5	8.0	8.7	8.3
FeO	3.7	3.6	3.7	3.7	3.8	3.9	3.9	3.8	4.1	4.0
MgO	15.6	15.7	15.7	15.6	15.0	14.6	14.6	14.7	14.7	14.7
CaO	20.4	20.1	20.2	20.1	20.7	20.7	20.4	21.1	20.2	20.4
Na_2O	1.1	1.1	1.1	1.1	1.1	1.1	1.0	1.0	1.1	1.0
K_2O									.03	.04
TiO_2	1.5	1.5	1.6	1.4	2.2	2.5	2.5	2.2	1.9	1.7
Cr_2O_3	.88	.92	.89	.99	.56	.20	.18	.26	.25	.20
NiO	.06	.05	.07	.04	.04	.06	.05	.03		
Total	100.24	99.97	100.56	100.13	100.60	100.86	100.73	100.63	100.38	99.94
Ca	45.3	44.9	45.0	45.0	46.5	47.0	46.6	47.4	46.1	46.4
Fe	6.4	6.3	6.4	6.5	6.7	6.9	7.0	6.7	7.3	7.1
Mg	48.2	48.8	48.6	48.5	46.8	46.1	46.4	45.9	46.6	46.5

CLINOPYROXENE

Loc., Sample[1]	63-9-2B	63-9-2B	63-9-3B	63-9-3B	63-9-4B	63-9-4B	63-9-5B	63-9-5B	63-9-6B	63-9-6B
Group[2]	Center	Edge	Center	Edge	Center	Edge	Center	Edge	Center	Edge
Rock Type[3]										
SiO_2	49.0	49.5	49.1	49.5	49.0	49.2	49.1	49.5	49.9	49.1
Al_2O_3	8.9	8.9	8.8	8.5	8.9	8.7	8.7	8.6	8.5	8.2
FeO	4.1	4.1	4.3	4.2	4.4	4.3	4.4	4.4	4.3	4.3
MgO	14.5	14.6	14.5	14.7	14.4	14.5	14.4	14.5	14.2	14.5
CaO	20.4	20.5	20.0	20.3	19.9	20.0	20.0	19.9	20.0	20.0
Na_2O	1.1	1.0	1.4	1.0	1.1	1.1	1.1	1.0	1.1	1.1
K_2O	.03	.03	.03	.03	.03	.03	.02	.02	.02	.01
TiO_2	2.0	1.6	1.9	1.7	1.9	1.9	1.9	1.7	1.9	1.8
Cr_2O_3	.08	.07	.08	.08	.10	.10	.16	.15	.23	.27
NiO										
Total	100.11	100.30	100.11	100.01	99.73	99.83	99.78	99.77	100.15	99.28
Ca	46.6	46.6	46.0	46.1	45.9	45.9	46.0	45.7	46.4	45.9
Fe	7.3	7.3	7.7	7.5	7.9	7.7	7.9	7.9	7.8	7.7
Mg	46.1	46.1	46.3	46.4	46.2	46.3	46.1	46.4	45.8	46.3

Loc., Sample	63-12-1	63-12-2	63-12-3	63-12-4	63-12-5	63-12-6	63-12-7	63-12-8	63-12-9	63-12-10
Group	Systematic			Systematic						
Rock Type	OWeb			OWeb						
SiO_2	50.3	51.2	51.7	52.4	52.3	51.3	51.8	52.0	52.1	50.4
Al_2O_3	5.9	5.9	5.7	5.6	5.8	5.8	5.9	5.9	5.9	6.2
FeO	3.9	4.0	4.0	4.0	4.1	4.0	4.1	4.1	4.1	3.8
MgO	15.5	15.7	15.9	16.0	15.9	15.9	15.9	15.9	16.0	15.7
CaO	20.7	20.6	20.8	21.2	20.9	21.1	21.0	21.1	20.8	20.7
Na_2O	.74	.73	.74	.73	.74	.74	.73	.74	.74	.72
K_2O	.02	.01	.02	.01	.02	.02	.02	.01	.02	
TiO_2	.53	.54	.53	.49	.47	.47	.50	.50	.46	.51
Cr_2O_3	.73	.72	.66	.65	.66	.69	.64	.66	.69	.72
NiO										
Total	98.32	99.40	100.05	101.08	100.89	100.02	100.59	100.91	100.81	98.87
Ca	45.7	45.2	45.2	45.5	45.2	45.5	45.3	45.4	45.0	45.5
Fe	6.7	6.9	6.8	6.7	6.9	6.7	6.9	6.9	6.9	6.6
Mg	47.6	47.9	48.0	47.8	47.9	47.7	47.8	47.7	48.1	47.9

CLINOPYROXENE

Loc., Sample[1]	63-12-11	63-12-12	63-12-13	63-12-14	63-17-1	63-17-2	63-17-3	63-17-4	63-17-1A	63-17-2A
Group[2]	Systemstic		Systematic		Systematic					Systematic
Rock Type[3]	D		OWeb		L					OWeb
SiO_2	50.6	50.8	49.8	50.5	52.0	51.9	51.8	52.1	52.4	52.0
Al_2O_3	6.0	6.1	6.2	6.4	6.1	6.0	6.2	6.1	5.9	5.9
FeO	3.7	3.8	3.7	3.8	3.3	3.3	3.3	3.3	3.2	3.2
MgO	15.8	15.7	15.4	15.6	15.8	15.7	15.8	15.9	15.8	15.8
CaO	20.4	21.0	20.6	21.2	20.4	20.5	20.5	20.3	20.3	20.2
Na_2O	.74	.74	.77	.80	1.1	1.1	1.1	1.1	1.1	1.1
K_2O										
TiO_2	.51	.53	.56	.58	.58	.59	.59	.59	.54	.56
Cr_2O_3	.61	.64	.72	.78	.76	.82	.77	.78	.77	.72
NiO	.11	.10	.09	.12	.07	.09	.09	.07	.08	.11
Total	98.47	99.41	97.84	99.78	100.11	100.00	100.15	100.24	100.09	99.59
Ca	45.1	45.8	45.7	46.2	45.4	45.6	45.5	45.1	45.3	45.2
Fe	6.5	6.4	6.5	6.5	5.7	5.7	5.7	5.7	5.6	5.6
Mg	48.5	47.7	47.8	47.2	48.9	48.6	48.8	49.2	49.1	49.2

Loc., Sample	63-17-3A	63-17-4A	63-17-5A	63-17-1B	63-17-2B	63-17-3B	63-17-4B	63-17-5B	63-17-1C	63-17-2C
Group	Systematic				Systematic			Systematic		
Rock Type	L				OWeb			L		
SiO_2	52.2	51.7	52.4	51.8	51.8	51.9	52.0	52.3	52.0	52.0
Al_2O_3	6.1	6.0	6.0	5.9	6.3	6.1	6.1	6.1	6.1	6.1
FeO	3.3	3.3	3.2	3.3	3.3	3.3	3.3	3.3	3.2	3.3
MgO	15.8	15.9	15.8	15.8	15.9	15.7	15.8	15.9	15.8	15.9
CaO	20.4	20.4	20.4	20.2	20.2	20.1	20.4	20.3	20.5	20.4
Na_2O	1.1	1.1	1.1	1.1	1.1	1.1	1.1	1.1	1.1	1.1
K_2O										
TiO_2	.55	.56	.54	.56	.52	.54	.54	.58	.56	.57
Cr_2O_3	.79	.74	.78	.75	.76	.77	.79	.73	.71	.75
NiO	.08	.08	.10	.08	.08	.07	.08	.10	.08	.08
Total	100.32	99.78	100.32	99.49	99.96	99.58	100.11	100.41	100.05	100.20
Ca	45.4	45.2	45.5	45.1	45.0	45.2	45.4	45.1	45.6	45.2
Fe	5.7	5.7	5.6	5.8	5.7	5.8	5.7	5.7	5.6	5.7
Mg	48.9	49.1	49.0	49.1	49.3	49.1	48.9	49.2	48.9	49.1

CLINOPYROXENE

Loc., Sample[1]	63-17-3C	63-17-1D	63-17-2D	63-17-3D
Group[2]				
Rock Type[3]				
SiO_2	52.0	52.0	51.9	52.0
Al_2O_3	6.0	6.2	6.1	6.3
FeO	3.3	3.4	3.3	3.4
MgO	16.1	15.7	15.7	15.7
CaO	20.3	20.1	20.2	20.1
Na_2O	1.2	1.2	1.2	1.2
K_2O				
TiO_2	.55	.58	.57	.56
Cr_2O_3	.75	.78	.75	.73
NiO	.11	.07	.08	.06
Total	100.31	100.03	99.80	100.05
Ca	44.8	45.1	45.3	45.1
Fe	5.7	5.9	5.8	5.9
Mg	49.5	49.0	48.9	49.0

Loc., Sample	
Group	
Rock Type	
SiO_2	
Al_2O_3	
FeO	
MgO	
CaO	
Na_2O	
K_2O	
TiO_2	
Cr_2O_3	
NiO	
Total	
Ca	
Fe	
Mg	

CLINOPYROXENE

Loc., Sample[1]	23-11-1	23-11-2	23-11-3	23-11-4	23-11-5	23-11-6	23-11-7	23-11-1A	23-11-2A	23-11-3A
Group[2]	Systematic									
Rock Type[3]	L									
SiO_2	50.6	51.1	51.2	50.9	50.1	51.1	51.6	51.4	51.2	51.1
Al_2O_3	6.9	6.7	7.0	6.9	7.0	7.2	6.7	7.7	7.6	7.5
FeO	5.1	5.0	5.1	4.7	4.6	4.2	3.9	3.6	3.6	3.6
MgO	14.7	15.3	14.8	15.0	14.9	15.0	15.5	15.2	15.2	15.2
CaO	19.4	19.4	18.9	19.3	19.3	19.3	19.4	18.9	19.0	19.3
Na_2O	1.4	1.4	1.4	1.3	1.4	1.4	1.3	1.6	1.6	1.5
K_2O										
TiO_2	.73	.69	.61	.40	.47	.50	.41	.74	.61	.61
Cr_2O_3	.66	.66	.66	.65	.65	.65	.60	.65	.65	.65
NiO	.08	.10	.11	.13	.11	.13	.10	.13	.11	.10
Total	99.57	100.35	99.78	99.28	98.53	99.48	99.51	99.92	99.57	99.56
Ca	44.2	43.6	43.4	44.0	44.2	44.4	44.0	44.1	44.2	44.7
Fe	9.2	8.7	9.2	8.4	8.3	7.6	6.9	6.6	6.5	6.4
Mg	46.6	47.6	47.4	47.6	47.5	48.0	49.1	49.3	49.2	48.9

Loc., Sample	23-11-4A	23-11-5A	23-11-1B	23-11-2B	23-11-3B
Group					
Rock Type					
SiO_2	51.1	51.8	51.9	52.1	51.0
Al_2O_3	7.6	6.9	7.6	7.8	7.6
FeO	3.6	3.6	3.6	3.6	3.6
MgO	15.2	15.5	15.3	15.1	15.2
CaO	18.9	19.3	19.0	18.8	19.1
Na_2O	1.6	1.4	1.5	1.6	1.5
K_2O					
TiO_2	.72	.50	.61	.74	.69
Cr_2O_3	.65	.60	.63	.67	.62
NiO	.11	.12	.12	.15	.09
Total	99.48	99.72	100.26	100.56	99.40
Ca	44.2	44.2	44.0	44.2	44.3
Fe	6.6	6.4	6.6	6.5	6.4
Mg	49.3	49.4	49.4	49.3	49.2

CLINOPYROXENE

Loc., Sample[1]	17-17-1	17-74-2	17-74-3	17-74-4	18-2-2	18-2-3	18-9-1	18-9-2	18-31-1
Group[2]	B-G						B-G		B-G
Rock Type[3]	L						L		Weh
SiO_2	51.1	52.2	51.9	51.5	52.1	51.4	52.3	53.0	49.8
Al_2O_3	6.3	6.0	6.6	6.0	2.3	2.7	3.3	3.4	6.6
FeO	4.7	4.8	4.7	4.9	5.4	3.5	3.3	3.4	4.7
MgO	18.3	18.8	18.3	18.7	20.2	20.1	20.3	20.1	18.8
CaO	16.4	16.3	16.3	17.3	18.0	18.0	18.5	18.6	16.0
Na_2O	.80	.80	.80	.70	.06	.32	.06	.05	.77
K_2O						.05	.03	.03	.03
TiO_2	.42	.29	.41	1.3	.01	.20	.03	.04	.40
Cr_2O_3	1.3	1.3	1.3	1.2	2.1	2.1	1.3	1.4	1.4
NiO	.08	.07	.09	.11					
Total	99.36	100.52	99.98	101.71	100.17	98.37	99.12	100.02	98.50
Ca	36.0	35.3	35.9	36.7	35.8	37.0	37.6	37.8	35.0
Fe	8.1	8.1	8.1	8.1	8.4	5.5	5.3	5.4	8.0
Mg	55.9	56.6	56.0	55.2	55.9	57.4	57.1	56.8	57.0

Loc., Sample	18-31-2	18-31-3	18-31-4	18-31-5	18-34-1	18-34-A	18-34-2	18-34-3
Group					B-G			
Rock Type					Weh			
SiO_2	51.2	51.1	50.4	51.6	49.9	50.7	49.8	50.1
Al_2O_3	6.3	6.1	7.1	6.3	6.8	7.2	6.9	7.7
FeO	4.6	4.6	4.7	4.7	4.6	3.6	4.7	5.0
MgO	18.8	18.9	18.6	18.9	18.3	19.9	18.1	18.6
CaO	15.6	15.9	16.0	15.8	15.9	14.7	15.8	15.0
Na_2O	.76	.77	.76	.76	.80	.96	.82	.90
K_2O	.03	.04	.02	.04	.03	.41	.04	.03
TiO_2	.43	.45	.43	.41	.42	.48	.42	.47
Cr_2O_3	1.4	1.4	1.3	1.4	1.6	1.5	1.5	1.4
NiO								
Total	99.12	99.26	99.31	99.91	98.35	99.45	98.08	99.20
Ca	34.3	34.7	35.0	34.5	35.3	32.5	35.4	33.6
Fe	8.0	7.8	8.0	8.0	8.0	6.3	8.2	8.7
Mg	57.7	57.4	57.0	57.5	56.6	61.2	56.4	57.7

CLINOPYROXENE

Loc., Sample[1]	18-34-4	18-34-5	18-34-6	18-34-7	18-75-1	18-75-2	18-78-3
Group[2]					B-G		Systematic
Rock Type[3]					L		L
SiO_2	50.0	51.1	50.5	50.6	50.7	51.1	52.0
Al_2O_3	7.2	7.5	7.4	7.1	5.5	5.5	6.7
FeO	4.8	4.9	4.8	4.8	4.3	4.1	4.4
MgO	18.3	17.9	18.3	17.7	18.8	18.6	16.3
CaO	15.7	14.4	15.9	17.1	16.7	16.8	17.3
Na_2O	.82	1.0	.81	.74	.77	.83	1.1
K_2O	.02	.11	.02	.02	.04	.04	.06
TiO_2	.43	.48	.42	.38	.17	.14	.61
Cr_2O_3	1.6	1.4	1.5	1.6	1.5	1.5	1.2
NiO							
Total	98.87	98.79	99.65	100.04	98.48	98.61	99.68
Ca	34.9	33.4	35.2	37.6	36.2	36.5	39.9
Fe	8.4	8.9	8.3	8.2	7.2	7.0	7.8
Mg	56.7	57.8	56.5	54.2	56.6	56.5	52.2

Loc., Sample
Group
Rock Type
SiO_2
Al_2O_3
FeO
MgO
CaO
Na_2O
K_2O
TiO_2
Cr_2O_3
NiO
Total
Ca
Mg
Fe

CLINOPYROXENE

Loc., Sample[1]	33-204-1	33-204-2
Group[2]	G	
Rock Type[3]	BWeb	
SiO_2	49.7	50.3
Al_2O_3	9.1	8.7
FeO	4.7	4.7
MgO	14.0	14.3
CaO	19.4	19.0
Na_2O	.92	1.0
K_2O	.03	.05
TiO_2	.55	.56
Cr_2O_3	.09	.10
NiO		
Total	98.49	98.71
Ca	45.6	44.7
Fe	8.6	8.6
Mg	45.8	46.7

Loc., Sample	
Group	
Rock Type	
SiO_2	
Al_2O_3	
FeO	
MgO	
CaO	
Na_2O	
K_2O	
TiO_2	
Cr_2O_3	
NiO	
Total	
Ca	
Fe	
Mg	

CLINOPYROXENE

Loc., Sample[1]	SAL-3	SAL-5	SAL-6	SAL-7	SAL-8	SAL-9-1	SAL-9-2	SAL-10	SAL-11	SAL-12
Group[2]	Systematic									
Rock Type[3]	L									
SiO_2	52.3	53.1	52.5	51.4	51.8	53.5	53.0	52.3	52.5	53.1
Al_2O_3	6.7	7.3	7.1	7.8	8.1	7.0	7.2	7.3	7.1	7.1
FeO	4.7	4.7	4.9	4.8	5.1	4.5	4.6	4.6	4.6	4.8
MgO	14.8	14.7	14.7	14.0	14.2	14.9	14.7	14.5	14.5	14.6
CaO	18.0	18.1	17.5	18.3	18.0	17.8	18.4	17.9	18.2	18.1
Na_2O	2.0	2.3	2.3	2.3	2.3	2.2	2.3	2.2	2.3	2.2
K_2O										
TiO_2	.60	1.1	.90	1.2	1.4	.77	.87	.89	.89	.97
Cr_2O_3	.98	.97	1.0	.82	.13	.99	1.0	.92	1.0	1.0
NiO	.08	.07	.09	.08	.08	.08	.08	.06	.09	.06
Total	100.16	102.34	100.99	100.70	101.11	101.74	102.15	100.69	101.18	101.93
Ca	42.6	42.9	41.9	44.1	43.1	42.3	43.4	43.0	43.4	42.9
Fe	8.9	8.7	9.2	9.0	9.5	8.4	8.5	8.6	8.6	8.9
Mg	48.7	48.4	48.9	46.9	47.3	49.3	48.2	48.4	48.1	48.2

Loc., Sample	SAL-13	SAL-14	SAL-15	SAL-16	SAL-17	SAL-1A	SAL-2A	SAL-3A	SAL-3AA	SAL-4A
Group						Systematic				
Rock Type						GCP				
SiO_2	52.2	52.0	51.9	52.5	51.6	52.1	52.1	52.2	51.4	51.8
Al_2O_3	7.3	7.2	8.1	7.3	7.5	8.1	8.0	7.8	8.9	7.8
FeO	4.8	4.8	4.9	5.0	4.9	5.7	5.0	5.2	6.8	7.2
MgO	14.6	14.6	14.1	14.7	14.5	14.2	14.4	14.6	13.5	13.6
CaO	17.9	17.9	18.0	18.0	18.1	17.7	17.7	17.6	16.6	17.4
Na_2O	2.3	2.3	2.4	2.3	2.2	2.3	2.3	2.3	2.6	2.4
K_2O										
TiO_2	1.0	.98	1.4	1.1	1.2	1.5	1.3	1.3	1.7	1.5
Cr_2O_3	.92	.93	.68	.56	.33	.10	.16	.20	.10	.06
NiO	.07	.07	.07	.06	.08	.06	.07	.06	.07	.06
Total	101.09	100.78	101.55	101.52	100.41	101.76	101.03	101.21	101.67	101.82
Ca	42.7	42.7	43.4	42.5	43.0	42.2	42.5	41.9	40.8	41.5
Fe	8.9	8.9	9.2	9.2	9.1	10.6	9.4	9.7	13.0	13.4
Mg	48.4	48.4	47.3	48.3	47.9	47.1	48.1	48.4	46.2	45.1

CLINOPYROXENE

Loc., Sample[1/]	SAL-4AA	SAL-5A	SAL-6A	SAL-7A	SAL-7AA	SAL-8	SAL-9	SAL-1B	SAL-2B	SAL-3B
Group[2/]										
Rock Type[3/]										
SiO_2	50.8	50.5	50.1	51.6	50.6	50.2	50.6	50.8	50.3	50.1
Al_2O_3	8.8	8.7	9.0	8.1	8.6	9.2	8.6	8.1	8.4	7.5
FeO	7.6	7.8	8.7	8.6	8.9	9.3	9.3	9.3	9.3	9.2
MgO	13.0	12.8	12.5	12.8	12.6	12.3	12.5	12.5	12.2	12.5
CaO	17.0	16.6	16.4	17.0	16.5	15.9	16.4	16.5	16.4	16.5
Na_2O	2.8	2.6	2.7	2.6	2.7	2.7	2.7	2.7	2.8	2.7
K_2O										
TiO_2	1.7	1.6	1.7	1.5	1.6	1.7	1.6	1.4	1.4	1.2
Cr_2O_3	.06	.07	.05	.09	.06	.08	.07	.10	.08	.07
NiO	.07	.06	.06	.06	.06	.05	.07	.06	.06	.06
Total	101.83	100.73	101.21	102.35	101.62	101.43	101.84	101.46	100.94	102.53
Ca	41.4	41.0	40.4	40.9	40.3	39.5	40.0	40.1	40.4	40.2
Fe	14.5	15.0	16.7	12.2	17.0	18.0	17.7	17.6	17.9	17.5
Mg	44.1	44.0	42.9	42.9	42.8	42.5	42.4	42.3	41.8	42.3

Loc., Sample	
Group	
Rock Type	
SiO_2	
Al_2O_3	
FeO	
MgO	
CaO	
Na_2O	
K_2O	
TiO_2	
Cr_2O_3	
NiO	
Total	
Ca	
Fe	
Mg	

ORTHOPYROXENE

Loc., Sample[1]	32-15-1	32-15-2	32-15-3	32-15-4	32-15-5	32-15-6	32-15-7	32-15-8	32-15-9
Group[2]	Systematic				Systematic				
Rock Type[3]	OWeb				OWeb				
SiO_2	53.7	53.9	53.7	53.9	54.3	54.3	53.8	53.7	54.2
Al_2O_3	5.1	5.0	5.2	5.2	5.1	5.2	5.3	5.2	4.9
FeO	8.0	8.0	7.9	8.2	7.6	7.3	7.4	8.0	8.2
MgO	32.1	32.2	32.1	32.0	32.5	32.8	32.4	32.1	32.0
CaO	.90	.96	.92	.88	.87	.85	.84	.88	.88
Na_2O	.08	.07	.07	.08	.84	.07	.07	.08	.08
K_2O									
TiO_2	.10	.10	.13	.10	.09	.08	.08	.13	.08
Cr_2O_3	.23	.22	.22	.23	.25	.23	.26	.24	.25
NiO	.09	.10	.09	.11	.84	.08	.10	.09	.10
MnO									
Total	100.20	100.55	100.33	100.70	102.39	100.91	100.25	100.42	100.69
Ca	1.7	1.7	1.8	1.7	1.7	1.6	1.6	1.7	1.7
Fe	12.0	12.0	11.9	12.4	11.4	10.9	11.2	12.1	12.3
Mg	86.3	86.3	86.3	85.9	86.9	87.5	87.2	86.2	86.0

Loc., Sample	32-22-4	32-22-7	32-22-8	32-22-9	32-22-10	32-24-1	32-24-1	32-24-2	32-24-3
Group	Cr-Di					Systematic			
Rock Type	L					OWeb			
SiO_2	53.9	54.7	55.0	54.8	54.7	55.2	54.8	55.5	55.2
Al_2O_3	4.2	4.0	4.0	3.9	4.1	4.7	4.7	4.7	4.8
FeO	6.3	6.3	6.3	6.3	6.4	6.4	6.4	6.4	6.4
MgO	34.7	33.8	33.9	34.0	33.9	33.8	33.7	33.9	33.7
CaO	.77	.68	.72	.69	.71	.78	.79	.77	.82
Na_2O		.08	.07	.07	.08	.06	.06	.06	.06
K_2O						.02	.02	.03	.02
TiO_2	.11	.08	.09	.09	.12	.18	.18	.17	.18
Cr_2O_3	.21	.35	.37	.32	.33				
NiO		.10	.11	.12	.12				
MnO						.12	.11	.12	.12
Total	100.19	100.09	100.56	100.29	100.46	101.26	100.76	101.65	101.30
Ca	1.4	1.3	1.4	1.3	1.3	1.5	1.5	1.5	1.6
Fe	9.1	9.3	9.3	9.3	9.4	9.5	9.5	9.4	9.5
Mg	89.5	89.4	89.3	89.4	89.2	89.1	89.0	89.1	89.0

ORTHOPYROXENE

Loc., Sample[1]	32-15-1	32-15-2	32-15-3	32-15-4	32-15-5	32-15-6	32-15-7	32-15-8	32-15-9	32-22-4
Group[2]	Systematic				Systematic					Cr-Di
Rock Type[3]	OWeb				OWeb					L
SiO_2										
Al_2O_3										
FeO										
MgO										
CaO										
Na_2O										
K_2O										
TiO_2										
Cr_2O_3										
NiO										
Total										
Ca										
Fe										
Mg										

Loc., Sample	32-22-7	32-22-8	32-22-9	32-22-10	32-24-1	32-24-1	32-24-2	32-24-3	32-24-1A
Group					Systematic				
Rock Type					OWeb				
SiO_2									55.2
Al_2O_3									4.6
FeO									6.3
MgO									33.2
CaO									.81
Na_2O									
K_2O									
TiO_2									.18
Cr_2O_3									
NiO									
Total									100.29
Ca									1.6
Fe									9.5
Mg									89.0

ORTHOPYROXENE

Loc., Sample[1]	32-24-2A	32-24-3A	32-24-4	32-24-5	32-24-6	32-24-7	32-24-8	32-24-9	32-29-1	32-29-2
Group[2]	Systematic								Al-Aug	
Rock Type[3]	OWeb								Web	
SiO_2	55.0	55.4	54.3	54.2	53.6	54.1	54.2	54.2	53.7	54.4
Al_2O_3	4.1	4.8	3.3	4.0	3.9	4.3	4.6	4.6	5.5	5.2
FeO	8.1	8.3	8.9	8.7	8.6	8.2	7.9	7.3	8.7	8.7
MgO	31.0	32.0	31.9	31.9	32.2	32.1	32.4	32.8	31.6	31.9
CaO	.98	.96	.90	.81	.90	.83	.81	.80	.81	.87
Na_2O			.09	.09		.09	.08	.07	.08	.07
K_2O									.04	.03
TiO_2	.15	.20	.08	.10		.09	.11	.11	.23	.24
Cr_2O_3			.27	.32	.27	.43	.30	.29		
NiO			.09	.09	.10	.11	.12	.12		
MnO									.16	.17
Total	99.33	101.66	99.83	100.21	99.57	100.25	100.52	100.29	100.82	101.58
Ca	1.9	1.8	1.7	1.5	1.7	1.6	1.6	1.5	1.6	1.7
Fe	12.5	12.5	13.3	13.1	12.8	12.3	11.8	10.9	13.2	13.0
Mg	85.5	85.7	85.0	85.4	85.5	86.1	86.6	87.5	85.2	85.3

Loc., Sample	32-29-3	32-29-4	32-29-5	32-48-1	32-48-2	32-48-3	32-52-1	32-52-2	32-52-3	32-57-2
Group				Cr-Di			Cr-Di			Transitional
Rock Type				L			L			L
SiO_2	54.1	54.0	54.2	52.3	53.0	53.0	54.7	54.5	54.8	53.0
Al_2O_3	5.4	5.7	5.3	3.4	3.8	3.3	4.3	3.9	4.1	5.3
FeO	8.7	8.7	8.5	5.7	5.6	5.6	7.2	8.0	7.5	8.4
MgO	31.8	31.5	31.9	35.0	34.6	34.5	33.3	32.8	32.4	31.7
CaO	.86	.85	.82	1.4	1.4	1.4	.80	.90	.90	1.4
Na_2O	.08	.08	.07				.08	.09	.06	
K_2O	.03	.02	.02				.01	.04	.02	
TiO_2	.22	.23	.22	.05	.04	.05	.11	.15	.11	.26
Cr_2O_3										
NiO										
MnO	.17	.16	.16				.25	.29	.26	
Total	101.36	101.24	101.19	97.85	98.44	97.85	100.75	100.67	100.15	100.06
Ca	1.7	1.7	1.6	2.6	2.6	2.6	1.5	1.7	1.7	2.7
Fe	13.1	13.2	12.8	8.2	8.1	8.1	10.7	11.8	11.3	12.6
Mg	85.2	85.1	85.6	89.3	89.3	89.3	87.8	86.5	87.0	84.7

ORTHOPYROXENE

Loc., Sample[1]	32-72-2	32-72-1	32-72-2	32-72-2A	32-72-3	32-72-4	32-72-A	32-72-5	32-72-6	32-72-7
Group[2]	Transitional	Systematic								
Rock Type[3]	L	L								
SiO_2	53.9	53.7	54.0	54.4	53.7	53.4	53.9	53.9	54.1	54.3
Al_2O_3	4.0	2.8	3.8	3.6	4.7	5.3	4.6	4.8	5.0	4.9
FeO	8.4	8.8	8.3	8.5	8.4	7.6	8.1	7.6	7.3	6.9
MgO	32.3	31.9	32.2	32.2	32.1	32.3	32.2	32.6	32.8	32.7
CaO	1.1	1.1	.95	1.0	.92	.98	.91	.89	.89	.91
Na_2O		.13	.02	.11	.11	.12	.12	.10	.11	.11
K_2O										
TiO_2		.16	.07	.09	.05	.17	.07	.08	.12	.10
Cr_2O_3		.08	.03	.24	.36	.38	.37	.34	.35	.33
NiO		.12	.34	.12	.10	.11	.10	.11	.15	
MnO	.32									
Total	100.02	98.79	99.71	100.26	100.44	100.36	100.37	100.42	100.82	100.25
Ca	2.1	2.0	1.8	1.9	1.8	1.9	1.7	1.7	1.7	1.7
Fe	12.5	13.1	12.5	12.7	12.5	11.4	12.2	11.3	10.9	10.4
Mg	85.4	84.9	85.7	85.4	85.7	86.7	86.0	87.0	87.4	87.9

Loc., Sample	32-72-1A	32-72-2A	32-72-3A	32-72-4A	32-72-0B	32-72-1B	32-72-2B	32-74-1	32-90-1	32-90-2
Group								Transitional	Cr-Di	
Rock Type								L	L	
SiO_2	54.0	53.8	53.9	53.9	54.0	54.0	54.0	53.8	55.8	56.0
Al_2O_3	5.1	4.9	4.9	4.9	4.8	5.0	5.0	5.7	2.8	3.0
FeO	6.7	6.8	6.9	7.1	7.2	6.9	7.0	7.2	5.8	5.8
MgO	33.0	33.1	32.9	32.7	32.7	32.7	32.7	31.6	35.9	34.8
CaO	.87	.90	.89	.90	.85	.89	.87	1.0	.75	.67
Na_2O	.18	.11	.15	.11	.10	.11	.11	.15		
K_2O								.01		
TiO_2	.12	.09	.10	.10	.10	.08	.13	.21	.08	.04
Cr_2O_3	.33	.30	.33	.31	.33	.32	.36	.35		
NiO	.13		.07	.12	.12	.14	.13			
Total	100.43	100.00	100.14	100.15	100.20	100.14	100.30	100.02	101.13	100.31
Ca	1.7	1.7	1.7	1.7	1.6	1.7	1.7	2.0	1.4	1.2
Fe	10.0	10.1	10.3	10.7	10.8	10.4	10.5	11.1	8.2	8.4
Mg	88.3	88.2	88.0	87.5	87.6	87.9	87.8	86.9	90.4	90.3

ORTHOPYROXENE

Loc., Sample[1]	32-90-3	33-1-1	31-1-2	33-1-3	33-1-4	33-1-5	33-1-6	33-1-7	33-1-1A	33-1-2A
Group[2]		Systematic								
Rock Type[3]		L								
SiO_2	56.0	54.0	54.6	54.5	54.6	53.5	54.4	54.5	54.4	55.0
Al_2O_3	3.0	3.3	3.2	3.3	4.1	4.5	4.3	4.3	4.8	4.6
FeO	5.7	9.1	8.9	8.7	8.6	8.0	7.8	7.6	6.4	6.6
MgO	34.7	31.7	32.2	32.2	32.3	32.4	32.7	32.8	33.6	33.5
CaO	.80	1.0	.99	1.0	.93	.88	.91	.90	.82	.86
Na_2O		.10	.09	.09	.09	.10	.08	.08	.09	
K_2O										
TiO_2	.01	.13	.09	.08	.07	.10	.06	.08	.12	.12
Cr_2O_3		.40	.30	.33	.37	.35	.35	.36	.37	.02
NiO		.11	.16	.14	.12	.11	.11	.10	.11	.42
Total	99.71	99.84	100.53	100.34	101.18	99.94	100.71	100.72	100.71	101.12
Ca	1.5	2.0	1.9	1.9	1.8	1.7	1.7	1.7	1.6	1.6
Fe	8.3	13.6	13.2	13.0	12.8	12.0	11.6	11.3	9.6	9.8
Mg	90.2	84.4	84.9	85.1	85.4	86.3	86.7	87.0	88.9	88.5

Loc., Sample	33-1-3A	33-1-4A	33-1-5A	33-1-1B	33-1-2B	33-1-3B	33-1-4B	33-1-1C	33-1-2C	33-1-3C
Group										
Rock Type										
SiO_2	54.3	54.2	54.4	54.6	54.7	54.4	54.9	54.9	54.7	55.0
Al_2O_3	4.9	4.8	4.3	4.6	5.0	4.9	4.6	4.7	4.6	4.7
FeO	6.9	7.2	7.5	6.4	6.4	6.3	6.3	6.3	6.3	6.4
MgO	33.2	33.0	32.9	33.5	33.6	33.6	33.6	33.7	33.7	33.7
CaO	.86	.85	.92	.88	.83	.85	.88	.87	.90	.87
Na_2O	.08	.09	.08	.09	.08	.08	.08	.09	.10	.08
K_2O										
TiO_2	.11	.11	.08	.10	.14	.12	.09	.11	.11	.11
Cr_2O_3	.37	.40	.37	.35	.39	.42	.37	.38	.36	.36
NiO	.12	.12	.13	.12	.13	.11	.14	.10	.18	.11
Total	100.84	100.77	100.68	100.64	101.27	100.78	100.96	101.15	100.95	101.33
Ca	1.6	1.6	1.8	1.7	1.6	1.6	1.7	1.7	1.7	1.6
Fe	10.3	10.8	11.2	9.6	9.4	9.4	9.4	9.3	9.3	9.4
Mg	88.0	87.6	87.0	88.7	89.0	89.0	88.9	89.0	89.0	88.9

ORTHOPYROXENE

Loc., Sample[1]	33-2-4	35-2-3	33-2-1	33-3-1	33-3-3	33-40-1	33-40-2	33-99-1	33-99-2	33-99-3
Group[2]	Al-Aug			Cr-Di		Cr-Di		Cr-Di		
Rock Type[3]	L			L		L		OP		
SiO_2	54.5	54.9	54.9	55.1	55.3	52.4	53.7	54.9	55.3	55.5
Al_2O_3	1.5	1.6	1.5	3.5	3.0	3.5	3.6	3.2	3.2	3.1
FeO	12.7	12.2	13.1	6.0	6.3	8.7	7.5	7.1	7.6	7.3
MgO	30.2	30.7	30.8	33.9	34.5	32.4	33.1	33.4	33.3	33.4
CaO	.60	.47	.54	.67	.60	1.1	.63	.85	.83	.85
Na_2O	.01	.02	.02			.08	.11	.11	.10	.09
K_2O								.03	.03	.03
TiO_2	.09	.05	.03	.19	.20	.23	.23	.18	.10	.15
Cr_2O_3	.11	.14	.18			.33	.29			
NiO										
MnO								.12	.14	.12
Total	99.71	100.08	101.07	99.36	99.90	98.74	99.16	99.89	100.60	100.54
Ca	1.1	.9	1.0	1.3	1.1	2.1	1.2	1.6	1.6	1.6
Fe	18.9	18.1	19.1	8.9	9.2	12.8	11.1	10.5	11.2	10.7
Mg	80.0	81.0	79.9	89.8	89.7	85.1	87.7	87.9	87.3	87.6

Loc., Sample	33-99-4	35-4-1	35-4-2	36-11-1	36-11-2	36-11-2E	36-12-1	36-12-1E	36-12-2	36-12-3
Group		Cr-Di		Al-Aug			Cr-Di			
Rock Type		L		Web			L			
SiO_2	55.5	54.4	53.6	51.4	52.0	51.6	54.9	54.7	55.0	54.8
Al_2O_3	2.9	4.9	4.8	6.6	6.3	6.3	5.2	5.2	5.2	5.1
FeO	7.3	6.7	6.8	12.2	12.1	12.1	6.6	6.6	6.6	6.5
MgO	33.5	33.2	32.6	28.3	28.6	28.5	33.2	33.1	33.1	33.1
CaO	.86	.99	.97	1.4	1.4	1.3	1.2	1.2	1.2	1.1
Na_2O	.10			.10	.10	.11	.11	.11	.11	.12
K_2O	.03			.02	.02	.02	.01	.01	.01	.02
TiO_2	.15	.19	.21	.46	.45	.45	.14	.15	.14	.15
Cr_2O_3										
NiO										
MnO	.14									
Total	100.48	100.38	98.98	100.48	100.87	100.38	101.36	101.07	101.36	100.89
Ca	1.6	1.9	1.9	2.8	2.8	2.6	2.3	2.3	2.3	2.1
Fe	10.7	10.0	10.3	18.9	18.7	18.7	9.8	9.8	9.8	9.7
Mg	87.7	88.1	87.8	78.3	78.6	78.7	87.9	87.9	87.9	88.2

ORTHOPYROXENE

Loc., Sample[1]	36-12-4	36-14-1	36-14-1E	36-14-2	36-14-4	36-14-5	36-18-3	36-18-4	36-18-5	36-18-6
Group[2]		Al-Aug					Cr-Di			
Rock Type[3]		CP					L			
SiO_2	54.7	51.0	51.2	51.5	51.0	51.4	54.9	54.4	54.0	54.5
Al_2O_3	5.1	6.6	6.7	6.7	6.8	6.6	4.5	4.8	5.0	5.1
FeO	6.6	13.2	13.3	13.3	13.2	13.3	6.7	6.4	6.4	6.5
MgO	33.0	27.6	27.6	27.5	27.6	27.6	33.5	32.3	32.2	32.2
CaO	1.1	1.3	1.3	1.4	1.4	1.3	.88	.81	.82	.84
Na_2O	.12	.11	.11	.11	.12	.10	.09	.10	.11	.10
K_2O	.01	.02	.02	.02	.02	.03	.01			
TiO_2	.16	.50	.50	.52	.53	.52	.14	.13	.13	.14
Cr_2O_3								.34	.36	.39
NiO							.07	.15	.13	.14
Total	100.81	100.33	100.73	101.05	100.67	100.85	100.79	99.43	99.15	99.91
Ca	2.3	2.6	2.6	2.8	2.8	2.6	1.7	1.6	1.6	1.7
Fe	9.9	20.6	20.7	20.7	20.6	20.7	9.9	9.9	9.9	9.9
Mg	87.8	76.8	76.7	76.5	76.6	76.7	88.4	88.5	88.5	88.4

Loc., Sample	36-18-7
Group	
Rock Type	
SiO_2	55.0
Al_2O_3	4.9
FeO	6.5
MgO	32.6
CaO	.83
Na_2O	.11
K_2O	
TiO_2	.12
Cr_2O_3	.37
NiO	.15
Total	100.62
Ca	1.6
Fe	9.9
Mg	88.5

ORTHOPYROXENE

Loc., Sample[1]	40-1-1	40-1-2	40-1-3	40-1-4	40-1-5	40-1-6	40-1-1A	40-1-2A	40-1-3A	40-1-4A
Group[2]	Systematic			Systematic			Systematic			Systematic
Rock Type[3]	OWeb			L			OWeb			L
SiO_2	55.2	55.1	55.2	55.3	55.5	55.5	56.0	55.4	55.3	55.9
Al_2O_3	3.4	3.6	3.4	3.4	3.6	3.6	3.2	3.2	3.7	3.3
FeO	5.9	6.0	6.0	6.0	6.0	6.0	6.0	5.9	5.9	6.0
MgO	34.5	34.2	34.5	34.5	34.3	34.1	34.5	34.5	34.2	34.4
CaO	.74	.89	.87	.86	.92	.90	.90	.87	.86	.90
Na_2O	.05	.05	.06	.06	.06	.06	.06	.06	.04	.06
K_2O										
TiO_2	.07	.07	.07	.06	.07	.07	.08	.08	.10	.10
Cr_2O_3	.42	.43	.40	.40	.40	.41	.47	.45	.50	.49
NiO	.09	.08	.10	.07	.08	.10	.10	.08	.07	.08
Total	100.37	100.42	100.60	100.65	100.93	100.74	101.31	100.54	100.67	101.23
Ca	1.4	1.7	1.6	1.6	1.7	1.7	1.7	1.6	1.6	1.7
Fe	8.6	8.8	8.7	8.7	8.8	8.8	8.7	8.6	8.7	8.8
Mg	90.0	89.5	89.6	89.6	89.5	89.5	89.6	89.8	89.7	89.5

Loc., Sample	40-1-5A	40-1-6A	40-4-3	40-127-1	40-127-2	40-127-3	40-127-4	40-127-5	40-127-A3	40-127-1A
Group			Cr-Di	Systematic						
Rock Type			L	L						
SiO_2	55.9	55.7	54.3	55.1	54.3	54.6	53.5	53.6	54.3	54.3
Al_2O_3	3.2	3.2	4.2	3.5	3.5	3.9	3.6	3.5	3.5	3.7
FeO	6.0	5.9	9.0	6.6	6.7	7.7	10.7	10.7	9.2	9.4
MgO	34.5	34.4	32.6	33.3	33.0	32.5	30.3	30.2	31.5	31.4
CaO	.83	.86	.84	.77	.75	.80	.89	1.3	.90	.79
Na_2O	.06	.06		.06	.05	.05	.06	.07	.05	.05
K_2O										
TiO_2	.09	.10	.28	.15	.16	.18	.21	.34	.16	.11
Cr_2O_3	.44	.44		.51	.51	.59	.45	.44	.50	.38
NiO	.08	.10		.06	.07	.05	.05	.05	.05	.09
Total	101.10	100.76	101.22	100.05	99.04	100.37	99.76	100.20	100.16	100.22
Ca	1.5	1.6	1.6	1.5	1.4	1.5	1.7	2.5	1.7	1.5
Fe	8.8	8.6	13.2	9.9	10.1	11.6	16.3	16.2	13.8	14.2
Mg	89.7	89.8	85.2	88.7	88.5	86.9	82.0	81.3	84.4	84.3

ORTHOPYROXENE

Loc., Sample[1]	40-127-2A	40-127-3A	40-127-4A	40-127-5A
Group[2]				
Rock Type[3]				
SiO_2	54.0	54.2	53.1	53.0
Al_2O_3	3.6	3.6	4.4	3.6
FeO	10.5	11.5	11.1	12.2
MgO	30.6	30.2	29.6	28.8
CaO	.85	.92	1.2	1.1
Na_2O	.06	.06	.08	.13
K_2O				
TiO_2	.11	.11	.34	.26
Cr_2O_3	.38	.36	.40	.24
NiO	.09	.08	.09	.05
Total	100.19	101.03	100.31	99.38
Ca	1.6	1.8	2.4	2.2
Fe	15.9	17.3	17.0	18.8
Mg	82.5	80.9	80.6	79.0

Loc., Sample	
Group	
Rock Type	
SiO_2	
Al_2O_3	
FeO	
MgO	
CaO	
Na_2O	
K_2O	
TiO_2	
Cr_2O_3	
NiO	
Total	
Ca	
Fe	
Mg	

ORTHOPYROXENE

Loc., Sample[1]	23-11-1	23-11-2	23-11-3	23-11-4	23-11-5	23-11-6	23-11-7	23-11-2A	23-11-3A	23-11-4A
Group[2]	Systematic									
Rock Type[3]	L									
SiO_2	53.3	52.9	53.0	52.9	52.6	53.8	52.9	53.2	54.4	54.3
Al_2O_3	3.7	3.6	3.5	4.7	5.1	5.0	5.0	5.1	5.0	5.1
FeO	9.5	9.4	9.3	9.0	8.4	8.0	7.4	6.7	6.7	6.7
MgO	31.4	31.6	31.6	31.4	31.8	32.3	32.5	33.0	33.3	33.2
CaO	1.1	1.0	1.1	1.0	.95	.96	.95	.91	.91	.89
Na_2O	.11	.10	.10	.11	.10	.11	.10	.10	.10	.11
K_2O										
TiO_2	.19	.15	.13	.12	.10	.12	.13	.13	.12	.12
Cr_2O_3	.25	.23	.22	.30	.30	.30	.30	.28	.30	.30
NiO	.11	.11	.10	.12	.12	.12	.13	.10	.13	.12
Total	99.66	99.09	99.05	99.65	99.47	100.71	99.41	99.52	100.96	100.84
Ca	2.1	2.0	2.1	2.0	1.8	1.8	1.8	1.7	1.7	1.7
Fe	14.3	14.0	13.9	13.6	12.7	12.0	11.1	10.1	10.0	10.1
Mg	83.6	84.0	84.0	84.4	85.4	86.2	87.1	88.2	88.3	88.2

Loc., Sample	23-11-5A	23-11-2B	23-11-3B	23-11-4B
Group				
Rock Type				
SiO_2	53.4	53.4	53.3	53.7
Al_2O_3	5.1	5.1	5.0	5.0
FeO	6.7	6.7	6.7	6.7
MgO	33.0	33.0	33.0	33.0
CaO	.90	.95	.91	.91
Na_2O	.10	.10	.11	.10
K_2O				
TiO_2	.12	.14	.11	.11
Cr_2O_3	.29	.32	.28	.31
NiO	.14	.12	.12	.13
Total	99.75	99.83	99.53	99.96
Ca	1.7	1.8	1.7	1.7
Fe	10.0	10.0	10.0	10.0
Mg	88.3	88.2	88.2	88.2

ORTHOPYROXENE

Loc., Sample[1]	66-10-1	66-10-2	66-10-3	66-10-1A	66-10-2A	66-10-3A	66-10-4A	66-123-1	66-123-2	66-123-3
Group[2]	Systematic							Systematic		
Rock Type[3]	L							L		
SiO_2	54.1	54.30	53.9	54.4	54.4	54.2	54.1	54.5	54.3	54.3
Al_2O_3	4.4	4.30	4.5	4.1	4.2	4.4	4.7	5.2	5.4	5.3
FeO	8.1	8.00	8.1	7.9	7.9	8.1	8.0	6.6	6.6	6.6
MgO	31.9	32.30	32.1	32.1	32.2	32.1	32.0	32.8	32.6	32.7
CaO	.73	.67	.75	.68	.67	.70	.76	.93	.90	.90
Na_2O	.32	.06	.06	.06	.05	.05	.06	.11	.10	.11
K_2O										
TiO_2	.20	.18	.19	.23	.25	.28	.31	.16	.19	.17
Cr_2O_3	.33	.30	.36	.32	.31	.23	.22	.42	.42	.39
NiO	.06	.05	.05	.06	.06	.05	.05	.06	.05	.05
Total	100.14	100.16	100.01	99.85	100.04	100.11	100.20	100.78	100.56	100.52
Ca	1.4	1.3	1.5	1.3	1.3	1.4	1.5	1.8	1.8	1.7
Fe	12.3	12.0	12.2	12.0	11.9	12.2	12.1	10.0	10.0	10.0
Mg	86.3	86.7	86.3	86.7	86.8	86.4	86.4	88.2	88.2	88.3

Loc., Sample	66-123-4	66-123-5	66-123-1A	66-123-2A	66-123-3A	66-123-4A	66-123-5A	67-7-1	67-7-2
Group	Systematic		Systematic		Systematic			Systematic	
Rock Type	OWEB		L		OWEB			OCP	
SiO_2	54.0	53.5	54.2	53.5	54.0	53.8	53.4	53.5	54.5
Al_2O_3	5.4	6.1	5.4	5.6	5.9	6.5	6.7	4.4	4.5
FeO	6.6	6.7	6.5	6.6	6.6	6.6	6.6	10.2	10.3
MgO	32.4	32.1	32.7	33.1	32.6	32.0	32.2	30.8	30.8
CaO	.91	.95	.95	.93	.87	.92	.86	.85	.88
Na_2O	.12	.12	.12	.11	.11	.12	.12		
K_2O									
TiO_2	.17	.17	.18	.18	.17	.19	.19	.39	.29
Cr_2O_3	.40	.47	.40	.42	.47	.52	.53		
NiO	.05	.05	.06	.05	.05	.05	.06		
Total	100.05	100.16	100.17	100.49	100.77	100.70	100.66	100.14	101.27
Ca	1.8	1.9	1.8	1.8	1.7	1.8	1.7	1.7	1.7
Fe	10.1	10.3	9.8	9.9	10.0	10.2	10.1	15.4	15.5
Mg	88.1	87.8	88.3	88.3	88.3	88.0	88.2	82.9	82.8

ORTHOPYROXENE

Loc., Sample[1]	67-7-3	67-7-4	67-7-1A	67-7-2A	67-7-3A	67-7-4A	67-84-1	67-84-2	67-84-1A	67-84-2A
Group[2]			Systematic				Systematic		Systematic	
Rock Type[3]			L				OCP		L	
SiO_2	54.4	53.6	54.2	54.7	54.8	54.5	54.1	5 .1	54.6	53.6
Al_2O_3	5.0	4.6	4.5	4.5	4.5	4.4	5.2	5.5	4.4	4.5
FeO	10.5	10.1	10.0	10.1	10.0	10.0	8.6	8.5	8.2	8.1
MgO	30.8	30.9	31.2	31.0	30.7	31.2	32.2	31.8	32.8	32.9
CaO	.78	.84	.83	.82	.86	.82	.70	.68	.73	.75
Na_2O							.05	.05	.05	.04
K_2O										
TiO_2	.38	.35	.27	.30	.32	.30	.33	.29	.22	.22
Cr_2O_3								.01		
NiO								.11		
MnO							.16		.19	.16
Total	101.86	100.39	101.00	101.42	101.18	101.22	101.34	100.04	101.19	100.27
Ca	1.5	1.6	1.6	1.6	1.7	1.6	1.3	1.3	1.4	1.4
Fe	15.8	15.3	15.0	15.2	15.2	15.0	12.9	12.9	12.1	12.0
Mg	82.7	83.1	83.4	83.2	83.1	83.4	85.8	85.8	86.5	86.6

Loc., Sample	67-84-3A	67-84-4A	67-84-5A	67-84-6A	67-84-7A	67-84-8A	67-84-9A	67-84-1B	67-84-2B	67-84-3B
Group	Systematic						Systematic			
Rock Type	OCP						L			
SiO_2	54.2	54.0	54.0	53.4	54.0	53.3	53.6	54.2	54.4	54.6
Al_2O_3	4.7	4.8	4.6	5.0	4.8	4.5	4.7	4.4	4.2	4.1
FeO	8.5	8.5	8.2	8.6	8.4	8.2	8.2	8.1	8.0	7.9
MgO	32.5	32.5	32.9	32.4	32.6	33.0	32.8	32.8	32.9	32.8
CaO	.76	.73	.74	.74	.74	.72	.71	.75	.70	.70
Na_2O	.05	.05	.05	.05	.04	.05	.05	.06	.04	.05
K_2O						.05	.05	.03	.03	.03
TiO_2	.25	.25	.27	.29	.27	.26	.25	.19	.17	.14
Cr_2O_3										
NiO										
MnO	.19	.17	.17	.18	.18	.18	.19	.15	.15	.16
Total	101.15	101.17	100.93	100.66	101.03	100.26	100.55	100.68	100.59	100.48
Ca	1.4	1.4	1.4	1.4	1.4	1.3	1.4	1.4	1.3	1.3
Fe	12.6	12.6	12.1	12.8	12.5	12.1	12.1	12.0	11.8	11.7
Mg	86.0	86.0	86.5	85.8	86.1	86.6	86.5	86.6	86.8	86.9

ORTHOPYROXENE

Loc., Sample[1]	67-136-2	67-136-3	67-136-4	67-136-5	67-136-6	67-136-2A	67-136-3A	67-136-4A	67-136-2B	67-136-2B
Group[2]	Systematic		Systematic							
Rock Type[3]	OCP		L							
SiO_2	53.0	52.8	53.1	53.1	53.0	54.2	54.4	53.7	54.2	54.4
Al_2O_3	4.9	4.8	4.6	4.9	4.6	4.5	4.4	4.0	3.9	4.1
FeO	9.6	9.8	9.3	9.4	9.4	8.0	8.1	8.0	7.9	7.9
MgO	31.4	31.2	31.7	31.6	31.6	32.7	32.6	32.5	33.0	32.7
CaO	.80	.86	.80	.83	.83	.76	.78	.80	.79	.79
Na_2O	.10	.04	.04	.04	.05	.04	.05	.04	.04	.05
K_2O										
TiO_2	.26	.27	.28	.28	.28	.24	.22	.19	.17	.18
Cr_2O_3	.20	.05	.14	.16	.20	.21	.22	.31	.35	.31
NiO	.05	.06	.06	.06	.06	.07	.08	.06	.07	.06
Total	100.31	99.88	100.07	100.37	100.02	100.72	100.85	99.60	100.42	100.49
Ca	1.5	1.7	1.5	1.6	1.6	1.5	1.5	1.5	1.5	1.5
Fe	14.4	14.7	13.9	14.1	14.1	11.9	12.1	11.9	11.7	11.8
Mg	84.0	83.6	84.5	84.3	84.3	86.6	86.4	86.5	86.8	86.7

Loc., Sample	67-136-3B	67-136-4B	67-162-5
Group			Cr-Di
Rock Type			L
SiO_2	53.4	54.0	54.2
Al_2O_3	4.2	4.4	4.6
FeO	8.0	8.0	7.0
MgO	32.5	32.7	33.3
CaO	.78	.77	.69
Na_2O	.04	.04	.13
K_2O			
TiO_2	.20	.21	.23
Cr_2O_3	.28	.22	.06
NiO	.09	.07	
Total	99.49	100.41	100.21
Ca	1.5	1.5	1.3
Fe	12.0	11.9	10.4
Mg	86.5	86.6	88.3

ORTHOPYROXENE

Loc., Sample[1]	63-3-1	63-3-2	63-3-3	63-3-4	63-3-1A	63-3-2A	63-3-3A	63-3-4A	63-3-5A	63-3-6A
Group[2]	Systematic				Systematic					
Rock Type[3]	L				L					
SiO_2	55.2	55.7	54.4	55.4	54.3	54.5	55.1	54.6	54.7	54.9
Al_2O_3	3.5	3.4	3.5	3.5	3.4	3.3	3.4	3.4	3.4	3.4
FeO	6.4	6.4	6.4	6.5	6.3	6.4	6.5	6.4	6.5	6.3
MgO	33.7	33.8	33.6	33.7	33.2	33.6	34.1	33.6	33.8	33.9
CaO	.85	.87	.88	.86	.87	.86	.88	.92	.88	.88
Na_2O	.05	.05	.05	.05	.05	.05	.04	.05	.05	.05
K_2O										
TiO_2	.10	.11	.11	.12	.15	.14	.14	.15	.13	.14
Cr_2O_3	.51	.51	.53	.52	.51	.46	.51	.50	.55	.55
NiO	.08	.11	.14	.11	.10	.13	.12	.08	.10	.09
Total	100.39	100.95	99.61	100.76	98.88	99.44	100.79	99.70	100.11	100.21
Ca	1.6	1.7	1.7	1.6	1.7	1.6	1.6	1.7	1.7	1.7
Fe	9.4	9.4	9.4	9.6	9.5	9.5	9.5	9.5	9.6	9.3
Mg	89.0	88.9	88.9	88.8	88.8	88.9	88.9	88.8	88.8	89.0

Loc., Sample	63-3-7A	63-3-8A	63-3-9A	63-3-10A	63-3-1B	63-3-2B	63-3-3B	63-3-4B	63-3-5B	63-3-6B
Group					Systematic					
Rock Type					OWeb					
SiO_2	55.0	55.1	54.2	54.5	53.5	53.8	54.9	53.4	54.4	52.5
Al_2O_3	3.3	3.3	3.4	3.4	4.0	4.1	4.3	4.6	4.6	4.7
FeO	6.6	6.5	6.4	6.4	6.6	6.4	6.5	6.6	6.7	6.6
MgO	34.0	33.9	33.5	33.6	33.7	33.6	33.3	33.3	33.2	33.1
CaO	.85	.86	.88	.88	.83	.87	.83	.83	.82	.84
Na_2O	.06	.04	.05	.05	.05	.07	.05	.05	.06	.06
K_2O										
TiO_2	.13	.12	.12	.14	.15	.14	.13	.14	.15	.15
Cr_2O_3	.50	.54	.52	.52	.49	.48	.46	.54	.55	.60
NiO	.12	.09	.11	.10	.11	.11	.12	.10	.11	.12
Total	100.56	100.45	99.18	99.59	99.43	99.57	100.58	99.56	100.59	98.67
Ca	1.6	1.6	1.7	1.7	1.6	1.7	1.6	1.6	1.6	1.6
Fe	9.7	9.6	9.5	9.5	9.7	9.5	9.7	9.8	10.0	9.9
Mg	88.7	88.8	88.8	88.8	88.7	88.8	88.8	88.6	88.4	88.5

ORTHOPYROXENE

Loc., Sample[1]	63-3-1C	63-3-2C	63-3-3C	63-3-4C	63-3-5C	63-3-6C	63-3-7C	63-3-8C	63-3-1D	63-3-2D
Group[2]	Systematic					Systematic			Systematic	
Rock Type[3]	L					OWeb			L	
SiO_2	54.2	54.6	54.7	55.2	54.7	54.7	55.0	54.7	54.0	54.5
Al_2O_3	3.5	3.4	3.5	3.5	3.6	3.4	3.3	3.3	3.6	3.6
FeO	6.7	6.6	6.7	6.6	6.5	6.6	6.5	6.5	6.6	6.7
MgO	33.5	33.7	33.6	33.7	33.5	33.8	33.7	33.7	33.4	33.5
CaO	.87	.83	.86	.85	.91	.87	.83	.84	.85	.85
Na_2O	.04	.04	.05	.04	.05	.04	.04	.05	.04	.05
K_2O										
TiO_2	.14	.14	.15	.13	.14	.13	.13	.13	.16	.18
Cr_2O_3	.46	.48	.51	.47	.64	.52	.50	.52	.50	.46
NiO	.09	.10	.11	.11	.09	.09	.11	.08	.09	.10
Total	99.50	99.89	100.18	100.60	100.13	100.15	100.11	99.82	99.24	99.94
Ca	1.7	1.6	1.6	1.6	1.7	1.6	1.6	1.6	1.6	1.6
Fe	9.9	9.7	9.9	9.7	9.6	9.7	9.6	9.6	9.8	9.9
Mg	88.4	88.7	88.5	88.7	88.6	88.6	88.8	88.8	88.6	88.5

Loc., Sample	63-3-3D	63-3-4D	63-3-5D	63-3-1E	63-3-2E	63-3-3E	63-3-4E	63-3-5E	63-3-6E	63-3-7E
Group										
Rock Type										
SiO_2	55.3	55.6	55.7	52.6	54.3	55.2	54.0	54.7	54.8	54.8
Al_2O_3	3.8	3.6	3.7	3.8	3.8	3.7	3.7	3.7	3.6	3.6
FeO	6.6	6.5	6.6	6.4	6.4	6.5	6.4	6.5	6.5	5.8
MgO	33.9	34.0	33.9	33.4	33.60	33.60	33.6	33.8	33.8	33.7
CaO	.88	.87	.85	.86	.89	.88	.82	.84	.85	.85
Na_2O	.05	.03	.04	.05	.05	.05	.05	.05	.06	.06
K_2O										
TiO_2	.16	.15	.15	.13	.14	.14	.14	.14	.13	.06
Cr_2O_3	.52	.49	.46	.49	.53	.54	.49	.53	.50	.50
NiO	.12	.10	.10	.09	.11	.14	.11	.11	.08	
Total	101.33	101.31	101.50	97.82	99.82	100.75	99.31	100.37	100.32	99.37
Ca	1.6	1.6	1.6	1.7	1.7	1.7	1.6	1.6	1.6	1.6
Fe	9.7	9.5	9.7	9.5	9.5	9.6	9.5	9.6	9.6	8.7
Mg	88.7	88.8	88.7	88.8	88.8	88.7	88.9	88.8	88.8	89.7

ORTHOPYROXENE

Loc., Sample[1]	63-6-1	63-6-2	63-6-3	63-6-1A	63-6-2A	63-6-3A	63-6-4A	63-6-1B	63-6-2B	63-6-3B
Group[2]	Systematic									Systematic
Rock Type[3]	H									OWeb
SiO_2	55.9	56.3	56.6	56.0	56.1	56.0	56.0	56.2	56.2	55.8
Al_2O_3	2.4	2.4	2.4	2.5	2.5	2.5	2.6	2.9	2.8	3.0
FeO	5.6	5.6	5.6	5.6	5.4	5.5	5.6	5.4	5.6	5.5
MgO	34.4	34.4	34.4	34.5	34.4	34.3	34.4	34.2	34.2	34.1
CaO	1.1	1.1	.97	1.0	1.0	1.0	1.0	.94	.95	.97
Na_2O	.07	.08	.07	.05	.06	.06	.05	.06	.05	.04
K_2O										
TiO_2	.07	.07	.07	.10	.10	.10	.10	.13	.13	.14
Cr_2O_3	.60	.62	.63	.57	.64	.60	.60	.85	.88	.92
NiO	.05	.37	.05	.06	.06	.05	.06	.05	.06	.05
Total	100.19	100.94	100.79	100.38	100.26	100.11	100.41	100.73	100.87	100.52
Ca	2.1	2.1	1.8	1.9	1.9	1.9	1.9	1.8	1.8	1.8
Fe	8.2	8.2	8.2	8.2	7.9	8.1	8.2	8.0	8.3	8.2
Mg	89.7	89.7	90.0	89.9	90.2	90.0	89.9	90.2	89.9	90.0

Loc., Sample	63-6-4B	63-6-1C	63-6-2C	63-6-3C	63-9-1	63-9-2	63-9-3	63-9-4	63-9-5	63-9-1A
Group					Systematic					
Rock Type					L					
SiO_2	55.4	54.8	54.9	55.1	53.8	53.8	53.6	53.5	53.6	53.0
Al_2O_3	3.5	4.1	4.2	4.0	4.3	4.2	4.3	4.2	4.1	5.1
FeO	5.6	5.9	5.9	5.9	7.8	7.8	7.9	7.8	7.7	8.0
MgO	34.1	33.6	33.6	33.7	32.1	32.1	32.5	32.4	32.4	31.9
CaO	.98	.96	1.0	.99	.94	.95	.98	.96	.95	.92
Na_2O	.04	.05	.05	.05	.07	.07	.07	.07	.07	.06
K_2O										
TiO_2	.16	.15	.13	.13	.43	.42	.42	.41	.41	.49
Cr_2O_3	.83	.60	.61	.55	.61	.68	.58	.64	.68	.48
NiO	.05	.06	.06	.06	.05	.04	.06	.05	.06	.04
Total	100.66	100.22	100.45	100.48	100.10	100.06	100.41	100.03	99.67	99.99
Ca	1.9	1.8	1.9	1.9	1.8	1.8	1.9	1.8	1.8	1.8
Fe	8.3	8.8	8.8	8.8	11.8	11.8	11.8	11.7	11.6	12.1
Mg	89.9	89.4	89.3	89.3	86.4	86.4	86.3	86.5	86.6	86.1

ORTHOPYROXENE

Loc., Sample[1]	63-9-2A	63-9-3A	63-9-4A	63-9-5A	63-9-6A	63-9-1B	63-9-2B	63-9-3B	63-9-4B	63-9-5B
Group[2]	Systematic		Systematic			Systematic				
Rock Type[3]	OWeb		L			OWeb				
SiO_2	53.2	53.7	53.5	53.3	52.9	52.7	52.7	52.8	53.2	52.9
Al_2O_3	5.4	5.6	5.6	5.3	5.5	5.8	6.1	5.9	5.7	5.9
FeO	8.0	8.0	8.0	8.1	8.0	8.5	8.6	8.8	8.9	8.7
MgO	31.7	31.2	31.4	31.4	31.5	31.5	31.4	31.2	31.3	31.4
CaO	.92	.89	.91	.92	.95	.97	.93	.89	.96	.97
Na_2O	.06	.06	.06	.06	.06	.09	.08	.07	.08	.07
K_2O										
TiO_2	.49	.52	.53	.50	.48	.42	.43	.43	.43	.43
Cr_2O_3	.33	.25	.32	.29	.26	.04	.05	.03	.07	.05
NiO	.05	.05	.05	.06	.04	.09	.10	.09	.12	.08
Total	100.15	100.27	100.37	99.93	99.69	100.11	100.39	100.21	100.76	100.50
Ca	1.8	1.8	1.8	1.8	1.9	1.9	1.8	1.7	1.9	1.9
Fe	12.2	12.3	12.3	12.4	12.2	12.9	13.1	13.4	13.5	13.2
Mg	86.0	85.9	85.9	85.8	85.9	85.2	85.1	84.8	84.6	84.9

Loc., Sample	63-9-6B	63-9-7B	63-12-1	63-12-2	63-12-3	63-12-4	63-12-5	63-12-6	63-12-7	63-12-8
Group			Systematic				Systematic			Systematic
Rock Type			OWeb				D			OWeb
SiO_2	52.8	52.9	53.7	53.9	53.9	53.9	54.6	54.5	54.7	53.7
Al_2O_3	5.9	5.8	4.2	4.5	4.4	4.2	4.3	4.1	4.2	4.3
FeO	8.8	8.8	8.2	8.3	8.1	8.1	8.3	8.2	8.3	8.0
MgO	31.2	31.3	32.2	32.2	32.1	32.2	32.8	32.7	32.9	31.9
CaO	.99	.96	.97	.99	1.0	.99	.95	.95	.94	1.1
Na_2O	.08	.07	.07	.07	.06	.07	.07	.07	.06	.08
K_2O										
TiO_2	.43	.44	.16	.16	.15	.16	.16	.15	.15	.16
Cr_2O_3	.05	.05	.37	.44	.40	.39	.36	.35	.38	.38
NiO	.11	.09	.07	.07	.06	.07	.07	.06	.07	.07
Total	100.36	100.41	99.94	100.63	100.17	100.08	101.61	101.08	101.70	99.69
Ca	1.9	1.9	1.8	1.9	1.9	1.9	1.8	1.8	1.8	2.1
Fe	13.4	13.4	12.3	12.4	12.2	12.1	12.2	12.1	12.2	12.1
Mg	84.7	84.7	85.9	85.7	85.9	86.0	86.0	86.1	86.0	85.8

ORTHOPYROXENE

Loc., Sample[1]	63-12-9	63-12-10	63-12-11	63-12-12	63-12-13	63-12-14	63-12-15	63-12-16	63-17-1	63-17-2
Group[2]						Systematic		Systematic	Systematic	
Rock Type[3]						D		OWeb	L	
SiO_2	54.0	54.5	53.1	53.1	53.2	54.2	54.3	53.6	54.8	54.4
Al_2O_3	4.3	4.3	4.5	5.1	4.6	4.8	4.7	4.7	4.6	4.5
FeO	8.2	8.4	8.2	8.0	8.0	8.1	8.1	8.1	6.8	6.7
MgO	32.3	32.5	31.7	31.6	31.8	31.1	31.3	31.2	33.5	33.0
CaO	1.0	.99	1.0	.98	.97	.86	.88	.88	.92	.92
Na_2O	.07	.07	.08	.08	.08	.05	.05	.05	.10	.10
K_2O										
TiO_2	.16	.14	.14	.14	.12	.17	.17	.14	.15	.15
Cr_2O_3	.36	.39	.42	.47	.46	.37	.35	.39	.41	.40
NiO	.07	.07	.06	.07	.07	.14	.12	.13	.11	.11
Total	100.46	101.36	99.20	99.54	99.30	99.79	99.97	99.19	101.39	100.28
Ca	1.9	1.9	1.9	1.9	1.9	1.7	1.7	1.7	1.7	1.8
Fe	12.2	12.4	12.4	12.2	12.1	12.5	12.5	12.5	10.0	10.0
Mg	85.9	85.7	85.7	85.9	86.0	85.8	85.8	85.7	88.2	88.2

Loc., Sample	63-17-1A	63-17-2A	63-17-3A	63-17-1B	63-17-2B	63-17-3B	63-17-1C	63-17-2C	63-17-1D	63-17-2D
Group		Systematic	Systematic		Systematic	Systematic				
Rock Type		OWeb	L		OWeb	L				
SiO_2	54.3	54.3	54.1	54.6	54.5	54.5	54.4	54.5	54.3	54.4
Al_2O_3	4.5	4.5	4.5	4.6	4.6	4.5	4.7	4.5	4.6	4.6
FeO	6.7	6.8	6.8	6.8	6.8	6.8	6.9	6.8	6.7	6.8
MgO	33.0	33.1	33.0	33.0	33.1	33.0	33.2	33.1	33.0	33.1
CaO	.88	.89	.92	.93	.92	.93	.85	.90	.87	
Na_2O	.09	.08	.09	.09	.09	.08	.09	.08	.08	.08
K_2O										
TiO_2	.14	.16	.16	.16	.15	.15	.15	.15	.16	.17
Cr_2O_3	.45	.41	.41	.41	.41	.39	.41	.40	.44	.39
NiO	.10	.08	.12	.10	.09	.10	.11	.12	.12	.15
Total	100.16	100.32	100.10	100.69	100.66	100.45	99.81	100.55	100.27	99.69
Ca	1.7	1.7	1.8	1.8	1.8	1.8	1.6	1.7	1.7	1.7
Fe	10.0	10.2	10.2	10.2	10.1	10.2	10.3	10.2	10.1	10.2
Mg	88.3	88.1	88.0	88.0	88.1	88.0	88.1	88.1	88.3	88.2

ORTHOPYROXENE

Loc., Sample[1]	4-80-1	4-80-2	4-80-3	4-80-4	4-80-5	4-80-6	4-80-7	4-80-1A	4-80-2A	4-80-3A
Group[2]	Systematic		Systematic							
Rock Type[3]	OWeb		L							
SiO_2	53.2	53.6	54.1	54.2	54.0	54.6	54.4	54.2	53.7	55.1
Al_2O_3	5.4	6.0	4.8	4.6	4.6	4.9	4.5	4.3	4.6	4.3
FeO	7.4	7.2	7.3	7.3	7.2	7.3	7.3	7.2	7.2	7.3
MgO	31.8	31.2	32.5	32.9	32.8	32.8	33.1	32.8	32.1	33.5
CaO	2.7	2.6	1.9	.90	.84	.84	.88	.92	.87	.88
Na_2O	.06	.13	.09	.06	.06	.06	.07	.09	.05	.07
K_2O										
TiO_2	.13	.13	.11	.08	.08	.09	.09	.11	.11	.11
Cr_2O_3	.25	.30	.28	.22	.24	.24	.22	.29	.31	.25
NiO	.12	.10	.09	.06	.10	.11	.11	.10	.12	.13
Total	101.06	101.26	101.17	100.32	99.92	100.94	100.77	100.01	99.06	101.64
Ca	5.1	5.0	3.6	1.7	1.6	1.6	1.7	1.8	1.7	1.7
Fe	10.9	10.9	10.8	10.9	10.8	10.9	10.8	10.8	11.0	10.7
Mg	83.9	84.1	85.6	87.4	87.6	87.5	87.5	87.4	87.3	87.6

Loc., Sample	4-80-4A	4-80-5A	4-80-6A	4-80-7A	4-80-8A
Group	Systematic				
Rock Type	OWeb				
SiO_2	54.5	54.8	54.2	54.6	54.1
Al_2O_3	4.4	4.3	4.6	4.6	4.9
FeO	7.2	7.2	7.3	7.4	7.5
MgO	33.1	33.1	33.0	32.9	32.7
CaO	.89	.85	.89	.89	.87
Na_2O	.06	.07	.06	.06	.08
K_2O					
TiO_2	.11	.10	.10	.09	.08
Cr_2O_3	.27	.31	.34	.28	.19
NiO	.10	.12	.11	.14	.12
Total	100.63	100.85	100.60	100.96	100.54
Ca	1.7	1.6	1.7	1.7	1.7
Fe	10.7	10.7	10.8	11.0	11.2
Mg	87.6	87.7	87.5	87.3	87.1

ORTHOPYROXENE

Loc., Sample[1]	18-2-1	18-2-1	18-2-4	18-9-3	18-9-4	18-9-5	18-9-6	18-25-1	18-25-4
Group[2]	B-G			B-G				B-G	
Rock Type[3]	L			L				H	
SiO_2	55.9	53.8	53.5	55.6	55.5	55.0	55.7	52.2	51.3
Al_2O_3	2.5	2.2	2.2	3.0	3.0	3.0	3.0	3.4	2.9
FeO	5.6	5.4	5.3	5.4	5.4	5.4	5.4	5.4	4.6
MgO	32.5	33.6	33.4	32.7	32.7	32.7	32.6	33.0	29.8
CaO	2.1	2.1	2.1	2.1	2.1	2.1	2.2	2.0	5.5
Na_2O	.06	.06	.06	.01	.01	.02	.01	.12	.59
K_2O	.02	.01	.01		.01	.02	.01	.02	.04
TiO_2	.01		.01	.01	.01	.01	.02	.12	.33
Cr_2O_3	1.4	1.1	1.1	1.1	1.1	1.1	1.1	1.1	1.3
NiO									
Total	100.09	98.27	97.68	99.92	99.83	99.35	100.04	97.36	96.36
Ca	4.1	4.0	4.0	4.1	4.1	4.1	4.2	3.8	10.9
Fe	8.4	8.0	7.9	8.1	8.1	8.1	8.2	8.0	7.1
Mg	87.4	88.1	88.2	87.8	87.8	87.8	87.6	88.1	81.9

Loc., Sample	18-25-6	18-25-7	18-75-2	18-75-3	18-75-4	18-75-5	18-77-1	18-77-2	18-77-3
Group			Systematic				B-G		
Rock Type			L				H		
SiO_2	52.50	53.9	53.4	53.2	53.8	53.6	54.7	55.0	55.2
Al_2O_3	3.5	3.5	4.8	4.8	4.9	4.8	3.0	3.0	3.0
FeO	5.6	5.6	6.2	6.1	6.0	6.2	5.5	5.5	5.5
MgO	33.0	32.9	31.7	32.6	32.5	33.0	33.3	32.9	32.8
CaO	2.0	2.0	1.9	1.9	1.8	1.8	2.0	2.0	2.0
Na_2O	.12	.13	.14	.14	.13	.14	.10	.10	.39
K_2O	.01	.03	.03	.03	.02	.02	.01	.02	.25
TiO_2	.11	.10	.07	.07	.06	.05	.14	.13	.30
Cr_2O_3	1.1	1.1	1.0	1.0	1.0	1.0	1.1	1.1	1.1
NiO									
Total	97.94	99.26	99.24	99.84	100.21	100.61	99.85	99.75	100.54
Ca	3.8	3.8	3.7	3.6	3.5	3.5	3.8	3.8	3.9
Fe	8.3	8.4	9.6	9.1	9.0	9.3	8.1	8.2	8.2
Mg	87.9	87.8	86.7	87.3	87.5	87.2	88.1	88.0	87.9

ORTHOPYROXENE

Loc., Sample[1]	18-78-1	18-78-2	18-78-01	18-78-S1	18-78-S2	18-78-3	18-78-4	18-78-5	18-78-6	18-78-7
Group[2]	Systematic									
Rock Type[3]	L									
SiO_2	52.7	53.1	53.1	53.2	53.4	54.1	53.6	52.8	53.1	53.1
Al_2O_3	5.4	5.0	5.3	5.4	5.0	4.8	5.1	5.3	5.4	6.3
FeO	6.8	7.7	7.5	7.9	7.5	7.5	7.7	8.0	7.5	7.1
MgO	28.7	32.2	31.3	31.2	31.5	31.8	32.1	32.2	31.4	30.5
CaO	5.5	1.6	1.6	1.6	1.6	1.7	1.7	1.6	1.7	1.6
Na_2O	.35	.14	.14	.13	.14	.13	.14	.15	.16	.13
K_2O	.02	.02	.02	.04	.03	.03	.03	.02	.04	.02
TiO_2	.51	.39	.40	.41	.39	.40	.40	.42	.41	.38
Cr_2O_3	.75	.67	.66	.66	.72	.79	.72	.66	.66	1.3
NiO										
Total	100.73	100.82	100.02	100.54	100.28	101.25	101.49	101.15	100.37	100.43
Ca	10.9	3.0	3.1	3.0	3.2	3.2	3.2	3.1	3.3	3.3
Fe	10.4	11.5	11.4	12.0	11.4	11.3	11.4	11.8	11.5	11.2
Mg	78.7	85.5	85.4	85.0	85.4	85.5	85.4	85.1	85.2	85.5

Loc., Sample
Group
Rock Type

SiO_2
Al_2O_3
FeO
MgO
CaO
Na_2O
K_2O
TiO_2
Cr_2O_3
NiO
Total
Ca
Fe
Mg

ORTHOPYROXENE

Loc., Sample[1]	SAL-1	SAL-2	SAL-3	SAL-4	SAL-5	SAL-6	SAL-7	SAL-8	SAL-9	SAL-10
Group[2]	Systematic									
Rock Type[3]	L									
SiO_2	54.2	54.3	53.9	54.0	54.0	53.9	53.6	53.6	54.1	53.3
Al_2O_3	4.3	4.4	4.6	4.7	4.8	4.8	4.8	4.7	4.3	4.3
FeO	8.3	8.3	8.6	8.5	8.6	8.8	8.8	8.8	8.7	8.7
MgO	32.2	32.1	31.8	32.2	32.2	32.2	31.7	31.9	32.3	31.3
CaO	.91	.94	.91	.97	.92	.92	.88	.89	.89	.89
Na_2O	.15	.17	.17	.17	.16	.17	.17	.15	.18	.16
K_2O										
TiO_2	.20	.19	.23	.27	.27	.31	.32	.33	.31	.32
Cr_2O_3	.52	.56	.59	.52	.49	.47	.40	.32	.20	.17
NiO	.08	.11	.10	.10	.10	.09	.09	.09	.08	.07
Total	100.86	101.07	100.90	101.43	101.54	101.66	100.76	100.78	101.07	99.21
Ca	1.7	1.8	1.8	1.9	1.8	1.8	1.7	1.7	1.7	1.7
Fe	12.4	12.5	12.9	12.7	12.9	13.0	13.2	13.2	12.9	13.3
Mg	85.9	85.7	85.3	85.4	85.4	85.2	85.1	85.1	85.4	85.0

Loc., Sample	SAL-11-1	SAL-11-2	SAL-11-3	SAL-13-1	SAL-13-2
Group					
Rock Type					
SiO_2	52.8	52.9	53.6	53.2	52.9
Al_2O_3	4.7	4.9	4.8	4.4	4.6
FeO	8.8	8.6	8.7	8.6	8.6
MgO	31.3	31.4	31.6	31.3	31.3
CaO	.89	.87	.92	.90	.87
Na_2O	.16	.17	.16	.17	.16
K_2O					
TiO_2	.32	.28	.28	.32	.30
Cr_2O_3	.27	.58	.47	.27	.42
NiO	.09	.09	.09	.08	.08
Total	99.33	99.79	100.62	99.24	99.23
Ca	1.7	1.7	1.8	1.8	1.7
Fe	13.4	13.2	13.1	13.2	13.1
Mg	84.9	85.1	85.1	85.1	85.2

ORTHOPYROXENE

Loc., Sample[1]	33-204-1	33-204-2
Group[2]	G	
Rock Type[3]	GWeb	
SiO_2	50.0	50.9
Al_2O_3	7.5	7.2
FeO	10.0	10.3
MgO	28.5	28.0
CaO	.94	.90
Na_2O		
K_2O		
TiO_2	.11	.07
Cr_2O_3		
NiO		
Total	97.05	97.37
Ca	2.0	1.9
Fe	16.1	16.8
Mg	81.9	81.3

Loc., Sample	
Group	
Rock Type	
SiO_2	
Al_2O_3	
FeO	
MgO	
CaO	
Na_2O	
K_2O	
TiO_2	
Cr_2O_3	
NiO	
Total	
Ca	
Fe	
Mg	

Spinel

Loc., Sample[1]	32-15-1	32-15-2	32-15-2a	32-15-3	32-15-4	32-15-5	32-15-6	32-15-7	32-15-8	32-15-9
Group[2]	Systematic									
Rock Type[3]	OWeb									
Al_2O_3	54.0	54.6	58.0	57.3	58.0	57.4	58.4	58.3	57.2	57.3
FeO	18.3	17.2	14.6	15.9	14.7	14.8	14.6	14.6	16.1	15.7
MgO	18.8	19.2	20.5	20.1	20.6	20.6	20.7	20.4	19.9	19.9
CaO	.16	.18	.15	.15	.16	.18	.15	.14	.12	.16
TiO_2	.07	.07	.08	.06	.07	.09	.08	.08	.09	.11
Cr_2O_3	7.9	8.2	6.4	6.4	6.3	6.7	5.6	5.7	6.1	6.0
NiO	.21	.20	.23	.22	.21	.22	.23	.22	.23	.23
MnO	.20	.18	.16	.16	.15	.15	.15	.16	.17	.16
Total	99.64	99.83	100.12	100.29	100.19	100.14	99.91	99.60	99.91	99.56

Loc., Sample	32-15-10	32-15-11	32-22-1	33-22-3	32-22-4	32-24-1	32-24-2	32-24-3	32-24-4	32-24-5
Group			Cr-Di			Systematic				Center
Rock Type			L			OWeb				
Al_2O_3	52.7	59.4	57.0	57.4	58.6	60.0	61.1	60.0	60.3	64.4
FeO	19.2	12.8	11.5	11.5	11.5	10.8	10.8	10.8	10.8	10.1
MgO	18.2	21.4	20.7	20.7	20.8	22.6	22.8	22.7	22.6	23.6
CaO	.18	.14								
TiO_2	.09	.09	.07	.09	.04	.13	.13	.14	.14	.10
Cr_2O_3	9.1	5.5	10.8	10.9	10.8	4.8	4.3	4.7	4.7	1.5
NiO	.20	.22	.11	.14	.13	.37	.38	.38	.37	.44
MnO	.23	.12	.02	.04	.04	.06	.06	.08	.11	.04
V_2O_5			.03		.01	.07	.10	.06	.07	.07
Total	99.90	99.67	100.23	100.77	101.92	98.83	99.67	98.86	99.09	100.25

Spinel

Loc., Sample[1] / Group[2] / Rock Type[3]	32-24-5 Edge	32-24-7	32-24-8	32-24-9	32-24-10	32-24-11	32-24-1A	32-24-2A	32-24-4A	32-24-5A
Al_2O_3	64.7	62.7	63.5	64.1	64.2	64.5	59.9	63.5	60.1	58.4
FeO	10.1	10.5	10.5	10.3	10.3	10.3	11.5	9.4	11.5	11.8
MgO	23.5	22.5	22.8	22.9	23.0	23.0	22.0	23.2	22.0	21.8
CaO	.05	.03	.02	.03	.05	.05	.04		.07	.04
TiO_2	.08	.10	.10	.08	.08	.09	.12	.21	.11	.14
Cr_2O_3	1.2	3.0	2.5	1.8	1.7	1.6	6.0	3.5	5.9	7.4
NiO	.44	.49	.51	.50	.55	.51	.47		.46	.44
MnO	.05	.07	.07	.07	.07	.07	.09	.27	.08	.08
V_2O_5	.08									
Total	100.20	99.39	100.00	99.78	99.95	100.12	100.12	100.08	100.22	100.10

Loc., Sample / Group / Rock Type	32-24-6A	32-24-7A	32-24-8A	32-24-9A	32-24-10A	32-24-11A	32-24-12A	32-24-13A	32-24-14A	32-24-5B
Al_2O_3	59.1	60.5	61.1	60.1	59.0	58.9	59.9	59.8	59.9	57.0
FeO	11.6	11.4	11.2	11.5	11.7	11.7	11.5	11.6	11.3	13.7
MgO	21.9	22.2	22.3	22.2	21.9	21.9	21.9	21.8	22.1	20.7
CaO	.04	.05	.07	.04	.04	.05	.04	.04	.06	.09
TiO_2	.15	.13	.12	.12	.13	.12	.12	.13	.12	.10
Cr_2O_3	6.8	5.4	5.1	5.8	6.9	6.9	6.0	6.1	5.9	7.5
NiO	.46	.46	.49	.46	.43	.46	.47	.45	.47	.45
MnO	.07	.09	.08	.09	.08	.09	.08	.08	.09	.11
V_2O_5										
Total	100.12	100.23	100.46	100.31	100.18	100.12	100.01	100.00	99.94	99.65

Spinel

Loc., Sample[1]	32-24-6B	32-24-7B	32-24-8B	32-24-9B	32-24-10B	32-24-11B	32-29-1	32-29-2	32-29-3	32-48-2
Group[2]							Al-Aug			Cr-Di
Rock Type[3]							Web			L
Al_2O_3	56.3	55.5	54.4	56.7	56.5	55.2	64.2	64.0	64.9	35.9
FeO	14.3	15.1	16.1	13.7	14.3	15.7	13.7	13.7	13.7	16.1
MgO	20.5	20.0	19.5	20.6	20.3	19.6	21.8	21.8	21.8	21.0
CaO	.06	.09	.09	.07	.06	.08	.07	.07	.07	
TiO_2	.11	.10	.09	.13	.12	.11	.20	.19	.20	.11
Cr_2O_3	7.8	8.3	8.8	7.5	7.6	8.3	.29	.31	.28	28.90
NiO	.43	.43	.50	.45	.45	.43	.37	.38	.40	.08
MnO	.12	.12	.14	.11	.12	.15	.06	.06	.07	
V_2O_5							.08	.08	.07	
Total	99.62	99.64	99.62	99.26	99.45	99.57	100.77	100.59	101.49	102.09

Loc., Sample	32-52-3	32-57-2	32-57-3	32-72-1	32-72-2	32-72-3	32-72-4	32-73-5	32-73-6	32-73-7
Group	Cr-Di	Cr-Di		Systematic						
Rock Type	L	L		L						
Al_2O_3	54.8	52.8	51.7	52.1	53.3	53.0	56.1	56.0	56.3	56.8
FeO	13.7	17.4	16.6	17.1	15.9	16.1	15.0	14.6	13.6	13.1
MgO	20.4	20.4	21.8	19.4	19.8	19.6	20.1	20.7	20.7	21.1
CaO										
TiO_2		.38	.24							
Cr_2O_3	12.4	9.3	8.9	11.0	9.6	10.1	8.9	8.5	8.2	7.8
NiO	.15	.22	.23	.27	.26	.26	.28	.29	.28	.29
MnO	.06									
V_2O_5	.02									
Total	101.53	100.50	99.43	99.87	98.86	99.06	100.38	100.09	99.08	99.09

Spinel

Loc., Sample[1]	32-72-8	32-72-1A	32-72-2A	32-72-3A	32-72-4A	32-72-5A	32-74-1	33-1-1	33-1-2	33-1-3
Group[2]							Cr-Di	Systematic		
Rock Type[3]							L	L		
SiO_2				1.3						
Al_2O_3	56.5	58.0	57.2	57.3	56.9	57.3	57.6	48.6	49.1	48.1
FeO	13.0	12.3	12.3	12.4	12.8	13.3	11.0	17.4	17.2	17.3
MgO	21.1	21.1	21.5	21.5	21.1	21.0	21.8	17.7	17.9	17.7
CaO					.15	.14	.15			
TiO_2					.10	.11	.10			
Cr_2O_3	7.6	7.7	7.8	7.8	7.7	7.8	7.5	15.1	14.5	15.5
NiO	.29	.29	.28	.27	.27	.29	.38	.18	.19	.17
MnO				.01	.20	.19	.22			
V_2O_5										
Total	98.49	99.39	99.08	99.27	98.77	99.69	99.59	99.43	99.33	99.24

Loc., Sample	33-1-4	33-1-1A	33-1-2A	33-1-3A	33-1-4A	33-1-5A	33-1-6A	33-1-7A	33-1-8A	33-1-9A
Group										
Rock Type										
Al_2O_3	51.3	53.4	53.1	54.5	54.3	54.4	55.3	55.4	54.7	54.5
FeO	15.3	14.8	14.3	14.5	14.0	13.7	13.2	13.0	13.0	12.9
MgO	18.6	19.5	19.7	20.1	20.2	20.1	20.4	20.6	20.2	21.0
CaO	.13	.11	.10	.11	.12	.11	.13	.11	.12	.09
TiO_2	.12	.10	.10	.10	.10	.11	.10	.09	.10	.10
Cr_2O_3	13.2	11.5	11.2	11.0	11.3	11.6	10.6	10.7	11.7	10.7
NiO	.22	.21	.20	.21	.21	.20	.21	.20	.19	.20
MnO	.18	.16	.16	.16	.15	.12	.13	.15	.13	.13
V_2O_5										
Total	99.05	99.78	98.86	100.68	100.38	100.34	100.07	100.25	100.14	99.62

Note:

1 Tabulation page 84 - plus are on J9b (a continuation of J9a) ② On the disk, screen - (to calc. w/tables) you must start on page 1 (copyright [illegible] page) ③ On the printout the [illegible] has been [illegible] ... start in page [illegible]

Disk-J-9b, xenolith2b,ryp, 3/15/84;HW/sw 4/16/84

Spinel

Loc., Sample[1]	33-1-1B	33-1-2B	33-1-3B	33-1-4B	33-1-5B	33-1-1C	33-1-2C	33-1-3C	33-2-5	33-2-7
Group[2]									Al-Aug	
Rock Type[3]									L	
Al_2O_3	54.7	55.5	54.2	55.2	55.9	54.9	55.5	54.4	49.6	49.3
FeO	12.4	12.4	12.3	12.0	12.7	11.8	12.0	12.1	22.3	23.8
MgO	20.3	20.9	20.7	21.0	21.2	20.4	21.0	20.6	18.3	16.0
CaO	.09	.08	.08	.10	.09	.09	.11	.10		
TiO_2	.10	.09	.07	.08	.09	.09	.09	.09	.34	.36
Cr_2O_3	11.2	10.8	11.3	10.5	10.4	10.6	10.6	10.6	9.0	9.4
NiO	.20	.19	.19	.21	.21	.21	.20	.20	.27	.32
MnO	.14	.11	.13	.13	.12	.11	.11	.12	.10	.10
V_2O_5									.07	.07
Total	99.13	100.07	98.97	99.22	100.71	98.20	99.61	98.21	100.25	99.35

Loc., Sample	33-2-7	33-2-9	33-2-13	33-2-14	33-2-15	33-2-16	33-3-1	33-3-2	33-3-3	33-40-1
Group							Cr-Di			Cr-Di
Rock Type							L			L
Al_2O_3	49.4	49.5	47.9	47.6	47.5	48.8	57.2	54.3	54.6	32.3
FeO	22.7	23.7	27.3	26.3	26.3	24.2	10.9	10.9	10.9	23.6
MgO	16.8	15.8	14.4	14.7	15.1	15.5	21.2	20.9	21.9	12.5
CaO										
TiO_2	.35	.30	.12	.17	.21	.28				.04
Cr_2O_3	9.1	9.7	10.1	10.0	10.0	9.2	12.4	12.4	12.0	29.8
NiO	.29	.31	.40	.37	.37	.36	.04	.01	.02	.21
MnO	.10	.11	.16	.14	.14	.11				.24
V_2O_5	.08	.08	.07	.08	.08	.11				.10
Total	97.82	99.50	100.45	99.36	99.70	98.56	101.74	98.51	99.42	98.79

Spinel

Loc., Sample[1]	33-40-2	33-40-3	35-1-1	35-1-2	35-1-3	36-11-1	36-11-2	36-11-3	36-11-3	36-12-1
Group[2]			Cr-Di			Al-Aug		Center	Edge	Cr-Di
Rock Type[3]			L			Web				L
Al_2O_3	31.6	33.2	57.5	55.7	57.9	57.9	58.2	58.5	58.4	54.9
FeO	23.9	20.6	12.7	13.0	12.8	20.8	20.8	20.8	20.8	12.4
MgO	12.5	14.0	21.7	22.0	22.1	18.2	18.2	18.2	18.0	21.6
CaO						.26	.28	.27	.22	.22
TiO_2	.05	.04	.07	.13	.12	.64	.62	.62	.58	.19
Cr_2O_3	30.2	30.5	8.5	8.9	8.3	.60	.65	.53	.57	10.4
NiO	.19	.20	.11	.10	.09	.31	.29	.29	.30	.39
MnO	.22	.20				.10	.08	.08	.08	.09
V_2O_5	.02	.03				.14	.15	.13	.14	.10
Total	98.68	98.77	100.58	99.83	101.30	98.85	99.27	99.42	99.09	100.48

Loc., Sample	36-12-2	36-12-3	36-12-3	36-14-1	36-14-2	36-14-3	36-14-3	36-18-1	36-18-2	36-18-2
Group		Center	Edge	Al-Aug		Center	Edge	Cr-Di	Center	Edge
Rock Type				CP				L		
Al_2O_3	54.8	54.8	54.9	58.0	58.2	57.6	57.5	56.1	56.1	56.1
FeO	12.4	12.4	12.4	22.3	22.3	22.3	22.3	11.5	11.5	11.5
MgO	21.6	21.7	21.7	17.7	17.7	17.7	17.7	21.6	21.6	21.6
CaO	.23	.24	.2	.27	.30	.25	.32	.18	.21	.22
TiO_2	.20	.18	.18	.69	.71	.68	.71	.17	.13	.13
Cr_2O_3	10.6	10.5	10.6	.06	.06	.07	.06	8.8	8.9	8.9
NiO	.35	.36	.36	.15	.14	.14	.15	.36	.35	.33
MnO	.08	.09	.08	.10	.09	.09	.09	.07	.08	.09
V_2O_5	.10	.11	.10	.16	.17	.16	.16	.09	.08	.09
Total	100.36	100.38	100.52	99.43	99.67	98.99	98.99	98.87	98.95	98.96

Spinel

Loc., Sample[1/]	36-18-3
Group[2/]	
Rock Type[3/]	
Al_2O_3	56.2
FeO	11.5
MgO	21.4
CaO	.21
TiO_2	.14
Cr_2O_3	9.0
NiO	.36
MnO	.08
V_2O_5	.09
Total	98.98

Loc., Sample	
Group	
Rock Type	
Al_2O_3	
FeO	
MgO	
CaO	
TiO_2	
Cr_2O_3	
NiO	
MnO	
V_2O_5	
Total	

Spinel

Loc., Sample[1/]	23-11-1	23-11-2	23-11-3	23-11-4	23-11-1A	23-11-2A	23-11-3A	23-11-4A	23-11-5A	23-11-6A
Group[2/]	Systematic									
Rock Type[3/]	L									
Al_2O_3	47.4	51.7	54.4	53.1	55.8	57.1	56.7	55.7	56.4	57.0
FeO	20.6	18.3	16.8	17.0	13.2	12.7	12.9	13.1	13.0	12.6
MgO	17.2	18.5	19.2	19.0	20.9	21.1	21.1	20.9	21.1	21.3
CaO	.43	.46	.46	.49	.47	.47	.50	.47	.46	.50
TiO_2	.22	.16	.12	.13	.09	.14	.09	.09	.09	.09
Cr_2O_3	13.5	10.8	8.8	10.0	9.1	8.1	8.4	9.4	8.8	8.2
NiO	.21	.17	.17	.17	.12	.11	.12	.13	.12	.11
MnO	.09	.09	.09	.07	.07	.05	.04	.06	.05	.04
V_2O_5										
Total	99.65	100.18	100.04	99.96	99.75	99.77	99.85	99.85	100.02	99.84

Loc., Sample	23-11-1B	23-11-2B	23-11-3B	23-11-4B	23-11-5B	23-11-6B
Group						
Rock Type						
Al_2O_3	57.8	57.8	58.1	58.5	57.9	57.9
FeO	12.4	12.7	12.6	12.4	12.8	12.4
MgO	21.4	21.5	21.5	21.4	21.6	21.5
CaO	.53	.52	.45	.47	.52	.53
TiO_2	.10	.13	.12	.12	.12	.12
Cr_2O_3	7.6	7.6	7.4	7.3	7.7	7.6
NiO	.11	.10	.11	.10	.10	.11
MnO	.05	.05	.06	.05	.05	.08
V_2O_5						
Total	99.99	100.40	100.34	100.34	100.79	100.24

Spinel

Loc., Sample[1]	66-10-1	66-10-2	66-10-3	66-10-1A	66-10-2A	66-10-3A	66-10-4A	66-10-5A	66-10-6A	66-10-7A
Group[2]	Systematic			Systematic			Systematic			
Rock Type[3]	L			OCP			L			
SiO_2				.22	.20	.14	.19	.14	.19	.18
Al_2O_3	56.1	56.5	57.6	62.0	65.2	63.9	60.9	59.2	57.0	56.6
FeO	14.4	14.3	14.4	12.5	12.1	13.0	13.4	13.8	14.4	14.5
MgO	20.1	20.2	20.3	21.5	22.0	21.7	21.3	20.9	20.5	20.3
CaO	.08	.09	.10	.13	.10	.07	.08	.08	.09	.09
TiO_2	.13	.13	.15	.13	.12	.18	.15	.20	.19	.20
Cr_2O_3	7.2	7.0	6.6	2.9	.26	1.2	3.7	5.0	7.0	7.2
NiO	.33	.36	.33	.35	.35	.34	.33	.34	.32	.33
MnO	.11	.11	.11	.09	.08	.09	.09	.10	.11	.11
V_2O_5	.12	.13	.14							
Total	98.57	98.82	99.73	99.82	100.41	100.62	100.14	99.76	99.80	99.51

Loc., Sample	66-13-1	66-123-1	66-123-2	66-123-3	66-123-1A	66-123-2A	66-123-3A	67-7-1a	67-7-2
Group	Cr-Di	Systematic		Systematic				Systematic	
Rock Type	L	L		Web				OCP	
SiO_2	1.6							1.7	
Al_2O_3	57.6	58.5	58.7	58.9	58.2	59.0	59.4	62.4	62.2
FeO	10.9	10.8	10.9	10.9	10.8	10.9	10.7	16.1	16.4
MgO	21.8	21.6	21.9	21.9	22.1	22.1	22.1	19.8	21.0
CaO		.06	.09	.06	.08	.04	.08		
TiO_2		.16	.16	.17	.16	.17	.13		.22
Cr_2O_3	8.0	6.5	6.5	6.4	6.4	5.9	5.9	.20	1.3
NiO	.34	.37	.36	.37	.37	.37	.41	.29	
MnO	.01	.08	.08	.08	.07	.08	.08	.01	
V_2O_5		.09	.08	.10	.08	.09	.09		
Total	100.25	98.16	98.77	98.88	98.26	98.65	98.89	100.50	100.12

Spinel

Loc., Sample[1]	67-7-1A	67-7-2A	67-7-3A	67-7-4A	67-84-3	67-84-4	67-84-5	67-84-6	67-84-7
Group[2]	Systematic				Systematic				
Rock Type[3]	L				OCP				
Al_2O_3	55.3	55.6	56.1	55.5	62.8	63.1	63.7	63.9	62.9
FeO	17.2	17.5	17.5	17.7	16.0	15.4	15.4	15.1	13.8
MgO	19.0	19.8	19.5	19.1	20.1	20.5	20.5	20.4	21.5
CaO					.08	.06	.10	.07	.04
TiO_2	.27	.25	.26	.28	.23	.22	.24	.21	.21
Cr_2O_3	6.8	6.8	6.1	6.7	.02	.03	.03	.02	.74
NiO					.10	.10	.11	.13	.20
MnO					.12	.12	.12	.11	.08
V_2O_5									
Total	98.57	99.95	99.46	99.28	99.45	99.53	100.20	100.34	99.41

Loc., Sample	67-84-8	67-84-9	67-84-10	67-84-11	67-84-5A	67-84-6A	67-84-7A	67-84-8A	67-84-9A
Group									
Rock Type									
Al_2O_3	63.8	63.2	63.2	62.6	63.1	63.4	63.5	63.6	63.4
FeO	13.8	14.0	14.5	13.5	14.4	14.6	14.2	14.0	13.8
MgO	21.0	21.0	20.9	20.9	20.9	21.2	21.0	21.0	20.1
CaO	.07	.07	.06	.05	.06	.07	.06	.08	.07
TiO_2	.18	.21	.20	.21	.17	.19	.18	.17	.20
Cr_2O_3	.31	.21	.03	.89	.04	.02	.03	.04	.15
NiO	.20	.19	.17	.17	.13	.15	.15	.17	.19
MnO	.10	.11	.11	.10	.12	.11	.11	.09	.10
V_2O_5									
Total	99.46	98.99	99.17	98.42	98.92	99.74	99.23	99.15	98.01

Spinel

Loc., Sample[1] / Group[2] / Rock Type[3]	67-84-10A	67-84-11A	67-84-12A	67-84-13A	67-84-14A	67-84-15A	67-84-16A	67-84-17A	67-84-18A	67-84-19A Systemati L
Al_2O_3	62.7	63.1	62.6	63.2	62.0	62.4	63.1	61.5	60.4	61.2
FeO	13.5	13.6	13.6	13.7	13.4	13.5	13.5	13.3	13.8	13.9
MgO	21.1	21.2	21.3	21.7	20.9	20.8	21.2	21.0	21.0	21.0
CaO	.09	.07	.07	.08	.08	.10	.15	.10	.06	.08
TiO_2	.19	.18	.19	.20	.20	.20	.20	.20	.23	.23
Cr_2O_3	.49	.27	.50	.68	1.7	1.3	.94	2.3	3.2	3.3
NiO	.20	.20	.20	.20	.21	.20	.20	.20	.18	.19
MnO	.12	.10	.12	.10	.10	.10	.10	.10	.12	.11
V_2O_5										
Total	98.39	98.72	98.58	99.86	98.59	98.60	99.39	98.70	98.99	100.01

Loc., Sample / Group / Rock Type	67-84-20A	67-84-21A	67-84-22A	67-84-23A	67-84-24A	67-84-25A	67-84-26A	67-84-27A	67-84-28A	67-84-29A
Al_2O_3	60.0	58.5	58.3	57.7	57.6	56.9	56.0	55.8	55.7	55.5
FeO	13.7	14.0	14.3	14.2	14.3	14.6	14.6	14.8	14.6	14.9
MgO	20.9	20.4	20.5	20.5	20.2	20.1	20.0	19.9	20.0	20.3
CaO	.07	.04	.06	.04	.06	.07	.07	.08	.06	.06
TiO_2	.21	.20	.22	.22	.22	.24	.24	.22	.24	.23
Cr_2O_3	3.8	5.1	5.6	5.9	6.3	7.0	7.4	7.7	8.0	8.2
NiO	.21	.20	.20	.20	.20	.18	.21	.18	.18	.21
MnO	.11	.12	.13	.11	.14	.13	.13	.15	.16	.15
V_2O_5										
Total	99.00	98.56	99.31	98.87	99.02	99.22	98.65	98.83	98.94	99.55

Spinel

Loc., Sample[1] / Group[2] / Rock Type[3]	67-84-30A	67-84-5B	67-84-6B	67-84-6aB	67-84-6bB	67-84-7B	67-84-8B	67-84-9B	67-84-9aB	67-84-9bB
Al_2O_3	58.6	54.8	55.7	55.2	56.3	56.8	56.7	57.0	57.3	56.8
FeO	13.9	15.1	14.7	15.1	14.6	14.5	14.9	15.0	14.8	14.6
MgO	20.5	19.8	19.8	19.9	19.7	19.8	20.0	19.9	20.1	19.7
CaO	.07	.08	.07	.10	.07	.08	.08	.07	.08	.08
TiO_2	.22	.18	.17	.17	.18	.20	.19	.19	.21	.20
Cr_2O_3	4.9	9.2	8.5	8.9	8.6	8.2	8.1	8.4	7.5	7.8
NiO	.22	.42	.45	.44	.43	.43	.41	.45	.43	.44
MnO	.14	.17	.15	.15	.15	.15	.15	.15	.16	.13
V_2O_5										
Total	98.55	99.75	99.54	99.96	100.03	100.16	100.53	101.16	100.58	99.75

Loc., Sample	67-84-10B	67-84-11B	67-84-12B	67-84-13B	67-136-1	67-136-2	67-136-3	67-136-4	67-136-1A	67-136-2A
Group					Systematic		Systematic		Systematic	
Rock Type					CP		L		CP	
Al_2O_3	56.7	56.1	56.6	55.4	62.5	59.5	58.3	57.4	63.2	62.0
FeO	14.9	15.1	14.9	15.0	15.2	15.8	15.1	15.4	14.0	13.5
MgO	19.8	19.7	20.0	19.9	20.5	20.0	19.9	19.7	21.1	21.3
CaO	.08	.09	.06	.09	.12	.15	.08	.08	.12	.12
TiO_2	.21	.20	.21	.20	.20	.31	.28	.30	.20	.18
Cr_2O_3	8.6	8.9	8.2	9.3	.05	2.5	4.4	5.3	.01	1.4
NiO	.45	.43	.44	.44	.25	.23	.24	.23	.28	.32
MnO	.16	.16	.13	.16	.07	.08	.09	.09	.06	.07
V_2O_5					.10	.12	.13	.13	.10	.12
Total	100.90	100.68	100.54	100.49	98.99	98.69	98.52	98.63	99.07	99.01

Spinel

Loc., Sample[1]	67-136-3A	67-136-4A	67-136-2B	67-136-3B	67-136-4B
Group[2]					
Rock Type[3]					
Al_2O_3	57.6	53.6	52.4	54.2	57.2
FeO	13.4	14.2	14.5	14.1	13.6
MgO	20.8	20.4	19.5	20.0	20.7
CaO	.09	.10	.13	.08	.10
TiO_2	.18	.27	.25	.26	.22
Cr_2O_3	6.0	9.7	11.2	9.3	6.9
NiO	.30	.27	.31	.28	.31
MnO	.08	.08	.10	.09	.08
V_2O_5	.10	.13	.12	.09	.12
Total	98.45	98.75	98.51	98.40	99.23

Loc., Sample	
Group	
Rock Type	
Al_2O_3	
FeO	
MgO	
CaO	
TiO_2	
Cr_2O_3	
NiO	
MnO	
V_2O_5	
Total	

Spinel

Loc., Sample[1]	40-1-1	40-1-2	40-1-3	40-1-4	40-1-1A	40-1-2A	40-1-3A	40-1-4A	40-2-1	40-2-2
Group[2]	Systematic		Systematic		Systematic		Systematic		Cr-Di	
Rock Type[3]	OWeb		L		OWeb		L		L-OWeb	
SiO_2										
Al_2O_3	50.1	51.0	51.7	52.1	48.4	46.7	45.0	44.2	29.3	26.2
FeO	12.0	12.0	11.9	11.9	12.2	12.5	12.8	13.0	14.2	14.9
MgO	20.5	20.7	20.9	21.1	20.4	20.1	20.2	19.8	18.4	18.5
CaO	.10	.11	.11	.10	.13	.11	.10	.12	.52	1.0
TiO_2	.14	.13	.12	.13	.14	.15	.18	.20	2.5	3.0
Cr_2O_3	15.0	14.6	13.8	13.7	16.2	17.4	18.7	19.1	34.3	35.6
NiO	.29	.32	.31	.32	.31	.31	.34	.31	.31	.32
MnO	.10	.09	.09	.09	.09	.11	.10	.11	.14	.14
V_2O_5	.09	.09	.09	.09	.11	.10	.13	.13	.34	.32
Total	98.32	99.04	99.02	99.53	97.98	97.48	97.55	96.97	100.01	100.01

Loc., Sample	40-4-1	40-4-2	40-4-4	40-4-5	40-127-1	40-127-2	40-127-3	40-127-5	40-127-6	40-127-7
Group	Cr-Di				Systematic			Systematic		Systematic
Rock Type	L				L			Gb		L
SiO_2					.20	.18	.20	.19	.24	.21
Al_2O_3	52.4	53.8	53.7	56.0	52.8	46.7	43.9	48.2	50.5	49.7
FeO	13.4	15.8	17.9	17.3	15.6	20.1	22.7	18.9	12.8	13.2
MgO	18.9	20.1	19.2	18.7	19.1	16.9	15.5	17.5	20.3	20.0
CaO					.13	.16	.15	.16	.16	.10
TiO_2	.22	.25	.22	.26	.19	.55	.67	.50	.26	.30
Cr_2O_3	12.5	11.8	10.8	9.1	10.2	13.9	15.2	13.4	14.3	15.0
NiO	.15	.13	.15	.17	.34	.32	.26	.29	.32	.35
MnO					.10	.15	.15	.15	.11	.10
V_2O_5										
Total	97.57	101.88	101.97	101.53	98.66	98.96	98.73	99.29	98.99	98.96

Spinel

Loc., Sample[1]	40-127-1A	40-127-1A	40-127-2A	40-127-2A	40-127-3A	40-127-3A	40-127-4A	40-127-4A
Group[2]	Center	Edge	Center	Edge	Center	Edge	Center	Edge
Rock Type[3]								
Al_2O_3	45.2	45.5	46.9	47.4	47.9	47.8	47.6	47.7
FeO	19.4	19.3	18.7	18.7	18.3	18.1	19.5	19.8
MgO	16.7	16.7	16.9	17.2	17.3	17.3	16.7	16.9
CaO	.18	.20	.20	.23	.21	.21	.19	.21
TiO_2	.34	.37	.30	.36	.28	.28	.34	.33
Cr_2O_3	13.6	13.4	13.2	13.0	13.3	13.2	12.9	12.9
NiO	.31	.32	.34	.33	.33	.31	.33	.32
MnO	.20	.19	.18	.20	.19	.18	.20	.19
V_2O_5	.14	.13	.14	.14	.13	.15	.14	.17
Total	96.07	96.11	96.86	97.56	97.94	97.53	97.90	97.82

Loc., Sample	40-127-5A	40-127-5A	40-127-6A	40-127-6A	40-127-7A	40-127-7A	40-127-8A
Group	Center	Edge	Center	Edge	Center	Edge	Center
Rock Type							
Al_2O_3	46.4	46.5	44.5	42.6	43.5	42.9	41.4
FeO	21.4	21.3	23.9	25.3	24.4	25.1	25.5
MgO	15.8	16.0	14.9	14.9	15.1	15.1	14.6
CaO	.18	.18	.24	.21	.32	.40	.25
TiO_2	.52	.53	.71	1.1	.82	1.1	.95
Cr_2O_3	12.9	12.4	12.5	12.5	12.4	12.1	15.1
NiO	.31	.32	.27	.26	.25	.25	.28
MnO	.19	.19	.23	.23	.23	.22	.23
V_2O_5	.15	.15	.18	.20	.22	.22	.23
Total	97.85	97.57	97.43	97.30	97.24	97.39	98.54

Spinel

Loc., Sample[1]	63-3-1	63-3-2	63-3-3	63-3-4	63-3-5	63-3-1A	63-3-2A	63-3-3A	63-3-4A	63-3-5A
Group[2]	Systematic									
Rock Type[3]	L									
Al_2O_3	42.3	42.9	42.8	42.9	43.4	43.4	44.1	44.6	44.4	43.7
FeO	14.4	14.5	14.7	14.6	14.6	14.2	14.3	14.2	14.1	14.2
MgO	18.4	18.4	18.4	18.3	18.5	18.5	18.5	18.5	18.7	18.6
CaO	.10	.10	.10	.10	.10	.10	.09	.11	.11	.10
TiO_2	.28	.29	.29	.30	.31	.27	.28	.30	.29	.29
Cr_2O_3	23.7	23.7	23.1	22.7	23.0	21.7	21.6	21.6	21.7	21.8
NiO	.36	.36	.37	.36	.36	.18	.17	.18	.19	.18
MnO	.19	.18	.19	.20	.20	.18	.18	.17	.16	.17
V_2O_5										
Total	99.73	100.43	99.95	99.46	100.46	98.53	99.22	99.66	99.65	99.04

Loc., Sample	63-3-6A	63-3-7A	63-3-8A	63-3-10A	63-3-1B	63-3-2B	63-3-3B	63-3-4B	63-3-5B	63-3-6B
Group					Systematic					
Rock Type					OWeb					
Al_2O_3	43.6	43.6	44.6	46.2	47.4	48.4	48.6	50.7	52.9	53.2
FeO	14.4	14.3	14.2	13.8	13.6	13.3	13.6	13.2	12.0	12.9
MgO	18.5	18.8	18.7	18.8	18.9	19.3	19.5	19.8	20.2	20.3
CaO	.11	.10	.12	.13	.12	.12	.10	.09	.09	.09
TiO_2	.29	.28	.31	.29	.27	.30	.26	.23	.23	.21
Cr_2O_3	22.4	22.0	21.3	20.5	18.1	17.9	17.7	15.2	12.8	13.1
NiO	.18	.21	.17	.18	.40	.39	.35	.38	.40	.40
MnO	.19	.19	.16	.16	.18	.18	.18	.15	.13	.15
V_2O_5										
Total	99.85	99.48	99.56	100.06	98.97	99.89	100.29	99.76	98.75	100.36

Spinel

Loc., Sample[1]	63-3-7B	63-3-8B	63-3-1C	63-3-2C	63-3-3C	63-3-4C	63-3-5C	63-3-6C	63-3-7C	63-3-8C
Group[2]									Systematic	
Rock Type[3]									L	
Al_2O_3	53.3	52.4	46.1	46.0	46.3	46.7	45.9	44.1	44.2	44.4
FeO	12.9	12.7	14.2	14.1	14.3	14.2	14.2	14.1	14.1	14.3
MgO	20.1	20.0	19.1	19.2	19.2	18.9	18.9	18.8	18.7	18.9
CaO	.07	.11	.09	.10	.09	.10	.11	.14	.09	.09
TiO_2	.23	.23	.28	.27	.26	.27	.27	.28	.29	.30
Cr_2O_3	13.3	14.0	19.5	19.5	19.5	19.5	20.2	21.3	21.1	21.7
NiO	.38	.38	.19	.18	.19	.17	.20	.05	.19	.20
MnO	.14	.14	.18	.17	.18	.18	.18	.15	.18	.17
V_2O_5										
Total	100.42	99.96	99.64	99.52	100.02	100.02	99.96	98.92	98.85	100.06

Loc., Sample	63-3-9C	63-3-10C	63-3-11C	63-3-1D	63-3-2D	63-3-3D	63-3-4D	63-3-5D	63-3-1E	63-3-2E
Group										
Rock Type										
Al_2O_3	44.6	44.1	43.8	47.2	47.1	47.2	46.6	46.0	45.9	45.1
FeO	14.4	14.5	14.4	13.9	14.0	14.0	14.0	14.2	13.8	14.1
MgO	19.0	19.0	18.9	19.1	19.1	19.0	19.2	19.2	18.9	18.9
CaO	.10	.11	.10	.07	.09	.09	.09	.08	.12	.11
TiO_2	.27	.28	.28	.30	.29	.29	.28	.30	.32	.31
Cr_2O_3	21.8	21.9	22.0	18.2	18.7	18.5	18.6	19.1	20.1	20.4
NiO	.18	.18	.18	.18	.18	.18	.19	.17	.38	.40
MnO	.18	.17	.18	.18	.17	.16	.17	.19	.16	.17
V_2O_5										
Total	100.53	100.24	99.84	99.13	99.63	99.42	99.13	99.24	99.68	99.49

Spinel

Loc., Sample[1] / Group[2] / Rock Type[3]	63-3-3E	63-3-4E	63-3-5E	63-3-6E	63-3-7E	63-6-1	63-6-2	63-6-3	63-6-1A	63-6-2A
						Systematic				
						L				
SiO_2										
Al_2O_3	44.8	44.5	44.6	43.8	44.6	30.5	30.5	30.1	31.9	32.0
FeO	14.2	14.1	14.2	14.3	13.7	14.3	14.3	14.3	14.4	14.4
MgO	18.9	18.6	18.5	18.7	18.8	17.0	16.9	17.1	17.5	17.3
CaO	.11	.12	.10	.09	.12	.20	.19	.17	.19	.19
TiO_2	.32	.36	.34	.35	.35	.29	.27	.26	.35	.37
Cr_2O_3	21.1	21.5	21.3	22.4	22.3	35.5	35.4	35.9	34.1	34.0
NiO	.35	.38	.34	.34	.34	.15	.16	.15	.16	.17
MnO	.18	.20	.18	.16	.18	.29	.29	.28	.28	.28
V_2O_5						.23	.24	.22	.23	.23
Total	99.96	99.76	99.56	100.14	100.39	98.46	98.25	98.48	99.11	98.94

Loc., Sample	63-6-3A	63-6-1B	63-6-2B	63-6-3B	63-6-4B	63-6-5B	63-6-1C	63-6-2C	63-6-3C	63-6-3C
Group					Systematic					Opposite
Rock Type					OWeb					Edge
SiO_2		.20	.21	.32	.33	.50				
Al_2O_3	32.2	31.5	31.7	31.7	34.0	38.4	50.0	49.7	49.8	49.5
FeO	14.4	14.1	14.0	14.1	13.5	12.6	10.8	11.5	11.5	11.6
MgO	17.3	17.5	17.7	17.6	18.2	19.2	20.8	20.4	20.5	20.5
CaO	.19	.22	.20	.21	.28	.22	.16	.17	.11	.16
TiO_2	.37	.47	.49	.45	.44	.37	.20	.18	.20	.20
Cr_2O_3	34.0	34.7	34.7	34.6	32.2	27.8	17.0	16.8	17.4	17.6
NiO	.17	.25	.25	.26	.24	.25	.20	.23	.19	.19
MnO	.28	.16	.15	.16	.15	.13	.19	.20	.18	.19
V_2O_5	.24						.14	.14	.12	.14
Total	99.15	99.10	99.40	99.40	99.34	99.47	99.49	99.32	100.00	100.08

Spinel

Loc., Sample[1]	63-9-1	63-9-2	63-9-3	63-9-4	63-9-5	63-9-1A	63-9-2A	63-9-3A	63-9-4A	63-9-5A
Group[2]	Systematic						Systematic		Systematic	
Rock Type[3]	L						OWeb		L	
SiO_2	.17	.29	.25	.25	.19	.23	.21	.25	.24	.25
Al_2O_3	49.8	46.7	48.2	45.0	43.6	55.6	60.0	60.0	59.1	58.2
FeO	14.7	15.6	15.1	15.7	16.1	13.7	12.9	13.0	13.2	13.4
MgO	19.4	18.5	19.1	18.3	18.1	20.4	21.0	21.0	20.9	20.8
CaO	.12	.11	.15	.13	.18	.10	.12	.08	.09	.10
TiO_2	.73	.82	.76	.87	.89	.56	.42	.47	.48	.49
Cr_2O_3	14.4	17.5	15.9	18.7	20.8	9.1	4.8	5.0	5.5	5.9
NiO	.31	.30	.30	.31	.30	.33	.33	.35	.33	.33
MnO	.11	.14	.12	.12	.12	.09	.08	.09	.09	.09
V_2O_5										
Total	99.74	99.96	99.88	99.38	100.38	100.11	99.86	100.24	99.93	99.56

Loc., Sample	63-9-1aB	63-9-1aB	63-9-1bB	63-9-1bB	63-9-1cB	63-9-1cB	63-9-2aB	63-9-2B	63-9-2bB
Group	Center	Edge	Center	Edge	Center	Edge	Systematic		
Rock Type							OWeb		
Al_2O_3	60.8	60.6	61.3	61.7	60.8	61.6	60.9	61.5	62.3
FeO	12.1	12.4	12.6	12.3	13.0	12.3	12.9	12.8	12.5
MgO	20.9	21.2	21.4	21.3	21.5	21.4	21.6	21.9	21.9
CaO	.07	.10	.10	.10	.07	.05	.09	.11	.14
TiO_2	.46	.42	.39	.42	.43	.43	.40	.38	.37
Cr_2O_3	3.7	3.7	3.1	3.1	3.9	3.8	3.5	3.0	1.9
NiO	.33	.32	.35	.33	.32	.30	.35	.32	.33
MnO	.11	.12	.11	.11	.13	.11	.12	.11	.11
V_2O_5	.10	.11	.09	.10	.10	.12	.09	.14	.11
Total	98.57	98.97	99.44	99.46	100.25	100.11	99.95	100.26	99.66

Spinel

Loc., Sample[1]	63-9-2cB	63-9-2dB	63-9-2eB	63-9-3B	63-9-3aB	63-9-3bB	63-9-3cB	63-9-4B	63-9-4aB	63-9-4bB
Group[2]										
Rock Type[3]										
Al_2O_3	63.1	64.3	64.1	63.7	63.6	63.6	63.5	63.2	63.0	62.9
FeO	12.7	12.7	12.9	12.9	13.2	13.1	13.6	13.2	13.5	13.6
MgO	22.1	22.1	22.2	22.1	22.0	22.0	22.3	21.8	21.8	21.6
CaO	.13	.11	.11	.14	.13	.13	.12	.08	.05	.10
TiO_2	.36	.34	.33	.31	.33	.35	.36	.38	.34	.38
Cr_2O_3	1.5	.89	.63	.61	.68	.82	.99	1.1	1.3	1.5
NiO	.32	.31	.30	.31	.30	.29	.30	.30	.30	.31
MnO	.11	.10	.11	.12	.10	.10	.08	.10	.10	.11
V_2O_5	.11	.10	.11	.10	.12	.10	.11	.12	.12	.11
Total	100.43	100.95	100.79	100.29	100.46	100.49	101.36	100.28	100.51	100.61

Loc., Sample	63-9-5bB	63-9-5cB	63-9-5dB	63-9-5eB	63-9-5fB	63-12-3	63-12-4	63-12-5	63-12-6	63-12-7
Group						Systematic	Systematic		Systematic	
Rock Type						OWeb	D		OWeb	
Al_2O_3	62.9	60.1	60.1	61.2	62.8	52.9	52.9	53.0	52.9	53.3
FeO	13.8	14.0	14.3	13.8	13.3	15.0	15.0	14.8	14.8	15.0
MgO	22.0	21.2	21.2	21.1	21.4	19.7	19.7	19.7	19.6	19.6
CaO	.07	.10	.13	.16	.09	.06	.09	.13	.08	.14
TiO_2	.38	.44	.42	.42	.38	.23	.22	.22	.20	.19
Cr_2O_3	1.5	3.7	4.0	2.9	1.6	11.0	11.0	10.9	11.0	10.4
NiO	.28	.28	.31	.29	.29	.38	.38	.39	.36	.35
MnO	.11	.12	.13	.12	.11	.16	.16	.15	.17	.17
V_2O_5	.11	.13	.12	.13	.11	.11	.11	.10	.10	.10
Total	101.15	100.07	100.71	100.12	100.08	99.54	99.56	99.39	99.21	99.25

Spinel

Loc., Sample[1]	63-12-9	63-12-10	63-12-11	63-12-12	63-12-13	63-17-1	63-17-2	63-17-3	63-17-4	63-17-2A
Group[2]						Systematic				
Rock Type[3]						L				
SiO_2						.27	.28	.23	.26	.24
Al_2O_3	53.6	53.7	53.2	53.0	53.4	56.0	55.7	54.8	54.2	55.3
FeO	14.7	15.3	15.1	15.4	14.0	11.7	11.6	11.8	11.8	11.1
MgO	19.7	19.0	19.1	18.9	19.2	20.6	20.6	20.7	20.6	20.6
CaO	.16	.13	.11	.07	.02	.11	.14	.10	.13	.18
TiO_2	.18	.20	.18	.22	.23	.20	.20	.20	.18	.19
Cr_2O_3	9.9	10.7	10.6	11.3	11.2	11.3	11.4	11.6	11.6	11.7
NiO	.38	.48	.47	.47	.52	.33	.34	.31	.32	.33
MnO	.16	.11	.12	.12	.11	.11	.12	.16	.11	.12
V_2O_5	.11									
Total	98.89	99.62	98.88	99.48	98.68	100.62	100.38	99.90	99.20	99.75

Loc., Sample	63-17-3A	63-17-4A	63-17-5A	63-17-6A	63-17-7A	63-17-1B	63-17-2B	63-17-3B	63-17-4B	63-17-5B
Group			Systematic		Systematic		Systematic		Systematic	
Rock Type			OWeb		L		OWeb		L	
SiO_2	.33	.25	.24	.24	.23	.21	.25	.29	.24	.26
Al_2O_3	55.5	55.7	54.6	55.0	55.3	55.7	55.5	54.7	55.1	55.1
FeO	11.8	11.8	11.8	11.8	12.0	11.9	11.8	11.7	11.7	11.7
MgO	20.8	20.7	20.6	20.6	20.8	20.9	20.7	20.6	21.0	20.4
CaO	.15	.19	.24	.11	.17	.15	.14	.19	.20	.12
TiO_2	.18	.19	.18	.19	.19	.17	.19	.17	.18	.19
Cr_2O_3	11.6	11.9	11.9	11.8	11.9	12.1	11.8	11.9	11.7	11.4
NiO	.32	.34	.33	.33	.32	.33	.35	.35	.31	.33
MnO	.14	.15	.11	.13	.12	.14	.13	.15	.12	.12
V_2O_5										
Total	100.82	101.22	100.00	100.20	101.03	101.60	100.86	100.05	100.55	99.62

Spinel

Loc., Sample[1]	63-17-1C	63-17-2C	63-17-3C	63-17-4C	63-17-5C	63-17-1D	63-17-2D	63-17-3D	63-17-4D	63-17-5D
Group[2]										
Rock Type[3]										
SiO_2	.37	.22	.24	.24	.26	.21	.20	.21	.26	.17
Al_2O_3	54.4	55.0	55.4	56.0	55.7	56.0	56.0	56.7	55.6	55.2
FeO	11.7	11.5	11.9	11.8	11.7	11.6	11.7	11.7	11.8	11.7
MgO	20.7	20.9	20.9	20.6	20.4	20.9	20.9	20.9	20.8	21.0
CaO	.16	.15	.14	.21	.24	.13	.13	.08	.14	.16
TiO_2	.19	.17	.19	.20	.20	.18	.17	.16	.18	.19
Cr_2O_3	11.4	11.5	12.0	11.7	11.7	10.8	10.9	11.2	11.2	11.2
NiO	.30	.33	.33	.33	.32	.32	.34	.36	.33	.36
MnO	.14	.13	.11	.12	.13	.14	.12	.14	.15	.11
V_2O_5										
Total	99.36	99.90	101.21	101.20	100.65	100.28	100.46	101.45	100.46	100.09

Loc., Sample
Group
Rock Type

Al_2O_3
FeO
MgO
CaO
TiO_2
Cr_2O_3
NiO
MnO
V_2O_5
Total

Spinel

Loc., Sample[1]	4-80-1	4-80-2	4-80-3	4-80-4	4-80-5	4-80-6	4-80-6a	4-80-7	4-80-8	4-80-9
Group[2]	Systematic						Systematic			
Rock Type[3]	OWeb						L			
Al_2O_3	60.6	60.4	61.9	62.9	62.2	61.5	60.6	61.8	61.1	60.7
FeO	11.7	11.9	11.5	11.4	11.4	11.7	11.7	11.6	11.4	11.6
MgO	21.2	21.1	21.4	21.4	21.5	21.3	21.2	21.4	21.2	21.4
CaO	.05	.05	.06	.08	.09	.07	.08	.10	.11	.08
TiO_2	.09	.09	.08	.07	.08	.08	.08	.08	.08	.08
Cr_2O_3	5.2	5.4	4.5	4.0	4.3	5.8	5.9	4.6	5.8	5.9
NiO	.26	.25	.25	.24	.22	.23	.24	.22	.23	.22
MnO	.10	.10	.10	.11	.10	.10	.10	.11	.10	.10
V_2O_5										
Total	99.20	99.29	99.79	100.20	99.89	100.78	99.90	99.91	100.02	100.08

Loc., Sample	4-80-10	4-80-11	4-80-12	4-80-13	4-80-14	4-80-15	4-80-1A	4-80-2A	4-80-3A	4-80-4A
Group						Systematic	Systematic			
Rock Type						OWeb	L			
Al_2O_3	60.1	59.5	60.8	61.4	61.1	60.9	58.0	58.7	59.1	58.1
FeO	11.5	11.5	11.5	11.4	11.6	11.5	11.7	11.9	11.8	11.8
MgO	21.3	21.3	21.5	21.3	21.3	21.1	20.7	21.0	20.7	20.9
CaO	.06	.08	.07	.09	.07	.06	.07	.08	.06	.08
TiO_2	.08	.10	.08	.10	.09	.09	.13	.11	.10	.11
Cr_2O_3	5.9	6.0	5.9	5.9	6.3	6.3	8.6	8.4	8.6	8.4
NiO	.22	.22	.21	.23	.21	.24	.22	.22	.21	.22
MnO	.10	.09	.11	.11	.12	.11	.11	.13	.11	.11
V_2O_5										
Total	99.26	98.79	100.17	100.53	100.79	100.30	99.75	100.54	100.68	99.72

Spinel

Loc., Sample[1]	4-80-5A	4-80-6A	4-80-6aA	4-80-7A	4-80-7aA	4-80-8A	4-80-9A	4-80-10A	4-80-11A
Group[2]	Systematic								
Rock Type[3]	OWeb								
Al_2O_3	58.3	59.7	59.5	58.3	58.4	58.9	59.8	61.5	60.4
FeO	11.8	11.9	11.9	11.7	11.7	11.8	11.6	11.7	11.7
MgO	20.9	20.9	20.9	20.8	21.0	21.1	21.3	21.1	21.4
CaO	.06	.07	.07	.10	.11	.09	.10	.10	.06
TiO_2	.12	.12	.10	.11	.09	.10	.09	.10	.09
Cr_2O_3	8.3	8.3	8.1	7.9	7.6	6.3	6.3	5.9	4.9
NiO	.24	.21	.21	.21	.22	.25	.25	.23	.22
MnO	.12	.10	.11	.11	.10	.10	.10	.10	.11
V_2O_5									
Total	99.84	101.30	100.89	99.23	99.22	98.64	99.54	100.73	98.88

Loc., Sample	4-80-12A	4-80-13A	4-80-15A
Group			
Rock Type			
Al_2O_3	61.8	60.8	60.7
FeO	11.5	11.5	11.5
MgO	21.3	21.2	21.1
CaO	.09	.06	.06
TiO_2	.09	.09	.08
Cr_2O_3	4.4	4.5	5.1
NiO	.24	.06	.23
MnO	.10	.15	.11
V_2O_5			
Total	99.52	98.36	98.88

Spinel

Loc., Sample[1]	18-2-1	18-2-2	18-2-3	18-34-1	18-34-6	18-75-1	18-78-1	18-78-2	18-78-3	18-78-4	18-78-5
Group[2]	B-G			B-G		Systematic	Cr-Di				
Rock Type[3]	L			Web		L	L				
Al_2O_3	18.5	18.3	18.5	42.2	38.1	40.5	44.5	43.4	41.1	42.5	43.9
FeO	13.7	17.8	17.7	15.1	16.5	15.4	18.0	18.1	18.3	17.8	17.6
MgO	15.0	15.0	14.9	19.1	17.5	19.4	18.6	18.0	18.7	18.5	17.9
Cr_2O_3	50.0	50.0	50.0	20.4	26.7	26.5	20.0	20.8	21.9	20.6	20.0
Total	97.20	101.10	101.10	96.80	98.80	101.80	101.80	100.30	100.00	99.40	99.40
Al	22.55	21.3	21.5	54.3	46.8	49.1	54.0	52.7	50.6	52.5	53.9
Cr	60.9	58.1	58.0	26.3	32.8	32.2	24.3	25.3	26.9	25.5	24.5
Fe	16.6	20.6	20.5	19.4	20.3	18.7	21.7	21.9	22.5	22.0	21.6

Loc., Sample

Group

Rock Type

Al_2O_3

FeO

MgO

Cr_2O_3

Total

Al

Cr

Fe

Spinel

Loc., Sample[1]	SAL-1	SAL-2	SAL-3	SAL-4	SAL-5	SAL-6	SAL-7	SAL-8	SAL-9	SAL-10
Group[2]	Systematic									
Rock Type[3]	L									
SiO_2	.27	.30	.29	.38	.28	.30	.29	.30	.30	.35
Al_2O_3	46.1	46.2	48.4	48.0	47.8	47.2	48.6	48.1	49.6	46.1
FeO	17.8	17.4	18.0	17.9	18.3	18.1	18.3	18.2	17.9	18.5
MgO	17.7	17.7	18.0	17.9	17.8	17.8	18.2	18.1	18.2	17.4
CaO	.20	.20	.23	.23	.18	.18	.24	.23	.20	.28
TiO_2	.59	.56	.64	.63	.67	.65	.72	.70	.68	.69
Cr_2O_3	16.4	16.6	15.3	14.9	15.5	15.1	14.3	13.7	12.7	16.2
NiO	.31	.30	.32	.32	.32	.32	.31	.31	.32	.28
MnO	.15	.16	.15	.15	.17	.17	.16	.16	.14	.15
V_2O_5										
Total	99.52	99.12	101.33	100.41	101.02	99.82	101.12	99.80	100.04	99.95

Loc., Sample	SAL-11	SAL-12	SAL-13	SAL-X	SAL-14	SAL-15	SAL-16
Group							
Rock Type							
SiO_2	.45	.35	.27	.31	.22	.34	.38
Al_2O_3	46.4	49.7	49.2	49.5	49.3	50.6	50.4
FeO	17.5	18.2	18.1	17.9	18.1	18.1	17.8
MgO	18.5	18.1	17.9	18.1	18.3	18.2	18.3
CaO	.19	.18	.22	.24	.23	.21	.20
TiO_2	.72	.68	.70	.68	.71	.70	.64
Cr_2O_3	15.6	12.8	13.8	12.8	13.3	12.8	12.3
NiO	.31	.31	.30	.31	.30	.32	.31
MnO	.16	.15	.15	.16	.16	.14	.15
V_2O_5							
Total	99.83	100.47	100.64	100.00	100.62	101.41	100.15

Spinel

Loc., Sample[1/]	33-204-1
Group[2/]	G
Rock Type[3/]	GWeb

Al_2O_3	63.9
FeO	14.3
MgO	18.9
CaO	
TiO_2	.01
Cr_2O_3	2.7
NiO	.26
MnO	
V_2O_5	
Total	100.07

Loc., Sample	
Group	
Rock Type	

Al_2O_3	
FeO	
MgO	
CaO	
TiO_2	
Cr_2O_3	
NiO	
MnO	
V_2O_5	
Total	

Amphibole

Loc., Sample[1]	32-72-1	32-72-2	32-72-3	32-72-4	32-72-5	32-72-6	32-72-7	32-72-8	32-72-9
Group[2]	Systematic		Systematic						
Rock Type[3]	Vein		L						
SiO_2	40.8	42.7	43.4	43.3	43.1	43.3	43.3	43.3	42.9
Al_2O_3	14.2	13.7	13.8	14.3	15.5	15.4	15.3	15.3	15.5
FeO	13.6	7.9	6.5	6.3	6.1	5.9	5.8	5.6	5.4
MgO	13.2	15.3	16.3	16.6	16.2	16.7	16.7	16.7	16.8
CaO	10.8	10.9	10.7	10.7	11.4	10.6	10.7	10.6	10.6
Na_2O	2.7	2.8	2.8	3.0	3.0	3.1	3.2	3.2	3.2
K_2O	1.3	1.2	1.2	1.1	.97	.76	.72	.69	.54
TiO_2	4.3	3.6	2.6	1.8	1.3	1.1	1.3	1.4	1.5
Cr_2O_3		.20	.57	.85	1.1	1.1	1.0	.99	1.0
MnO									
Total	100.90	98.30	97.87	97.95	98.67	97.96	98.02	97.78	97.44

Loc., Sample	32-72-1A	32-72-2A	32-72-3A	32-72-1B	32-72-2B	32-72-3B	32-72-4B	32-72-5B
Group			Systematic	Systematic				
Rock Type			Vein	L				
SiO_2	43.2	43.1	40.9	43.1	43.0	42.7	43.1	42.9
Al_2O_3	15.4	13.7	14.1	15.5	15.4	15.3	15.5	15.3
FeO	5.2	6.4	10.5	4.9	4.9	4.9	5.0	5.1
MgO	16.9	16.3	13.4	16.8	16.8	16.9	16.8	16.8
CaO	10.6	10.8	11.0	10.7	10.7	10.8	10.9	10.6
Na_2O	3.3	2.8	2.7	3.1	3.1	3.2	3.2	3.1
K_2O	.43	1.2	1.3	.72	.67	.56	.55	.56
TiO_2	1.8	2.8	4.4	1.9	2.0	2.0	2.0	1.9
Cr_2O_3	.95	.50	.01	.95	.94	.89	.98	.91
MnO								
Total	97.78	97.60	98.31	97.67	97.51	97.25	98.03	97.17

Amphibole

Loc., Sample[1]	32-72-1	32-72-2	32-72-3	32-72-4	32-72-5	32-72-6	32-72-7	32-72-8	32-72-9	32-72-1A
Group[2]	Systematic		Systematic							
Rock Type[3]	Vein		L							
SiO_2	40.8	42.7	43.4	43.3	43.1	43.3	43.3	43.3	42.9	43.2
Al_2O_3	14.2	13.7	13.8	14.3	15.5	15.4	15.3	15.3	15.5	15.4
FeO	13.6	7.9	6.5	6.3	6.1	5.9	5.8	5.6	5.4	5.2
MgO	13.2	15.3	16.3	16.6	16.2	16.7	16.7	16.7	16.8	16.9
CaO	10.8	10.9	10.7	10.7	11.4	10.6	10.7	10.6	10.6	10.6
TiO_2	4.3	3.6	2.6	1.8	1.3	1.1	1.3	1.4	1.5	1.8
Cr_2O_3		.2	.57	.85	1.1	1.1	1.0	.99	1.0	.95
Na_2O	2.7	2.8	2.8	3.0	3.0	3.1	3.2	3.2	3.2	3.3
K_2O	1.3	1.2	1.2	1.1	.97	.76	.72	.69	.54	.43
Total	100.9	98.3	97.87	97.95	98.67	97.96	98.02	97.78	97.44	97.78

Loc., Sample	32-72-2A	32-72-3A	32-72-1B	32-72-1B	32-72-2B	32-72-3B	32-72-4B	32-72-5B	32-72-6B	33-1-1
Group		Systematic	Systematic							Systematic
Rock Type		Vein	L							Vein
SiO_2	43.1	40.9	43.1	43.0	42.7	43.1	42.9	42.8	43.5	39.9
Al_2O_3	13.7	14.1	15.5	15.4	15.3	15.5	15.3	15.3	15.3	13.5
FeO	6.4	10.5	4.9	4.9	4.9	5.0	5.1	5.1	5.4	9.8
MgO	16.3	13.4	16.8	16.8	16.9	16.8	16.8	16.8	16.8	13.8
CaO	10.8	11.0	10.7	10.7	10.8	10.9	10.6	10.7	10.7	10.9
TiO_2	2.8	4.4	1.9	2.0	2.0	2.0	1.9	1.9	2.0	3.7
Cr_2O_3	.50	.01	.95	.94	.89	.98	.91	.89	.89	.12
Na_2O	2.8	2.7	3.1	3.1	3.2	3.2	3.1	3.1	3.2	2.7
K_2O	1.2	1.3	.72	.67	.56	.55	.56	.54	.51	1.3
Total	97.60	98.31	97.67	97.51	97.25	98.03	97.17	97.13	98.30	95.72

Amphibole

Loc., Sample[1]	33-1-2	33-1-3	33-1-4	33-1-5	33-1-6	33-1-7	33-1-8	33-1-9	33-1-10	33-1-11
Group[2]				Systematic						
Rock Type[3]				L						
SiO_2	41.1	42.1	42.9	42.9	43.2	42.7	43.3	42.9	42.9	43.0
Al_2O_3	13.4	13.0	13.0	12.9	13.4	13.8	14.4	14.8	14.9	15.0
FeO	9.2	8.1	7.0	7.1	6.8	6.8	6.6	6.2	6.0	5.7
MgO	14.6	15.6	16.2	16.4	16.5	16.7	16.7	16.8	16.9	17.1
CaO	10.9	10.9	11.0	10.9	10.8	10.8	10.7	10.8	10.8	10.8
TiO_2	3.6	3.2	2.9	2.8	2.0	1.6	1.2	1.2	1.3	1.4
Cr_2O_3	.09	.29	.46	.56	1.0	1.1	1.1	1.2	1.2	1.1
Na_2O	2.7	2.8	2.8	2.8	2.9	3.0	3.0	3.2	3.3	3.4
K_2O	1.4	1.3	1.3	1.3	1.1	1.0	.76	.53	.40	.29
Total	96.99	97.29	97.56	97.66	97.70	97.50	97.76	97.63	97.70	97.79

Loc., Sample	33-1-12	33-1-1A	33-1-2A	33-1-3A	33-1-4A	33-1-5A	33-1-1B	33-1-2B	33-1-3B	33-1-4B
Group										
Rock Type										
SiO_2	43.0	42.7	42.9	43.0	42.5	42.9	42.7	43.0	43.5	43.7
Al_2O_3	15.0	15.3	15.4	15.3	15.2	15.1	15.5	15.3	15.4	15.5
FeO	5.7	4.8	4.9	5.2	5.4	5.6	4.7	4.7	4.8	4.7
MgO	16.9	17.0	17.0	17.0	16.8	17.0	17.1	17.3	17.5	17.4
CaO	10.8	10.8	10.9	10.8	10.9	10.8	10.9	11.0	10.9	10.9
TiO_2	1.4	1.8	1.7	1.6	1.5	1.4	1.7	1.8	1.8	1.7
Cr_2O_3	1.1	1.1	1.2	1.1	1.1	1.2	1.2	1.1	1.1	1.2
Na_2O	3.3	3.5	3.5	3.5	3.4	3.4	3.5	3.5	3.5	3.5
K_2O	.28	.04	.05	.08	.15	.26	.03	.02	.01	.02
Total	97.48	97.04	97.55	97.58	96.95	97.66	97.33	97.72	98.51	98.62

	Amphibole									
Loc., Sample[1]	33-1-1C	33-1-2C	33-1-3C	33-1-4C	33-2-1	32-52-1	33-52-2	33-52-3	32-52-4	33-104-1
Group[2]					Al-Aug	Cr-Di				Systematic
Rock Type[3]					L	L				L
SiO_2	43.4	43.4	43.5	43.6	40.2	41.0	41.4	44.5	41.7	38.5
Al_2O_3	15.3	15.2	15.5	15.2	15.1	15.0	15.1	15.3	14.8	15.1
FeO	4.7	4.6	4.7	4.6	7.8	5.6	5.6	5.3	5.4	13.8
MgO	17.3	17.3	17.4	17.3	15.9	17.9	17.8	17.8	18.0	11.4
CaO	10.6	10.8	10.9	10.8	11.1	10.7	10.9	10.7	10.3	10.2
TiO_2	1.8	1.8	1.7	1.9	2.7	1.3	1.1	1.0	1.1	5.9
Cr_2O_3	1.1	1.1	1.1	1.1	.56	1.0	1.2	1.0	.92	
Na_2O	3.5	3.6	3.5	3.6	2.6	3.4	3.3	3.1	3.1	2.1
K_2O	.02	.02	.03	.03	.99	.28	.27	.46	.52	1.50
MnO					.09	.05	.04	.04	.03	.26
Total	97.72	97.82	98.33	98.13	97.04	96.23	96.71	99.20	95.87	98.76

Loc., Sample	33-104-2	33-104-3	33-104-4	33-104-5	33-104-6	33-104-1V	33-104-2V	33-104-3V
Group						Systematic		
Rock Type						Vein		
SiO_2	38.4	42.5	41.8	43.2	43.2	39.1	40.4	43.1
Al_2O_3	13.8	13.1	14.2	13.2	14.6	14.0	14.4	12.6
FeO	12.5	7.6	7.0	7.3	6.4	12.4	11.3	6.8
MgO	12.8	15.3	16.2	15.7	16.3	12.0	13.6	16.5
CaO	11.2	10.0	10.8	10.5	10.9	10.5	10.7	10.8
TiO_2	5.9	3.5	1.5	3.0	1.6	5.4	5.4	3.3
Cr_2O_3								
Na_2O	2.3	2.7	2.9	2.8	3.1	2.6	2.6	2.7
K_2O	1.2	1.3	.93	1.3	.89	1.5	1.4	1.2
MnO	.21	.20	.09	.16	.09			
Total	98.31	96.20	95.42	97.16	97.08	97.50	99.80	97.00

Amphibole

Loc., Sample[1]	23-11-1	23-11-2	23-11-3	23-11-4	23-11-5	23-11-6	23-11-7	23-11-8	23-11-9	23-11-10
Group[2]	Systematic						Systematic			
Rock Type[3]	Vein						L			
SiO_2	42.1	42.6	42.0	42.6	42.5	43.3	42.6	42.8	43.2	42.7
Al_2O_3	13.8	13.5	13.6	13.5	13.5	13.9	14.9	15.1	15.6	15.6
FeO	7.2	7.0	6.9	7.1	7.0	6.8	6.8	6.4	6.1	5.5
MgO	15.6	15.9	15.9	16.0	16.1	16.2	16.0	16.5	16.6	17.0
CaO	10.9	11.0	10.9	11.0	10.9	10.8	10.8	10.8	10.7	10.9
TiO_2	3.6	3.5	3.5	3.5	3.4	2.6	1.8	1.7	1.6	1.8
Cr_2O_3	.23	.33	.36	.37	.41	.70	.98	.76	.90	.83
Na_2O	2.6	2.6	2.7	2.7	2.7	2.8	2.9	2.9	2.9	3.1
K_2O	1.4	1.4	1.4	1.4	1.3	1.2	1.1	.97	.81	.68
Total	97.43	97.83	97.26	98.17	97.81	98.30	97.88	97.93	98.41	98.11

Loc., Sample	23-11-11	23-11-1A	23-11-2A	23-11-3A	23-11-4A	23-11-5A	23-11-1B	23-11-3B	23-11-4B	23-11-5B
Group							Systematic	Systematic		
Rock Type							Vein	L		
SiO_2	42.3	42.4	43.3	42.4	42.9	43.0	42.3	42.3	43.9	43.6
Al_2O_3	15.3	15.4	15.9	15.6	15.6	15.7	14.1	15.6	15.7	15.8
FeO	5.3	4.8	4.9	4.8	4.9	4.8	7.9	4.8	5.0	5.0
MgO	17.0	17.2	17.1	17.1	17.0	17.2	15.1	17.2	17.2	17.2
CaO	10.8	11.0	11.0	10.9	10.9	10.8	11.1	10.7	10.6	10.7
TiO_2	2.1	2.2	1.6	2.0	2.2	2.1	4.0	2.4	2.4	2.3
Cr_2O_3	.80	.84	.93	.82	.83	.83	.13	.63	.80	.87
Na_2O	3.2	3.2	3.1	3.0	3.1	3.1	2.5	1.8	3.4	3.2
K_2O	.52	.54	.85	.91	.63	.68	1.4	.11	.36	.35
Total	97.32	97.58	98.68	97.53	98.06	98.21	98.53	95.54	99.36	99.32

	Amphibole								
Loc., Sample[1/]	23-11-6B	23-11-7B	23-11-8B	23-11-9B	28-2-1	28-4-1	28-4-2	28-6-1	28-6-3
Group[2/]					Al-Aug	Al-Aug		Al-Aug	
Rock Type[3/]					CP	CP		CP	
SiO_2	43.9	43.0	44.2	43.5	37.5	39.9	38.0	39.0	39.9
Al_2O_3	16.0	16.0	16.0	15.6	13.9	14.8	14.6	14.1	13.9
FeO	5.0	4.9	4.8	4.8	13.3	12.5	12.0	13.7	13.8
MgO	17.2	17.2	17.2	17.3	12.1	12.7	12.7	12.0	11.9
CaO	10.7	10.8	10.9	10.8	13.3	10.4	10.4	10.9	10.2
TiO_2	2.3	2.2	2.1	2.2	7.1	5.3	5.5	5.3	5.1
Cr_2O_3	.83	.85	.83	.80		.01	.00		
Na_2O	3.3	3.3	3.2	3.2	2.4	2.7	2.7	2.5	2.4
K_2O	.38	.45	.45	.68	.96	.99	.85	1.3	1.1
MnO					.08				
Total	99.61	98.70	99.68	98.88	100.56	99.30	96.75	98.80	98.30

Loc., Sample	
Group	
Rock Type	
SiO_2	
Al_2O_3	
FeO	
MgO	
CaO	
TiO_2	
Cr_2O_3	
Na_2O	
K_2O	
Total	

Amphibole

Loc., Sample[1]	Ag-2-1	Ag-2-2
Group[2]	Cr-Di	
Rock Type[3]	L	
SiO_2	44.6	41.7
Al_2O_3	10.2	14.5
FeO	10.3	9.9
MgO	15.5	15.8
CaO	12.4	11.2
TiO_2	1.7	1.4
Cr_2O_3	.51	.49
Na_2O	2.5	2.9
K_2O	.64	.36
Total	98.35	98.25

Loc., Sample
Group
Rock Type
SiO_2
Al_2O_3
FeO
MgO
CaO
TiO_2
Cr_2O_3
Na_2O
K_2O
Total

PHLOGOPITE

Loc., Sample[1]	33-2-1	33-2-1	33-40-1	63-27-1	Ag-2-1	Ag-2-1	Ag-2-2	Ag-2-2
Group[2]	Al-Aug		Cr-Di		Cr-Di			
Rock Type[3]	L		L		L			
	Center	Edge			Center	Edge	Center	Edge
SiO_2	39.8	39.7	39.9	40.4	41.1	38.7	42.8	37.0
Al_2O_3	15.6	16.2	15.9	16.2	13.6	12.5	13.5	12.3
FeO	7.2	6.9	5.8	3.1	4.9	11.0	4.7	10.6
MgO	20.9	21.3	22.9	23.1	24.1	15.9	24.0	16.6
CaO					.19	.29	.13	.14
Na_2O	1.2	1.2	1.3	.49	1.9	2.1	2.2	2.3
K_2O	8.8	8.3	8.1	9.5	9.8	9.2	9.7	9.0
TiO_2	2.7	1.1	.70	1.8	2.2	7.8	2.2	8.1
Cr_2O_3	.61	1.1	1.3	2.6	.66		.68	.02
MnO	.03	.05	.06	.03				
F				.24				
Rb	.03	.03	.03	.01				
Total	96.87	95.88	95.99	97.47	98.45	97.49	99.91	96.06

Analyzed by Martin Prinz

INTERSTITIAL GLASS

Loc., Sample[1]	33-2-1	33-40-1
Group[2]	Al-Aug	Cr-Di
Rock Type[3]	L	L
SiO_2	45.6	50.2
Al_2O_3	22.4	22.9
FeO	7.1	5.8
MgO	6.4	4.8
CaO	11.1	8.7
Na_2O	3.2	5.2
K_2O	2.7	.96
TiO_2	1.8	.44
MnO	.11	.10
P_2O_5	.07	
Total	100.48	99.10

Analyzed by Martin Prinz

Loc., Sample[1]	17-1	17-1	17-1	17-1	17-1	17-5	17-5	17-5	17-8
Group[2]	B-G					B			B-G
Mineral[3]	Cpx					Cpx			Cpx
SiO_2	51.2	51.5	52.1	51.1	51.4	50.4	50.4	50.5	51.0
Al_2O_3	5.8	6.0	6.4	6.3	5.9	6.6	6.9	6.6	7.6
FeO	4.2	4.3	4.3	4.3	4.3	4.5	4.6	4.5	4.6
MgO	17.2	17.3	17.6	17.7	17.5	16.3	17.0	16.3	17.2
CaO	17.5	17.4	17.4	17.6	17.3	18.5	18.5	18.5	17.4
Na_2O	.77	.79	.74	.74	.82	.77	.78	.76	.74
K_2O	.07	.07	.03	.03	.07	.07	.07	.07	.02
TiO_2	.43	.46	.42	.42	.49	.48	.59	.60	.53
Cr_2O_3	1.4	1.4	1.4	1.4	1.4	.76	.76	.77	.99
Total	98.57	99.22	100.39	99.59	99.18	98.38	99.6	98.6	100.08
Ca	39.2	38.9	38.5	38.5	38.5	41.4	40.4	41.4	38.8
Mg	53.5	53.6	54.1	54.1	54.1	50.7	51.7	50.7	53.2
Fe	7.3	7.5	7.4	7.3	7.5	7.9	7.9	7.9	8.0

Loc., Sample	17-8	17-8	17-13	17-13	17-13	33-103	33-103	34-103	34-103
Group			B-G			Al-Aug		Al-Aug	
Mineral			Cpx			Amph.		Amph.	
						Center	Edge	Center	Edge
SiO_2	51.2	50.4	51.9	52.0	52.0	40.1	42.0	38.9	38.5
Al_2O_3	7.5	7.5	5.7	5.5	6.0	14.6	14.7	14.1	14.2
FeO	4.6	4.6	4.4	4.2	4.4	9.9	9.9	12.8	12.5
MgO	17.1	17.3	17.9	17.6	18.0	13.2	13.6	12.1	11.8
CaO	17.7	17.5	17.2	17.0	17.3	11.0	11.1	10.8	10.7
Na_2O	.73	.75	.87	.84	.88	2.3	2.3	1.6	2.3
K_2O	.03	.02	.09	.06	.08	1.8	1.8	1.6	1.7
TiO_2	.49	.50	.46	.43	.46	6.8	6.6	6.2	6.4
Cr_2O_3	.96	.98	1.5	1.6	1.4				
Total	100.31	99.55	100.02	99.23	100.52	99.70	102.00	98.10	98.10
Ca	39.3	38.7	37.7	38.0	37.8				
Mg	52.7	53.3	54.8	54.7	54.7				
Fe	7.9	8.0	7.5	7.3	7.5				

GARNET

Loc., Sample[1]	33-204-1	33-204-2	33-204-3
Group[2]	G		
Rock Type[3]	GWeb		
SiO_2	41.1	41.1	41.2
Al_2O_3	25.2	24.9	23.7
FeO	11.7	11.7	11.5
MgO	18.2	18.7	18.1
CaO	5.5	5.6	5.6
TiO_2	.15	.06	.21
Cr_2O_3	.06	.07	.08
Na_2O			
K_2O			
Total	102.31	102.47	100.79

GARNET

Loc., Sample[1]	SAL-1	SAL-2	SAL-3	SAL-4	SAL-5	SAL-6	SAL-7	SAL-8	SAL-9
Group[2]	Systematic								
Rock Type[3]	GCP								
SiO_2	41.0	40.8	40.6	40.7	40.7	41.7	41.9	42.1	42.5
Al_2O_3	20.4	20.1	20.2	20.2	20.3	21.1	21.0	21.4	21.7
FeO	14.9	16.2	17.2	17.2	17.3	12.9	12.5	12.1	11.3
MgO	17.7	16.7	16.3	16.2	16.3	19.1	19.6	19.8	20.3
CaO	4.8	5.0	4.8	4.8	4.8	4.6	4.7	4.8	4.6
TiO_2	.42	.43	.41	.38	.37	.38	.35	.38	.34
Cr_2O_3	.11	.39	.18	.15	.14	.13	.14	.14	.15
Na_2O	.04	.04	.05	.03	.05	.05	.04	.04	.04
Total	99.71	100.01	100.09	100.01	100.31	100.32	100.58	101.12	101.29
Ca	11.7	12.2	11.7	11.8	11.7	11.2	11.3	11.5	11.0
Fe	28.3	20.9	32.8	32.9	33.0	24.4	23.4	22.6	21.2
Mg	60.0	56.8	55.5	55.3	55.3	64.4	65.4	65.9	67.8

Loc., Sample	SAL-3A	SAL-4A	SAL-5A	SAL-6A
Group				
Rock Type				
SiO_2	40.8	40.4	40.6	40.7
Al_2O_3	20.5	20.5	20.6	20.5
FeO	17.5	17.5	17.4	17.3
MgO	16.0	15.9	16.0	16.2
CaO	4.9	5.0	5.0	4.7
TiO_2	.35	.36	.35	.37
Cr_2O_3	.08	.12	.10	.15
Na_2O	.04	.04	.04	.04
Total	100.54	100.16	100.44	100.30
Ca	12.0	12.3	12.2	11.5
Fe	33.5	33.5	33.3	33.2
Mg	54.5	54.2	54.5	55.3

Appendix VI. Systematic Mineral Compositional Trends in Composite Xenoliths

Composite Xenoliths Containing Members of More Than One Main Group

As described in Appendix III, composite xenoliths containing more than one subtype of the same group, whether mafic or ultramafic, are of widespread occurrence. Moreover, composite xenoliths that contain different textural variants of the same subtypes are also found. In addition to these, we have sought and collected a comparatively large number of composite xenoliths that contain members of more than one main group. These important rocks help establish relative ages of the main groups, intergradations between main groups, and establish the close proximity of different rock types in their place of origin.

Gabbroids with igneous textures have been found as thin veins in Cr-diopside peridotite (fig. VI-1a, b), Al-augite clinopyroxenite (fig. VI-1c), olivine-rich Al-augite wehrlite, and Al-augite olivine websterite. The gabbroid veins resemble gabbroids that form isolated xenoliths at the same localities.

Composite xenoliths in which metagabbroids are in contact with Cr-diopside peridotite are scarce but are more common than unmetamorphosed gabbroids in contact with peridotite. Such xenoliths (fig. VI-1d, e) have been found at three localities (Table 1, nos. 2, 40, 67). At two of these localities (nos. 1, 40) the metagabbroids were thin dikes that subsequently have been metamorphosed. In one example, a partly metamorphosed gabbroid dike crosscuts two thin Cr-diopside websterite layers in lherzolite. A single composite xenolith from Kilbourne Hole (loc. 67) consists of two layers of lherzolite interleaved in sharp contact with two layers of metagabbronorite grading to metawebsterite. The metagabbro component of this composite xenolith (fig. VI-1f) is closely similar to many larger isolated metagabbro xenoliths from the same locality. At two of these localities (nos. 40, 67) both peridotite and gabbroid xenoliths are abundant, and diligent search may turn up more composite xenoliths (8 have been found at locality no. 40, 1 at locality 67). Two thin feldspathic veins in peridotite were found at locality 2 although isolated gabbroid xenoliths are uncommon there; several lherzolite xenoliths are feldspathic. This is also true of locality nos. 39 and 40, but no feldspathic lherzolites are known from Kilbourne Hole (no. 67).

The most common composite xenoliths with members of two groups in contact are hornblendite (kaersutite ± Ti-phlogopite) veins of the Al-augite group in Cr-diopside or peridotite transitional between the Cr-diopside and Al-augite group (fig. VI-1g, h), and less commonly in Al-augite pyroxenites. Systematic compositional variations occur in peridotite adjacent to some xenoliths veined by hornblendite (Best, 1974b; Francis, 1976; Stewart and Boettcher, 1977; Boettcher and others, 1979; Wilshire and others, 1980) yielding transitional peridotites but this relationship is not always distinguishable in hand specimen. Crosscutting relationships clearly indicate that the hornblendites post-date anhydrous mineral layering in the peridotite; moreover, they commonly post-date the youngest metamorphic event in the peridotite (Wilshire and Trask, 1971). Composite xenoliths of this type are known from 8

localities (nos. 25, 28, 32, 33, 40, 41, 63, 64).

Al-augite pyroxenite dikes occur in Cr-diopside lherzolite at Pinchot (no. 11), Kilbourne Hole (no. 67), San Carlos (no. 63), and Wikieup (no. 42). In most samples, the pyroxenite is separated from Cr-diopside lherzolite by a zone of comparatively Fe-rich peridotite that is assigned to the Al-augite group (Wilshire and Shervais, 1974); however, other A1-Aug pyroxenite dikes are in direct contact with Cr-diopside peridotite. Rare xenoliths show Al-augite pyroxenite dikes crosscutting layering of Cr-diopside websterite and lherzolite. More commonly, Al-augite pyroxenites crosscut metamorphic foliation of Cr-diopside peridotite.

Composite xenoliths with feldspathic peridotite are rare; two examples (locality no. 40) have feldspathic olivine websterite in contact with nonfeldspathic lherzolite. Composite xenoliths of Cr-diopside peridotite and members of the bottle-green pyroxene group are not known, but would be extremely difficult to recognize because of the lack of distinctive characteristics of bottle-green pyroxene peridotite. However, locality 39 yielded one xenolith with bottle-green pyroxene pyroxenite in planar contact with Al-augite pyroxenite. Composite xenoliths composed of garnetiferous rocks and peridotite are rare but xenoliths with garnet pyroxenite in contact with spinel lherzolite occur at Salt Lake Crater, Oahu.

Systematic compositional data were obtained on seven composite xenoliths containing two or more subtypes of the Cr-diopside group, three composite xenoliths containing subtypes of the Al-augite group, three composite xenoliths in which the peridotite member is transitional between Cr-diopside and Al-augite groups, one peridoitite cut by a pyroxenite of the "bottle green" pyroxene group, one peridotite of the Cr-diopside group in contact with garnet clinopyroxenite, three peridotites of the Cr-diopside or transitional groups cut by hornblendite veins, and one xenolith composed of two pyroxenitic subtypes of the Al-augite group and a hornblendite vein. The complete mineral analyses are given in Appendix V.

Cr-diopside Group Subtypes.

Sample Ep-1-123, Potrillo maar, New Mexico is a fragment of a cored bomb. The core is a well-rounded composite xenolith measuring 8 X 6 X 5 cm that consists of a lherzolite layer about 2 cm thick and an olivine websterite layer about 3 cm thick (fig. VI-1i; Table VI-1). The contact between the two lithologies is gradational over a short distance. Textures of both lithologies are allotriomorphic granular. The lherzolite has scattered, strongly deformed relics of olivine; the websterite has more deformed relics of olivine and also has deformed relics of orthopyroxene with exsolution lamellae of clinopyroxene.

Probe traverses cross the contact between the two lithologies over a linear distance of 2.6 cm in two thin sections (fig. VI-2). Cr and Al in spinel vary antithetically, with the Al/Cr ratio decreasing substantially in the websterite toward the contact with lherzolite. Mg/(Mg+Fe) ratios of orthopyroxene and clinopyroxene increase slightly from websterite into lherzolite. The Ca content of olivine varies widely with a possible trend to higher average values from websterite to lherzolite. Ti and Cr contents of clinopyroxene do not vary significantly across the contact.

Sample SQ-1-80, San Quintin, Baja, California is a bomb, the core of which is a blocky, subangular composite xenolith 13 X 12 X 6 cm. An olivine websterite layer 2.6 cm thick is sandwiched by lherzolite with less distinct layers of olivine websterite as much as 1 cm thick (Table VI-2). All layers are parallel and have gradational contacts with lherzolite (fig. VI-1j). Textures of both lithologies are porphyroclastic. The peridotite has relics of deformed olivine, orthopyroxene and clinopyroxene in a foliated matrix. The websterite has a much highr proportion of relic grains. Pyroxene relics have exsolution lamellae.

Probe traverses cross from lherzolite through the main websterite layer, into lherzolite and part of one of the more diffuse layers, a linear distance of 6.1 cm. Significant antithetic variations of Cr and Al occur in spinel (fig. VI-3) with Al/Cr decreasing greatly in the websterite toward the lherzolite. Spinels in lherzolite between the websterite layers have marked trends toward lower Al/Cr with distance from the websterites, but a a similar change to lower Al/Cr occurs within the opposite side of the main websterite layer. Mg/(Mg+Fe) of both pyroxenes increases from a minimum in the center of the main websterite layer to higher values in the lherzolite. There is no variation in Mg/(Mg+Fe) in pyroxenes or olivine, or in Ti and Cr of clinopyroxene on one side of the central websterite layer. Al contents of both pyroxenes decrease significantly from the main websterite layer into adjacent lherzolite. Incomplete Ca determinations for olivine indicate rapid decrease of this component from websterite to lherzolite.

Sample Sc-1-6, San Carlos, Arizona is a broken fragment of an inclusion from the upper mesa-capping lava flow (Frey and Prinz, 1976) whose original triaxial dimensions were greater than 18 X 9 X 9 cm. The xenolith consists of olivine websterite more than 8 cm thick and harzburgite more than 10 cm thick. A layer of olivine-rich harzburgite about 3 cm thick along the contact with websterite grades into coarser-grained harzburgite that contains about 5% more orthopyroxene (fig. VI-1k; Table VI-3). The contacts between these lithologies are fairly sharp but gradational, and are parallel to one another. The texture of the peridotite is allotriomorphic granular grading to porphyroclastic with development of unfoliated polygonally recrystallized texture. The websterite has an equigranular mosaic texture.

Probe traverses span parts of a linear distance of 10 cm across all the lithologic variants. The principal chemical variations occur within the websterite and a narrow border zone with the olivine-rich harzburgite fig VI-4). The trends extend farther into harzburgite, but for some elements the differences are too small to be reliably detected by probe techniques. The Al/Cr ratio of spinel decreases markedly within the websterite toward the harzburgite, the steepest gradient occurring in a zone 1.5 cm thick adjacent to the harzburgite. Mg/(Mg+Fe) ratios of both pyroxenes and olivine increase from the center of the websterite toward harzburgite, and Ti of clinopyroxene decreases and Cr may increase in websterite toward the harzburgite. Al contents of both pyroxenes decrease in websterite toward the harzburgite, and the Ca content of olivine decreases from websterite into harzburgite.

Sample SC-1-3, San Carlos, Arizona is a blocky, subangular inclusion from the upper, mesa-capping lava flow. Triaxial dimensions are 18 X 8.5 X 6 cm. The xenolith consists of lherzolite cut by two intersecting olivine websterite layers (fig. VI-1l; Table 4). The older layer is a thin (70 mm) olivine-poor

websterite that is crosscut and offset 2.8 cm by a 5 cm thick websterite layer. The thicker layer is gradationally zoned from olivine + clinopyroxene-rich margins to a more orthopyroxene-rich core. Contacts between websterite and lherzolite are moderately sharp and irregular. The textures of all lithologies are porphyroclastic. The peridotite has relics of deformed olivine in a polygonally recrystallized matrix. The pyroxenite has scarce pyroxene relics with exsolution lamellae in an unfoliated polygonally recrystallized matrix. The websterites are finer grained than the lherzolite.

Two probe traverses cross lherzolite and the thickest websterite layer and lherzolite between the thin and thick websterites for a total linear distance of 8.4 cm. The Al/Cr ratio in spinels in the thickest websterite are asymmetrical within the layer, but decrease markedly into lherzolite on both sides of the layer (fig. VI-5). The Al/Cr ratio in spinels across 2 cm of lherzolite separating the websterites (right side of figure VI-5) is abnormal due to proximity to the pyroxenites. The Mg/(Mg+Fe) ratios for both pyroxenes and olivine show minima that are asymmetrically disposed in the thick websterite, but the ratios increase in lherzolite from the thicker toward the thinner websterite. Cr and Ti of clinopyroxene are not antithetic, but vary systematically with proximity to the websterites. Alumina contents of both pyroxenes decrease slightly from the websterites into lherzolite. Ca content of olivines is erratic and does not show a systematic trend across lithologies.

Sample Ki-5-1, Cima volcanic field, California is a subrounded block collected from unconsolidated ejecta. It is 5 X 4 X 0.8 cm, and consists of two 5 mm-thick layers of olivine websterite separated by harzburgite 2.5 mm thick. The websterite layers are also bounded by harzburgite about 10 mm thick which grades away from the layers into lherzolite (fig. VI-1m; Table VI-5). The lherzolite is distinctly foliated parallel to the lithologic layering. Textures of all lithologies are protogranular transitional to porphyroclastic.

Probe traverses cross all lithologies of the xenolith for a linear distance of 4 cm. Significant compositional trends are not symmetrical with respect to the websterite layers (fig. VI-6). Al/Cr ratios of spinel change markedly across the websterite layers but are much higher in lherzolite on one side of the layers than on the other. The Mg/(Mg+Fe) ratio of pyroxenes increases from one layer into lherzolite, but does not vary across the other. The Al content of clinopyroxene decreases from one websterite into lherzolite, and increases in the other websterite to values similar to those in lherzolite, whereas the Al content of orthopyroxene is erratic in one websterite and does not vary across the other websterite and lherzolite adjacent to it. The Ca content of olivine decreases slightly from both websterites into lherzolite.

Sample SC-1-12, San Carlos, Arizona is a fragment of an inclusion from the upper, mesa-capping lava flow. Its original triaxial dimensions were greater than 9 X 7 X 7 cm. The xenolith consists of olivine websterite cut by a 1.3 cm thick dunite layer with moderately sharp, irregular contacts (fig. VI-1n; Table VI-6). The textures of both lithologies are porphyroclastic with pyroxene and olivine relics in a weakly foliated matrix.

Probe traverses cross a linear distance of 2.5 cm. Substantial variation is seen only in Ca content of olivine and Al content of orthopyroxene, but

neither trend is symmetrical with respect to the dunite (fig. VI-7).

Sample SC-1-17, San Carlos, Arizona is a fragment of an inclusion from the upper, mesa-capping lava flow. Its original triaxial dimensions were greater than 9.5 X 8.4 X 6 cm. The inclusion consists of lherzolite cut by intersecting olivine websterite layers 0.5 and 0.6 cm thick, one of which is diffuse (fig. VI-1o; Table VI-7). Contacts with the lherzolite are irregular and gradational over short distances. Textures of all lithologies are porphyroclastic wth olivine and pyroxene relics in an unfoliated polygonally recrystallized matrix.

Probe traverses cross all lithologies over a linear distance of 11.6 cm There are no compositional trends systematically related to the websterite layers (fig. VI-8). Spinels and clinopyroxenes have small variations in alumina (to nearly 3 wt. %) and Cr (to 1 wt. %), and the Ca content of olivine varies erratically across the traverse. Other compositional parameters do not vary significantly across the entire traverse.

Al-augite Group Subtypes.

Sample Ba-1-24, Dish Hill, California is a volcanic bomb, the core of which is a blocky subangular xenolith measuring 12 X 8 X 8 cm. The xenolith consists of four layers to 1.5 cm thick of olivine websterite in more olivine-rich olivine websterite (fig. VI-1p; Table VI-8); all lithologies contain minor amphibole that has been partly melted. Contacts between lithologies are moderately sharp. The olivine-poor websterites are coarse-grained and have allotriomorphic-granular textures. Relic clinopyroxenes have well-developed exsolution textures. The texture of the olivine-rich websterite is similar except for the absence of relic clinopyroxenes and the presence of deformed relics of olivine. Amphiboles occur as partial rims on spinel.

Probe traverses cross olivine-rich and olivine-poor websterite over a linear distance of 4.8 cm. The Al/Cr ratio in spinel decreases markedly from olivine-poor websterite toward olivine-rich websterite (fig. VI-9); the trend is flat for 2 cm within the olivine-rich websterite, but then Al/Cr decreases systematically for 2 cm into the olivine-rich rock creating a distinct compositional gradient. Mg/(Mg+Fe) of clinopyroxene and olivine decreases slightly within the olivine-poor websterite, and then the Mg/(Mg+Fe) ratio of both pyroxenes and olivine is constant for about 2 cm into olivine-rich websterite and then decreases rapidly toward the edge of the xenolith. The Ti and Cr contents of clinopyroxene vary antithetically; Ti is high in the olivine-poor websterite. Ti and Cr also are high in the olivine-rich websterite beyond the 2 cm distance. Al content of clinopyroxene decreases from the olivine-poor websterite into olivine-rich websterite, and the Al content of both pyroxenes decreases beyond the 2 cm distance. The Ca content of olivine decreases in the olivine-poor websterite toward olivine-rich websterite, and increases beyond the 2 cm discontinuity toward the edge of the xenolith.

Sample Ep-3-7, Kilbourne Hole, New Mexico is a fragment of a block collected from the ejecta of the Kilbourne Hole maar. The original triaxial dimensions of the block were greater than 14 X 12 X 11 cm. The xenolith consists of lherzolite cut by two branching or intersecting veins of olivine clinopyroxenite from 0.9 to 4 cm thick (fig. VI-1q; Table VI-9). Partial

melting along clinopyroxene-spinel boundaries in the pyroxenites was quenched to olivine, plagioclase, and glass (?). Contacts between the pyroxenites and lherzolite are moderately sharp and regular. The texture of the lherzolite is fine-grained tabular equigranular in which there are scattered pyroxene relics with exsolution lamellae. The thicker pyroxenite has an inequigranular mosaic texture whereas the thinner one has allotriomorphic-granular texture transitional to inequigranular mosaic.

Probe traverses over a linear distance of 3.5 cm cross the thicker pyroxenite and adjacent lherzolite show marked reduction of the Al/Cr ratio in spinel from the pyroxenite into the lherzolite(fig. VI-10). The Mg/(Mg+Fe) ratio of both pyroxenes and olivine increases from pyroxenite into lherzolite. Ti and Cr of clinopyroxenes vary antithetically and the Ti content decreases from pyroxenite into lherzolite. The Al content of both pyroxenes decreases from pyroxenite into lherzolite, whereas the Ca content of olivine increases in the same direction.

Sample Ep-3-84, Kilbourne Hole, New Mexico is a bomb, the core of which measures 10.5 X 9 X 7 cm. It consists of olivine clinopyroxenite 6 cm wide in sharp but irregular contact with lherzolite 4 cm wide (fig. VI-1r; Table VI-10). The texture of the lherzolite is fine-grained tabular, whereas that of the clinopyroxenite is mosaic. Foliation in the lherzolite is truncated at the contact with clinopyroxenite.

Probe traverses cross the two lithologies over a linear distance of 7 cm. Marked reduction of the Al/Cr ratio of spinel from the clinopyroxenite into the lherzolite is evident in figure VI-11. There is very little variation of spinel composition in the pyroxenite. The Mg/(Mg+Fe) ratio of olivine and both pyroxenes increases from the pyroxenite into the lherzolite. The Ti and Cr contents of clinopyroxene vary antithetically and the Ti/Cr ratio decreases from pyroxenite into lherzolite. The Al contents of both pyroxenes decrease from pyroxenite into lherzolite, whereas the Ca content of olivine appears to have a minimum near the contact between the two lithologies.

Samples Transitional Between Cr-diopside and Al-augite Groups.

Sample SC-1-9, San Carlos, Arizona is a fragment of an inclusion from the upper mesa-capping flow. The original triaxial dimensions of the inclusion were greater than 9.2 X 8.5 X 5.5 cm. The inclusion consists of lherzolite and olivine websterite cut by branching veins of olivine clinopyroxenite to 3.5 cm thick (fig. VI-1s: Table VI-11). The thicker pyroxenite veins crosscut a faint foliation in the peridotite, whereas the thin offshoots from the main pyroxenite (fig. VI-1s) appear to be parallel to the foliation. Peridotite between the cluster of pyroxenite veins (to the lower left of the scale in figure VI-1s) is richer in pyroxene than peridotite on the opposite side of the thick pyroxenite. The colors of its constituent minerals as seen in hard specimen are duller than those of the Cr-diopside group, but not as dark as those of the Al-augite group. In the direction away from the pyroxenite, the clinopyroxene and olivine of the other peridotite layers grade to the bright greens more characteristic of the Cr-diopside group. Contacts between lithologies are sharp to diffuse, and are irregular. The peridotite has a porphyroclastic texture with deformed relics of orthopyroxene and olivine to 8 mm across in a matrix of irregular to polygonal olivine and pyroxene with an average grain size of about 1 mm. The olivine pyroxenites are finer-grained

(range 0.1 to 2 mm) than the peridotite, and have an allotriomorphic-granular texture with no evidence of deformation.

Probe traverses cross the different lithologies over a linear distance of 4.7 cm. Spinel has major antithetic variations of Al and Cr (fig. VI-12); the Al/Cr ratio decreases from pyroxenite to peridotite, but reaches values characteristic of the Cr-diopside group for only short distances in the peridotite due to the influence of multiple pyroxenite veins. Although the thinner peridotite layers sandwiched by pyroxenite veins reverse the Al/Cr trends in spinel, the ratios remain far removed from those of the Cr-diopside group. The Mg/(Mg+Fe) ratios of principal silicate phases all increase from pyroxenite into peridotite, but the values in the peridotite depend on the distance between pyroxenite veins. The Ti/Cr ratio of clinopyroxene varies in the same manner as Al/Cr in spinel. Al contents of both pyroxenes decrease substantially from pyroxenite to peridotite, with thin peridotite layers yielding intermediate values. The Ca content of olivine is variable.

Sample Ep-3-136, Kilbourne Hole, New Mexico is a fragment of a block from the ejecta of the Kilbourne Hole maar. The original triaxial dimensions of the inclusions were larger than 5.5 X 4.0 X 3.0 cm. The inclusion consists of lherzolite of the Cr-diopside group and lherzolite transitional between the Cr-diopside and Al-augite groups cut by an olivine clinopyroxenite layer 2.2 cm thick (fig. VI-1t; Table VI-12). The transitional peridotite sandwiches the Cr-diopside peridotite and grades into it on one side of the pyroxenite. The pyroxenite contains minor amphibole as reaction rims on spinel. The pyroxenite layer crosscuts a prominent foliation and has sharp contacts with the transitional peridotite. The lherzolite has a fine-grained tabular texture with an average grain size of about 0.8 mm (range 0.5 to 2.0m). The pyroxenite has an allotriomorphic-granular texture with an average grain size of about 1.5 mm (ranges 0.5 to 3.0 mm, with a coarser grain size toward the center of the layer). The larger clinopyroxenes have exsolution lamellae of orthopyroxene, but small grains of orthopyroxene along grain boundaries of clinopyroxene indicate that minor recrystallization has taken place after emplacement of pyroxenite.

Probe traverses cross the different lithologies over a linear distance of 4.5 cm, and show the typical antithetic relationship between Al and Cr of spinel with the Al/Cr ratio decreasing from the pyroxenite into the peridotite(fig. VI-13). The Mg/(Mg+Fe) ratios of both pyroxenes and olivine increase from pyroxenite into peridotite, but are lower in the transitional lherzolite than in lherzolite of the Cr-diopside group into which it grades. Ti and Cr in clinopyroxene vary antithetically so that the Ti/Cr ratio is higher in the pyroxenite. Al content of both pyroxenes decreases from pyroxenite into peridotite, as does the Ca content of olivine.

Sample Ep-1-10, Potrillo maar, New Mexico is a fragment of an inclusion collected from the ejecta deposits. The original triaxial dimensions of the inclusion were greater than 9.0 X 5.5 X 4.8 cm. The inclusion consists of lherzolite that appears in hand specimen to be transitional between the Cr-diopside and Al-augite groups cut by an olivine clinopyroxenite layer of the Al-augite group (fig. VI-1u; table VI-13). The contact is sharp, regular, and parallel to a weak foliation in the peridotite. The texture of the peridotite is tabular, with a grain size range of 0.5 to 1.0 mm. About 1 and 2 cm from the contact with pyroxenite the foliation is slightly weaker, the grain size

increases somewhat, and the pyroxene content increases (Table VI-13); The grain size is nevertheless finer than tipical for cr-diopside lherzolites. The pyroxenite has an allotriomorphic-granular texture with a coarse to very coarse grain size.

Probe traverses cross both lithologies over a linear distance of 4.5 cm. The Al/Cr ratio of spinel decreases markedly from the pyroxenite into the peridotite (fig. VI-14). The Mg/(Mg+Fe) ratio of clinopyroxene and olivine decreases slightly within the pyroxenite in the direction of the peridotite. The Mc/Mg+Fe ratio of clinopyroxene is variable in the lherzolite, but that of orthopyroxene and olivine does not vary in the peridotite. The Ti/Cr ratio of clinopyroxene decreases from pyroxenite to peridotite. The Al contents of both pyroxenes decrease into the peridotite. The Ca content of olivine also decreases from the pyroxenite into peridotite, but shows marked, apparently random variations in the peridotite.

Bottle-green Pyroxene Group Subtypes.

Sample TM-2-78, Black Rock Summit volcanic field, Nevada, is a small bomb collected from the ejecta of an unnamed cone immediately north of U.S. Highway 50 at Black Rock Summit. Its original major and minor axes were larger than 3.5 X 2.7 cm. The xenolith consists of a layer of spinel pyroxenite 6 mm thick with a single, straight contact with harzburgite 1.8 cm thick. The contact is macroscopically sharp, but microscopically gradational. The textures of both lithologies are allotriomorphic granular, but both show local polygonal recrystallization. Olivine is strongly deformed.

Probe traverses cross the pyroxenite and harzburgite for a linear distance of 2.0 cm. A rapid drop in Al/Cr ratio of spinel occurs within the pyroxenite as the contact with peridotite is approached (fig. VI-15); there is no spinel in the peridotite in the one probe mount prepared. The Mg/(Mg+Fe) ratio of olivine decreases slightly from the pyroxenite into the peridotite. The Cr and Al contents of orthopyroxene vary antithetically within the pyroxenite: Cr reaches a maximum and Al a minimum within the pyroxenite. Within the peridotite Cr and Al vary sympathetically. However, without one point that is abnormally high in both Cr and Al, the smoothed trends would be antipathetic with a slight drop in Al and slight increase in Cr in orthopyroxene away from the pyroxenite. Ca in olivine shows a single point minimum near the contact between pyroxenite and peridotite.

Feldspathic Ultramafic Group Subtypes.

Sample Ki-5-127, Cima volcanic field California, is a small block collected from the ejecta of the "Red Rose" cone. The xenolith is subrounded and measures 5.5 X 3.5 X 3.0 cm. It consists of Cr-diopside lherzolite cut by two feldspathic olivine clinopyroxenite veins, 1.4 cm and 0.2 cm thick (Fig. VI-1v; Table VI-14). Thin offshoots of pyroxenite connect the two veins to form a netvein complex. Plagioclase, olivine, and opaque minerals crystallized from an interstitial and globular melt, the residue of which was quenched to glass. Contacts between pyroxenite and peridotite are sharp but irregular. The texture of the peridotite is porphyroclastic with deformed olivine relics to 4 mm. The veins have an allotriomorphic granular texture.

Probe traverses cross the lherzolite and both veins over a linear

distance of 3.0 cm. Both Al and Cr in spinel increase from the thin vein into peridotite on both sides, but this trend is reversed in peridotite with proximity to the thick vein (fig. VI-16). The Mg/(Mg+Fe) ratio varies substantially for both pyroxenes and olivine, and increases markedly from the veins into the peridotite. The Ti/Cr ratio of clinopyroxene decreases from the veins into peridotite, and the Al contents of both pyroxenes drop from the veins into peridotite. The Ca content of olivine also drops from the veins into peridotite. Negligible to moderate zoning of minerals both in the veins and the peridotite is observed (Appendix V).

Garnetiferous Ultramafic Group Subtypes

Sample 68-SAL-11, Salt Lake Crater, Oahu, is a small block collected from the ejecta of Salt Lake Crater. The xenolith is subrounded and had original triaxial dimensions of 8.5 X 7.0+ X 6.5 cm. It consists of garnet clinopyroxenite 5.6 cm thick and spinel lherzolite of the Cr-diopside group 9 mm thick (Table VI-15). The contact is sharp and slightly irregular. The texture of both lithologies is allotriomorphic granular with local polygonal recrystallization. Olivine is strongly deformed. Spinel occurs interstitially and as inclusions in other minerals.

Probe traverses cross both lithologies for a linear distance of 5.6 cm. A rapid decrease in Al/Cr ratio of spinel occurs in the lherzolite away from the pyroxenite (fig. VI-17), and a marked decrease of the Fe/Mg ratio in garnet of the pyroxenite as the contact with lherzolite is approached. The Mg/(Mg+Fe) ratio of clinopyroxene increases from the pyroxenite into the lherzolite, and that of orthopyroxene increases in the lherzolite away from the pyroxenite. The Ti/Cr ratio of clinopyroxene decreases from the pyroxenite into the lherzolite. Al contents of clinopyroxene and orthopyroxene decrease away from the pyroxenite, whereas that of garnet increases in the pyroxenite toward the lherzolite. The Ca content of olivine is variable but may generally decrease in the lherzolite away from the pyroxenite.

Xenoliths with Amphibole Veins.

Sample Ba-2-1, Dish Hill, California is an angular block 17.0 X 16.0 X 9.5 cm. It consists of foliated Cr-diopside lherzolite with a thin amphibole selvage on one flat surface (Fig. VI-1w; Table VI-16). The selvage cuts the foliation of the peridotite at a high angle; it contains about 5% phlogopite and about 5% apatite unevenly distributed through the amphibole. Amphibole grain size reaches 2.3 cm, whereas the largest phlogopites are 3 cm across. The selvage has a macroscopically sharp contact with the peridotite. The contact is microscopically gradational, and the abundance of amphibole drops off rapidly in the peridotite but is present in at least trace amounts throughout the xenolith (Wilshire and others, 1980). The texture of the peridotite is allotriomorphic granular with an average grain size of 3-5 mm. The texture of the selvage is allotriomorphic granular with an average grain size of 3-5 mm.

Probe traverses cross the selvage and peridotite for a linear distance of 9.0 cm. The Al/Cr ratio of spinel increases with distance from the selvage (fig. VI-18), and the Mg/(Mg+Fe) ratio increases in all the principal silicate phases away from the selvage. The K_2O/Na_2O ratio and Ti content of amphibole

decrease markedly away from the selvage, whereas the Cr contents of amphibole and clinopyroxene increase away from the selvage. The Al contents of amphibole and both pyroxenes increase away from the selvage.
Sample DL-5-11, Deadman Lake, California is an angular block collected from the ejecta of a small unnamed crater. The triaxial dimensions of the xenolith are 11.0 X 5.4 X 4.2 cm. It consists of Cr-diopside lherzolite with a thin (1-2 mm) selvage of amphibole on one flat surface (Fig. VI-1x). The contact of the selvage with the peridotite is macroscopically sharp and microscopically gradational; the abundance of amphibole drops off rapidly into the peridotite. The texture of the peridotite is porphyroclastic with pyroxene and olivine relics in a very weakly foliated matrix. The average grain size is 4-6 mm. The texture of the selvage is allotriomorphic granular with an average grain size of .75-1.5 mm.

Probe traverses cross the selvage and peridotite for a linear distance of 8 cm. A steep gradient in Al/Cr ratio of spinel occurs near the selvage, and a gradual increase in the ratio more than 1 cm away from the selvage (fig. VI-19). The Mg/(Mg+Fe) ratio of all silicate phases and of spinel increases away from the selvage. The K_2O/Na_2O ratio of amphibole decreases for 3 cm away from the selvage, as do the Ti contents of amphibole and clinopyroxene in the vicinity of the selvage. The Al contents of amphibole and both pyroxenes increase away from the selvage.

Sample Ba-1-72, Dish Hill, California, is a fragment of a bomb, the peridotite core of which had original triaxial dimensions larger than 12.5 X 7.5 X 7.5 cm. The xenolith consists of foliated Cr-diopside lherzolite with amphibole selvages to 7 mm thick on two parallel surfaces of the peridotite (Table VI-17). The selvages cut the foliation of the peridotite at a high angle. Contacts between amphibole selvages and peridotite are microscopically gradational and the amphibole content drops off rapidly into the peridotite. The texture of the peridotite is allotriomorphic-granular with local development of porphyroclastic textures. The average grain size is 3-5 mm. The amphibole selvages have allotriomorphic granular textures with an average amphibole grain size of 3-6 mm.

Probe traverses cross the selvages and peridotite over a linear distance of 4 cm. The Al/Cr ratio of spinel and the Mg/(Mg+Fe) of all principal phases increase rapidly away from the selvage (fig. VI-20). The K_2O/Na_2O ratio of amphibole, and Ti contents of amphibole and clinopyroxene drop markedly away from the selvage. Al contents of amphibole and both pyroxenes increase away from the selvage.

Xenoliths with Hydrous and Anhydrous Veins.

Sample Ba-1-15, Dish Hill, California, is a fragment of a block whose original triaxial dimensions were greater than 7.0 X 6.0 X 3.0 cm. The xenolith consists of Al-augite olivine websterite in contact with Al-augite wehrlite and a thin amphibole selvage that cuts across the anhydrous mineral layers at a high angle (Table VI-18). The wehrlite is separated from olivine websterite by 5 mm wide "depletion" zones that contain much less pyroxene than the websterite. Contacts between the various lithologies are macroscopically sharp but microscopically gradational. Websterite, wehrlite, and the amphibole selvage all have allotriomorphic granular textures.

Probe traverses made normal to the contact between websterite and wehrlite over a linear distance of 1.5 cm show a sympathetic decrease in Al and Cr of spinel away from the wehrlite, with both rising in the websterite farthest from the wehrlite (fig. VI-21). The Mg/(Mg+Fe) ratio of orthopyroxene and clinopyroxene decrease slightly in the wehrlite toward the websterite, then increase through about 1 cm of the websterite and then drop again. The Ti/Cr ratio of clinopyroxene decreases in websterite away from the wehrlite, and the Al contents of pyroxenes increase change little. The Ca content of olivine has a minimum within the wehrlite.

Disk 10 p7-24; xenoliths; Wilshire-sw; 2/15/84;2/2184;3/7/84

Table VI-1. Modal and Chemical Composition, Composite Xenolith EP-1-123

Chemical Composition			CIPW Norm			Modal Composition		
	1	2		1	2		1	2
SiO_2	44.4	52.3	or			Olivine	69.3	26.9
Al_2O_3	3.9	8.4	ab	1.7	6.6	Clinopyroxene	22.3	53.3
Fe_2O_3	.45	.73	an	9.9	19.9	Orthopyroxene	5.0	18.3
FeO	7.7	4.3	lc			Spinel	2.7	1.8
MgO	39.2	22.2	ne					
CaO	2.6	8.9	wo	1.2	10.4			
Na_2O	.20	.77	di en	18.5	49.9			
K_2O	.00	.00	fs	2.6	6.3			
H_2O+	.27	.33	hy en					
H_2O-	.01	.03	fs					
TiO_2	.10	.35	ol fo	56.3	4.5			
P_2O_5	.02	.02	fa	8.8	.6			
			mt	.7	1.1			
			il	.2	.7			
MnO	.13	.11	cs					
CO_2	.04	.03	cm					
Cl			cc	.1				
			ap					
Less O	.00	.00						
Total	99.02	98.47						

Analyst: Rapid Rock Analysis Laboratory, Leonard Shapiro, Project Leader

1. Cr-diopside lherzolite. 2. Cr-diopside olivine websterite.

Table VI-2. Modal and Chemical Composition, Composite Xenolith SQ-1-80

Chemical Composition			CIPW Norm			Modal Composition		
	1	2		1	2		1*/	2
SiO_2	43.91	49.11	or	.1	.1	Olivine	91	28.6
Al_2O_3	3.04	9.14	ab	1.2	2.7	Clinopyroxene	6	38.7
Fe_2O_3	1.09	1.32	an	7.6	23.4	Orthopyroxene	2	29.6
FeO	8.30	5.38	lc			Oxide	1	3.1
MgO	39.45	26.72	ne			Garnet		
CaO	3.21	7.14	wo	3.3	4.9	Amphibole		
Na_2O	.14	.33	di en	15.8	38.5	Plagioclase		
K_2O	.02	.02	fs	2.4	4.9	Glass		
H_2O+	.07	.04	en			Secondary		
H_2O-	.06	.02	hy fs					
TiO_2	.08	.16	fo	57.8	19.6			
P_2O_5	.05	.02	ol fa	9.5	2.7			
MnO	.14	.12	cs					
Cr_2O_3	.28	.53	mt	1.6	1.9			
NiO	.28	.10	il	.2	.3			
CO_2	.01	.01	cm	.4	.8			
Cl	.00	.01	cc					
F	.00	.00	ap	.1	.1			
S	.00	.00						
Less 0	.00	.00						
Total	100.13	100.17						

Analyst: Elaine L. Brandt

1. Cr-diopside lherzolite. 2. Cr-diopside olivine websterite.
*/ Mode is a field estimate

Table VI-3. Modal and Chemical Composition, Composite Xenolith SC-1-6

Chemical Composition				CIPW Norm				Modal Composition		
	1	2	3		1	2	3		1	
SiO_2	43.1	43.3	49.6	or	.1	.5	.4	Olivine	78.0	12.3
Al_2O_3	1.0	1.6	4.0	ab	.3	1.7	3.8	Clinopyroxene	3.6	67.8
Fe_2O_3	1.2	.60	2.2	an	2.5	3.0	8.7	Orthopyroxene	17.5	18.1
FeO	6.8	7.4	2.8	lc				Oxide	.9	2.0
MgO	46.0	45.8	27.7	ne				Garnet		
CaO	.78	.62	12.4	wo	.3		21.8	Amphibole		
Na_2O	.04	.20	.45	di en	14.3	10.3	33.5	Plagioclase		
K_2O	.02	.09	.06	fs	1.5	1.2	1.6	Glass		
H_2O+	.42	.27	.22	en				Secondary		
				hy						
H_2O-	.10	.12	.08	fs						
TiO_2	.03	.00	.26	fo	70.5	73.0	24.9			
				ol						
P_2O_5	.10	.00	.11	fa	8.0	9.4	1.3			
MnO	.18	.10	.17	cs						
				mt	1.7	.9	3.2			
				il	.1		.5			
CO_2		.01		cm						
Cl				cc						
F				ap	.2		.3			
S	.00									
Less O										
Total	99.77	100.11	100.05							

Analyst: Rapid rock Analysis Laboratory, Leonard Shapiro, Project Leader

1. Cr-diopside lherzolite. 2. Cr-diopside lherzolite. 3. Cr-diopside olivine websterite.

Table VI-4. Modal Composition, Composite Xenolith SC-1-3

	1	2
Olivine	72.9	14.0
Clinopyroxene	8.6	32.3
Orthopyroxene	16.8	50.6
Oxide	1.7	3.0
Garnet		
Amphibole		
Plagioclase		
Glass		
Secondary		

1. Cr-diopside lherzolite 2. Cr-diopside websterite

Table V1-5. Modal and Chemical Composition of Composite Xenolith Ki-5-1

Chemical Composition	1	2	3
SiO_2	42.0	43.2	46.7
Al_2O_3	2.3	2.5	6.6
Fe_2O_3	.50	1.4	1.7
FeO	8.1	7.8	5.0
MgO	46.2	44.0	33.0
CaO	.76	1.4	5.7
Na_2O	.03	.06	.28
K_2O	.12	.09	.12
H_2O+	.26	.22	.32
H_2O-	.05	.04	.03
TiO_2	.04	.04	.15
P_2O_5	.00	.00	.00
MnO	.05	.08	.07
Cr_2O_3			
NiO			
CO_2	.02	.06	.04
Cl			
F			
S			
Less O			
Total	100.43	100.89	99.71

CIPW Norm		1	2	3
	or	.7	.5	.7
	ab	.3	.5	2.4
	an	3.6	6.2	16.5
	lc			
	ne			
	wo		.1	4.9
di	en	6.3	11.9	27.2
	fs	.8	1.4	2.5
hy	en			
	fs			
ol	fo	75.9	67.8	38.7
	fa	10.5	9.0	4.0
	cs			
	mt	.7	2.0	2.5
	il	.1	.1	.3
	cm			
	cc			.1
	ap			

Modal Composition	1	2	3
Olivine	88.8	81.8	16.5
Clinopyroxene	2.4	5.6	43.6
Orthopyroxene	6.9	9.9	32.1
Oxide	1.9	2.7	7.8
Garnet			
Amphibole			
Plagioclase			
Glass			
Secondary			

Analyst: Rapid rock Analysis Laboratory, Leonard Shapiro, Project Leader

1. Cr-diopside Harzburgite 2. Cr-diopside lherzolite. 3. Cr-diopside olivine websterite.

Table VI-6. Modal and Chemical Compositons, Composite Xenolith SC-1-12

Chemical Composition	1	2	3
SiO_2		52.4	53.5
Al_2O_3		6.4	6.3
Fe_2O_3		2.2	2.5
FeO		3.6	5.0
MgO		20.7	28.5
CaO		13.7	3.5
Na_2O		.51	.09
K_2O		.06	.03
H_2O+		.26	.28
H_2O-		.05	.05
TiO_2		.33	.23
P_2O_5		.00	.00
MnO		.07	.09
Cr_2O_3			
NiO			
CO_2		.02	.02
Cl			
F			
S			
Total		100.30	100.09

CIPW Norm		1	2	3
	or		.4	.2
	ab		4.3	.8
	an		15.0	16.7
	lc			
	ne			
	wo		22.0	.2
di	en		46.6	70.7
	fs		4.0	6.9
	en			
hy	fs			
	fo		3.4	.2
ol	fa		.3	
	cs			
	mt		3.2	3.6
	il		.6	.4
	cm			
	cc			
	ap			

Modal Composition	1	2	3
Olivine	93.2	13.0	8.4
Clinopyroxene	5.8	73.4	56.2
Orthopyroxene		12.4	35.6
Oxide	.7	1.2	
Garnet			
Amphibole			
Plagioclase			
Glass			
Secondary			

Analyst: Radid Rock Analysis Laboratories, Leonard Shapiro, Project Leader

1. Cr-diopside dunite. 2. Cr-diopside olivine websterite. 3. Cr-diopside olivine websterite.

Table VI-7. Modal and Chemical Compositons, Composite Xenolith SC-1-17

Chemical Composition	1	2	3
SiO_2	43.2	47.8	
Al_2O_3	1.7	11.6	
Fe_2O_3	.70	1.1	
FeO	8.2	4.3	
MgO	44.5	24.3	
CaO	.69	10.7	
Na_2O	.20	.48	
K_2O	.07	.07	
H_2O^+	.34	.32	
H_2O^-	.17	.14	
TiO_2	.00	.11	
P_2O_5	.00	.00	
MnO	.10	.08	
Cr_2O_3			
NiO			
CO_2	.02	.01	
Cl			
F			
S			
Less O			
Total	99.89	101.01	

CIPW Norm		1	2	3
	or	.4	.4	
	ab	1.7	4.0	
	an	3.3	29.1	
	lc			
	ne			
	wo		9.9	
di	en	11.7	22.2	
	fs	1.6	2.6	
hy	en			
	fs			
ol	fo	69.9	26.6	
	fa	10.2	3.4	
	cs			
	mt	1.0	1.6	
	il		.2	
	cm			
	cc			
	ap			

Modal Composition	1*/	2	3
Olivine	88	30.0	50.3
Clinopyroxene	4	26.0	35.9
Orthopyroxene	7	40.6	11.5
Oxide	1	3.3	2.2
Garnet			
Amphibole			
Plagioclase			
Glass			
Secondary			

Analyst: Rapid Rock Analysis Laboratories, Leonard Shapiro, Project Leader

1. Cr-diopside lherzolite. 2. Cr-diopside olivine websterite. 3. Cr-diospide olivine websteri

*/ Mode is a field estimate

Table VI-8. Modal and Chemical Compositons, Composite Xenolith Ba-1-24

Chemical Composition			CIPW Norm			Modal Composition		
	1	2		1	2		1*/	2
SiO_2	44.12	43.71	or	.1		Olivine	82	15.7
Al_2O_3	3.42	14.91	ab	1.7		Clinopyroxene	8	50.7
Fe_2O_3	1.02	2.52	an	8.4	36.0	Orthopyroxene	10	11.6
FeO	8.18	2.24	lc		.1	Oxide		19.6
MgO	39.63	18.59	ne		4.7	Garnet		
CaO	2.46	15.69	wo	1.4	14.5	Amphibole		2.5
Na_2O	.20	1.03	di en	17.1	12.3	Plagioclase		
K_2O	.02	.03	fs	2.5	.3	Glass		
H_2O+	.02	.13	en			Secondary		
			hy					
H_2O-	.06	.06	fs					
TiO_2	.11	.64	fo	57.2	23.8			
			ol					
P_2O_5	.01	.01	fa	9.3	.7			
MnO	.17	.09	cs		2.1			
Cr_2O_3	.28	.20	mt	1.5	3.7			
NiO	.24	.15	il	.2	1.2			
CO_2	.04	.05	cm	.4	.3			
Cl	.00	.00	cc	.1	.1			
F	.01	.01	ap					
S								
Less O								
Total	99.99	100.06						

Analyst: Vertie C. Smith

1. Al-augite olivine websterite. 2. Al-augite olivine websterite.
*/ Mode is a field estimate

Table VI-9 Modal and Chemical Composition, Composite Xenolith Ep-3-7

Chemical Composition			CIPW Norm			Modal Composition		
	1	2			1	2		1	2
SiO_2	41.22	42.82		or	.1		Olivine	75.9	12.4
Al_2O_3	3.96	12.87		ab	2.6		Clinopyroxene	18.2	68.7
Fe_2O_3	1.51	3.04		an	9.4	31.8	Orthopyroxene	3.0	.9
FeO	12.06	5.20		lc			Oxide	2.8	17.1
MgO	36.19	18.65		ne		3.3	Garnet		
CaO	3.88	15.41		wo	3.9	14.8	Amphibole		
Na_2O	.31	.73	di	en	4.5	11.7	Plagioclase	.1	.9
K_2O	.01	.00		fs	1.0	1.5	Glass		
H_2O+	.00	.00		en			Secondary		
H_2O-	.01	.03	hy	fs					
TiO_2	.26	.95		fo	60.0	24.3			
P_2O_5	.02	.01	ol	fa	15.4	3.4			
MnO	.23	.15		cs		2.7			
Cr_2O_3	.22	.06		mt	2.2	4.4			
NiO	.14	.08		il	.5	1.8			
CO_2	.06	.06		cm	.3	.1			
Cl	.00	.00		cc	.1	.1			
F	.01	.01		ap					
S									
Less O									
Total	100.09	100.07							

Analyst: Vertie C. Smith

1. Al-augite lherzolite. 2. Al-augite wehrlite.

Table VI-10. Modal and Chemical composition, Composite Xenolith Ep-3-84

Chemical Composition			CIPW Norm				Modal Composition		
	1	2			1	2		1	2
SiO_2	45.1	42.3		or	.1		Olivine	64.8	11.3
Al_2O_3	3.3	17.1		ab	.4		Clinopyroxene	15.6	65.9
Fe_2O_3	1.3	3.6		an	8.8	43.5	Orthopyroxene	7.0	2.2
FeO	8.8	3.6		lc		.1	Oxide	2.6	18.5
MgO	36.8	14.1		ne		3.0	Garnet		
CaO	3.3	17.1		wo	3.1	13.0	Amphibole		2.1
Na_2O	.05	.66	di	en	25.3	10.8	Plagioclase		
K_2O	.02	.02		fs	4.2	.6	Glass		
H_2O+	.40	.54		en			Secondary		
			hy						
H_2O-	.04	.07		fs					
TiO_2	.14	1.2		fo	46.9	17.0			
			ol						
P_2O_5	.04	.02		fa	8.6	1.0			
MnO	.19	.12		cs		3.0			
Cr_2O_3				mt	1.9	5.2			
NiO				il	.3	2.3			
CO_2				cm					
Cl				cc					
F				ap	.1				
S									
Less O									
Total	99.48	100.43							

Analyst: Rapid Rock Analysis Laboratories, Leonard Shapiro, Project Leader

1. Al-augite lherzolite. 2. Al-augite olivine clinopyroxenite

Table VI-11. Modal and Chemical Composition, Composite Xenolith SC-1-9

Chemical Composition				CIPW Norm					Modal Composition			
	1	2	3			1	2	3		1	2*/	3
SiO_2	42.9	43.2	44.4		or		.2	.2	Olivine	80.0	83	11.2
Al_2O_3	2.5	3.6	12.3		ab	.2	.7	5.4	Clinopyroxene	2.3	15	74.6
Fe_2O_3	.15	.90	2.4		an	4.2	6.3	29.4	Orthopyroxene	15.0		3.6
FeO	10.5	10.2	4.3		lc				Oxide	2.7	2	10.6
MgO	40.9	38.5	19.0		ne			1.7	Garnet			
CaO	.90	1.3	13.6		wo			16.1	Amphibole			
Na_2O	.02	.08	1.0	di	en	18.4	21.4	13.1	Plagioclase			
K_2O	.00	.03	.03		fs	3.5	4.0	1.1	Glass			
H_2O+	.18	1.3	.08		en				Secondary			
H_2O-	.04	.05	.04	hy	fs							
TiO_2	.15	.24	1.4		fo	59.8	53.4	24.4				
P_2O_5	.04	.03	.03	ol	fa	12.4	11.0	2.2				
MnO	.15	.16	.12		cs							
Cr_2O_3					mt	.2	1.3	3.5				
NiO					il	.3	.5	2.7				
CO_2	.02	.01	.03		cm							
Cl					cc			.1				
F					ap	.1	.1	.1				
S												
Less O												
Total	98.45	99.60	98.73									

Analyst: Rapid Rock Analysis Laboratories, Leonard Shapiro, Project Leader

1. Al-augite lherzolite. 2. Al-augite lherzolite. 3. Al-augite olivine clinopyroxenite.
*/ Mode is a field estimate

Table VI-12. Modal and Chemical Composition, Composite Xenolith Ep-3-136

Chemical Composition	1	2	3
SiO_2	44.0	43.6	42.5
Al_2O_3	2.3	2.3	16.9
Fe_2O_3	1.4	1.1	3.6
FeO	8.9	10.0	3.0
MgO	40.4	39.9	14.2
CaO	2.0	2.2	17.5
Na_2O	.00	.02	.50
K_2O	.07	.05	.10
H_2O+	.34	.43	.43
H_2O-	.03	.02	.04
TiO_2	.11	.15	1.1
P_2O_5	.04	.03	.03
MnO	.26	.19	.11
Cr_2O_3			
NiO			
CO_2			
Cl			
F			
S			
Less O			
Total	99.85	99.99	100.01

CIPW Norm		1	2	3
	or	.4	.3	
	ab		.2	
	an	6.1	6.0	43.6
	lc			.5
	n3			2.3
	wo	1.5	2.0	13.6
di	en	20.1	17.5	11.5
	fs	3.1	3.1	.3
hy	en			
	fs			
ol	fo	56.6	57.4	16.7
	fa	9.6	11.2	.5
	cs			3.3
	mt	2.0	1.6	5.2
	il	.2	.3	2.1
	cm			
	cc			
	ap	.1	.1	.1

Modal Composition	1	2	3
Olivine	66.0		6.7
Clinopyroxene	11.9		72.8
Orthopyroxene	18.3		3.0
Oxide	3.8		17.4
Garnet			
Amphibole			
Plagioclase			.2
Glass			
Secondary			

Analyst: Rapid Rock Analysis Laboratories, Leonard Shapiro, Project Leader

1. Al-augite lherzolite far from contact with 3. 2. Al-augite lherzolite close to contact w
   3. Al-augite olivine clinopyroxenite.

Table VI-13. Modal and Chemical Composition, Composite Xenolith Ep-1-10

Chemical Composition				CIWP Norm					Modal Composition			
	1	2	3			1	2	3		1	2	3
SiO_2	44.9	43.5	40.5		or	.2	.2		Olivine	63.2	68.3	8.2
Al_2O_3	3.6	3.0	20.8		ab	1.8	1.2		Clinopyroxene	8.6	6.8	75.1
Fe_2O_3	1.1	1.2	2.1		an	8.9	7.5	52.3	Orthopyroxene	24..	1.0	.7
FeO	8.1	8.4	2.9		lc			.3	Oxide	4.1	3.9	13.3
MgO	35.6	39.0	15.7		ne			4.1	Garnet			
CaO	4.0	2.9	15.8		wo	4.5	2.8	1.8	Amphibole			
Na_2O	.21	.14	.90	di	en	23.3	16.8	1.5	Plagioclase			tr
K_2O	.03	.03	.07		fs	3.7	2.5	.1	Glass			
H_2O+	1.1	.54	.43		en				Secondary			2.7
H_2O-	.04	.04	0.8	hy	fs							
TiO_2	.24	.17	.97		fo	46.3	56.9	26.3				
P_2O_5	.05	.05	.04	ol	fa	8.0	9.4	1.7				
MnO	.19	.20	.14		cs			6.6				
Cr_2O_3					mt	1.6	1.8	3.0				
NiO					il	.5	.3	1.8				
CO_2					cm							
Cl					cc							
F					ap	.1	.1	.1				
S												
Less O												
Total	99.16	99.27	100.43									

Analyst: Rapic Rock Analysis Laboratories, Leonard Shapiro, Project Leader

1. Al-augite lherzolite, coarse-grained, pyroxene-rich. 2. Al-augite lherzolite, fine-grain adjacent to 3. 3. Al-augite olivine clinopyroxenite.

Disk 10 xenoliths; p.7-24; (page 20 on screen); xenoliths; Wilshire/sw

Table VI-14. Modal and Chemical Composition, Composite Xenolith Ki-5-127

Chemical Composition				CIPW Norm				Modal Composition			
	1	2	3		1	2	3		1	2	3
SiO_2	41.69	41.62	45.58	or	.2	.1	2.2	Olivine		63.3	18.3
Al_2O_3	2.67	2.32	6.70	ab	1.6	1.8	8.3	Clinopyroxene		13.2	58.9
Fe_2O_3	1.20	1.22	2.27	an	6.3	5.3	12.0	Orthopyroxene		20.9	
FeO	12.99	15.55	10.69	lc				Oxide		2.1	.8
MgO	37.99	35.39	19.43	ne			.6	Garnet			
CaO	2.52	2.91	11.85	wo	2.2	3.7	19.2	Amphibole			
Na_2O	.19	.21	1.11	di en	8.5	9.0	13.2	Plagioclase		.5	7.8
K_2O	.03	.02	.38	fs	2.1	2.9	4.4	Glass			14.2
H_2O+	.08	.08	.19	en				Secondary			
H_2O-	.02	.01	.07	hy fs							
TiO_2	.16	.16	1.16	fo	60.3	55.3	24.7				
P_2O_5	.03	.02	.13	ol fa	16.3	19.3	9.1				
MnO	.21	.25	.22	cs							
Cr_2O_3	.20	.20	.15	mt	.7	1.8	3.3				
NiO	.20	.20	.03	il	.3	.3	2.2				
CO_2				cm	.3	.3	.2				
Cl	.00	.00	.01	cc	.2						
F	.01	.01	.02	ap	.1		.3				
S	.00	.01	.02								
Less O		.01	.02								
Total	100.19	100.17	99.99								

Analyst: Edythe E. Engleman

1. Cr-diopside lherzolite. 2. Cr-diopside lherzolite between pyroxenites. 3. Al-augite feldspathic olivine clinopyroxenite.

Table VI-15 Modal and Chemical Composition, Composite Xenolith 68-SAL-11
(Beeson and Jackson, 1970)

Chemical Composition		CIPW Norm		Modal Composition	
	1		1		1
SiO_2	44.57	or	.1	Olivine	.4
Al_2O_3	13.61	ab	14.3	Clinopyroxene	61.2
Fe_2O_3	4.17	an	29.5	Orthopyroxene	
FeO	8.49	lc		Oxide	1.9
MgO	13.34	ne		Garnet	36.5
CaO	11.42	wo	11.2	Amphibole	
Na_2O	1.69	di en	7.9	Plagioclase	
K_2O	.02	fs	2.3	Glass	
H_2O+	.29	en	3.0	Secondary	
H_2O-	.14	hy fs	.9		
TiO_2	1.76	fo	15.6		
P_2O_5	.02	ol fa	5.0		
MnO	.21	cs			
Cr_2O_3	.06	mt	6.1		
NiO	.04	il	3.3		
CO_2	.03	cm	.1		
Cl	.00	cm	.1		
F	.01	ap	.1		
S					
Less O					
Total	99.87				

1. Garnet clinopyroxenite

Table VI-16. Modal Composition, Composite Xenolith Ba-2-1

Modal Composition

	1
Olivine	55.5
Clinopyroxene	15.5
Orthopyroxene	19.1
Oxide	1.6
Garnet	
Amphibole	8.2
Plagioclase	
Glass	
Secondary	

1. Cr-diopside lherzolite adjacent to amphibole selvage.

Table VI-17. Modal and Chemical Composition, Composite Xenolith Ba-1-72

Chemical Composition		CIPW Norm			Modal Composition	
	1			1		1
SiO_2	44.08		or	.1	Olivine	51.3
Al_2O_3	3.62		ab	2.5	Clinopyroxene	19.3
Fe_2O_3	1.06		an	8.5	Orthopyroxene	20.6
FeO	8.21		lc		Oxide	1.8
MgO	39.06		ne		Garnet	
CaO	2.85		wo	2.2	Amphibole	7.1
Na_2O	.29	di	en	15.4	Plagioclase	
K_2O	.01		fs	2.3	Glass	
H_2O+	.01		en		Secondary	
H_2O-	.01	hy	fs			
TiO_2	.12		fo	57.3		
P_2O_5	.01	ol	fa	9.4		
MnO	.16		cs			
Cr_2O_3	.36		mt	1.5		
NiO	.25		il	.2		
CO_2	.03		cm	.5		
Cl	.00		cc	.1		
F	.01		ap			
S						
Less O						
Total	100.14					

Analyst: Elaine L Brandt

1. Cr-diopside lherzolite adjacent to amphibole selvage.

Table VI-18. Modal and Chemical Composition, Composite Xenolith Ba-1-15

Chemical Composition			CIPW Norm			Modal Composition		
	1	2			1	2		1	2
SiO_2	43.7	47.0		or	.5	.5	Olivine	83.3	18.0
Al_2O_3	4.5	10.1		ab	.8	2.6	Clinopyroxene	12.7	38.0
Fe_2O_3	1.1	1.9		an	11.6	26.1	Orthopyroxene	2.2	37.0
FeO	7.8	5.0		lc			Oxide	1.7	7.0
MgO	37.8	27.2		ne			Garnet		
CaO	4.4	7.4		wo	4.3	4.5	Amphibole		
Na_2O	.10	.31	di	en	13.1	29.0	Plagioclase		
K_2O	.08	.08		fs	1.9	3.3	Glass		
H_2O+	.02	.36		en			Secondary		
H_2O-	.44	.09	hy	fs					
TiO_2	.01	.07		fo	57.1	27.5			
P_2O_5	.00	.00	ol	fa	9.1	3.5			
MnO	.14	.14		cs					
Cr_2O_3				mt	1.6	2.8			
NiO				il		.1			
CO_2	.01	.03		cm					
Cl				cc		.1			
F				ap					
S									
Less O									
Total	100.10	99.68							

Analyst: Rapid Rock Analysis Laboratories, Leonard Shapiro, Project Leader

1. Al-augite wehrlite. 2. Al-augite olivine websterite.

Figure VI-1. Photomicrographs and outcrop photographs of xenoliths. Number at bottom of photomicrographs indicates the width of the field of view. a) Thin vein of fine-grained gabbro in Cr-diopside spinel lherzolite. Isolated patches of plagioclase-clinopyroxene intergrowths occur in the lherzolite. Both lithologies contain patches and stringers of glass. b) Thin vein of plagioclase, clinopyroxene, olivine, spinel in Cr-diopside lherzolite. Single elongate anhedral plagioclases commonly enclose smaller mafic minerals. c) Contact between gabbro (left) and Al-augite clinopyroxenite. Gabbro forms a 1 cm thick band in the coarser pyroxenite. Both lithologies contain accessory amphibole. Green spinel is abundant in both. d) Partly recrystallized(?) fine-grained olivine gabbro vein in Cr-diopside spinel lherzolite. e) Thin polygonally recrystallized plagioclase-clinopyroxene vein in Cr-diopside lherzolite. f) Granoblastic texture in olivine metagabbro interleaved with pyroxenite. g) Cr-diopside spinel lherzolite with a kaersutite selvage (black and along bottom of xenolith above scale). Note sharp, straight contact between peridotite and kaersutite selvage. h) Loose-knit amphibole vein at contact between Cr-diopside lherzolite and olivine websterite; vein is not parallel to this contact. Amphiboles are marginally fused. i) Composite sample Ep-1-123 (see text for description). j) Composite sample SQ-1-80 (see text for description). k) Composite sample SC-1-6 (see text for description). l) Composite sample SC-1-3 (see text for description). m)Composite sample Ki-5-1 (see text for description). n) Composite sample SC-1-12 (see text for description). o) Composite sample SC-1-17 (see text for description). p) Composite sample Ba-1-24 (see text for description). q) Composite sample Ep-3-7 (see text for description). r) Composite sample Ep-3-84 (see text for description). s) Composite sample SC-1-9 (see text for description). t) Composite sample Ep-3-136 (see text for description). u) Composite sample Ep-1-10 (see text for description). v) Composite sample Ki-5-127 (see text for description). w) Composite sample Ba-2-1 (see text for description). x) Composite sample DL-5-11 (see text for description).

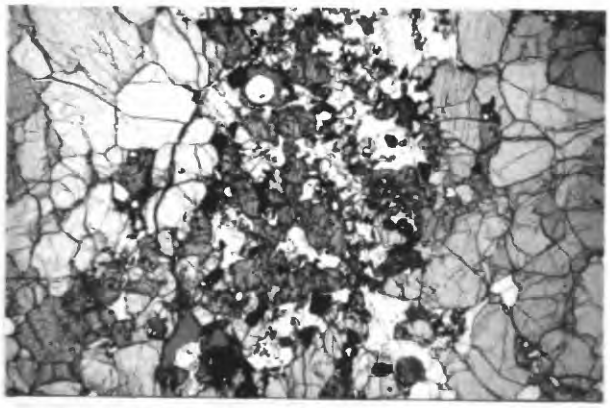

Ki-5-126-2 8.3mm a

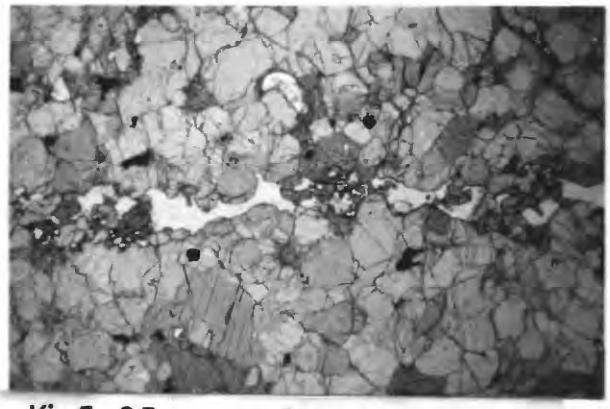

Ki-5-35 8.3mm b

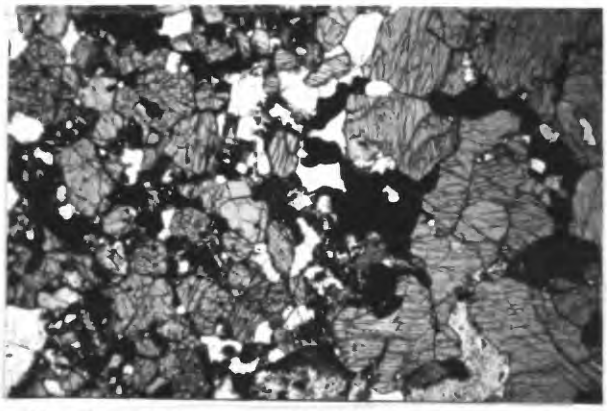

Ki-2-104 8.3mm c

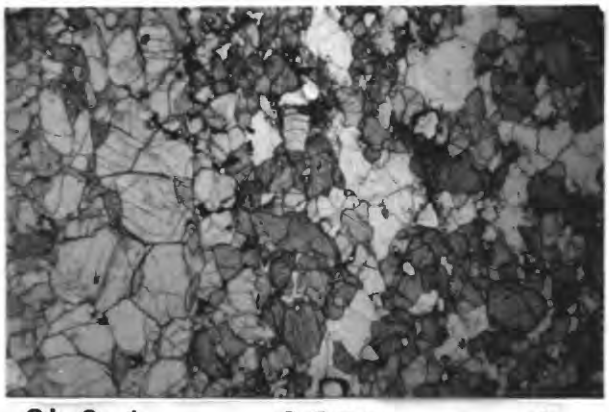

Gi-2-1 2.2mm d

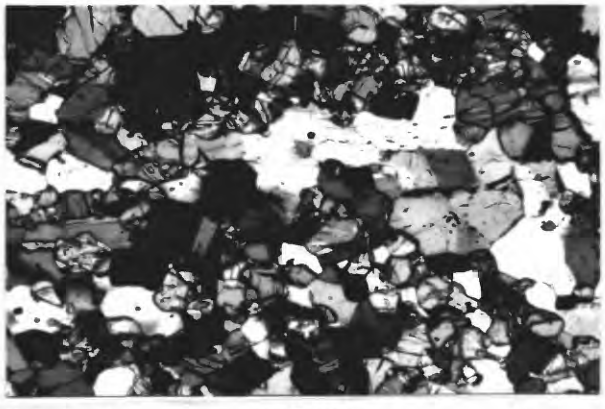

Ki-5-4 8.3mm e

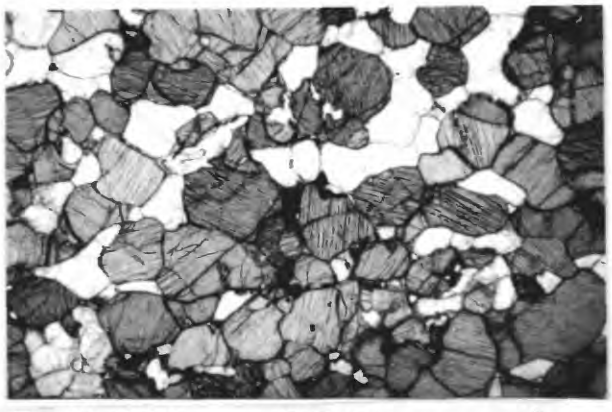

Ep-3-162 8.3mm f

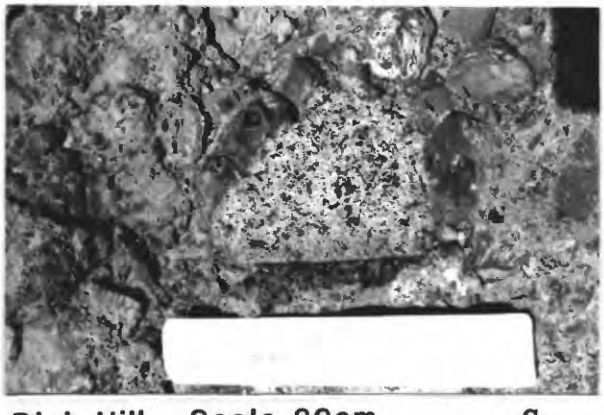

Dish Hill Scale 30cm g

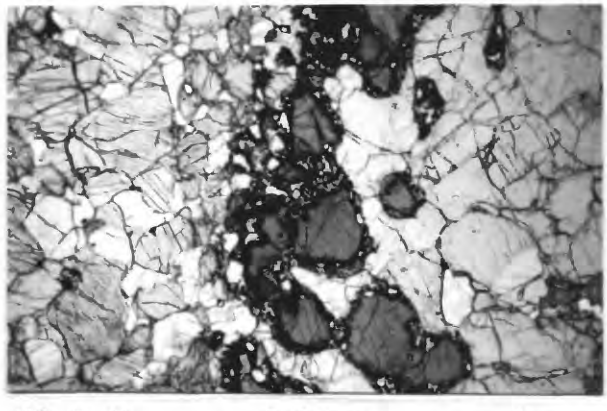

Ki-5-2 8.3mm h

Ep-1-123 i

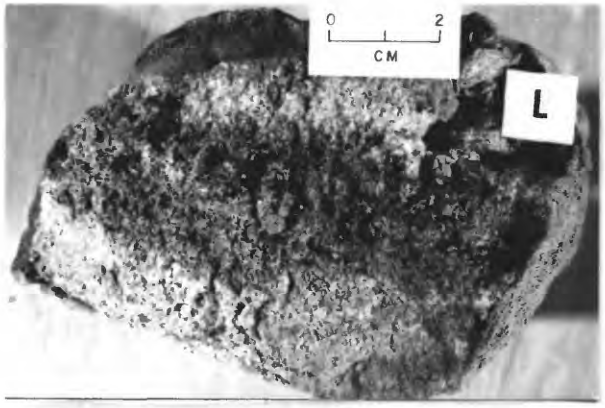

SQ-1-80 j

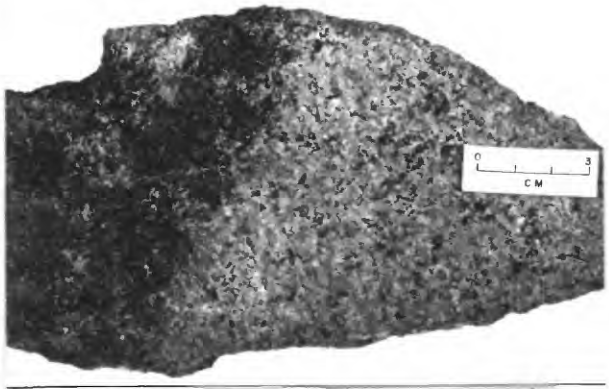

SC-1-6 k

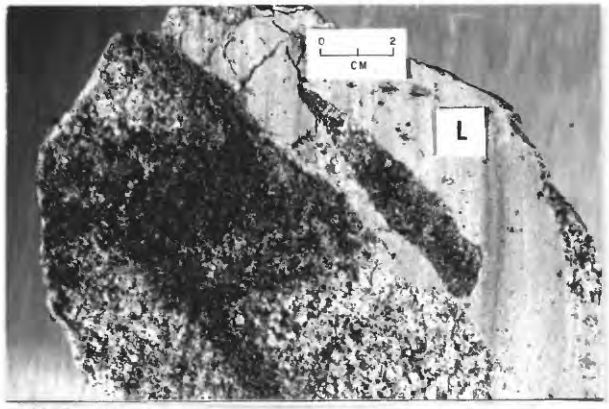

SC-1-3 l

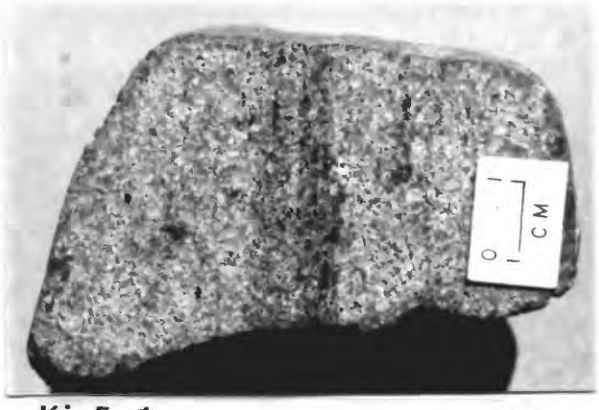

Ki-5-1 m

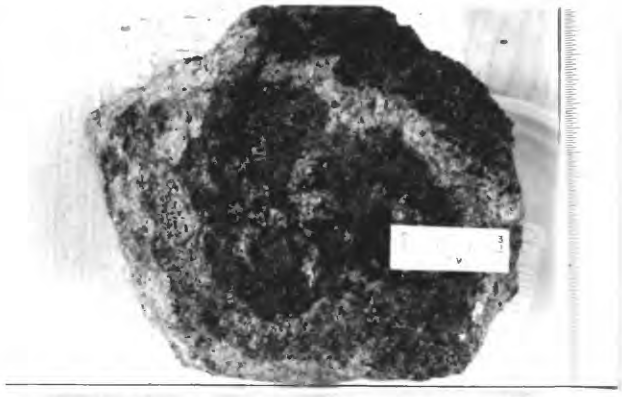

SC-1-12 n

SC-1-17 o

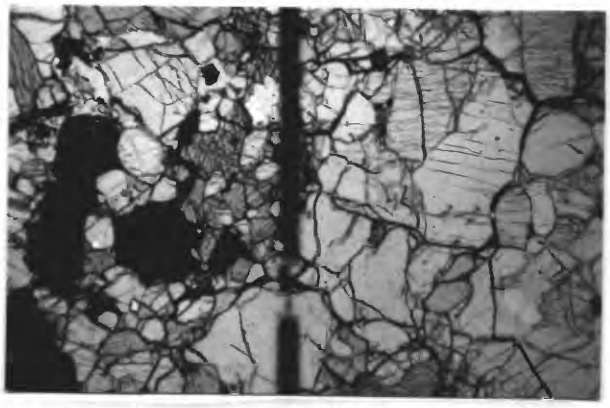

Ba-1-24 8.3mm p

VI-1

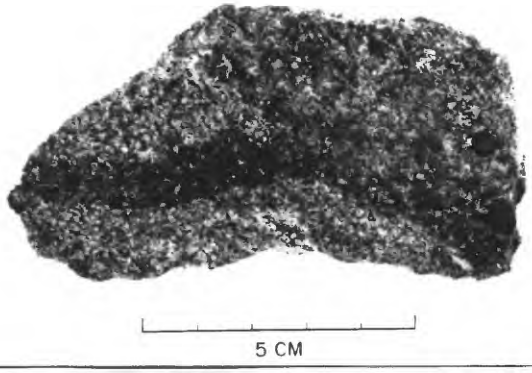

Ep-3-7 q

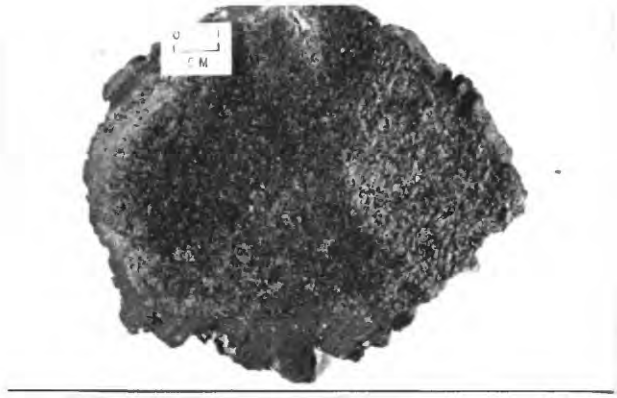

Ep-3-84 r

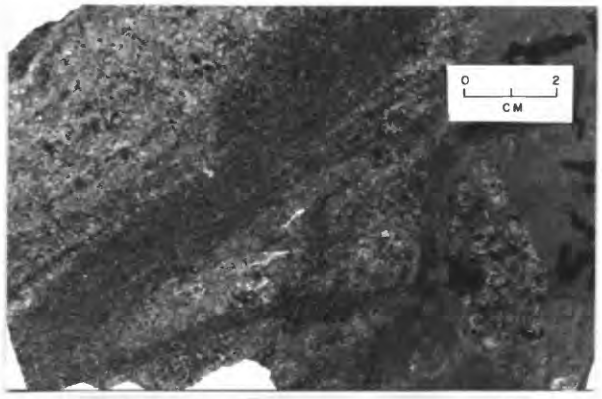

SC-1-9 s

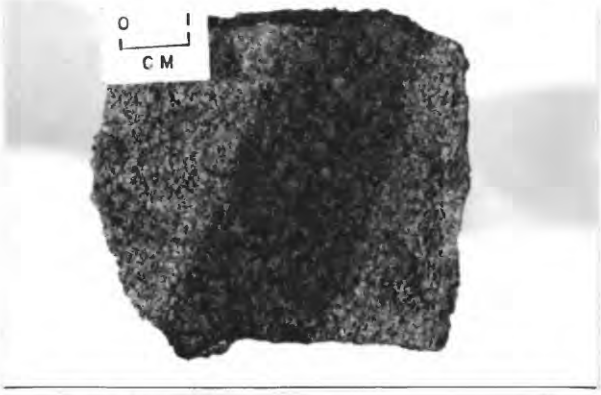

Ep-3-136 t

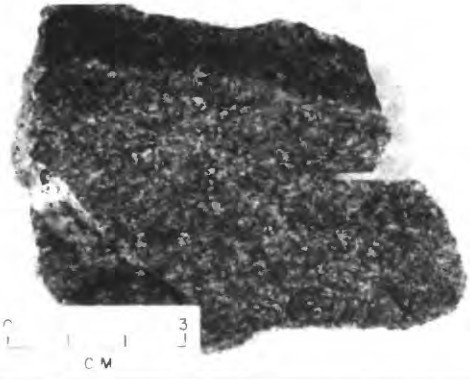

Ep-1-10 u

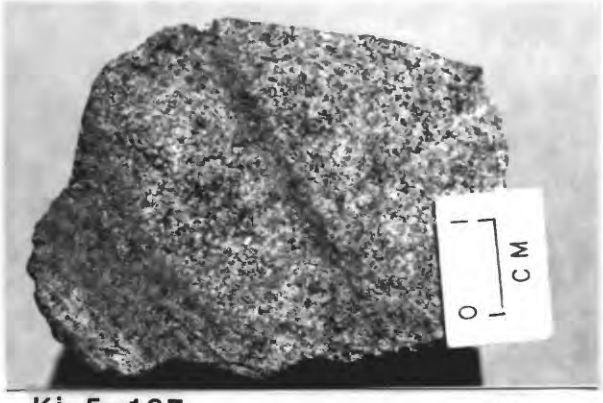

Ki-5-127 v

Ba-2-1 w

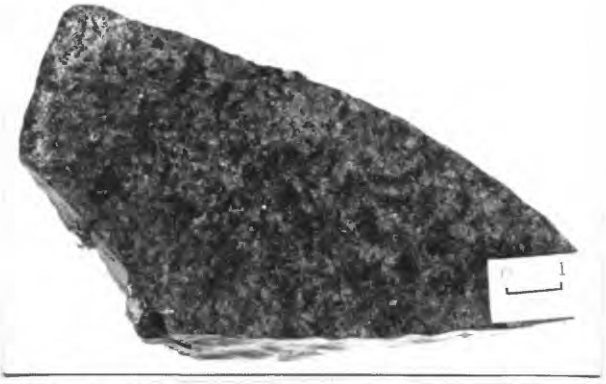

DL-5-11 x

VI-1

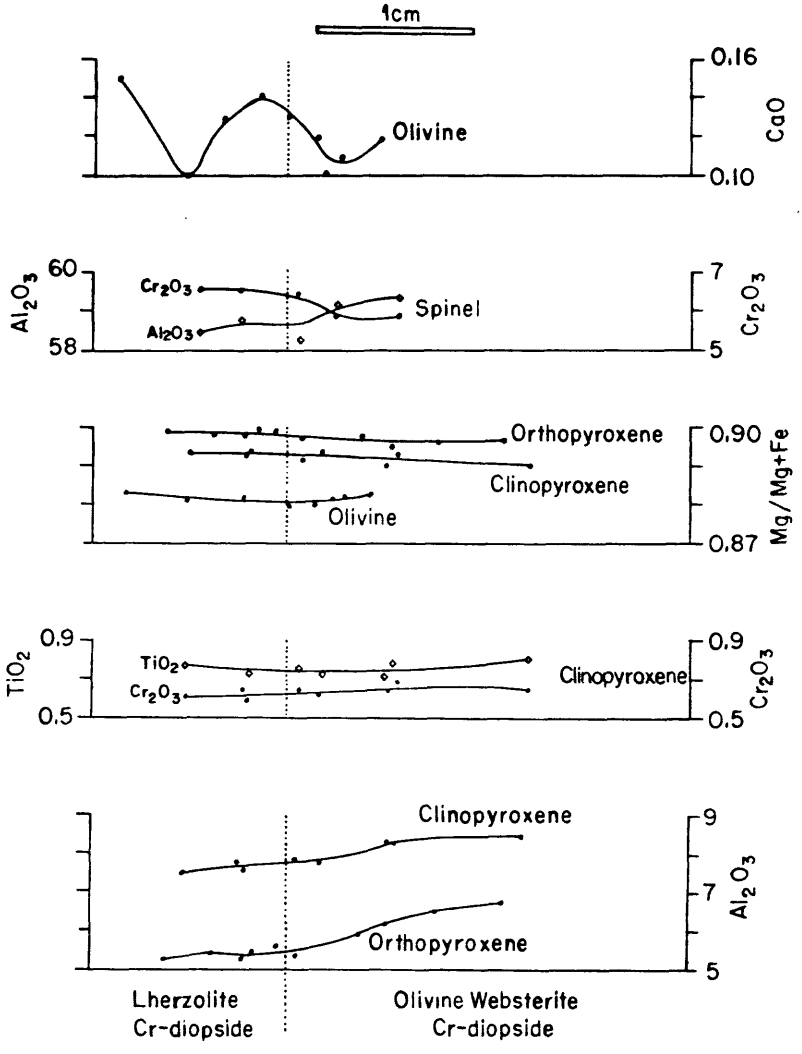

Fig. VI-2. Chemical variations across contact between Cr-diopside lherzolite and Cr-diopside olivine websterite, composite sample Ep-1-123.

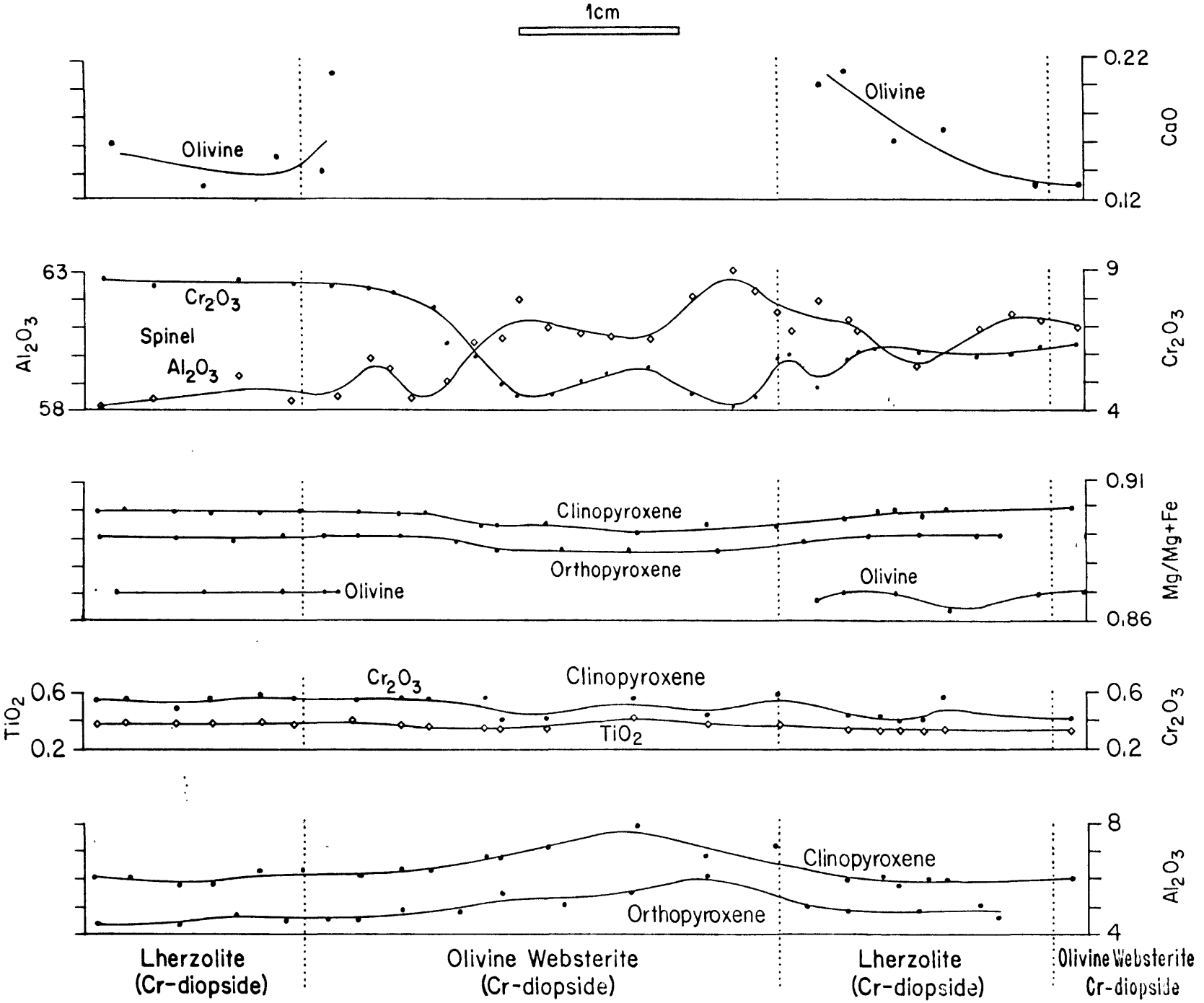

Fig. VI-3. Chemical variations across Cr-diopside olivine websterite band sandwiched by Cr-diopside lherzolite, composite sample SQ-1-80.

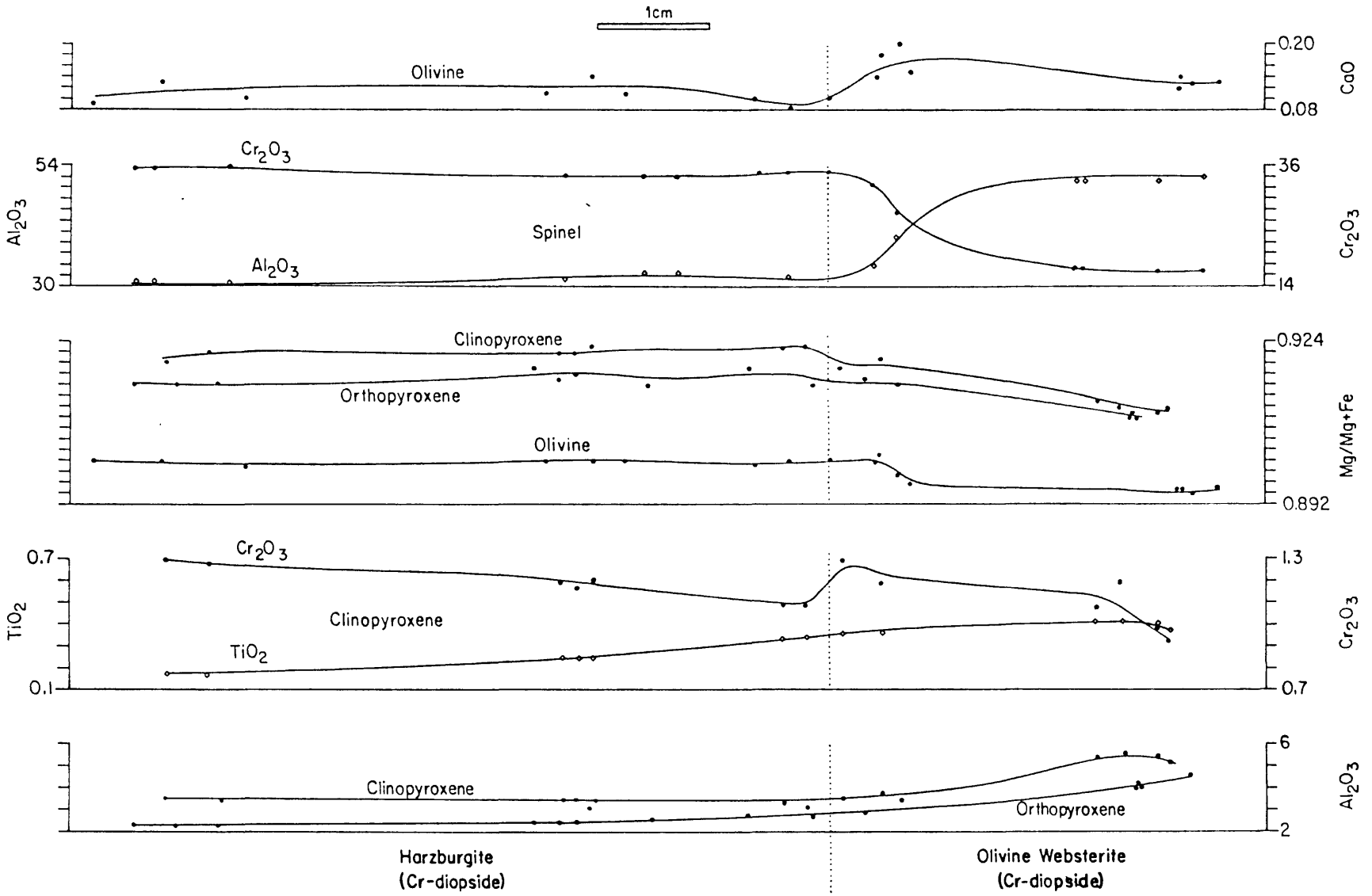

Fig. VI-4. Chemical variations across contact between Cr-diopside harzburgite and Cr-diopside olivine websterite, composite sample SC-1-6.

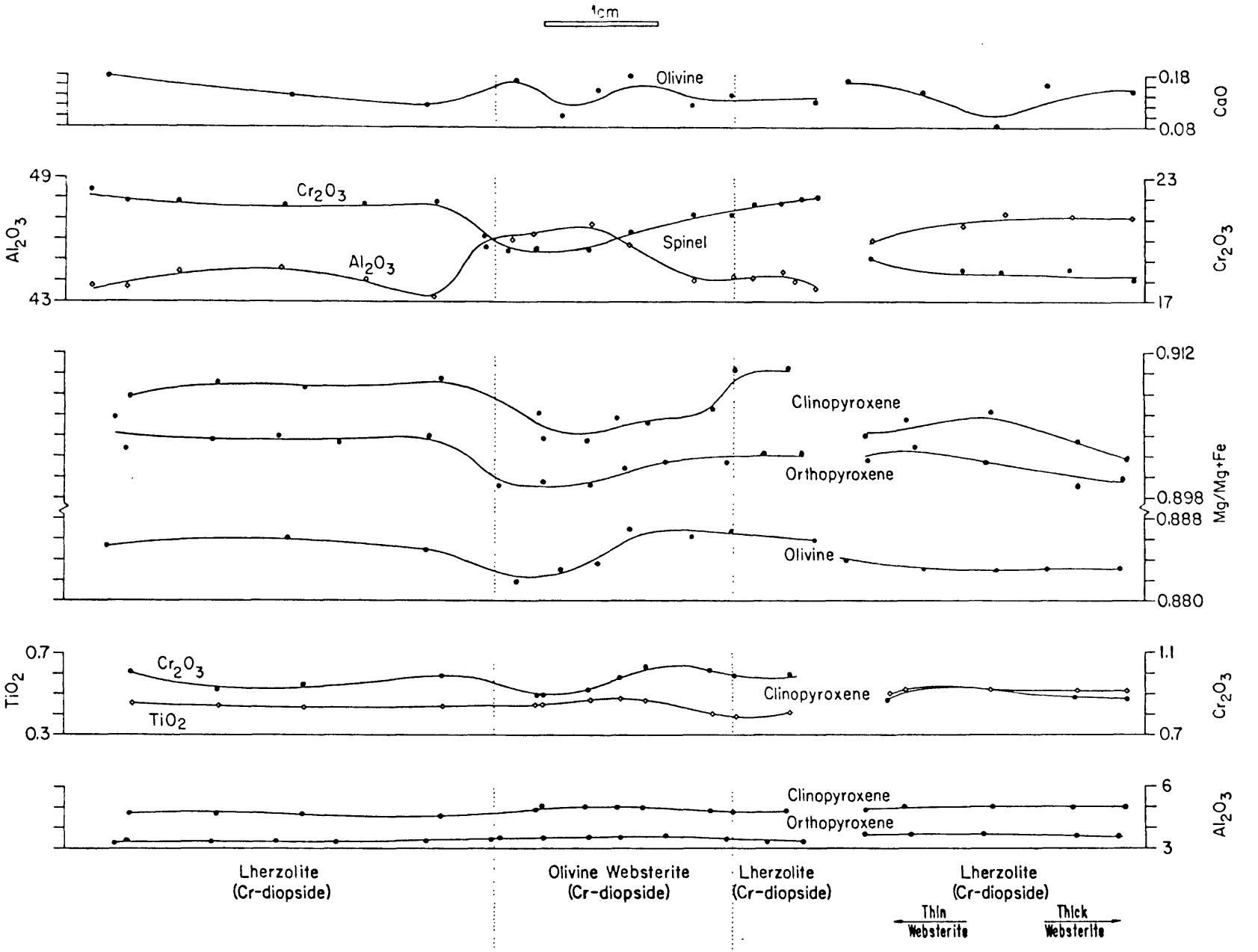

Fig. VI-5. Chemical variations across banded Cr-diopside lherzolite and olivine websterite, composite sample SC-1-3.

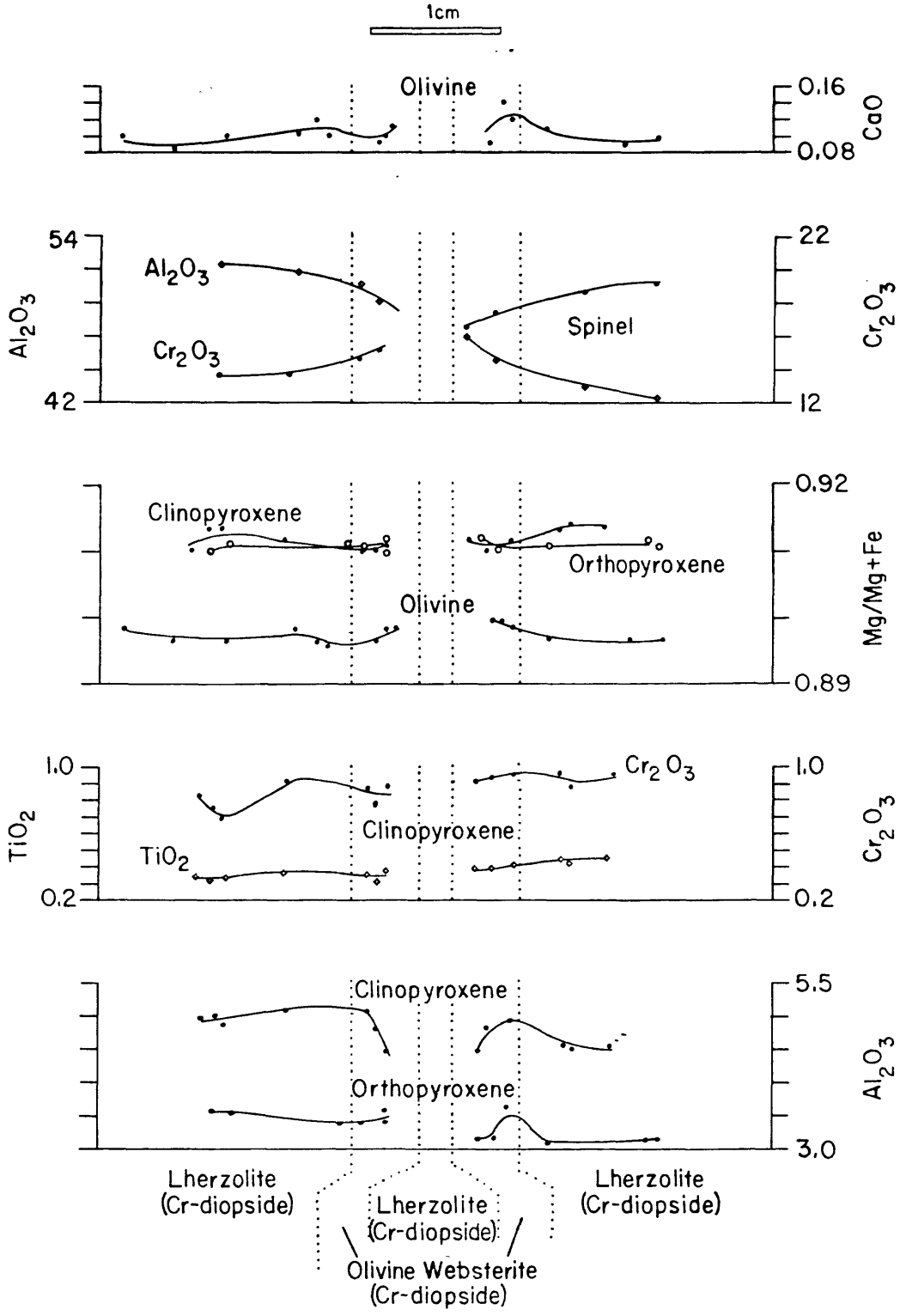

Fig. VI-6. Chemical variations across banded Cr-diopside lherzolite and Cr-diopside olivine websterite, composite sample Ki-5-1.

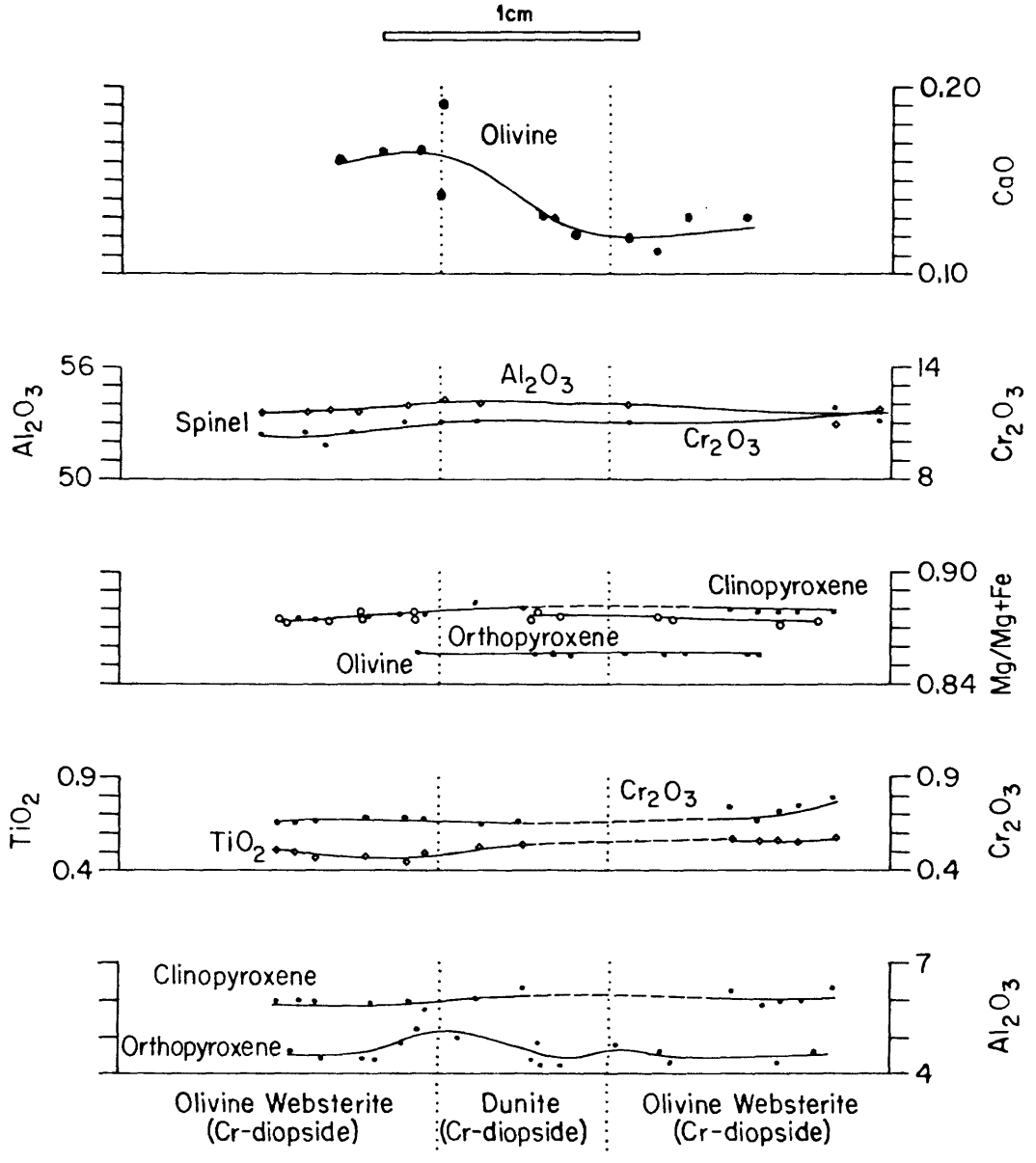

Fig. VI-7. Chemical variations across Cr-diopside dunite sandwiched by Cr-diopside olivine websterite, composite sample SC-1-12.

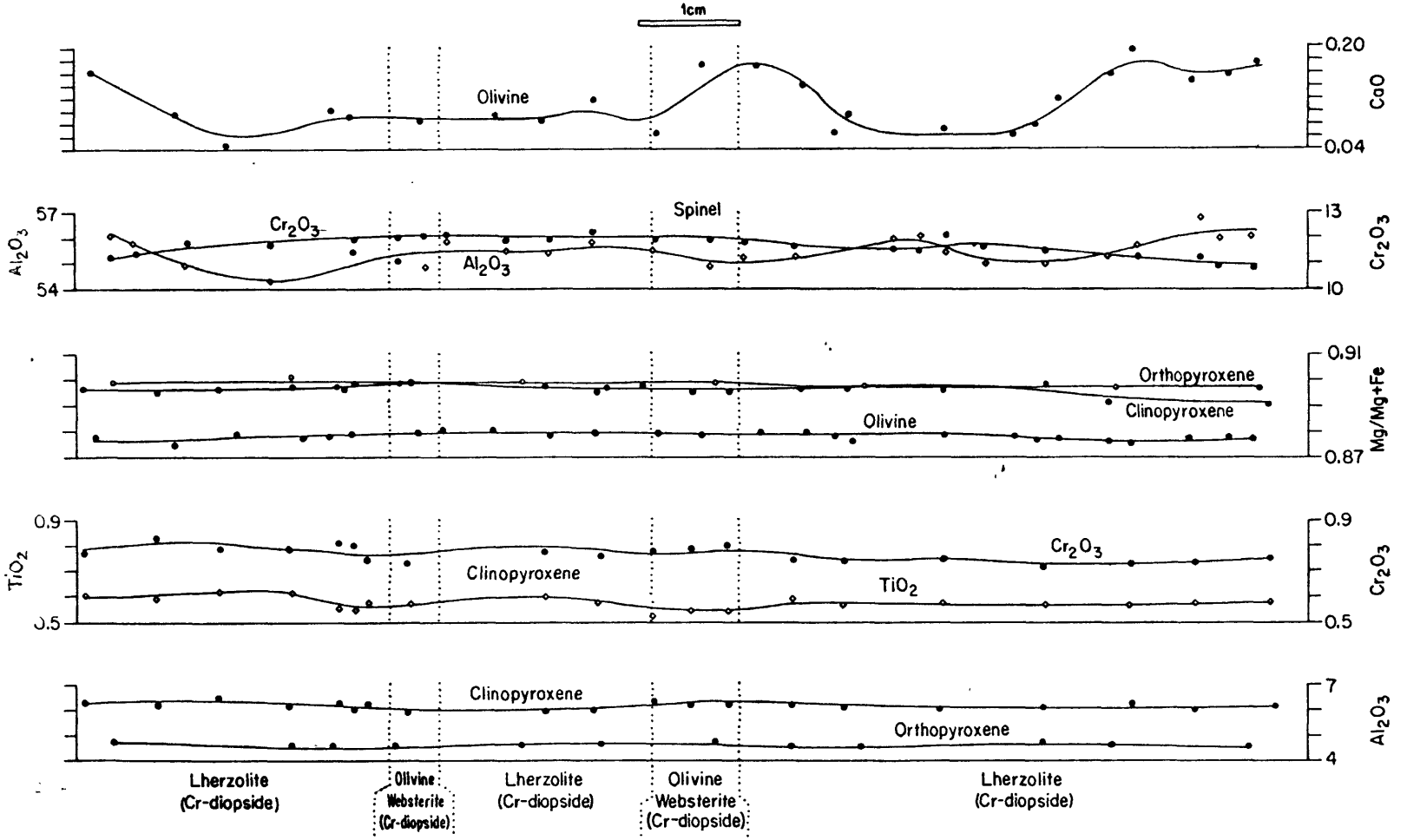

Fig. VI-8. Chemical variations across banded Cr-diopside lherzolite and Cr-diopside olivine websterite, composite sample SC-1-17.

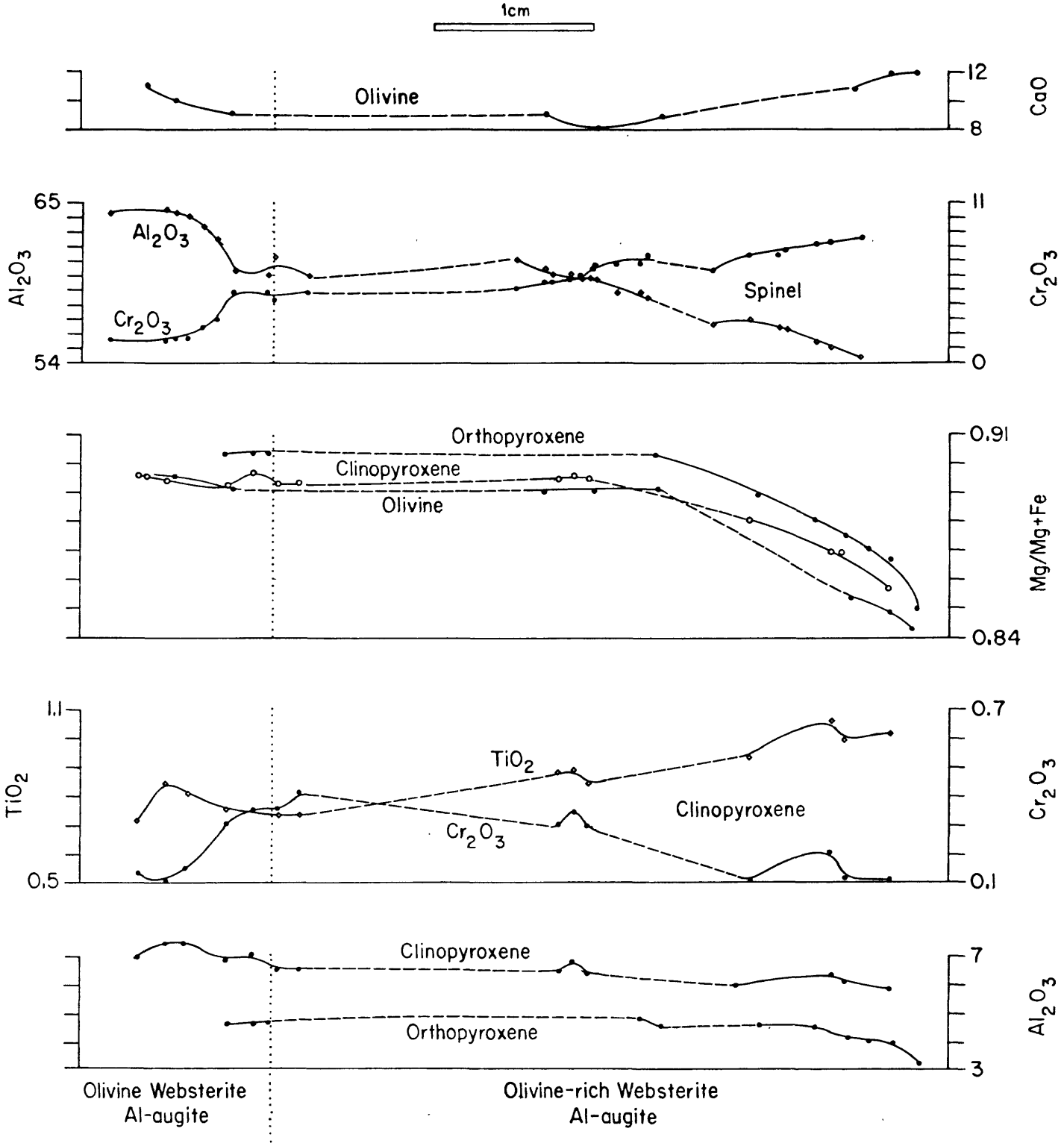

Fig. VI-9. Chemical variations across contact between Al-augite olivine websterite and olivine-rich Al-augite olivine websterite, composite sample Ba-1-24.

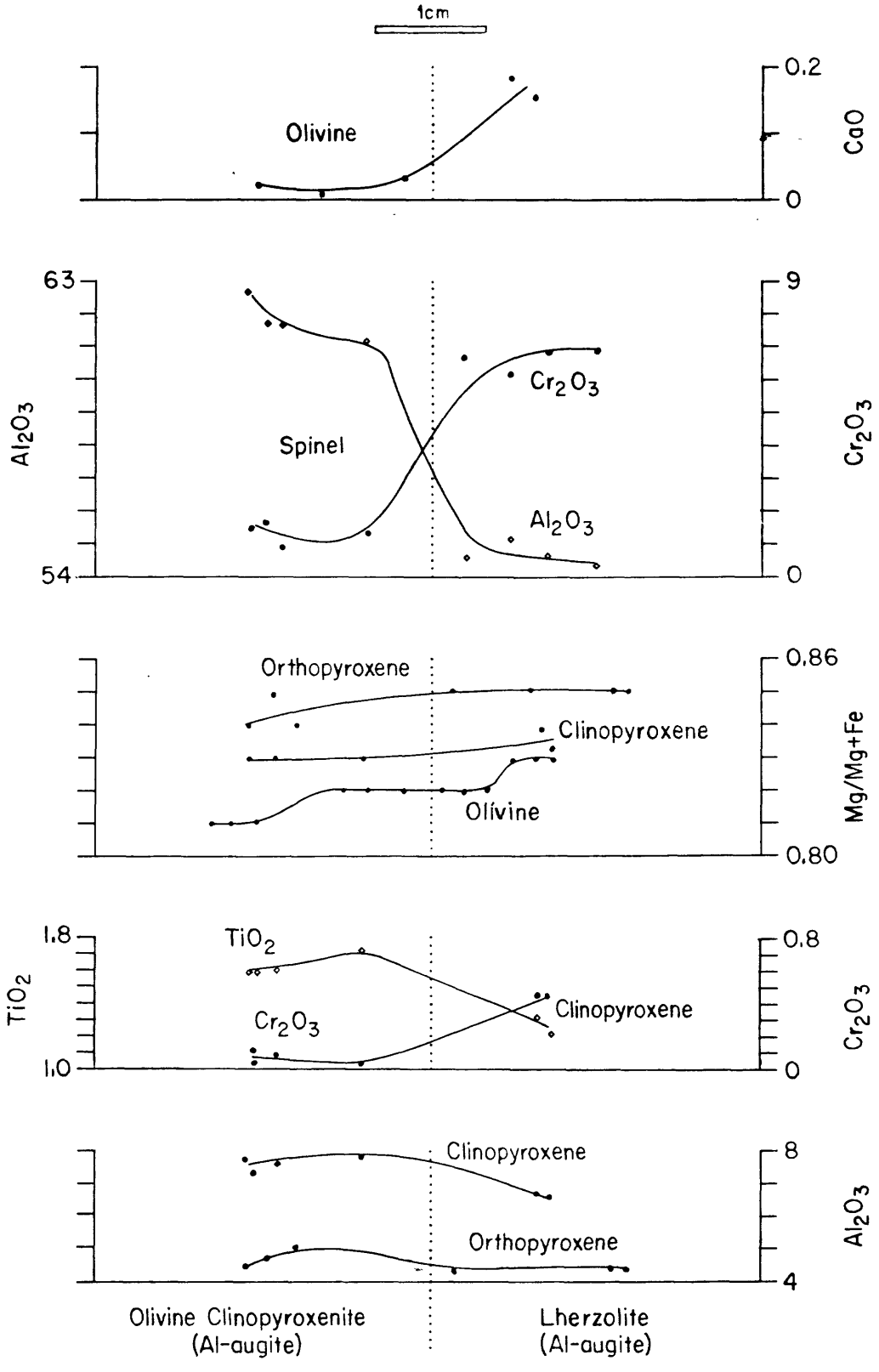

Fig. VI-10. Chemical variations across contact between Al-augite lherzolite and Al-augite olivine clinopyroxenite, composite sample Ep-3-7.

Fig. VI-11. Chemical variations across contact between Al-augite lherzolite and Al-augite olivine clinopyroxenite, composite sample Ep-3-84.

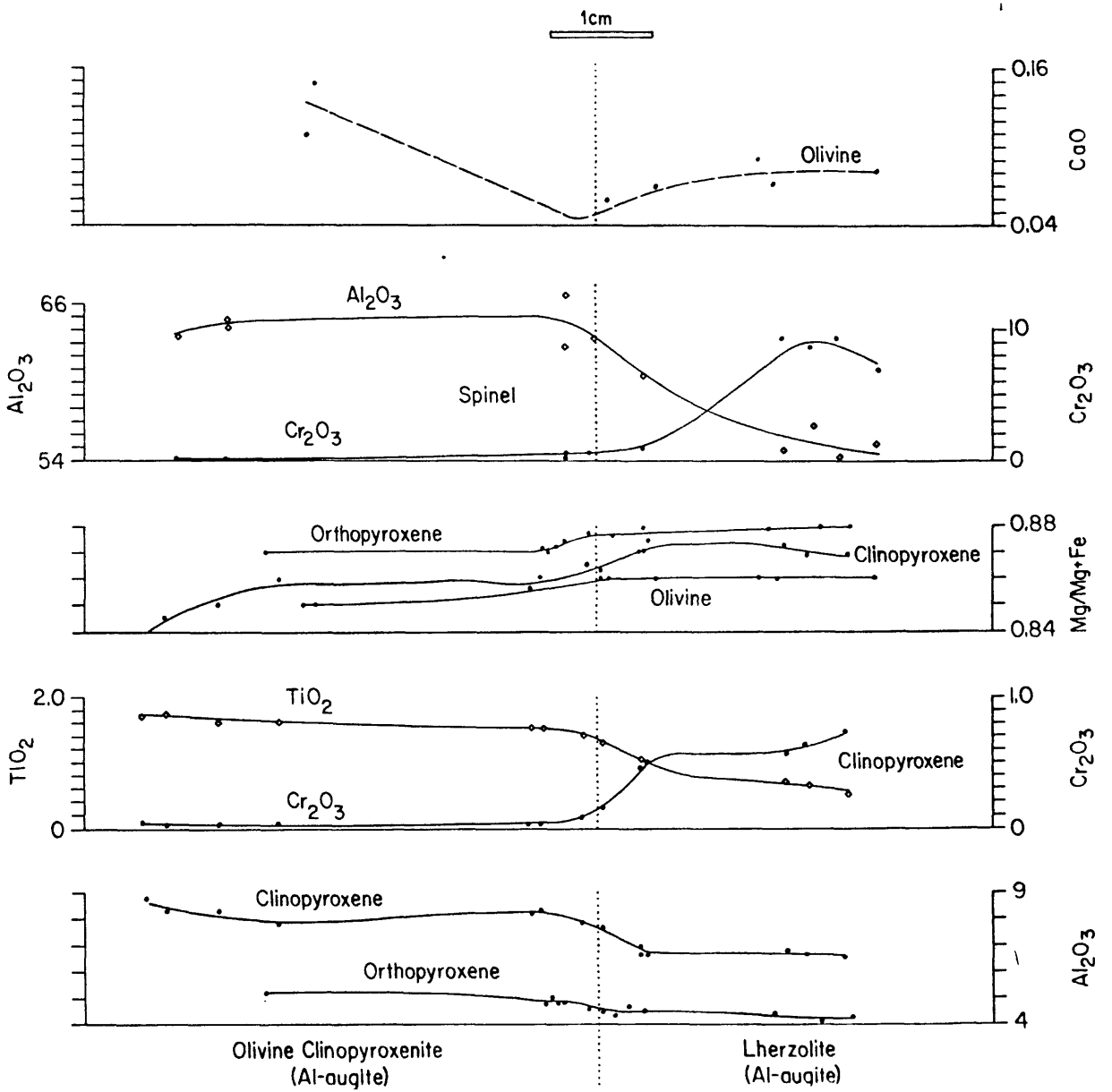

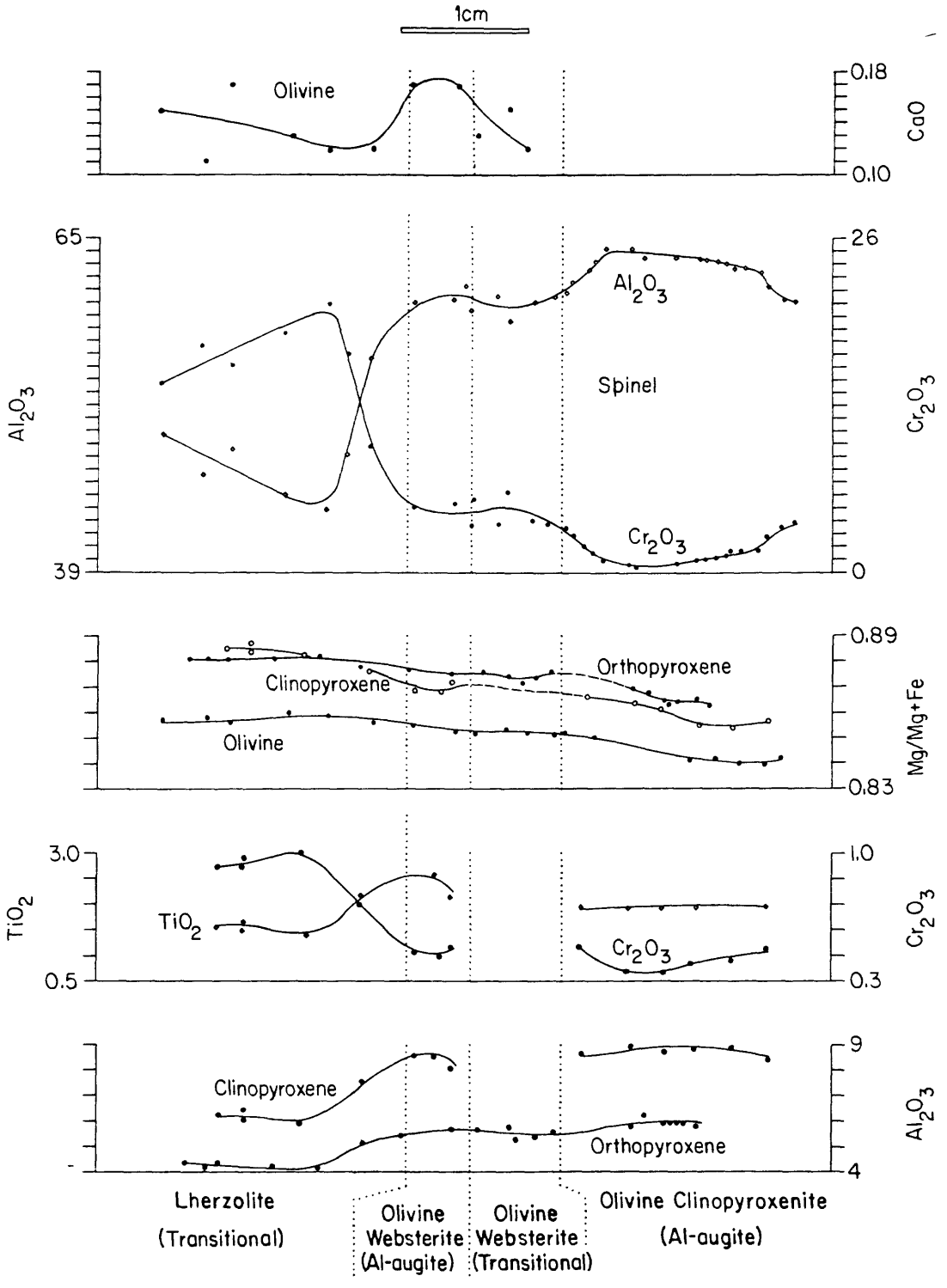

Fig. VI-12. Chemical variations across Al-augite clinopyroxenite and olivine websterite interbanded with lherzolite and olivine websterite transitional between Al-augite and Cr-diopside groups, composite sample SC-1-9.

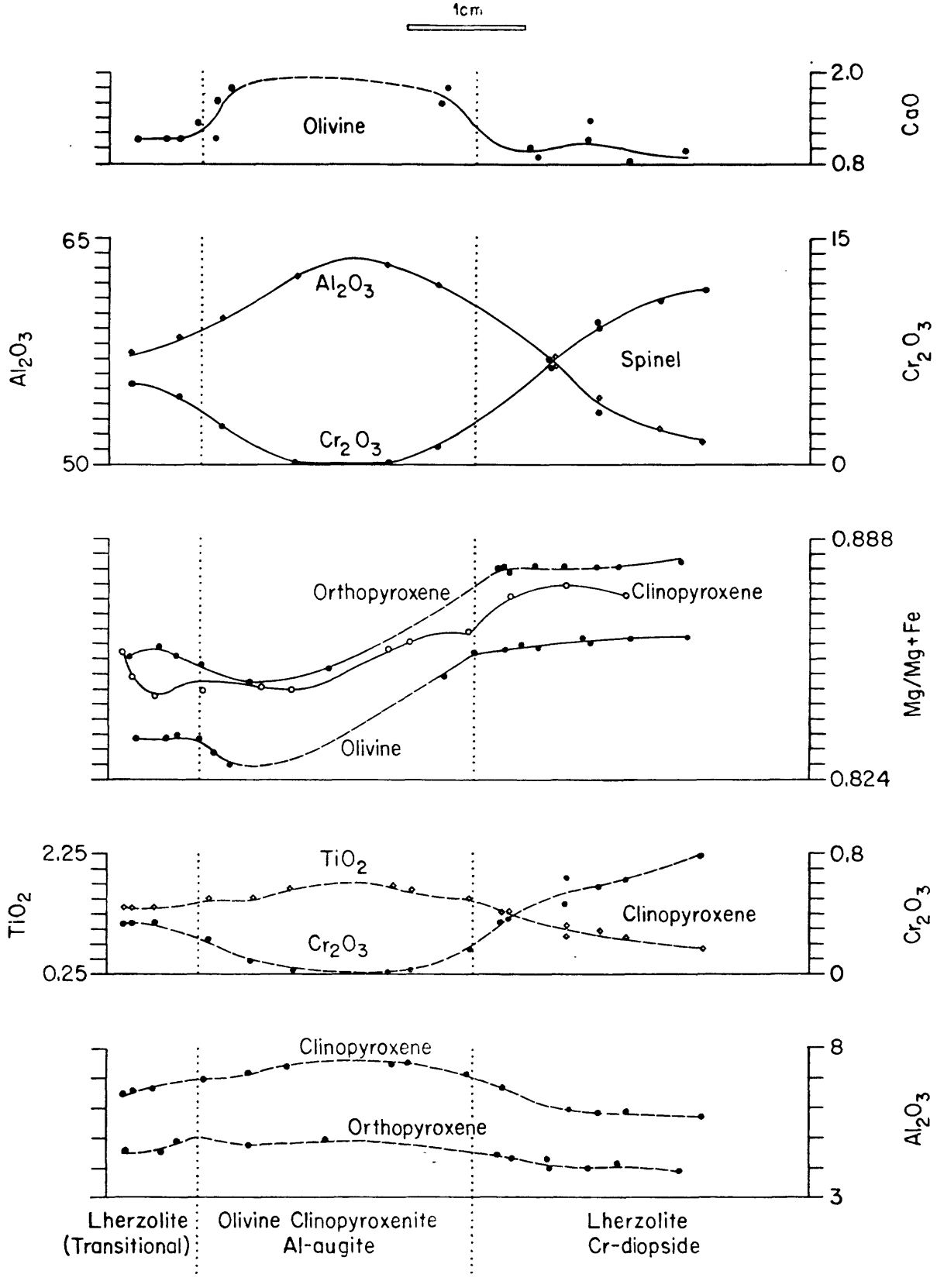

Fig. VI-13. Chemical variations across lherzolite transitional between Cr-diopside and Al-augite lherzolite, Al-augite olivine clinopyroxenite, and Cr-diopside lherzolite, composite sample Ep-3-136.

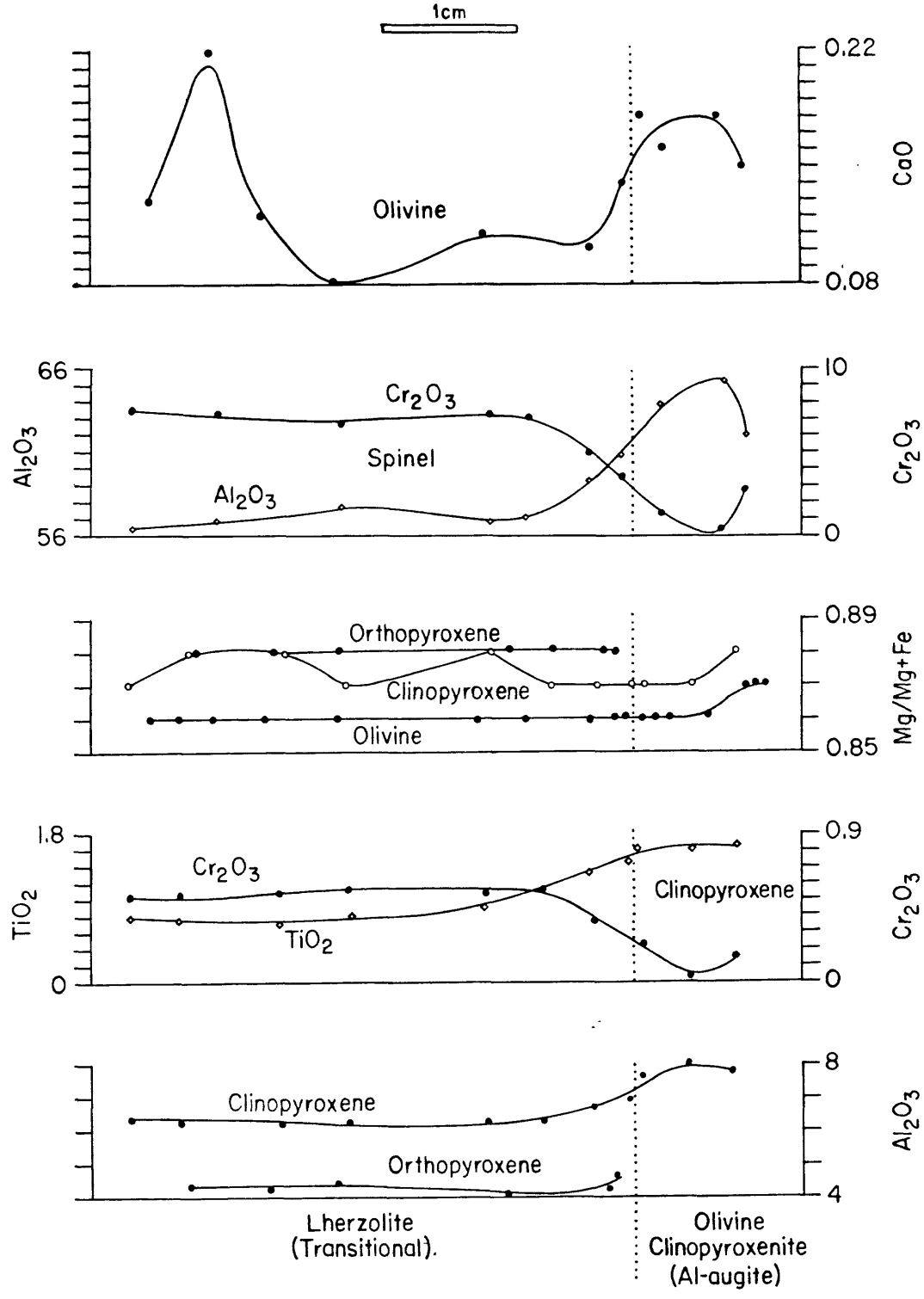

Fig. VI-14. Chemical variations across lherzolite transitional between Cr-diopside and Al-augite groups and Al-augite olivine clinopyroxenite, composite sample Ep-1-10.

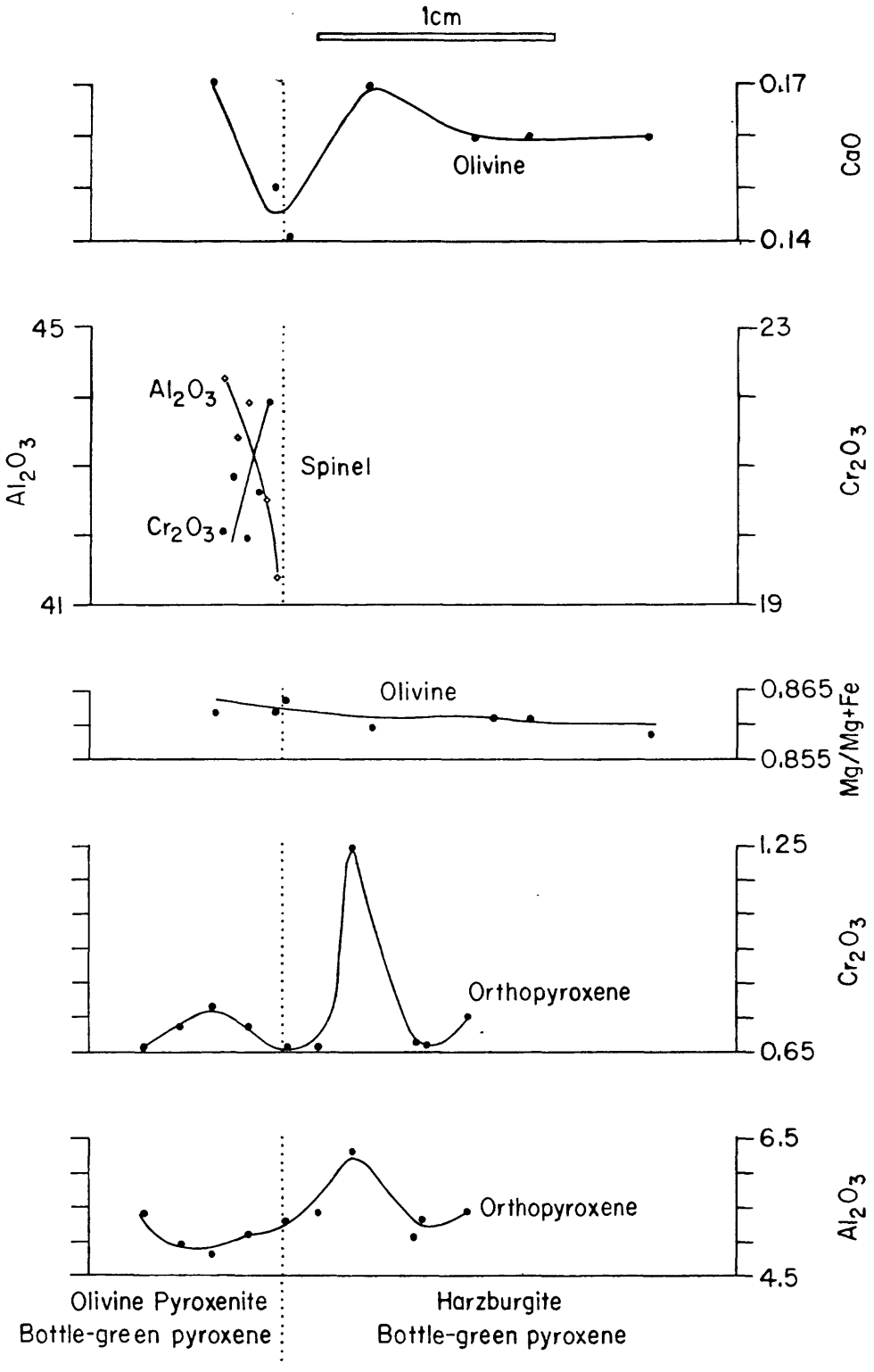

Fig. VI-15. Chemical variations across contact between bottle-green pyroxene olivine pyroxenite and harzburgite, composite sample Tm-2-78.

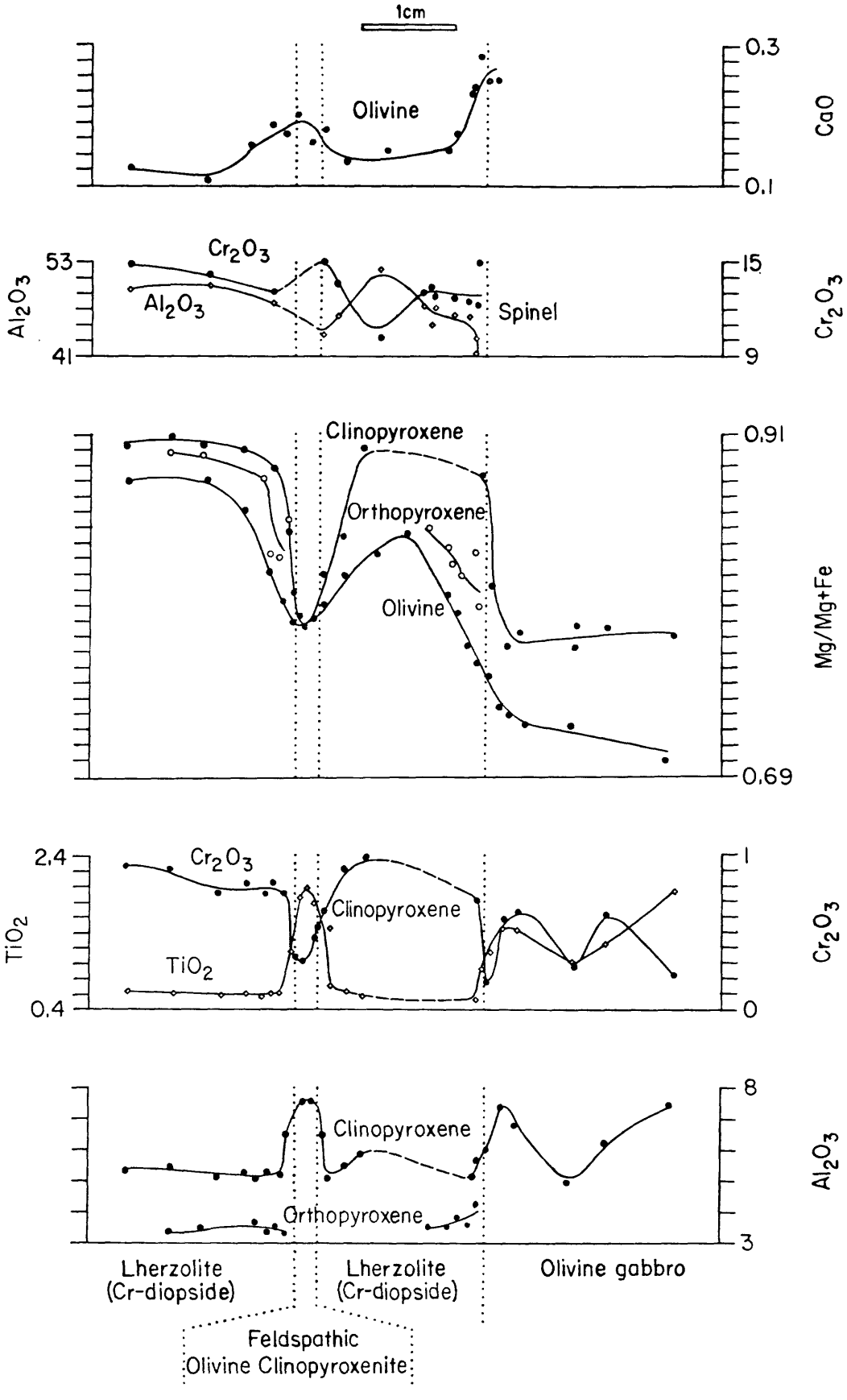

Fig. VI-16. Chemical variations across banded Cr-diopside lherzolite, feldspathic olivine clinopyroxenite, and olivine gabbro, composite sample Ki-5-127.

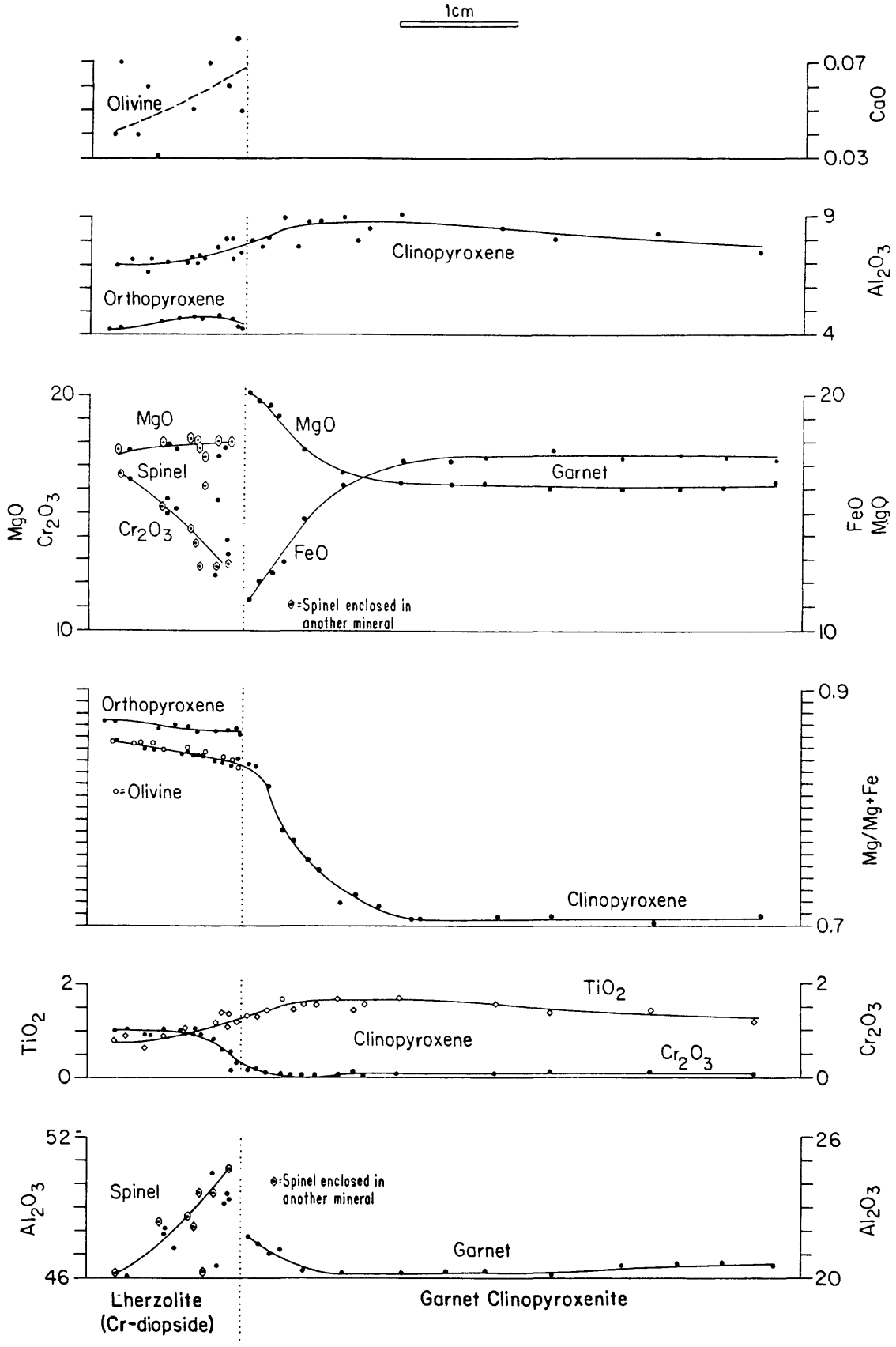

Fig. VI-17. Chemical variations across contact between Cr-diopside lherzolite and garnet clinopyroxenite, composite sample 68-SAL-11.

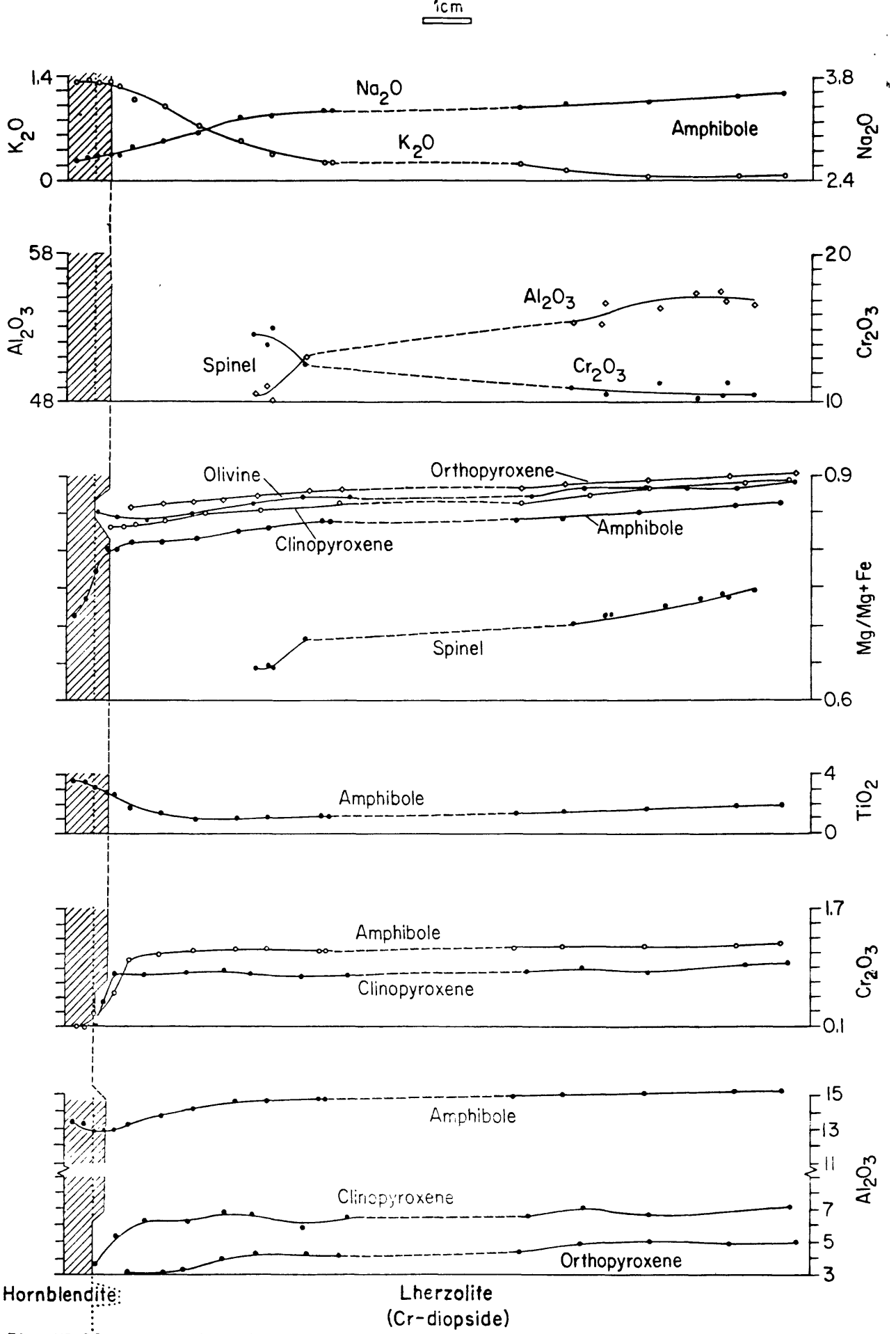

Fig. VI-18. Chemical variations across a kaersutite selvage on Cr-diopside lherzolite, composite sample Ba-2-1.

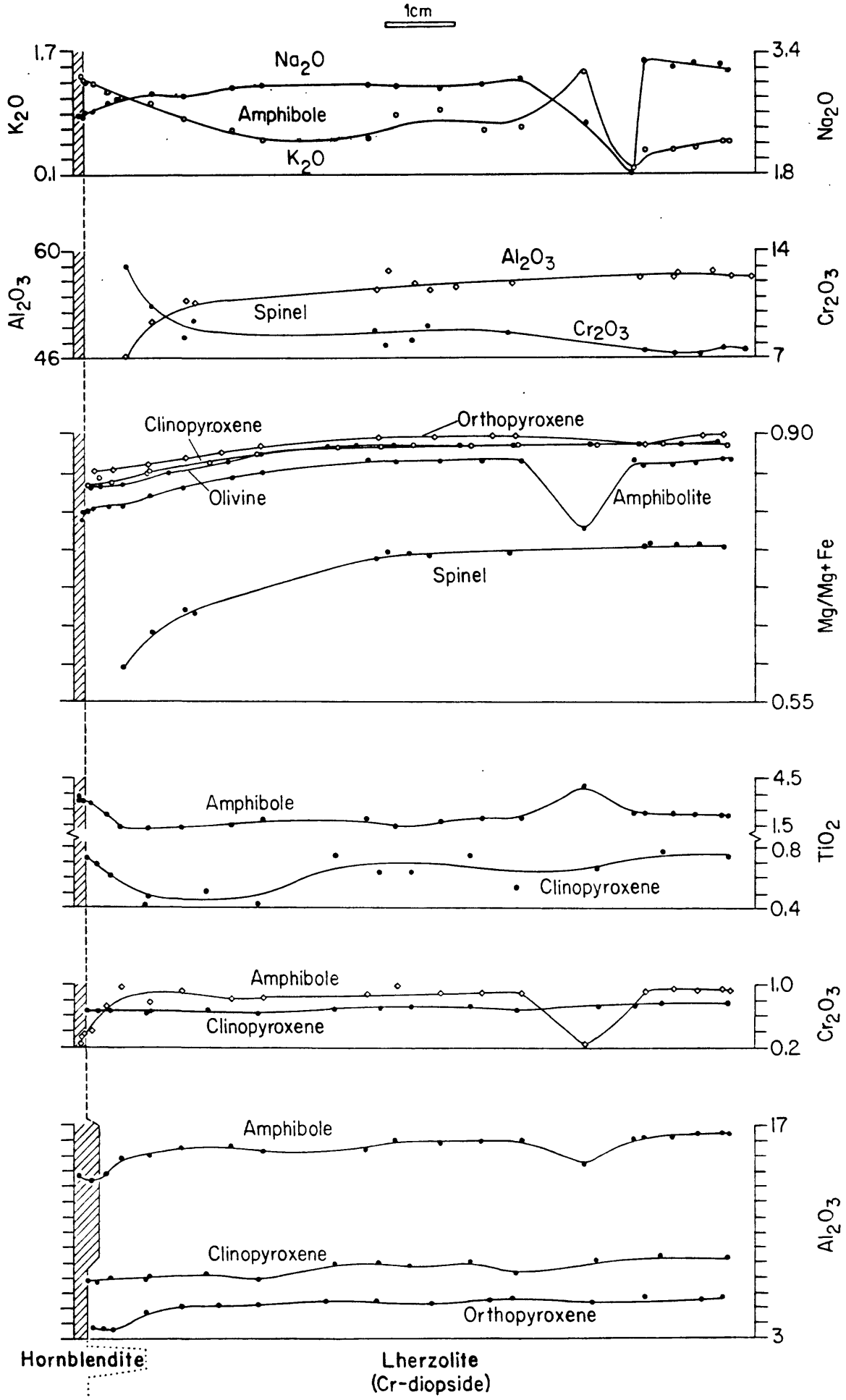

Fig. VI-19. Chemical variations across a kaersutite selvage on Cr-diopside lherzolite, composite sample DL-5-11.

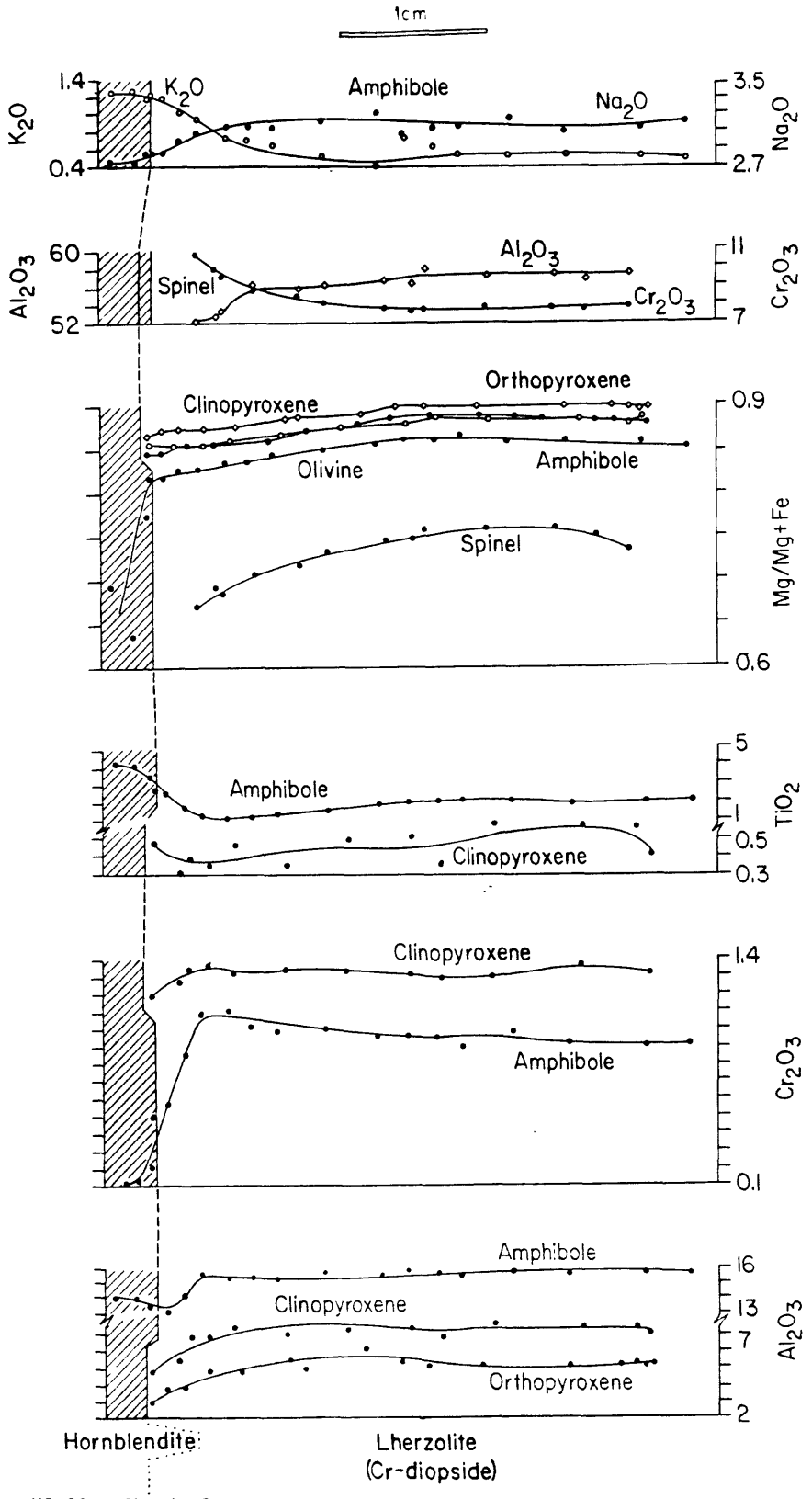

Fig. VI-20. Chemical variations across a kaersutite selvage on Cr-diopside lherzolite, composite sample Ba-1-72.

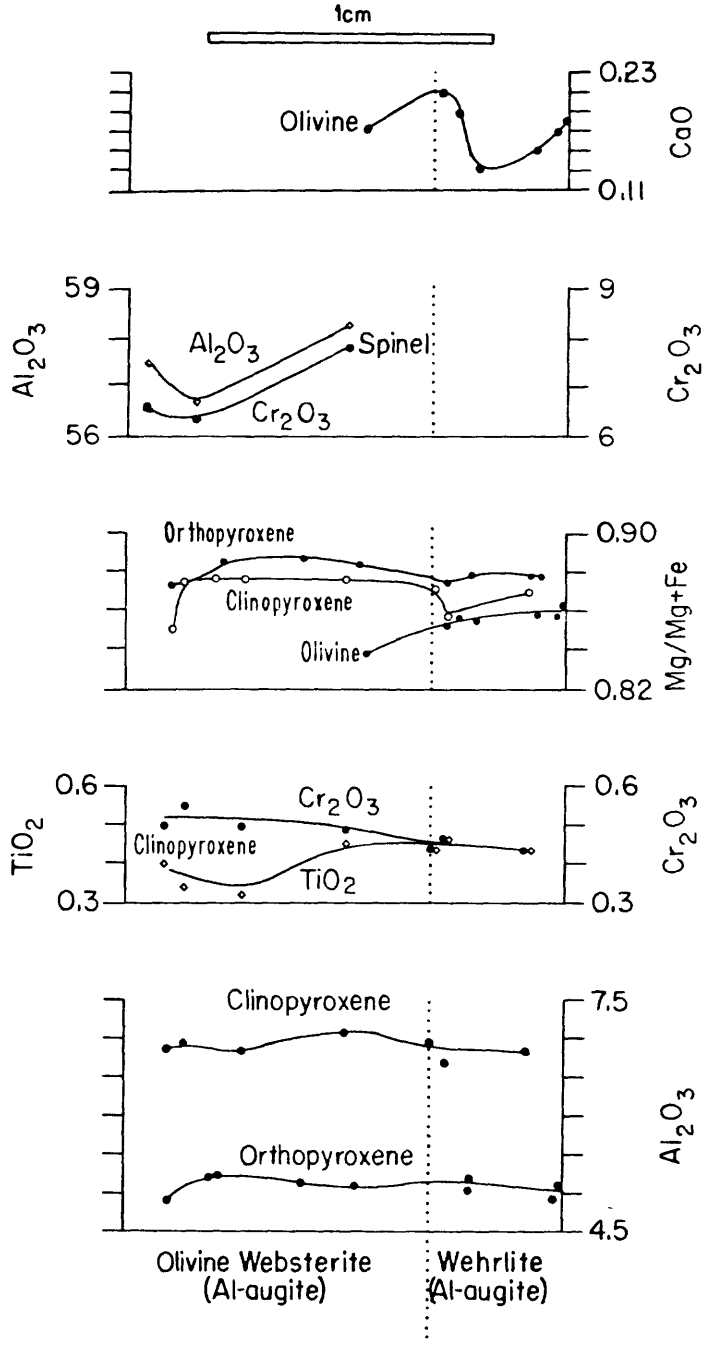

Fig. VI-21. Chemical variations across contact between Al-augite olivine websterite and Al-augite wehrlite, composite sample Ba-1-15.

Appendix VII. Trace Element and Isotopic Data for Host Rocks, Xenoliths, and Megacrysts.

Rare earth element (REE) data have been reported for basaltic host rocks of xenoliths from localities 19, 32, 55, 64, 65, and 67 (Table VII-1A), xenoliths of the Cr-diopside group from localities 32, 64, 65, 66, and 67 (Table VII-1B), xenoliths of the Al-augite group from localities 64, 65, and 67 (Table VII-1C), and mineral separates from xenoliths and megacrysts from localities, 16, 32, 41, 55, 64, 65, and 67, (Table VII-1D).

Sr isotopic data have been reported for basaltic host rocks of xenoliths from localities 4, 20, 32, 41, 48, 57, 63, and 67 (Table VII-2A), whole rock Cr-diopside group xenoliths from localities 4, 20, 57, and 58 (Table VII-2B), whole rock Al-augite group xenoliths from localities 57 and 63 (Table VII-2C), whole rock bottle green pyroxene group xenoliths (Table VII-2D), mineral components of Cr-diopside group xenoliths from localities 4, 32, 63, and 67 (Table VII-2E, nos. 1-31), mineral components of Al-augite group xenoliths and megacrysts from localities 4, 23, 32, 41, 48, and 63 (Table VII-2E, no. 34-37), and mineral components of feldspathic ultramafic group xenoliths from locality 4 (Table 2E nos. 32-33).

Sr and/or Nd isotopic data have been reported for basaltic host rocks of xenoliths from localities 9 and 65 (Table VII-3A) and minerals separated from xenoliths of the Cr-diopisde and Al-augite groups from localities 32 and 65 (Table VII-3B). Whole rock data are reported on garnetiferous xenoliths from locality 9, and from a Cr-diopisde lherzolite (Table VII-3C).

$\delta^{18}O$ values have been determined for host basaltic rocks from localities 4, 16, 32, 63 and 67 (Table VII-4A), whole rock Cr-diopside group xenoliths from localities 4, 32, 63, and 67 (Table VII-4B), whole rock Al-augite group xenoliths from localities 32, 40, 47, and 63 (Table VII-4C), and mineral separates and megacrysts from localities 4, 16, 23, 32, 40, 41, 44, 63, and 67 and two unnumbered localities (dike, west Texas, Irving, 1977; Riley maar, west Potrillo Mountains, New Mexico, Boettcher and O'Neil, 1980) (Table VII-4D).

Table VII - 1A. Rare earth elements in host rocks

Sample (Reference)	1(2)	2(2)	3(5)	4(5)	5(5)	6(5)	7(5)	8(5)	9(7)	10(7)	11(7))	12(7)
La	32.6	38.5	39.4	39.3	34.6	43.2	59	71	60	43.17		
Ce	82	67	77	73	67	84	106	131	120	90.9	53.4	60.3
Pr												
Nd	37	33	35	33	32	32	40	49	43.2	40.7	21.4	31.4
Pm											8	
Sm	7.85	7.17	6.46	5.67	6.20	6.65	6.81	8.26	8.59	8.01	4.83	7.29
Eu	2.23	2.28	2.18	1.99	2.14	2.27	2.25	2.81	2.93	2.61	1.72	2.51
Gd										5.46	7.45	
Tb	1.1	1.1	0.87	0.79	0.87	0.88	0.90	0.98	1.21	1.04		
Dy	1.1	1.1	5.4	4.8	5.3	5.7	5.6	6.2	6.56	6.18	4.56	7.03
Ho												
Er										2.52	3.47	
Tm												
Yb	2.3	2.0	2.57	2.46	2.50	2.84	3.02	3.29	3.36	2.57	2.02	2.95
Lu	0.38	0.30	0.33	0.29	0.35	0.40	0.44	0.44	0.45	0.30		

Samples: 1-2. Basalts, San Carlos, Arizona; 3-8, Basalts, San Bernardino field, Arizona. 9-13. Basalts, Lunar Crater field, Nevada. 14. Minette, The Thumb, Arizona. 15. Basalt, Kilbourne Hole, New Mexico. 16. Basalts, Alpine, Texas. 17. Mt. Riley, New Basalt, Mexico. 18. Basalt, 96 Ranch, Texas, 19. Basalt, Dish Hill, California. 20-21. Basalts, San Bernardino field, Arizona. References: (1) Jagoutz and others (1979); (2) Frey and Prinz (1979); (3) Reid and Frey (1971); (4) A. J. Irving (written communication, 1979); (5) W. R. Nash (written communication, 1981); (6) Irving (1980); (7) Bergman (1982); Bergman and others (1981); (8) Ehrenberg (1982); (9) Irving and Frey (1984). (10) Menzies and others (1984).

Sample (Reference)	13(7)	14(8)	15(9)	16(9)	17(9)	18(9)	19(9)	20(10)	21(10)
La		186	37.1	27.6	29.4	59	47.5	29.0	49.3
Ce	56.4	313	70	69.6	60	118	85.3	63.6	96.5
Pr									
Nd	28.4		31.8	35.2		50	34.2	28.6	42.7
Pm									
Sm	6.11	28.1	6.96	8.00	5.96	8.8	8.08	5.71	7.85
Eu	2.15	6.3	2.42	2.57	1.96	2.66	2.57	1.90	2.47
Gd	5.46				7.96			4.43	6.45
Tb		1.9	1.02	1.25	0.87	1.10	1.05		
Dy	4.97								5.59
Ho			1.60			1.2			
Er	2.36							2.45	3.34
Tm									
Yb	2.02	2.1	2.76	2.48	2.10	2.50	2.75	2.23	2.73
Lu		0.25	0.45	0.388	0.31	0.41	0.40		

Table VII - 1B Rare earth elements in Cr-diopside group xenoliths

Sample Reference)*	1(1)	2(2)	3(2)	4(2)	5(2)	6(2)	7(2)	8(2)	9(2)	10(2)
La	0.51	0.98	0.85	0.84	0.21	1.36	0.08	0.90	0.15	1.8
Ce	1.70	1.7	1.5	2.0	0.79	0.99	0.34	1.9	0.41	6.3
Pr	0.31	0.25	0.21	0.36	0.18	0.34	0.034	0.30	0.066	0.93
Nd		0.88	0.81	1.5	1.2	1.5	0.22	1.25	0.35	4.7
Pm										
Sm	0.54	0.163	0.171	0.342	0.461	0.314	0.118	0.279	0.114	1.38
Eu	0.20	0.056	0.061	0.119	0.228	0.101	0.046	0.103	0.041	0.49
Gd	0.69	0.17	0.20	0.39	0.89	0.36	0.28	0.34	0.21	1.75
Tb	0.12	0.022	0.032	0.060	0.16	0.055	0.048	0.055	0.035	0.27
Dy	0.77									
Ho	0.17	0.028	0.033	0.096	0.23	0.076	0.072	0.095	0.070	0.33
Er	0.44	0.082	0.093	0.24	0.62	0.27	0.21	0.25	0.21	0.98
Tm		0.011	0.015	0.038	0.092	0.041	0.022	0.041	0.033	0.12
Yb	0.47	0.083	0.098	0.27	0.54	0.27	0.17	0.32	0.26	0.62
Lu	0.071	0.016	0.02	0.041	0.098	0.07	0.026	0.05	0.040	0.13

Samples: 1. Lherzolite, San Carlos, Arizona. 2. Dunite, San Carlos, Arizona. 3-6. Lherzolite, San Carlos, Arizona. 7-9. Olivine orthopyroxenite and websterite, San Carlos, Arizona. 10-12, Olivine clinopyroxenite and websterite, San Carlos, Arizona. 13-14, Lherzolite, San Carlos, Arizona. 15. Orthopyroxenite, San Carlos, Arizona. 16. Harzburgite, San Carlos, Arizona. 17-21. Lherzolite, San Carlos, Arizona. 22. Lherzolite, Potrillo Maar, New Mexico. 23-42 Lherzolite, Kilbourne Hole, New Mexico. 43-44. Lherzolite, San Bernardino field, Arizona. 45. Websterite, San Bernardino field, Arizona. 46. Lherzolite, Dish Hill, California. 47. Lherzolite, San Quintin, Baja California.

*References same as Table VII - 1A

Table VII - 1B Rare earth elements in Cr-diopside group xenoliths (cont'd)

Sample Reference)	11(2)	12(2)	13(4)	14(4)	15(6)	16(6)	17(6)	18(6)	19(6)	20(6)
La	2.1		0.60	0.25	0.147	0.089	0.25	0.147	0.58	0.280.35
Ce		5.8	2.11	0.57				1.4	1.35	
Pr	1.07	0.45								
Nd	5.14	2.6							0.95	
Pm										
Sm	1.45	0.95	0.120	0.126	0.112	0.117	0.127	0.154	0.278	0.164
Eu	0.53	0.355	0.046	0.043	0.047	0.033	0.046	0.056	0.120	0.072
Gd	1.95	1.20								
Tb	0.30	0.21						0.035	0.068	
Dy										
Ho	0.41	0.29								
Er	1.02	0.70								
Tm	0.12	0.097								
Yb	0.66	0.60	0.084	0.083	0.12	0.084	0.083	0.24	0.29	0.32
Lu	0.11	0.086	0.014	0.016	0.019	0.014	0.016	0.043	0.051	0.059

Table VII - 1B Rare earth elements in Cr-diopside group xenoliths (cont'd)

Sample (Reference)	21(6)*	22(1)	23(1)	24(4)	25(4)	26(4)	27(4)	28(4)	29(4)	30(4)
La	0.51	0.081	0.051	0.048	0.045	0.275	0.095	0.19	0.054	0.52
Ce		0.48	0.21		0.27	0.87			0.54	
Pr		0.094	0.081							
Nd										
Pm										
Sm	0.56	0.27	0.27	0.291	0.193	0.265	0.245	0.225	0.235	0.479
Eu	0.20	0.12	0.11	0.124	0.083	0.103	0.110	0.094	0.092	0.175
Gd		0.47	0.41							
Tb	0.14	0.10	0.092							
Dy		0.64	0.64							
Ho		0.12	0.14							
Er		0.44	0.50							
Tm										
Yb	0.43	0.45	0.50	0.42	0.31	0.30	0.33	0.36	0.39	0.34
Lu	0.073	0.069	0.073	0.078	0.054	0.062	0.058	0.061	0.065	0.052

Table VII - 1B Rare earth elements in Cr-diopside group xenoliths (cont'd)

Sample (Reference)	31(4)	32(4)	33(4)	34(4)	35(4)	36(4)	37(4)	38(4)	39(4)	40(6)
La	0.070	0.151	0.099	0.159	0.88	0.091	0.028	0.134	0.157	0.30
Ce					2.6	0.63		0.51		
Pr										
Nd										
Pm										
Sm	0.260	0.263	0.199	0.182	0.478	0.231	0.140	0.220	0.240	0.257
Eu	0.108	0.112	0.079	0.080	0.152	0.095	0.067	0.097	0.103	0.096
Gd										
Tb										
Dy										
Ho										
Er										
Tm										
Yb	0.40	0.33	0.32	0.31	0.36	0.34	0.34	0.31	0.36	0.28
Lu	0.064	0.055	0.058	0.056	0.063	0.061	0.062	0.050	0.060	0.054

Table VII - 1B Rare earth elements in Cr-diopside group xenoliths (cont'd)

Sample (Reference)	41(6)	42(6)	43(5)	44(4)	45(5)	46(4)	47(4)
La	0.41	0.86		0.087	6	0.103	0.123
Ce		3.2	20		13	0.41	
Pr							
Nd					6		
Pm							
Sm	0.247	0.78	0.20	0.198	1.77	0.125	0.147
Eu	0.099	0.26	0.09	0.091	0.83	0.052	0.063
Gd							
Tb			0.05		0.33		
Dy			0.5		2.3		
Ho							
Er							
Tm							
Yb	0.32	0.43	0.31	0.28	0.91	0.28	0.26
Lu	0.055	0.071		0.047	0.13	0.049	0.048

Table VII - 1C Rare earth elements in Al-augite group xenoliths

Sample (Reference)*	1(2)	2(2)	3(2)	4(2)	5(2)	6(2)	7(6)	8(6)	9(6)	10(3)
La	2.81	5.13	4.23	9.18	3.74	5.7	3.46	1.53	1.38	4.80
Ce	6.9	14	10.1	25.1	9.5	11.0	12.2	5.1	3.9	15.42
Pr				4.1	1.75					2.88
Nd	4.8	10.6	7.6	18.6	8.9	10.6				15.41
Pm										
Sm	1.33	3.07	2.10	4.96	2.74	3.35	4.13	1.39	0.94	3.94
Eu	0.47	1.15	0.767	1.63	1.00	1.17	1.44	0.49	0.34	1.42
Gd				6.0	4.0					6.62
Tb	0.20	0.65	0.38	0.96	0.66	0.53	0.88	0.23	0.14	0.85
Dy										
Ho	0.24	0.72	0.48	0.99	0.72	0.43				0.95
Er				2.5	1.77					2.02
Tm				0.35	0.24					0.34
Yb	0.64	1.30	0.78	2.09	1.31	0.78	1.96	0.65	0.43	1.87
Lu	0.095	0.22	0.15	0.31	0.22	0.11	0.31	0.091	0.071	0.30

Samples: 1. Kaersutite wehrlite, San Carlos, Arizona. 2. Clinopyroxenite, San Carlos, Arizona. 3. Olivine Kaersutite websterite, San Carlos, Arizona. 4. Olivine kaersutite clinopyroxenite, San Carlos, Arizona. 5. Olivine clinopyroxenite, San Carlos, Arizona. 6. Kaersutite peridotite, San Carlos, Arizona. 7. Clinopyroxenite, San Carlos, Arizona. 8-9. Poikilitic wehrlite, San Carlos, Arizona. 10. Clinopyroxenite, Kilbourne Hole, New Mexico. 12. Olivine clinopyroxenite, Kilbourne Hole, New Mexico. 13. Alkali gabbro, San Bernardino field, Arizona. 14. Clinopyroxenite, San Bernardino field, Arizona. 15. Olivine kaersutite clinopyroxenite, San Bernardino field, Arizona.

*References same as Table VII - 1A.

Table VII - 1C Rare earth elements in Al-augite group xenoliths (cont'd)

Sample (Reference)	11(6)	12(6)	13(5)	14(5)	15(5)
La	3.02	3.46		4	9
Ce	10.7	11.5	5	13	20
Pr					
Nd		11	7	10	15
Pm					
Sm	3.37	3.55	1.33	2.74	3.49
Eu	1.11	1.26	0.51	1.03	1.27
Gd					
Tb	0.57	0.67	0.30	0.55	0.61
Dy			2.2	3.7	4.0
Ho					
Er					
Tm					
Yb	1.58	1.56	0.91	1.50	1.68
Lu	0.24	0.23	0.11	0.17	0.19

Table VII - 1D Rare earth elements in crystal separates from xenoliths and megacrysts

Sample (Reference)	1(2)	2(2)	3(2)	4(2)	5(2)	6(5)	7(5)	8(5)	9(5)	10(5)
La	4.32	1.39	0.91	0.19	0.14			5.7	14	10.6
Ce	8.8	1.6	2.0	0.20	0.15		8	18	43	9.5
Pr	1.47	0.646	0.618							
Nd	6.36	4.22	3.29	0.35	0.31		6	22	34	1.3
Pm										
Sm	1.99	1.98	1.18	0.46	0.45	0.01	1.77	6.09	8.36	0.10
Eu	0.743	0.770	0.448	0.62	0.58		0.67	2.32	2.92	2.39
Gd	2.36	3.12	1.63							
Tb	0.32	0.59	0.28	0.74	0.81		0.35	1.03	1.24	
Dy							2.5	6.5	7.7	
Ho	0.343	0.797	0.362	0.79	0.85					
Er	0.99	2.15	1.01							
Tm	0.131	0.315	0.134							
Yb	0.91	2.05	0.79	0.67	0.72		0.96	2.16	2.96	
Lu	0.41	0.29	0.13	0.69	0.74		0.12	0.28	0.42	

Samples: 1-2. Clinopyroxene from Cr-diopside lherzolite, San Carlos, Arizona. 3. Clinopyroxene from Cr-diopside websterite, San Carlos, Arizona. 4. Clinopyroxene from Al-augite olinopyroxenite, San Carlos, Arizona. 5. Clinopyroxene from Al-augite peridotite, San Carlos, Arizona. 6. Olivine megacryst, San Bernardino field, Arizona. 7. Clinopyroxene megacryst, San Bernardino field, Arizona. 8-9. Kaereutite megacrysts, San Bernardino field, Arizona. 10-12. Feldspar megacrysts, San Bernardino field, Arizona. 13-14. Al-augite olinopyroxene megacrysts, Lunar Crater field, Nevada. 15-16. Kaersutite megacrysts, Lunar Crater field, Nevada. 17-18. Bottle green olinopyroxene megacrysts, Lunar Crater field, Nevada. 19. Feldspar megacryst, Lunar Crater field, Nevada. 20-26. Clinopyroxene from coarse garnet lherzolite, The Thumb, Arizona. 27-30. Clinopyroxene from garnet olinopyroxenite, The Thumb, Arizona. 31-33. Clinopyroxene from ultra coarse peridotite, The Thumb, Arizona. 34-39. Clinopyroxene megacrysts, The Thumb, Arizona. 40-47. Clinopyroxene from sheared garnet lherzolite, The Thumb, Arizona. 48-53. Garnet from coarse garnet lherzolite, The Thumb, Arizona. 54-56. Garnet from garnet olinopyroxenite, The Thumb, Arizona. 57-62. Garnet from sheared garnet lherzolite, The Thumb, Arizona. 63. Kaersutite megacryst, Dish Hill, California. 64. Kaersutite vein, Dish Hill, California. 65. Kaersutite megacryst, Kilbourne Hole, New Mexico. 66. Kaersutite, megacryst, Mt. Riley, New Mexico. 67. Kaersutite megacryst, 96 Ranch, Texas. 68. Kaersutite megacryst, Hoover Dam, Arizona. 69-71. Clinopyroxene megacryst, Kilbourne Hole, New Mexico. 72. Clinopyroxene megacryst, San Carlos, Arizona. 73. Orthopyroxene megacryst, Alpine, Texas. 74. Mica megacryst, 96 Ranch, Texas. 74. Mica megacryst, 96 Ranch, Texas. 75. Anorthoclase megacryst, 96 Ranch, Texas. 76. Anorthoclase megacryst, San Carlos, Arizona. 77. Apatite megacryst, 96 Ranch, Texas. 78. Apatite megacryst, San Carlos, Arizona. 79. Clinopyroxena from Cr-diopside lherzolite, San Bernardino field, Arizona. 80. Amphibole, same xenolith as 79. 81. Apatite, same xenolith as 79. 82-84. Clinopyroxenes from Cr-diopside-lherzolites, San Bernardino field, Arizona. 85. Clinopyroxene from Cr-diopside lherzolite, Dish Hill, California. 86. Amphibole from same xenolith as 85. 87-88. Clinopyroxenes from Cr-diopside lherzolites, San Bernardino field, Arizona. 89. Mica from Cr-diopside lherzolite, San Bernardino field, Arizona. 90. Clinopyroxene from same xenolith as 89. 91. Clinopyroxene from Cr-diopside lherzolite, San Bernardino field, Arizona. 92. Apatite from Cr-diopside lherzolite xenolith, San Bernardino field, Arizona. 93. Amphibole from same xenolith as 92. 94. (same as sample 64) kaersutite vein, Dish Hill, California. 95. Clinopyroxene from Cr-diopside lherzolite in contact with 94. 96. Clinopyroxene, Al-augite pyroxenite, San Bernardino field, Arizona. 99. Clinopyroxene from peridotite in contact with 98. 100. Amphibole megacryst, San Bernardino field, Arizona. 101-102. Amphiboles from peridotites, San Bernardino field, Arizona.

Table VII - 1D Rare earth elements in crystal separates from xenoliths and megacrysts (cont'd)

Sample (Reference)	11(5)	12(5)	13(7)	14(7)	15(7)	16(7)	17(7)	18(7)	19(7)
La	10.2	18.2	3.7	2.7	8.21	8.2	2.26	1.46	10.35
Ce	8.1	15.1	7.4	9.0	25.6	29.0	4.67	4.9	10.16
Pr									
Nd	1.1	1.8	9.7	7.5	22.4	26.6	3.7	5.4	0.6
Pm									
Sm	0.06	0.11	3.42	2.68	6.41	7.05	1.30	1.43	0.06
Eu	1.95	0.82	1.33	0.98	2.4	2.63	0.50	0.53	2.22
Gd									
Tb			0.66	0.44	.95	1.10	0.32	0.26	
Dy			4.77	2.97	6.10	6.54	1.80	1.79	0.23
Ho									
Er									
Tm									
Yb			1.88	1.18	2.05	2.17	0.60	0.68	0.01
Lu			0.25	0.17	0.25	0.29	0.10	0.12	

Table VII - 1D Rare earth elements in crystal separates from xenoliths and megacrysts (cont'd)

Sample (Reference)	20(8)	21(8)	22(8)	23(8)	24(8)	25(8)	26(8)	27(8)	28(8)	29(8)
La	3.6	2.6	4.2	3.8	4.5	2.7	4.3	2.2	2.3	2.3
Ce	5.6	7.2	11.2	10.8	11.8	6.6	12.0	5.9	7.2	6.1
Pr										
Nd										
Pm										
Sm	1.14	1.0	2.0	0.80	2.7	1.6	2.5	1.8	2.3	2.0
Eu	0.21	0.25	0.49	0.19	0.60	0.50	0.75	.63	0.71	0.68
Gd										
Tb		0.080	0.14		0.20	0.096	0.19	0.22	0.28	0.25
Dy										
Ho										
Er										
Tm										
Yb			0.10		0.16	0.18	0.21	0.33	0.24	0.26
Lu	0.0056		0.012		0.013	0.019	0.032	0.038	0.030	0.040

Table VII - 1D Rare earth elements in crystal separates from xenoliths and megacrysts (cont'd)

Sample (Reference)	30(8)	31(8)	32(8)	33(8)	34(8)	35(8)	36(8)	37(8)	38(8)	39(8)
La	2.7	4.5	4.8	2.8	3.8	2.8	5.8	6.1	4.8	3.5
Ce	7.7	12.3	10.5	8.7	9.1	9.3	13.1	13.9	12.3	9.7
Pr										
Nd										
Pm										
Sm	2.5	2.7	2.2	2.6	2.3	2.6	3.0	2.8	2.9	2.8
Eu	0.75	0.88	0.72	0.77	0.71	0.76	0.96	1.10	1.00	0.97
Gd										
Tb	0.25	0.32	0.31	0.25	0.29	0.31	0.38	0.40	0.34	0.38
Dy										
Ho										
Er										
Tm										
Yb	0.29	0.28	0.29	0.24		0.25	0.26	0.26	0.32	
Lu	0.030	0.024	0.029	0.038		0.023	0.029	0.027	0.035	

Table VII - 1D Rare earth elements in crystal separates from xenoliths and megacrysts (cont'd)

Sample (Reference)	40(8)	41(8)	42(8)	43(8)	44(8)	45(8)	46(8)	47(8)
La	3.9	4.2	4.4	3.4	2.8	2.7	2.7	3.0
Ce	11.8	10.4	10.4	8.9	7.7	7.4	7.7	10.5
Pr								
Nd								
Pm								
Sm	3.8	2.9	3.5	2.9	2.6	2.4	2.4	2.7
Eu	0.94	0.92	1.10	0.91	0.78	0.76	0.75	0.83
Gd								
Tb	0.29	0.22	0.38	0.33	0.29	0.30	0.26	0.31
Dy								
Ho								
Er								
Tm								
Yb	0.17	0.10	0.33	0.22	0.28	0.26	0.24	0.27
Lu			0.047	0.031	0.061	0.047	0.036	0.031

Table VII - 1D Rare earth elements in crystal separates from xenoliths and megacrysts (cont'd)

Sample (Reference)	48(8)	49(8)	50(8)	51(8)	52(8)	53(8)
La	0.101	0.068	1.43	0.046	0.075	0.074
Ce						
Pr						
Nd						
Pm						
Sm	0.73	0.63	0.95	0.65	0.67	0.48
Eu	0.37	0.32	0.40	0.28	0.34	0.28
Gd						
Tb			0.31		0.38	0.43
Dy						
Ho						
Er						
Tm						
Yb	0.90	0.54	1.00	1.10	2.8	2.7
Lu	0.20		0.17	0.16	0.50	0.46

Table VII - 1D Rare earth elements in crystal separates from xenoliths and megacrysts (cont'd)

Sample (Reference)	54(8)	55(8)	56(8)	57(8)	58(8)	59(8)	60(8)	61(8)	62(8)
La	0.46	0.41	0.18	0.70	0.090	0.072	0.070	0.110	0.039
Ce									
Pr									
Nd									
Pm									
Sm	1.42	1.60	1.51	2.13	0.84	1.56	1.11	1.07	0.96
Eu	0.83	0.81	0.88	0.73	0.46	0.95	0.70	0.66	0.40
Gd									
Tb	1.02	1.15	0.93	0.43	0.61	0.69	0.53	0.81	0.35
Dy									
Ho									
Er									
Tm									
Yb	5.0	5.1	5.4	2.2	3.0	3.0	2.9	3.6	3.0
Lu	0.77	0.82	0.77	0.27	0.55	0.46	0.48	0.61	0.52

Table VII - 1D Rare earth elements in crystal separates from xenoliths and megacrysts (cont'd)

Sample (Reference)	63(9)	64(9)	65(9)	66(9)	67(9)	63(9)
La	6.55	13.1	5.1	8.1	13.8	6.35
Ce	22.7	41.5	17.1	25.4	47.3	22.0
Pr						
Nd			14.2			
Pm						
Sm	5.60	8.6	4.47	6.2	10.1	5.32
Eu	1.95	2.77	1.67	2.17	3.54	1.75
Gd						
Tb	1.00	1.32	0.71	1.03	1.44	0.89
Dy						
Ho						
Er						
Tm						
Yb	1.57	2.2	1.59	2.0	2.48	1.49
Lu	0.25	0.30	0.23	0.28	0.37	0.23

Table VII - 1D Rare earth elements in crystal separates from xenoliths and megacrysts (cont'd)

Sample (Reference)	69(9)	70(9)	71(9)	72(9)	73(9)	74(9)	75(9)	76(9)	77(9)	78(9)
La	1.24	1.25	1.24	2.38	0.037	0.36	13.2	14	517	712
Ce	5.1	5.4	5.3	7.8		0.55	13.9	11.3	1205	1540
Pr										
Nd	5.5	5.4	5.8	10.1					614	
Pm										
Sm	1.80	1.80	1.88	3.71	0.159	0.034	0.034	0.13	104	121
Eu	0.71	0.72	0.73	1.36	0.071	0.097	0.097	1.8	30.9	34.9
Gd									81.7	
Tb	0.34	0.37	0.42	0.62					10.3	14.2
Dy										
Ho	0.40	0.37	0.45	0.74						
Er										
Tm										
Yb	1.03	1.13	1.16	1.81	0.50				11.3	19.4
Lu	0.19	0.19	0.22	0.25	0.096				1.52	2.38

Table VII - 1D Rare earth elements in crystal separates from xenoliths and megacrysts (cont'd)

Sample (Reference)	79(10)	80(10)	81(10)	82(10)	83(10)	84(10)	85(10)	86(10)	87(10)	88)10)
La	2.24	24.30	899	0.966	2.97	0.304		20.3	3.34	5.35
Ce	5.57	74.0	1940	3.62	10.5	1.31	3.81	55.1	7.87	17.2
Pr										
Nd	4.44	50.9	815	4.18	10.2	2.51	3.52	40.0	3.13	12.8
Pm										
Sm	1.59	11.7	128	1.46	3.73	1.28	1.37	9.24	0.573	2.94
Eu	0.664	3.67	32.9	0.604	1.40	0.525	0.565		0.184	0.914
Gd	2.42		93.5		5.04	2.34	2.18	9.13	0.428	2.76
Tb										
Dy	3.25	9.74	67.4	2.70	4.67	2.97	3.23	7.63	0.650	2.37
Ho										
Er	2.16	4.97	30.4	1.72	2.30	1.91	2.18	3.75	0.473	1.17
Tm										
Yb	1.81	4.02	20.4	1.66	1.80	1.68	1.96	2.93	0.482	0.90
Lu										

Table VII - 1D Rare earth elements in crystal separates from xenoliths and megacrysts (cont'd)

Sample (Reference)	89(10)	90(10)	91(10)	92(10)	93(10)	94(10)	95(10)	96(10)	97(10)	98(10)
La	2.42		5.47	1040	15.7	20.7	11.8	0.459	0.355	1.54
Ce	5.36	13.0	14.1	1970	57.7	48.8	28.1	1.91	1.53	5.65
Pr										
Nd	2.01	7.82	7.63	800	41.8	32.4	15.4	3.41	2.83	5.78
Pm										
Sm	0.386	2.01	1.87	119	9.8	8.92	3.34	1.54	1.39	1.96
Eu	0.145	0.91	0.723	34.1	3.24	2.96	1.25	0.645	0.592	0.797
Gd	0.366	2.46	2.80	98.9	9.45	8.67	3.30	2.64	2.53	3.01
Tb										
Dy	0.301	2.68	2.77	62.5	8.27	7.43	4.14	3.17	3.12	3.40
Ho										
Er	0.174	1.65	1.70	27.5	4.3	3.50	2.55	1.94	1.99	1.83
Tm										
Yb	0.184	1.51	1.52	19.8	3.53	2.64	2.45	1.75	1.75	1.52
Lu										

Table VII - 2E Rb, Sr, Sr isotopes, Mineral Separates from Xenoliths and Megacrysts

Sample (Reference)	Rb	Sr	Rb/Sr	$^{87}Sr/^{86}Sr$	(References)	Rb	Sr	Rb	$^{87}Sr/^{86}Sr$
1(1)	.221	224	.0010	.7030	32(2)	.042	342.32	.0001	.70407±7(AW)
2(1)	.121	1.46	.083		33(2)	.046	13.04	.004	.70425±13(AW)
3(1)	.070	.237	.295		34(2)	.049	18.707	.003	.70413±8(AW)
4(1)	.120	24.6	.0048	.7025	35(2)	.049	22.144	.002	.70445±5(AW)
5(1)	.299	3.01	.099	.7080	36(1)	.134	52.5	.0025	.7032
6(1)	.130	1.65	.079	.7096	37(1)	.085	1.62	.052	.7043
7(1)	.067	43.7	.0015	.7025	38(3)	4.48	711.4	.006	.70271±5
8(1)	.079	1.17	.067	.7058	39(1)	.166	32.7	.0051	.7024
9(1)	.085	1.07	.079	.7060	40(3)	9.23	511.8	.018	.70288±6
10(3)	68.96	150.1	.459	.70325±7	41(3)	11.23	487.9	.023	.70273±5
11(3)	1.09	132.22	.008	.70328±9	42(3)	13.04	769.4	.017	.70266±5
12(4)	1.0	74	.014	.7016	43(2)	12.776	2503	.005	.70317±9
13(4)	1.2	2.4	.5	.708	44(3)	7.64	577	.013	.70275±5
14(4)	1.5	11	.14	.7087	45(5)				.70273
15(9)	2.40	169.5	.014	.7030±72	46(6)		2900		.7027
16(2)	.038	1.703	.022	.70261±8(AW)*	47(6)		2500		.7029
17(2)	.034	.322	.106	----(AW)	48(3)	9.64	516.3	.019	.70264±8
18(2)	.018	.233	.077	----(AW)	49(10)	5.35	9255	.001670	.70355±6
19(2)	.050	2.136	.023	.70484±10(AW)	50(10)	4.01	9383	.001236	.70355±4
20(2)	.083	2.976	.028	.70717±14(AW)	51(10)		8147		.70352±5
21(2)	.044	1.301	.034	.70555±12(AW)	52(10)		2652		.70349±4
22(2)	.054	5.295	.010	.70196±11(AW)	53(10)		1183		.70458±6
23(2)	.057	1.51	.038	.70579±7(AW)	54(10)		2367		.70329±5
24(2)	.035	.953	.037	.70585±18(AW)	55(10)	0.225	75.62	.00859	.70356±4
25(2)	.011	7.353	.001	.70230±6(AW)	56(10)	0.0536	58.33	.00266	.70352±6
26(2)	.003	.338	.009	.70302±13(AW)	57(10)	0.444	64.08	.0200	.70376±6
27(2)	.050	.189	.265	.70644±16(AW)	58(10)	1.134	67.63	.0485	.70387±4
28(2)	.059	5.643	.010	.70275±9(AW)	59(10)	1.117	74.83	.0432	.70382±4
29(2)	.073	21.99	.003	.70295±7(AW)	60(10)	0.051	0.437	.318	.70520+19-15
30(7)				.7084	61(10)	10.71	749.0	.04134	.70336±6
31(7)	1.2	2.9	.414	.7083	62(10)	3.3	1032	.00927	.70324±4

Samples: 1. Clinopyroxene, Cr-diopside lherzolite(?), San Carlos, Arizona. 2. Orthopyroxene, same xenolith as 1. 3. Olivine, same xenolith as 1. 4. Clinopyroxene, Cr-diopside lherzolite(?), San Carlos, Arizona. 5. Orthopyroxene, same xenolith as 4. 6. Olivine, same xenolith as 4. 7. Clinopyroxene, Cr-diopside lherzolite(?), Kilbourne Hole, New Mexico. 8. Orthopyroxene, same xenolith as 7. 9. Olivine, same xenolith as 7. 10. Phlogopite, Cr-diopside pyroxenite, Kilbourne Hole, New Mexico. 11. Clinopyroxene, same xenolith as 10. 12. Clinopyroxene, Cr-diopside lherzolite, Dish Hill, California. 13. Orthopyroxene, same xenolith as 12. 14. Olivine, same xenolith as 12. 15. Amphibole from Cr-diopside lherzolite, Dish Hill, California. 16. Clinopyroxene, Cr-diopside lherzolite,San Quintin, Baja California. 17. Orthopyroxene, same xenolith as 16. 18. Olivine, same xenolith as 16. 19. Clinopyroxene, Cr-diopside lherzolite, San Quintin, Baja California. 20. Orthopyroxene, same xenolith as 19. 21. Olivine, same xenolith as 19. 22. Clinopyroxene, Cr-diopside lherzolite, San Quintin, Baja California. 23. Orthopyroxene, same xenolith as 22. 24. Olivine, same xenolith as 22. 25. Clinopyroxene, Cr-diopside lherzolite,, San Quintin, Baja California. 26. Orthopyroxene, same xenolith as 25. 27. Olivine, same xenolith as 25. 28. Clinopyroxene, Cr-diopside lherzolite, San Quintin, Baja California. 29. Clinopyroxene, Cr-diopside clinopyroxenite, San Quintin, Baja California. 30. Orthopyroxene, Cr-diopside lherzolite,, Cerro Negro, New Mexico. 31. Olivine, same xenolith as 30. 32. Plagioclase, Feldspathic ultramafic group lherzolite, San Quintin, Baja California. 33. Clinopyroxene, same xenolith as 32. 34. Clinopyroxene, Al-augite clinopyroxenite, San Quintin, Baja California.. 35. Clinopyroxene, Al-augite clinopyroxenite, San Quintin, Baja California.. 36. Clinopyroxene, Al-augite wehrlite, Crater 160, Arizona. 37. Olivine, same xenolith as 36. 38. Kaersutite megacryst, San Carlos, Arizona. 39. Clinopyroxene megacryst (Al-augite), Kilbourne Hole, New Mexico. 40-42. Kaersutite megacrysts, Dish Hill, California. 43. Plagioclasm megacryst, San Quintin, Baja California. 44-45. Kaersutite megacrysts, Black Canyon (Hoover Dam), Arizona. 46-47. Feldspar megacrysts, Bandera, New Mexico. 48. Kaersutite megacryst, Deadman Lake, California. 49-54. Feldspar megacrysts, Lunar Crater, Nevada. 55-56. Al-augite clinopyroxene megacrysts Lunar Crater, Nevada. 57-59. Bottle green pyroxene clinopyroxene megacrysts (classified Cr-diopside by author), Lunar Crater field, Nevada. 60. Olivine megacryst, Lunar Crater field, Nevada. 61-62. Kaersutite megacrysts, Lunar Crater field, Nevada.

*AW=acid-washed.

Table VII - 2C Rb, Sr, Sr isotopes, Al-augite Group Xenoliths

Sample (Reference)	Rb	Sr	Rb/Sr	$^{87}Sr/^{86}Sr$	Sample Reference	Rb	Sr	Rb/Sr	$^{87}Sr/^{86}Sr$
1(3)	9.56	601.6	.016	.70269±5	4(10)	11.8	644	.0530	.70356±7
2(9)	9.42	416.0	.023	.70323±15	5(10)	4.4	556	.0225	.70369±5
3(6)		80		.7033	6(10)	12.8	210	.1763	.70368±6
					7(10)	2.8	516	.0157	.70331±5
					8(10)	10.0	301	.0961	.70354±4
					9(10)	5.8	345	.0486	.70335±6

Samples: 1-2. Hornblendite vein-amphibole, Dish Hill California. 3. Gabbro, Bandera, New Mexico. 4. Hornblendite, Lunar Crater field, Nevada. 5. Kaersutite clinopyroxenite, Lunar Crater field, Nevada. 6-8. Kaersutite gabbros, Lunar Crater field, Nevada. 9. Kaersutite wehrlite, Lunar Crater field, Nevada.

Table VII - 2D Rb, Sr, Sr isotopes, Bottle Green Pyroxene Group

Sample (Reference)	Rb	Sr	Rb/Sr	$^{87}Sr/^{86}Sr$
1(10)	.359	27.20	.0384	.70912±15
			.0377	.70896±5
2(10)	.280	11.8	.0683	.70418±5
3(10)	.152	23.57	.0186	.70502±6
4 (6)		38		.7023
5 (6)		110		.7040
6 (5)		47		.7023
7 (6)		108		.7031

Samples: 1. Harzburgite, Lunar Crater field, Nevada. 2. Dunite, Lunar Crater field, Nevada. 3. Lherzolite, Lunar Crater field, Nevada (Nos. 1-3 classified by author as cr-diopside group. 4-7. Green spinel lherzolite, Bandera, New Mexico.)

Table VII - 2A Rb, Sr, Sr isotopes, Host Rocks

Sample (Reference)	Rb	Sr	Rb/Sr	$^{87}Sr/^{86}Sr$	Sample (References)	Rb	Sr	Rb/Sr	$^{87}Sr/^{86}Sr$
1(1)	28.7	872	.033	.7028	12(6)			390	.7034
2(1)	27.0	540	.050	.7030	13(6)			620	.7028
3(3)	51.56	978.6	.053	.7033	14(7)	25	430	.058	.7039
				.70379±5					
4(4)	62	940	.066	.7031	15(7)				.7040
5(9)				.7028±11	16(8)				.7033±6
6(9)				.7031±18	17(1)	17.7	785	.022	.7031
7(2)	35.96	611.7	.059	.70311±8	18(10)	42.6	907.0	.1236	.70357±5
8(2)	26.58	560.7	.047	.70314±7	19(10)	17.18	484.1	.1026	.70454±6
9(3)	34.06	923.6	.037	.70399±8	20(10)	24.17	589.7	.1234	.70502±4
10(5)				.70456					
				.70316(AW)*					
11(6)		430		.7030					

Samples: 1. San Carlos, Arizona. 2. Kilbourne Hole, New Mexico. 3-6. Dish Hill, California. Nos. 3 and 5 are of the same sample. 7-8. San Quintin, Baja California. 9-10. Black Canyon (Hoover Dam) Arizona. 11-13. Bandera, New Mexico. 14-15. Cerro Negro (Puerco Plugs), New Mexico. 16. Malapai Hill, California. 17. Crater 160, Arizona.

References: 1. Stueber and Ikramuddin (1974). 2. Basu (1979). 3. Basu (1978). 4. Peterman and others (1970). 5. Foland and others (1980). 6. Laughlin and others (1971). 7. Kudo and others (1972). 8. Stull and Davis (1973). 9. M. A. Lanphere, unpublished data. 10. Bergman (1982).

*AW=acid-washed.

Table VII - 2B Rb, Sr, Sr isotopes, Cr-diopside Group Xenoliths

Sample (Reference)	Rb	Sr	Rb/Sr	$^{87}Sr/^{86}Sr$
1(2)	.043	1.591	.027	.70452±8 (AW)*
2(6)		20		.7045
3(6)		25		.7049
4(6)		100		.7055
5(7)	2.8	3.2	.875	.7090
				.7088
6(7)	0.8	5.9	.136	.7083
				.7082
7(7)				.7068
8(7)				.7069
9(7)	2.0	10.05	.199	.7070
				.7068
10(8)				.7043±8

Samples: 1. Lherzolite, San Quintin, Baja California. 2-4. Red spinel lherzolite, Bandera, New Mexico. 5-8, Lherzolite, Cerro Negro (Puerco Plugs), New Mexico. 9. Websterite, Cerro Negro, New Mexico. 10. Lherzolite, Malapai Hill, California.

*AW=Acid-washed

Table VII - 1D Rare earth elements in crystal separates from xenoliths and megacrysts (cont'd)

Sample (Reference)	99(10)	100(10)	101(10)	102(10)
La	1.50		7.22	6.14
Ce	4.65	27.7	28.2	19.4
Pr				
Nd	4.12	21.10	22.1	16.4
Pm				
Sm	1.57	5.61	5.47	4.81
Eu	0.683	1.92	1.84	1.66
Gd	2.73			
Tb				
Dy	3.16	5.29	5.3	5.06
Ho				
Er	1.96	2.83	2.75	2.68
Tm				
Yb	1.72	1.91	2.1	1.83
Lu				

Table VII - 3A Sr and Nd isotope ratios in host rocks

Sample (Reference)	$^{87}Sr/^{86}Sr$	$^{143}Nd/^{144}Nd$	Sm/Nd
1(1)	0.7029±2	0.513001±18	0.200
2(1)	0.70324±5	0.51289±28	0.183
3(1)	0.70310±3	0.512904±20	
4(1)		0.513053±12	
5(1)	0.70321±3		
6(2)	0.70296	0.513021±8	
7(2)	0.70304	0.513033±20	
8(2)	0.70295	0.513031±18	
9(2)	0.70321		
10(2)	0.70289		
11(2)	0.70285	0.513037±10	
12(2)	0.70327	0.5130025±20	
13(3)	0.70564±17	0.51269±1	
14(5)	0.70328±4	0.512980±33	0.218
		0.512970±32	
		0.512940±31	
15(5)	0.70339±7	0.512948±39	0.213
		0.512944±23	
16(5)	0.70375±6	0.512992±46	0.228

SAMPLES: 1-12, basalts, San Bernardino field, Arizona; 13, trachyandesite, Big Creek, California. 14-16, basalt rinds on xenoliths, Kilbourne Hole, New mexico.

References: (1) Menzies and others (1984); (2)Menzies and others (1983); (3) Domenick and others (1983); (4) Jagoutz and others (1980); (5) Roden and others (1984b).

Table VII - 3B. Sr and Nd isotope ratios in minerals separated from xenoliths, and megacrysts

Sample (Reference)	$^{87}Sr/^{86}Sr$	$^{143}Nd/^{144}Nd$	Sm/Nd
1(1)	0.70276±3	0.513118±16	0.358
2(1)	0.70287±3	0.513033±18	0.230
3(1)	0.70280±4	0.513003±28	0.157
4(1)	0.70308±3	).512983±14	0.349
5(1)	0.70277±4	0.513109±10	0.365
6(1)	0.70242±3	0.513285±12	0.510
7(1)	0.70197±4	0.513350±88	0.389
8(1)	0.70281±3	0.512965±20	0.231
9(1)	0.70321±4		
10(1)	0.70351±3	0.512778±42	0.182
	0.70346±6		
11(1)AW	0.70343±9	0.512740±14	
12(1)	0.70470±9	0.512603±12	0.230
		0.512652±32	
13(1)AW	0.70488±9	0.512584±30	
14(1)	0.70329±3	0.512945±66	0.192
15(1)	0.70274±6	0.512704±12	0.257
16(1)AW	0.70286±6	0.512704±12	
17(1)	0.70277±4	0.512931±34	0.245
18(1)	0.70289±3	0.513001±16	0.275
19(1)	0.70282±4	0.513045±24	0.216
20(1)	0.70317±3	0.512969±22	0.452
21(1)	0.70301±4	0.513085±22	0.491
22(1)	0.70297±4	0.512954±12	0.339
23(1)	0.70276±4	0.513161±42	0.381
24(1)	0.70331±3	0.512843±50	
25(1)	0.70303±5	0.512844±42	
26(1)	0.70305±5	0.512988±30	
27(1)	0.70286±4	0.513003±14	
28(1)	0.70292±4	0.513022±12	
29(1)	0.70289±3	0.513015±30	
30(1)	0.70299±3	0.513011±28	
31(1)	0.70288±4		
32(4)	0.70229±6	0.513308±15	0.52
33(4)	0.70361±4	0.513301±21	0.9200
34(4)	0.70255±9	0.513319±21	0.530
35(4)	0.70501±4	0.512764±11	0.360
36(4)		0.512763±24	0.360
37(5)	0.70286±7	0.513011±51	0.325
38(5)	0.70296±6		
	0.70295±9	0.513058±19	
	0.70284±7		
39(5)	0.70284±5	0.512987±30	0.305
40(5)	0.70284±8		
	0.70273±7	0.513073±31	0.306
	0.70268±7		

Samples: 1. Clinopyroxene, Cr-diopside lherzolite, San Bernardino field, Arizona. 2. Amphibole, same xenolith as 1. 3. Apatite, same xenolith as 1. 4-6. Clinopyroxenes, Cr-diopside lherzolite, San Bernardino field, Arizona. 7. Clinopyroxene Cr-diopside lherzolite Dish Hill, California. 8. Amphibole, vein, same xenolith as 7. 9. Mica, vein, same xenolith as 7. 10-11. Clinopyroxene, Cr-diopside lherzolite, San Bernardino field, Arizona; 11 is acid-washed. 12- 13. Clinopyroxene, Cr-diopside lherzolite, San Bernardino field, Arizona; 13 is acid-washed. 14. Mica, Clinopyroxene, Cr-diopside lherzolite, San Bernardino field, Arizona. 15-16. Clinopyroxene, same xenolith as 14; 16 is acid-washed. 17. Clinopyroxene, Cr-diopside lherzolite, San Bernardino field, Arizona. 18. Amphibole, vein, Cr-diopside lherzolite, Dish Hill, California. 19. Clinopyroxene, same xenolith as 18. 20. Clinopyroxene, Cr-diopside pyroxenite layer. 21. Clinopyroxene, Cr-diopside lherzolite in contact with 20. 22. Clinopyroxene, Al-augite pyroxenite layer. 23. Clinopyroxene, Cr-diopside lherzolite in contact with 22. 24. Clinopyroxene, Al-augite pyroxenite layer. 25. Clinopyroxene, Al-augite peridotite in contact with 24. 26. Amphibole, periodotite, San Bernardino field, Arizona. 27. Amphibole, vein, San Bernardino field, Arizona. 28-29. Amphiboles, peridotites, San Bernardino field, Arizona. 30-31. Kaersutite megacrysts, San Bernardino field, Arizona. 32. Clinopyroxene, Cr-diopside lherzolite, Kilbourne Hole, New Mexico. 33. Orthopyroxene, same xenolith as 32. 34. Whole rock, Cr-diopside lherzolite, same xenoliths as 32. 35. Clinopyroxene, Cr-diopside lherzolite San Carlos, Arizona. 36. Whole rock, Cr-diopside lherzolite, same xenolith as 35. 37. Clinopyroxene, Al-augite clinopyroxenite, Kilbourne Hole, new Mexico. 38. Clinopyroxene, Al-augite clinopyroxenite, Kilbourne Hole, New Mexico. 39. Clinopyroxene, lherzolite, composite with 38. 40. Clinopyroxene, Al-augite olinopyroxenite, Kilbourne Hole, New Mexico. 41. Clinopyroxene, lherzolite, composite with 40. 42-44. Clinopyroxenes, coarse grained Cr-diopside lherzolites, Kilbourne Hole, New Mexico. 45-46. Clinopyroxenes, fine-grained Cr-diopside lherzolites, Kilbourne Hole, New Mexico.

References: Same as Table VII - 3A

Table VII - 3B Sr and Nd isotope ratios in minerals separated from xenoliths (cont'd.)

41(5)	0.70280±5	0.513084±19	0.312
42(5)	0.70178±9		
	0.70176±6	0.513122±18	0.466
	0.70194±7		
43(5)	0.70389±9	0.512924±17	0.319
	0.70375±7		
44(5)	0.70210±6	0.513326±28	0.424
45(5)	0.70304±6	0.513054±14	0.302
46(5)	0.70451±4	0.512797±26	0.229

VII - 3C. Sr and Nd isotope ratios of xenoliths

Sample Reference)	$^{87}Sr/^{86}Sr$	$^{143}Nd/^{144}Nd$	Sm/Nd
1(1)	0.70351±4	0.513048±10	
2(3)	0.70312±9	0.51306±3	
3(3)	0.70409±11		
	0.70418±12		
	0.70419±10		
4(3)AW	0.70631±15	0.51233±1	
5(3)	0.70505±11	0.51269±1	
	0.70504±14		
	0.70506±9		

Samples: 1. Cr-diopside lherzolite, San Bernardino Field, Arizona. Same xenolith as samples 1-3, Table VII - 3B. 2. Cr-diopside lherzolite Pinchot, California. 3. Garnet lherzolite, Big Creek, California. 4. Carbonate-bearing garnet pyroxenite, Big Creek, California. 5. Garnet pyroxenite, Big Creek, California.

Table VII - 4A ^{18}O, Host rocks

Sample (Reference)	^{18}O
1(1)	+6.0
2(4)	6.3
3(2)	5.6±.3
4(2)	6.4±.1
5(4)	5.8
6(1)	6.2
7(1)	5.8
8(1)	5.9
9(1)	6.4

Samples: 1-4, San Carlos, Arizona. 5. Kilbourne Hole, New Mexico. 6 Dish Hill, California. 7-9. San Quintin, Baja California.

References: 1. Kyser and others (1981). 2. Rumble and others (1979). 3. Boettcher and O'Neil (1980). 4. Kyser (1980).

Table VII - 4B ^{18}O, Cr-diopside Group Xenoliths

Sample (Reference)	Whole Rock (calc)	^{18}O Spinel	Olivine	Clinopx	Orthopx
1(1)	5.7	5.3	6.0	5.7	5.6
2(1)	5.6		5.3	5.7	5.7
3(1)	5.4		5.2	5.4	
4(1)	5.5	4.6	4.9	5.4	5.6
5(1)	5.2	4.8	5.6	5.8	5.6
6(1)	5.3	4.0	5.1	5.6	6.1
7(1)	6.0		5.9	5.8	6.1
8(1)	6.5		6.4	6.5	6.4
9(1)	6.2	5.3	6.3	5.6	5.7
10(1)	7.0		7.2	5.8	5.9
11(1)	6.5	5.3	6.7	5.6	5.3
12(1)	6.0	4.9	6.1	5.9	5.6
13(1)	5.9		6.1	5.9	6.1

Samples: 1-3, lherzolite, San Carlos, Arizona. 4-6, lherzolite, Kilbourne Hole, New Mexico. 7-8. lherzolite, Dish Hill, California. 9-13, lherzolite, San Quintin, Baja California.

Table VII - 4C $\delta^{18}O$, Al-augite Group Xenoliths

Sample (Reference)	Rock (calc)	Spinel	Olivine	Clinopx	Orthopy	Plag.	Amphib.	Mica
1(1)	5.6		5.6	5.5	5.4	5.1	5.8	
2(1)	5.6	4.2		5.6				
3(1)	5.5	5.4		5.5				
4(1)	5.6		4.8	5.6			5.8	
5(4)	5.7		5.8				5.5	
6(2)	5.7±2							
7(3)						5.57	6.11	
8(3)						5.12		
9(3)						6.01		

Samples: 1. Olivine ##los, Arizona. 3. (Plag.) clinopyroxenite, San Carlos, Arizona. 4. Olivine kaersutite (plag.) clinopyroxenite, San Carlos, Arizona. 5. Kaersutite peridotite, San Carlos, Arizona. 6. Clinopyroxenite, San Carlos, Arizona. 7. Kaersutite and phlogopite, hornblendite vein, Dish Hill, California. 8. Kaersutite, kaersutite-clinopyroxene xenolith, Williams, Arizona. 9. Kaersutite, hornblendite vein, Cima, California.

Table VII - 4D $\delta^{18}O$, Megacrysts

Sample (Reference)	$\delta^{18}O$
1(3)	4.73
2(3)	4.65
3(3)	5.55
4(3)	5.13
5(1)	5.8
6(1)	5.9
7(1)	6.7
8(1)	6.6
9(1)	5.7
10(3)	4.65
11(3)	5.40
12(3)	4.76
13(3)	4.77
14(3)	5.39

Samples: 1. Kaersutite megacryst, Black Canyon (Hoover Dam), Arizona. 2-4. Kaersutite megacryst, Deadman Lake, California. 5. Olivine megacryst, Black Rock Summit, Nevada. 6. Clinopyroxene megacrysts (Al-augite), Black Rock Summit, Nevada. 7. Anorthoclase megacryst Black Rock Summit, Nevada. 8. Clinopyroxene megacryst (bottle green pyroxene; classified Cr-diopside by author), Black Rock Summit, Nevada. 9. Clinopyroxene megacryst (Al-augite), Dish Hill, California. 10. Kaersutite megacryst, Cima, California. 11-12. Kaersutite megacryst,, Vulcans Throne, Arizona. 13. Kaersutite megacryst, West Potrillo Mts., New Mexico. 14. Kaersutite megacryst, dike, West Texas (Irving, 1977).